Eduardo Antonio Pina

Thermoeconomic and environmental synthesis and optimization of polygeneration systems supported with renewable energies and thermal energy storage applied to the residential-commercial sector

Departamento

Ingeniería Mecánica

Director/es

Lozano Serrano, Miguel Ángel
Serra de Renobales, Luis María

Tesis Doctoral

THERMOECONOMIC AND ENVIRONMENTAL SYNTHESIS AND OPTIMIZATION OF POLYGENERATION SYSTEMS SUPPORTED WITH RENEWABLE ENERGIES AND THERMAL ENERGY STORAGE APPLIED TO THE RESIDENTIAL-COMMERCIAL SECTOR

Autor

Eduardo Antonio Pina

Director/es

Lozano Serrano, Miguel Ángel
Serra de Renobales, Luis María

UNIVERSIDAD DE ZARAGOZA

Ingeniería Mecánica

2019

Universidad Zaragoza
1542

Doctoral Thesis

Thermoeconomic and environmental synthesis and optimization of polygeneration systems supported with renewable energies and thermal energy storage applied to the residential-commercial sector

Author

Eduardo Antonio Pina

Advisors

Miguel Ángel Lozano Serrano
Luis María Serra de Renobales

UNIVERSIDAD DE ZARAGOZA

Ph.D. Program in Mechanical Engineering

2019

ACKNOWLEDGEMENTS

Completing a PhD thesis is a real milestone in life, but this is the outcome of the effort and sacrifices required, the good and even the bad experiences that we have, and the collective work of countless people. I am very fortunate to have met amazing people that have supported me in my personal and academic life over these years.

First, I would like to express my heartfelt gratitude to my PhD supervisors, Prof. Miguel A. Lozano and Prof. Luis M. Serra, without whom this thesis would not have been possible. Thank you for the time invested in me, the patience, the spot-on insights, and the thorough reviews.

I would also like to thank Prof. Silvia Nebra, from the Universidade Federal do ABC, for her invaluable mentoring since I was an undergraduate student in Brazil. I also thank my former master's degree supervisor, Prof. Marcelo Modesto, for encouraging me to follow my PhD studies abroad. From the Politécnico di Torino, in Italy, I would like to thank Prof. Vittorio Verda and post-doc fellow Elisa Guelpa for receiving me during my research stay in 2018.

My heartfelt thanks to the professors, fellow colleagues and friends from the GITSE (Thermal Engineering and Energy Systems Group) and the University of Zaragoza for welcoming me to the group, the coffee breaks, the dinners, and the friendship.

I would like to thank my parents for the sound foundation, for giving me the freedom to make my own choices, and for supporting me even when one of those decisions meant moving abroad. To my friends back in Brazil, I thank you for our strong friendship even after four years and 8500 km apart.

And Jon, you were always there. I could not have gotten through this PhD without you.

ABSTRACT

Residential-commercial sector buildings are responsible for a significant share of the world energy consumption and yet there is a largely untapped potential for energy savings. Advanced energy systems, such as polygeneration systems (in which two or more energy services are produced from a common energy resource) assisted with on-site renewable energy sources (RES) and thermal energy storage (TES), are regarded as key alternatives to supply the buildings' energy demands efficiently and in a way that promotes higher economic savings and reduced environmental impacts. However, determining the best configuration and operational strategy of polygeneration systems is a complex task owing to the multiple technology options available and their feasible interrelations, and the dynamic operating conditions of buildings and their surroundings (e.g. variable energy demands, climatic conditions, energy and equipment prices, CO_2 emission factors). Once the system configuration and operational planning are established, the additional issue remains of the appropriate way to allocate the costs of the energy resources consumed to the final products obtained. In this context, the overall aim of this thesis is to develop methodologies for the synthesis and optimization of polygeneration systems in residential-commercial buildings that capture their dynamic behavior and local-based constraints, thereby addressing several research gaps: multi-objective optimization models with balanced objective functions; accurate representation of dynamic operating conditions; realistic representation of the thermal requirements of the energy supply and demand in the superstructure; and rational cost allocation approaches for an equitable share of costs among the final consumers. As a conceptual approach, simple trigeneration systems are first analyzed, outlining the potential benefits and the challenges involved in incorporating different types of technologies. Also, the thermoeconomic analysis of a simple trigeneration system with TES is carried out, seeking clarity of the concepts and explaining the role of the TES in achieving the optimal economic cost solution. More complex polygeneration systems are then proposed for two case studies, one consisting of a multi-family building in Zaragoza (Spain) and the other consisting of a university hospital in Campinas (Brazil). A multi-objective optimization procedure is developed, in which mixed integer linear programming (MILP) models are developed to determine the optimal system configuration (based on real commercially available equipment) and multi-period operational planning from the economic (total annual cost) and environmental (total annual CO_2 emissions) viewpoints. The technical, economic, and environmental feasibility of renewable-based polygeneration systems in Brazil is assessed with a careful representation of the Brazilian electricity sector regulations. This thesis' main contributions to the synthesis and operation optimization subject include the development of the MILP models with a view to ensuring the same level of detail, flexibility, and a more realistic representation of the thermal integration. Regarding the thermoeconomic analysis subject, this thesis contributed by proposing cost allocation approaches for the incorporation of TES units, free RES, components with different products for different operation modes, and joint production of energy services in dynamic energy systems.

RESUMEN

Los edificios del sector residencial-comercial son responsables de una parte importante del consumo energético mundial y, a su vez, existe un gran potencial de ahorro energético en este sector que está todavía en gran medida sin explotar. Los sistemas de poligeneración (en los que dos o más servicios energéticos se producen a partir de un recurso energético común) con fuentes de energía renovable (RES) y almacenamiento de energía térmica (TES), constituyen alternativas clave para atender las demandas de energía de los edificios de manera eficiente y que promueva mayores ahorros económicos y menores impactos ambientales. No obstante, obtener la mejor configuración y estrategia de operación de estos sistemas es una tarea compleja debido a la gran variedad de tecnologías y sus posibles interrelaciones, y a las condiciones dinámicas de operación del edificio y de su entorno (demandas de energía, condiciones climáticas, precios de energía y equipos, factores de emisión de CO_2). Una vez establecidas la configuración del sistema y la estrategia de operación queda la cuestión de cómo asignar los costes de los recursos energéticos a los productos finales. En este sentido, el objetivo de esta tesis es desarrollar metodologías de síntesis y optimización de sistemas de poligeneración en edificios del sector residencial-comercial que consideren su comportamiento dinámico y sus restricciones locales, abordando así aspectos poco investigados hasta la fecha: modelos de optimización multiobjetivo con funciones objetivo equilibradas; representación precisa de las condiciones dinámicas de operación; representación realista de los requisitos térmicos de la oferta y demanda en la superestructura; y propuestas de asignación de costes para un reparto justo entre los consumidores finales. Desde un enfoque conceptual, se analizan sistemas de trigeneración simples, describiendo las ventajas potenciales y los desafíos involucrados en la incorporación de diferentes tipos de tecnologías. Además, se lleva a cabo el análisis termoeconómico de un sistema de trigeneración simple con TES, buscando la claridad de los conceptos y explicando el papel que juega el TES para conseguir la solución óptima. A continuación, se proponen sistemas de poligeneración complejos para dos estudios de caso, un edificio multifamiliar en Zaragoza (España) y un hospital universitario en Campinas (Brasil). Se desarrolla un procedimiento de optimización multiobjetivo en el que se elaboran modelos de programación lineal entera mixta (PLEM) para determinar la configuración óptima del sistema (basada en equipos reales disponibles en el mercado) y la estrategia de operación multiperiodo desde las perspectivas económica (coste total anual) y ambiental (emisión de CO_2 total anual). La viabilidad técnica, económica y ambiental de los sistemas de poligeneración basados en energías renovables en Brasil se evalúa con una minuciosa representación del reglamento del sector eléctrico brasileño. Las principales aportaciones de esta tesis al campo de la síntesis y optimización consisten en el desarrollo de modelos de PLEM con el fin de garantizar el mismo nivel de detalle, flexibilidad, y una representación realista de la integración térmica. Con respecto al análisis termoeconómico, esta tesis presenta contribuciones novedosas al proponer y establecer criterios de asignación de costes para la incorporación de TES, la operación con RES, equipos multiproducto con distintos modos de operación, y producción conjunta de servicios energéticos en sistemas dinámicos.

TABLE OF CONTENTS

LIST OF FIGURES

LIST OF TABLES

LIST OF ACRONYMS

AB	Auxiliary boiler
ABD	Double-effect absorption chiller
ABS	Single-effect absorption chiller
ABT	Triple-effect absorption chiller
AC	Single-effect absorption chiller
AD	Double-effect absorption chiller
ANEEL	Brazilian Electricity Regulatory Agency
AS	Single-effect absorption chiller
BH	Biomass hot water boiler
BV	Biomass steam boiler
CCHP	Combined Cooling, Heat and Power
CHP	Combined Heat and Power
CM	Cogeneration module
COP	Coefficient of Performance
CS	Chilled water storage tank
CT	Cooling tower
DES	Distributed Energy System
DHW	Domestic hot water
EC	Mechanical chiller
EECS	Electrical Energy Compensation System
EER	Energy Efficiency Ratio
EES	Engineering Equation Solver
GB	Natural gas boiler
GE	Cogeneration module
GH	Natural gas hot water boiler
GHG	Greenhouse gas emissions
GV	Natural gas steam boiler
HP	Reversible heat pump
HPQ	Heat pump in heating mode
HPR	Heat pump in cooling mode
HS	Hot water storage tank
HTF	Heat Transfer Fluid
ICE	Internal Combustion Engine
IDAE	Institute for the Diversification and Saving of Energy
IEA	International Energy Agency
LCA	Life Cycle Assessment
LHV	Lower Heating Value
LP	Linear programming
MILP	Mixed integer linear programming
MINLP	Mixed integer non-linear programming
MOO	Multi-objective optimization
NLP	Non-linear programming
PM	Prime mover
PT	Parabolic trough collector
PV	Photovoltaic panel
RES	Renewable energy sources

CHAPTER 1

Introduction

1   INTRODUCTION

This thesis explores the synthesis and optimization of polygeneration systems for residential-commercial buildings with special consideration for the integration of thermal energy storage and renewable energy sources. In this introductory chapter, Section 1.1 states the problem addressed; Section 1.2 provides a general background to the undertaken research; Section 1.3 declares the objectives and contributions of this thesis; and Section 1.4 outlines the structure of this work.

1.1   PROBLEM STATEMENT

Energy demand is increasing worldwide owing to demographic and economic exponential growth. The current world population of 7.6 billion is expected to reach 9.8 billion in 2050, half of which being attributable to developing countries (UN, 2017). As human development and energy consumption are closely linked, over the last decades our society has been facing the challenge of improving quality of life while lowering environmental impacts in an economical and efficient manner. Still, fossil fuels continue to play a dominant role in the world energy supply. As of 2016, the global total primary energy supply was 13,761 Mtoe, 81.4% of which corresponded to fossil fuels (IEA, 2018). Such dependence brings forth concerns about the depletion of current fossil fuel resources, the effects of geopolitics and/or global energy markets on energy supply security and prices, and the potential damaging impacts of climate change induced by greenhouse gas (GHG) emissions.

In this respect, industrialized countries have committed to reducing their GHG emissions while also procuring energy security and energy equity. To this end, there can be identified three main top priority actions in the transition to sustainable energy systems (EU, 2010; IEA, 2017a; WEC, 2016): (i) the transformation of energy supply, characterized by the diversification of the primary energy supply and electricity generation through renewable energy sources (RES) and non-conventional energy resources (e.g. waste heat); (ii) energy efficiency measures; and (iii) the decarbonization of the energy sector.

A paradigm shift is currently taking place on two levels in the energy sector, as illustrated in Figure 1.1: on the one hand, there is a shift from single-fuel single-product energy systems to multiple-fuels multiple-products energy systems (Hemmes et al., 2007; Mancarella, 2014); and on the other hand, there is a shift from conventional centralized power systems to Distributed Energy Systems (DES) (Chicco and Mancarella, 2009; Manfren et al., 2011).
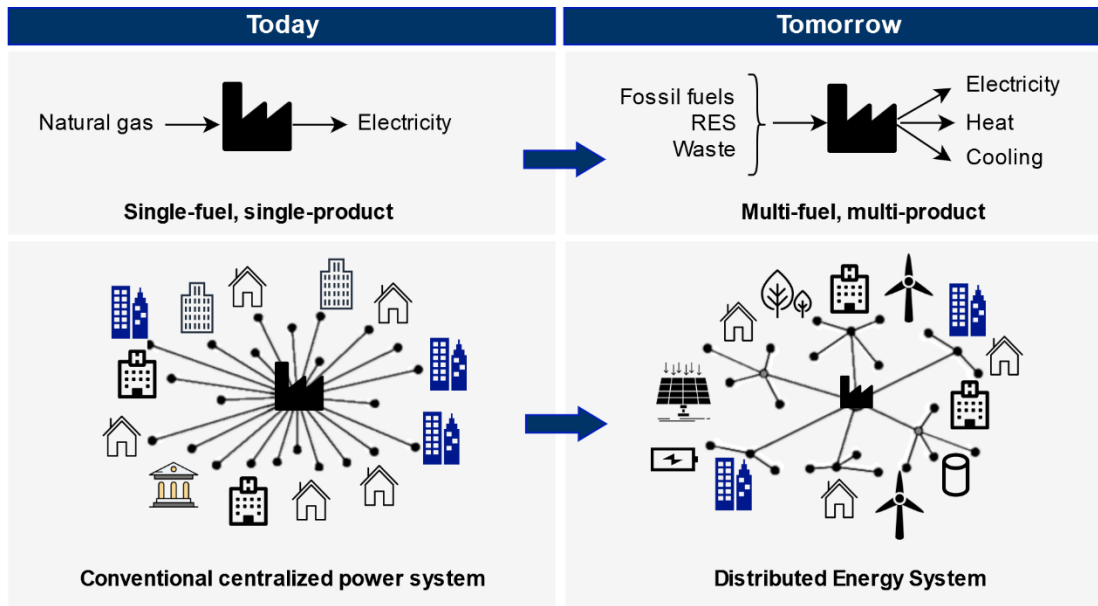
Figure 1.1: Paradigm shift in the energy sector.

Conventional centralized power systems follow a top-down unidirectional electricity supply from large-scale generators to a broad consumer base. For example, a central power plant consuming one fuel, such as natural gas, supplying one product, such as electricity, and dissipating waste heat into the environment, while household heating and cooling demands are generally covered by individual production at the consumer level through gas boilers, electric heaters, air conditioning units, etc. In contrast, DES are located in or near end-users, providing electricity and thermal energy through technologies of various rated capacities scattered over the territory. District Heating and Cooling Systems are typical examples of DES located close to end-users. As a result, numerous benefits can be derived from DES over centralized power supply systems (Angrisani et al., 2012; Chicco and Mancarella, 2009; Liu et al., 2013; Wu and Wang, 2006): (i) reduction in transmission and distribution energy losses, as well as in the associated costs; (ii) increased renewable energy deployment; (iii) improved electric grid reliability and flexibility; (iv) backup services; and (v) access to energy in remote areas.

DES may be divided into two major overlapping categories (Wu and Wang, 2006): one is related to on-site renewable energy systems (e.g. photovoltaic panels, solar thermal collectors, wind turbine generators), while the other concerns high-efficiency energy systems, such as cogeneration and trigeneration systems. It must be noted, however, that these systems are not exclusively decentralized, as such classification depends on their location, size, and application.

Cogeneration and trigeneration fit into the broader concept of polygeneration, which corresponds to the combined production of two or more energy services from a common energy resource. Owing to an appropriate energy integration between the constituting devices and energy flows, polygeneration systems can achieve higher energy efficiency, lower primary energy consumption,

lower unit costs of the final products, and lower environmental burdens relative to the conventional separate production (Mancarella, 2014; Rong and Lahdelma, 2016; Serra et al., 2009).

Despite the obvious benefits, the application of polygeneration systems in residential-commercial buildings is still incipient. This is mainly due to the considerable complexity of the design problem for buildings applications, which calls for novel cross-disciplinary approaches that take into account the multi-faceted nature of the problem, characterized by multiple energy resources, multiple energy products, multiple technology options, and multiple operation periods. Additionally, an inherent problem of such highly integrated energy systems is the appropriate way to allocate the resources consumed to the internal flows and final products. The way in which allocation is made is important because it directly affects the costs of the final products obtained and, thus, the final consumers' behavior and policy makers' decisions.

This thesis aims to address the aforementioned issues by proposing methodologies for the synthesis, optimization, and thermoeconomic analysis of polygeneration systems in residential-commercial buildings applications. Close attention will be given to the integration of renewable energy sources and thermal energy storage, given the dynamic operating conditions entailed by these technologies. Moreover, the appropriate ways to allocate the costs of the resources consumed by the system to its internal flows and final products will be proposed, tackling issues that have not been deeply studied so far in thermoeconomics regarding the presence of thermal energy storage units, the deployment of free energy resources (e.g. solar radiation), the integration of a device that has different products for different operation modes (e.g. a reversible heat pump that produces heat in heating mode and cooling in cooling mode), and the joint production of energy services in dynamic operating conditions. As a result, it is expected that this thesis can promote a more widespread understanding and adoption of polygeneration systems by the society.

1.2 BACKGROUND

This section provides a background to the main topics addressed in this thesis, namely the application of polygeneration systems in residential-commercial buildings (Section 1.2.1), the integration of thermal energy storage and renewable energy sources (Section 1.2.2), the synthesis and optimization of polygeneration systems (Section 1.2.3), and the thermoeconomic analysis (Section 1.2.4).

1.2.1 Polygeneration systems in residential-commercial buildings

The term buildings generally refers to residential and commercial buildings, which include a variety of applications such as households, offices, hotels, restaurants, hospitals, shopping centers, schools, universities, sports center, and government buildings. Depending on their application and geographic location (e.g. climatic conditions, local regulations), these buildings may differ on size, technical standards, building envelope, occupancy, and installed equipment (lighting and appliances), among others. These aspects determine the types and quantities of energy services demanded by the buildings.

Energy consumption in buildings includes electricity (e.g. for lighting, cooking, and appliances) and thermal energy (e.g. space heating, hot water, and space cooling). Space heating and domestic hot water account for half to two thirds of energy use in households of Europe and the United States (EEA, 2016; Harvey, 2012). Although less prominent, space cooling has seen a sharp increase over the last years owing to higher standards of living, cheaper air-conditioning units and more frequent occurrence of hot weather conditions, and is likely to double between 2016 and 2020 according to the International Energy Agency (IEA, 2017a).

The case is that buildings are progressively being recognized as relevant actors in the world energy consumption. As a matter of fact, buildings account for a substantial share of the world energy consumption, comprising about 25-40% of the final energy consumption in developed countries (EU, 2012; Harvey, 2012; IEA, 2017b). What is more, space heating and space cooling account for 9% and 2%, respectively, of the global final energy use (IEA, 2017a).

As reported by the IEA (2017c), there is a considerable potential for energy savings in heating and cooling that remains largely untapped. In the context of promoting energy efficiency in buildings, it becomes imperative to develop alternative ways to attend the increasing energy demands in an economical and environmentally sound manner. This need is addressed by the European Union Directive 2010/31/EU (EU, 2010), which establishes that member states must improve the energy performance of buildings through high-efficiency alternative energy systems, such as cogeneration and trigeneration, and on-site renewable energy systems.

Cogeneration, also known as Combined Heat and Power (CHP), generally refers to the joint production of electricity (and/or mechanical energy) and heat from a common resource. A typical extension of cogeneration is trigeneration, or Combined Cooling, Heating and Power (CCHP), which usually refers to the combined production of electricity, heat and cooling.

Simple cogeneration and trigeneration systems are depicted in Figure 1.2. The core of a cogeneration system is the cogeneration module, composed of a prime mover (e.g. reciprocating

internal combustion engine, stirling engine, gas turbine, microturbine, fuel cell), in which the chemical energy of the fuel is converted into shaft power, coupled to an electricity generator and a heat recovery system. Trigeneration systems extend the thermal and/or mechanical/electrical coverage of cogeneration systems by incorporating a thermally activated technology (TAT), such as an absorption chiller, and/or a mechanical chiller. Thus, they are particularly interesting for applications with heating demands restricted to a few winter months and significant need for cooling during the summertime (e.g. Mediterranean countries) or throughout the year (e.g. tropical countries). Auxiliary equipment, such as steam or hot water boilers and heat pumps, are often included to guarantee supply and avoid oversizing the cogeneration module.
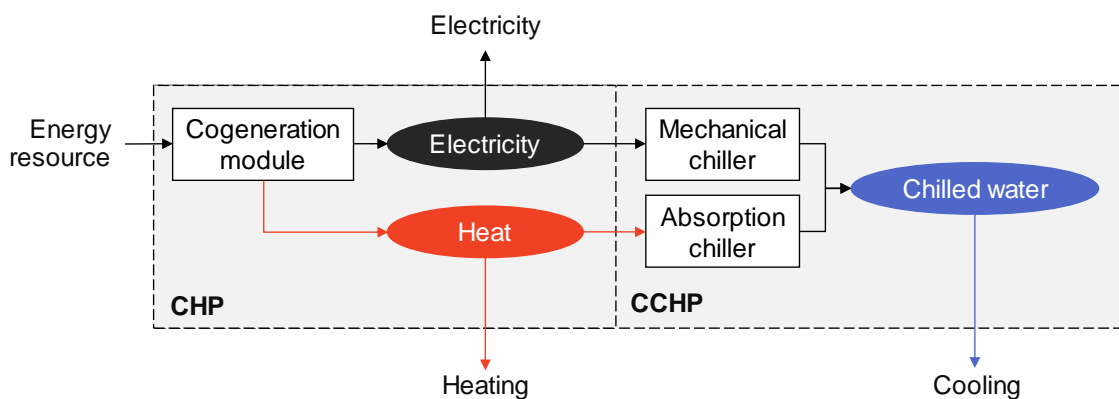
Figure 1.2: CHP and CCHP diagrams.

Several classifications of cogeneration systems have been defined in the technical and scientific literature with respect to their sizes (maximum electric power output); for instance, in accordance with Liu et al. (2014) these may be micro-scale (under 20 kW_{el}), small-scale (between 20 kW_{el} and 1 MW_{el}), medium-scale (between 1 and 10 MW_{el}) and large-scale (larger than 10 MW_{el}) systems. Knight et al. (2005) and Murugan and Horák (2016) reviewed micro-cogeneration systems for single- and multi-family residential applications. Trigeneration systems of various sizes and for different applications have been reviewed by Wu and Wang (2006), Liu et al. (2014) and Jradi and Riffat (2014), who have also considered development status and barriers around the world, especially Europe, the United States and China. In particular, micro-trigeneration systems have been reviewed by Angrisani et al. (2012), Gluesenkamp et al. (2013) and Sonar et al. (2014). A review of TATs for trigeneration systems has been developed by Deng et al. (2011), demonstrating their potential also in obtaining energy savings and environmental protection. Examples of polygeneration systems and their benefits are discussed by Serra et al. (2009), Rong and Lahdelma (2016) and Jana et al. (2017).

An overview of the potential benefits that can be derived from polygeneration systems for buildings applications in the sustainable energy scenario, the main conditions for their success, and the limiting factors for their full implementation is provided in Table 1.1.

Table 1.1: Benefits, enabling conditions and difficulties of polygeneration systems.

Potential benefits	- High flexibility, reliability and efficiency - High energy integration and recoverable waste heat - High economic performance - High RES deployment - Low negative environmental impacts - Rational use of energy resources
Conditions for success	- Final consumers are also the owners of the energy supply system - Economic stability of the business - Favorable market conditions - Stable and favorable regulatory environment
Limiting factors	- High initial investment costs - Low technical training or absence of qualified staff - Misleading belief that individual energy supply provides greater reliability - Insufficient political and administrative support mechanisms

1.2.2   Integration of thermal energy storage and renewable energy sources

Renewable energy sources, apart from high-efficiency cogeneration, also play a fundamental role in the transition towards sustainable energy systems. Renewable energy technologies (RETs) based on solar (e.g. photovoltaic panels, solar thermal collectors, hybrid photovoltaic/thermal), wind (e.g. wind turbine generator) and biomass (e.g. biomass boiler), among others, are increasingly being integrated in polygeneration systems, promoting higher flexibility as well as energy, economic, and environmental performances (Jana et al., 2017). An interesting example of a renewable-based polygeneration system integrated into district systems is the Marstal plant, which included solar thermal collectors, biomass (wood chips), seasonal storage, heat pump, and CHP (Nielsen, 2014).

There are many ways in which solar energy can be effectively deployed to cover multiple energy demands directly (e.g. photovoltaic panels producing electricity; solar thermal collectors producing hot water for space heating) and/or by coupling to heating/cooling technologies (e.g. photovoltaic panels coupled to an electric heat pump for hot water production; solar thermal collectors producing hot water to drive an absorption chiller). Solar systems for both heating and cooling generation optimally exploit the solar radiation throughout the year, producing cooling in the summertime and heating in the wintertime. Solar-powered air-conditioning systems also benefit greatly from the high correlation between solar radiation and cooling loads in the summer.

Other examples of solar energy-based heat and power generation systems in various applications have been reviewed by Modi et al. (2017), also including ground-source heat pump, biomass boiler, and Organic Rankine Cycle.

However, fully renewable energy systems based on intermittent RES, such as solar and wind, are found incapable of appropriately following the dynamic consumer load profiles in a reliable way (Modi et al., 2017). In this context, coupling dispatchable cogeneration systems with intermittent RES, in so-called hybrid energy systems, increases the flexibility of the system as well as its energy, economic and environmental performances (Chicco and Mancarella, 2009). Further benefits can be derived from the integration of energy storage, such as higher energy security, higher overall system performance and lower operation costs, as well as a reduction in the installed capacity of other technologies (Buoro et al., 2014; Rubio-Maya et al., 2011).

Commonly used energy storage technologies include electric energy storage (EES) units, such as electric batteries, and thermal energy storage (TES) units, such as hot water storage tank, chilled water storage tank and ice storage tank. The incorporation of TES units results in a better utilization of intermittent RES, thus overcoming the mismatch problem between energy services production and consumption (Buoro et al., 2014). Likewise, TES can improve the utilization of cogeneration by absorbing excess waste heat in times when production surpasses demand, allowing the prime mover to operate in a more continuous way and avoiding frequent occurrence of transient behavior during start-up and shutdown (Crespo Del Granado et al., 2016; Haeseldonckx et al., 2007). In addition, cooling systems may take advantage of the possibility to store energy in the TES to shift operation to nighttime periods, with higher energy efficiency and possibly lower electricity prices (Khan et al., 2004; Lozano et al., 2010). Environmental benefits can also be derived from TES integration, for example in the reduction of CO_2 emissions associated with the operation of cogeneration facilities connected to the electric grid (Haeseldonckx et al., 2007; Voorspools and D'Haeseleer, 2002).

A technology review of both EES and TES was presented by Gallo et al. (2016), who have also addressed applications and development status. Regarding TES, Arteconi (2012) and Li and Zheng (2016) reviewed various TES integration forms and applications. In particular, recent publications have investigated the integration of TES in cogeneration (Bianchi et al., 2013; Buoro et al., 2014; Capuder and Mancarella, 2014; Wakui et al., 2016), trigeneration (Lai and Hui, 2010; Liu et al., 2015; Lozano et al., 2010) and polygeneration systems (Barberis et al., 2016; Rivarolo et al., 2013; Rubio-Maya et al., 2011), as well as district heating systems (Olsthoorn et al., 2016). Overall, it has been shown that the proper sizing of the storage volume and prime mover capacity is one of the key factors to achieve the energy benefits and economic profitability of TES in polygeneration systems (Arteconi et al., 2012; Bianchi et al., 2013).

The connection to the electric grid and the possibility to inject or sell electricity to the grid are also regarded as essential factors to achieve not only better energy use and reliability but also economic benefits, thus improving the economic feasibility of polygeneration systems (Gallo et al., 2016; Jiménez Navarro et al., 2017; Mendes et al., 2011).

Figure 1.3 illustrates the complexity that arises from the integration of RETs and TES in polygeneration systems, as there are many available technologies and different combinations between them. Not evident in the figure but nonetheless important, there is the issue of the temporary variations in environmental conditions (ambient temperature, solar radiation, etc.) and its effect on technologies' output and conversion efficiency. In particular, the production of solar-based RETs depends not only on the solar resource availability but also on the collector working temperature and ambient temperature. This intrinsic characteristic of solar-based RETs is often overlooked in many studies that choose to consider constant efficiency ratios regardless of the operating conditions in the corresponding time interval.
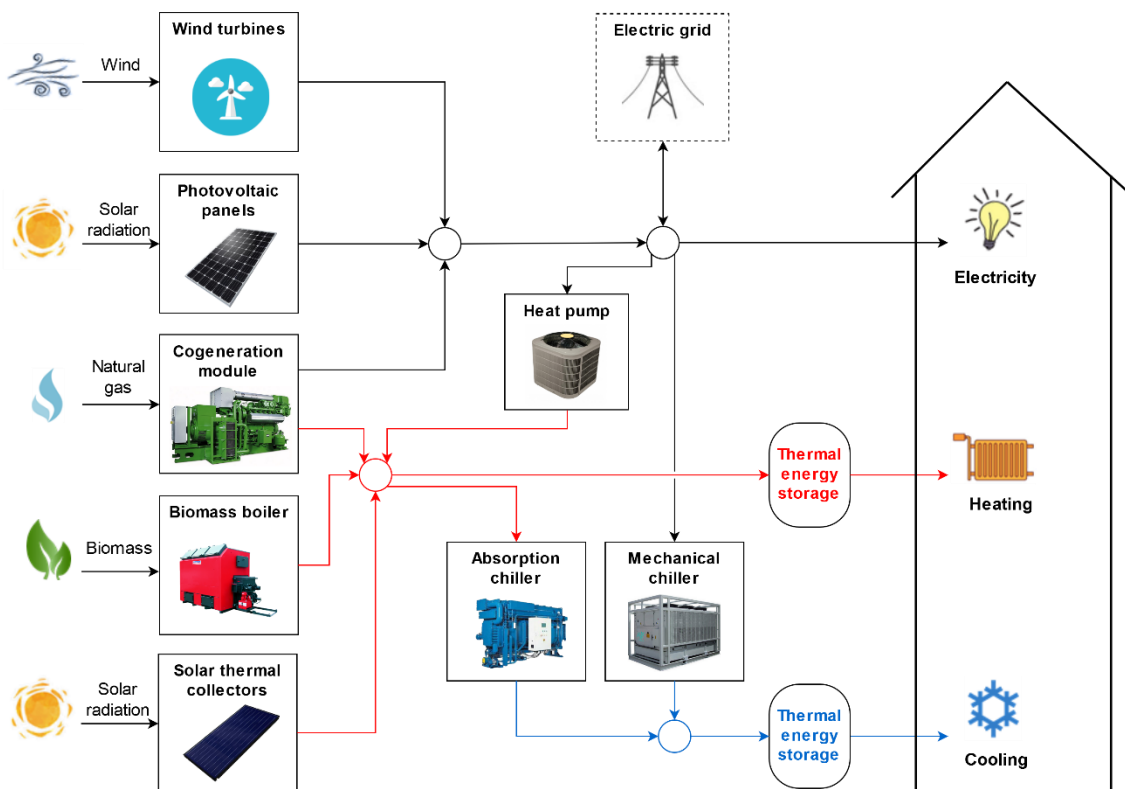
Figure 1.3: Integration of renewables and thermal energy storage in a CCHP system.

Thus, novel systematic approaches for the design of polygeneration systems assisted with RETs and TES must be developed, tackling the increasingly elaborate problem of determining the optimal configuration and operational strategy of polygeneration systems, as described in the following section.

1.2.3   Synthesis and optimization of polygeneration systems

The optimization of polygeneration systems has been effectively applied in industrial and district heating sectors for decades, providing economic and environmental benefits to industrial applications typically characterized by steady or quasi-steady operation, often isolated from the economic environment, owned by individual parties, and sometimes with availability of non-commercial residual fuels (Bruno et al., 1998). On the other hand, energy systems in residential-commercial buildings fundamentally differ from the industry's in aspects such as: (i) consumer behavior: the variability of energy demands requires that devices operate often at partial load or even be turned off for some periods; (ii) economic environment: the energy system is often inserted in an economic market that dictates the energy prices, which vary over time and may change in the future; and (iii) ownership: multiple decision makers must reach an agreement in commonly operated energy systems, e.g. a trigeneration system supplying energy services for a multi-family building. This calls for further development of optimization methodologies that take into account the increasingly elaborate problem of the synthesis of polygeneration systems supported with RETs and TES for buildings applications (Liu et al., 2013; Rong and Su, 2017).

A general representation of a polygeneration system for buildings applications is depicted in Figure 1.4, indicating typical energy resources and energy demands. Given the various trajectories available for the production of energy services, the design procedure must provide systems that are flexible, efficient and reliable. In this respect, two fundamental issues must be addressed (Lozano et al., 2009c; Wakui et al., 2016; Yokoyama et al., 1994): the synthesis of the plant configuration (installed technologies and capacities, etc.) and the operational planning (strategy concerning the operational state of the equipment, energy flow rates, purchase/selling of electricity, etc.). For new plants, these issues are not independent, but for existing plants the operational planning is the only concern.

Finding the optimal configuration and operational planning of polygeneration systems in buildings applications is a complex task because of the multi-faceted nature of these systems: multiple energy resources (renewable and non-renewable), multiple energy products (electricity, steam, hot water, chilled water), multiple technology options (dispatchable, intermittent, storage technologies), and multiple operation periods (hourly and seasonal variations in energy resources, energy demands, and climatic conditions, and temporal variations in energy prices). An overall view of this problem is given in Figure 1.5 with a non-exhaustive list of the main location, technology, economy and environment related aspects.
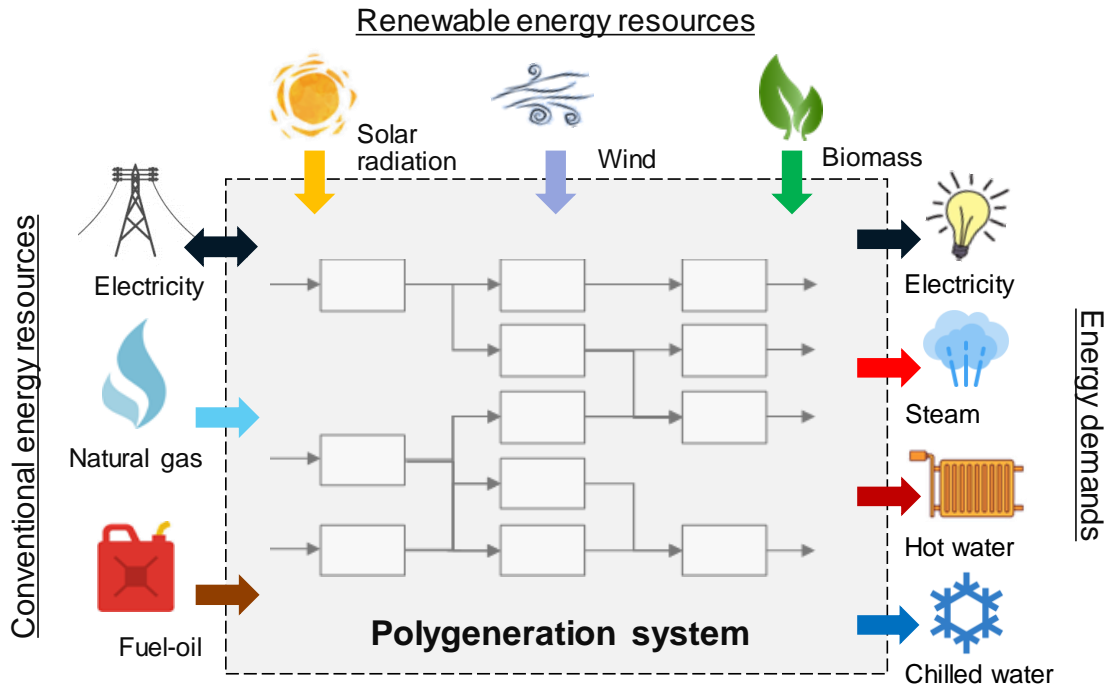
Figure 1.4: General representation of a polygeneration system for buildings.
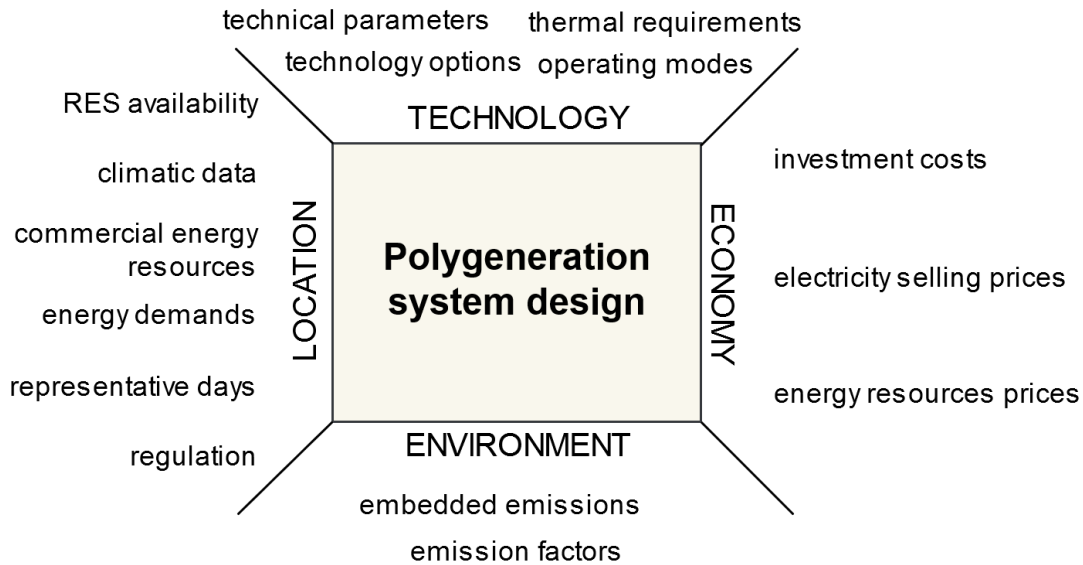
Figure 1.5: Polygeneration systems design aspects.

For a system that does not include TES, the multiple operation periods are always independent from each other. However, the integration of TES introduces dynamic constraints relative to the charging and discharging history of the storage tank (Ito et al., 1994; Lozano et al., 2010; Pina et al., 2017). In this way, the operation of the system in an hourly period may be affected by others, meaning that the multi-period operational planning must be assessed as a whole.

There are three main approaches for the design of polygeneration systems (Andiappan, 2017):

- Heuristics: Utilize rules based on the experience and previous knowledge of the designer. Therefore, they cannot guarantee finding the optimal solution. Moreover, the method may not be applicable to new or not established processes;

- Thermodynamic-based: employ thermodynamic principles to obtain energy targets of the system. Probably the most prominent thermodynamic-based method, Pinch Analysis (Kemp, 2007; Linnhoff et al., 1982) is used to thermally integrate an energy process and determine its heating and cooling requirements. Although this method has proved to be effective, simple and achieve great energy savings, it does not provide a common framework to assess alternative configurations in a systematic manner; and

- Mathematical optimization: Involve the definition of a superstructure, containing the candidate technologies, and the search for a solution fulfilling an objective function (e.g. economic cost, environmental impact, thermodynamic efficiency, primary energy consumption) that is to be minimized or maximized.

Examples of mathematical formulations include linear programming (LP), non-linear programming (NLP), mixed integer linear programming (MILP), and mixed integer non-linear programming (MINLP). In particular, MILP models are suitable for modelling and analyzing energy systems by representing all possible configuration options and operation modes through binary and integer variables, while all physical, economic and environmental quantities are expressed by continuous variables (Ashouri et al., 2013; Biegler and Grossmann, 2004; Lozano et al., 2010; Wakui et al., 2016). The reviews by Chicco and Mancarella (2009), Hinojosa et al. (2007), Olsthoorn et al. (2016), and Ünal et al (2015) describe the characteristics of the optimization models for polygeneration systems presented in the scientific literature, indicating the solution method, the objective function, and the time scale, among others.

The feasibility of a project is commonly evaluated based on its economic performance; for this reason, economic aspects are predominantly considered in optimization studies. However, the growing concern about sustainability-related issues in recent years is promoting a shift in the decision-making process to also take into consideration environmental and societal aspects (Azapagic, 2010; Ng and Martinez Hernandez, 2016). The issue is that the minimization of economic costs is often opposed to the minimization of environmental impacts, such as CO_2 emissions, which means that there is no optimal solution fulfilling both objectives. Multi-objective optimization tackles the issue of conflicting objectives by providing a set of non-dominated solutions, also called Pareto set, which provides flexibility and allows the decision-makers' judgement and expertise into the optimization problem (Alarcon-Rodriguez et al., 2010; Hennen

et al., 2017; Wang et al., 2009). For such trade-off solutions, no improvement in one objective can be achieved without a negative impact on the other.

The above discussion highlighted the necessary conditions for a reliable synthesis approach. Concerning the inherently dynamic behavior of residential-commercial buildings, it is necessary to use local-based information (the energy demands of the consumer center, the available energy resources, climatic data, energy prices, regulatory aspects, etc.) with sufficient level of detail, such as hour by hour and day by day time scales for energy demands, solar radiation, etc. These dynamic operating conditions also affect the behavior of the technologies installed, so it is necessary to take into account the effect of variations in environmental conditions (ambient temperature, solar radiation, etc.) on the technologies' production capacities and performances. Finally, another condition is to respect the Second Law of Thermodynamics by considering the temperature levels of the thermal flows supplied/required by the technologies.

Once the system configuration and operational planning have been determined, the issue of the appropriate way to allocate the resources consumed to the internal flows and final products of the system arises. Such challenging question is addressed in the following section.

1.2.4 Thermoeconomic analysis

Thermoeconomics combines thermodynamic principles with economic analysis aiming at revealing opportunities of energy and cost savings in the analysis, diagnosis, and optimization of energy conversion systems that are not available through conventional methods (El-Sayed, 2003; Gaggioli, 1983; Lozano and Valero, 1993; Tsatsaronis and Winhold, 1985). Thermoeconomic provides powerful tools for the analysis (Deng et al., 2008; Lozano et al., 2009a; Wang and Lior, 2007), diagnosis (Lozano et al., 1994; Reini and Taccani, 2004; Verda and Borchiellini, 2007), and optimization (El-Sayed and Evans, 1970; Frangopoulos, 1987; Lozano et al., 1996; Rovira et al., 2011) of energy conversion systems.

The objective of thermoeconomics is to explain the cost formation process throughout the system, from the resources consumed to the final products obtained (Gaggioli, 1983). The fundamental problem of cost allocation can be formulated as follows (Lozano and Valero, 1993): Given a system whose limits have been defined and a level of aggregation that specifies the constituting subsystems, how to obtain the cost of all flows becoming interrelated in such structure. A simple illustration of the problem is shown in Figure 1.6.
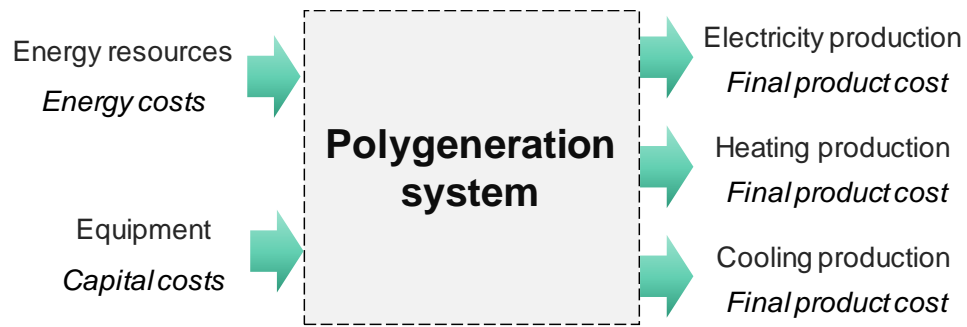
Figure 1.6: Cost allocation problem in polygeneration systems for buildings applications.

As energy systems become more and more complex the problem of the appropriate way to distribute the resources consumed to the internal flows and final products of the system increases. The way in which allocation is made is important because it directly affects the prices of the final products obtained and, thus, the final consumers' behavior and policy makers' decisions. Widespread acceptance of polygeneration systems in buildings applications requires that consumers (Lozano et al., 2014, 2011): (i) be offered cheaper energy services prices relative to other alternatives available in the market, and (ii) be given informative indications on the rational, economic and environmentally friendly consumption of energy services.

In polygeneration systems, common resources are consumed to produce different products and there is no way, based on pertinent facts, to identify the share of resources consumed associated with each product flow. The allocation of costs in joint production is thus always arbitrary (Gochenour, 2003; Horngren, 2009; Itami and Kaplan, 1980; Thomas, 1969). In this regard, numerous methodologies have been proposed (Amundsen et al., 2011; da Gama Cerqueira and Nebra, 1999; Gochenour, 2003; Holmberg et al., 2012; Li et al., 2015; Lozano et al., 2014; Tereshchenko and Nord, 2015), e.g. energy method, exergy method, power bonus method, fuel chargeable to power method, benefit distribution method, market-based prices method. However, no consensus has been reached as to a universally accepted approach. An appropriate allocation criterion should: (i) allow all products to remain competitive and profitable relative to their alternatives in the market (Gochenour, 2003; Thomas, 1969), (ii) consider the context in which joint production takes place, as well as value judgements (Frischknecht, 2000), and (iii) be evaluated on a case-by-case basis, so that there is no approach suitable for every situation (Ardente and Cellura, 2012). Ultimately, the decision on the allocation method must be made in accordance with the objectives of the analysis.

Obtaining unit costs of internal flows and final products of energy systems is a cornerstone of several thermoeconomic methodologies that have been presented in the literature (Lozano et al., 2009b). Unit costs represent the amount of resources that must be consumed to produce one unit of a flow. Three different approaches to determine the unit costs of internal flows and final

products of a simple trigeneration system were presented in Lozano et al. (Lozano et al., 2009a), namely marginal cost analysis, valuation of production according to their market prices, and internal costs calculation. From the various results obtained for each approach, it was concluded that there is no general rule to decide which approach is the best, as it depends on the objectives of the analysis. Carvalho (2011) demonstrated the utility of interpreting the shadow prices (or dual prices) provided by the optimization computational tool as the marginal costs of the internal flows and final products, aiming at identifying their optimal production paths and their relationship with appropriate cost allocation criteria.

To date, most of the thermoeconomic analysis methodologies for energy systems (Abusoglu and Kanoglu, 2009; El-Sayed, 2003; Gaggioli, 1983; Lazzaretto and Tsatsaronis, 2006; Lozano and Valero, 1993) have focused on large industrial systems, characterized by steady or quasi-steady operation, often isolated from the economic environment, owned by individual parties, and sometimes with non-commercial energy resources. As previously mentioned, energy systems in buildings applications differ fundamentally from the ones in the industry in that the variability of energy demands requires that components operate at partial load or even be turned off for some time; also, these systems are inserted in an economic environment that dictates the energy resources prices, which vary hourly and may change in the future. Therefore, further development and refinement of existing thermoeconomic methodologies are required (Lozano et al., 2011; Piacentino and Cardona, 2007).

The fundamentals of thermoeconomics for energy systems with variable energy demands or operated at partial load have been examined in detail by Piacentino and Cardona (2007) and Lozano et al. (2011); these works also addressed the issue of the appropriate way to allocate capital costs of components considering variable annual operation. In the context of tertiary sector buildings, the proposed cost assessment methodologies have been applied to trigeneration systems that cover the energy demands of a large-scale hotel (Piacentino and Cardona, 2007) and a medium-size hospital (Lozano et al., 2011). Wang and Mao (2015) discussed cost allocation in a trigeneration system based on biomass gasification with different operating modes. Examples of thermoeconomic analysis considering off-design operation conditions include a combined cycle power plant based on gas turbine (Rovira et al., 2011), a district heating system based on cogeneration for a university campus (Tereshchenko and Nord, 2015), and a cogeneration steam cycle in a desalination plant (Catrini et al., 2017).

Although thermoeconomic analysis has been traditionally used for the allocation of economic and energy (exergy) resources, there is no limitation to the incorporation of environmental loads or impacts, such as CO_2 emissions and other pollutants, obtained through Life Cycle Assessment (LCA) (Azapagic and Clift, 1999). Lozano et al. (2014) demonstrated the application of

thermoeconomic analysis to allocate environmental costs in simple trigeneration systems. Allocation is also an important issue in LCA-related studies (Ardente and Cellura, 2012; Azapagic and Clift, 1999; Beretta et al., 2014; da Silva et al., 2017; González et al., 2003; Holmberg et al., 2012; Ubando et al., 2013).

Apart from the variable load operation of polygeneration systems for buildings applications, there are several aspects to these systems that have not been deeply studied so far. One aspect is the incorporation of thermal energy storage units, which adds a new dimension to the cost allocation problem: by decoupling energy services production from consumption, it becomes necessary to determine not only the device that is producing the energy flow, but also the time in which the production took place. Another aspect concerns the fact that some RES (e.g. solar radiation, wind) do not have an established market value, which implies attributing them a cost. A third aspect derives from technologies with different products for different operating modes, as is the case of a reversible heat pump that produces heat in heating mode and cooling in cooling mode. Finally, there is also the issue of the appropriate way to allocate the capital costs of the technologies to their products.

1.3 OBJECTIVES

The energy system synthesis and optimization should carefully represent the dynamic conditions that govern the selection of technologies and the operational planning of the system, which ultimately affect the objective function. It is not uncommon, however, to find studies in the literature that ignore or oversimplify key aspects of the synthesis procedure to the detriment of a more realistic solution. In this regard, the following research gaps have been identified:

Unbalanced objective functions

The embedded CO_2 emissions in the manufacturing process of the technologies are seldom taken into account, so that the environmental objective function is represented only in terms of the CO_2 emissions associated with the consumption of energy resources in the operation of the system. This not only results in an imbalance between the economic and the environmental aspects, in which the former is assessed for both investment and operation costs, while the latter only accounts for operation emissions, but also compromises the accuracy of the environmental optimal, in which technologies are installed as if they had no environmental impact whatsoever. This situation becomes clear when solar-based RETs are considered, such as photovoltaic panels and solar thermal collectors, because they consume an energy resource that has zero cost and zero emissions. Some interesting works that have thoroughly approached CO_2 emissions include

the LCA optimization of a solar-assisted hybrid CCHP system (Wang et al., 2015), and the multi-objective optimization of a renewable hybrid CHP system (González et al., 2016) and a CCHP system (Carvalho et al., 2012) based on economic and environmental aspects.

Constant electricity CO_2 emission factors

The importance of an appropriate characterization of the electricity GHG emission factors to evaluate the environmental performance of energy systems has been demonstrated by Voorspools and D'haeseleer (2003) and Haeseldonckx et al. (2007) for CHP systems in Belgium; Messagie et al. (2014) performed the hourly LCA of electricity production also in Belgium; Gordon and Fung (2009) estimated the hourly emission factors in Ontario, Canada, for the integration of RETs; Kopsakangas-Savolainen et al. (2017) calculated hourly-based GHG emission factors of the electricity produced in Finland and used these values to estimate potential emissions savings in households and companies; and Khan et al. (2018) analyzed the time-varying carbon intensity of electricity in New Zealand.

Even though it is true that sufficiently accurate data is difficult to obtain, all energy system optimization studies consulted for this thesis considered annual average values for the electricity CO_2 emissions, thus completely ignoring the dynamic interaction between the energy system and the electric grid as well as the potential benefits. Nevertheless, it is also interesting to analyze the various methods employed in the literature to determine the average CO_2 emission factors: the most common approach is to consider the electricity power mix of a region or a country (Carvalho et al., 2012; Maroufmashat et al., 2015; Sigarchian et al., 2018), but Casisi et al. (2018) adopted the main thermoelectric of the region, and Wang et al. (2015) considered a coal power plant.

To the best of the author's knowledge, dynamic electricity CO_2 emission factors have never been taken into account in energy systems optimization studies. It is well-known that the power dispatch is a dynamic process in which the electric generation of different types of power plants must be carefully coordinated to meet the current electricity demand in a certain region/country. Depending on the resource consumed and the power plant type, the produced electricity will have different CO_2 emissions content. It should prove straightforward to acknowledge that the electricity available in the electric grid will present fluctuating CO_2 emissions content depending on the dispatch at the considered time interval. Taking the Spanish electric grid as an example, Figure 1.7 presents the hourly CO_2 emission factors for the year 2016, as well as the annual average value. Therefore, in the same way that variable electricity prices enable the polygeneration system to achieve potential economic savings by operating in cheap electricity hours, so do the fluctuating CO_2 emissions allow for potential environmental benefits.
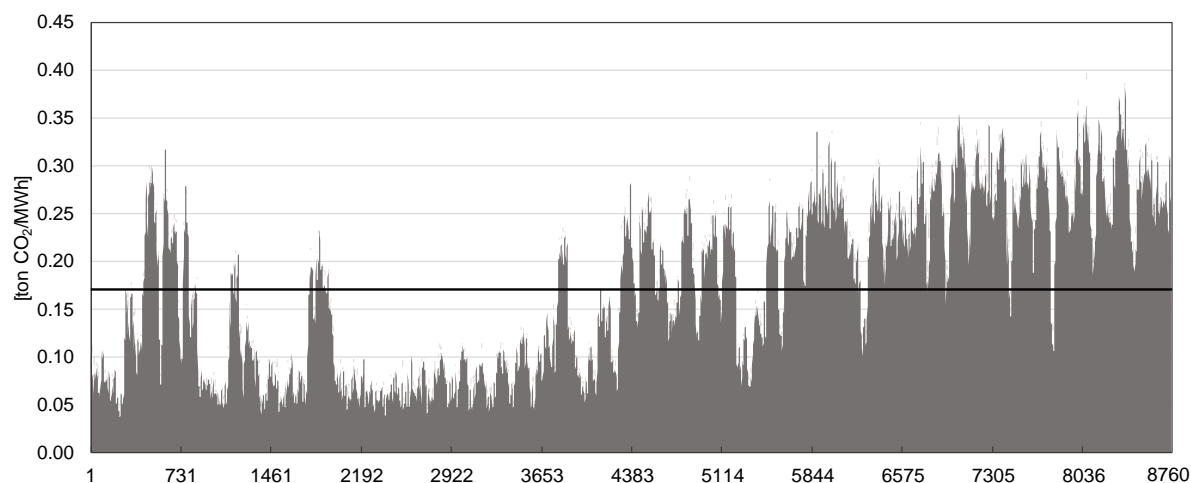
Figure 1.7: Hourly CO_2 emissions of the electricity available in the Spanish electric grid and annual average value in 2016 (REE, 2018).

Disregard for dynamic climatic conditions on the performance of solar-based RETs

Several studies disregard the effect of dynamic climatic conditions, such as hourly and seasonal variations in the ambient temperature and solar radiation, on the performance of solar-based RETs. A temporal and dynamic approach to the operation of solar-based RETs, such as photovoltaic panels and solar thermal collectors, is needed to enhance the optimization procedure and the benefits that can be derived from their integration in energy systems. There are some examples in the literature of studies that have effectively integrated solar-based RETs, such as the economic optimization of a CHP system for a commercial building in Portugal (Safaei et al., 2013), a micro-CHP system for a residential application in Italy (Brandoni and Renzi, 2015), and a CCHP for a commercial building in Switzerland (Ashouri et al., 2013); and in the multi-objective optimization of a distributed CHP system considering economic and environmental aspects (Casisi et al., 2018), and a CCHP system considering economic and exergetic aspects (Sanaye and Sarrafi, 2015).

Thermodynamic oversimplification

Another important issue concerning the synthesis and optimization of polygeneration systems is the necessity of an appropriate thermal integration that accounts for both the quantity of energy produced (e.g. in kWh) and the quality (temperature). In fact, several works have highlighted the importance of an appropriate match between the prime mover and the TAT based on their working temperatures (Deng et al., 2011; Gluesenkamp et al., 2013; Li et al., 2014; Wu and Wang, 2006).

However, studies available in the literature generally considered fixed layouts for the heat recovery between the equipment supplying and demanding heat. As a result, there is a thermodynamic oversimplification in which the heat flows (and their respective temperatures) are set before the optimization procedure even begins. To the best of the author's knowledge, an appropriate evaluation of the various possibilities of heat integration in polygeneration systems has not been performed, except for a few cases in industrial systems (Iyer and Grossmann, 1998; Liew et al., 2017; Maréchal, 1995; Picón-Núñez and Medina-Flores, 2013; Varbanov and Klemeš, 2011).

According to Ramos (2012), the efficiency of cogeneration facilities is limited not only by the recoverable heat quantity from the prime mover but also by the thermal characteristics of the heat demand at the consumer level. Consequently, the temperature of the required heat and the way in which heat is delivered will influence the choice of the prime mover and other technologies of the system. Moreover, the types of solar thermal collectors installed must also be chosen in accordance with the temperature level of the energy services required, as their performances are deeply affected by their working temperatures.

Limited thermoeconomic cost allocation

The system configuration and operational strategy are directly linked to the objective functions defined for the analysis, typically economic and/or environmental. Thus, the question arises how the values obtained for the objective functions could be rationally distributed between its internal flows and final products. To appropriately answer this question, several aspects must be taken into account which have not been deeply studied so far, thus requiring the development and refining of existing thermoeconomic cost allocation methodologies. These aspects are the following:

- The presence of the TES unit causes the cost formation process to be extended over the time intervals, so that the production time becomes as relevant as the device that produced the energy flow;

- The cost formation process depends on the operating conditions of the devices, especially regarding: (i) the joint production of energy services (electricity, heat and cooling); and (ii) devices with different products for different operation modes (e.g. a reversible heat pump producing heat in heating mode and cooling in cooling mode);

- The allocation of costs in joint production is always arbitrary and must be made in accordance with the objectives of the analysis;

- Some renewable energy resources are consumed with no established market value;

- The allocation of the capital costs of the technologies must consider their operating conditions and purposes.

The following objectives are established in order to answer the previously mentioned research questions:

1. Develop synthesis and operation optimization methodologies for polygeneration systems in residential-commercial applications that appropriately represent: (i) the buildings' dynamic behavior, as well as local climatic, economic, environmental and regulatory conditions; (ii) the thermal integration aspects between the heat supply and demand in terms of both energy quantity and quality; (iii) the operation of solar-based RETs; and (iv) the economic and environmental criteria with the same level of model detail.

2. Propose rational cost allocation approaches through an in-depth study of the cost formation process from the resources consumed to the final products obtained with particular attention to: (i) the joint production of energy services that takes place in the cogeneration module; (ii) the incorporation of TES units, which adds a new dimension to the cost allocation problem, as by decoupling energy services production from consumption it becomes necessary to know not only the amount of energy produced, but also the time in which the production took place; (iii) the incorporation of freely available RES, such as solar radiation, as they do not have an established market value and, therefore, their introduction in polygeneration systems entails the fundamental problem of attributing an economic value to them; and (iv) the allocation of capital costs of the equipment to their main products.

3. Demonstrate the application of the developed synthesis and operation optimization methodologies to selected case studies, assessing the technical, economic and environmental feasibility of the integration of cogeneration units, RETs, TES, heat pumps, absorption chillers, among others, for residential-commercial applications.

1.4   STRUCTURE

This thesis can be divided into two parts. The first part comprises Chapters 2 and 3, which take a more conceptual approach to the synthesis, optimization, and thermoeconomic analysis problem.

Chapter 2 addresses the main issues concerning the optimal synthesis of energy supply systems for buildings applications. First, the benefits that can be derived from the integration of different

types of technologies are discussed, including the case for the joint production, thermally activated technologies, thermal energy storage units, renewable energy technologies, and heat pumps. Then, a multi-objective synthesis framework is outlined, encompassing the stages of the superstructure definition, data compilation and elaboration, mathematical model development, and optimal decision-making.

Chapter 3 uses a simple trigeneration system to formulate and demonstrate the application of cost allocation approaches with special attention to the thermal energy storage unit. First, the simple trigeneration system is described and an optimization model is developed to determine the optimal operation of the system for a day of the year. Based on the results obtained, the marginal cost analysis is carried out, explaining the reasons for the optimal operation as well as the role of the thermal energy storage unit in achieving it. The thermoeconomic analysis based on average costs calculation is then performed. First, the productive structure is defined, with a careful consideration for the joint production of energy services and the interconnection of operation periods through the thermal energy storage unit. The cost formation process is unveiled, obtaining the hourly and daily unit costs of all internal flows and final products of the system.

Chapters 4 and 5 compose the second part of this thesis, in which the methodologies proposed in the first part are complemented and applied to more realistic polygeneration systems in two case studies, one in Spain and another in Brazil.

Chapter 4 develops a multi-objective synthesis and thermoeconomic analysis of a trigeneration system that must attend the energy demands of a residential building located in Zaragoza, Spain. Based on the synthesis framework outlined in Chapter 2, the superstructure is defined, and all the necessary data are collected and elaborated. The multi-period multi-objective optimization model is developed using the MILP formulation to determine the optimal system configuration and operational planning from the economic and environmental viewpoints. Special attention is given to the careful representation of dynamic operating conditions and to structural and operational restrictions. The results are presented in two parts: first, the single-objective solutions are obtained by minimizing each objective function; then, the Pareto curve is obtained, and the preferred trade-off solutions are selected. Finally, thermoeconomic cost allocation approaches are proposed and applied to the trigeneration system, determining the hourly, monthly and annual unit costs of the internal flows and final products of the system.

Chapter 5 develops a multi-objective optimization model to the assessment of the technical, economic and environmental feasibility of renewable-based polygeneration systems. The case study corresponds to a university hospital located in Campinas, Brazil. First, the case study is described, including all the necessary data regarding the energy demands, local climatic

conditions, local regulations, and economic and environmental data. The definition of the superstructure is carried out with appropriate consideration for the temperature levels of the thermal flows supplied/required by the technologies. The MILP model is formulated with an innovative approach to the thermal integration of technologies and utilities in the superstructure, thus combining Pinch Analysis techniques, by means of the problem table algorithm, with mathematical programming, based on MILP formulation, to achieve a more realistic representation of the heat supply and demand in the system. The results obtained focus on different modalities of power exchange with the electric grid (e.g. only electricity purchase is allowed; electricity purchase and sale are allowed); the optimal economic cost solutions are analyzed and sensitivity analyses are carried out to assess the effect of variations in the model's key parameters on the optimal solutions.

Chapter 6 summarizes the results and the main conclusions drawn from the study, followed by the contributions and future work developments.

CHAPTER 2

Optimal synthesis framework of energy supply systems in buildings

2 OPTIMAL SYNTHESIS FRAMEWORK OF ENERGY SUPPLY SYSTEMS IN BUILDINGS

Chapter 2 addresses the main issues concerning the optimal synthesis of polygeneration systems for residential-commercial applications. First, Section 2.1 discusses the benefits that can be derived from the integration of different technologies in a conventional energy system that covers the energy demands of a consumer center. Then, Section 2.2 presents the multi-objective synthesis framework of energy supply systems encompassing the stages of superstructure definition (Section 2.2.1), data compilation and elaboration (Section 2.2.2), mathematical model development (Section 2.2.3), and optimal decision-making (Section 2.2.4). Finally, Section 2.3 draws the conclusions of this chapter.

2.1 IMPROVING FLEXIBILITY IN POLYGENERATION SYSTEMS

A defining characteristic of polygeneration systems is the joint production of two or more energy services from a common resource. The joint production, along with appropriate process integration between the processes and energy flows involved, enables polygeneration systems to achieve primary energy savings, higher energy efficiency, lower unit costs of the final products, and lower environmental burdens relative to the conventional separate production (Andiappan, 2017; Mancarella, 2014; Rong and Lahdelma, 2016; Serra et al., 2009).

These benefits can potentially be enhanced by introducing further flexibility into the system. Flexibility corresponds to the capacity of the system to meet unexpected changes during operation, such as energy demands, prices of energy resources, intermittent generation, climatic conditions, among others (Grossmann et al., 1983; Lai and Hui, 2009). It is important to consider flexibility aspects still at the synthesis stage because, according to Lewis (2004), the decisions made at the earliest project phases will have the highest potential benefits on the system's performance with the lowest implementing costs.

System flexibility can be increased, for instance, by coupling thermal energy storage (TES) units and/or transformation technologies, which convert one energy service into another, such as absorption chillers and electric heat pumps (Capuder and Mancarella, 2014; Lai and Hui, 2009; Mancarella, 2014). The interconnection with the electric grid through electricity purchase and/or sale is another essential factor in providing flexibility to the system. Such a high level of integration is translated into a more stable and efficient system operation. Flexibility can also create economic value, for example, by reducing operation costs and installed capacities (Capuder and Mancarella, 2014; Houwing, 2010).

In this context, this section aims to describe the benefits that can be derived from the integration of different types of technologies in energy systems that cover the energy demands (e.g. electricity, heating, and cooling) of a consumer center (e.g. residential building).

A conventional energy system is taken as base case in Section 2.1.1, and the selected technologies are progressively incorporated in the following sections. Table 2.1 summarizes the six energy system configurations analyzed herein, including: auxiliary boiler AB, electric chiller EC, cogeneration module CM (composed of a prime mover, an alternator, and a heat recovery system), thermally activated technology TAT, thermal energy storage TES, renewable energy technology RET (solar-, wind- and biomass-based), and reversible electric heat pump HP. This list is by no means exhaustive. Also indicated in Table 2.1 is the system's interaction with the electric grid through the permission to purchase P and/or sale S electricity.

Table 2.1: Energy system configurations.

System configuration	Technologies included							Grid	
	AB	**EC**	**CM**	**TAT**	**TES**	**RET**	**HP**	**P**	**S**
S0 – Conventional	x	x	-	-	-	-	-	x	-
S1 – Simple cogeneration	x	-	x	-	-	-	-	x	x
S2 – Simple trigeneration	x	x	x	x	-	-	-	x	x
S3 – Simple trigeneration with storage	x	x	x	x	x	-	-	x	x
S4 – Simple trigeneration with renewables	x	x	x	x	x	x	-	x	x
S5 – Simple trigeneration with heat pump	x	-	x	x	x	x	x	x	x

In the aforementioned configurations, the label "simple" is used to indicate that generic assumptions have been made seeking clarity in the comprehension of concepts. These simple configurations should, therefore, be regarded as representative energy systems; their analyses in concrete situations provide the basis for the optimal synthesis of energy systems, which is developed further in Chapter 4. The simplifying assumptions are the following: (i) the equipment can modulate between minimal load (zero) and nominal load; (ii) the equipment efficiency is constant regardless of the operation load; (iii) the equipment produce thermal energy at the required temperature level to meet the heating and cooling demands; (iv) the energy demands of the consumer center and climatic conditions (e.g. ambient temperature and solar radiation) are known beforehand; and (v) purchase and selling prices of electricity are constant.

2.1.1 Conventional system – S0

The conventional system considered herein is depicted in Figure 2.1. This system is characterized by the conventional separate production of energy services: (i) the electricity demand is covered by electricity purchased from the grid; (ii) the heating demand is covered by the boiler AB

consuming fuel-oil; and (iii) the cooling demand is covered by the electric chiller EC with purchased electricity.
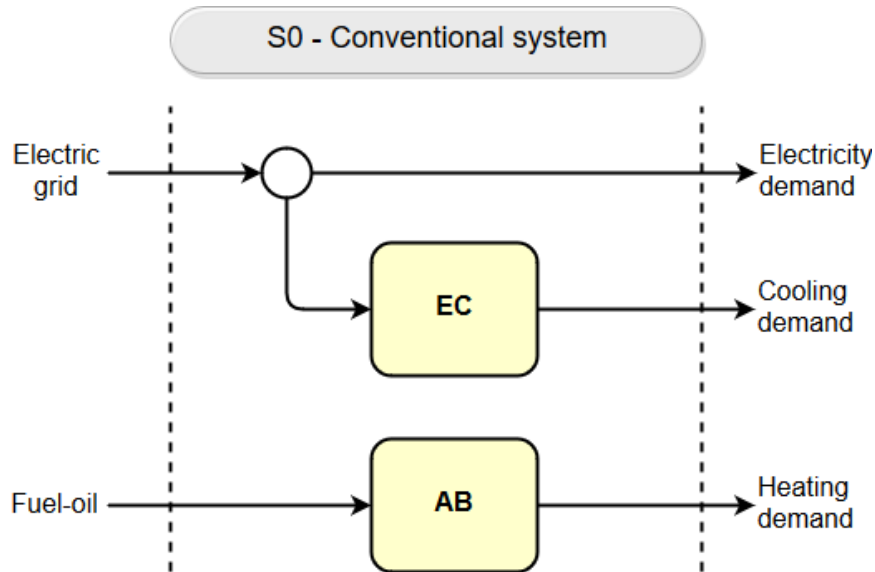
Figure 2.1: Conventional system – S0.

This configuration has been selected for being representative of most applications in residential-commercial buildings over the last decades; nevertheless, other common conventional configurations may include, for instance, the use of electric heaters and/or electric heat pumps to satisfy the thermal loads instead of the AB. Also, the fuel-oil consumed in the AB is just one example among several fossil fuels typically used in residential-commercial buildings, such as natural gas, liquified petroleum gases (propane), and kerosene.

2.1.2 Simple cogeneration system – S1

The simple cogeneration system considered herein has been originally studied by Lozano (2001) and subsequently by Lozano and Ramos (2010). The energy system configuration is depicted in Figure 2.2. The cogeneration module CM, which consists of a prime mover (natural gas internal combustion engine) coupled to a heat recovery system, consumes natural gas and produces cogenerated electricity and cogenerated heat. It is considered that a part of the electricity produced can be sold to the grid and a part of the cogenerated heat can be dissipated into the environment. The auxiliary boiler AB and the electric grid support the operation of the CM. As can be seen, this configuration can only attend the electricity and the heating demands of the consumer center.
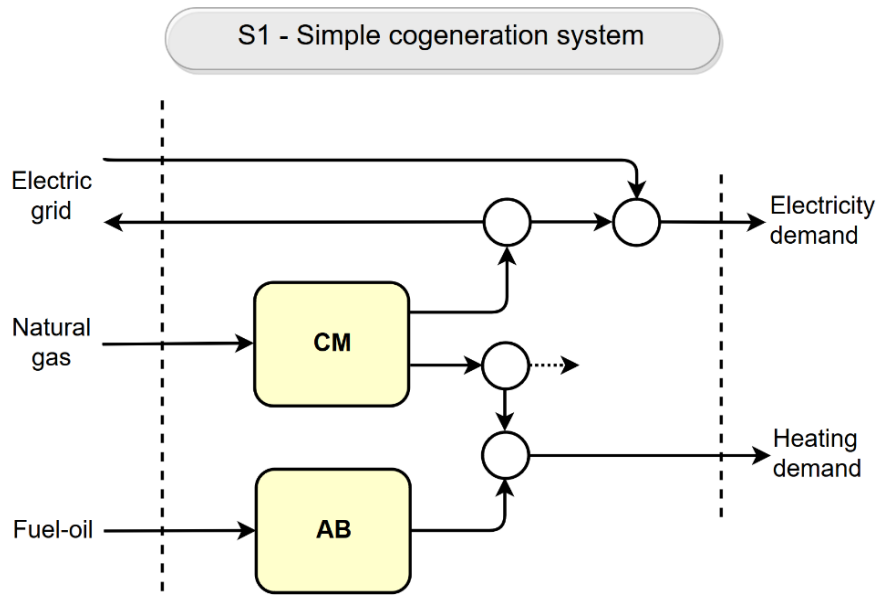
Figure 2.2: Simple cogeneration system – S1.

The core of any cogeneration system is the CM, in which the joint production of energy services takes place. The enhanced fuel consumption efficiency, which leads to primary energy savings and pollutant emissions reduction, is one of the main benefits of the joint production of energy services. In this regard, it is important to understand the conditions that enable cogeneration systems to achieve such benefits.

First, the difference between joint production and combined production must be clarified: in joint production the share of co-product outputs is always fixed, while in combined production this share is independently variable (Frischknecht, 2000). Thus, it is reasonable to infer that a cogeneration system composed exclusively of a CM is unlikely to successfully meet the dynamic energy demands of the consumer center, characterized by a potential non-coincidence of thermal and electric loads; in all probability, there will be periods of excess/shortage of one of the energy services, which will jeopardize potential benefits.

A way around this problem is to introduce auxiliary equipment to support the operation of the CM, such as the AB for heat production. The electric grid also plays a critical role, especially in the preferable case in which both electricity purchase and sale are possible. This list is by no means exhaustive; indeed, further procedures will be discussed in later sections. Such improved flexibility will allow for: (i) an increase in the CM load factor, as it can be sized to cover the base load; (ii) a reduction in heat dissipation; (iii) a reduction in the dependency on the electric grid; and (iv) a reduction in the installed capacity of the auxiliary equipment.

2.1.3   Simple trigeneration system – S2

For applications that also require cooling, in addition to the electricity and heating demands, the introduction of TATs in the simple cogeneration system is another way to enhance the flexibility of the system. In this way, the thermal coverage can be extended to meet the cooling demands, thus reducing cogenerated heat dissipation and increasing the CM load factor and the system overall performance.

The simple trigeneration system depicted in Figure 2.3 has been originally evaluated by Lozano et al. (2009a, 2009b) and later by Lozano et al. (2014). This energy system configuration is obtained by including in the simple cogeneration system of Figure 2.2 an electric chiller EC and a TAT, which in this case is a single-effect absorption chiller AC. Thus, cooling can be produced in two ways: (i) in the EC with cogenerated electricity from the CM and/or electricity purchased from the grid; and (ii) in the AC with cogenerated heat from the CM and/or heat from the AB.
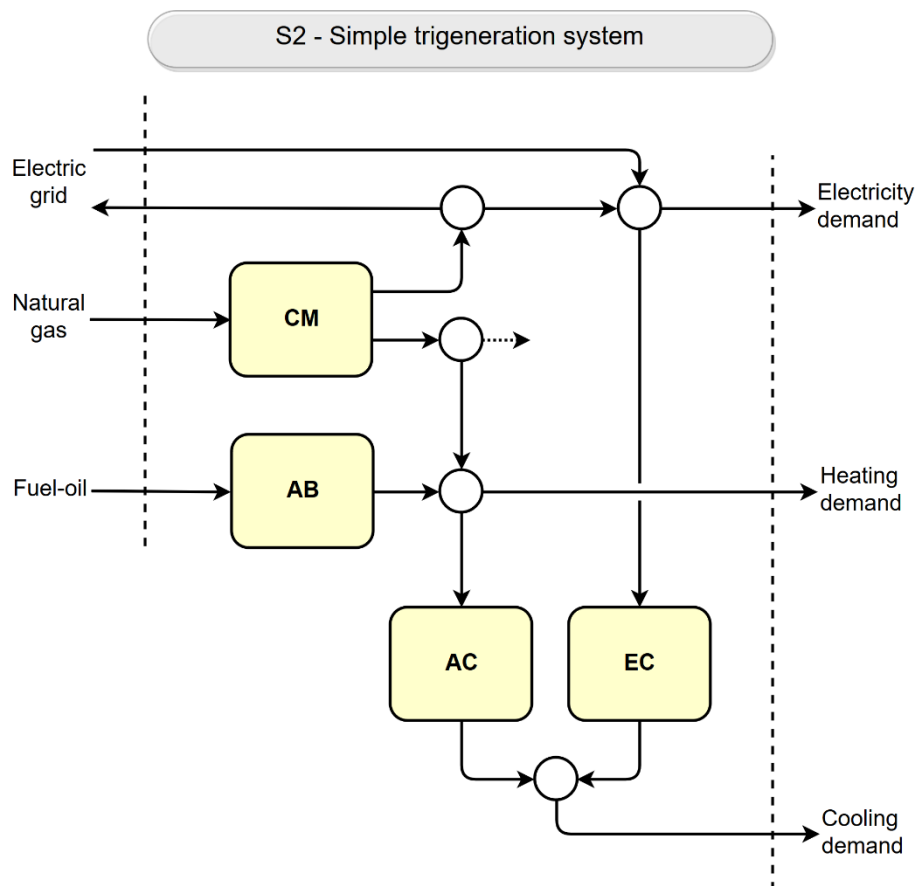
Figure 2.3: Simple trigeneration system – S2.

At first glance, the introduction of an EC may generate a competition with the AC for cooling production. Nevertheless, having two or more technologies producing the same product from different energy resources is worthwhile because it provides the system with alternative production routes. Therefore, based on the current operation conditions, the system can choose

one production route or another (or both) to achieve more interesting economic and/or energy results. For example, cooling can be produced in the EC during off-peak electricity prices or when there is surplus cogenerated electricity, and in the AC when there is excess cogenerated heat.

2.1.4   Simple trigeneration system with thermal energy storage – S3

This thesis builds upon the previously mentioned studies by extending their analyses to more varied system configurations which include key technologies to the development of polygeneration systems in residential-commercial buildings.

In this regard, the simple trigeneration system depicted in Figure 2.4 was obtained by introducing a TES unit for heat TSQ and another for cooling TSR in the simple trigeneration system of Figure 2.3. This energy system configuration (without the TSQ) has been analyzed by Pina et al. (2018b, 2017), as described later in Chapter 3.
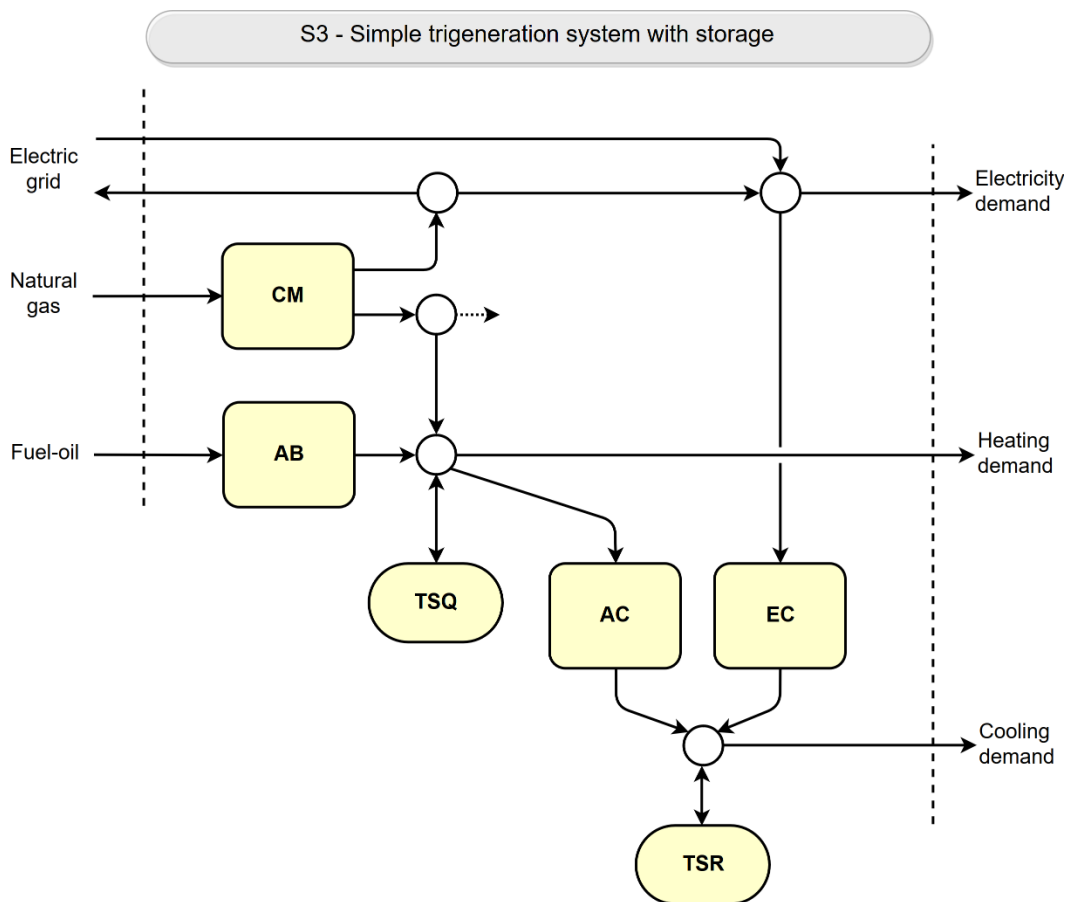
Figure 2.4: Simple trigeneration system with thermal energy storage – S3.

The integration of TES units improves the flexibility of the system as it decouples energy services production from consumption. This integration generally leads to an enhanced overall system performance, which is due to: (i) a better utilization of cogeneration by storing excess cogenerated

heat, thus allowing the CM to operate in a more continuous way; (ii) the possibility of producing cooling in the EC during the night with potentially higher energy efficiency and lower electricity prices; and (iii) electric load management through the EC operation. Such improved energy performance reflects positively on the economic operation of the system. Further economic benefits can be derived by: (i) taking advantage of time-of-use electricity tariffs to produce cooling in the EC at lower electricity prices; and (ii) allowing the CM to produce surplus electricity, which is sold to the grid generating profits (if legally allowed), without the need to dissipate cogenerated heat.

Additional benefits of TES units can be derived from their ability to act as peak-shaving mechanisms, by which it is possible to reduce the installed capacity required, and thus the investment costs.

2.1.5 Simple trigeneration system with thermal energy storage and renewables – S4

Based on the simple trigeneration system with storage (Figure 2.4), the system depicted in Figure 2.5 incorporates the following RETs: photovoltaic panel PV, solar thermal collector ST, wind turbine WT, and biomass boiler BB. The environmental benefits associated with the deployment of RES are fairly clear. In economic terms, the introduction of renewable energy can reduce operation costs by displacing other conventional technologies.

RETs based on intermittent RES greatly benefit from the presence of TES units and the interconnection with the electric grid, particularly when surplus electricity can be sold or injected to the grid. TES units can store excess production from RETs, thus avoiding power curtailment and overcoming the mismatch problem between energy service production and consumption. The interconnection with the electric grid is a decisive factor in the energy and economic feasibility of these technologies.

2.1.6 Simple trigeneration system with thermal energy storage, renewables and heat pump – S5

Apart from TES and RETs, the incorporation of a reversible electric heat pump HP can also provide considerable benefits to trigeneration systems. In fact, there is a great synergy between these three technologies in the sense that the HP can absorb excess electricity from the intermittent RETs to produce heating/cooling, which is then stored in the TES units for later use. This ensures a higher penetration of RES, as well as avoids power curtailment.
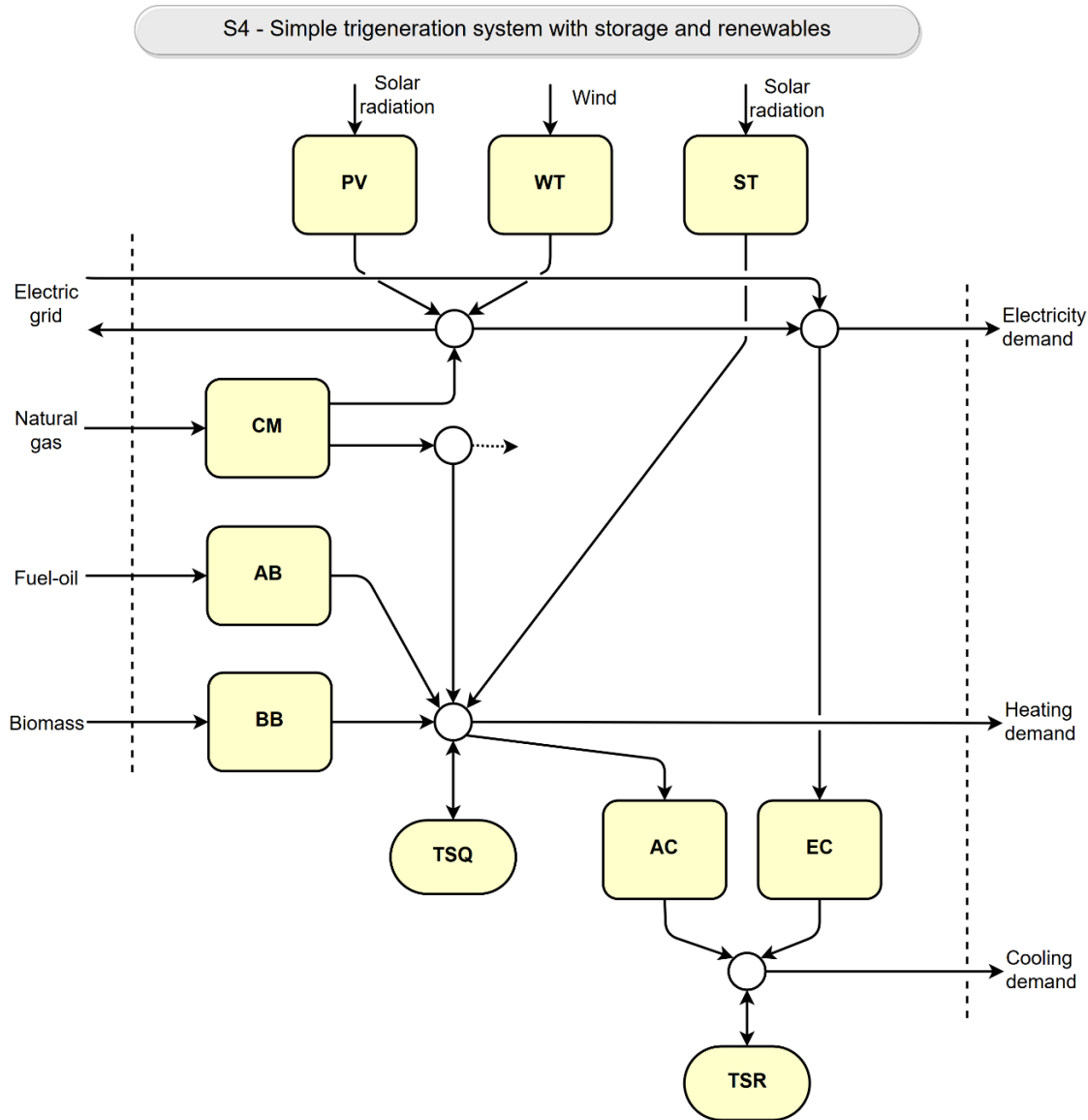
Figure 2.5: Simple trigeneration system with thermal energy storage and renewables – S4.

In this context, the energy system depicted in Figure 2.6 was obtained by replacing the EC with a reversible electric heat pump HP in the trigeneration system of Figure 2.5.

The HP can operate either in heating mode or in cooling mode; thus, the complementary operation modes allow the HP to achieve a potentially higher load factor relative to other technologies with only one operation mode, e.g. EC operating only during the summer, when cooling is required.

On the other hand, it should not be overlooked that heat pumps generally produce low-temperature heat (about 45 °C), which is suitable for underfloor heating systems but not for single-effect absorption chillers; hence the connection of the HP closer to the heating demand in Figure 2.6. This highlights the importance of a well-designed energy system with appropriate considerations for the different temperature levels of the thermal energy flows produced and consumed by the technologies, as well as supplied to the consumer center.
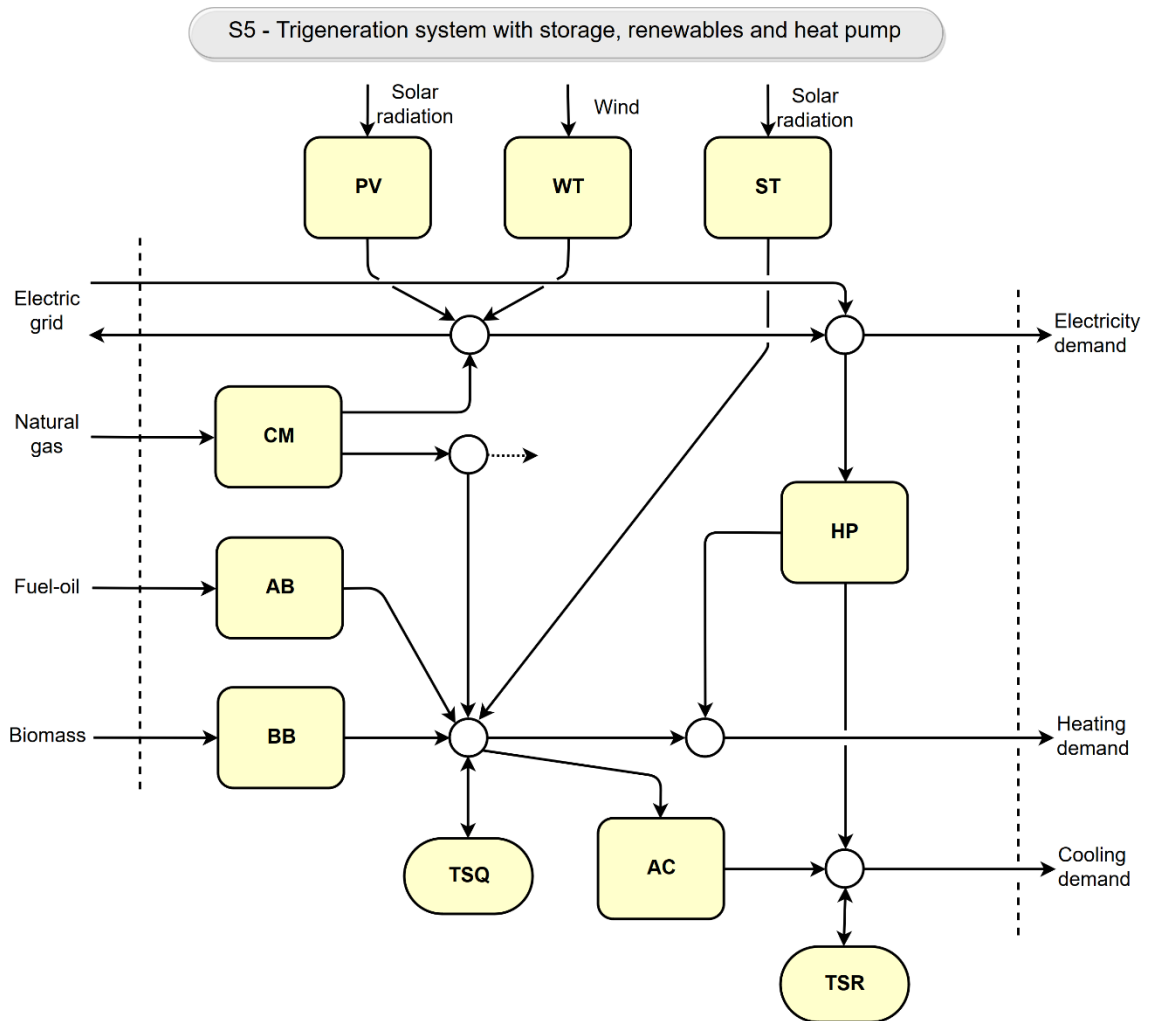
Figure 2.6: Simple trigeneration system with thermal storage, renewables and heat pump – S5.

The electricity that drives the HP has three possible sources: (i) the electric grid; (ii) the cogeneration module CM; and/or (iii) the RETs, namely PV and WT. Consequently, the products of the HP could be labeled as conventional when the electricity is supplied mostly by the electric grid, as cogenerated when the electricity is supplied mostly by the CM, and as renewable when the electricity is supplied mostly by the RETs.

2.2   OPTIMAL SYNTHESIS FRAMEWORK

It becomes clear from the discussion developed in the previous section that there are multiple alternative ways to produce the required energy services in polygeneration systems and that some technologies play a key role in enhancing the flexibility and the benefits of these systems. Nevertheless, it does not mean that all those technologies must be installed in every case, as this should be the result of the optimization process. Therefore, the following questions arise:

- What technologies should be installed to produce the required energy services?

- What is the size and number of units of each technology?

- What is the suitable operational planning of the technologies and the corresponding consumption of energy services?

This constitutes a combinatorial problem that aims at identifying the best solution among all feasible alternatives. In this context, two fundamental issues must be addressed (Lozano et al., 2009b; Wakui et al., 2016; Yokoyama et al., 1994): the synthesis of the plant configuration (installed technologies and capacities, etc.) and the operational planning (strategy concerning the operational state of the equipment, energy flow rates, purchase/selling of electricity, etc.). For new plants, these issues are not independent, but for existing plants the operational planning is the only concern. An appropriate synthesis procedure should neither underestimate the installed capacity, which would prevent the system from covering peak demands, nor overestimate it, which would incur high investment costs, thus compromising the economic feasibility of the system (Liu et al., 2013). Ultimately, the optimization process must provide energy systems that are flexible, efficient and reliable.

The synthesis and operation optimization of polygeneration systems in residential-commercial buildings involves a great number of variables related to the system itself and to its surroundings, for instance (Carvalho, 2011; Ramos, 2012): (i) the energy demands of the consumer center that must be attended; (ii) the energy resources available to the system, i.e. fuels purchased from the economic market, electricity purchased from the electric grid, and locally available renewable energy sources; (iii) purchase prices of the energy resources consumed; (iv) capital costs of the installed technologies; (v) technical parameters of the installed technologies; (vi) local climatic data; and (vii) regulatory aspects involving, for example, the installation of cogeneration facilities and the interconnection with the electric grid.

This calls for the development of innovative systematic optimization approaches that are able to address the complex interactions and variables involved (Andiappan, 2017; Ng and Martinez Hernandez, 2016). In this respect, superstructure-based optimization approaches, based on mathematical programming techniques, promote a suitable evaluation of multiple technology alternatives, as well as provide the global optimal configuration. Mixed integer linear programming (MILP) models capture the complexities of the design problem by using binary variables to consider the multiple possible plant configuration alternatives and operational strategies, and continuous variables to express energy, economic, and environmental flows (Biegler and Grossmann, 2004; Gong and You, 2015; Liu et al., 2007; Wakui et al., 2016).

Superstructure-based optimization approaches generally consist of four main steps, as illustrated in Figure 2.7: (i) superstructure definition in accordance with the defined energy design targets

and the available energy resources; (ii) data compilation and elaboration regarding the established optimization criteria and objective functions; (iii) mathematical model development in line with the nature of the problem (i.e. single- or multi-objective optimization); and (iv) optimal decision-making. These steps are discussed in detail in the following sections.
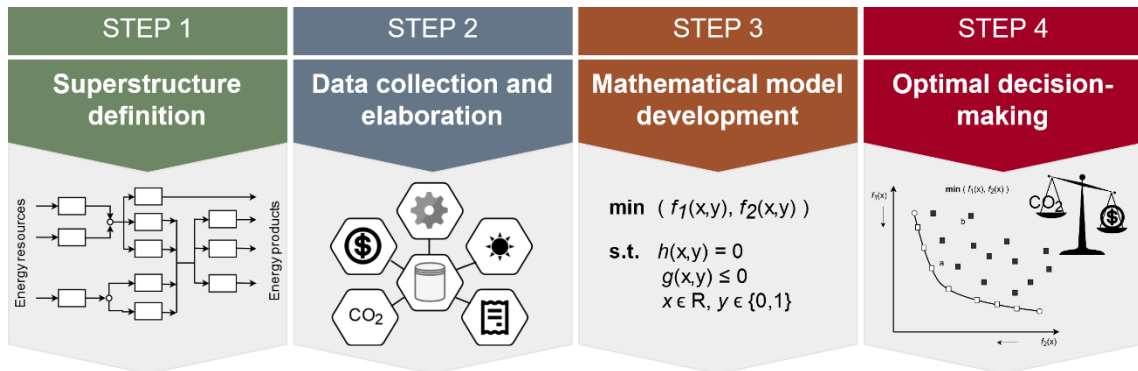
Figure 2.7: Multi-objective synthesis framework of energy supply systems.

2.2.1 Superstructure definition

As a first approach to the synthesis problem, the superstructure of the energy system must be defined (Iyer and Grossmann, 1998; Lozano et al., 2010; Yokoyama et al., 2015). Basically, the superstructure consists of a variety of potential technologies and the feasible connections between them to match the energy demand requirements. After the optimization procedure, the superstructure is reduced to the optimal configuration.

An appropriate definition of the superstructure is important for two reasons: On the one hand, it is necessary to provide the optimization model with sufficient information so that the best combination of technologies and interactions between them can be determined; a poorly defined superstructure will lead to solutions that fail to fully address the problem. On the other hand, the superstructure definition must also limit the scope of the problem because the more technologies are incorporated in the superstructure, the more complicated the optimization model becomes; therefore, there is a trade-off between variety of technologies and computational efficiency (Liu et al., 2013).

In this context, it is first necessary to establish the conditions that are imposed on the system, thus limiting the scope of the problem and reducing the complexity of the superstructure. These conditions include the types and quantities of energy services that the system must produce (i.e. energy targets), and the energy resources that are available to the system.

The energy targets correspond to the energy demands of the consumer center. In the case of residential-commercial applications, these energy demands typically include electricity, domestic

hot water (DHW), space heating (SH), and chilled water. The energy resources available to the system may include locally available RES, fossil fuels, electricity from the electric grid, among others. Possible restrictions may apply depending on local conditions and/or regulatory aspects, such as the permission to sell or inject electricity to the grid.

Once the energy targets have been established, the next step is to select the candidate technologies to be included in the superstructure taking into account the complex interactions between them, e.g. synergies, competitions, temperature levels, operation modes. Three general types of technologies can be identified:

- Generation technologies: Convert the energy resource into intermediate or final products. Depending on the energy resource's availability, the generation technologies can be classified as dispatchable (e.g. reciprocating internal combustion engines, microturbines, gas turbines, boilers) and non-dispatchable or intermittent (e.g. photovoltaic panels, solar thermal collectors);

- Transformation technologies: Convert the energy resource or intermediate product into a final product. Examples of transformation technologies include TATs (e.g. absorption chillers), mechanical chillers, and heat pumps.

- Storage technologies: Store the energy service produced by generation and transformation technologies. For instance, hot water storage tank, chilled water storage tank, ice storage, electric batteries, etc.

The consideration of the synergies and competitions between technologies provide practical guidance on the appropriate selection of candidate technologies. Section 2.1 outlined typical integration examples. In addition, the integration of thermal and/or electric energy storage units, which decouple energy service production from consumption, enhances the potential benefits derived from cogeneration and intermittent RETs. Energy cascading contributes by allowing the product of a technology to be used as fuel for another, for instance photovoltaic panels that produce electricity and an electric heat pump that produces heating or cooling. By contrast, some technologies can be mutually exclusive in the sense that they may compete to attend the same energy service or product, for instance a cogeneration module and a solar thermal collector, both producing low temperature heat. Still, it is important to provide component redundancy to increase the level of system reliability.

For analyses comprising longer time spans (months, seasons, years), different operation modes of the equipment may be considered. A fine example is the reversible heat pump, which can be set to operate in cooling mode during the summer and in heating mode for the rest of the year.

Likewise, solar thermal collectors can be set to operate at a higher temperature during the summer to drive an absorption chiller and support cooling production, and at a lower temperature for the rest of the year to attend the heating demand.

The combination of generation, transformation, and storage technologies in polygeneration systems for buildings applications is shown in Figure 2.8.
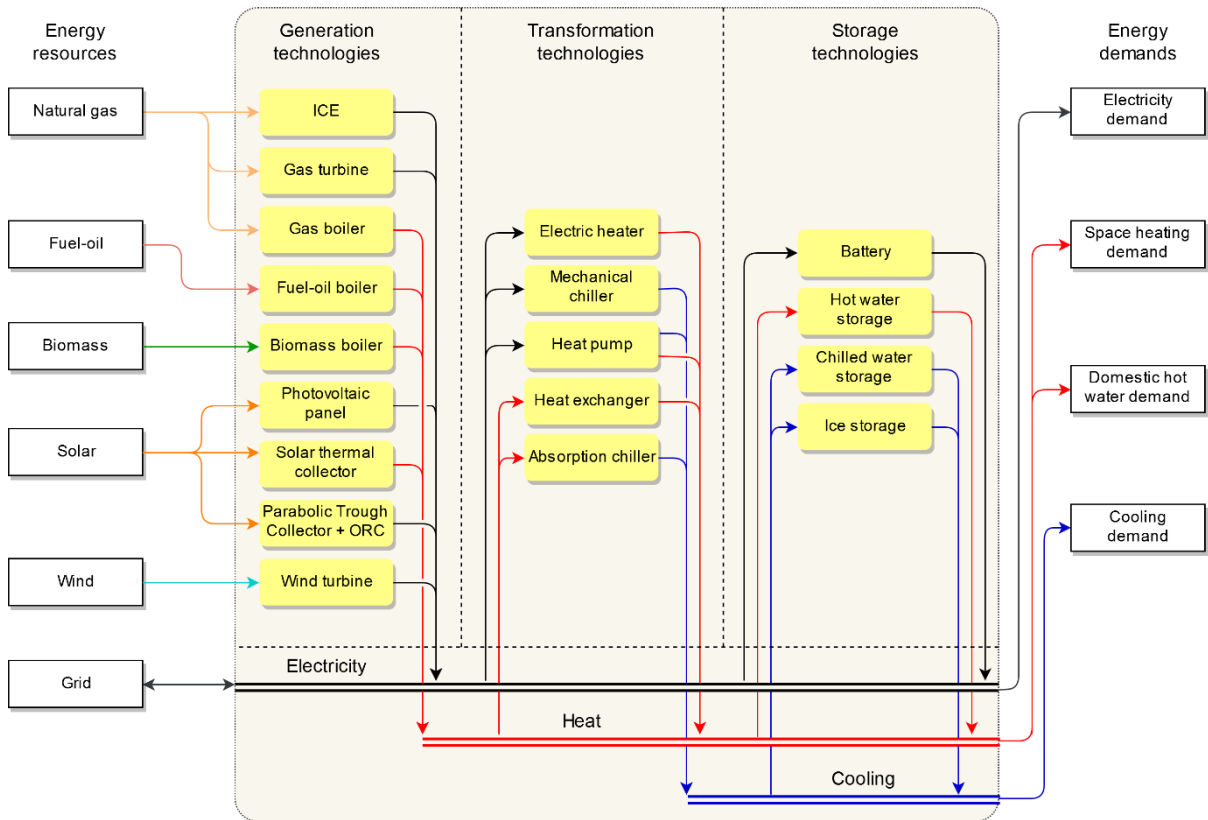
Figure 2.8: Combination of technologies in polygeneration systems for buildings.

As can be seen, Figure 2.8 illustrates a generic representation of the thermal energy flows that does not differentiate between the different temperature levels. In reality, thermal energy flows in polygeneration systems are available/required at different temperature levels according to the technologies that supply/consume them, thereby imposing physical and structural constraints on the system configuration and operation. Therefore, process integration techniques for the appropriate match between the technologies' heat supply/consumption and the consumer center's thermal demands are required.

The multiple possible applications of the consumer center's thermal energy demands make it essential to take into account (Ramos, 2012; Voll et al., 2015): (i) the technologies installed at the consumer level to deliver the thermal energy; and (ii) the corresponding temperature levels of the thermal energy flows. For example, as depicted in Figure 2.9, underfloor heating requires a hot water supply at about 30-40 °C, while hot water radiators require a hot water supply at about 60-

90 °C; chilled water for heating, ventilation and air-conditioning applications is typically supplied at 6-8 °C. These aspects must not be overlooked, as they will influence the selection of technologies in the superstructure and their operation.
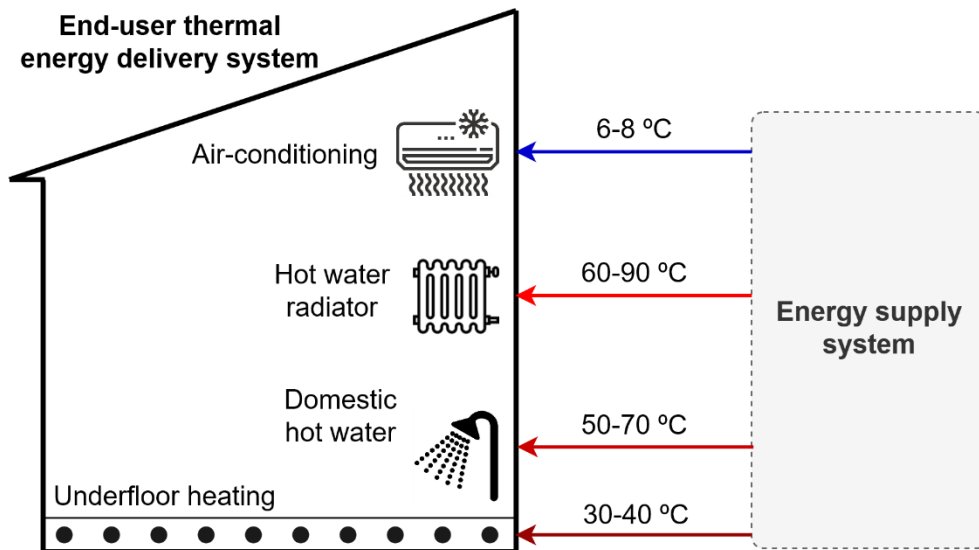
Figure 2.9: End-user's thermal energy services and supply temperatures.

Among the previously described technologies, the cogeneration module plays a critical role in the definition of the superstructure as its type will open up or eliminate the possibility of installing related technologies, such as TATs, as discussed by Deng et al. (2011), Gluesenkamp et al. (2013), Li et al. (2014), and Wu and Wang (Wu and Wang, 2006). The selection of the cogeneration module must consider several factors regarding (Ramos, 2012): (i) the consumer center: it is necessary to account for its thermal and power load profiles, as well as the quality of the thermal energy required, and other possible user-demand constraints; (ii) the technological aspects: these include the quantities and the quality of the recoverable heat, rated size ranges, and heat-to-power rates; and (iii) the energy services production: it is necessary to consider not only the energy services required by the consumer center, but also the production of additional energy services that might be used by other technologies, for example the production of steam to drive a double-effect absorption chiller for cooling production.

Table 2.2 matches the average recoverable heat temperature from different types of prime movers with typical applications in residential-commercial buildings.

Cogeneration modules based on internal combustion engines require especial consideration owing to their dispersed heat sources (exhaust gas, charge air, jacket cooling water, and lubricating oil) at different temperature levels. The result is that the amount of recoverable heat from the engine and its use depend on the required temperature level. For example, Figure 2.10 depicts the heat supply of a gas engine with gross electrical power of 5120 kWe. The usable heat

sources, indicated in both quantity (kW) and quality (thermal level) for full load operation conditions, could be used in the production of the following energy services (Lozano et al., 2019): (i) hot water at 35 °C with return at 30 °C, for climatized swimming pools; (ii) hot water at 45 °C with return at 35 °C, for underfloor heating; (iii) hot water at 95 °C with return at 55 °C, for central heating with hot water radiators or single-effect absorption chiller; and (iv) saturated steam at 10 bar (T_{sat} = 180 °C) from hot water at 95 °C, for double-effect absorption chiller.

Table 2.2: Recoverable heat temperatures of prime movers with matching applications (Wu and Wang, 2006).

Application	Supply temperature °C	Prime movers				
		GT 540 °C	SOFC 480 °C	MT 320 °C	SE 90 °C	PEMFC 60 °C
Underfloor heating	30-40	x	x	x	x	x
Domestic hot water	50-70	x	x	x	x	x
Space heating	60-90	x	x	x	x	x
Single-effect absorption (hot water)	80-90	x	x	x	x	-
Double-effect absorption (steam)	160-180	x	x	x	-	-
Triple-effect absorption (steam)	195-215	x	x	x	-	-

Abbreviations: GT = gas turbine; SOFC = solid oxide fuel cell; MT = microturbine; SE = stirling engine; PEMFC = PEM fuel cell.
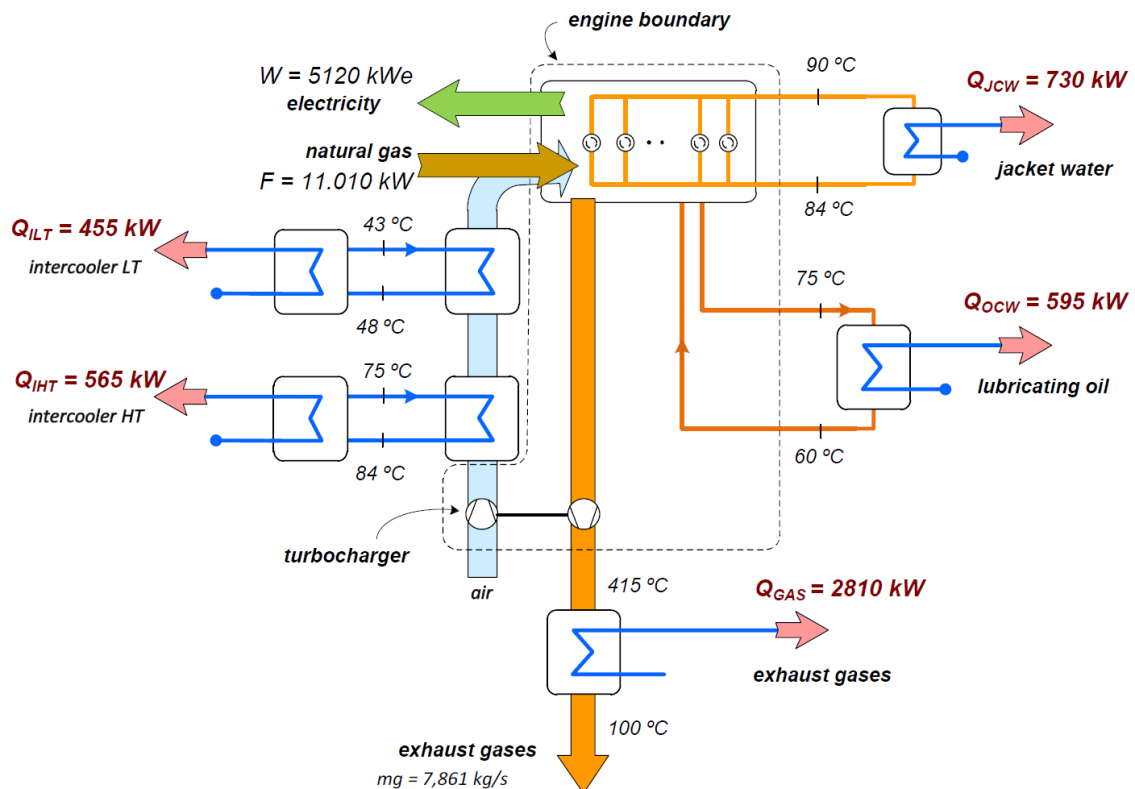
Figure 2.10: Usable heat sources of a gas engine with gross electrical power of 5120 kWe (adapted from Ramos (2012)).

Appropriate thermal integration requirements must also be satisfied for solar thermal applications, as the type of solar collector and its working temperature establish different production routes. Examples of solar thermal cooling alternatives are shown in Figure 2.11, featuring three types of solar collectors (one flat-plate and two parabolic trough collectors PT), as well as three absorption chillers (single-effect ABS, double-effect ABS, and triple-effect ABT). The continuous line for each collector corresponds to a medium irradiance.

RASE: Single-effect absorption chiller   RADE: Double-effect absorption chiller   RATE: Triple-effect absorption chiller

FPC: Flat-plate collector   PTC: Parabolic trough collector
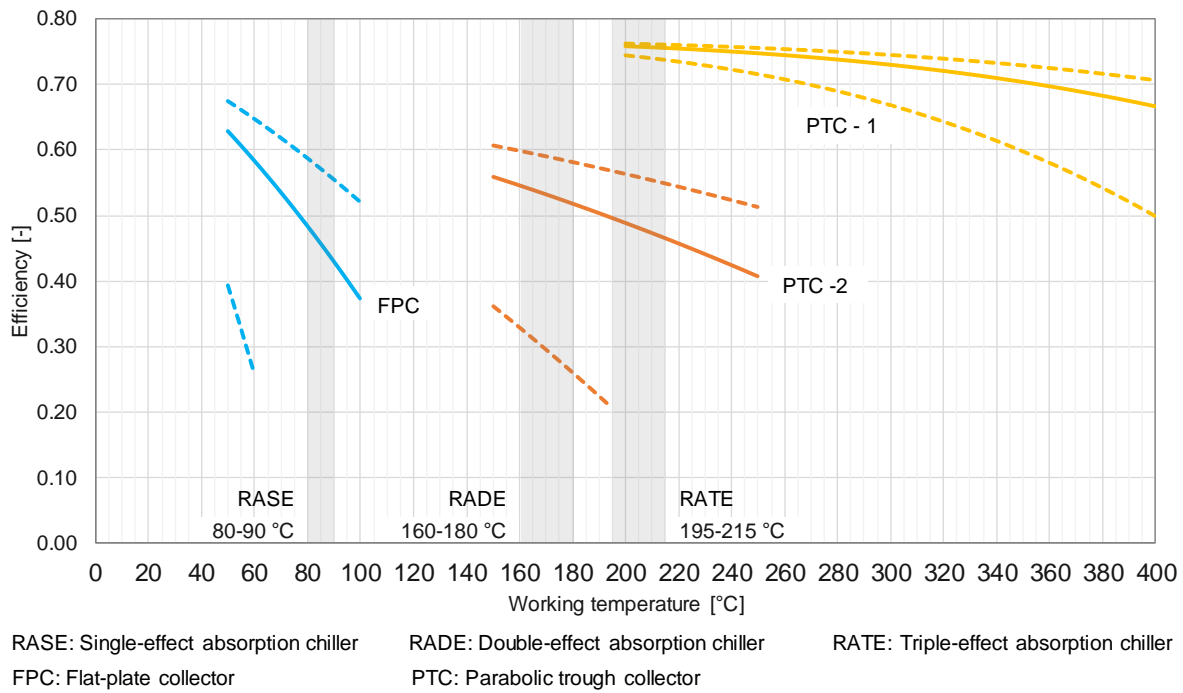
Figure 2.11: Solar collector efficiency at different working temperatures (adapted from Lozano et al. (2019)).

2.2.2 Data compilation and elaboration

Having defined the superstructure of the system, the next step is to gather additional and more specific data that will serve as input to the optimization model. Generally, this information may be collected from the literature, supply companies, manufacturers' catalogues, experimental and/or simulation works, government official reports, among others. Clearly, this step plays a key role in the design of energy systems because the quality of the data directly affects the credibility of the results obtained.

The required information must provide the necessary description of the system and the consumer center, including the types and quantities of (i) the energy demands of the consumer center; (ii) the energy resources available in the economic market; (iii) locally available RES; as well as (iv) technical parameters of the candidate technologies in the superstructure; (v) local climatic data; (vi) local regulations regarding environmental protection, the interconnection with the electric

grid, etc.; and (vii) other possible constraints, such as the consumer center's building envelope characteristics. Additionally, relevant data must be gathered in accordance with the criteria chosen for the analysis; in the case of the sustainable energy design, these criteria typically include economic and environmental data on the equipment manufacturing and installation, and the operation of the system (e.g. energy resources consumption).

The consumer center's load profiles represent the basis of the design procedure. For new buildings, real demand data are evidently not available and, thus, must be estimated through the use of modeling methods, such as the heating and cooling degree-days, or simulation tools, such as TRNSYS and EnergyPlus (ASHRAE, 2009). For existing buildings, however, energy demand data can be measured in situ through data acquisition systems.

At the stage of data collection and elaboration, two important considerations must be taken into account: The first regards the level of model detail, as explained in Section 2.2.2.1, and the second regards the nature of the analysis, as explained in Section 2.2.2.2.

2.2.2.1 Level of model detail

The level of model detail includes the definition of the time span (e.g. a day, a month, a year) and the temporal resolution (e.g. 10-minute basis, hourly basis, daily basis) of the analysis. Due to the dynamic nature of the problem, the accuracy and the reliability of the results obtained by the optimization model tend to increase with the number of operation periods. Nevertheless, it must be noted that the greater the number of operation periods, the greater the computational effort required to solve the model. Another aspect is that this information is not always available with the desired level of detail.

The hourly period is the temporal resolution typically considered in optimization studies (Liu et al., 2013; Ünal et al., 2015). For a whole-year operation, this would require 8760 hourly periods (365 days x 24 hourly periods), which would incur considerable computational effort. To tackle this issue, the method of representative days (also referred to as typical days or type-days) is commonly used with the purpose of reducing the size of the optimization problem. This method assumes that each day in a certain period (e.g. month, season) has the same characteristics (e.g. energy demand profiles, energy prices, climatic conditions) of the representative day of this period. In this way, by considering one representative day per month of the year, the total number of hourly periods can be reduced from 8760 to 288 (12 representative days x 24 hourly periods).

Different definitions of representative days have been proposed in the literature: Lozano et al. (2009c) analyzed the hourly energy demands of a Spanish hospital consisting of 24 representative

days (one working day and one holiday per month of the year); Barberis et al. (2016) analyzed the hourly energy demands of an Italian university campus based on 12 representative days (one for each month of the year); Santo (2014) considered 8 representative days (one working day and one holiday for each season of the year) to describe the hourly energy demands of a Brazilian university hospital; and Wakui et al. (2016) considered 5 representative days (summer day, summer peak day, winter day, winter peak day, and mid-season day) to represent the energy demands of a small residence in Japan.

Even though the method of representative days successfully reduces the number of operational periods, thus improving computational efficiency, it may compromise the accuracy of the model due to loss of information. Therefore, an appropriate number of representative days must be defined in a way that balances computational effort and model accuracy. The appropriate selection of representative days has been discussed by Domínguez-Muñoz et al. (2011), Ortiga et al. (2011), and Poncelet et al. (2017), to name a few examples. Their results indicate that the accuracy of the optimization results not only depends on the number of representative days, but also on the ability of those days to reproduce/resemble the corresponding period.

In this regard, other factors that complicate or even hinder the definition of representative days include: (i) the incorporation of seasonal storage, which stores energy from one period of the year to another (e.g. from summer to winter); (ii) the deployment of RES characterized by highly dynamic behavior, such as wind; and (iii) real-time electricity tariffs. The issue involving these factors is related to the difficulty of establishing representative values for any period. For instance, unlike solar radiation, which presents a strong correlation with the season of the year, increasing during the summer and decreasing during the winter, wind energy has a considerably more irregular behavior. Also, real-time electricity tariffs, as opposed to time-of-use electricity tariffs (in which the electricity price changes according to previously established hours of the day and months of the year), are more difficult to forecast and to determine a representative value.

The level of model detail also concerns the description of the technologies in the superstructure. It is widely known that the performance of several technologies typically used in polygeneration systems (e.g. prime movers, absorption chillers, electric heat pumps) vary with their load factors and ambient conditions (Liu et al., 2014; Wu and Wang, 2006). However, a very detailed description introduces non-linear equations which considerably increase the computational effort required to solve the model. For this reason, it is common to find studies in the literature that choose to simplify the operational behavior of technologies by considering constant performance parameters to the detriment of result accuracy. Therefore, there is a trade-off between accurate technology description and computational efficiency.

Furthermore, if the aim of the procedure is not to select the actual number of devices and their corresponding installed capacities (design), but rather to identify the types of technologies that must be included and estimate their installed capacities (synthesis), then it makes no sense to further complicate the optimization model with, for example, the issue of partial load behavior.

2.2.2.2   Nature of the analysis

Every optimization procedure is based on a certain criterion (or criteria), which typically consists of economic, environmental, and/or energy efficiency aspects. Once the criteria have been selected, it is necessary to define a measure to represent the objective function of the model. Examples of objective functions for such criteria include (Rong and Su, 2017): (i) economic criterion: total annual cost, net present cost, profit, etc.; (ii) environmental criterion: total annual pollutant emissions, pollutant emissions reduction, etc.; and (iii) energy efficiency criterion: primary energy consumption, primary energy savings, etc.

Thus, the nature of the analysis involves the criteria and the objective functions that have been selected for the analysis. It follows that data must be collected accordingly. For example, the total annual cost objective function is typically composed of a fixed term, which accounts for equipment investment and maintenance costs (capital cost), and a variable term, which accounts for the operation of the system (fuel and electricity purchase costs, electricity selling revenues).

When two or more criteria are incorporated into the optimization model, it is essential to ensure that all aspects are treated at the same level of detail. In the case of the energy design with economic and environmental considerations, for example, it means that the economic data must have their counterpart in the environmental data and vice versa. This is a challenging task because the information is not always easily obtained or identified. For instance, the electricity purchased from the grid is generally rated using time-of-use tariffs, in which the price changes according to the hours of the day and months of the year; it follows that the environmental data must also include the CO_2 emissions associated with the electricity available in the grid per hour of the year. The issue is that while hourly electricity prices are well-established and easily obtainable, the associated hourly CO_2 emissions very often are not.

2.2.3   Mathematical model development

The first step in the optimal decision-making process is to develop a mathematical model representing the behavior of all elements in the superstructure in accordance with the level of model detail and nature of the analysis defined. Then, the model is applied in the search for a solution fulfilling an objective function, which is to be maximized or minimized.

As presented in Section 2.2.2.2, various objective functions can be chosen from economic-, environmental-, and energy efficiency- based criteria. A mathematical model whose objective function exclusively reflects a single criterion is typically referred to as single-objective optimization (SOO). Depending on the mathematical nature of the model, it can be classified in terms of: (i) continuous and discrete variables; and (ii) linear and non-linear functions. Continuous optimization models include linear programming (LP) and non-linear programming (NLP); regarding discrete problems, these include mixed-integer linear programming (MILP) and mixed-integer non-linear programming (MINLP). Biegler and Grossmann (2004) provided a general classification of mathematical optimization problems, including typical applications in the field of process systems engineering, as well as a review of solution methods.

MILP is particularly suitable for the design of energy systems, as these models include (Ashouri et al., 2013; Biegler and Grossmann, 2004; Lozano et al., 2010): (i) binary variables to represent the selection of technologies, the permission to purchase/sell electricity to the grid, among others; (ii) integer variables to represent, for example, the number of pieces of technology installed; and (iii) continuous variables to represent all other physical and economic quantities. The general formulation corresponding to a mixed-integer optimization problem is presented below:

Min $\qquad\qquad Z = f(x, y)$ $\qquad\qquad\qquad\qquad\qquad\qquad\qquad\qquad$ (2.1)

Subject to $\qquad\quad h(x, y) = 0$ $\qquad\qquad\qquad\qquad\qquad\qquad\qquad\qquad$ (2.2)

$\qquad\qquad\qquad g(x, y) \leq 0$ $\qquad\qquad\qquad\qquad\qquad\qquad\qquad\qquad$ (2.3)

$\qquad\qquad\qquad x \in X, y \in \{0,1\}$ $\qquad\qquad\qquad\qquad\qquad\qquad\qquad$ (2.4)

where *f(x,y)* is the objective function to be minimized (e.g. total annual cost), *h(x,y)* corresponds to equality constraints (e.g. energy demands), and *g(x,y)* corresponds to inequality constraints (e.g. capacity limits). The variables *x* are continuous (e.g. state variables), while the variables *y* are binary (e.g. technology selection).

All logical, physical, and economic relations relative to the technologies in the superstructure and to the operation of the system are translated into equality and inequality constraints. In this way, the system modelling and the objective function are linked through the design variables. The basic constraints of the optimization problem include equipment constraints (e.g. capacity limits, production restrictions) and energy balances (e.g. electricity, heating, cooling). Additional constraints are related to the interconnection of the system with the electric grid (e.g. connected or isolated, permission to sell or inject surplus electricity), technical and environmental regulations (e.g. minimum equivalent electrical efficiency, minimum thermal efficiency, minimum

self-consumption of electricity), and operation modes of the equipment (e.g. heat pump in cooling mode during the summer and in heating mode for the rest of the year).

As previously mentioned, there are several factors that increase the computational effort necessary to solve the optimization model, for instance the number of operation periods, the number of technologies in the superstructure, and the accuracy of technology description using linear or non-linear functions. Additionally, the model complexity also increases with the number of binary variables included. Another aspect that must be taken into account is the role of the TES unit in the hourly operation of the energy system. For a system that does not include energy storage, the hourly operation periods are always independent from each other; thus, they can be evaluated individually. However, the incorporation of TES units allows energy service production to be decoupled from consumption, so that the operation of the system in an hourly period may be affected by others; now, the hourly operation periods cannot be assessed individually, but as a whole.

2.2.4 Optimal decision-making

Solving the MILP-based SOO problem brings the "best" solution to the established objective function. In the case of the energy system design for the minimum total annual cost, the optimal solution will include the set of technologies and the operational strategy that minimize capital and operational costs throughout the system's operational lifetime. Nevertheless, the mathematical optimal solution deviates from the real-world optimal solution for several reasons: (i) a mathematical model is never a perfect representation of the real-world problem; (ii) the analyst cannot possibly identify and introduce all the constraints that affect the system; (iii) the mathematical model only reflects the current situation, even though constraints (energy demands, energy prices, etc.) are bound to change in the future; and (iv) the global optimal solution does not give any information about its surroundings and robustness. These aspects have been addressed by Hamming (1973), Frangopoulos et al. (2002), Savic (2002), Carvalho et al. (2013), Pfenninger et al. (2014), and Voll et al. (2015). In this context, as stressed by Hamming (1973) and Savic (2002), optimization tools should be used with the purpose of providing insight rather than numbers, thus supporting the decision-making process.

Furthermore, real-world problems are seldom based on a single criterion; what is more, the multiple criteria involved are often conflicting, as is the case of the energy systems design with sustainability considerations, which typically involves economic and environmental aspects. Therefore, there is the need to consider two or more objective functions in so-called multi-objective optimization (MOO) problems.

There are numerous objective functions that can be used to evaluate an energy system. Nevertheless, the complexity of the optimization model increases with the number of objective functions. Thus, there is a trade-off between the accuracy of the model as regards the multiple conflicting criteria involved and the computational effort required to solve this model (Hennen et al., 2017). In addition, as demonstrated by Pintarič and Kravanja (2015, 2006), the choice of the objective function has a major impact on the results of the optimization procedure: considering the same criterion (e.g. economic costs), the different objective functions that can be used (e.g. total annual cost, net present value, profits) significantly affect the results obtained. This calls for a careful consideration of the criteria types and number, as well as the corresponding objective functions.

In contrast with the SOO, in MOO there is no single optimal solution. The interactions between the different objectives provide a set of trade-off solutions from which the decision-maker can choose. At this stage, one of the difficulties lies in determining if one solution is better than others. In this case, the concept of "dominance" is used: a solution a is said to dominate a solution b if the following two are true (Alarcon-Rodriguez et al., 2010): (i) a is no worse than b in all objectives; and (ii) a is better than b in at least one objective. A dominated solution is also said to be "sub-optimal". The result of a MOO problem is the set of non-dominated solutions, also known as Pareto-optimal solutions. These solutions constitute the Pareto set, or Pareto frontier, in which no improvement can be achieved in one objective without sacrificing the other (Andiappan, 2017). This concept is illustrated in Figure 2.12.
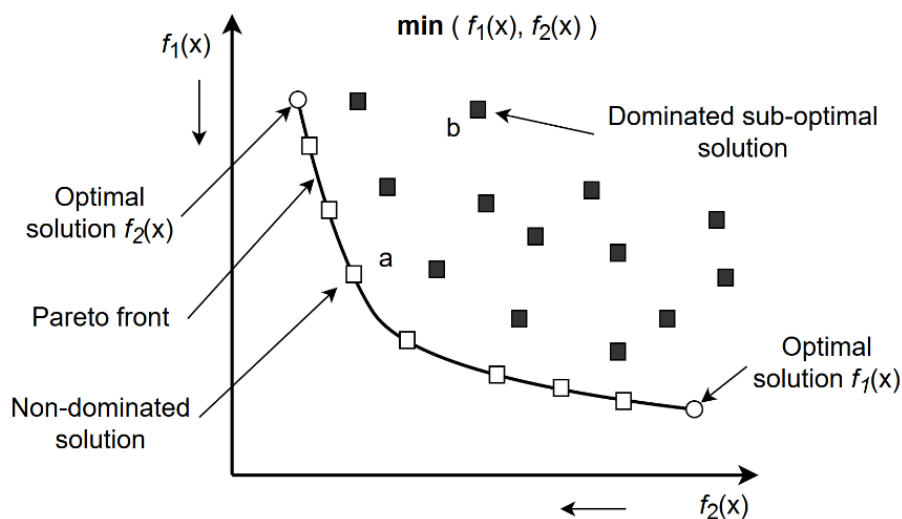
Figure 2.12: Pareto frontier indicating dominated and non-dominated solutions, and single-objective solutions.

Pareto optimization has been extensively applied in the literature concerned with MOO and many methods are available for solving this kind of problem. The solution to the MOO problem typically

involves converting the MOO into a series of SOO problems. An important question is the role of the decision-maker in the procedure. In this regard, *a posteriori* approaches for generating Pareto-optimal solutions are preferred. Among them, the ε-constraint method has been applied by various authors in the optimization of energy supply systems (Alarcon-Rodriguez et al., 2010; Buoro et al., 2013; Carvalho et al., 2012; Fazlollahi et al., 2012; Gebreslassie et al., 2012). In this approach, the problem is optimized with respect to one of the objective functions, while upper/lower bounds are set (ε-constraints) for the rest of the objective functions. The problem is repeatedly solved for different ε values, obtaining the different trade-off solutions that compose the Pareto set.

It follows that finding as many Pareto-optimal solutions in the Pareto set as possible is crucial to provide a more realistic representation of the problem. However, identifying the entire Pareto set is practically impossible due to its size, apart from the fact that the ε-constraint method is very time-consuming. Therefore, in accordance with Konak et al. (2006) and Alarcon-Rodriguez et al. (2010), the decision-maker should investigate the Pareto curve aiming for diverse solutions that cover the whole spectrum of the Pareto set.

Based on the Pareto-optimal solutions obtained, the decision-maker has more information to judge the different trade-off solutions and make a more informed decision. Given the great number of optimal solutions obtained, it may be interesting to define a metric to value these solutions. In this regard, the marginal and the average costs can be evaluated. The marginal cost represents the cost of moving from one Pareto-optimal solution to the next in the Pareto set, while the average cost represents the cost of moving from a specific Pareto-optimal solution to another. Considering the different circumstances under which the system operates, for instance local subsidies for CO_2 emissions savings and/or stock market prices of CO_2 emissions, the marginal cost could be the metric used to choose from the various trade-off solutions obtained.

2.3 CONCLUSIONS

The potential benefits of polygeneration systems relative to the conventional separate production are attributable to the inherent characteristics of the installed devices (e.g. joint production of energy services), their feasible interconnections (e.g. waste heat recovery), and the way in which they are operated over time. Naturally, the increased complexity of polygeneration systems is an issue that must be addressed in order to achieve the system's full potential. In this context, this chapter started with a brief discussion of the main benefits, as well as the associated challenges, that can be derived from the integration of different types of technologies. These technologies consisted of a cogeneration module, a thermally activated technology (e.g. absorption chiller), TES units, RETs, and a heat pump. Then, a multi-objective optimization synthesis framework was

outlined, composed of four steps: superstructure definition, data collection and elaboration, mathematical model development, and optimal-decision making. The synthesis framework will provide the basis for the optimization models developed in Chapters 4 and 5.

Once the system configuration and operational strategy are established, the question remains about the appropriate way to allocate the costs of the energy resources consumed to the internal flows and final products of the system. This issue is addressed in the next chapter through a simple trigeneration system with thermal energy storage.

CHAPTER 3

Thermoeconomic analysis of simple trigeneration systems with thermal storage

3 THERMOECONOMIC ANALYSIS OF SIMPLE TRIGENERATION SYSTEMS WITH THERMAL STORAGE

As explained in Chapter 2, there are several factors that increase the complexity of the design of energy systems, such as the incorporation of renewable energy sources (RES) and thermal energy storage (TES), the multiple energy resources available, the fluctuations in energy demands of the consumer center (both hourly and monthly), the variability of energy prices, among others. Once the configuration and operational state of the plant are obtained, along with the energy resources prices, the fundamental question of the appropriate way to allocate the costs of the resources consumed to the internal flows and final products of the system remains.

In this regard, thermoeconomics unveils the cost formation process from the resources consumed to the final products obtained. Given the potentially high complexity of polygeneration systems, it is proposed in this chapter to start with a simple energy system configuration. This approach allows for interesting analyses and conceptual interpretations, thus providing the base for the application of the cost allocation proposals to more complex case studies, which will be studied further in Chapter 4.

The simple trigeneration system analyzed by Lozano et al. (2009b) and Carvalho (2011) has been chosen for the present study. This thesis builds upon those works by incorporating a TES unit. The presence of a storage device adds a new dimension to the cost allocation problem, as it becomes necessary to determine not only the device that is producing the energy flow, but also the time interval in which the production took place.

The goal of this chapter is, thus, to formulate and demonstrate the application of cost allocation approaches for energy systems assisted with TES units. The chapter is structured as follows: Section 3.1 describes the simple trigeneration system analyzed herein, including the optimization model and the optimal operation of the systems for a day of the year. In Section 3.2, the analysis of the marginal costs obtained from the optimization model is used to explain the optimal operation of the simple trigeneration system, as well as the role of the TES unit in achieving the optimal solution. In Section 3.3 the cost allocation proposals are formulated and the application of the thermoeconomic analysis is demonstrated, obtaining the hourly and daily unit costs of all internal flows and final products of the system. Finally, Section 3.4 draws the conclusions from this chapter.

3.1 SIMPLE TRIGENERATION SYSTEM WITH THERMAL STORAGE

Trigeneration systems are distinguished by the numerous incorporated alternative devices and existing configuration modes (Wu and Wang, 2006). Basically, a trigeneration system is composed

of a cogeneration module and a thermally activated technology. The cogeneration module consists of a prime mover (e.g. reciprocating internal combustion engine, gas turbine, micro-turbine, fuel cell), which converts the chemical energy of the fuel into shaft power, an electricity generator, and a heat recovery system. Thermally activated technologies (e.g. absorption chillers, adsorption chillers, desiccant dehumidifiers) are responsible for providing cooling and must be chosen in accordance with the prime mover (Liu et al., 2014). Auxiliary devices commonly incorporated in trigeneration systems are boilers and electric chillers.

For the present study, the following simplifying assumptions were made: (i) the operation of the system is considered for a day of the year composed of 24 consecutive periods of 1-hour duration; (ii) the devices can modulate between zero and full load with no impact on their performances; (iii) the prices of the energy resources are considered constant throughout the day, especially in the case of the electricity; and (iv) only the operational planning is taken into account, thus excluding capital costs.

It goes without saying that the optimization model could have been more complex; nevertheless, in accordance with Lozano et al. (2009b), increasing the complexity of the model would not provide more relevant conclusions and would hide, to some extent, the clarity of the analysis.

3.1.1   System description

The simple trigeneration system analyzed herein is depicted in Figure 3.1. The system is composed of a cogeneration module CM, an auxiliary boiler AB, a single-effect absorption chiller AC, a mechanical chiller EC, and a chilled water storage tank TS.

The simple trigeneration system was designed to attend the electricity E_d, heating Q_d, and cooling R_d demands of a consumer center (e.g. multi-family building). It is considered that the system is interconnected with the electric grid, so purchase E_p and sale E_s of electricity are allowed. The CM consumes natural gas F_c and produces cogenerated electricity W_c and heat Q_c. A part of the cogenerated electricity W_c can be sold E_s to the grid; the part that is not sold W_{cc}, along with the electricity purchased from the grid E_p, is used to attend the electricity demand E_d and/or drive the EC E_r. The AB consumes fuel-oil F_a and produces conventional heat Q_a. Regarding the cogenerated heat Q_c, a part of it Q_{cl} can be dissipated into the environment. The part that is not wasted Q_{cc}, along with the conventional heat Q_a, is used to attend the heating demand Q_d and/or drive the AC Q_r. The cooling produced by the AC R_q and EC R_e are used to cover the cooling demand R_d and/or charge the TS. The TS can be either charging R_{in} or discharging R_{out} in each hourly period; energy losses R_s are proportional to the stored energy S_r and to the TS energy loss factor τ_{TS}.
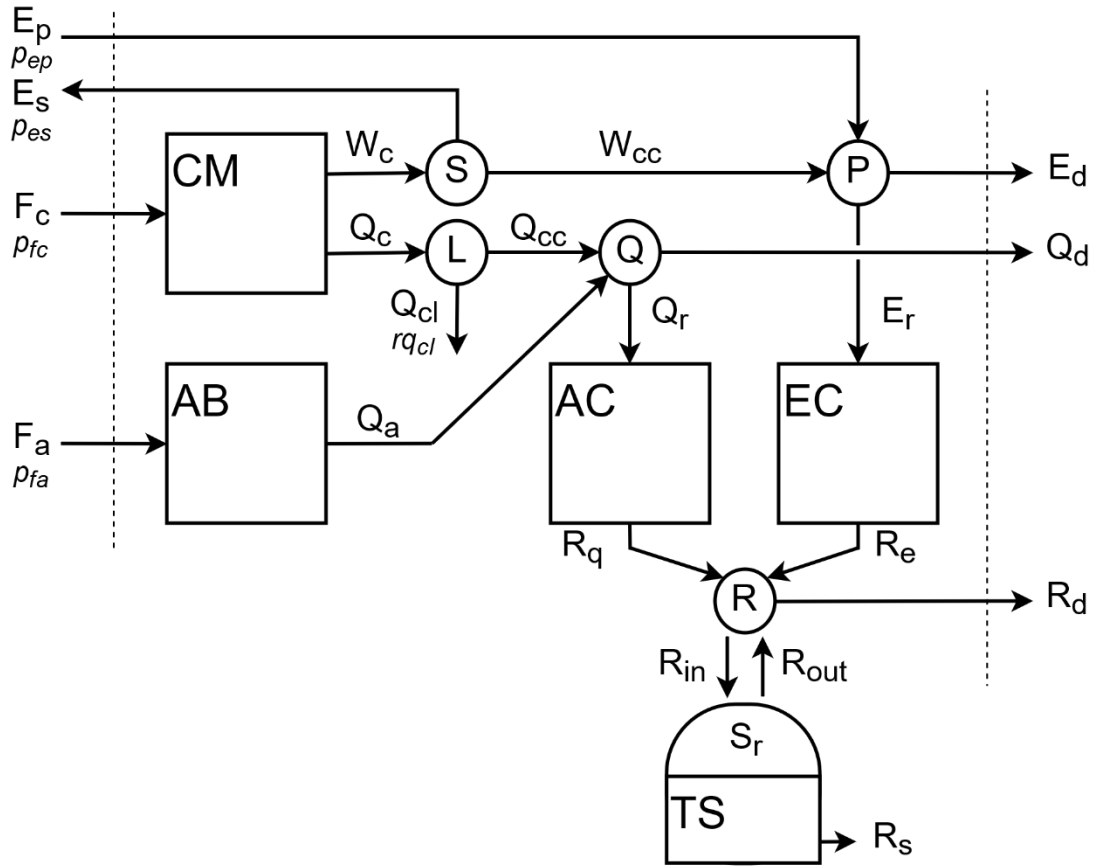
Figure 3.1: Diagram of the simple trigeneration system.

All system devices can modulate between zero and full load with constant performance factors. Table 3.1 presents the technical parameters and capacity limits of the system's devices.

Table 3.1: Technical parameters and capacity limits.

Device	Technical parameter	Value	Capacity limit
CM	Electric power efficiency	$\alpha_w = W_c/F_c = 0.35$	$W_{max} = 350$ kW
CM	Thermal efficiency	$\alpha_q = Q_c/F_c = 0.40$	
AB	Thermal efficiency	$\eta_q = Q_a/F_a = 0.80$	$Q_{max} = 400$ kW
AC	COP	$COP_q = R_q/Q_r = 0.625$	$R_{q,max} = 250$ kW
EC	COP	$COP_e = R_e/E_r = 5$	$R_{e,max} = 250$ kW
TS	Energy loss factor	$\tau_{TS} = 0.01$ h^{-1}	$V_{max} = 2000$ kWh

It is important to emphasize the reasons for including a TES unit for chilled water and not for hot water (or both). First, the cooling demand considered herein presents higher variations throughout the day than the heating demand. Secondly, the aim of this Section is to demonstrate the marginal cost analysis and thermoeconomic cost allocation methodologies, so the inclusion of two or more TES units would hinder the clarity of the analysis.

The simple trigeneration system interacts with the economic environment through the purchase of natural gas F_c, fuel-oil F_a, and electricity E_p, as well as through the sale of electricity E_s. The

corresponding energy prices are given in Table 3.2. Moreover, it was considered that no cost was associated with the dissipation of cogenerated heat to the environment $rq_{cl} = 0$ €/kWh.

Table 3.2: Energy prices, in €/kWh.

Purchased natural gas	Purchased fuel-oil	Purchased electricity	Sold electricity
$p_{fc} = 0.025$	$p_{fa} = 0.020$	$p_{ep} = 0.100$	$p_{es} = 0.080$

The energy demands of the consumer center E_d, Q_d, and R_d for a day of the year are described by 24 consecutive periods of 1-hour duration and are given in Table 3.3. As can be seen, E_d is required all through the day, Q_d is required at hours 1 and 7 to 24, and R_d is required between hours 14 and 22.

3.1.2   Optimal operation model

Given the various resources available and devices that constitute the simple trigeneration system, it becomes evident that many alternative production routes can take place to supply the energy demands of the consumer center. For instance, the heating demand Q_d can be covered with: (i) useful cogenerated heat Q_{cc} from the CM, consuming natural gas F_c at price p_{fc}; and/or (ii) conventional heat Q_a from the AB, consuming fuel-oil F_a at price p_{fa}.

Mathematical models based on LP are generally used to obtain a rational operational strategy, which is always linked to an objective function (e.g. minimum operation cost, minimum environmental loads). A rational, complete, and exact operational strategy constitutes essential data when addressing the cost allocation issue in energy systems.

The developed LP model determines the hourly operational strategy of the simple trigeneration system for a day of the year that minimizes the daily operation cost DC, given by Eq. (3.1). The daily operation cost corresponds to the sum of the hourly operation cost $HC(h)$ for the 24 consecutive periods h ($NP = 24$) of 1-hour duration ($NHP = 1$) that comprise the day.

$$Min\ DC = NHP \cdot \sum_{h=1}^{NP} HC(h) \tag{3.1}$$

For each hourly period h, $HC(h)$ includes the costs of purchasing electricity, natural gas, and fuel-oil, the cost associated with the dissipation of cogenerated heat, and the income from selling electricity to the grid, as expressed by Eq. (3.2).

$$HC(h) = p_{ep}(h) \cdot E_p(h) + p_{fc}(h) \cdot F_c(h) + p_{fa}(h) \cdot F_a(h) + rq_{cl}(h) \cdot Q_{cl}(h) - p_{es}(h) \cdot E_s(h) \tag{3.2}$$

Table 3.3: Optimal operation of the simple trigeneration system. Energy flows in kWh and cost in €.

Hour	E_d	Q_d	R_d	E_{grid}	F_c	W_c	W_{cc}	Q_c	Q_{cc}	Q_{cl}	F_a	Q_a	Q_r	R_q	E_r	R_e	R_{TS}	R_s	S_{rf}	Cost
1	253.6	168.4	0.0	-96.4	1000	350	253.6	400	400	0	0.0	0.0	231.6	144.8	0.0	0.0	144.8	2.4	385.7	17.3
2	247.0	0.0	0.0	-103.0	1000	350	247.0	400	400	0	0.0	0.0	400.0	250.0	0.0	0.0	250.0	3.9	631.9	16.8
3	241.7	0.0	0.0	-108.3	1000	350	241.7	400	400	0	0.0	0.0	400.0	250.0	0.0	0.0	250.0	6.3	875.6	16.3
4	237.7	0.0	0.0	-112.3	1000	350	237.7	400	400	0	0.0	0.0	400.0	250.0	0.0	0.0	250.0	8.8	1116.8	16.0
5	253.6	0.0	0.0	-96.4	1000	350	253.6	400	400	0	0.0	0.0	400.0	250.0	0.0	0.0	250.0	11.2	1355.6	17.3
6	262.9	0.0	0.0	-87.1	1000	350	262.9	400	400	0	0.0	0.0	400.0	250.0	0.0	0.0	250.0	13.6	1592.1	18.0
7	286.8	168.4	0.0	-63.2	1000	350	286.8	400	400	0	0.0	0.0	231.6	144.8	0.0	0.0	144.8	15.9	1720.9	19.9
8	324.0	244.0	0.0	-6.1	1000	350	343.9	400	400	0	0.0	0.0	156.0	97.5	19.9	99.4	196.9	17.2	1900.6	24.5
9	377.1	378.0	0.0	27.1	1000	350	350.0	400	400	0	0.0	0.0	22.0	13.7	0.0	0.0	13.7	19.0	1895.3	27.7
10	468.7	570.5	0.0	118.7	1000	350	350.0	400	400	0	213.1	170.5	0.0	0.0	0.0	0.0	0.0	19.0	1876.3	41.1
11	494.0	446.8	0.0	144.0	1000	350	350.0	400	400	0	58.5	46.8	0.0	0.0	0.0	0.0	0.0	18.8	1857.6	40.6
12	454.1	309.3	0.0	104.1	1000	350	350.0	400	400	0	0.0	0.0	90.7	56.7	0.0	0.0	56.7	18.6	1895.7	35.4
13	369.1	202.8	0.0	19.1	1000	350	350.0	400	400	0	0.0	0.0	197.2	123.3	0.0	0.0	123.3	19.0	2000.0	26.9
14	325.3	405.5	719.8	0.0	1000	350	350.0	400	400	0	6.9	5.5	0.0	0.0	24.7	123.4	-596.4	20.0	1383.6	25.1
15	313.4	319.6	644.0	0.0	1000	350	350.0	400	400	0	0.0	0.0	80.4	50.2	36.6	183.2	-410.6	13.8	959.1	25.0
16	338.6	299.0	698.2	0.0	1000	350	350.0	400	400	0	0.0	0.0	101.0	63.1	11.4	57.0	-578.0	9.6	371.5	25.0
17	414.3	240.6	614.4	112.4	1000	350	350.0	400	400	0	0.0	0.0	159.4	99.7	48.1	240.7	-274.0	3.7	93.7	36.2
18	468.7	299.0	359.0	168.7	1000	350	350.0	400	400	0	0.0	0.0	101.0	63.1	50.0	250.0	-45.8	0.9	47.0	41.9
19	452.8	405.5	296.5	152.8	1000	350	350.0	400	400	0	6.9	5.5	0.0	0.0	50.0	250.0	-46.5	0.5	0.0	40.4
20	455.5	508.6	243.3	154.1	1000	350	350.0	400	400	0	135.8	108.6	0.0	0.0	48.7	243.3	0.0	0.0	0.0	43.1
21	418.3	405.5	247.9	117.8	1000	350	350.0	400	400	0	6.9	5.5	0.0	0.0	49.6	247.9	0.0	0.0	0.0	36.9
22	361.2	319.6	177.0	36.5	1000	350	350.0	400	400	0	0.0	0.0	80.4	50.2	25.3	126.7	0.0	0.0	0.0	28.7
23	308.1	240.6	0.0	-41.9	1000	350	308.1	400	400	0	0.0	0.0	159.4	99.7	0.0	0.0	99.7	0.0	99.7	21.6
24	273.5	168.4	0.0	-76.5	1000	350	273.5	400	400	0	0.0	0.0	231.6	144.8	0.0	0.0	144.8	1.0	243.4	18.9
Day	8400	6100	4000	364.3	24000	8400	7608.8	9600	9600	0	428.0	342.4	3842.4	2401.5	364.3	1821.5	223	223	22302	660.8

The objective function is subject to equipment constraints (capacity limits and production restrictions) and balance equations, as described below.

Equipment constraints

For each hourly period *h*, the devices' productions are limited to their capacity limits (Table 3.1), as expressed by Equations (3.3)-(3.6). In the case of the TS, the energy stored at the end of each hourly period $S_{rf}(h)$ is limited to the maximum storage capacity V_{max}, according to Eq. (3.7).

CM_Wmax:	$W_c(h) \leq W_{max}$	(3.3)
AB_Qmax:	$Q_a(h) \leq Q_{max}$	(3.4)
AC_Rqmax:	$R_q(h) \leq R_{q,max}$	(3.5)
EC_Remax:	$R_e(h) \leq R_{e,max}$	(3.6)
Srf_Vol:	$S_{rf}(h) \leq V_{max}$	(3.7)

Production restrictions are expressed by Equations (3.8)-(3.12), taking the technical parameters from Table 3.1.

CM_W:	$\alpha_w \cdot F_c(h) - W_c(h) = 0$	(3.8)
CM_Q:	$\alpha_q \cdot F_c(h) - Q_c(h) = 0$	(3.9)
AB_Q:	$\eta_q \cdot F_a(h) - Q_a(h) = 0$	(3.10)
AC_R:	$COP_q \cdot Q_r(h) - R_q(h) = 0$	(3.11)
EC_R:	$COP_e \cdot E_r(h) - R_e(h) = 0$	(3.12)

The energy losses $R_s(h)$ in each hourly period *h* are equal to the energy stored at the end of the previous period $S_{rf}(h-1)$ multiplied by the TS energy loss factor τ_{TS}:

$$R_s(h) = \tau_{TS} \cdot S_{rf}(h-1) \tag{3.13}$$

Given the daily regularity of the energy demands, it was considered that the TS must return to its initial state after the daily cycle; in this way, the energy stored at the end of the day $S_{rf}(24)$ must be equal to the energy stored at the beginning of the day $S_{ri}(1)$, as expresses Eq. (3.14). Also, given the continuous operation of the TS, it follows that the energy stored at the beginning of an hourly period $S_{ri}(h)$ must be equal to the energy stored at the end of the previous period $S_{rf}(h-1)$, according to Eq. (3.15).

$$S_{ri}(1) = S_{rf}(24) \tag{3.14}$$
$$S_{ri}(h) = S_{rf}(h-1) \tag{3.15}$$

Balance equations

The energy balances in the junctions and distributors of the system are expressed as

S:	$W_c(h) - E_s(h) - W_{cc}(h) = 0$	(3.16)
P:	$W_{cc}(h) + E_p(h) - E_r(h) - E_d(h) = 0$	(3.17)
L:	$Q_c(h) - Q_{cc}(h) - Q_{cl}(h) = 0$	(3.18)
Q:	$Q_a(h) + Q_{cc}(h) - Q_r(h) - Q_d(h) = 0$	(3.19)
R:	$R_q(h) + R_e(h) + R_{out}(h) - R_{in}(h) - R_d(h) = 0$	(3.20)

The energy balance in the TS provides Eq. (3.21), in which the stored energy $S_{ri}(h)$ and $S_{rf}(h)$, in kWh, are divided by the number of hours per period $NHP = 1$, thus obtaining the corresponding value in kW.

$$TS: \quad S_{ri}(h)/NHP + R_{in}(h) - R_{out}(h) - R_s(h) - S_{rf}(h)/NHP = 0 \qquad (3.21)$$

3.1.3 Optimal operation of the simple trigeneration system

The optimization model was solved using the software LINGO (Schrage, 1999). A daily operation cost DC of 660.8 €/day was obtained, of which: (i) 600 €/day is due to the purchase of natural gas F_c for the CM; (ii) 115.6 €/day is due to the purchase of electricity from the grid E_p; (iii) 8.6 €/day is due to the purchase of fuel-oil F_a for the AB; and (iv) 63.3 €/day corresponds to the income generated by selling of cogenerated electricity E_s.

The hourly energy flows of the optimal operation are presented in Table 3.3, in which E_{grid} represents the net electricity exchanged with the electric grid (negative values mean sale E_s and positive values mean purchase E_p), and R_{TS} indicates whether the TS is charging (positive values, R_{in}) or discharging (negative values, R_{out}).

The hourly electricity and heat energy flows (production and energy demands) in the optimal operation of the system are presented, respectively, in Figure 3.2 and Figure 3.3. The cogeneration module CM operates at full load all through the day (daily load factor of 100%), consuming 24,000 kWh/day of natural gas F_c and simultaneously producing 8400 kWh/day of cogenerated electricity W_c and 9600 kWh/day of cogenerated heat Q_c. From hours 1 to 8 and 23 to 24, the system sells 791.2 kWh/day of surplus cogenerated electricity E_s, which represents 9.4% of the total electricity produced W_c. On the other hand, from hours 9 to 13 and 17 to 22, the system must purchase 1155.5 kWh/day of electricity E_p, which represents 13.2% of the total electricity consumed ($E_d + E_r$). Regarding the heat production in the CM, no cogenerated heat is wasted into the environment ($Q_{cl} = 0$ kWh/day). Additionally, the available cogenerated heat Q_{cc} represents 96.6% of the total heat consumed by the system ($Q_d + Q_r$). The remaining 3.4% (342.4 kWh/day) is supplied by the AB (daily load factor of 4%), which operates marginally to cover peak heat demands (e.g. hours 10, 11, and 20).
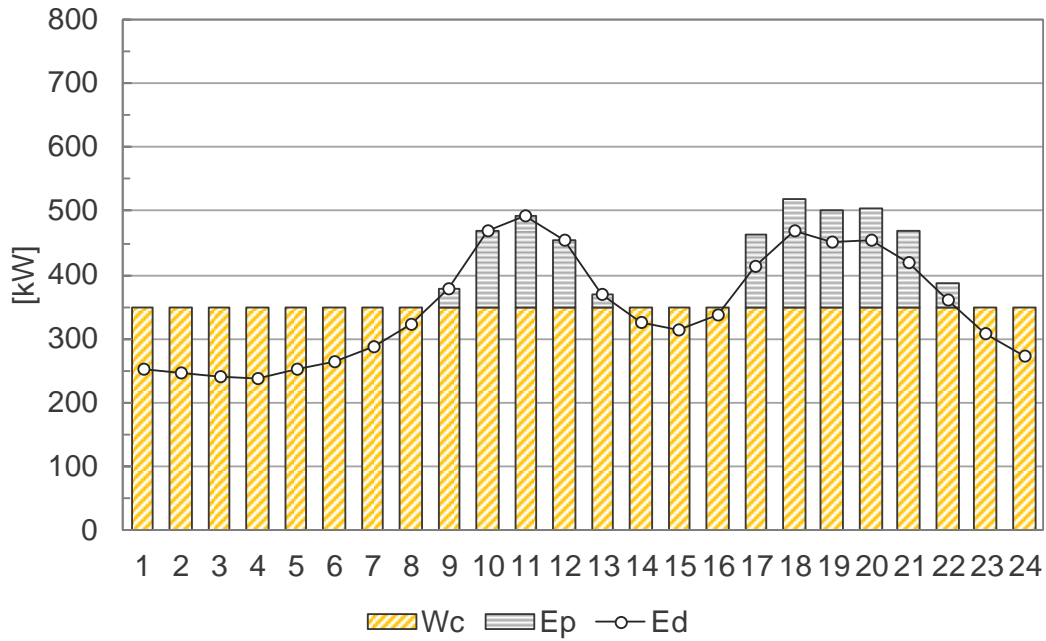
Figure 3.2: Hourly electricity flows.
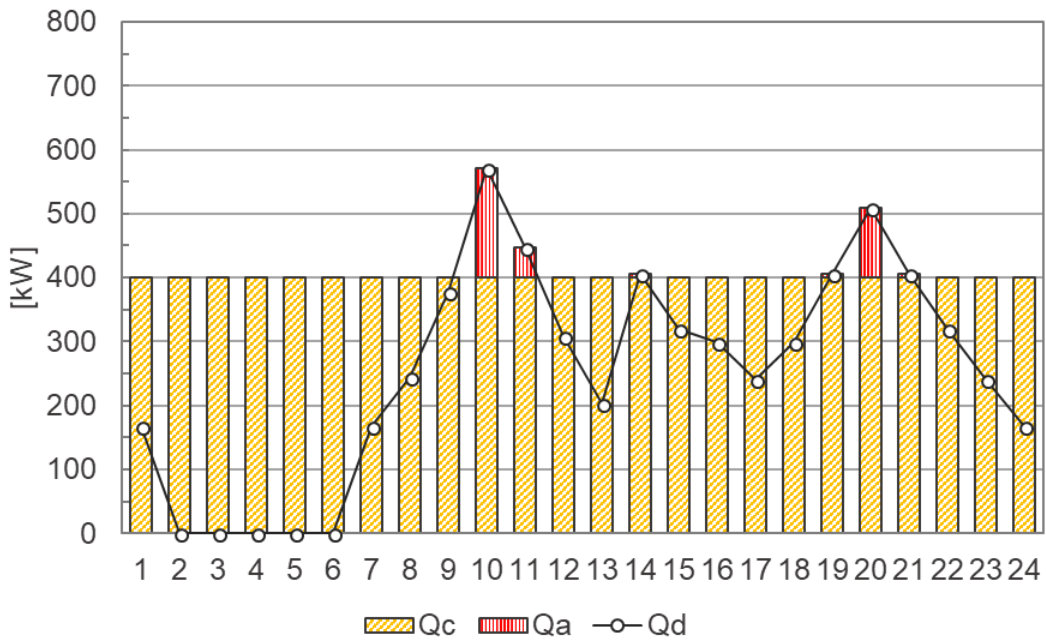
Figure 3.3:Hourly heat flows.

The hourly cooling production and demand throughout the day are presented in Figure 3.4. Even though the consumer center only requires cooling R_d between hours 14 and 22, its production also takes place at previous hours to charge the TS. Considering the cooling produced by the system, 56.9% (2401.5 kWh/day) is produced in the AC (daily load factor of 40%) and 43.1% (1821.5 kWh/day) is produced in the EC (daily load factor of 30%). The EC cooling production R_e takes place at hours 8 and 14 to 22. It is interesting to note the different electricity sources available for the EC at different hours: on the one hand, at hours 8 and 14 to 16, the system is not purchasing

electricity (E_p = 0 kWh), so all cooling R_e is produced with cogenerated electricity W_{cc}; on the other hand, at hours 17 to 22, cooling R_e is produced with both purchased E_p and cogenerated W_{cc} electricity flows. In the case of the AC, cooling R_q is produced at hours 1 to 9, 12, 13, 15 to 18, and 22 to 24. Although there is no physical limitation to the use of cogenerated Q_{cc} and/or conventional Q_a heat flows, it can be seen that, in the optimal operation, the AB is never used to drive the AC, which means that all R_q is produced with cogenerated heat Q_{cc}.
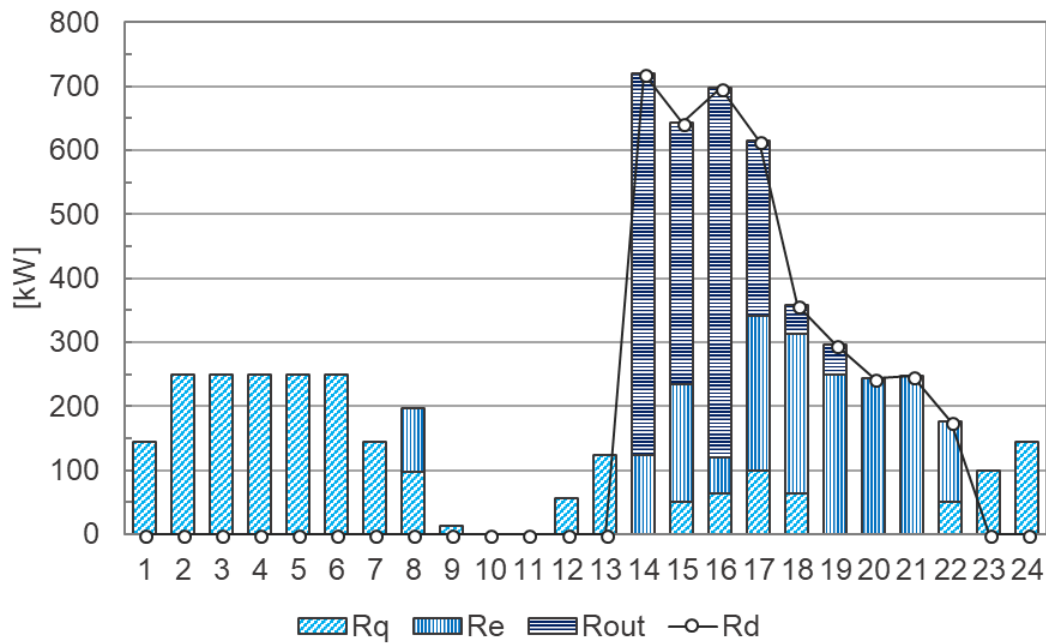
Figure 3.4: Hourly cooling flows.

The energy stored at the end of each hourly period S_{rf} is shown in Figure 3.5. As can be seen, charging of the TS takes place for 13 hours, beginning at hour 23 of the previous day until hour 9 and continuing at hours 12 and 13 until the TS is fully charged with 2000 kWh. Discharging takes place for 6 hours, beginning at hour 14 along with the cooling demand R_d, until hour 19. Considering the daily demand R_d, 48.8% of it is supplied by the TS, meaning that it was produced at different previous hours. By the end of the discharging period the TS is fully discharged and remains in this way until hour 23, when the charging cycle begins again. Following from the explanation provided in the previous paragraph, it is also interesting to note the different types of cooling stored: hour 8 is characterized by production of both R_q (with cogenerated heat Q_{cc}) and R_e (with cogenerated electricity W_{cc}); the rest of the charging hours are characterized exclusively by R_q production (with cogenerated heat Q_{cc}).
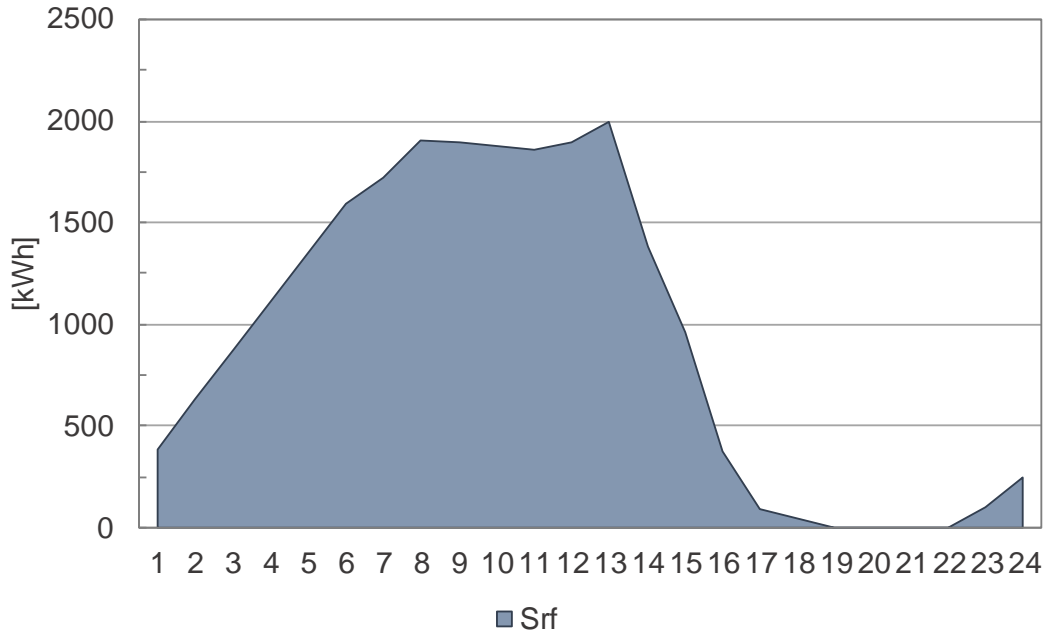
Figure 3.5: Energy stored at the end of the hourly period S_{rf}.

3.1.4 Reference system

The reference system considered in this analysis corresponds to the separate conventional production of energy services, as depicted in Figure 3.6. In this way, considering the same energy resources prices and technical parameters of the devices as for the simple trigeneration system: (i) the electricity demand E_d is covered by purchase from the electric grid; (ii) the heating demand Q_d is covered by the boiler AB consuming fuel-oil F_a; and (iii) the cooling demand R_d is covered by the mechanical chiller EC consuming electricity purchased from the grid E_p.
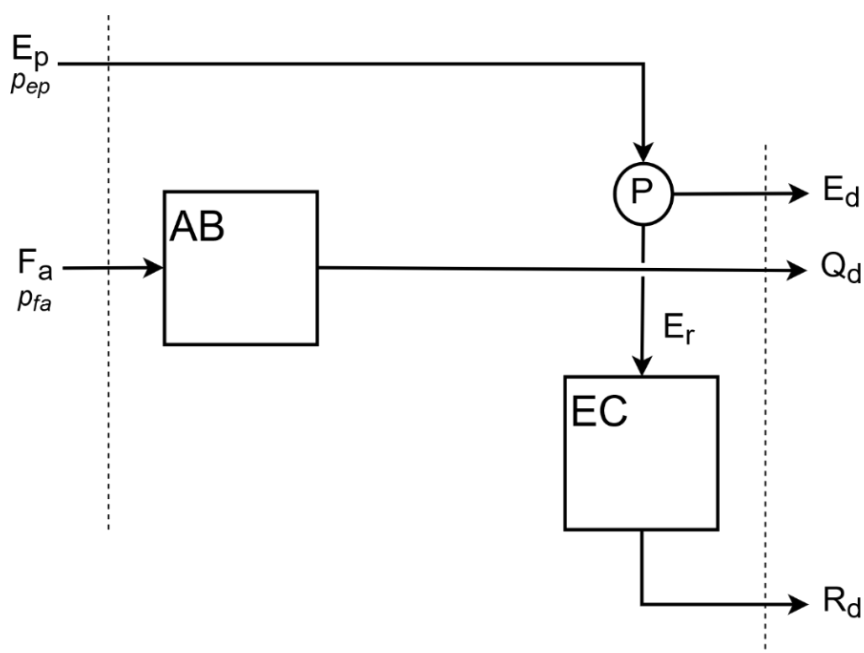
Figure 3.6: Reference system.

Therefore, the production costs of the energy services in the reference system can be determined as follows: (i) electricity: purchase price from the electric grid $(cW)_{ref} = p_{ep}$ = 0.100 €/kWh; (ii) heat: production cost in the AB consuming fuel-oil $(cQ)_{ref} = p_{fa}/\eta_{AB}$ = 0.025 €/kWh; and (iii) cooling: production cost in the EC consuming electricity purchased from the grid $(cR)_{ref} = p_{ep}/COP_e$ = 0.020 €/kWh.

3.2 MARGINAL COST ANALYSIS

Thermoeconomics combines thermodynamic principles with economic analysis, aiming at revealing opportunities of energy and cost savings in the analysis, diagnosis, and optimization of energy conversion systems that are not available through conventional methods (Gaggioli, 1983; Lozano and Valero, 1993).

Obtaining unit costs of internal flows and final products of energy systems is a cornerstone of several thermoeconomic methodologies that have been presented in the literature (Lozano et al., 2009b). Three different approaches to determine the unit costs of internal flows and final products of a simple trigeneration system were presented in Lozano et al. (2009a): (i) marginal cost analysis based on the optimal operation of the system; (ii) products valuation according to their market prices; and (iii) internal costs calculation. From the various results obtained for each approach, it was concluded that there is no general rule to decide which approach is the best, as it depends on the objectives of the analysis.

It is important to distinguish between unit (or average) and marginal costs: unit cost is a ratio that corresponds to the unit (or average) production cost of a flow, calculated by dividing the total cost by the total quantity produced, while the marginal cost is a derivative that corresponds to the cost of producing one more unit of a flow.

Unit cost calculation in energy systems with joint production, such as trigeneration systems, can only be achieved by establishing arbitrary allocation rules. Furthermore, unit costs do not explain the reasons for the optimal operation mode of the plant, nor do they provide information about the behavior of the system's operation given a change in external circumstances (e.g. energy demand changes).

On the other hand, marginal costs offer a clear route to understanding and managing the behavior of costs throughout the system. Consequently, they are able to (Li et al., 2015): (i) motivate investments in infrastructure and equipment, improving efficiency and reducing operational costs; (ii) express variation in production costs; and (iii) reflect variations in the market prices of the resources.

Marginal costs have been used to provide information about the operation of energy systems in the building sector (Lozano et al., 2009b), waste facilities (Martinez-Sanchez et al., 2016), power plants (site model) (Hui, 2000), site utility systems focusing on steam production (Varbanov et al., 2004), and district heating facilities (Li et al., 2015; Sjödin and Henning, 2004), to name a few examples. Quelhas et al. (2006) used marginal costs to analyze the influence of the various fuel networks (production, transportation, and delivery of fossil fuels to the power plants) on the electric network.

Owing to the fact that marginal costs are intrinsically related to the operation of the system, a "marginal path" can be traced, linking the point at which the marginal change is required (e.g. consumer center's energy demand), via one or more items of the system's equipment, to the system boundary where changes in the fuel and/or electricity purchases can be evaluated; the term "marginal path" is generally reserved to the one which incurs the smallest marginal cost (Rossiter and Ranade, 1988).

On the downside, marginal costs are difficult to calculate, given the multiple possibilities of production paths, especially in systems with high level of energy integration. Computational tools facilitate the calculation of marginal costs and the analysis of the influences of changes in the input data.

Along with the optimal operation of the system, the LINGO solution report provides a dual price figure for each constraint of the model. This dual price figure indicates the amount by which the objective function (in this case, the daily operation cost DC) would change as the constant term of the constraint is increased by one unit. If a constraint expresses the production of a flow, then its dual price can be interpreted as the marginal cost λ of this flow. The following sections present a detailed interpretation of the dual prices associated with the system's constraints and final products.

3.2.1   Marginal costs of the final products

The dual prices of the constraints P (Eq. (3.17)), Q (Eq. (3.19)), and R (Eq. (3.20)), presented in Table 3.4, can be interpreted as the marginal costs of the electricity λE_d, heat λQ_d, and cooling λR_d, respectively. Examples of the interpretation of the marginal costs for selected hours are presented in the following paragraphs.

Table 3.4: Dual prices of balance equations P, Q and R, in €/kWh.

Hour	P (λE_d)	Q (λQ_d)	R (λR_d)
1	0.0800	0.0093	0.0149
2	0.0800	0.0094	0.0151
3	0.0800	0.0095	0.0152
4	0.0800	0.0096	0.0154
5	0.0800	0.0097	0.0155
6	0.0800	0.0098	0.0157
7	0.0800	0.0099	0.0158
8	0.0800	0.0100	0.0160
9	0.1000	0.0101	0.0162
10	0.1000	0.0250	0.0163
11	0.1000	0.0250	0.0165
12	0.1000	0.0104	0.0167
13	0.1000	0.0105	0.0168
14	0.0970	0.0250	0.0194
15	0.0980	0.0123	0.0196
16	0.0990	0.0124	0.0198
17	0.1000	0.0125	0.0200
18	0.1000	0.0126	0.0202
19	0.1000	0.0250	0.0204
20	0.1000	0.0250	0.0200
21	0.1000	0.0250	0.0200
22	0.1000	0.0125	0.0200
23	0.0800	0.0091	0.0146
24	0.0800	0.0092	0.0148

Figure 3.7, Figure 3.8, and Figure 3.9 graphically explain the "marginal paths" of the final products of the simple trigeneration system for hours 8, 9, and 15, respectively. In the three figures, the "marginal paths" of the electricity, heat, and cooling are represented by bold, dashed, and dotted lines, respectively. It should be noted that marginal costs are evaluated individually; therefore, the aforementioned figures present the marginal costs of the individual production of each final product, and not of the simultaneous production of all three. In addition, the bold, normal-size, and dotted outlines in the system's devices indicate, respectively, that the device is operating at full load, at partial load, and not operating.

3.2.1.1 Hour 8: Of simultaneous energy service production and supply

At hour 8 electricity is sold to the electric grid, the CM is operating at full load (hence the bold outline), the AB is not operating (hence the dotted outline), and cooling is produced in both the AC and EC. The marginal cost of the electricity is λE_d = 0.080 €/kWh, which indicates that if an additional unit of electricity is required, one less unit will be sold to the market; thus, λE_d is interpreted as the selling price p_{es} (λE_d = 1·p_{es} = 0.080 €/kWh). The marginal cost of the heat λQ_d

= 0.010 €/kWh is interpreted as follows: If an additional unit of heat is required, one less unit will be directed to the AC, resulting in $1 \cdot COP_q$ = 0.625 kWh less of cooling produced; the cooling depletion will be covered by the EC with $0.625/COP_e$ = 0.125 kWh less of electricity available to be sold to the electric grid ($\lambda Q_d = 0.125 \cdot p_{es}$ = 0.010 €/kWh). The marginal cost of the cooling is λR_d = 0.016 €/kWh, which means that the additional unit of cooling will be provided by the EC with $1/COP_e$ = 0.200 kWh of electricity at selling price ($\lambda R_d = 0.200 \cdot p_{es}$ = 0.016 €/kWh).
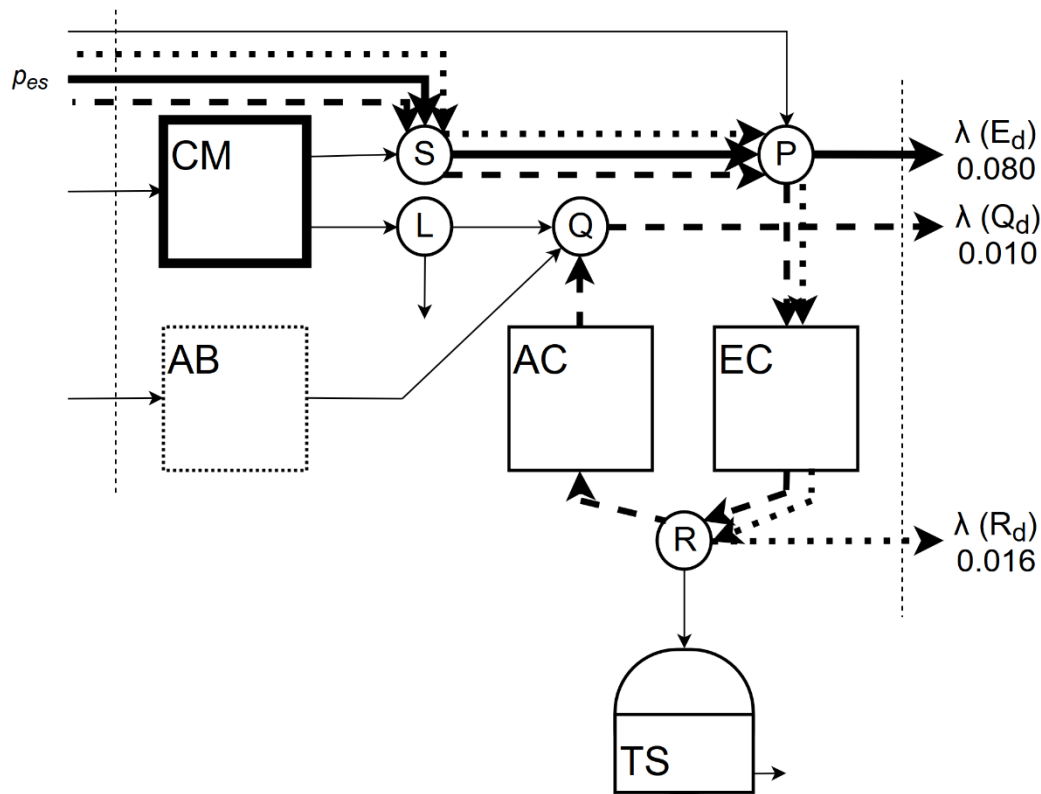
Figure 3.7: Marginal paths for hour 8; marginal costs in €/kWh.

Alternative production paths can be identified in Figure 3.7 and proved to be more costly than their respective "marginal paths". For example, the additional unit of heat could be supplied by the AB with the consumption of $1/\eta_q$ = 1.250 kWh of fuel-oil valued at price p_{fa} = 0.020 €/kWh, thus resulting in a marginal cost of 0.025 €/kWh, which is more than double the actual λQ_d. The additional cooling could be supplied by the AC with $1/COP_q$ = 1.6 kWh of heat from the AB, which would require $1.6/\eta_q$ = 2 kWh of fuel-oil at price p_{fa} = 0.020 €/kWh, thus resulting in a marginal cost of 0.040 €/kWh, which is more than double the actual λR_d; in particular, this shows that cooling production in the EC with electricity (either at purchasing p_{ep} or selling p_{es} price) is more profitable than in the AC with heat from the AB. This is the reason that whenever cooling is required at hour 8 it is produced in the EC rather than in the AC.

Less obvious production paths can be traced by including the TES unit and connecting the system's operation at hour 8 to other hourly periods. However, these would also prove to be more

costly than the "marginal paths" obtained. Examples of how and why production should be advanced or delayed by using the TS to supply cheaper energy services are given below for hours 9 and 15.

3.2.1.2   Hour 9: Of why energy service production should be advanced

Even though the TS is charging at hour 8, it does not directly affect the marginal costs of the final products of the trigeneration system at that hour, i.e. it is not included in the "marginal path". By contrast, Figure 3.8 shows that the "marginal paths" of the heat and the cooling supplied at hour 9 are linked to the system's operation at hour 8 through the TS.

At hour 9, the marginal cost of the electricity is λE_d = 0.1000 €/kWh, which indicates that if an additional unit of electricity is required, it will be purchased from the electric grid at purchasing price ($\lambda E_d = 1 \cdot p_{ep}$ = 0.1000 €/kWh). In this case, both the purchase and the supply of the marginal electricity take place within hour 9.

On the other hand, the "marginal paths" of the heat and the cooling include the TS, meaning that energy services production is shifted in time. The marginal cost of the heat λQ_d = 0.0101 €/kWh can be interpreted as follows: If an additional unit of heat is required, one less unit will be directed to the AC, resulting in $1 \cdot COP_q$ = 0.625 kWh less of cooling produced; because the TS is being charged at hour 9, 0.625 kWh less of cooling will be stored. The cooling depletion must be offset at hour 8, when cooling can be produced in the EC with electricity at selling price p_{es}. However, because there are energy losses in the TS, more than 0.625 kWh of cooling must be produced and stored at hour 8. Given the required discharge at hour h, $R_{out}(h)$, Eq. (3.22) provides the amount of cooling that must be produced and stored at hour k, $R_{in}(k)$:

$$R_{out}(h) = R_{in}(k) \cdot (1 - \tau_{TS})^{(h-k)} \tag{3.22}$$

It follows that to compensate for the lack of 0.625 kWh of cooling at hour 9, 0.6313 kWh of cooling must be produced and stored at hour 8 with the consumption of 0.1263 kWh of electricity at selling price ($\lambda Q_d = 0.1263 \cdot p_{es}$ = 0.0101 €/kWh). The same reasoning applies to the marginal cost of cooling λR_d = 0.0162 €/kWh: supplying an additional unit of cooling at hour 9 reduces the storage in the same amount, which must be compensated by producing 1.0101 kWh of cooling (1 kWh + energy losses) at hour 8 with 0.2020 kWh of electricity at selling price ($\lambda R_d = 0.2020 \cdot p_{es}$ = 0.0162 €/kWh).
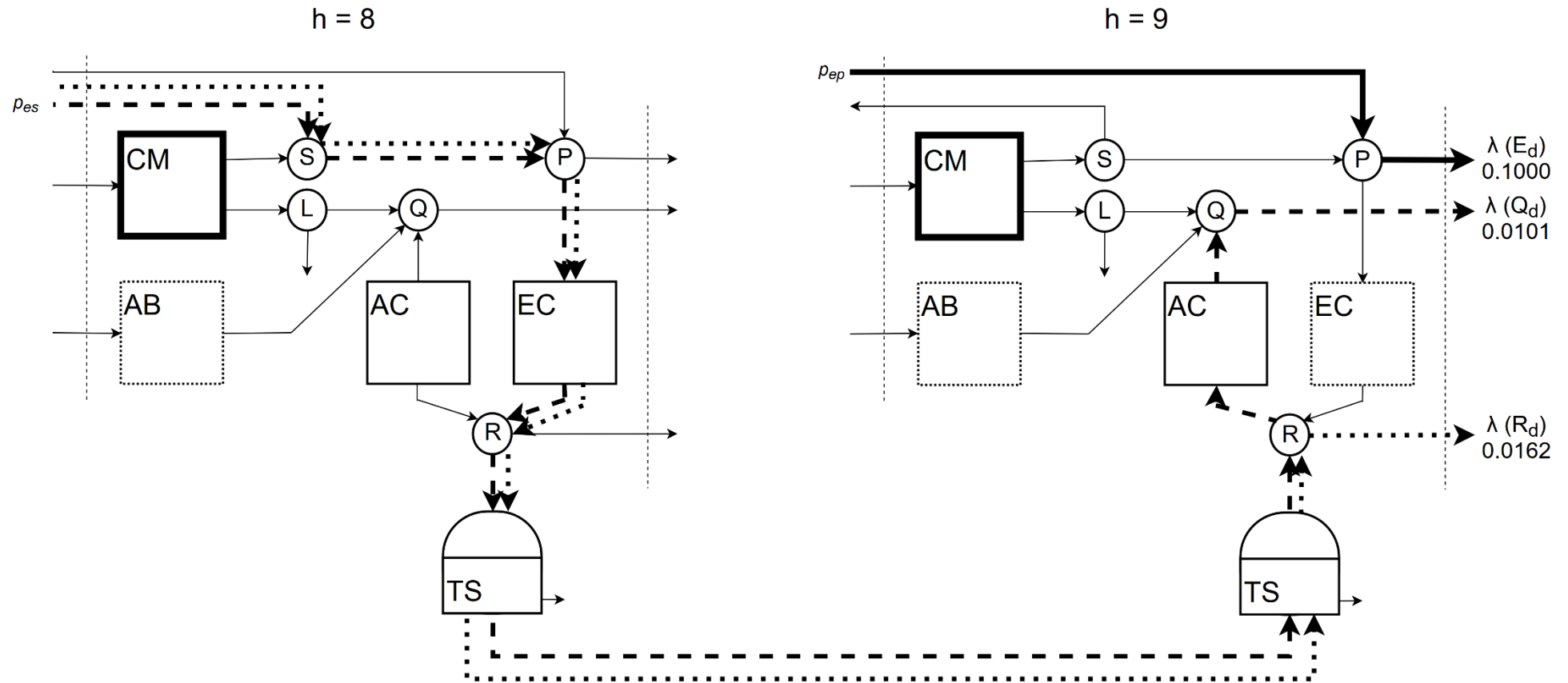
Figure 3.8: Marginal paths for hour 9, marginal costs in €/kWh.

Alternative (and more costly) production paths can be identified in Figure 3.8 for hour 9, similarly to those explained for hour 8 (Figure 3.7). It becomes clear that even though at hour 9 the devices AB, AC, and EC are able to supply the marginal heating and cooling, production must be advanced to hour 8 in order to achieve lower costs.

3.2.1.3   Hour 15: Of why energy service production should be delayed

As shows Figure 3.9, the "marginal paths" of electricity, heat, and cooling supplied at hour 15 are linked to the system's operation at hour 17 through the TS.

At hour 15, the CM operates at full load, both the AC and EC operate at partial load, and the TS is discharging (discharging takes place from hour 14 to 19). Moreover, there is neither purchase nor sale of electricity. The marginal cost of the electricity λE_d = 0.0980 €/kWh can be interpreted as follows: If an additional unit of electricity is required at hour 15, the system will reduce EC consumption by 1 kWh and compensate lack of $1 \cdot COP_e$ = 5 kWh of cooling by increasing the discharge from the TS in the same amount. Consequently, there will be less cooling stored in the following hours, which will ultimately affect the system's operation at the end of the discharging period (i.e. hour 19). Therefore, that is the most appropriate time for the compensation to take place. Nevertheless, at hour 19 the EC operates at full load and, thus, its production cannot be increased. The same is true for hour 18. Finally, the production in the EC must take place at hour 17 with electricity purchased from the grid. It is interesting to notice that, because now storage time has reduced from five hours (originally between hours 14 and 19) to two (between hour 17 to 19), the production will be smaller than the corresponding consumption. The exact figure can be determined through Eq. (3.22), whose application in this particular case of the delayed production gives how much energy must be produced at hour k, $R_{in}(k)$, in order to compensate for a discharge at a previous hour h, $R_{out}(h)$.

It follows that to compensate for the discharge $R_{out}(15)$ = 5 kWh at hour 15, $R_{in}(17)$ = 4.9050 kWh must be produced at hour 17; the corresponding electricity consumption in the EC 4.9050/COP_e = 0.9810 kWh valued at purchasing price gives the marginal cost of the electricity supplied at hour 15 (λE_d = 0.9810·p_{ep} = 0.0980 €/kWh).

Thus, the correct interpretation of the arrows in Figure 3.9 is that production is being delayed by increasing the discharge of energy that is already stored, and not that energy is being stored from hour 17 to hour 15.
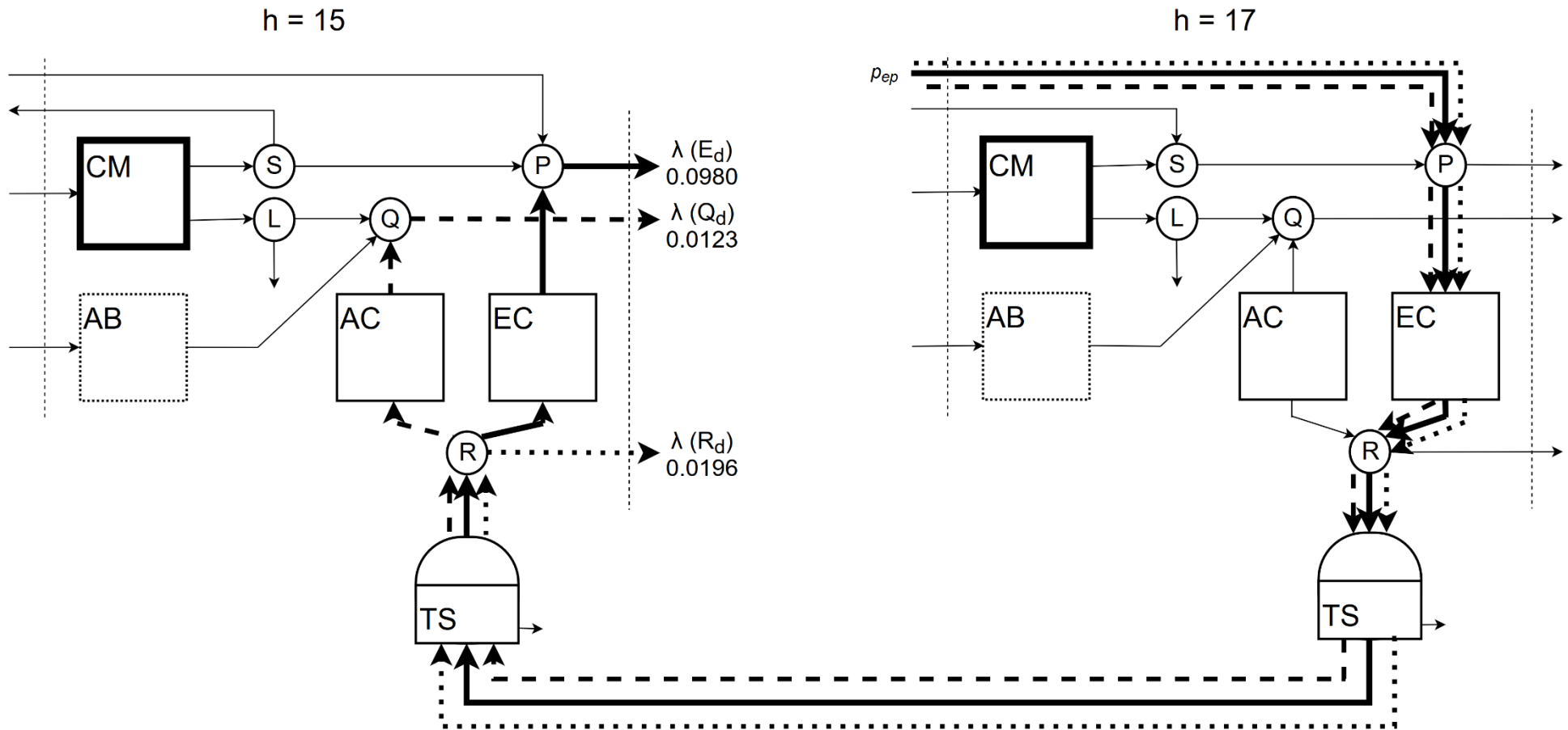
Figure 3.9: Marginal paths for hour 15, marginal costs in €/kWh.

The marginal cost of the heat λQ_d = 0.0123 €/kWh and cooling λR_d = 0.0196 €/kWh can be understood following the same logic. By consuming an additional unit of heat at hour 15, $1 \cdot COP_q$ = 0.625 kWh less of cooling is produced, which must be compensated by increasing the discharge from the TS. At hour 17, 0.6125 kWh of cooling must be produced in the EC with 0.1225 kWh of purchased electricity (λQ_d = 0.1225·p_{ep} = 0.0123 €/kWh). Similarly, the additional consumption of 1 kWh of cooling at hour 15 increases consumption of purchased electricity in the EC at hour 17 by 0.1960 kWh (λR_d = 0.1960·p_{ep} = 0.0196 €/kWh).

3.2.2 Cyclical view of the operation with TS

Both hours 9 and 15 use the TS to shift marginal production in time. However, while the shift that takes place from hour 9 to 8 advances production, the one from hour 15 to 17 delays it. There lies a fundamental difference. By advancing production, the storage time increases and so do the energy losses. Therefore, the production that takes place at hour 8 is higher than the corresponding supply at hour 9 (production at hour 8 = marginal supply at hour 9 + energy losses). This situation can only be profitable if: (i) the energy resource is cheaper enough at a previous hour than at the hour of supply as to compensate for energy losses (e.g. hour 8 p_{es} versus hour 9 p_{ep}); or (ii) it is more profitable to sustain a higher operation cost due to energy losses than to increase installed capacity. On the other hand, by delaying production, the storage time decreases and so do the energy losses. Therefore, production at hour 17 will be smaller than the corresponding supply at hour 15 (production at hour 17 = marginal supply at hour 15 – energy losses).

With these key hours explained, a more general approach to the marginal costs of the 24-hour operation of the system can be taken. Figure 3.10, Figure 3.11, and Figure 3.12 present the marginal costs from Table 3.4 of the electricity, heat, and cooling, respectively, and highlight the interconnection between the hourly periods through the TS. The enclosed numbers represent the operation hours, while the numbers on the outside express the corresponding marginal costs in €/kWh.

In each figure, different shades of gray are used to represent different origins of the marginal final products of the trigeneration system. In the case of the electricity (Figure 3.10), the periods in white are those in which the marginal electric demand is covered by internal production at the same hour, that is, there is no shift in production. Therefore, following the same logic as explained for hour 8, the marginal cost of electricity in such periods can be interpreted at the selling price p_{es} = 0.080 €/kWh. In black periods, the marginal cost of the electricity can be interpreted as the purchasing price p_{ep} = 0.100 €/kWh because the marginal electricity comes from the electric grid, as explained for hour 9. Lastly, light gray periods are those in which it is possible to delay

production to hour 17, as explained for hour 15. It can be seen that the marginal costs of the electricity increase from hours 14 to 17, as the time difference between the supply and the corresponding production shortens.
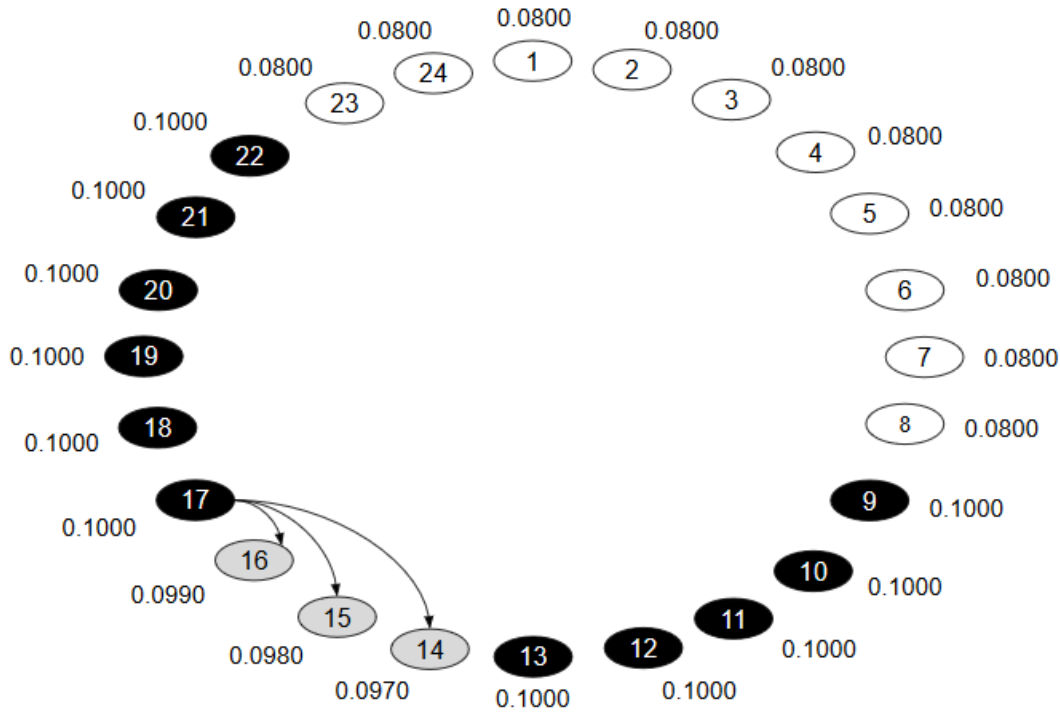
Figure 3.10: Hourly marginal costs of the electricity, in €/kWh.

Regarding the heat production (Figure 3.11), the same concepts as described for the white and light gray periods in Figure 3.10 apply. In the case of white periods, the marginal cost varies according to the different resources consumed: (i) at hour 8, the marginal cost of the heat is related to the production of cooling in the EC with electricity at selling price p_{es} = 0.080 €/kWh; (ii) hours 17 and 22 follow the same logic as hour 8 but with electricity purchased from the electric grid at p_{ep} = 0.100 €/kWh; and (iii) for the rest of the white periods, the marginal heat is produced by the AB at p_{fa}/η_q = 0.025 €/kWh. The marginal cost of the heat in periods that delay production (light gray periods) or advance it (dark gray periods) are related to the price of the resource consumed in the period in which the production takes place. For example, hours 1 to 7, 23, and 24 delay production to hour 8, in which electricity is sold at p_{es} = 0.080 €/kWh, so their marginal costs will be lower than $\lambda Q_d(8)$ = 0.0100 €/kWh. Likewise, hours 15 and 16 advance consumption from hour 17, when the system purchases electricity p_{ep} = 0.100 €/kWh, so their marginal costs will be lower than $\lambda Q_d(17)$ = 0.0125 €/kWh. The same considerations are valid for the marginal costs of the cooling (Figure 3.12).
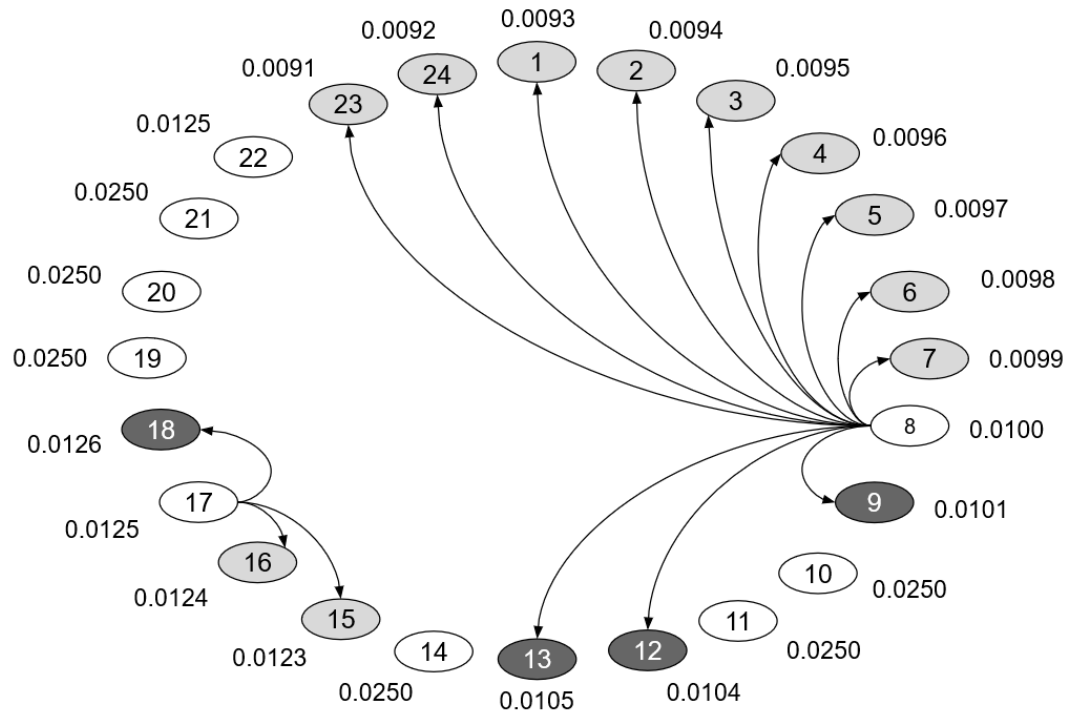
Figure 3.11: Hourly marginal costs of the heat, in €/kWh.
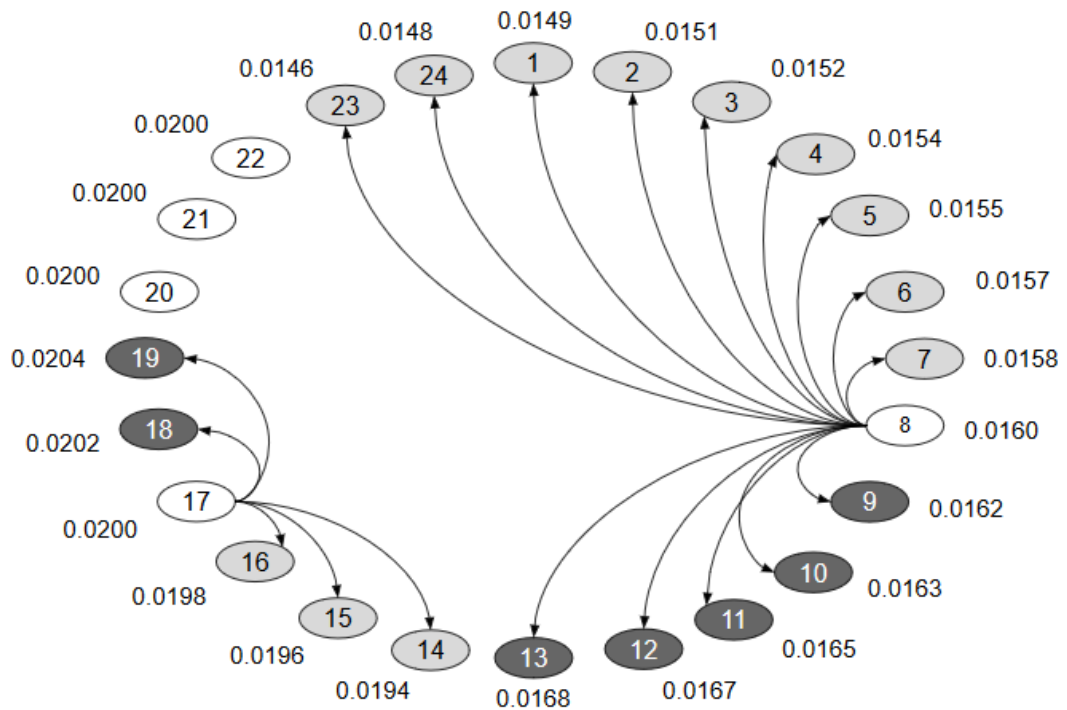
Figure 3.12: Hourly marginal costs of the cooling, in €/kWh.

It becomes clear that even though only a TES unit for cooling is included, the thermal integration in the trigeneration system allows to extend the benefits of the storage to the other utilities, e.g. electricity and heat.

3.2.3   Internal constraints

The marginal costs of the internal flows can be obtained by interpreting the dual prices corresponding to Eqs. (3.3)-(3.21) of the optimization model. The following paragraphs provide examples of interpretation of the dual prices obtained.

3.2.3.1   Capacity limits

Capacity limits impose an upper limit to the device's production. Increasing the right-hand side of the constraint (or the constant term) allows the device to increase its maximum production. Therefore, the associated dual price can be interpreted as the marginal cost of producing an additional unit of product. Table 3.5 presents the dual prices of the installed capacity constraints.

Table 3.5: Dual prices of installed capacity constraints, in €/kWh.

Hour	CM_Wmax	AB_Qmax	AC_Rqmax	EC_Remax	Srf_Vol
1	-0.0192	-	-	-	-
2	-0.0193	-	-	-	-
3	-0.0194	-	-	-	-
4	-0.0195	-	-	-	-
5	-0.0197	-	-	-	-
6	-0.0198	-	-	-	-
7	-0.0199	-	-	-	-
8	-0.0200	-	-	-	-
9	-0.0401	-	-	-	-
10	-0.0571	-	-	-	-
11	-0.0571	-	-	-	-
12	-0.0405	-	-	-	-
13	-0.0406	-	-	-	-
14	-0.0542	-	-	-	-0.0024
15	-0.0406	-	-	-	-
16	-0.0417	-	-	-	-
17	-0.0429	-	-	-	-
18	-0.0430	-	-	-0.0002	-
19	-0.0571	-	-	-0.0004	-
20	-0.0571	-	-	-	-
21	-0.0571	-	-	-	-
22	-0.0429	-	-	-	-
23	-0.0190	-	-	-	-
24	-0.0191	-	-	-	-

Of course, only active restrictions present non-zero dual prices (i.e. only when the corresponding device operates at full load, otherwise it would make no difference to increase the installed capacity). In fact, dual prices of constraints AB_Qmax (Eq. (3.4)) and AC_Rqmax (Eq. (3.5)) are

always zero because neither device reaches its maximum capacity. Moreover, it should be noted that the analysis carried out in this paper only considers operation costs and not capital costs.

Constraint CM_Wmax (Eq. (3.3)) limits the production of electricity W_c in the CM to a maximum W_{max}. Increasing W_{max} by one unit leads to:

- An increase in the production of electricity of 1 kWh.

- An increase in the consumption of natural gas of $1/\alpha_w$ = 2.8570 kWh.

- An increase in the production of cogenerated heat of α_q/α_w = 1.1428 kWh.

While the additional consumption of natural gas increases the total operation cost, producing more electricity and cogenerated heat creates savings that can be valued at the marginal costs of electricity and heat, respectively. For each hourly period, the marginal cost associated with the restrictions CM_Wmax can be interpreted as the economic impact that the three effects have on the objective function:

$$\lambda CM\_Wmax(h) = 2.8570 \cdot p_{fc} - 1 \cdot \lambda E_d(h) - 1.1428 \cdot \lambda Q_d(h) \tag{3.23}$$

For example, at hour 8 the cost associated with the increase in the consumption of natural gas is $2.8570 \cdot p_{fc}$ = 0.0714 €/kWh, the increase in electricity and cogenerated heat productions allow for savings of $1 \cdot \lambda E_d(8)$ = 0.0800 €/kWh and $1.1428 \cdot \lambda Q_d(8)$ = 0.0114 €/kWh, respectively. This results in a decrease of 0.0200 €/kWh in the total operation cost. The negative sign in $\lambda CM\_Wmax(8)$ = -0.0200 €/kWh shows that an increase in the capacity limit W_{max} would lead to an improvement in the objective function (i.e. reduction of the total operation cost).

The EC operates at full load at hours 18 and 19. At these hours, the dual prices associated with the constraint EC_Remax (Eq. (3.6)) are -0.0002 €/kWh and -0.0004 €/kWh, respectively. The interpretation is that, because hours 18 and 19 advance production to hour 17, increasing cooling production in the EC by 1 kWh at such hours would decrease the production at hour 17. For example, at hour 18 the additional cooling would be produced with 0.2000 kWh of purchased electricity, thus reducing the purchase of electricity at hour 17 by 0.2020 kWh, at p_{ep} = 0.1000 €/kWh. Therefore:

$$\lambda EC\_Remax(18) = 0.200 \cdot p_{ep} - 0.202 \cdot p_{ep} = -0.0002 \ €/kWh \tag{3.24}$$

As can be seen, this change results in a reduction of 0.0002 €/kWh in the total operation cost, which is equal to the marginal cost associated with restriction EC_REmax at hour 18.

The constraint Srf_Vol (Eq. (3.7)) only has a non-zero dual price at hour 14, when the TS is fully charged. At that hour, it would be profitable to be able to store an additional unit of energy, which would allow to increase cooling production and storage at hour 8 (with electricity at p_{es} = 0.080 €/kWh) and reduce cooling production at hour 17 (with purchased electricity at p_{ep} = 0.100 €/kWh).

3.2.3.2   Production constraints

Production constraints are associated with the production efficiency in each device. By increasing the right-hand side of the constraint, either the device consumption increases in order to keep the production unchanged or the production decreases in order to maintain consumption. Unlike capacity constraints, the marginal cost associated with production constraints have a negative impact on the objective function (i.e. increase the total operation cost). Table 3.6 presents the dual prices associated with the production constraints.

Table 3.6: Dual prices of production constraints, in €/kWh.

Hour	CM_W	CM_Q	AB_Q	AC_R	EC_R
1	0.0608	0.0093	0.0250	0.0149	-
2	0.0607	0.0094	0.0250	0.0151	-
3	0.0606	0.0095	0.0250	0.0152	-
4	0.0605	0.0096	0.0250	0.0154	-
5	0.0603	0.0097	0.0250	0.0155	-
6	0.0602	0.0098	0.0250	0.0157	-
7	0.0601	0.0099	0.0250	0.0158	-
8	0.0600	0.0100	0.0250	0.0160	0.0160
9	0.0599	0.0101	0.0250	0.0162	-
10	0.0429	0.0250	0.0250	-	-
11	0.0429	0.0250	0.0250	-	-
12	0.0595	0.0104	0.0250	0.0167	-
13	0.0594	0.0105	0.0250	0.0168	-
14	0.0429	0.0250	0.0250	-	0.0194
15	0.0574	0.0123	0.0250	0.0196	0.0196
16	0.0573	0.0124	0.0250	0.0198	0.0198
17	0.0571	0.0125	0.0250	0.0200	0.0200
18	0.0570	0.0126	0.0250	0.0202	0.0200
19	0.0429	0.0250	0.0250	-	0.0200
20	0.0429	0.0250	0.0250	-	0.0200
21	0.0429	0.0250	0.0250	-	0.0200
22	0.0571	0.0125	0.0250	0.0200	0.0200
23	0.0610	0.0091	0.0250	0.0146	-
24	0.0609	0.0092	0.0250	0.0148	-

The constraint CM_W (Eq. (3.8)) is associated with the efficiency of electricity production in the CM. By increasing the right-hand side of Eq. Eq. (3.8) by one unit, either W_c is kept unchanged and F_c is increased or W_c is decreased and F_c is kept constant. It can be demonstrated that the former alternative is more profitable because: (i) the electricity from the CM is cheaper than the purchase and selling prices of electricity (if the cost of fuel consumption were allocated entirely to the electricity production, its unit cost would be 0.0714 €/kWh, which is lower than both p_{es} and p_{ep}), so reducing its production would incur in a greater cost; and (ii) by increasing the fuel consumption by $1/\alpha_w$ = 2.8570 kWh, the production of cogenerated heat increases accordingly α_q/α_w = 1.1428 kWh, displacing production in another device.

For each hourly period, the marginal cost of constraint CM_W can be interpreted as the economic impacts of the consumed fuel 2.8570 kWh, valued at p_{fc} = 0.025 €/kWh, and the produced heat 1.1428 kWh, valued at the corresponding marginal cost $\lambda Q_d(h)$. For example, at hour 8:

$$\lambda CM\_W(8) = 2.8570 \cdot p_{fc} - 1.1428 \cdot \lambda Q_d(8) = 0.0600 \text{ €}/kWh \tag{3.25}$$

Constraint CM_Q (Eq. (3.9)) is associated with the production efficiency of cogenerated heat in the CM. By increasing the right-hand side of Eq. (3.9) by one unit, the cogenerated heat Q_c would decrease by the same amount. This happens because the consumption of natural gas is defined by the electric production W_c, which, as previously explained, remains constant. The lack of cogenerated heat must be compensated by production elsewhere at the corresponding marginal cost $\lambda Q_d(h)$.

Whenever the AB operates, the dual price associated with restriction AB_Q (Eq. (3.10)) will be that of producing 1 kWh of heat Q_a, that is $(1/\eta_q) \cdot p_{fa}$ = 0.0250 €/kWh. The interpretation is that by increasing the right-hand side of Eq. (3.10) by one unit, the AB increases fuel-oil consumption accordingly.

Regarding constraints AC_R (Eq. (3.11)) and EC_R (Eq. (3.12)), it can be seen in Table 3.6 Table 3.4 that dual prices are only provided when the device operates, as it makes no sense to evaluate the effect of production efficiency in a non-operative device.

Increasing the right-hand side of restriction AC_R by one unit leads to a reduction in the cooling production R_q, which would have to be compensated by production elsewhere at the corresponding marginal cost $\lambda R_d(h)$. This situation takes place because, as explained earlier, it is more profitable to produce cooling in the EC than in the AC. However, by increasing the right-hand side of restriction EC_R by one unit, the production R_e is kept constant, while the consumption of electricity is increased by $1/COP_e$ = 0.200 kWh. The marginal cost associated with restriction EC_R

can be interpreted as the economic impact of the increase in electricity consumption valued at the marginal cost of the electricity ($\lambda EC\_R(h) = 0.200 \cdot \lambda E_d(h)$).

The energy losses in the TS for each hourly period is expressed by Eq. (3.13). The corresponding dual price can be interpreted as the marginal cost of wasting energy in the TS, which will bring the same marginal cost as that of the cooling $\lambda R_d(h)$

3.2.3.3 Balance constraints

The dual prices associated with balance constraints can be interpreted as the marginal cost of the corresponding internal product or energy service. Therefore, the dual prices of junctions S (Eq. (3.16)) and P (Eq. (3.17)) correspond to the marginal cost of electricity $\lambda E_d(h)$, the dual prices of junctions L (Eq. (3.18)) and Q (Eq. (3.19)) correspond to the marginal cost of heat $\lambda Q_d(h)$, and the dual price of junction R (Eq. (3.20)), corresponds to the marginal cost of cooling $\lambda R_d(h)$. Further, the dual prices associated with the energy balance in the TES (Eq. (3.21)) can be interpreted as the marginal cost of cooling $\lambda R_d(h)$.

3.3 THERMOECONOMIC COST ALLOCATION

Cost accounting tackles the problem of allocating the costs of the resources consumed to the internal flows and final products of the system. The difficulty of cost allocation increases when different products are obtained from common resources, as it is the case with polygeneration systems. The way in which allocation is made is important because it will directly affect the results obtained.

As explained in Section 3.2, marginal costs give valuable insight into the operation of the system, explaining how and why the system operates given a change in external conditions (e.g. increase in the consumer center's energy demand). On the downside, marginal costs are generally not sufficient to explain the actual production of the system (Hui, 2000; Lozano et al., 2009b; Pina et al., 2017), apart from not being conservative (Lozano et al., 2009a).

Unit costs, however, provide valuable information to explain the way the system is operating. Based on the cost conservation principle, the total cost of the resources exchanged with the economic environment must be equal to the total cost of the products obtained. Considering the daily operation cost DC from Eq. (3.1), the following expression holds true:

$$DC = \sum_h \sum_i c_i(h) \cdot R_i(h) = \sum_h \sum_j c_j(h) \cdot P_j(h) \tag{3.26}$$

in which $c_i(h)$ and $R_i(h)$ are, respectively, the unit cost and the energy flow of the resource i exchanged with the economic environment at the hourly period h; and $c_j(h)$ and $P_j(h)$ are, respectively, the unit cost and the energy flow of the product obtained j at the hourly period h.

In the case of the simple trigeneration system analyzed herein, the energy resources are natural gas, fuel-oil, and electricity purchased from the electric grid, and the energy products are the electricity sold to the grid and the energy demands of the consumer center (i.e. electricity, heating, and cooling). Provided that all energy flows R_i and P_j in each hourly period h are known, as well as the unit costs of the resources c_i, the aim is to objectively determine the unit costs of the products c_j. In this regard, it is essential to connect the product flow that is being valued to the different resources consumed, so that each product flow receives its corresponding share of costs.

The productive structure is the tool that is generally used in thermoeconomics to unveil the distribution of resources to the internal flows and final products of an energy system. Identifying the appropriate productive structure is crucial when performing a thermoeconomic analysis (Lozano et al., 2011, 2014; Lozano and Valero, 1993). Once the productive structure has been defined, the application of cost conservation balance to its elements allows for the determination of the unit costs of product flows, unveiling the cost formation process.

The definition of the productive structure and the issues faced in the process are described in Section 3.3.1. The cost allocation proposals for the simple trigeneration system are presented in Section 3.3.2. Then, the results obtained are discussed in Sections 3.3.3 and 3.3.4.

3.3.1   Definition of the productive structure

Figure 3.1 shows the physical structure of the simple trigeneration system including TES analyzed herein. The physical structure depicts the devices that constitute the system and the energy flows that connect the devices with each other and the system with its boundaries (economic environment and the consumer center). The productive structure, on the other hand, consists of defining the main product (or the productive purpose) of each device with aim of allocating the resources consumed throughout the plant. Thus, the productive structure is not necessarily equal to the physical structure and several possible productive structures can be proposed depending on the objective of the analysis. Clearly, different costs of the final products are obtained for different productive structures. This underlines the importance of appropriately defining the productive structure of the energy conversion system, so that the results obtained are in accordance with the objective of the analysis.

The internal flows and final products of the productive structure must be expressed in terms of an extensive magnitude, e.g. mass, volume, energy or exergy content, number of moles. In this work, the productive structure is composed of energy flows and, thus, the associated unit costs are expressed in terms of energy. The reason for expressing the unit costs in terms of energy is that this is the most typical billing mechanism perceived by the final consumers (final consumers pay for their energy resources per unit of energy consumed), which are the ones that will ultimately make the decision on whether to consume energy services from the trigeneration system.

The joint production of energy services that takes place in polygeneration systems is achieved through appropriate energy integration of the production processes (Mancarella, 2014; Serra et al., 2009). Such a high level of integration hinders the determination of a logical distribution of the resources consumed towards the cogenerated products. The true purpose of this analysis is to achieve a fair cost-and-benefit apportionment of the joint production costs to the energy services produced. This requires: (i) the definition of a productive structure with the highest possible disaggregation level, so as to connect the resources consumed to the final products obtained through the various existing productive trajectories (Lozano and Valero, 1993); and (ii) the definition of fair allocation criteria, so as not to favor or prioritize any resource/product (Amundsen et al., 2011; Gochenour, 2003; Horngren, 2009).

Thus, it becomes clear that to connect the resources consumed by the simple trigeneration system to its internal flows and final products one must tackle the issues of: (i) the joint production of electricity and heat that takes place in the cogeneration module; (ii) the disaggregation of energy flows and devices; and (iii) the interconnection between charging and discharging periods due to the incorporation of a TES unit. These aspects are analyzed in detail in the following sections.

3.3.1.1   Joint production in the cogeneration module

As described by Lozano et al. (2011, 2014), the fundamental device of a cogeneration system is the cogeneration module CM, in which the joint production of electricity (and/or mechanical energy) and heat takes place. By incorporating a TAT, such as an absorption chiller AC, the cogenerated heat can be extended to cooling production. The combination CM+AC thus make the trigeneration subsystem.

For the work developed in this Thesis, it was proposed to expand the aforementioned trigeneration subsystem to include a mechanical chiller EC, so that cogenerated electricity can also be used to produce cooling. In this way, both CM products can contribute to cooling

production. The combination CM+AC+EC thus forms the trigeneration subsystem considered in the productive structure and depicted in Figure 3.13.
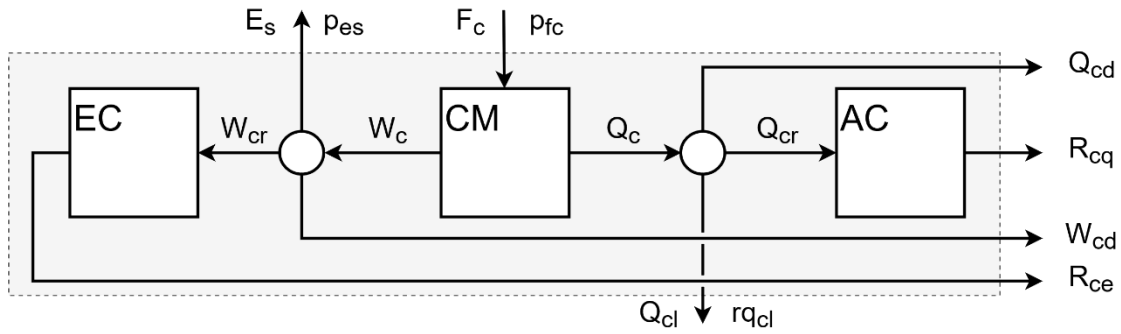
Figure 3.13: Trigeneration subsystem.

In the simple trigeneration system analyzed herein, the CM consumes natural gas F_c to produce cogenerated electricity W_c and cogenerated heat Q_c. The cogenerated electricity W_c can be: (i) sold to the electric grid E_s; (ii) used in the EC to produce cooling R_{ce}; and (iii) used to cover the electricity demand W_{cd}. In the case of the cogenerated heat Q_c, there are three possible destinations: (i) attend the heat demand Q_{cd}; (ii) produce cooling R_{cq} in the AC; and (iii) be dissipated to the environment Q_{cl}. As mentioned earlier, the purchase price of natural gas p_{fc} and the price of the electricity sold to the grid p_{es} are defined by the market (see Table 3.2); also, heat dissipation can occur with no associated cost (rq_{cl} = 0 €/kWh). Therefore, the four cogenerated products to which costs should be allocated are W_{cd}, Q_{cd}, R_{ce}, and R_{cq}.

3.3.1.2 Aggregation level

When it comes to precisely allocating resources to internal flows and final products, defining the productive structure requires the highest possible disaggregation level of physical flows and devices. This is done so that the productive structure reflects the various productive trajectories which, in an integrated energy system, connect the resources consumed to the final products obtained. Avoiding the disaggregation by combining devices and/or processes only hides the problem and, thus, is not recommended.

Supporting the production of the trigeneration subsystem are the auxiliary boiler and the electric grid. So, when the cogeneration module CM and the auxiliary boiler AB are both in operation, there are two heat sources available to drive the absorption chiller AC and to attend the heat demand Q_d. Analogously, when the CM is operating and the system is purchasing electricity from the grid E_p, there are two electricity sources available to drive the mechanical chiller EC and to attend the electricity demand E_d. Therefore, in accordance with Lozano et al. (Lozano et al., 2011, 2014), the

AC and the EC can each be divided into two virtual devices; in this way, each virtual device will consume energy from its specific source.

The productive structure obtained is depicted in Figure 3.14, which includes the trigeneration subsystem defined in Section 3.3.1.1 (enclosed in the gray box), the conceptual division of the absorption chiller AC and mechanical chiller EC, and the corresponding virtual flows. Additionally, the productive structure is composed of three fundamental components: (i) productive units (white rectangles), associated with an energy transformation process, in which the input flows are consumed to produce a specific product; (ii) junctions (rhombs), where two or more flows merge into one output flow; and (iii) distributors (circles), where a homogeneous flow is divided into two or more output flows.

An important limitation imposed to the definition of the productive structure is that it must be possible to evaluate all flows of the productive structure unequivocally in relation to the state of the plant, as defined by the physical structure (Lozano and Valero, 1993). The relations that define the virtual flows in the productive structure are explained in the following paragraphs.

The absorption chiller AC is divided into two virtual devices: ACc, which consumes cogenerated heat Q_{cr} and produces cogenerated absorption cooling R_{cq}, and ACa, which consumes conventional heat Q_{ar} and produces conventional absorption cooling R_{aq}. Both virtual heat flows compose the Q_r in Figure 3.1, so that

$$Q_r(h) = Q_{cr}(h) + Q_{ar}(h) \tag{3.27}$$

The mechanical chiller EC is divided into two virtual devices: ECc, which consumes cogenerated electricity W_{cr} and produces cogenerated mechanical cooling R_{ce}, and ECp, which consumes purchased electricity E_{pr} and produces auxiliary cooling R_{pe}. Both virtual electricity flows compose the E_r in Figure 3.1, so that

$$E_r(h) = W_{cr}(h) + E_{pr}(h) \tag{3.28}$$

Despite the inclusion of additional virtual flows and/or devices in the productive structure, in each hourly period the same amount of energy resources (natural gas, fuel-oil, and electricity) is consumed to attend the energy services (electricity, heating, and cooling demands) as in the physical structure's optimal operation described in Section 3.1.3. With these aspects "fixed", there are various ways in which the disaggregation of internal flows can take place while satisfying the operation state of the plant. Therefore, the energy flows distribution in distributors Q2, Q3, E2 and E3 are inevitably arbitrary.
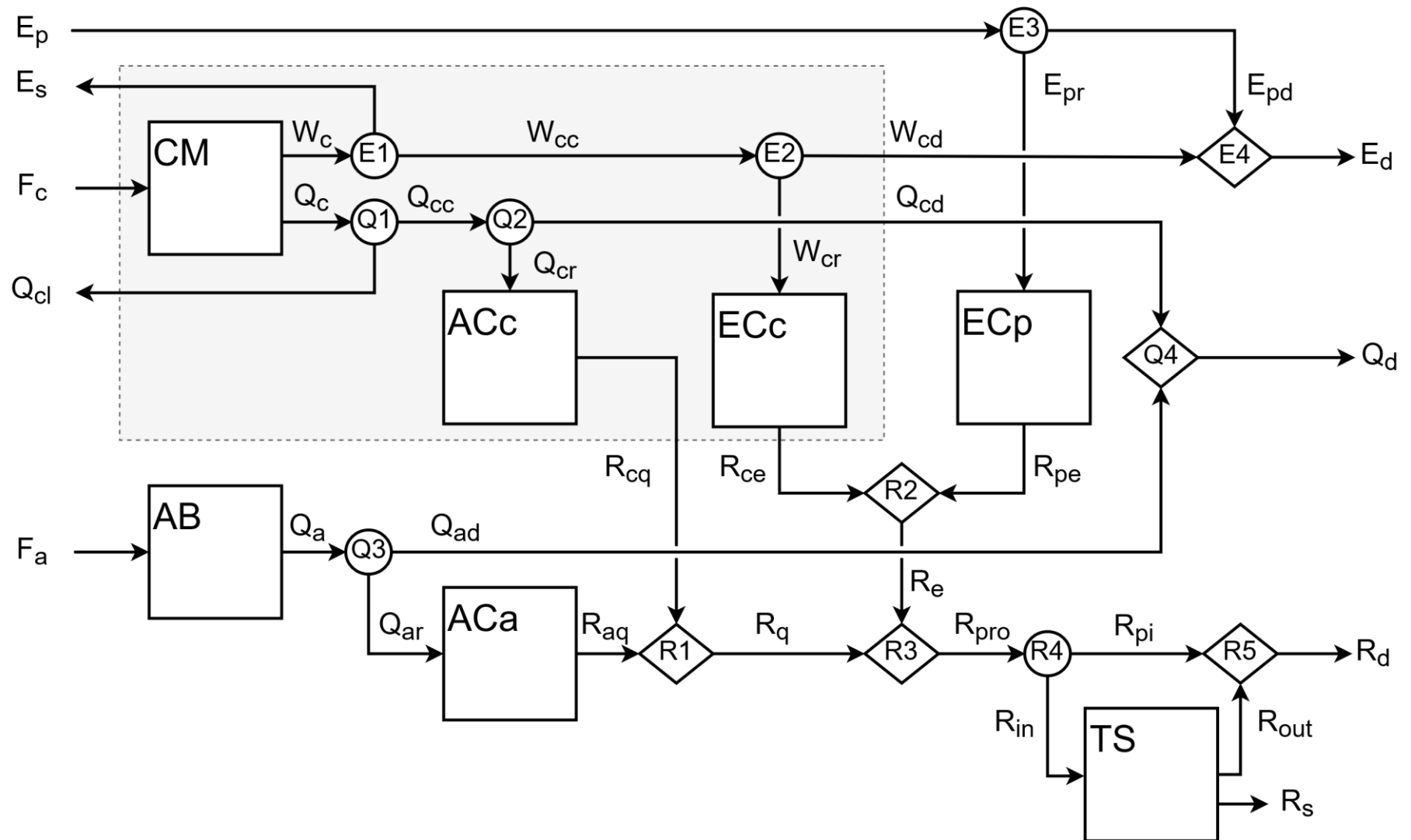
Figure 3.14: Productive structure of the simple trigeneration system.

In accordance with the core objective of this study, which is to promote a fair cost-and-benefit apportionment of costs in the trigeneration system, it is proposed to distribute the cogenerated heat Q_{cc}, the conventional heat Q_a, the cogenerated electricity W_{cc} and the purchased electricity E_p in distributors Q2, Q3, E2 and E3 (see Figure 3.14), respectively, in a way that: (i) no energy resource is prioritized in the production of energy services; and (ii) no energy service is prioritized in the use of energy resources. As a result, no energy service gets favored with a lower cost due to an also arbitrary decision to prioritize its production with the consumption of a cheaper energy resource.

Two parameters are defined for the distribution of heat and electricity, respectively: (i) δ_1 expresses the share of heat that covers the heat demand in proportion to the total heat demanded (Eq. (3.29)); and (ii) δ_2 expresses the share of electricity that attends the electricity demand in proportion to the total electricity demanded (Eq. (3.30)).

$$\delta_1(h) = Q_d(h)/(Q_d(h) + Q_r(h)) \tag{3.29}$$
$$\delta_2(h) = E_d(h)/(E_d(h) + E_r(h)) \tag{3.30}$$

The available cogenerated heat Q_{cc} and the conventional heat Q_a are distributed between the consumer center and the AC as follows:

$$Q_{cd}(h) = \delta_1(h) \cdot Q_{cc}(h) \tag{3.31}$$
$$Q_{cr}(h) = \left(1 - \delta_1(h)\right) \cdot Q_{cc}(h) \tag{3.32}$$
$$Q_{ad}(h) = \delta_1(h) \cdot Q_a(h) \tag{3.33}$$
$$Q_{ar}(h) = \left(1 - \delta_1(h)\right) \cdot Q_a(h) \tag{3.34}$$

The cogenerated electricity W_{cc} and the purchased electricity E_p are distributed between the consumer center and the EC as follows:

$$W_{cd}(h) = \delta_2(h) \cdot W_{cc}(h) \tag{3.35}$$
$$W_{cr}(h) = \left(1 - \delta_2(h)\right) \cdot W_{cc}(h) \tag{3.36}$$
$$E_{pd}(h) = \delta_2(h) \cdot E_p(h) \tag{3.37}$$
$$E_{pr}(h) = \left(1 - \delta_2(h)\right) \cdot E_p(h) \tag{3.38}$$

The cooling produced from cogenerated heat R_{cq} and the cooling produced from conventional heat R_{aq} are determined as follows:

$$R_{cq}(h) = COP_q \cdot Q_{cr}(h) \tag{3.39}$$
$$R_{aq}(h) = COP_q \cdot Q_{ar}(h) \tag{3.40}$$

The cooling produced from cogenerated electricity R_{ce} and the cooling produced from purchased electricity R_{pe} are

$$R_{ce}(h) = COP_e \cdot W_{cr}(h) \tag{3.41}$$
$$R_{pe}(h) = COP_e \cdot E_{pr}(h) \tag{3.42}$$

The cooling produced by the absorption chillers R_q and by the mechanical chillers R_e compose the total cooling produced in the hourly period R_{pro} (Eq. (3.43)). Part of R_{pro} can be charged to the TS R_{in}; the part that is not charged is the cooling produced and consumed in the hourly period R_{pi} (Eq. (3.44)). In this way, the charged cooling R_{in} in an hourly period has the same characteristics as the cooling produced at that time. In turn, the discharge R_{out} will depend on the charged cooling of previous hourly periods. This connection between charging and discharging periods is implicit in the productive structure defined herein and is explored in the following section.

$$R_{pro}(h) = R_q(h) + R_e(h) \tag{3.43}$$
$$R_{pi}(h) = R_{pro}(h) - R_{in}(h) \tag{3.44}$$

The virtual flows and the distribution parameters previously defined were calculated and their values are given in Table 3.7.

3.3.1.3 Interconnection between hourly periods through the TES unit

The hourly operation of an energy system can be described in terms of the operational state of the devices (full load, part load, off), production rates, resource consumption, etc. For a system that does not include energy storage, the hourly operation periods are always independent from each other. However, the incorporation of energy storage allows energy service production to be decoupled from consumption, so that the operation of the system in an hourly period may be affected by others; now, the hourly operation periods cannot be assessed individually, but as a whole.

This is particularly relevant for the cost allocation problem involving energy storage because connecting the resources consumed to the internal flows and final products requires analyzing the temporal connection between charging and discharging hourly periods. Therefore, the presence of the energy storage unit incorporates a new dimension to the cost allocation problem, as it becomes necessary to know not only the amount of energy that must be charged and discharged in each hourly period, but also the origin period of the discharged energy. By doing so, the resources consumed to produce the charged flow can be forwarded to the discharging periods and to the final products.

Table 3.7: Virtual flows of the productive structure and distribution parameters. Energy flows in kWh.

Hour	W_{cd}	W_{cr}	E_{pd}	E_{pr}	Q_{cd}	Q_{cr}	Q_{ad}	Q_{ar}	R_{ce}	R_{pe}	R_{cq}	R_{aq}	R_{pro}	R_{pi}	δ_1	δ_2
1	253.6	0.0	0.0	0.0	168.4	231.6	0.0	0.0	0.0	0.0	144.8	0.0	144.8	0.0	0.42	1.00
2	247.0	0.0	0.0	0.0	0.0	400.0	0.0	0.0	0.0	0.0	250.0	0.0	250.0	0.0	0.00	1.00
3	241.7	0.0	0.0	0.0	0.0	400.0	0.0	0.0	0.0	0.0	250.0	0.0	250.0	0.0	0.00	1.00
4	237.7	0.0	0.0	0.0	0.0	400.0	0.0	0.0	0.0	0.0	250.0	0.0	250.0	0.0	0.00	1.00
5	253.6	0.0	0.0	0.0	0.0	400.0	0.0	0.0	0.0	0.0	250.0	0.0	250.0	0.0	0.00	1.00
6	262.9	0.0	0.0	0.0	0.0	400.0	0.0	0.0	0.0	0.0	250.0	0.0	250.0	0.0	0.00	1.00
7	286.8	0.0	0.0	0.0	168.4	231.6	0.0	0.0	0.0	0.0	144.8	0.0	144.8	0.0	0.42	1.00
8	324.0	19.9	0.0	0.0	244.0	156.0	0.0	0.0	99.4	0.0	97.5	0.0	196.9	0.0	0.61	0.94
9	350.0	0.0	27.1	0.0	378.0	22.0	0.0	0.0	0.0	0.0	13.7	0.0	13.7	0.0	0.95	1.00
10	350.0	0.0	118.7	0.0	400.0	0.0	170.5	0.0	0.0	0.0	0.0	0.0	0.0	0.0	1.00	1.00
11	350.0	0.0	144.0	0.0	400.0	0.0	46.8	0.0	0.0	0.0	0.0	0.0	0.0	0.0	1.00	1.00
12	350.0	0.0	104.1	0.0	309.3	90.7	0.0	0.0	0.0	0.0	56.7	0.0	56.7	0.0	0.77	1.00
13	350.0	0.0	19.1	0.0	202.8	197.2	0.0	0.0	0.0	0.0	123.3	0.0	123.3	0.0	0.51	1.00
14	325.3	24.7	0.0	0.0	400.0	0.0	5.5	0.0	123.4	0.0	0.0	0.0	123.4	123.4	1.00	0.93
15	313.4	36.6	0.0	0.0	319.6	80.4	0.0	0.0	183.2	0.0	50.2	0.0	233.4	233.4	0.80	0.90
16	338.6	11.4	0.0	0.0	299.0	101.0	0.0	0.0	57.0	0.0	63.1	0.0	120.1	120.1	0.75	0.97
17	313.6	36.4	100.7	11.7	240.6	159.4	0.0	0.0	182.2	58.5	99.7	0.0	340.4	340.4	0.60	0.90
18	316.3	33.7	152.5	16.3	299.0	101.0	0.0	0.0	168.7	81.3	63.1	0.0	313.1	313.1	0.75	0.90
19	315.2	34.8	137.6	15.2	400.0	0.0	5.5	0.0	174.0	76.0	0.0	0.0	250.0	250.0	1.00	0.90
20	316.2	33.8	139.2	14.9	400.0	0.0	108.6	0.0	168.9	74.4	0.0	0.0	243.3	243.3	1.00	0.90
21	312.9	37.1	105.4	12.5	400.0	0.0	5.5	0.0	185.4	62.4	0.0	0.0	247.9	247.9	1.00	0.89
22	327.0	23.0	34.1	2.4	319.6	80.4	0.0	0.0	114.8	12.0	50.2	0.0	177.0	177.0	0.80	0.93
23	308.1	0.0	0.0	0.0	240.6	159.4	0.0	0.0	0.0	0.0	99.7	0.0	99.7	0.0	0.60	1.00
24	273.5	0.0	0.0	0.0	168.4	231.6	0.0	0.0	0.0	0.0	144.8	0.0	144.8	0.0	0.42	1.00
Day	7317.4	291.4	1082.6	72.9	5757.6	3842.4	342.4	0.0	1456.9	364.6	2401.5	0.0	4223.0	2048.5	0.61	0.96

In the case of the simple trigeneration system analyzed in this paper, the optimal operation model provides the amount of energy that must be charged R_{in} or discharged R_{out} in each hourly period. In order to lift the veil on how the stored energy is distributed between the hourly periods, a charging and discharging network was considered, as shown in Figure 3.15. The network is composed of nodes and pairs. Source nodes (circles) receive the charged energy R_{in} and distribute it to the sink nodes (rhombs), from which the discharged energy R_{out} leaves. Between the source and the sink nodes, there are intermediate nodes (squares) at the beginning of each hourly period from which energy losses r_s are deduced. The charged energy flows from source to sink nodes through pairs called *IN*, when they leave the source node, and called *OUT*, when they enter the sink node.

The charging and discharging network in Figure 3.15 can be represented in algebraic form as follows: The discharged energy $R_{out}(h)$ in period h is equal to the sum of all pairs *OUT(z,h)* that originate in previous periods z and arrive in period h (Eq. (3.45)). The charged energy $R_{in}(z)$ in period z may be divided into pairs *IN(z,h)* that originate in period z and are directed to discharging periods h (Eq. (3.46)). Energy losses $r_s(z,h,k)$ are evaluated along the path *(z,h)* at the beginning of each hourly period k according to Eq. (3.47), for $k > z$, or Eq. (3.48), for $k < z$. It holds true that for the path *(z,h)* the charged energy pair *IN(z,h)* is equal to the discharged pair *OUT(z,h)* plus the energy losses $r_s(z,h,k)$ along the path (Eq. (3.49)).

$$R_{out}(h) = \sum_{z \neq h} OUT(z,h) \tag{3.45}$$

$$R_{in}(z) = \sum_{h \neq z} IN(z,h) \tag{3.46}$$

$$r_s(z,h,k) = IN(z,h) \cdot \tau_{TS} \cdot (1 - \tau_{TS})^{(k-z-1)}, \text{ for } k > z \tag{3.47}$$

$$r_s(z,h,k) = IN(z,h) \cdot \tau_{TS} \cdot (1 - \tau_{TS})^{(k-z-1+NP)}, \text{ for } k < z \tag{3.48}$$

$$IN(z,h) = OUT(z,h) + \sum_{k \neq z} r_s(z,h,k) \tag{3.49}$$

These equations can be either included in the optimization model or solved separately. It must be noted that: (i) solving the equation set does not change the optimal operation of the system; and (ii) the feasible solution obtained is not unique, as numerous combinations of paths *(z,h)* may exist to fulfill the charging and discharging requirements. In order to guarantee a unique feasible solution, the first in first out (FIFO) method was imposed, which determines that the first unit of energy to be charged must be the first unit of energy to be discharged.
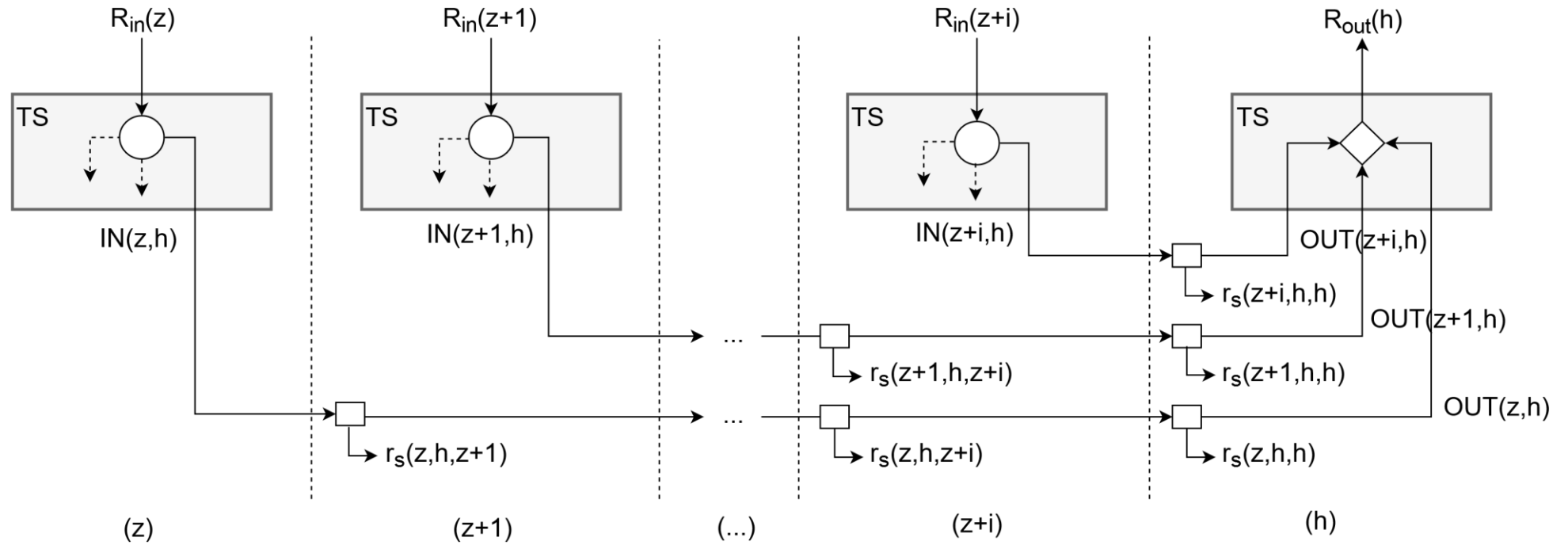
Figure 3.15: Charging and discharging network.

Solving the equation set with R_{in} and R_{out} from the optimal operation of the system as input data yields the energy flows that compose the charging and discharging network. In the case analyzed herein, the interconnection between hourly periods through the TES unit TS is presented in Figure 3.16. An example of interpretation of the results is provided as follows: The energy charged at hour 3 $R_{in}(3)$ = 250 kWh is directed to hours 14 (*IN(3,14)* = 40.56 kWh) and 15 (*IN(3,15)* = 209.44 kWh). The discharged energy at hour 15 $R_{out}(15)$ = 410.64 kWh proceeds from hours 3 (*OUT(3,15)* = 185.64 kWh), 4 (*OUT(4,15)* = 223.83 kWh), and 5 (*OUT(5,15)* = 1.16 kWh).

3.3.2 Cost allocation proposals in the simple trigeneration system

The cost conservation principle applied to the elements in the productive structure allows the cost formation process to be transparent throughout the system, from the resources consumed to the final products obtained. The unit energy costs of the internal flows and final products are thus obtained, representing the amount of resources that must be consumed to produce one unit of the flow. The unit cost name of the flows in the productive structure of Figure 3.14 is obtained by adding the letter *c* at the beginning of the energy flow name.

The first and foremost requirement to performing cost allocation is the knowledge of the operational state of the system, which means that all energy flows in each hourly period must be known. For the trigeneration system analyzed herein, the energy flows were provided in Table 3.3 and Table 3.7. The market-based prices of the electricity, natural gas, and fuel-oil have been defined in Table 3.2.

The cost conservation principle is applied to all junctions (rhombs), distributors (circles), and productive units (white rectangles) of the productive structure, allowing the following cost balance equations to be formulated:

Junctions

E4: $\quad cW_{cd}(h) \cdot W_{cd}(h) + cE_{pd}(h) \cdot E_{pd}(h) - cE_d(h) \cdot E_d(h) = 0$ $\hfill$ (3.50)

Q4: $\quad cQ_{cd}(h) \cdot Q_{cd}(h) + cQ_{ad}(h) \cdot Q_{ad}(h) - cQ_d(h) \cdot Q_d(h) = 0$ $\hfill$ (3.51)

R1: $\quad cR_{aq}(h) \cdot R_{aq}(h) + cR_{cq}(h) \cdot R_{cq}(h) - cR_q(h) \cdot R_q(h) = 0$ $\hfill$ (3.52)

R2: $\quad cR_{ce}(h) \cdot R_{ce}(h) + cR_{pe}(h) \cdot R_{pe}(h) - cR_e(h) \cdot R_e(h) = 0$ $\hfill$ (3.53)

R3: $\quad cR_q(h) \cdot R_q(h) + cR_e(h) \cdot R_e(h) - cR_{pro}(h) \cdot R_{pro}(h) = 0$ $\hfill$ (3.54)

R5: $\quad cR_{pi}(h) \cdot R_{pi}(h) + cR_{out}(h) \cdot R_{out}(h) - cR_d(h) \cdot R_d(h) = 0$ $\hfill$ (3.55)

Considering that the unit costs of the entering flows are known, the unit cost of the junction's product is directly obtained from the cost balance equation.

		1	2	3	4	5	6	7	8	9	10	11	12	13	14	15	16	17	18	19	20..22	23	24	1...
(1,14)	IN, OUT	144.76													127.03									
	rs		1.45	1.43	1.42	1.40	1.39	1.38	1.36	1.35	1.34	1.32	1.31	1.30	1.28									
(2,14)	IN, OUT		250.00												221.60									
	rs			2.50	2.47	2.45	2.43	2.40	2.38	2.35	2.33	2.31	2.28	2.26	2.24									
(3,14)	IN, OUT			40.56											36.32									
	rs				0.41	0.40	0.40	0.39	0.39	0.39	0.38	0.38	0.37	0.37	0.37									
(3,15)	IN, OUT			209.44												185.64								
	rs				2.09	2.07	2.05	2.03	2.01	1.99	1.97	1.95	1.93	1.91	1.89	1.88								
(4,15)	IN, OUT				250.00											223.83								
	rs					2.50	2.47	2.45	2.43	2.40	2.38	2.35	2.33	2.31	2.28	2.26								
(5,15)	IN, OUT					1.28										1.16								
	rs						0.01	0.01	0.01	0.01	0.01	0.01	0.01	0.01	0.01	0.01								
(5,16)	IN, OUT					248.72											222.69							
	rs						2.49	2.46	2.44	2.41	2.39	2.37	2.34	2.32	2.30	2.27	2.25							
(6,16)	IN, OUT						250.00										226.10							
	rs							2.50	2.47	2.45	2.43	2.40	2.38	2.35	2.33	2.31	2.28							
(7,16)	IN, OUT							141.49									129.26							
	rs								1.41	1.40	1.39	1.37	1.36	1.35	1.33	1.32	1.31							
(7,17)	IN, OUT							3.26										2.95						
	rs								0.03	0.03	0.03	0.03	0.03	0.03	0.03	0.03	0.03	0.03						
(8,17)	IN, OUT								196.86									179.83						
	rs									1.97	1.95	1.93	1.91	1.89	1.87	1.85	1.83	1.82						
(9,17)	IN, OUT									13.73								12.67						
	rs										0.14	0.14	0.13	0.13	0.13	0.13	0.13	0.13						
(12,17)	IN, OUT												56.69					53.91						
	rs													0.57	0.56	0.56	0.55	0.54						
(13,17)	IN, OUT													25.69				24.68						
	rs														0.26	0.25	0.25	0.25						
(13,18)	IN, OUT													48.19					45.83					
	rs														0.48	0.48	0.47	0.47	0.46					
(13,19)	IN, OUT													49.39						46.50				
	rs														0.49	0.49	0.48	0.48	0.47	0.47				
(23,14)	IN, OUT														85.70							99.65		
	rs	0.99	0.98	0.97	0.96	0.95	0.94	0.93	0.92	0.91	0.90	0.89	0.88	0.87	0.87								1.00	
(24,14)	IN, OUT														125.76								144.76	
	rs	1.45	1.43	1.42	1.40	1.39	1.38	1.36	1.35	1.34	1.32	1.31	1.30	1.28	1.27								1.00	
Rin(h)		144.76	250.00	250.00	250.00	250.00	250.00	144.76	196.86	13.73	-	-	56.69	123.27	-	-	-	-	-	-	-	99.65	144.76	
Rout(h)		-	-	-	-	-	-	-	-	-	-	-	-	-	596.40	410.64	578.04	274.05	45.83	46.50	-	-	-	
Rs(h)		2.43	3.86	6.32	8.76	11.17	13.56	15.92	17.21	19.01	18.95	18.76	18.58	18.96	20.00	13.84	9.59	3.71	0.94	0.47	0.00	0.00	1.00	

Figure 3.16: Interconnection between charging and discharging periods through the TS – Energy flows, in kW.

Distributors

E3: $\quad p_{ep} \cdot E_p(h) - cE_{pr}(h) \cdot E_{pr}(h) - cE_{pd}(h) \cdot E_{pd}(h) = 0$ (3.56)

Q3: $\quad cQ_a(h) \cdot Q_a(h) - cQ_{ar}(h) \cdot Q_{ar}(h) - cQ_{ad}(h) \cdot Q_{ad}(h) = 0$ (3.57)

R4: $\quad cR_{pro}(h) \cdot R_{pro}(h) - cR_{in}(h) \cdot R_{in}(h) - cR_{pi}(h) \cdot R_{pi}(h) = 0$ (3.58)

For the distributors, a generally accepted accounting principle, which states that the unit costs of the products from the same line are equal, is applied. The following auxiliary equations are thus obtained:

$cE_{pr}(h) = cE_{pd}(h)$ (3.59)

$cQ_{ar}(h) = cQ_{ad}(h)$ (3.60)

$cR_{pi}(h) = cR_{in}(h)$ (3.61)

Productive units

AB: $\quad p_{fa} \cdot F_a(h) - cQ_a(h) \cdot Q_a(h) = 0$ (3.62)

ACa: $\quad cQ_{ar}(h) \cdot Q_{ar}(h) - cR_{aq}(h) \cdot R_{aq}(h) = 0$ (3.63)

ECp: $\quad cE_{pr}(h) \cdot E_{pr}(h) - cR_{pe}(h) \cdot R_{pe}(h) = 0$ (3.64)

The AB, ACa and ECp have only one product. In this case, the unit cost of the product is directly obtained from the cost balance equation, provided the unit costs of the consumed flows are known. The ACc and ECc also have only one product, but because they are inserted in the trigeneration subsystem the unit costs of their products are calculated differently, as will be explained below.

As already mentioned, the trigeneration subsystem and the TES unit TS impose some issues to the cost allocation problem that have not been deeply studied in thermoeconomics so far, namely (i) the joint production of energy services in dynamic trigeneration systems; and (ii) the incorporation of a TES unit. These aspects are analyzed in detail in the next paragraphs.

(i) Joint production in the trigeneration subsystem

The cost balance equation associated with the trigeneration subsystem is expressed by Eq. (3.65).

Tri-sub: $\quad \begin{aligned} &p_{fc} \cdot F_c(h) - p_{es} \cdot E_s(h) + rq_{cl} \cdot Q_{cl}(h) - cW_{cd}(h) \cdot W_{cd}(h) - cQ_{cd}(h) \cdot Q_{cd}(h) \\ &\quad - cR_{cq}(h) \cdot R_{cq}(h) - cR_{ce}(h) \cdot R_{ce}(h) = 0 \end{aligned}$ (3.65)

No costs are incurred to the dissipation of cogenerated heat Q_{cl} to the ambient (rq_{cl} = 0 €/kWh). Considering that the resources consumed by the trigeneration subsystem must be allocated to its useful cogenerated products (W_{cd}, Q_{cd}, R_{cq}, R_{ce}) three auxiliary equations are needed to determine their unit costs (cW_{cd}, cQ_{cd}, cR_{cq}, cR_{ce}).

In accordance with the objective of promoting widespread acceptance of polygeneration systems in society through a fair cost-and-benefit apportionment of joint production costs, it was proposed to apply the same discount d to all products of the trigeneration subsystem with respect to a reference cost of the corresponding energy services production. In previous papers (Lozano et al., 2014, 2011, 2009a), the authors have applied the discount method in similar thermoeconomic analyses of trigeneration systems.

$$d = 1 - cW_{cd}(h)/(cW)_{ref} = 1 - cQ_{cd}(h)/(cQ)_{ref} = 1 - cR_{cq}(h)/(cR)_{ref}$$
$$= 1 - cR_{ce}(h)/(cR)_{ref} \tag{3.66}$$

According to (Gochenour, 2003; Itami and Kaplan, 1980), the discount method, or benefit distribution method, is practicable for allocating variable costs because it results in sharing the benefits of joint production among all cogenerated products. Moreover, based on the cost allocation decision guide given in (Frischknecht, 2000; Horngren, 2009), the benefit distribution method can be justified under the fairness or equity criterion, which establishes that when several parties participate in a joint production process, an allocation procedure that satisfies all of them is required.

In the present analysis, the final consumers are the owners of the trigeneration system and thus all of them must receive the benefits of the joint production, which should be translated as lower unit costs of energy services relative to the conventional separate production cost. Therefore, the reference costs considered herein correspond to the energy services production cost of the reference system, as presented in Section 3.1.4. The three auxiliary equations are thus obtained from Eq. (3.66).

$$cW_{cd}(h)/(cW)_{ref} = cQ_{cd}(h)/(cQ)_{ref} \tag{3.67}$$
$$cW_{cd}(h)/(cW)_{ref} = cR_{cq}(h)/(cR)_{ref} \tag{3.68}$$
$$cW_{cd}(h)/(cW)_{ref} = cR_{ce}(h)/(cR)_{ref} \tag{3.69}$$

(ii) Incorporation of a TES unit

The cost allocation in the TS follows from the methodology developed in Section 3.3.1.3, which considers the interconnection between hourly periods through the TS as a charging and discharging network.

As expresses Eq. (3.61), the unit cost of the charged cooling cR_{in} is equal to the unit cost of the cooling produced cR_{pi} in the hourly period. This reflects the fact that the energy stored in the TS may have different unit costs according to the hourly period in which it was produced. Considering that the penalty for energy wasting in the TS must be allocated to its useful products, no cost was

allocated to the energy losses R_s ($cR_s = 0$ €/kWh). The unit cost of the discharged cooling cR_{out} was obtained by tracing the discharged flow back to its origin periods, as expresses Eq. (3.70).

$$cR_{out}(h) \cdot R_{out}(h) = \sum_{z \neq h} cR_{in}(z) \cdot IN(z, h) \tag{3.70}$$

3.3.3 Application to the simple trigeneration system

This section presents and discusses the results obtained from the application of the cost allocation approach proposed in Section 3.3.2 to the simple trigeneration system.

The hourly unit costs of the internal flows and final products of the simple trigeneration system were obtained by solving the linear equation system proposed in Section 3.3.2 using the software Engineering Equation Solver (EES, 2017). The allocation proposal allowed the operation cost to be distributed between the internal flows and final products of the system in each hourly period. Table 3.8 presents the main unit costs obtained.

Figure 3.17 presents the hourly unit costs obtained for the final products of the trigeneration system and their respective reference costs (separate production costs defined in Section 3.3.2). As can be seen, the hourly cE_d, cQ_d, and cR_d were always lower than their respective reference costs. The consolidated daily values cE_d, cQ_d, and cR_d resulted 38%, 41%, and 36% lower than $(cW)_{ref}$, $(cQ)_{ref}$, and $(cR)_{ref}$, respectively.

Regarding the trigeneration subsystem, its operation cost (consumption of natural gas) and revenue (sale of cogenerated electricity to the electric grid) were allocated to the cogenerated products in an equitable manner. Figure 3.18 presents the hourly unit costs of the cogenerated products and their respective reference costs. It was verified that the unit costs of the cogenerated products were always lower than the associated reference costs; the discount d being, on average, 44%.

It is worth noting that even though the trigeneration subsystem has four cogenerated products (W_{cd}, Q_{cd}, R_{cq}, and R_{ce}), it does not mean that all four are produced in the same hourly period. For example, at hours 8, 15 to 18, and 22 the four cogenerated products are produced, whereas at hours 2 to 6, 10, and 11 only two cogenerated products are produced. This affects the unit costs obtained, as the operation cost and revenue will be distributed between two, three, or four products. As can be seen from Figure 3.18, when both R_{cq} and R_{ce} are produced, their unit costs are the same; this follows from the application of the discount d (Eq. (3.66)), which considered the same reference cost $(cR)_{ref}$ to both types of cooling produced.

Table 3.8: Hourly unit costs of the internal flows and final products of the simple trigeneration system, in €/kWh.

Hour	Final products			Trigeneration subsystem products				Other internal flows								Stored energy
	cE_d	cQ_d	cR_d	cW_{cd}	cQ_{cd}	cR_{cq}	cR_{ce}	cQ_a	cE_{pr}	cR_{pe}	cR_e	cR_q	cR_{pro}	cR_{in}	cR_{out}	cS_{rf}
1	0.0533	0.0133	-	0.0533	0.0133	0.0107	-	-	-	-	-	0.0107	0.0107	0.0107	-	0.0110
2	0.0564	-	-	0.0564	-	0.0113	-	-	-	-	-	0.0113	0.0113	0.0113	-	0.0112
3	0.0560	-	-	0.0560	-	0.0112	-	-	-	-	-	0.0112	0.0112	0.0112	-	0.0113
4	0.0557	-	-	0.0557	-	0.0111	-	-	-	-	-	0.0111	0.0111	0.0111	-	0.0113
5	0.0569	-	-	0.0569	-	0.0114	-	-	-	-	-	0.0114	0.0114	0.0114	-	0.0114
6	0.0576	-	-	0.0576	-	0.0115	-	-	-	-	-	0.0115	0.0115	0.0115	-	0.0115
7	0.0557	0.0139	-	0.0557	0.0139	0.0112	-	-	-	-	-	0.0112	0.0112	0.0112	-	0.0116
8	0.0578	0.0144	-	0.0578	0.0144	0.0116	0.0116	-	-	-	0.0116	0.0116	0.0116	0.0116	-	0.0117
9	0.0591	0.0140	-	0.0559	0.0140	0.0112	-	-	-	-	-	0.0112	0.0112	0.0112	-	0.0118
10	0.0668	0.0172	-	0.0556	0.0139	-	-	0.0250	-	-	-	-	-	-	-	0.0120
11	0.0685	0.0151	-	0.0556	0.0139	-	-	0.0250	-	-	-	-	-	-	-	0.0121
12	0.0669	0.0143	-	0.0570	0.0143	0.0114	-	-	-	-	-	0.0114	0.0114	0.0114	-	0.0122
13	0.0609	0.0147	-	0.0588	0.0147	0.0118	-	-	-	-	-	0.0118	0.0118	0.0118	-	0.0123
14	0.0556	0.0140	0.0124	0.0556	0.0139	-	0.0111	0.0250	-	-	0.0111	-	0.0111	-	0.0126	0.0123
15	0.0568	0.0142	0.0121	0.0568	0.0142	0.0114	0.0114	-	-	-	0.0114	0.0114	0.0114	-	0.0125	0.0124
16	0.0572	0.0143	0.0124	0.0572	0.0143	0.0114	0.0114	-	-	-	0.0114	0.0114	0.0114	-	0.0126	0.0123
17	0.0683	0.0145	0.0128	0.0581	0.0145	0.0116	0.0116	-	0.1000	0.0200	0.0137	0.0116	0.0131	-	0.0125	0.0122
18	0.0711	0.0143	0.0135	0.0572	0.0143	0.0114	0.0114	-	0.1000	0.0200	0.0142	0.0114	0.0137	-	0.0124	0.0124
19	0.0691	0.0140	0.0136	0.0556	0.0139	-	0.0111	0.0250	0.1000	0.0200	0.0138	-	0.0138	-	0.0125	-
20	0.0691	0.0163	0.0138	0.0556	0.0139	-	0.0111	0.0250	0.1000	0.0200	0.0138	-	0.0138	-	-	-
21	0.0668	0.0140	0.0134	0.0556	0.0139	-	0.0111	0.0250	0.1000	0.0200	0.0134	-	0.0134	-	-	-
22	0.0609	0.0142	0.0120	0.0568	0.0142	0.0114	0.0114	-	0.1000	0.0200	0.0122	0.0114	0.0120	-	-	-
23	0.0558	0.0139	-	0.0558	0.0139	0.0112	-	-	-	-	-	0.0112	0.0112	0.0112	-	0.0112
24	0.0548	0.0137	-	0.0548	0.0137	0.0110	-	-	-	-	-	0.0110	0.0110	0.0110	-	0.0111
Day	0.0620	0.0147	0.0127	0.0563	0.0141	0.0113	0.0113	0.0250	0.1000	0.0200	0.0130	0.0113	0.0120	0.0113	0.0126	0.0118
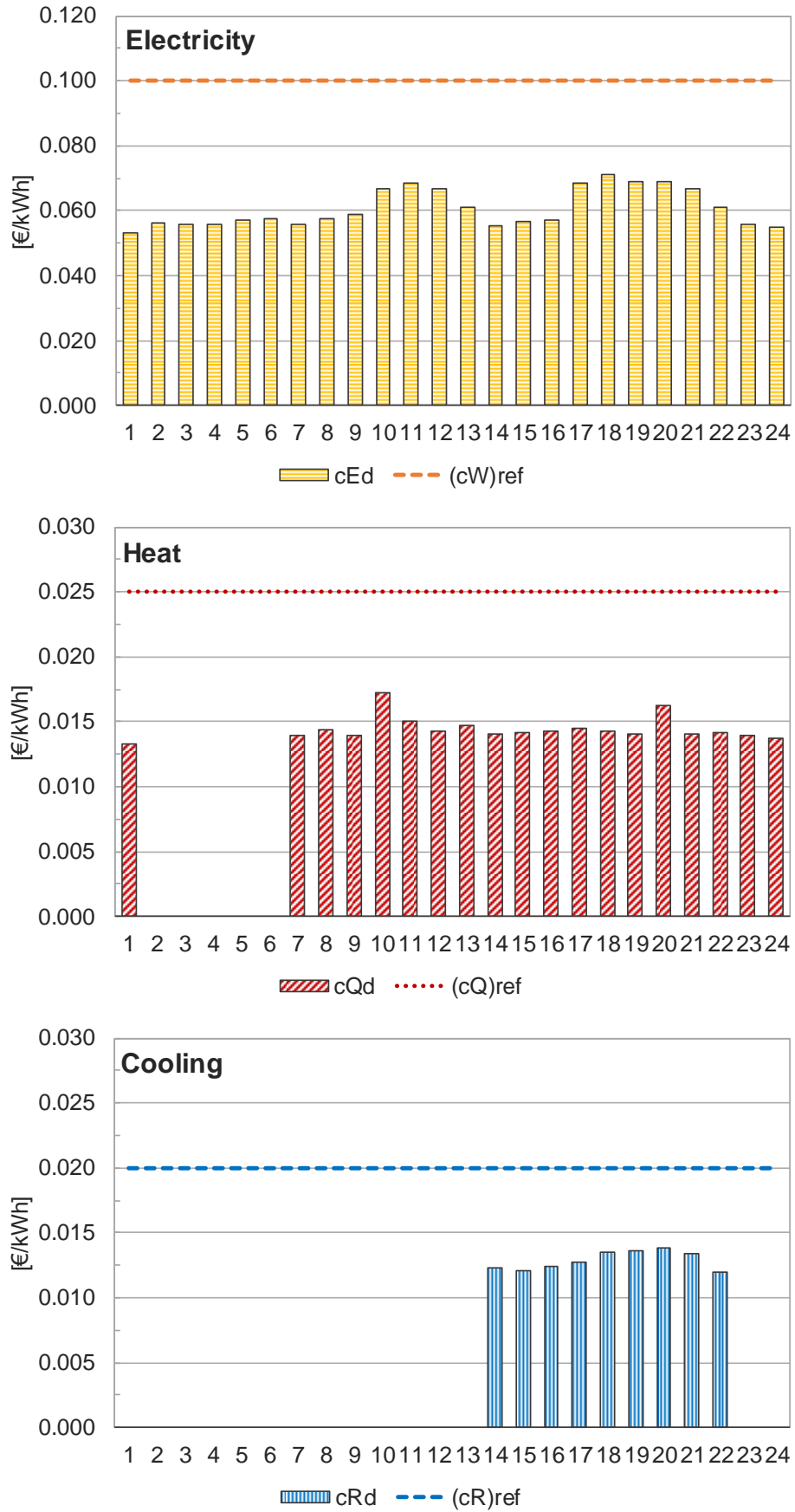
Figure 3.17: Hourly unit costs of the final products of the simple trigeneration system and reference costs.
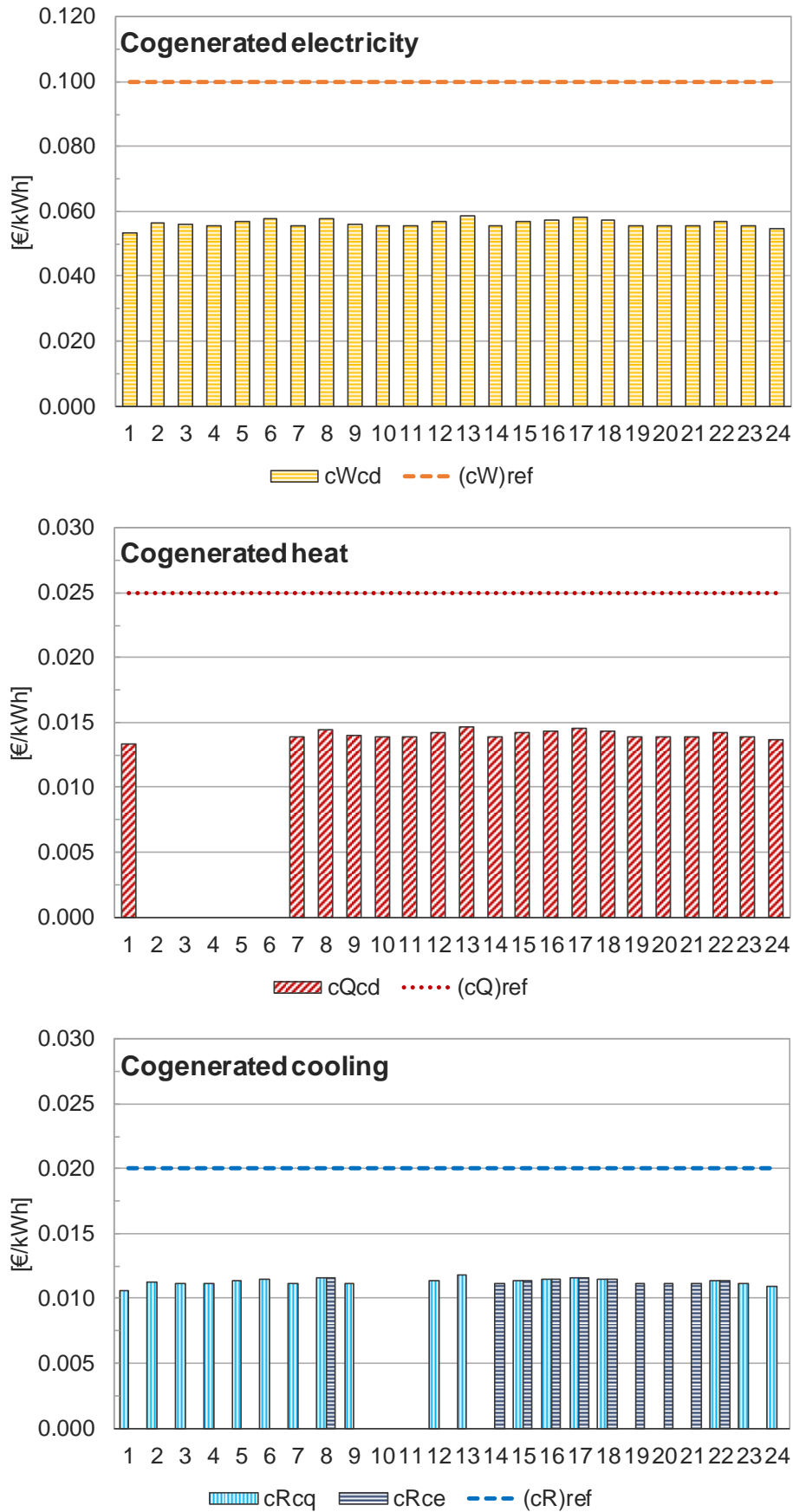
Figure 3.18: Hourly unit costs of the cogenerated products and reference costs.

The unit cost of the discharged energy cR_{out} in each hourly period was determined from the interconnection between hourly periods through the TS. By knowing the origin periods of the discharged energy and the unit costs of the charged energy in those periods, the cR_{out} could be assessed. Similar to Figure 3.16, Figure 3.19 shows the unit costs of the charged cR_{in} and discharged cR_{out} cooling, and of the associated pairs *cIN* and *cOUT.*

As can be seen from Figure 3.19, the unit costs of the discharged energy cR_{out} were always lower than the reference cost of cooling $(cR)_{ref}$, about 37% on average. Also, the unit cost of the discharged energy *cOUT* was always greater than that of the corresponding *cIN*. This is due to the energy losses along the path, which increase with the storage time. Therefore, the longer the storage time, the higher the increase in *cOUT* relative to *cIN*, which can also be interpreted as the penalty over *cOUT* due to energy wasting. For example, the energy discharged at hour 14 has been stored for, on average, 13 hourly periods, which implies an average penalty of 14% over the unit cost of the corresponding charged energy; on the other hand, the energy discharged at hour 19 has been stored for, on average, 6 hourly periods, which implies an average penalty of 6%.

3.3.4 Exergy-based unit costs

Exergy is recognizably the most applied magnitude in thermoeconomic cost allocation studies found in the academic literature. However, the discussion about what is the most appropriate base in which unit costs should be expressed (e.g. energy or exergy) is secondary to this study because whenever an unambiguous relation between two extensive magnitudes *X* and *Y* can be established, the unit costs base change from one to another is obvious: $c_y = c_x \cdot X/Y$. When exergy flows are considered, the Carnot factor related to the temperature level of the heating and cooling loads must be defined. Therefore, the cost allocation methodology proposed herein can be solved regardless of energy- or exergy-based approach and the same equivalent results would be obtained. This is demonstrated in this section.

First, the energy flows of the productive structure must be converted to exergy. In the case of the electricity, its exergy content is equal to its energy content.

The exergy content *Ex* of heating can be obtained by multiplying its energy content *En* by the Carnot factor:

$$\frac{Ex}{En} \equiv 1 - \frac{T_0}{T_H} = 1 - \frac{297}{360} = 0.1750 \tag{3.71}$$

where, T_0 is the reference ambient temperature (297 K) and T_H is the average temperature for the heat (360 K).

		1	2	3	4	5	6	7	8	9	10	11	12	13	14	15	16	17	18	19	20..22	23	24	1...
(1,14)	cIN, cOUT	0.0107													0.0121									
(2,14)	cIN, cOUT		0.0113												0.0127									
(3,14)	cIN, cOUT			0.0112											0.0125									
(3,15)	cIN, cOUT			0.0112												0.0126								
(4,15)	cIN, cOUT				0.0111											0.0124								
(5,15)	cIN, cOUT					0.0114										0.0126								
(5,16)	cIN, cOUT					0.0114											0.0127							
(6,16)	cIN, cOUT						0.0115										0.0127							
(7,16)	cIN, cOUT							0.0112									0.0122							
(7,17)	cIN, cOUT							0.0112										0.0123						
(8,17)	cIN, cOUT								0.0116									0.0126						
(9,17)	cIN, cOUT									0.0112								0.0121						
(12,17)	cIN, cOUT												0.0114					0.0120						
(13,17)	cIN, cOUT													0.0118				0.0122						
(13,18)	cIN, cOUT													0.0118					0.0124					
(13,19)	cIN, cOUT													0.0118						0.0125				
(23,14)	cIN, cOUT														0.0130							0.0112		
(24,14)	cIN, cOUT														0.0126								0.0110	
cRin(h)		0.0107	0.0113	0.0112	0.0111	0.0114	0.0115	0.0112	0.0116	0.0112	-	-	0.0114	0.0118	-	-	-	-	-	-	-	0.0112	0.0110	
cRout(h)		-	-	-	-	-	-	-	-	-	-	-	-	-	0.0126	0.0125	0.0126	0.0125	0.0124	0.0125	-	-	-	

Figure 3.19: Interconnection between charging and discharging periods through the TS – Unit costs, in €/kWh.

The exergy content Ex of cooling can be obtained by dividing its energy content En by the Carnot cycle COP:

$$\frac{Ex}{En} \equiv \frac{T_0}{T_C} - 1 = \frac{297}{280} - 1 = 0.0607 \tag{3.72}$$

where, T_C is the average temperature for the cooling (280 K).

The exergy content of the natural gas can be obtained by multiplying its energy content F_c by 1.0352, which corresponds to the ratio of its specific exergy 39,330 kJ/kg to its LHV (lower heating value) 37,991 kJ/kg. In the case of the fuel-oil its exergy content can be obtained by multiplying its energy content F_a by 1.0616 (specific exergy 46,149 kJ/kg and LHV 43,472 kJ/kg).

Secondly, the exergy-based prices of the energy resources consumed can be obtained by dividing the energy-based prices from Table 3.2 (electricity purchase p_{ep}, electricity sale p_{es}, natural gas p_{fc} and fuel-oil p_{fa}) by the corresponding factor from the previous paragraph; in the case of the electricity, the exergy-based price is equal to the energy-based one.

The reference costs considered in this work (Section 3.1.4), related to the separate production of energy services, can also be assessed in terms of exergy by dividing the energy-based reference cost by the corresponding factor from Eq. (3.71) and Eq. (3.72):

- Energy-based unit cost of the electricity 0.100 €/kWh → Exergy-based unit cost of the electricity 0.100 €/kWh;

- Energy-based unit cost of the heat 0.025 €/kWh → Exergy-based unit cost of the heat 0.1429 €/kWh; and

- Energy-based unit cost of the cooling 0.020 €/kWh → Exergy-based unit cost of the cooling 0.3294 €/kWh.

Finally, the thermoeconomic model has been solved using the software EES (EES, 2017), obtaining the hourly exergy unit costs of the internal flows and final products of the trigeneration system. The aggregated daily values of the energy and exergy flows and unit costs of the final products of the trigeneration system are presented in Table 3.9. Analogously, Table 3.10 compares the energy and exergy flows and unit costs of the trigeneration subsystem products.

As can be seen, the final products, as well as the trigeneration subsystem products, present lower exergy-based unit costs than the corresponding exergy-based reference costs. The discount d of the cogenerated products being, on average, about 44%. Thus, it becomes clear that considering the base change from energy- to exergy-based unit costs, the results obtained are the same. This

highlights the core issue approached in this work, which is not to discuss the base in which unit costs should be expressed (e.g. energy or exergy), but rather to propose fair criteria for the distribution of joint production costs among the final consumers.

Table 3.9: Daily energy and exergy flows and unit costs of the final products.

Final products	Energy, kWh	Unit energy cost, €/kWh	Exergy, kWh	Unit exergy cost, €/kWh
E_d	8400.0	0.0620	8400.0	0.0620
Q_d	6100.0	0.0147	1067.5	0.0838
R_d	4000.0	0.0127	242.9	0.2095

Table 3.10: Daily energy and exergy flows and unit costs of the trigeneration subsystem products.

Trigeneration subsystem products	Energy, kWh	Unit energy cost, €/kWh	Exergy, kWh	Unit exergy cost, €/kWh
W_{cd}	7317.4	0.0563	7317.4	0.0563
Q_{cd}	5757.6	0.0141	1007.6	0.0803
R_{cq}	2401.5	0.0113	145.8	0.1859
R_{ce}	1456.9	0.0113	88.5	0.1862

3.4 CONCLUSIONS

This chapter developed a thermoeconomic analysis of a simple trigeneration system including TES based on marginal cost analysis and average costs calculation. A simple trigeneration system was chosen to allow for interesting analyses and conceptual interpretations. First, a linear programming model was developed to determine the optimal hourly operation of the system that minimized the daily operation cost. The dual prices of the constraints provided by the optimization solver were interpreted, thereby obtaining the marginal costs of the internal flows and final products. The analysis of the marginal costs provided valuable insight into the operation of the system and the role of the TES. It was possible to identify time intervals in which the system took advantage of its ability to store energy to achieve a better economic result, for instance, there were hourly periods in which energy services production was advanced (produced in a time interval and stored for consumption later) and hourly periods in which it was delayed (consumed the energy already stored and postpone the production).

Regarding the average costs calculation, a cost allocation approach was proposed based on an equitable share of the benefits and inefficiencies of the combined production between the final products of the system. The presence of the TES added a new dimension to the cost formation process, as the energy stored in the TES carries a production cost. This is made clear in Figure 3.20, which shows how production costs are distributed between the hourly periods.

	Resources	TES		Products
	F_c, F_a, E_p/E_s	Q_{in}	Q_{out}	E_d, Q_d, R_d
h = 1	17.3 €	-1.5 €		15.7 €
h = 2	16.8 €	-2.8 €		13.9 €
h = 3	16.3 €	-2.8 €		13.5 €
h = 4	16.0 €	-2.8 €		13.2 €
h = 5	17.3 €	-2.8 €		14.4 €
h = 6	18.0 €	-2.9 €		15.2 €
h = 7	19.9 €	-1.6 €		18.3 €
h = 8	24.5 €	-2.3 €		22.2 €
h = 9	27.7 €	-0.2 €		27.6 €
h = 10	41.1 €			41.1 €
h = 11	40.6 €			40.6 €
h = 12	35.4 €	-0.6 €		34.8 €
h = 13	26.9 €	-1.5 €		25.5 €
h = 14	25.1 €		7.5 €	32.7 €
h = 15	25.0 €		5.1 €	30.1 €
h = 16	25.0 €		7.3 €	32.3 €
h = 17	36.2 €		3.4 €	39.7 €
h = 18	41.9 €		0.6 €	42.4 €
h = 19	40.4 €		0.6 €	41.0 €
h = 20	43.1 €			43.1 €
h = 21	36.9 €			36.9 €
h = 22	28.7 €			28.7 €
h = 23	21.6 €	-1.1 €		20.5 €
h = 24	18.9 €	-1.6 €		17.3 €
Day	**660.8 €**	-24.5 €	24.5 €	**660.8 €**

Figure 3.20: Energy resources' costs displaced through the TES.

The cost allocation approaches proposed herein are applied in Chapter 4 to a more complex trigeneration system, addressing additional challenges, including the allocation of capital (investment) costs to the products obtained.

CHAPTER 4

Multi-objective synthesis and thermoeconomic analysis
of trigeneration systems

4   MULTI-OBJECTIVE SYNTHESIS AND THERMOECONOMIC ANALYSIS OF TRIGENERATION SYSTEMS

The optimal synthesis framework outlined in Chapter 2 provides the base for the case study developed in Chapter 4, in which a multi-objective optimization model is developed using mixed integer linear programming (MILP) formulation to determine the optimal system configuration and multi-period operational planning, from the economic and environmental viewpoints, of trigeneration systems including renewable energy technologies (RETs) and thermal energy storage (TES). The methodology is applied to a case study of a multi-family residential building located in Zaragoza, Spain, that requires electricity, heating, and cooling.

The model uses binary variables to impose structural (e.g. permission to install technologies or not) and operational (e.g. different operating modes of technologies) restrictions, and continuous variables to represent the energy, economic, and environmental flows. The multi-period operation reflects the way in which the production of energy services is adjusted, within established limits, to dynamic operating conditions, such as the variability of climatic conditions, energy resources, and energy demands, as well as changes in energy resources prices, CO_2 emission factors, and technologies' performances. Also, local regulatory aspects involving, for example, the installation of cogeneration facilities and the interconnection with the electric grid are considered. The single-objective solutions provide the minimum total annual cost and minimum total annual CO_2 emissions of installing and operating the system, a breakdown of capital and operation costs and emissions, as well as the hourly, monthly, and annual energy flows. In turn, the multi-objective trade-off solutions are identified and plotted on the Pareto curve.

Based on a similar figure by Wakui et al. (2016), Figure 4.1 presents a general overview of the synthesis and optimization framework developed herein: (i) superstructure definition in accordance with the defined energy design targets and the available energy resources; (ii) data compilation and elaboration regarding the established optimization criteria and objective functions; (iii) optimization model development in line with the nature of the problem (i.e. single- or multi-objective optimization); and (iv) optimal decision-making.

It is worth mentioning that this approach is intended as a pre-design method: the solutions obtained do not correspond to final designs; on the contrary, they provide the basis for a subsequent more in-depth optimization process, which establishes the actual number of devices and their corresponding installed capacities, and takes into account part-load operating conditions.
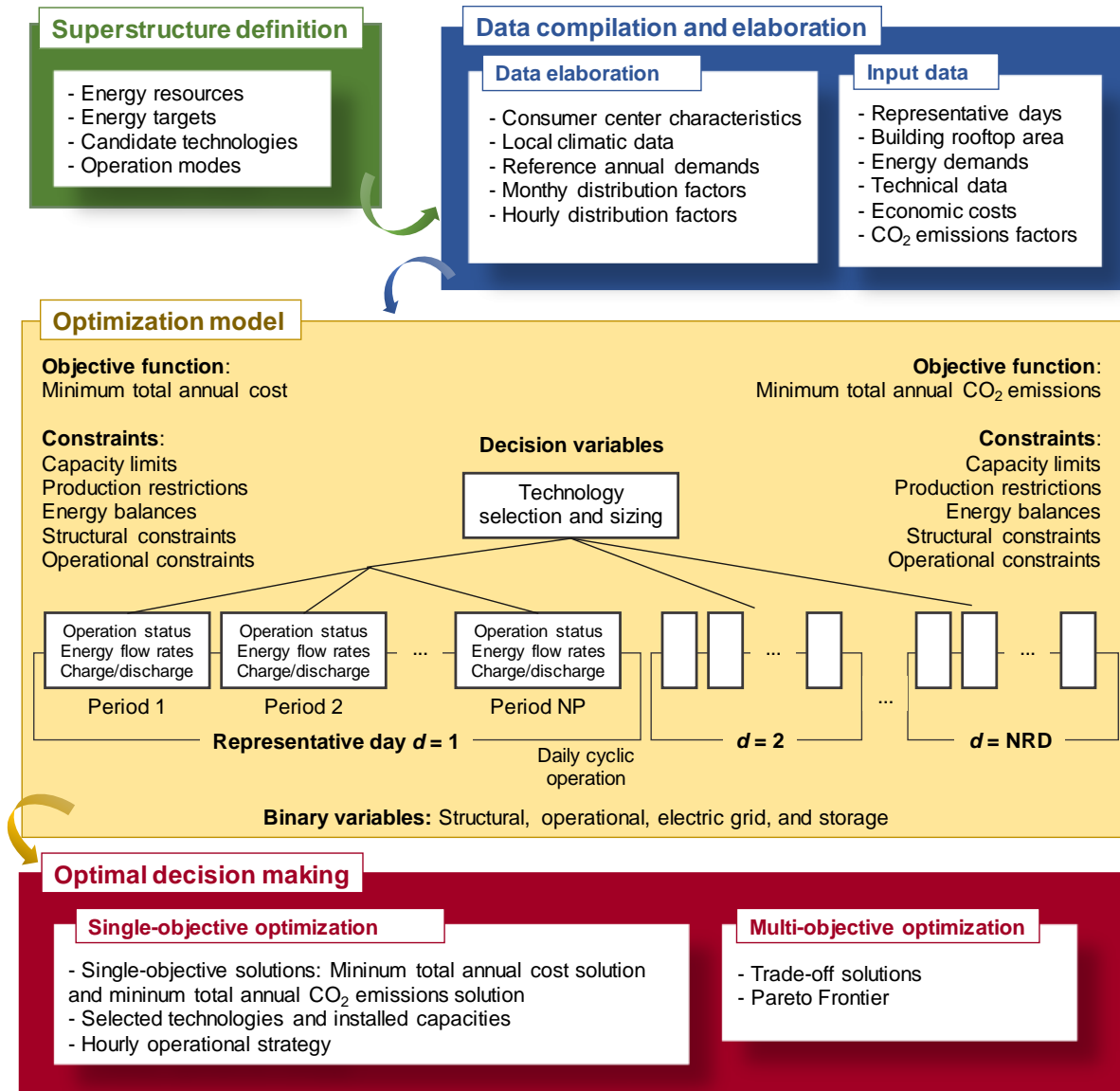
Figure 4.1: Multi-objective synthesis framework.

Thus, the main contributions and novelties of the methodology developed in this chapter include the appropriate consideration for:

- Economic and environmental aspects: the objective functions are represented with the same level of model detail, that is, both the economic and the environmental objective functions account for the costs and the CO_2 emissions of installing and operating the system;

- Electricity prices and CO_2 emissions: apart from considering hourly electricity prices, the hourly CO_2 emission factors of the electricity available in the electric grid are also included; and

- Climatic conditions: the hourly ambient temperature and hourly solar radiation are reflected in the dynamic operation of the system, as well as their effect on technologies' performances.

Finally, once the configuration and operational state of the trigeneration systems are determined, the cost allocation approaches for simple energy systems proposed in Chapter 3 are extended to tackle these systems of higher complexity levels. The issue of the appropriate ways to distribute capital costs is addressed, thereby proposing novel capital cost allocation approaches and demonstrating their applications. This part of the study has been published in Pina et al. (2018a).

The synthesis and optimization framework encompasses Sections 4.1 through 4.5: Section 4.1 defines the superstructure of the trigeneration system; Section 4.2 introduces the case study and describes the input data used in the optimization model; Section 4.3 develops the mathematical formulation of the MILP model, explaining the objective functions and the model constraints; Section 4.4 presents and discusses the results obtained for the single-objective solutions, namely optimal economic cost and optimal environmental solutions; and Section 4.5 develops the multi-objective optimization, obtains the Pareto curve, and identifies the preferred trade-off solutions. The economic cost allocation approaches are proposed and applied in Section 4.6. Finally, Section 4.7 draws the conclusions from this study. The data elaboration process for the case study analyzed herein is developed in Appendix A.

4.1   SUPERSTRUCTURE OF THE TRIGENERATION SYSTEM

Following the explanation provided in Section 2.2.1, the superstructure of the trigeneration system analyzed herein is defined taking into account: (i) the energy resources available; (ii) the type, quantity, and quality of the energy services required by the consumer center; and (iii) an appropriate process integration between the technologies in the superstructure and the thermal energy flows.

As depicted in Figure 4.2, the superstructure of the trigeneration system consists of a cogeneration module GE (natural gas reciprocating engine coupled to a heat recovery system), a natural gas boiler GB, a single-effect absorption chiller ABS, a reversible heat pump HP, photovoltaic panels PV, flat-plate solar thermal collectors ST, hot water storage tank TSQ, and chilled water storage tank TSR. The trigeneration system must attend the electricity E_d, heating Q_d, and cooling R_d demands of the consumer center. The following energy resources are available to the system: natural gas F_p, and solar radiation F_{pv} and F_{st}. Regarding the electric grid conditions, it is considered that both electricity purchase E_p and sale E_s are allowed.
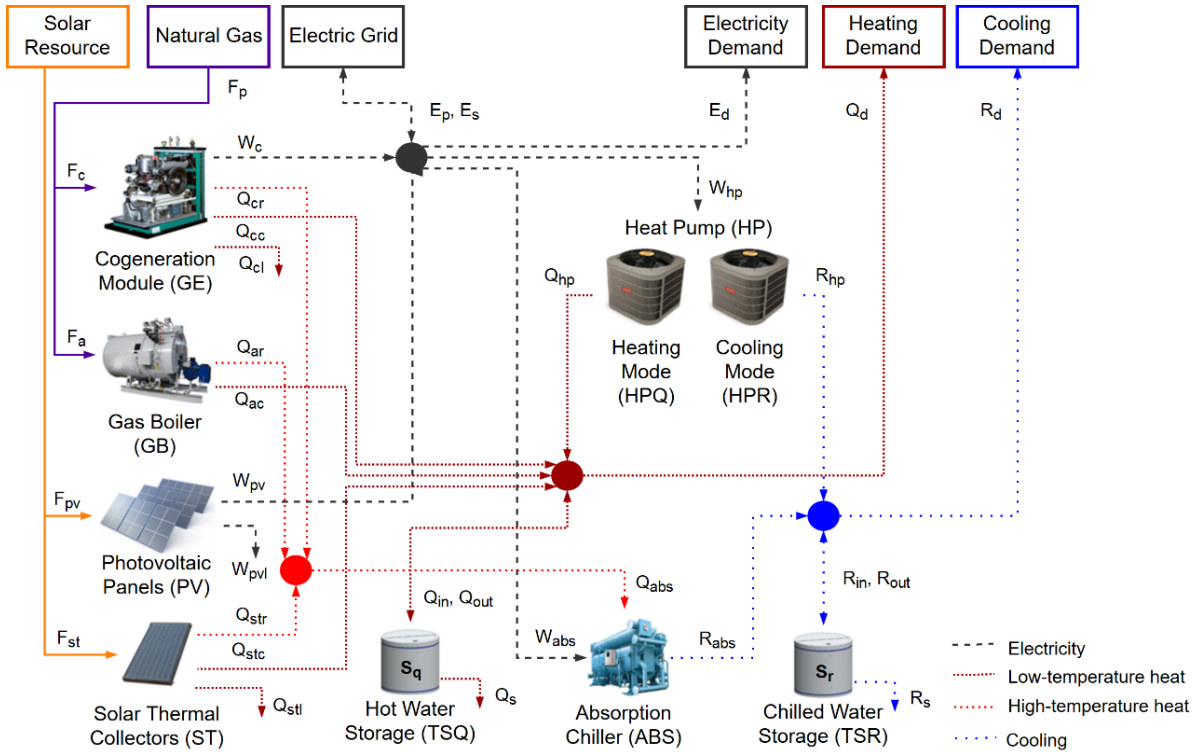
Figure 4.2: Superstructure of the trigeneration system.

Heat production takes place at two temperature levels: low-temperature heat at 60 °C, which is used exclusively to attend the heating demand, and high-temperature heat at 85 °C, which is used to drive the ABS for cooling production. The cogeneration module GE, the gas boiler GB, and the flat-plate solar thermal collectors ST can produce both low- and high-temperature heat flows, while the reversible heat pump HP can only produce low-temperature heat.

The cogeneration module GE consumes natural gas F_c and produces cogenerated electricity W_c, low-temperature heat Q_{cc}, and high-temperature heat Q_{cr}; also, a part of the total heat produced can be dissipated into the environment Q_{cl}. The gas boiler GB consumes natural gas F_a and produces low-temperature heat Q_{ac} and high-temperature heat Q_{ar}. The photovoltaic panels PV produce electricity W_{pv} from the incident solar radiation F_{pv}; there is the possibility of wasting a part of the photovoltaic electricity produced W_{pvl}, if necessary. The single-effect absorption chiller ABS consumes high-temperature heat Q_{abs} to produce cooling R_{abs}; also, an auxiliary electricity consumption W_{abs} is considered for this technology. Regarding the reversible heat pump HP and the flat-plate solar thermal collectors ST, two operation modes are considered according to the month of the year:

- From January to May and from October to December: The HP operates in heating mode (HPQ) consuming electricity W_{hp} to produce low-temperature heat Q_{hp}. The ST produce low-temperature heat Q_{stc} from the incident solar radiation F_{st};

- From June to September: The HP operates in cooling mode (HPR) consuming electricity W_{hp} to produce cooling R_{hp}. The ST can produce both low- and high- temperature heat Q_{stc} and Q_{str}, respectively.

Both operation modes of the ST allow heat to be dissipated into the environment Q_{stl}, if necessary. Concerning the thermal energy storage tanks, the TSQ is charged Q_{in} and discharged Q_{out} with low-temperature heat, while the TSR is charged R_{in} and discharged R_{out} with cooling. For both devices, charge and discharge cannot take place simultaneously. Energy losses Q_s and R_s are proportional to the energy stored S_q and S_r at the previous hourly period.

4.2 DATA COMPILATION AND ELABORATION

As can be seen from Figure 4.1, the data compilation and elaboration step is composed of two sub-items. The data elaboration corresponds to a preliminary step in which the input data required by the optimization model is identified and assessed. It is convenient to separate this step from the synthesis problem, which can be solved with MILP techniques suitable for its combinatorial nature. In fact, non-linear equations may be solved in the data elaboration step, thus preventing the higher complexity of employing mixed integer non-linear programming techniques to obtain the global solution.

Therefore, the information relating to the data elaboration process is explained in detail in Appendix A, including: (i) the consumer center's building and geographic characteristics; (ii) the assessment of local climatic data such as hourly ambient air temperature, hourly wet-bulb temperature, and hourly solar radiation; (iii) the evaluation of the consumer center's energy demands for the representative days of the months of the year, based on annual reference values and monthly and hourly distribution profiles; and (iv) a technical description of the technologies included in the superstructure.

The input data are described throughout this section: First, a brief description of the consumer center is given in Section 4.2.1, followed by the hourly energy demands for the representative days of the months of the year, in Section 4.2.2. The technical parameters of the candidate technologies in the superstructure are given in Section 4.2.3. Finally, Sections 4.2.4 and 4.2.5 provide information regarding the criteria chosen for the multi-objective optimization procedure, namely economic and environmental data, respectively.

4.2.1   Consumer center

The case study analyzed herein consists of a multi-family residential building complex located in Zaragoza (latitude 41.6°), Spain. The complex consists of 100 dwellings, each one with 100 m² of surface area, distributed between five identical buildings. Considering the geometry of the residential buildings, a total rooftop area AA = 2000 m² is available for the installation of photovoltaic panels and solar thermal collectors.

4.2.2   Energy demands

The energy demands of the consumer center represent the core of the design procedure, as they provide the necessary information to determine: (i) the selection of technologies that must be installed; (ii) their corresponding installed capacities; and (iii) the operational strategy of the system following the energy demands' hourly and monthly variations. Therefore, the estimation of energy demands data plays a critical role in ensuring the economic and environmental feasibility of the trigeneration system.

The energy demands required by the consumer center correspond to electricity, heating, and cooling. The heating demand is composed of both domestic hot water (DHW) and space heating (SH) loads, which are supplied to the consumer center at 60 °C. The cooling demand corresponds to chilled water at 7 °C. Moreover, the electricity demand excludes the consumption of electricity for thermal production, e.g. electric chiller for cooling production, electric heat pump for heat production; thus, the electricity demand considers only the dwellings' electric consumption for home appliances, lighting, etc.

Following the procedure described in Section A.3 of Appendix A, the estimation of the annual, monthly, and hourly energy demands took into account the following information: (i) climatic data for the geographical location in Spain (e.g. hourly ambient air temperature and monthly cold water temperature of the supply network); (ii) building characteristics (e.g. number of dwellings, surface areas, occupancy rate); (iii) reference values of annual energy consumption; and (iv) monthly and hourly energy demands profiles.

The present study covers the period of one year described by 12 representative days, each one composed of 24 consecutive periods of 1-hour duration. Each representative day d is attributed to a month of the year and no distinction is made between working days and weekends; in this way, the number of representative days type d per year NRY is equal to the number of days in the corresponding month: $NRY(Jan, Feb, Mar, ..., Dec)$ = 31, 28, 31, ..., 31.

The energy demands were estimated for the representative days of the months of the year. As the name implies, these representative days only account for typical energy demand values, which may hide, to some extent, sporadic peak demands. In order for these extreme demand conditions to be taken into account, two extra representative days were included, one for wintertime and another for summertime, as described in Section 4.2.2.4.

The annual electricity, heating, and cooling demands are 254.96 MWh/yr, 573.50 MWh/yr, and 113.99 MWh/yr, respectively. Table 4.1 presents the daily energy demands for the 12 representative days corresponding to the months of the year. The following sections describe the hourly profiles of each energy service.

Table 4.1: Energy demands of the consumer center per representative day.

Day type d	Number of days per year *NRY*	Heating Demand		Electricity demand		Cooling demand	
		Total, kWh/day	Mean, kW	Total, kWh/day	Mean, kW	Total, kWh/day	Mean, kW
Jan	31	4061.80	169.24	776.10	32.34	0.00	0.00
Feb	28	3366.70	140.28	776.00	32.33	0.00	0.00
Mar	31	1916.80	79.87	776.10	32.34	0.00	0.00
Apr	30	1065.90	44.41	694.30	28.93	0.00	0.00
May	31	456.80	19.03	694.00	28.92	0.00	0.00
Jun	30	424.00	17.67	626.00	26.08	559.90	23.33
Jul	31	351.50	14.65	626.00	26.08	1538.50	64.10
Aug	31	312.40	13.02	626.00	26.08	1144.30	47.68
Sep	30	382.10	15.92	626.00	26.08	467.50	19.48
Oct	31	422.40	17.60	694.00	28.92	0.00	0.00
Nov	30	2327.80	96.99	694.30	28.93	0.00	0.00
Dec	31	3873.20	161.38	776.10	32.34	0.00	0.00
Year	365	573.50 MWh/yr	65.47 kW	254.96 MWh/yr	29.11 kW	113.99 MWh/yr	13.01 kW

4.2.2.1 Electricity demand

The hourly electricity demand for the representative days of the months of the year is given in Table A.17. The same information is depicted in Figure 4.3, which allows for a clearer visualization of the monthly and hourly variations. As can be seen, electricity is required all year round. The representative days with the highest electricity demand correspond to the months from December to March (wintertime), while the representative days with the lowest electricity demand correspond to the months from June to September (summertime).

An example is provided in Figure 4.4 for the hourly electricity demand in January. The peak demand within the representative day takes place at hour 22 and corresponds to 52.0 kW.
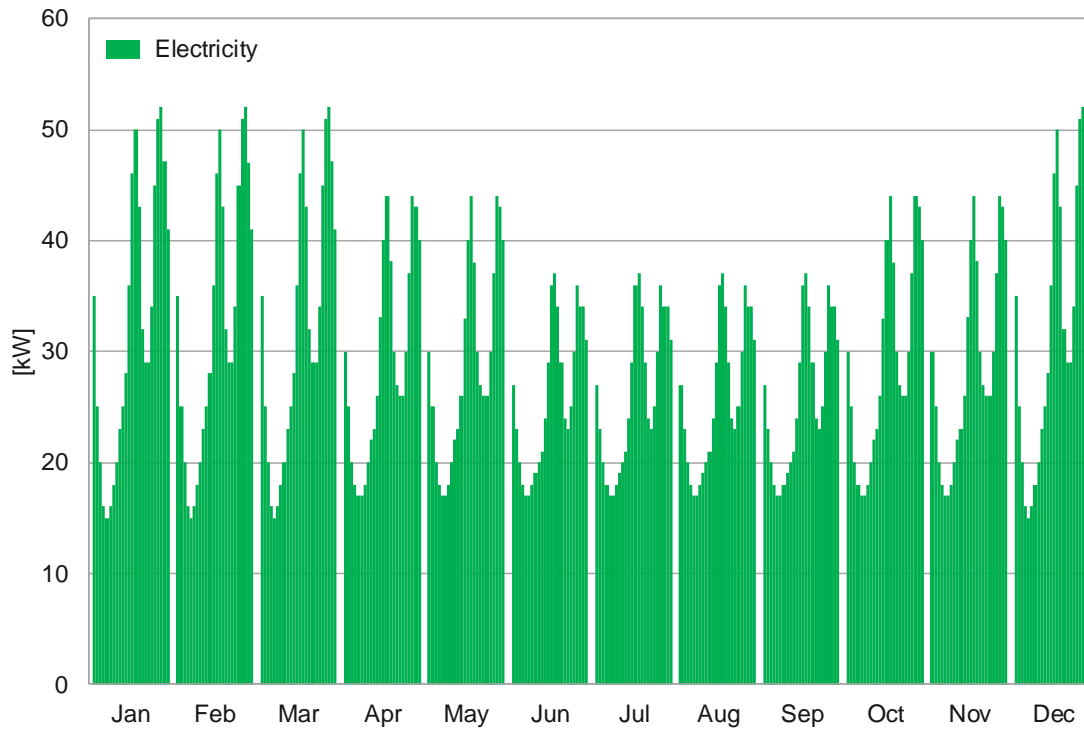
Figure 4.3: Annual electricity demand on an hourly basis.
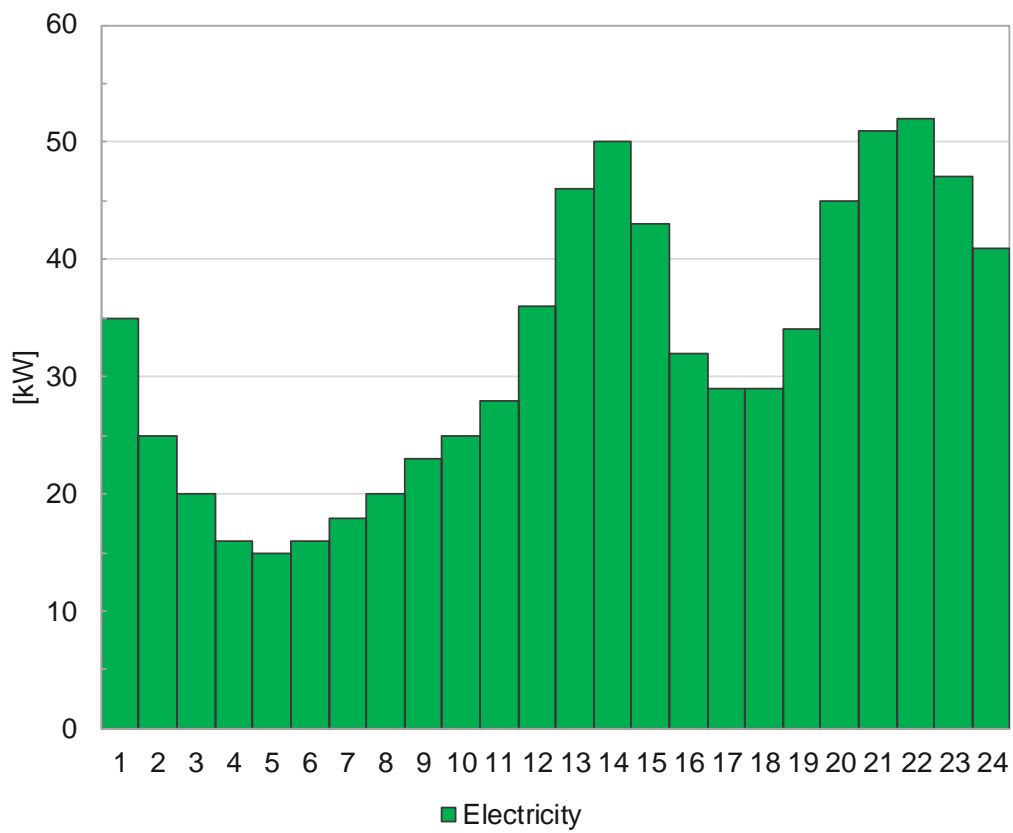
Figure 4.4: Hourly electricity demand for a representative day in January.

It is also interesting to analyze the energy demand's load duration curve, which is a graphic representation of the load over the time in descending order of magnitude, thus being a useful tool to estimate the duration of the energy load and to size the technologies' installed capacity.

Figure 4.5 depicts the electricity demand load duration curve. As can be seen, the electricity demand highest and lowest values throughout the year are 52 kW and 15 kW, respectively.
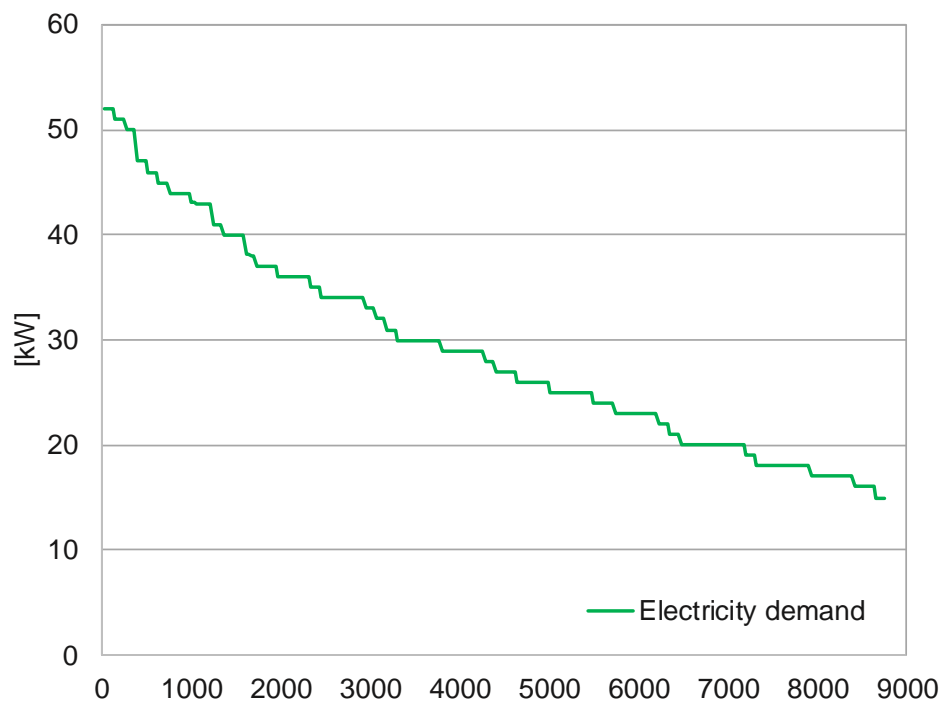
Figure 4.5: Load duration curve for the electricity demand.

4.2.2.2 Heating demand

The hourly heating demand for the representative days of the months of the year is given in Table A.23. The hourly and monthly variations of the heating demand, composed of DHW and SH demands, are also shown in Figure 4.6. As can be seen, the DHW is required all year round, while SH is only required from November to April.

An example is provided in Figure 4.7 for the hourly heating demand in January. The peak demand within the representative day takes place at hour 19 and corresponds to 313.0 kW.
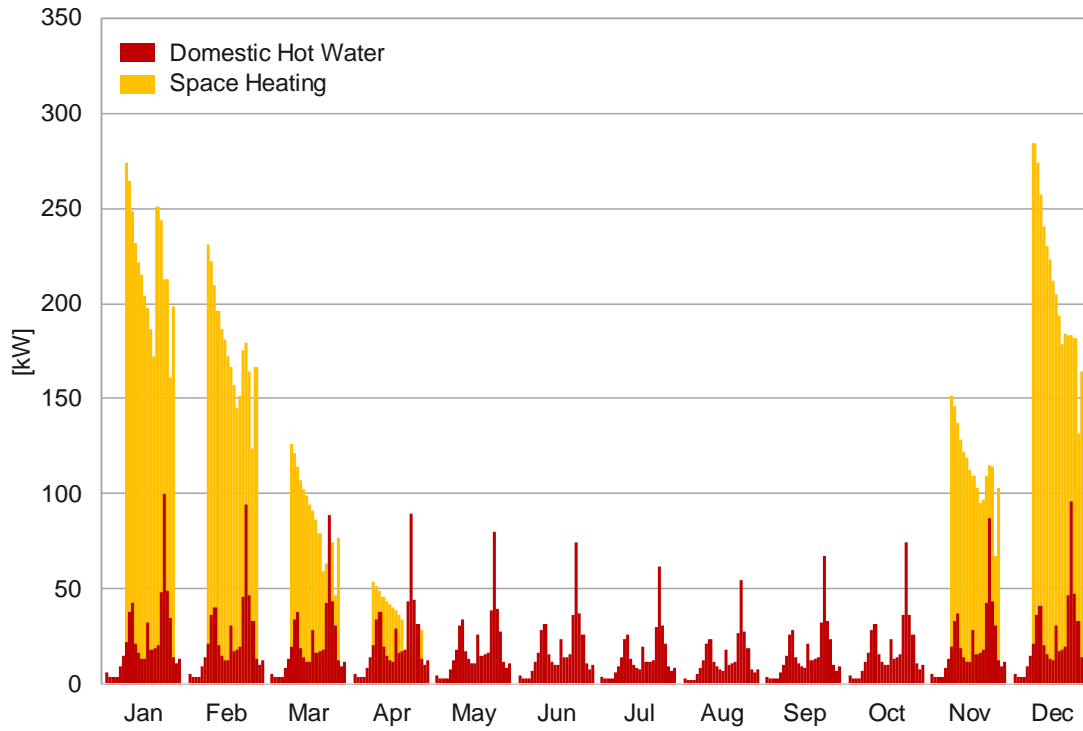
Figure 4.6: Annual heating demands on an hourly basis.
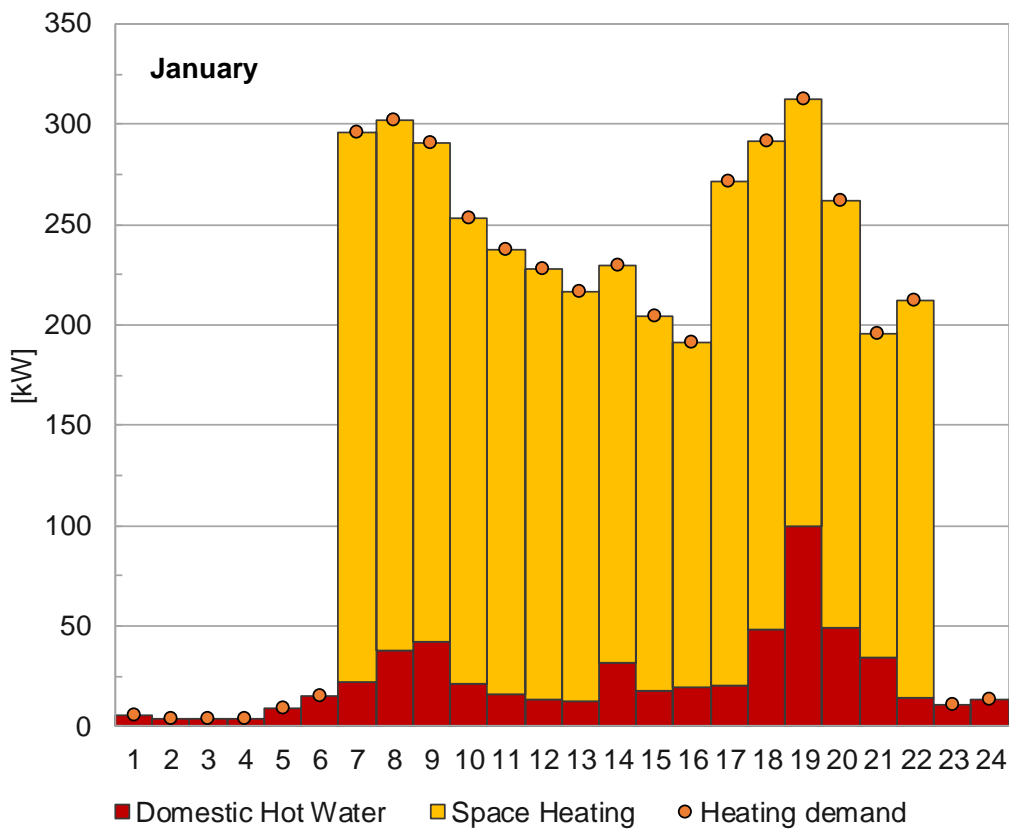
Figure 4.7: Hourly heating demands for a representative day in January.

From the 573.50 MWh/yr of annual heating demand, 406.0 MWh/yr corresponds to SH and the rest, 167.5 MWh/yr, to DHW. As can be seen from the heating demand load duration curve depicted in Figure 4.8, the SH load takes place for about 3000 h/yr; even though DHW is required all through the year, its peak demands are restricted to only 400 h/yr (5% of the year). Furthermore, it is important to highlight the non-simultaneity between the SH and DHW loads. For this reason, the highest heating demand value in Figure 4.8, 313.0 kW, is not equal to the sum of the highest SH and DHW demands, 285.0 kW and 100.0 kW, respectively. As shown in Figure 4.7, the SH and DHW peak demands within the representative day of January take place at different hours: hour 7 for the SH and hour 19 for the DHW.
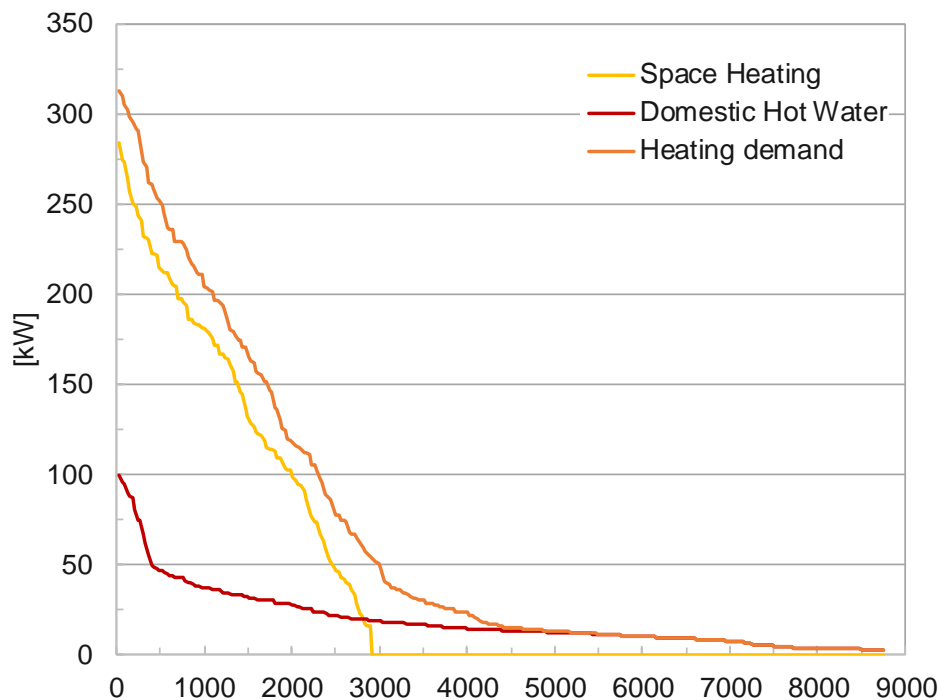
Figure 4.8: Load duration curve for the heating demands.

4.2.2.3 Cooling demand

The hourly cooling demand for the representative days of the months of the year is given in Table A.25. The hourly and monthly variations of the cooling demand are also given in Figure 4.9. As can be seen, the cooling demand is required from June to September (summertime), being highest in July.

For the representative day associated with the month of July, Figure 4.10 provides the hourly cooling demands. The peak demand within the representative day takes place at hour 16 and corresponds to 266.6 kW.
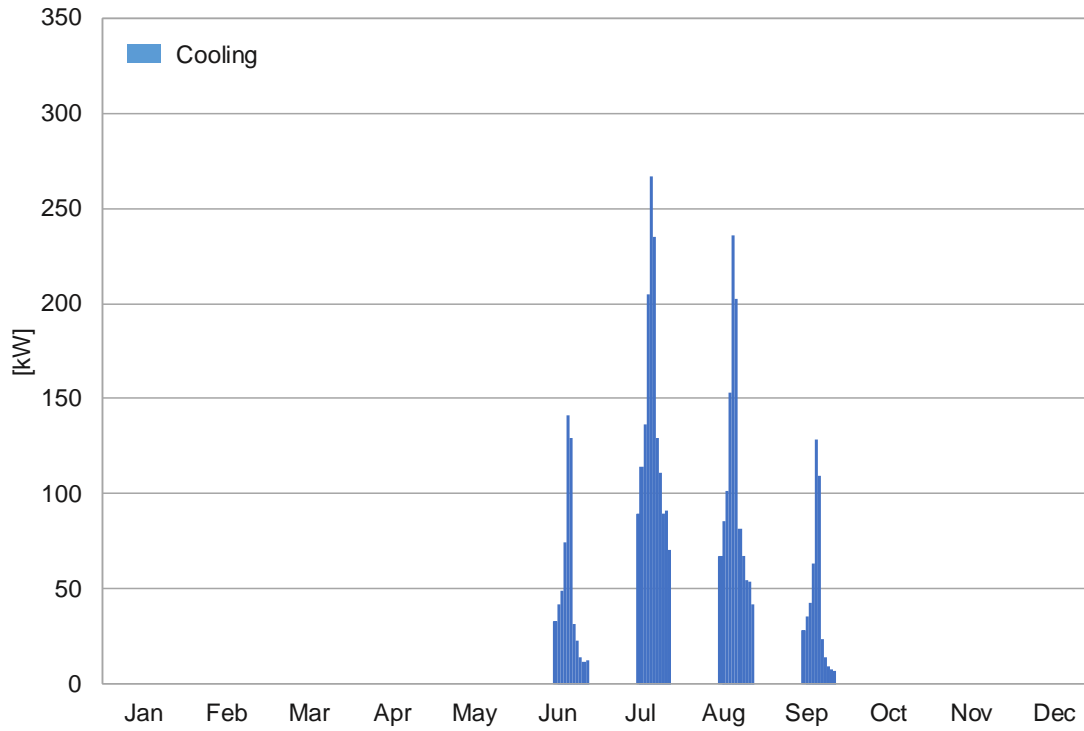
Figure 4.9: Annual cooling demands on an hourly basis.
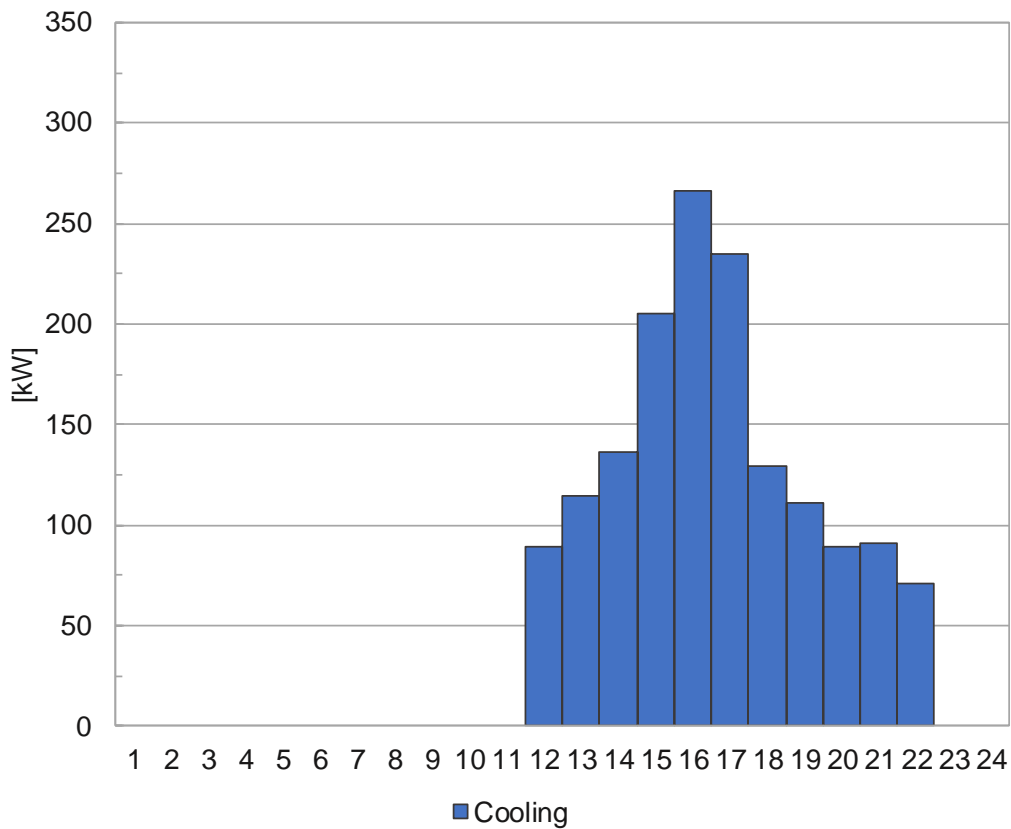
Figure 4.10: Hourly cooling demand for a representative day in July.

The cooling demand load duration curve is depicted in Figure 4.11. As can be seen, the consumer center requires cooling for about 1350 h/yr, with peak cooling loads restricted to a fairly short time frame (about 300 h/yr).
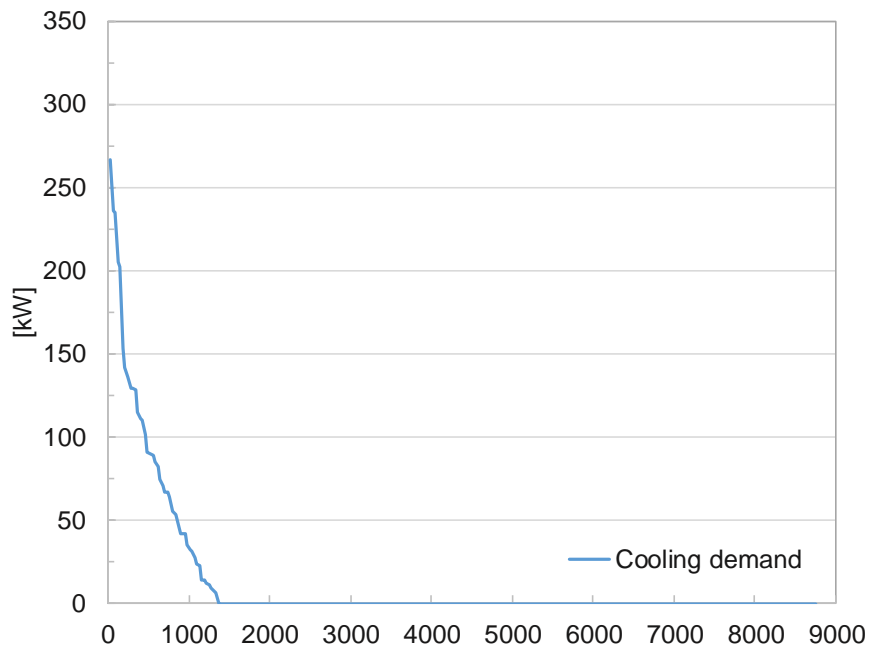
Figure 4.11: Load duration curve for the cooling demand.

4.2.2.4 Extreme demand conditions

As explained in Chapter 2, the high level of process integration that characterizes trigeneration systems makes it easier for these systems to cope with unexpected changes in energy demands and in other operation conditions. The incorporation of extreme demand representative days guarantees that an additional capacity is installed for safety power margin, thus increasing the total investment cost of the system. Nevertheless, they are not taken into account in the system's annual operation cost.

Therefore, in addition to the 12 representative days that describe the annual energy demands of the consumer center, two more were defined with the purpose of accounting for extreme demand conditions. The assessment of the extreme demand representative days considered the representative day with the highest hourly demand of each energy service. Then, for the identified representative days, all energy services were increased by 20%. For example:

- The representative day with the highest hourly electricity demand is January (hour 22), so an extreme demand representative day was created in which the hourly electricity, heating, and cooling demands of the whole day are 20% higher than the ones in January;

- The representative day with the highest hourly heating demand is also January (hour 19), so there was no need to create an additional extreme demand representative day;

- The representative day with the highest hourly cooling demand is July (hour 16), so an extreme demand representative day was created in which the hourly electricity, heating, and cooling demands of the whole day are 20% higher than the ones in July.

Table 4.2 presents the daily values obtained for both extreme demand representative days. Because they are intended to affect only the installed capacity of the technologies and not the annual operation cost of the system, an $NRY = 0$ was applied.

Table 4.2: Extreme demand representative day, daily basis.

Day type d	Number of days per year NRY	Heating demand		Electricity demand		Cooling demand	
		Total, kWh/day	Mean, kW	Total, kWh/day	Mean, kW	Total, kWh/day	Mean, kW
xJan	0	4874	203	931	39	0	0
xJul	0	422	18	751	31	1846	77

4.2.3   Technical data

This section provides the technical data concerning the technologies included in the superstructure. The technologies' technical parameters are given in Section 4.2.3.1, and the adjustment factors for the performances of the absorption chiller and reversible heat pump are briefly described in Sections 4.2.3.2 and 4.2.3.3, respectively. The reader is referred to Section A.4 of Appendix A for a more detailed explanation.

4.2.3.1   Technical parameters of the technologies included in the superstructure

The technical, economic, and environmental parameters of the technologies included in the superstructure defined in Section 4.1 are based on real, commercially available devices, which are described in detail in Section A.4.1. These devices were carefully selected to suit appropriate capacity ranges, which have been estimated from the consumer center's energy demands.

Table 4.3 presents the main technical parameters of the technologies included in the superstructure, as well as their maximum installable capacity CAP_{MAX} values. The information follows the nomenclature of the mathematical model that will be developed later in Section 4.3.

Table 4.3: Main technical parameters of the technologies in the superstructure.

Tech.	Parameter	Value	CAP_{MAX}
GE	α_w: Electric power efficiency	0.26	500 kW$_{el}$
	α_q Thermal efficiency	0.61	
GB	η_q: Thermal efficiency	0.95	500 kW
HP	COP_{hpq}: COP (heating mode)	3.24	500 kW
	EER_{hpr}: EER (cooling mode)	3.19	
	$RCAP_{rq}$: Cooling/heating capacity ratio	0.90	
ABS	COP_{abs}: COP	0.69	500 kW
	$kwabs$: Unit auxiliary electricity consumption	0.03	
TSQ	$fpacuQ$: Hourly energy loss factor	0.01 h^{-1}	1000 kWh
TSR	$fpacuR$: Hourly energy loss factor	0.01 h^{-1}	1000 kWh
PV	rpv: PV rooftop area usage	3.1250 m^2 roof/m^2 PV	AA = 2000 m^2
ST	rst: ST rooftop area usage	2.2676 m^2 roof/m^2 ST	rooftop

For each technology in the superstructure, its installed capacity *CAP* is limited to a maximum installable capacity *CAP$_{MAX}$*, which is also given in Table 4.3. In the case of the PV and ST, their installation is limited to the rooftop area available *AA*, defined in Section 4.2.1. As described in Section A.4.4, the PV and ST surface areas and tilt were used to estimate the rooftop area occupied by each square meter of module *rpv* and *rst*.

Except for the solar-based RETs (i.e. PV and ST), the technologies can be operated between zero and nominal load with no effect on their performances. Based on the manufacturers' catalogues, the performances of some technologies have been adjusted for off-nominal operating conditions, such as: (i) different operating modes, in the case of the reversible heat pump HP; and (ii) variable hourly ambient temperature, in the case of the HP and single-effect absorption chiller ABS. Therefore, adjustment factors were introduced for the ABS and HP as described in Sections 4.2.3.2 and 4.2.3.3, respectively.

In the case of the PV and ST, because of the intermittent behavior of the solar resource, their production varies according to the available solar radiation and conversion efficiency, which depends not only on the incident solar radiation but also on the collector working temperature and ambient air temperature. In order to account for their dynamic behavior, the technologies' technical parameters and local climatic data (hourly ambient temperature and hourly solar radiation) were used to calculate the PV and ST hourly specific productions per m^2 of module installed, as described in Section A.4.3.

The PV specific production $x_{pv}(d,h)$ for each hourly period of each representative day is given in Table A.43. In the case of the ST, $x_{stq}(d,h)$ corresponds to the specific production for low-temperature operation, while $x_{str}(d,h)$ corresponds to the specific production for high-

temperature operation. The values of $x_{stq}(d,h)$ and $x_{str}(d,h)$ obtained are given in Table A.44 and Table A.45, respectively.

4.2.3.2   Adjustment factors for the single-effect absorption chiller ABS

Table 4.4 presents the single-effect absorption chiller's operation parameters at nominal conditions and the ones considered in the case study. As can be seen, the ABS's cooling capacity *CAP(ABS)* and COP_{abs} must be adjusted according to the following changes in operation conditions: (i) the inlet cooling water temperature $T_{cw,in}(d,h)$ is considered to be 5 °C above the hourly wet-bulb temperature *Twb(d,h)*; (ii) the inlet hot water temperature is equal to 85 °C; and (iii) the temperature difference in the hot water circuit is equal to 10 °C.

Table 4.4: Operation conditions for the single-effect absorption chiller.

Parameter	Nominal	Case study
Inlet cooling water temperature	29.4 °C	$T_{cw,in}(d,h) = Twb(d,h) + 5$ °C
Inlet hot water temperature	90.6 °C	85 °C
Temperature difference in the hot water circuit	5.6 °C	10 °C

Processing the data collected from the manufacturer's catalogue, as explained in Section A.4.2, allowed Eq. (4.1) to be obtained, which yields the adjustment factor for the cooling capacity $fCAP_{abs}(d,h)$ as a function of $T_{cw,in}(d,h)$.

$$fCAP_{abs}(d,h) = 0.3311 + 0.1211 \cdot T_{cw,in}(d,h) - 0.0033 \cdot T^2_{cw,in}(d,h) \tag{4.1}$$

It must be noted, however, that due to a lack of technical information provided by the manufacturer, the COP_{abs} was considered constant regardless of the operation conditions.

The adjustment factors $fCAP_{abs}(d,h)$ obtained for each hourly period *h* of each representative day *d* can be found in Table A.38.

4.2.3.3   Adjustment factors for the reversible heat pump HP

The heat pump has two operation modes: heating and cooling modes. Regarding the heating mode, Table 4.5 presents the operation parameters at nominal conditions and the ones considered in the case study. As can be seen, the HP's heating capacity *CAP(HPQ)* and COP_{hpq} must be adjusted according to the following changes in operation conditions: (i) the ambient air temperature *Ta(d,h)* is considered to vary hourly and monthly; and (ii) the outlet hot water temperature is equal to 55 °C.

Table 4.5: Operation conditions for the reversible heat pump in heating mode.

Parameter	Nominal	Case study
Ambient air temperature	7 °C	*Ta(d,h)*
Outlet hot water temperature	45 °C	55 °C

Processing the data collected from the manufacturer's catalogue, as explained in Section A.4.2, allowed Eq. (4.2) and Eq. (4.3) to be obtained, which yield the adjustment factors for the HP's heating capacity $fCAP_{hpq}(d,h)$ and COP $fCOP_{hpq}(d,h)$, respectively, as a function of $Ta(d,h)$.

$$fCAP_{hpq}(d,h) = 0.8435 + 0.0184 \cdot Ta(d,h) \qquad (4.2)$$
$$fCOP_{hpq}(d,h) = 0.7050 + 0.0133 \cdot Ta(d,h) \qquad (4.3)$$

The adjustment factors $fCAP_{hpq}(d,h)$ and $fCOP_{hpq}(d,h)$ obtained for each hourly period h of each representative day d can be found in Table A.39 and Table A.40, respectively.

Regarding the cooling mode, the only difference in the operation conditions is the hourly ambient temperature: its nominal value is a constant 35 °C, while it is considered that $Ta(d,h)$ varies on hourly and monthly basis. Therefore, the HP's cooling capacity $CAP(HPQ)$ and EER_{hpr} must be adjusted as a function of $Ta(d,h)$.

Analogous to the heat pump in heating mode, Eq. (4.4) and Eq. (4.5) yield the HP's cooling capacity $fCAP_{hpr}(d,h)$ and EER $fEER_{hpr}(d,h)$, respectively, as a function of $Ta(d,h)$.

$$fCAP_{hpr}(d,h) = 1.4825 - 0.0138 \cdot Ta(d,h) \qquad (4.4)$$
$$fEER_{hpr}(d,h) = 1.9146 - 0.0256 \cdot Ta(d,h) \qquad (4.5)$$

The $fCAP_{hpr}(d,h)$ and $fEER_{hpr}(d,h)$ obtained for each hourly period h of each representative day d can be found in Table A.41 and Table A.42, respectively.

4.2.4 Economic data

The total annual cost of installing and operating the trigeneration system is composed of a fixed term (or capital term), relative to the investment and maintenance costs of the technologies, and a variable term (or operation term), relative to the hourly operation cost of the system.

The capital and the operation costs for the case study developed herein are given in Sections 4.2.4.1 and 4.2.4.2, respectively.

4.2.4.1   Investment and maintenance costs

As explained in Section 4.2.3.1, the technical, economic, and environmental parameters of the technologies included in the superstructure are based on real, commercially available devices, which have been described in Section A.4.1 of Appendix A.

The bare module cost CI of each technology i corresponds to the unit investment cost CU adjusted by a simple module factor f_M, which takes into account transportation, installation, connection, insulation costs, among others. Table 4.6 presents the technologies' investment costs, obtained from the manufacturers' catalogues and from the literature.

Table 4.6: Investment costs of the technologies in the superstructure.

	Technology i	**Unit investment cost** CU	**Simple module factor** f_M	**Bare module cost** CI
GE	Cogeneration module	2000 €/kW	1.35 [1]	2700 €/kW
GB	Gas boiler	55 €/kW	1.40 [2]	77 €/kW
HP	Heat pump	370 €/kW	1.30 [3]	481 €/kW
ABS	Absorption chiller	370 €/kW	1.40 [4]	518 €/kW
PV	Photovoltaic panel	170 €/m²	1.55 [5]	264 €/m²
ST	Solar thermal collector	330 €/m²	1.75 [6]	578 €/m²
TSQ	Hot water storage tank	130 €/kWh	1.15 [2]	150 €/kWh
TSR	Chilled water storage tank	260 €/kWh	1.15 [2]	300 €/kWh

References: [1]Average values from Darrow et al. (2015), Pehnt et al. (2006), and Ramos (2012); [2]Obtained from the manufacturer's catalogue; [3]The same consideration as the mechanical chiller from Ramos (2012); [4]Estimated from Ramos (2012); [5]Average values from Harvey (2012) and Kaltschmitt et al. (2007); [6]Average values from Kaltschmitt et al. (2007) and Peuser et al. (2005).

The optimization model determines which technologies should be selected and their corresponding installed capacities. The total investment cost of the plant is increased by a factor of 20% (f_{IC} = 0.20), which takes into account indirect costs of the plant, such as engineering and supervision expenses, legal expenses, contractor's fees and contingencies (Carvalho, 2011). Further, the total investment cost is multiplied by the amortization and maintenance factor fam, composed of the capital recovery factor f_{CR} and the maintenance and operation costs factor f_{mo}.

$$fam = f_{CR} + f_{mo} \qquad (4.6)$$

The operation and maintenance costs are assumed to be 3.25% of the total investment cost of the plant (f_{mo} = 0.0325 yr^{-1}). The capital recovery factor f_{CR} is determined by Eq. (4.7) considering, for all technologies, an interest rate iyr = 0.10 yr^{-1} and an operational lifetime nyr = 20 yr.

$$f_{CR} = \frac{iyr \cdot (1 + iyr)^{nyr}}{(1 + iyr)^{nyr} - 1}$$

(4.7)

The obtained capital recovery factor is f_{CR} = 0.1175 yr^{-1}. Finally, the *fam* is equal to 0.15 yr^{-1}.

4.2.4.2 Gas and electricity rates

The trigeneration system purchases natural gas from the economic market. It is considered that electricity can be purchased from and sold to the electric grid without restrictions. Therefore, it is necessary to establish the natural gas and electricity purchase prices, as well as the electricity selling price, applicable to the case study.

In Spain, both electricity and natural gas markets are liberalized, which means that consumers are free to choose from the available local distributors or to remain connected to the regulated market. For Zaragoza, Spain, the gas and electricity prices considered herein were taken from the distributor EDP (2017), under the free market modality.

In the case of the natural gas, the purchase price with taxes c_g is given in Table 4.7. The applicable taxes correspond to the hydrocarbons tax and the VAT (Value Added Tax).

Table 4.7: Natural gas price for the local distributor (EDP, 2017).

Concept		Price
	Price without taxes	0.0444 €/kWh (LHV)
Taxes	Hydrocarbons tax	0.00234 €/kWh (LHV)
	VAT	21%
	Price with taxes c_g	0.0566 €/kWh (LHV)

Regarding the electricity, the access rate 3.0A was chosen based on a preliminary estimation of the consumer center's peak electricity demands. According to this access rate, the day is composed of three hourly periods with different electricity prices: (P1) On-peak; (P2) Mid-peak; and (P3) Off-peak. The distribution of rating periods P1, P2 and P3 changes according to the month of the year, as shown in Table 4.8, but no distinction is made between working days and weekends/holidays.

Table 4.8: Annual distribution of rating periods for the access rate 3.0A, Zone 1 – Peninsular – ITC/2794/2007 (Spanish Industry Office, 2007).

Hours	Winter			Summer							Winter	
	Jan	Feb	Mar	Apr	May	Jun	Jul	Aug	Sep	Oct	Nov	Dec
1-8	P3	P3	P3	P3	P3	P3	P3	P3	P3	P3	P3	P3
9-11	P2	P2	P2	P2	P2	P2	P2	P2	P2	P2	P2	P2
12-15	P2	P2	P2	P2	P1	P1	P1	P1	P1	P1	P2	P2
16-18	P2	P2	P2	P2	P2	P2	P2	P2	P2	P2	P2	P2
19-22	P1	P1	P1	P1	P2	P2	P2	P2	P2	P2	P1	P1
23-24	P2	P2	P2	P2	P2	P2	P2	P2	P2	P2	P2	P2

The electricity prices with taxes c_{ep} are given in Table 4.9 for each rating period. The applicable taxes include the electricity tax, the tax base factor, and the VAT. The selling price of the electricity c_{es} was assumed to be the same as the purchase price at the corresponding period.

Table 4.9: Time-of-use electricity prices for the local distributor (EDP, 2017).

	Concept	On-peak P1	Mid-peak P2	Off-peak P3
	Initial price	0.1372 €/kWh	0.1172 €/kWh	0.0912 €/kWh
Taxes	Electricity tax		4.864%	
	Tax base factor		1.05113	
	VAT		21%	
	Final price c_{ep}	0.1830 €/kWh	0.1563 €/kWh	0.1216 €/kWh

4.2.5 Environmental data

In addition to the economic data described in Section 4.2.4, the other aspect considered in the multi-objective optimization procedure concerns the environmental impacts associated with the installation and operation of the trigeneration system, expressed by the total annual CO_2 emissions. Analogous to the total annual cost, the total annual CO_2 emissions is also composed of a fixed (or capital) term, relative to the emissions associated with the manufacturing of the technologies, and a variable (or operation) term, relative to the emissions generated in the operation of the system, i.e. consumption of natural gas and electricity from the electric grid.

For each technology *i* from the superstructure, Table 4.10 presents the unit CO_2 emissions *CO2U*, which expresses the amount of CO_2 emissions associated with the manufacturing of the technology per unit of capacity installed. The *CO2U* values were estimated from different works available in the literature for the devices described in Section A.4.1.

Table 4.10: Unit CO_2 emissions of the technologies in the superstructure.

	Technology i	Unit CO_2 emissions $CO2U$	Reference
GE	Cogeneration module	65 kg CO_2/kW	Carvalho (2011)
GB	Gas boiler	10 kg CO_2/kW	Carvalho (2011)
HP	Heat pump	160 kg CO_2/kW	Carvalho (2011)
ABS	Absorption chiller	165 kg CO_2/kW	Carvalho (2011)
PV	Photovoltaic panel	285 kg CO_2/m²	Ito et al. (2009)
ST	Solar thermal collector	95 kg CO_2/m²	Guadalfajara (2016)
TSQ	Hot water storage tank	150 kg CO_2/kWh	Guadalfajara (2016)
TSR	Chilled water storage tank	300 kg CO_2/kWh	Guadalfajara (2016)

Regarding the hourly operation of the system, it is necessary to determine the CO_2 emissions associated with the consumption of natural gas and electricity from the electric grid.

The environmental cost associated with the consumption of natural gas is constant throughout the year $kgCO2_g$ = 0.252 kg CO_2/kWh (LHV). This is a Spanish national value provided by IDAE (2016).

In the case of the electricity purchased from the electric grid, *Red Eléctrica de España* (REE) provides real-time data on the national electric generation and the associated CO_2 emissions on a 10-minute basis (REE, 2018). Such emissions are calculated by associating each technology with the corresponding emission factor established in the Spanish Renewable Energy Plan 2005-2010, in line with the Decision of the European Commission 2007/589/CE. Figure 4.12 shows a screenshot of the online tool indicating the demand curves (actual demand, demand forecast, and hourly operating schedule), the generation mix, and the associated CO_2 emissions.

Figure 4.12: Electricity demand tracking in real time (REE, 2018).

The annual data for the year of 2016 were exported from the online tool to a spreadsheet file. Then, the information was processed to obtain the unit CO_2 emissions $kgCO2_e(d,h)$ associated with the electricity available in the electric grid for each hourly period h of each representative day d. The obtained unit CO_2 emissions $kgCO2_e(d,h)$ are shown in Figure 4.13 and in Table 4.11.

Selling electricity displaces the consumption of electricity from the electric grid; therefore, the hourly CO_2 emissions associated with the electricity sold to the grid were considered to be equal to the emissions associated with the purchased electricity.
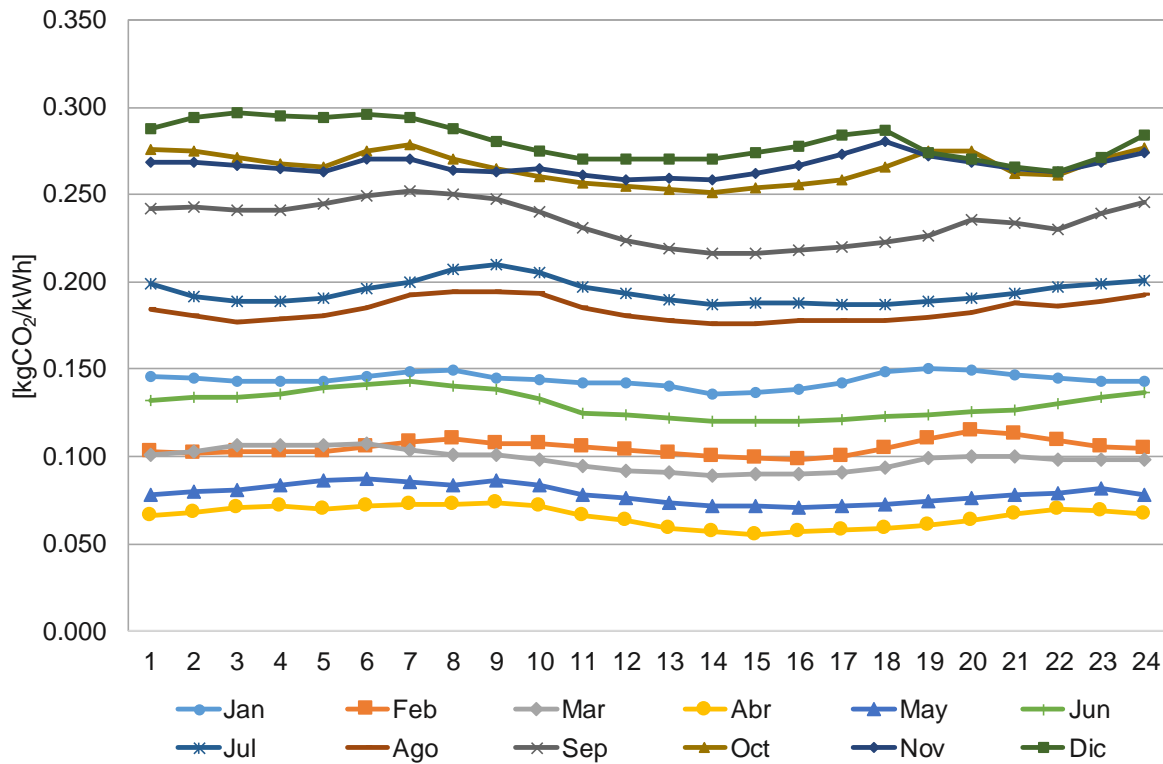
Figure 4.13: Hourly CO_2 emissions $kgCO2_e$ of the electricity in the Spanish electric grid of each representative day of the year 2016, in kg CO_2/kWh.

Table 4.11: Unit CO_2 emissions of the electricity in the Spanish electric grid for each representative day of the year 2016, in kg CO_2/kWh.

Hour	Jan	Feb	Mar	Apr	May	Jun	Jul	Aug	Sep	Oct	Nov	Dec
1	0.1459	0.1032	0.1009	0.0663	0.0777	0.1325	0.1990	0.1845	0.2420	0.2758	0.2689	0.2880
2	0.1452	0.1022	0.1029	0.0684	0.0798	0.1344	0.1920	0.1810	0.2425	0.2754	0.2682	0.2940
3	0.1435	0.1024	0.1062	0.0703	0.0812	0.1341	0.1890	0.1771	0.2407	0.2709	0.2672	0.2969
4	0.1435	0.1024	0.1061	0.0713	0.0837	0.1356	0.1891	0.1786	0.2416	0.2677	0.2649	0.2953
5	0.1429	0.1027	0.1062	0.0702	0.0863	0.1392	0.1907	0.1804	0.2445	0.2659	0.2635	0.2944
6	0.1463	0.1054	0.1071	0.0719	0.0871	0.1411	0.1958	0.1853	0.2494	0.2753	0.2705	0.2960
7	0.1486	0.1086	0.1036	0.0722	0.0850	0.1433	0.2002	0.1925	0.2523	0.2783	0.2704	0.2946
8	0.1492	0.1098	0.1008	0.0727	0.0837	0.1401	0.2072	0.1947	0.2500	0.2707	0.2641	0.2879
9	0.1450	0.1074	0.1007	0.0738	0.0859	0.1389	0.2100	0.1947	0.2471	0.2648	0.2631	0.2801
10	0.1439	0.1072	0.0978	0.0720	0.0832	0.1326	0.2052	0.1935	0.2402	0.2603	0.2650	0.2750
11	0.1425	0.1056	0.0943	0.0663	0.0782	0.1248	0.1969	0.1855	0.2312	0.2569	0.2610	0.2708
12	0.1420	0.1034	0.0919	0.0630	0.0759	0.1237	0.1935	0.1803	0.2233	0.2552	0.2587	0.2702
13	0.1404	0.1017	0.0906	0.0590	0.0731	0.1223	0.1901	0.1776	0.2192	0.2531	0.2592	0.2702
14	0.1361	0.1001	0.0894	0.0569	0.0714	0.1206	0.1872	0.1758	0.2163	0.2512	0.2583	0.2701
15	0.1363	0.0993	0.0897	0.0556	0.0718	0.1206	0.1879	0.1764	0.2166	0.2536	0.2619	0.2738
16	0.1382	0.0983	0.0898	0.0570	0.0706	0.1200	0.1878	0.1782	0.2185	0.2562	0.2663	0.2782
17	0.1419	0.0999	0.0906	0.0575	0.0713	0.1209	0.1872	0.1783	0.2196	0.2588	0.2734	0.2845
18	0.1485	0.1049	0.0938	0.0591	0.0727	0.1226	0.1871	0.1783	0.2227	0.2658	0.2806	0.2865
19	0.1505	0.1098	0.0990	0.0603	0.0745	0.1242	0.1888	0.1800	0.2269	0.2753	0.2725	0.2740
20	0.1496	0.1143	0.1003	0.0632	0.0759	0.1258	0.1904	0.1823	0.2352	0.2754	0.2682	0.2706
21	0.1465	0.1127	0.1004	0.0673	0.0783	0.1264	0.1936	0.1881	0.2334	0.2623	0.2646	0.2658
22	0.1445	0.1091	0.0986	0.0699	0.0786	0.1305	0.1970	0.1864	0.2297	0.2615	0.2633	0.2634
23	0.1435	0.1056	0.0981	0.0691	0.0815	0.1342	0.1992	0.1893	0.2389	0.2708	0.2689	0.2710
24	0.1432	0.1046	0.0985	0.0674	0.0783	0.1367	0.2006	0.1924	0.2456	0.2772	0.2740	0.2844

4.3   MATHEMATICAL MODEL

Having defined the superstructure of the trigeneration system and having collected and elaborated the necessary data on the consumer center, the next step is to develop a mathematical model representing the behavior and performances of all elements considered in the system. Chapter 2 presented the general formulation of a MILP model, which is composed of an objective function to be maximized or minimized, subject to equality and inequality constraints.

For the present study, a MILP model was developed to determine the optimal configuration of the system (installed technologies and their corresponding capacities) and the optimal hourly operation strategy throughout the year from the economic and environmental viewpoints. The MILP model employs binary variables to impose specific conditions on the structure (e.g. permission to install the technologies in the superstructure or not) and operation (e.g. operation modes of the reversible heat pump and flat-plate solar thermal collectors) of the system. Additionally, continuous variables are used to represent the energy, economic, and environmental flows. The MILP model was implemented and solved using the software LINGO (Schrage, 1999).

Some important assumptions have been made to reach a good compromise between model accuracy and computational effort: (i) the hourly energy demands, climatic data (ambient temperature and solar radiation), energy prices, and CO_2 emission factors are known before-hand and are considered constant in each time interval; (ii) the technologies' unit investment costs and the unit CO_2 emissions are independent from their corresponding installed capacities; (iii) the TES units work as a buffer in which thermal energy is stored (with losses) and consumed later at the same temperature level; and (iv) a daily cyclic operation of the TES units is considered assuming that the energy stored at the end of the representative day must be the same as the energy stored at the beginning of that day.

The economic and environmental aspects of installing and operating the trigeneration system are evaluated through the minimum total annual cost and minimum total annual CO_2 emissions, respectively, as described in Section 4.3.1. The objective functions are subject to equipment constraints, energy balances, and structural and operational restrictions, described in Section 4.3.2.

4.3.1   Objective functions

The economic objective function minimizes the total annual cost CTE_{tot} (in €/yr), which is the sum of the annual fixed cost CTE_{fix} and the annual operation cost CTE_{ope}, as expressed in Eq. (4.8).

$$CTE_{tot} = CTE_{fix} + CTE_{ope} \tag{4.8}$$

The annual fixed cost CTE_{fix} is expressed by Eq. (4.9).

$$CTE_{fix} = fam \cdot (1 + f_{IC}) \cdot \sum_i CI(i) \cdot CAP(i) \tag{4.9}$$

where $CAP(i)$ is the installed capacity of technology i.

As previously explained, it is assumed that the energy demands and the operation of the system are described by 12 representative days d (NRD = 12), each one composed of 24 consecutive periods h (NP = 24) of 1-hour duration ($NHP(h)$ = 1). The annual operation cost CTE_{ope} can be calculated according to Eq. (4.10).

$$CTE_{ope} = \sum_{d=1}^{NRD} \sum_{h=1}^{NP} NRY(d) \cdot NHP(h) \cdot CTE_{dh}(d,h) \tag{4.10}$$

where $CTE_{dh}(d,h)$ is the operation cost of the hourly period h of the representative day d, calculated according to Eq. (4.11), in which the first and second terms correspond to the purchase cost of natural gas and electricity and the third term corresponds to the revenue generated by selling electricity to the grid.

$$CTE_{dh}(d,h) = F_p(d,h) \cdot c_g + E_p(d,h) \cdot c_{ep}(d,h) - E_s(d,h) \cdot c_{es}(d,h) \tag{4.11}$$

Regarding the environmental objective, the goal is to minimize the total annual CO_2 emissions $CO2_{tot}$ (in kg CO_2/yr), expressed by Eq. (4.12), which is the sum of the annual fixed emissions $CO2_{fix}$ and the annual operation emissions $CO2_{ope}$.

$$CO2_{tot} = CO2_{fix} + CO2_{ope} \tag{4.12}$$

The annual fixed CO_2 emissions $CO2_{fix}$ is given by Eq. (4.13).

$$CO2_{fix} = \sum_i \frac{CO2U(i) \cdot CAP(i)}{nyr} \tag{4.13}$$

The annual CO_2 emissions $CO2_{ope}$ is expressed by Eq. (4.14).

$$CO2_{ope} = \sum_{d=1}^{NRD} \sum_{h=1}^{NP} NRY(d) \cdot NHP(h) \cdot CO2_{dh}(d,h) \tag{4.14}$$

where $CO2_{dh}(d,h)$ corresponds to the CO_2 emissions associated with the operation of the system in the hourly period h of the representative day d, calculated according to Eq. (4.15), in which the

first and second terms correspond to the emissions associated with the consumption of natural gas and the net electricity exchange with the electric grid, respectively.

$$CO2_{dh}(d,h) = F_p(d,h) \cdot kgCO2_g + \left(E_p(d,h) - E_s(d,h)\right) \cdot kgCO2_e(d,h) \tag{4.15}$$

4.3.2   System constraints

The objective functions are subject to equipment constraints (capacity limits and production restrictions), balance equations, and structural and operational restrictions, described in the following subsections.

4.3.2.1   Installed capacity limits

The common constraint to all technologies in the superstructure is the installed capacity limit, expressed by Eq. (4.16). For each technology *i*, the installed capacity *CAP(i)* is limited to the maximum installable capacity value $CAP_{MAX}(i)$, defined in Table 4.3.

$$CAP(i) \leq yINS(i) \cdot CAP_{MAX}(i) \tag{4.16}$$

where the binary variable *yINS(i)* expresses the permission to install or not the technology *i*.

Specific capacity limits apply to the reversible heat pump HP, photovoltaic panels PV, and flat-plate solar thermal collectors ST, as explained below.

Reversible heat pump – heating mode (HPQ) and cooling mode (HPR)

The HP's nominal capacity *CAP* and maximum installable capacity CAP_{MAX} have different values for heating mode (HPQ) and for cooling mode (HPR), which are related through the cooling/heating capacity ratio *RCAPrq*:

$$CAP_{MAX}(HPR) = RCAP_{rq} \cdot CAP_{MAX}(HPQ) \tag{4.17}$$
$$CAP(HPR) = RCAP_{rq} \cdot CAP(HPQ) \tag{4.18}$$

Photovoltaic panels (PV) and flat-plate solar thermal collectors (ST)

In the case of the PV and ST, their installation is limited to the rooftop area available *AA*, as expressed by Eq. (4.19). The ratios *rpv* and *rst* are used to relate the rooftop area occupied per m² of PV and ST module installed, respectively.

$$rpv \cdot CAP(PV) + rst \cdot CAP(ST) \leq AA \tag{4.19}$$

4.3.2.2   Production restrictions

The candidate technologies' production restrictions are described below, applicable to each hourly period h of each representative day d. The technical parameters of the technologies were previously presented in Table 4.3. The identifiable energy flows were described in Section 4.1.

Cogeneration module (GE)

The electricity produced by the cogeneration module $W_c(d,h)$ is limited to the installed capacity *CAP(GE)*, as expressed by Eq. (4.20). The electricity production depends on the GE electric power efficiency α_w, according to Eq. (4.21); likewise, the heat production depends on the GE thermal efficiency α_q, according to Eq. (4.22). The total cogenerated heat $Q_{cx}(d,h)$ produced by the technology corresponds to the sum of the low-temperature $Q_{cc}(d,h)$, high-temperature $Q_{cr}(d,h)$, and wasted $Q_{cl}(d,h)$ heat flows, as expressed by Eq. (4.23).

$$W_c(d,h) \leq CAP(GE) \tag{4.20}$$
$$\alpha_w \cdot F_c(d,h) - W_c(d,h) = 0 \tag{4.21}$$
$$\alpha_q \cdot F_c(d,h) - Q_{cx}(d,h) = 0 \tag{4.22}$$
$$Q_{cx}(d,h) = Q_{cc}(d,h) + Q_{cr}(d,h) + Q_{cl}(d,h) \tag{4.23}$$

Gas boiler (GB)

The total heat produced by the gas boiler $Q_{ax}(d,h)$ is limited to the installed capacity *CAP(GB)*, according to Eq. (4.24). In turn, the production in the GB is a function of its thermal efficiency η_q, as expressed by Eq. (4.25). The heat flow $Q_{ax}(d,h)$ is the sum of the low-temperature $Q_{ac}(d,h)$ and the high-temperature $Q_{ar}(d,h)$ heat flows, as expressed by Eq. (4.26).

$$Q_{ax}(d,h) \leq CAP(GB) \tag{4.24}$$
$$\eta_q \cdot F_a(d,h) - Q_{ax}(d,h) = 0 \tag{4.25}$$
$$Q_{ax}(d,h) = Q_{ac}(d,h) + Q_{ar}(d,h) \tag{4.26}$$

Reversible heat pump – heating mode (HPQ) and cooling mode (HPR)

The reversible heat pump consumes electricity to produce hot water when operating in heating mode (HPQ) and chilled water when operating in cooling mode (HPR). The operation modes are defined by the binary variables *yHPQ(d)* and *yHPR(d)*, given as input data for each representative day d, satisfying the restriction *yHPQ(d) + yHPR(d) ≤ 1*.

The heat $Q_{hp}(d,h)$ produced by the HPQ is limited to its installed capacity, which must be adjusted by the factor *fCAP_{hpq}(d,h)*, according to Eq. (4.27). The adjustment factor is given as input data to the optimization model; it takes into account off-nominal operation conditions, as explained in

Section 4.2.3.3. The same reasoning applies to the chilled water $R_{hp}(d,h)$ produced by the HPR, determined by Eq. (4.28).

$$Q_{hp}(d,h) \leq yHPQ(d) \cdot fCAP_{hpq}(d,h) \cdot CAP(HPQ) \tag{4.27}$$
$$R_{hp}(d,h) \leq yHPR(d) \cdot fCAP_{hpr}(d,h) \cdot CAP(HPR) \tag{4.28}$$

As expressed in Eq. (4.29), the electricity $W_{hp}(d,h)$ consumed by the HPQ and its production $Q_{hp}(d,h)$ are related through the COP_{hpq}, which must also be adjusted by a factor $fCOP_{hpq}(d,h)$, previously defined in Section 4.2.3.3. Analogously, Eq. (4.30) expresses the relation between the consumed electricity $W_{hp}(d,h)$ and the chilled water produced $R_{hp}(d,h)$ in the HPR.

$$Q_{hp}(d,h) = fCOP_{hpq}(d,h) \cdot COP_{hpq}(HPQ) \cdot W_{hp}(d,h) \tag{4.29}$$
$$R_{hp}(d,h) = fEER_{hpr}(d,h) \cdot EER_{hpr}(HPR) \cdot W_{hp}(d,h) \tag{4.30}$$

Single-effect absorption chiller (ABS)

The cooling produced $R_{abs}(d,h)$ is limited to the installed capacity *CAP(ABS)* adjusted by the factor *fCAP_{abs}(d,h)*, which takes into account the effect of varying ambient temperature, as expressed by

$$R_{abs}(d,h) \leq fCAP_{abs}(d,h) \cdot CAP(ABS) \tag{4.31}$$

The heat consumed by the absorption chiller $Q_{abs}(d,h)$ and its production $R_{abs}(d,h)$ are related through the COP_{abs}:

$$COP_{abs} \cdot Q_{abs}(d,h) - R_{abs}(d,h) = 0 \tag{4.32}$$

In addition, an auxiliary electricity consumption $W_{abs}(d,h)$ was considered for the operation of the absorption chiller, determined through the unit electricity consumption *kwabs*, as expressed by

$$W_{abs}(d,h) - kwabs \cdot R_{abs}(d,h) = 0 \tag{4.33}$$

Photovoltaic panels (PV)

The electricity produced by the photovoltaic panels *W_{pvx}(d,h)* is related to the hourly specific production per m² *x_{pv}(d,h)* and to the installed capacity *CAP(PV)* (Eq. (4.34)). From the total electricity produced *W_{pvx}(d,h)*, a part is used by the system *W_{pv}(d,h)* and, if necessary, a part may be wasted *W_{pvl}(d,h)* (Eq. (4.35)).

$$x_{pv}(d,h) \cdot CAP(PV) - W_{pvx}(d,h) = 0 \tag{4.34}$$
$$W_{pvx}(d,h) = W_{pv}(d,h) + W_{pvl}(d,h) \tag{4.35}$$

Flat-plate solar thermal collectors (ST)

As explained in Section 4.1, the solar thermal collectors can operate at high-temperature during the summer, to attend the cooling production, and at low-temperature for the rest of the year, to attend the thermal demand. The operation mode in each representative day *d* is defined by binary variables given as input data to the model: (i) *ySTR(d)*, for high-temperature operation; and (ii) *ySTQ(d)*, for low-temperature operation; satisfying the restriction *ySTQ(d) + ySTR(d) ≤ 1*.

The total heat produced $Q_{stx}(d,h)$ by the ST is assessed for the operation mode in the corresponding representative day *d* (Eq. (4.36)). Eq. (4.37) expresses the three components of the total heat produced, namely high-temperature heat *Qstr(d,h)*, low-temperature heat *Qstc(d,h)*, and dissipated heat *Qstl(d,h)*. An additional restriction is introduced by Eq. (4.38), which limits the heat production *Qstr(d,h)* in high-temperature operation to the installed capacity *CAP(ST)* and to the hourly specific production per m² *xstr(d,h)*.

$$\big(ySTQ(d) \cdot x_{stq}(d,h) + ySTR(d) \cdot x_{str}(d,h)\big) \cdot CAP(ST) - Q_{stx}(d,h) = 0 \qquad (4.36)$$
$$Q_{stx}(d,h) = Q_{str}(d,h) + Q_{stc}(d,h) + Q_{stl}(d,h) \qquad (4.37)$$
$$Q_{str}(d,h) \leq ySTR(d) \cdot x_{str}(d,h) \cdot CAP(ST) \qquad (4.38)$$

Thermal energy storages – hot water (TSQ) and chilled water (TSR)

Regarding the hot water storage tank TSQ, the energy stored $S_q(d,h)$ at the end of any hourly period is limited to the installed capacity *CAP(TSQ)*, as expressed by

$$S_q(d,h) \leq CAP(TSQ) \qquad (4.39)$$

The energy losses $Q_s(d,h)$ are equal to the stored energy at the end of the previous hourly period *Sq(d,h-1)* multiplied by the energy loss factor *fpacuQ*.

$$Q_s(d,h) = fpacuQ \cdot S_q(d,h-1) \qquad (4.40)$$

The energy balance in the TSQ is given by Eq. (4.41). The charged *Qin(d,h)*, discharged *Qout(d,h)*, and losses *Qs(d,h)* energy flows, in kW, are multiplied by the duration of the period *NHP(h)* in order to convert them to the same units as the stored energy *Sq(d,h)*, kWh. Considering the daily cyclical characteristic of the thermal energy storage, the energy stored at the beginning must be equal to the energy stored at the end of each representative day.

$$S_q(d,h-1) + \big(Q_{in}(d,h) - Q_{out}(d,h) - Q_s(d,h)\big) \cdot NHP(h) - S_q(d,h) = 0 \qquad (4.41)$$

The same considerations are made for the chilled water storage tank TSR, thus obtaining the following equations:

$$S_r(d,h) \leq CAP(TSR) \tag{4.42}$$

$$R_s(d,h) = fpacuR \cdot S_r(d,h-1) \tag{4.43}$$

$$S_r(d,h-1) + \big(R_{in}(d,h) - R_{out}(d,h) - R_s(d,h)\big) \cdot NHP(h) - S_r(d,h) = 0 \tag{4.44}$$

4.3.2.3   Energy balances

Equations (4.45)-(4.49) express the electricity, natural gas, low-temperature heat, high-temperature heat, and cooling balances in each time interval, respectively.

$$E_p(d,h) + W_c(d,h) + W_{pv}(d,h) - E_s(d,h) - W_{hp}(d,h) - W_{abs}(d,h) - E_d(d,h) = 0 \tag{4.45}$$

$$F_p(d,h) - F_c(d,h) - F_a(d,h) = 0 \tag{4.46}$$

$$Q_{cc}(d,h) + Q_{ac}(d,h) + Q_{hp}(d,h) + Q_{stc}(d,h) + Q_{out}(d,h) - Q_{in}(d,h) - Q_d(d,h) = 0 \tag{4.47}$$

$$Q_{cr}(d,h) + Q_{ar}(d,h) + Q_{str}(d,h) - Q_{abs}(d,h) = 0 \tag{4.48}$$

$$R_{abs}(d,h) + R_{hp}(d,h) + R_{out}(d,h) - R_{in}(d,h) - R_d(d,h) = 0 \tag{4.49}$$

4.3.2.4   Structural and operational restrictions

The MILP model employs binary variables to represent: (i) structural conditions, such as the permission to install the candidate technologies in the superstructure; and (ii) operational conditions, such as the operation modes of the technologies (e.g. HP in heating mode or in cooling mode; ST operating at high-temperature or low-temperature), the interconnection with the electric grid (e.g. whether electricity purchase and sale are allowed or not), and the TES units charging and discharging operation mode.

Structural restrictions

The structural restriction is given by Eq. (4.16), in which *yINS(i)* corresponds to the binary variable 1/0 indicating that the technology *i* can/cannot be installed.

For the case study analyzed herein, all candidate technologies were allowed to be installed, thus: $yINS(i) = 1, \forall\, i$.

Operational restrictions

Operational restrictions apply for the reversible heat pump HP and for the flat-plate solar thermal collectors ST.

In the HP's operational restrictions, given by Eq. (4.27) and Eq. (4.28), *yHPQ(d)* is the binary variable 1/0 expressing that the HP operates/does not operate in heating mode in the representative day *d*, and *yHPR(d)* is the binary variable 1/0 expressing that the HP operates/does not operate in cooling mode in the representative day *d*.

In accordance with the explanation provided in Section 4.1, Table 4.12 shows the binary variables' values for the representative days of the months of the year.

Table 4.12: Binary variables for the HP's operation modes for each representative day.

Binary variable	1	2	3	4	5	6	7	8	9	10	11	12
yHPQ	1	1	1	1	1	0	0	0	0	1	1	1
yHPR	0	0	0	0	0	1	1	1	1	0	0	0

The ST's operational restrictions are given by Eq. (4.36) and Eq. (4.37), in which *ySTQ(d)* is the binary variable 1/0 indicating that the ST operates/does not operate at low-temperature in the representative day *d*, and *ySTR(d)* is the binary variable 1/0 indicating that the ST operates/does not operate at high-temperature in the representative day *d*.

In accordance with the explanation provided in Section 4.1, Table 4.13 shows the binary variables' values for the representative days of the months of the year.

Table 4.13: Binary variables for the ST's operation modes for each representative day.

Binary variable	1	2	3	4	5	6	7	8	9	10	11	12
ySTQ	1	1	1	1	1	0	0	0	0	1	1	1
ySTR	0	0	0	0	0	1	1	1	1	0	0	0

Electric grid restrictions

The permission to purchase electricity from the grid and the permission to sell electricity to the grid are expressed by Eq. (4.50) and Eq. (4.51), respectively.

$$E_p(d,h) \leq yp \cdot \left(W_{hp}(d,h) + W_{abs}(d,h) + E_d(d,h) \right) \tag{4.50}$$

$$E_s(d,h) \leq ys \cdot \left(W_c(d,h) + W_{pv}(d,h) \right) \tag{4.51}$$

where *yp* is the binary variable 1/0 indicating that the system can/cannot purchase electricity from the grid, and *ys* is the binary variable 1/0 indicating that the system can/cannot sell electricity to the grid.

As previously explained, for the case study analyzed herein the system is allowed to both purchase and sell electricity, thus: $yp = 1$ and $ys = 1$.

Nevertheless, electricity purchase and sale cannot take place simultaneously in each hourly period. Therefore, the binary variables *yep(d,h)* and *yes(d,h)* were used to indicate that the system is/is not purchasing electricity and is/is not selling electricity, respectively, at the corresponding hourly period *h* of the representative day *d*. Their values are defined by the optimization model, satisfying the following condition:

$$yep(d,h) + yes(d,h) \leq 1 \tag{4.52}$$

In order to avoid a nonlinearity, the constant *BIGM*, with a very large value (i.e. 1,000,000), was introduced. The following equations were thus obtained:

$$E_p(d,h) \leq yep(d,h) \cdot BIGM \tag{4.53}$$
$$E_s(d,h) \leq yes(d,h) \cdot BIGM \tag{4.54}$$
$$yep(d,h) \leq yp \tag{4.55}$$
$$yes(d,h) \leq ys \tag{4.56}$$

TES charging and discharging restrictions

Regarding the TES units, there is an imposed condition which establishes that charging and discharging cannot take place simultaneously. Therefore, for the operation of the TSQ, the binary variables *yqin(d,h)* and *yqout(d,h)* were used to indicate that the tank is/is not charging and is/is not discharging at the hourly period *h* of the representative day *d.* Their values are defined by the optimization model, satisfying the following condition:

$$yqin(d,h) + yqout(d,h) \leq 1 \tag{4.57}$$

As previously explained, the constant *BIGM* was used in Eq. (4.58) and Eq. (4.59) to avoid nonlinearities.

$$Q_{in}(d,h) \leq yqin(d,h) \cdot BIGM \tag{4.58}$$
$$Q_{out}(d,h) \leq yqout(d,h) \cdot BIGM \tag{4.59}$$

The same reasoning was applied to the TSR, thus defining the binary variables *yrin(d,h)* and *yrout(d,h)*, which appear in the following Equations:

$$yrin(d,h) + yrout(d,h) \leq 1 \tag{4.60}$$
$$R_{in}(d,h) \leq yrin(d,h) \cdot BIGM \tag{4.61}$$
$$R_{out}(d,h) \leq yrout(d,h) \cdot BIGM \tag{4.62}$$

4.4   SINGLE-OBJECTIVE OPTIMIZATION

As a first approach to the multi-objective optimization, the objective functions were assessed individually. The single-objective optimization solutions obtained were analyzed and compared with each other and with the reference system considered herein, thus providing essential information for the determination of the trade-off solutions between them.

Table 4.14 presents the main results obtained for the minimization of the total annual cost and the total annual CO_2 emissions. The following subsections provide an in-depth explanation of the results.

Table 4.14: Main results, single-objective optimization solutions.

	Technology	Optimal total annual cost (B)				Optimal total annual CO_2 emissions (A)			
		Installed capacity	Load factor	Investment cost €/yr	CO_2 emissions kg CO_2/yr	Installed capacity	Load factor	Investment cost €/yr	CO_2 emissions kg CO_2/yr
GE	Cogeneration module	4.2 kW_{el}	0.88	2050.8	13.7	0.0 kW_{el}	-	-	-
GB	Gas boiler	204.8 kW	0.13	2838.1	102.4	49.3 kW	0.00	683.1	24.6
HP	Heat pump	162.1 kW	0.50	14,031.7	1296.5	269.6 kW	0.40	23,343.1	2156.9
ABS	Absorption chiller	94.0 kW	0.02	8761.6	775.2	48.8 kW	0.07	4554.4	403.0
PV	Photovoltaic panels	0.0 m^2	-	-	-	461.2 m^2	0.17	21,873.1	6571.6
ST	Solar thermal collectors	0.0 m^2	-	-	-	246.5 m^2	0.10	25,618.8	1170.7
TSQ	Hot water storage tank	0.4 kWh	-	10.8	3.0	314.0 kWh	-	8449.1	2354.8
TSR	Chilled water storage tank	39.9 kWh	-	2148.9	598.9	0.0 kWh	-	-	-
Annual fixed cost CTE_{fix} and emissions $CO2_{fix}$				29,841.9	2789.8			84,521.6	12,681.6

Energy resource	Consumption kWh/yr	Energy cost €/yr	CO_2 emissions kg CO_2/yr	Consumption kWh/yr	Energy cost €/yr	CO_2 emissions kg CO_2/yr
Natural gas	363,285.1	20,557.7	91,547.8	124.2	7.0	31.3
Purchased electricity	355,040.0	54,667.3	60,728.1	355,919.7	54,606.8	63,048.5
Sold electricity	-	-	-	9348.0	1505.1	1521.3
Annual operation cost CTE_{ope} and emissions $CO2_{ope}$	75,225.0	152,275.9		53,108.7	61,558.5
Total annual cost CTE_{tot} and emissions $CO2_{tot}$	**105,066.9**	155,065.7		137,630.2	**74,240.1**

4.4.1   Economic cost optimization

The main results obtained for the total annual cost optimal solution are shown in Table 4.14, including both the capital (installed technologies) and the operation (energy services consumption) aspects of the system. This information is complemented by Figure 4.14, which depicts the optimal configuration of the system, indicating the installed capacities of the technologies and the annual energy flows.
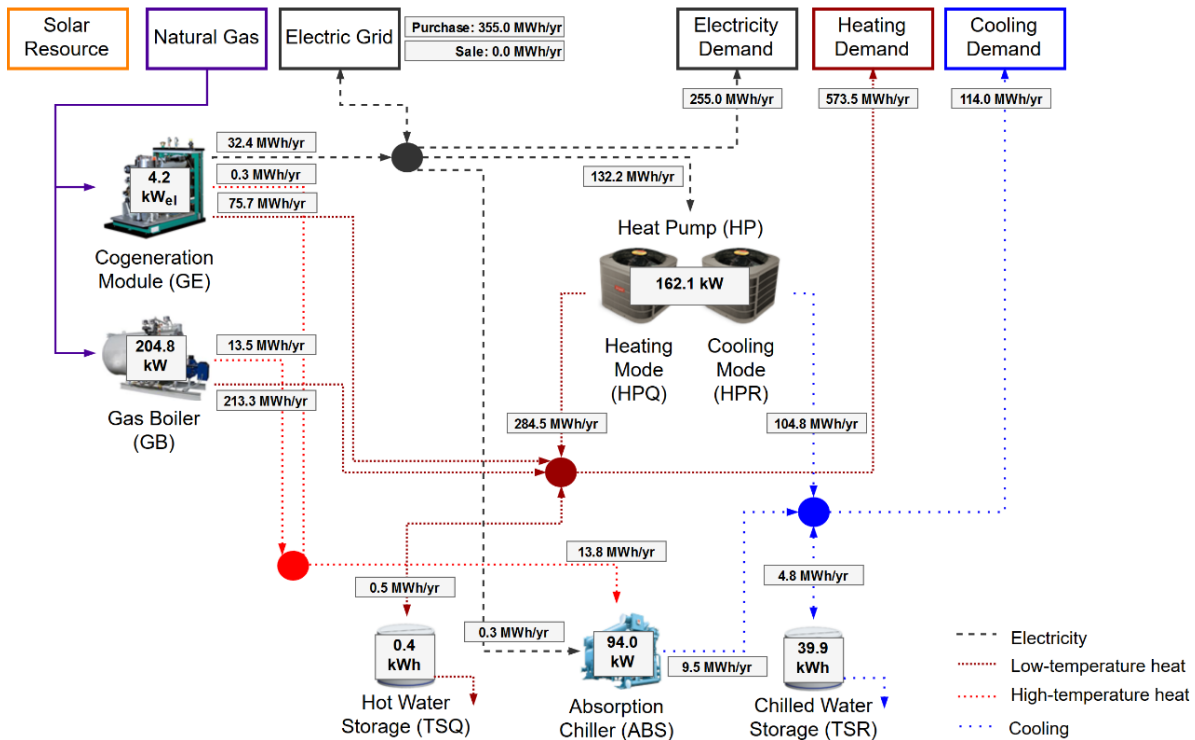
Figure 4.14: Installed capacities and annual energy flows – Optimal total annual cost solution.

The minimum total annual cost CTE_{tot} of 105,066.9 €/yr was obtained, 72% of which corresponds to energy consumption costs and 28% to the investment cost. The corresponding total annual CO_2 emissions $CO2_{tot}$ was equal to 155,065.7 kg CO_2/yr, the vast majority of which (98%) being attributable to the purchased electricity and natural gas.

For the optimal total annual cost solution, all candidate technologies were included except for the RETs (PV and ST); additionally, the TSQ installed capacity is so small (0.4 kWh) that it can be neglected. Regarding the annual investment cost, 47% is due to the installation of HP, followed by the ABS, with 29%, and the GB, with 10%. Taking into account the annual CO_2 emissions relative to the manufacturing of each technology, the HP also accounts for the highest share of emissions (46%), followed by the ABS, with 28%, and the TSR, with 21%. As regards the annual consumption of energy resources, the optimal total annual cost solution heavily relies on natural gas and electricity from the electric grid. Furthermore, all the electricity produced by the system (i.e. in the cogeneration module GE) is consumed, so there is no sale to the grid. The annual operation

cost shows that the purchased electricity accounts for 73%, the remaining 27% being associated with the purchase of natural gas. Conversely, the associated CO_2 emissions are mostly attributed to the natural gas consumption (60%).

Analyzing the annual operation of the system, the GE, GB, and HP operate all year round, while the ABS and the TSR operate only during the summertime (from June to September), when cooling is required. Considering the electricity consumption (internal consumption and electricity demand), 8.4% is produced by the GE and the rest is purchased from the electric grid. Even though the installed capacity of GE is relatively small, it operates with the highest load factor (88%) compared to the other technologies. Regarding the heat production, the HP and the GB are the major producers, with 48.4% and 38.6%, respectively. The GB, on the other hand, presents a relatively low load factor (13%), as it operates mostly during the wintertime, when the heating demand is higher. The cooling production takes place almost entirely in the HP (91.7%), being the ABS only used to attend peak demands in July and August with heat produced by the GB, hence the low load factor (2%). The dual operation of the HP (i.e. heating mode and cooling mode) allows for a prolonged operation throughout the year, resulting in a load factor of 50%. Considering the total cooling produced by the system, 4.5% of it is stored in the TSR.

The annual energy flows are obtained by consolidating the hourly operation of the system for each representative day of the year. Two examples are provided: (i) Figure 4.15 presents the optimal hourly electricity and heating productions of the system in January; and (ii) Figure 4.16 presents the optimal hourly electricity, heating, and cooling productions of the system in July.

In January, only electricity E_d and heating Q_d are required by the consumer center. The hourly electricity production is characterized by purchase from the electric grid E_p and by a continuous operation of the GE throughout the day, producing cogenerated electricity W_c and heat Q_{cc}. In particular, between hours 6 and 24, the GE operates at full load. It is interesting to notice the increase in E_p at hours 7 and 8, which corresponds to: (i) the end of the off-peak electricity rate (see Table 4.8); and (ii) the beginning of the heating demand Q_d. Apart from the electricity demand, electricity is also consumed by the HP from hour 6 to 20 for heat production Q_{hp}. The heat production is also supported by the GB with Q_{ac} and Q_{ar}. The HP's load increases in the afternoon, after hour 11; it also complements the heat production when the GB is operating at full load, e.g. hours 9 to 11 and 19 to 20.

In the month of July, electricity E_d, heating Q_d and cooling R_d are required by the consumer center. The GE operation is similar to the one in January, and the system also purchases electricity E_p throughout the day. In the summertime (from June to September), the HP operates in cooling mode, thus consuming electricity W_{hp} to produce cooling R_{hp}. The heat production is covered by

the GE and the GB. The HP provides most of the required cooling, leaving the ABS to cover the peak demands with heat from the GB, at hours 15 to 17, when the HP is at full load. It is interesting to notice that even though the cooling demand starts at hour 12, its production begins earlier in the day at hour 8. This hour corresponds to the end of the off-peak electricity rate period (see Table 4.8), so the system can take advantage of the TSR to store cooling produced with cheaper electricity and use it at hour 15 to displace the more expensive operation of the ABS.
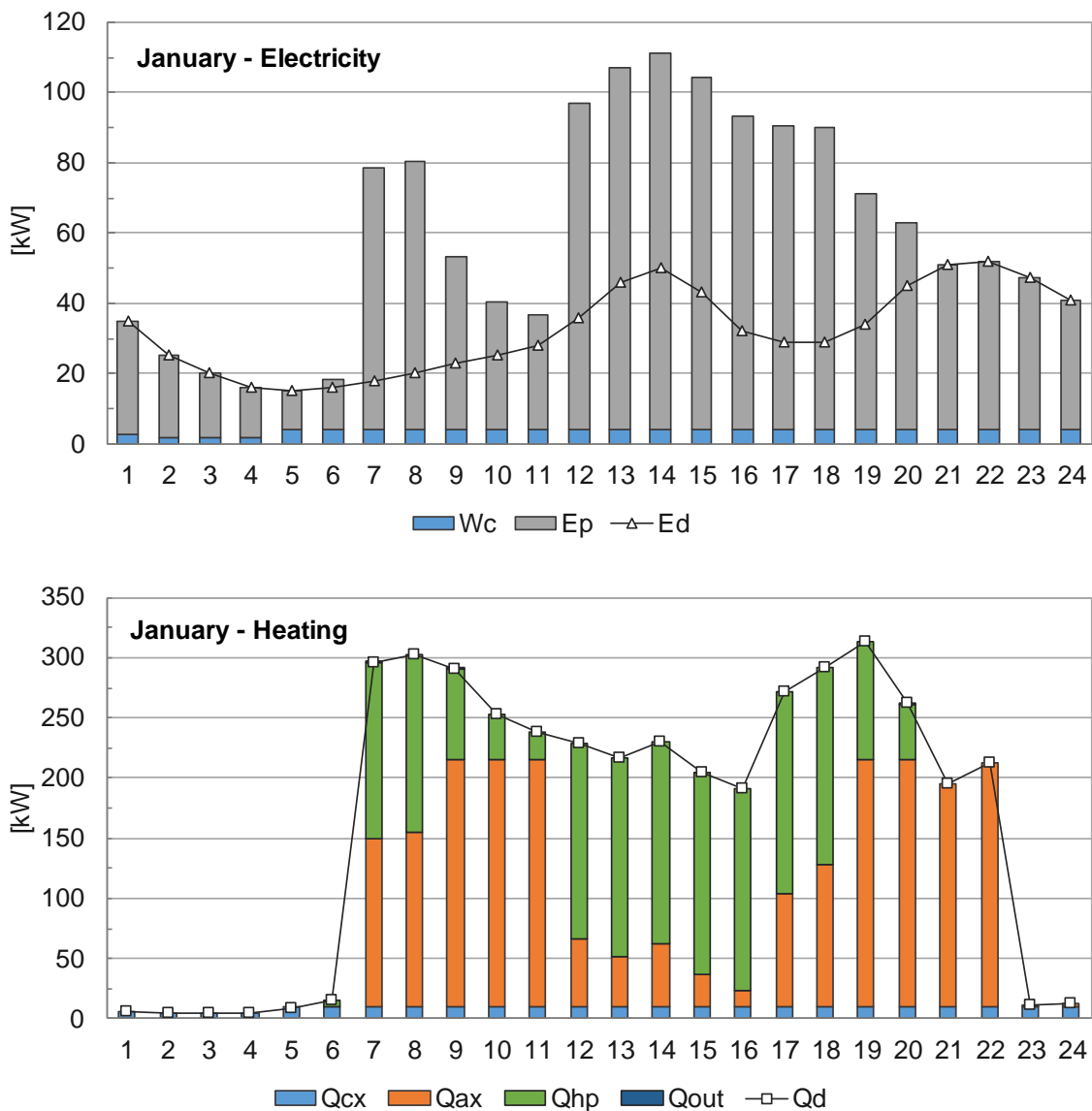
Figure 4.15: Hourly electricity and heating productions in January – Optimal total annual cost solution.
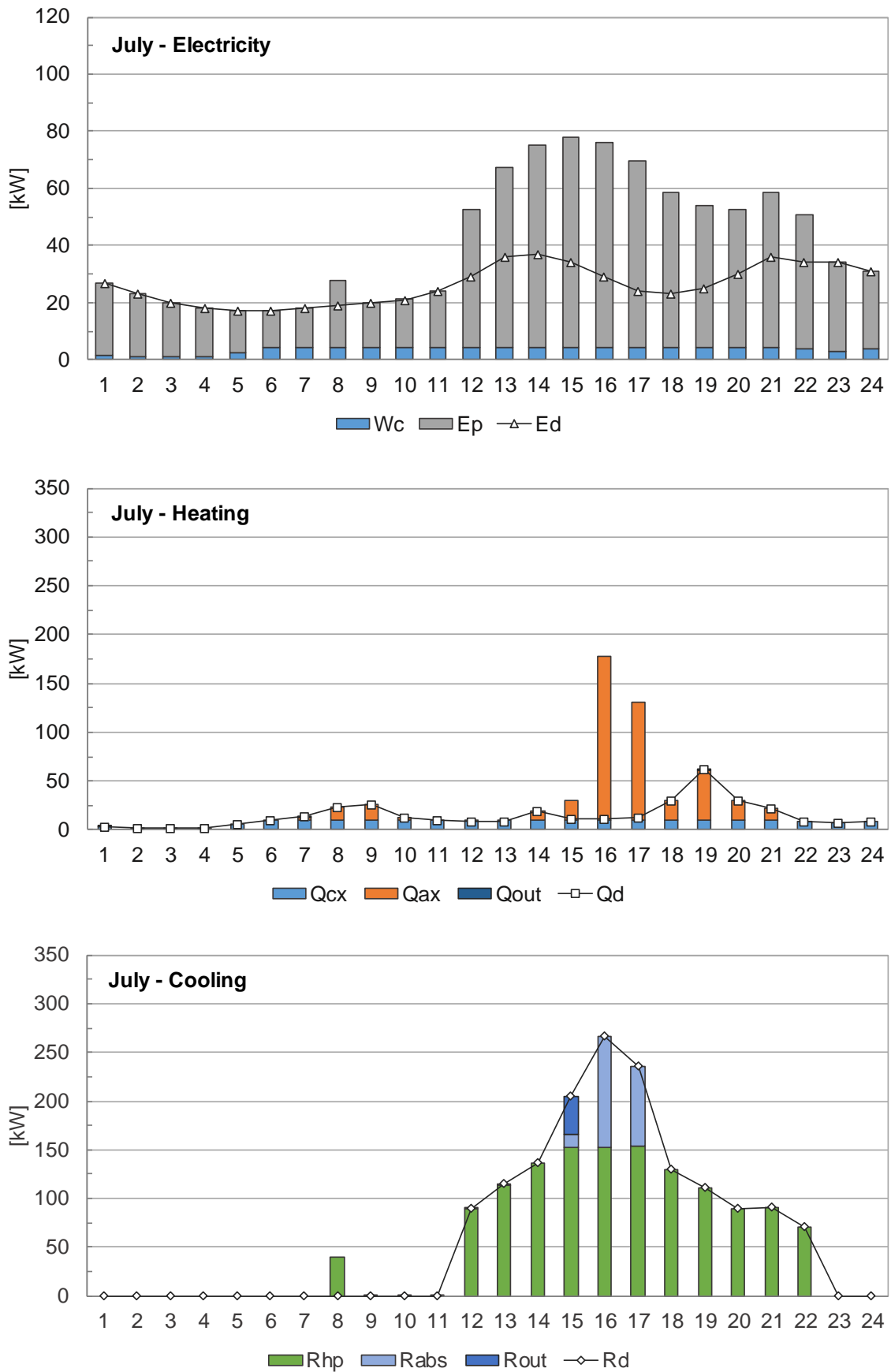
Figure 4.16: Hourly electricity, heating, and cooling productions in July – Optimal total annual cost solution.

4.4.2 Environmental optimization

Analogous to the economic cost optimization, the main results for the optimal total annual CO_2 emissions solution are shown in Table 4.14 and Figure 4.17.
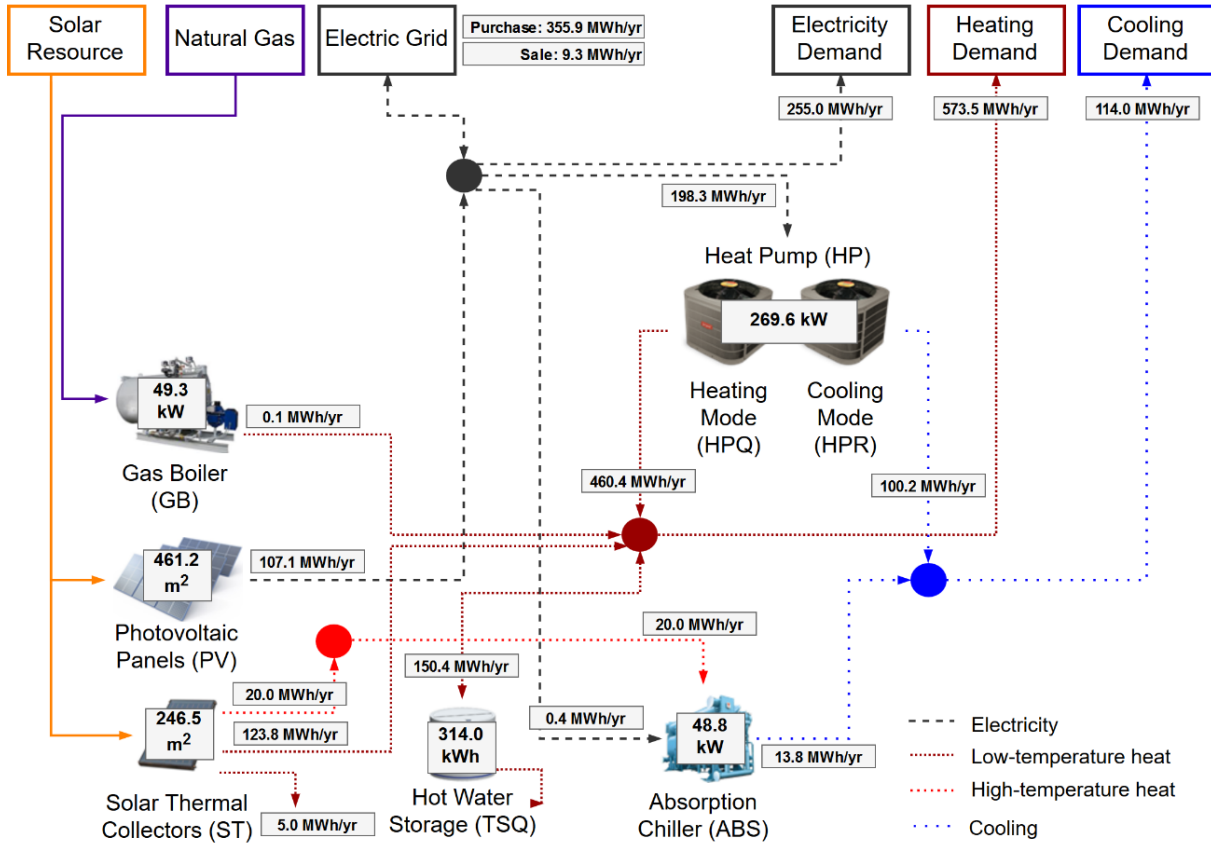
Figure 4.17: Installed capacities and annual energy flows – Optimal total annual CO_2 emissions solution.

The minimum total annual CO_2 emissions $CO2_{tot}$ equal to 74,240.1 kg CO_2/yr was obtained, 83% of which being attributable to the annual operation of the system and the remaining 17% to the technologies manufacturing and installation. The corresponding total annual cost CTE_{tot} was equal to 137,630.2 €/yr, being 61% related to the investment cost and 39% to the annual operation of the system.

In the case of the optimal total annual CO_2 emissions solution, all candidate technologies were included except for the GE and TSR. It is interesting to notice that all the rooftop area is used for the installation of PV and ST. Regarding the annual investment cost, the three highest shares are attributable to the installation of ST (30%), HP (28%), and PV (26%). By contrast, considering the annual CO_2 emissions associated with the manufacturing of the technologies, the three highest shares are the following: PV (52%), TSQ (19%), and HP (17%). As regards the annual consumption of energy resources, the optimal total annual CO_2 emissions solution heavily relies on the

electricity purchased from the electric grid. On the other hand, there is virtually no consumption of natural gas. Consequently, the economic cost and CO_2 emissions associated with the annual operation of the system are almost entirely due to the purchase of electricity from the grid. There are, however, hours in which the electricity produced is sold to the electric grid. In fact, 8.7% of the electricity produced by the system is sold to the grid, generating 1505.1 €/yr of economic profits and displacing 1521.3 kg CO_2/yr of emissions associated with the electricity available in the electric grid.

Analyzing the annual operation of the system, the PV, ST, and TSQ operate all year round; the HP also operates throughout the year, except for the month of May; the ABS operates all summer, except for September; and the GB operates marginally in June to cover heat peak demands. It is worth mentioning that there is dissipation of heat Q_{stl} from the ST in May (33.1% of the heat produced by the ST in the month). The PV produces 23.6% of the electricity consumed by the system (internal consumption and electricity demand), while the rest is purchased from the electric grid. The HP is responsible for 76.2% of the heat produced by the system, followed by the ST with 23.8%; the GB has a negligible share. From the total heat produced by the system, 26.7% is stored in the TSQ. Cooling is produced mostly in the HP (87.9%), the rest being covered by the ABS with solar heat Q_{str} from the ST.

The annual energy flows are obtained by consolidating the hourly operation of the system for each representative day of the year. Two examples are provided herein: (i) Figure 4.18 presents the optimal hourly electricity and heating productions of the system in January; and (ii) Figure 4.19 presents the optimal hourly electricity, heating, and cooling productions of the system in July.

In January, only electricity E_d and heating Q_d are required by the consumer center. The system must purchase electricity E_p from the grid throughout the day. The PV electricity production W_{pv} peaks at hours 12 and 13. Apart from the electricity demand E_d, electricity is also consumed by the HP to produce heating Q_{hp}. As can be seen, heating is produced and stored at several hours of the day (hours 4, 5, 13 to 17, and 24). The reason for this operation strategy is derived from the hourly CO_2 emissions associated with the electricity available in the electric grid, as depicted in Figure 4.13. In fact, these hours are the ones with the lowest CO_2 emissions, so the system takes advantage of its storage capacity to produce heating with lower related environmental impacts. The TSQ is discharged Q_{out} at hours 7 to 9 and 18 to 20, when the electricity-related CO_2 emissions are the highest. Regarding the solar heating production Q_{stx}, it peaks at hour 13.

Now, in July, cooling R_d is also required, apart from the E_d and Q_d. The PV electricity production W_{pv} is considerably higher than in January, which enables the system to sell electricity to the electric grid from hour 8 to 11. Likewise, the solar heat produced by the ST is enough so that it can

cover the whole daily heating demand (instantaneously and through the storage in the TSQ), as well as a part of the cooling demand through the ABS. Regarding the cooling production, the HP provides most of the cooling required. The ABS at hours 13 to 16 displaces HP production, thus reducing the amount of electricity purchased from the grid and, consequently, the corresponding CO_2 emissions.
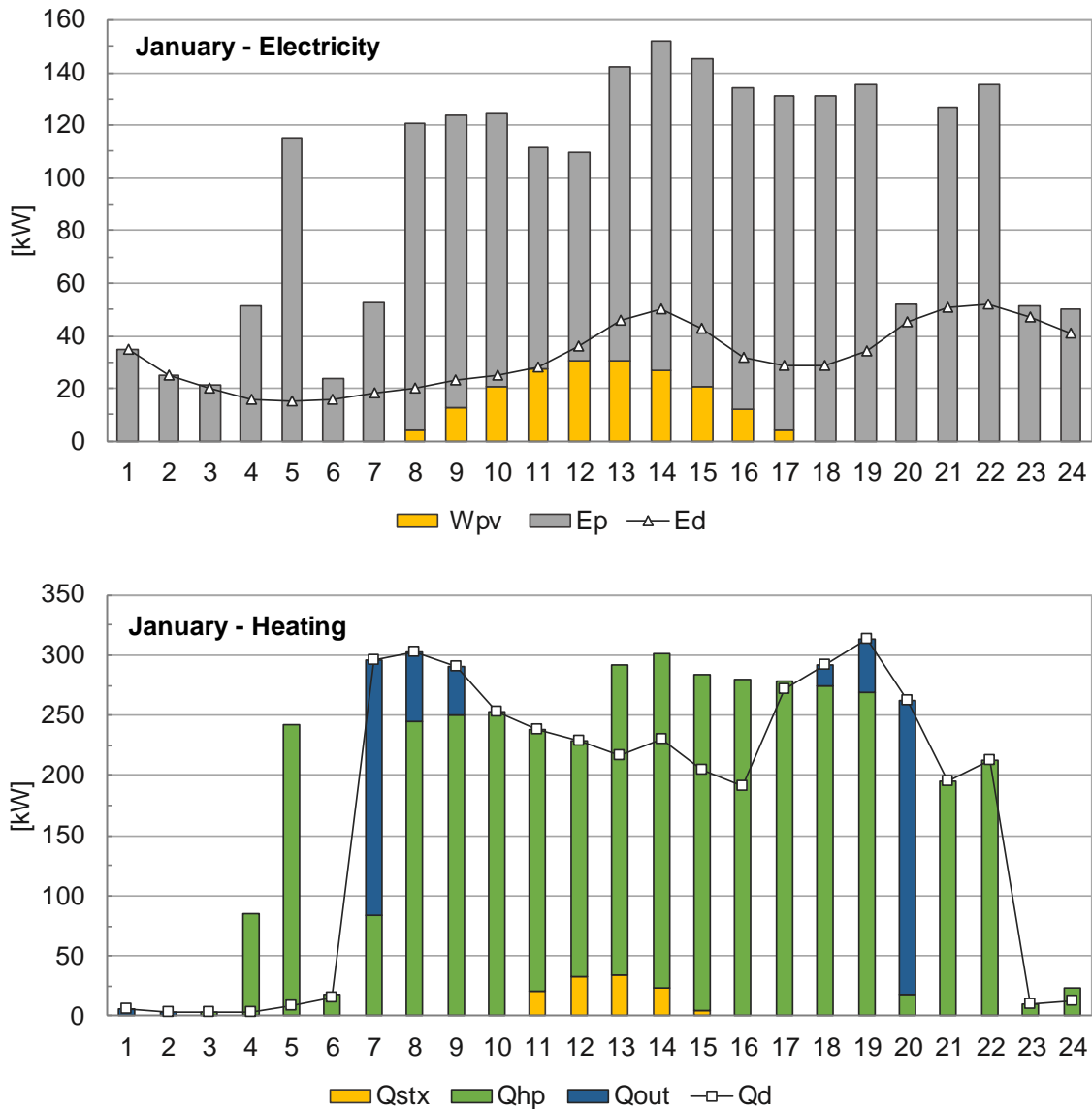
Figure 4.18: Hourly electricity and heating productions in January – Optimal total annual CO_2 emissions solution.
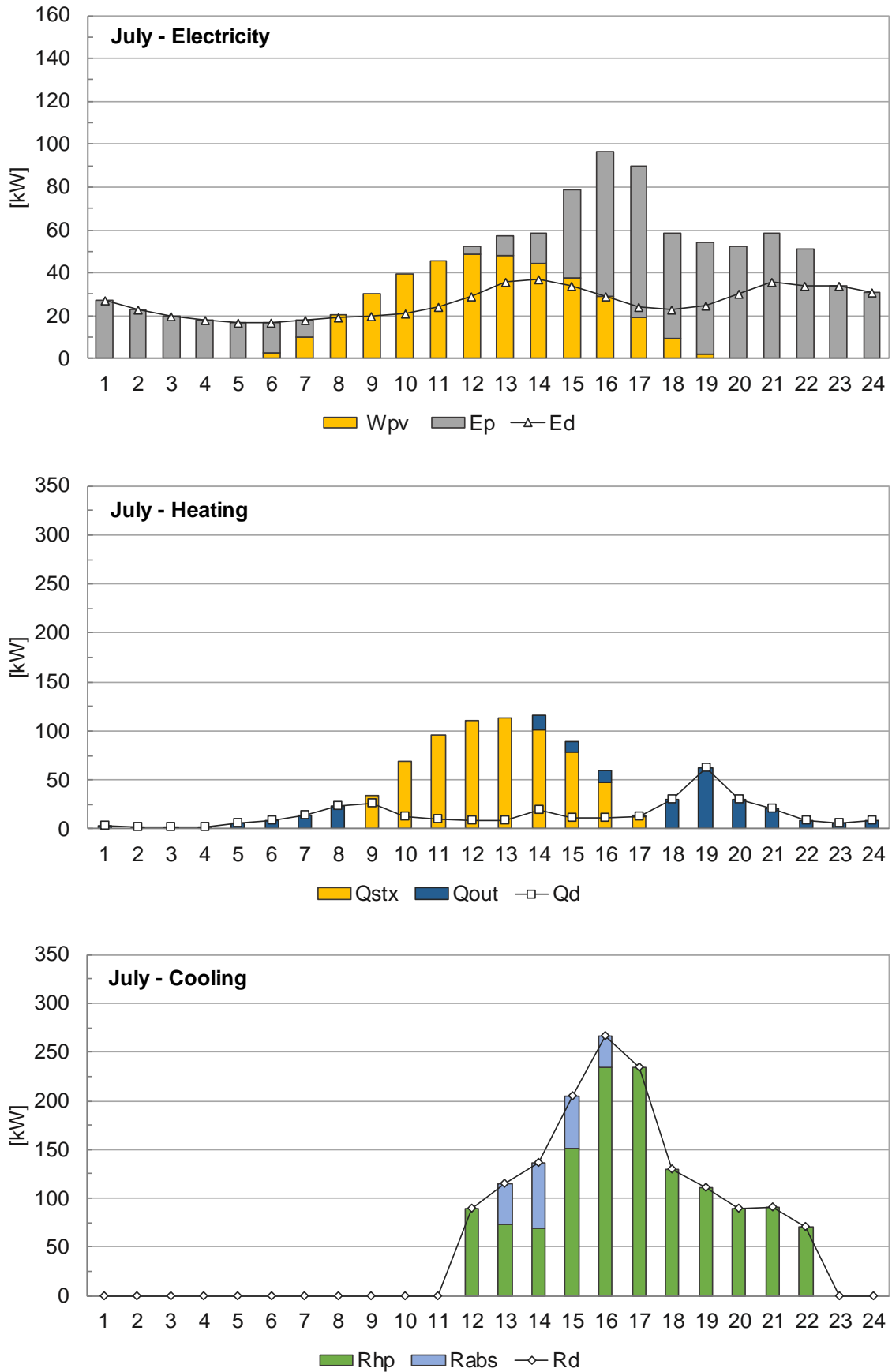
Figure 4.19: Hourly electricity, heating, and cooling productions in July – Optimal total annual CO_2 emissions solution.

4.4.3   Optimal economic and environmental solutions comparison

The following points were drawn from the analysis of the single-objective solutions obtained:

- The optimal annual cost solution included the cogeneration module GE, but not the renewable energy technologies (PV and ST), while the optimal environmental solution included both the PV and ST, but not the GE. In fact, the installation of PV and ST occupied all the available rooftop area, reaching the upper constraint of maximum installable capacity;

- Compared with the optimal annual cost solution, the optimal environmental solution presented a higher installed capacity of HP and lower installed capacities of GB and ABS, which suggests that, for the conditions considered herein, electricity-based heating and cooling production is a more environmentally sound alternative to natural gas;

- Also, there was a significant shift in the use of thermal energy storage not only in type but also in quantity (from 39.9 kWh of TSR in the optimal annual cost solution to 314.0 kWh of TSQ in the optimal environmental solution);

- Regarding the consumption of energy resources, both solutions are highly dependent on the electricity from the electric grid. Nevertheless, the optimal annual cost solution is also significantly dependent on the purchase of natural gas. Even though a small quantity, the optimal environmental solution is able to sell electricity to the grid, thus generating economic profit and avoiding CO_2 emissions relative to the purchase of electricity from the grid;

- In both economic and environmental optimal solutions, the systems take advantage of time-varying electricity prices and CO_2 emissions to achieve lower operating costs and lower environmental impacts; these effects mostly take place in the HP either producing heating or cooling;

- The optimal environmental solution presents a total annual cost 31% higher than the optimal annual cost solution, while the CO_2 emissions are 52% lower. The shift towards a more environmentally sound configuration leads to an increase of 183% in the annual fixed cost and 354% in the annual CO_2 emissions relative to manufacturing and installation of technologies. On the other hand, such increased costs are offset by a better energy use throughout the operation of the system, which is translated into a decrease of 29% in the annual operation costs and 59% in the annual CO_2 emissions associated with the operation of the system; and

- While annual fixed CO_2 emissions in the optimal annual cost solution represent only 1.8% of the total annual emissions, they are more significant in the optimal environmental solution (17.1%).

4.5   MULTI-OBJECTIVE OPTIMIZATION

The multi-objective optimization tackles the issue of conflicting objectives, such as the minimization of total annual cost and total annual CO_2 emissions. As explained in Chapter 2, for such cases there is not a single optimal solution that fulfills both objectives, but a set of trade-off solutions that constitute the Pareto set in which no improvement in one objective can be achieved without sacrificing the other (Andiappan, 2017).

Following the procedure explained in Section 2.2.3, the ε-constraint method was applied herein to determine the Pareto set. Considering the total annual cost as the objective function, the other objective function was converted into an inequality constraint, thus imposing an upper limit to the total annual CO_2 emissions of the system. The single-objective optimization solutions described in the previous section constitute the limits of the Pareto set. As depicted in Figure 4.20, the Pareto set is found within an upper limit of 155.1 ton CO_2/yr (relative to the optimal annual cost solution) and a lower limit of 74.2 ton CO_2/yr (relative to the optimal environmental solution).
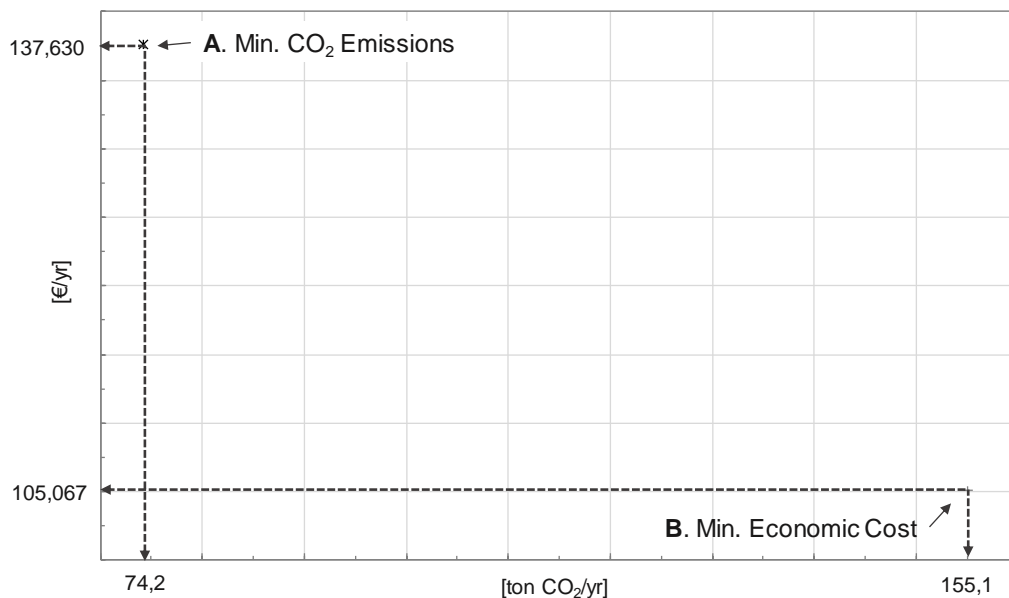
Figure 4.20: Single-objective optimization solutions – Superior and inferior limits to the Pareto set.

The interval between upper and lower limits have been divided and the model was repeatedly solved. Table 4.15 presents the complete set of results obtained, indicating the ε values considered in the procedure starting from the optimal annual cost solution (point B) towards the optimal annual CO_2 emissions solution (point A). Along the Pareto set, different solutions are obtained with different configurations and installed capacities. Figure 4.21 shows the Pareto set obtained, in which equal symbols represent the same configuration (with different installed capacities). As can be seen from Table 4.15, a total of 33 ε values were evaluated, obtaining 9 different configurations. Moreover, the different installed capacities along the Pareto set were plotted in the graphs of Figure 4.22.

The analysis of the trade-off solutions that constitute the Pareto set shows that each candidate technology was included in at least one solution; on the other hand, there was no solution that simultaneously included the eight candidate technologies. The GB and the HP were included in all solutions obtained, and the TSR was present in most of them. It is worth noticing that the GE was not included in any solution together with the PV and/or ST.
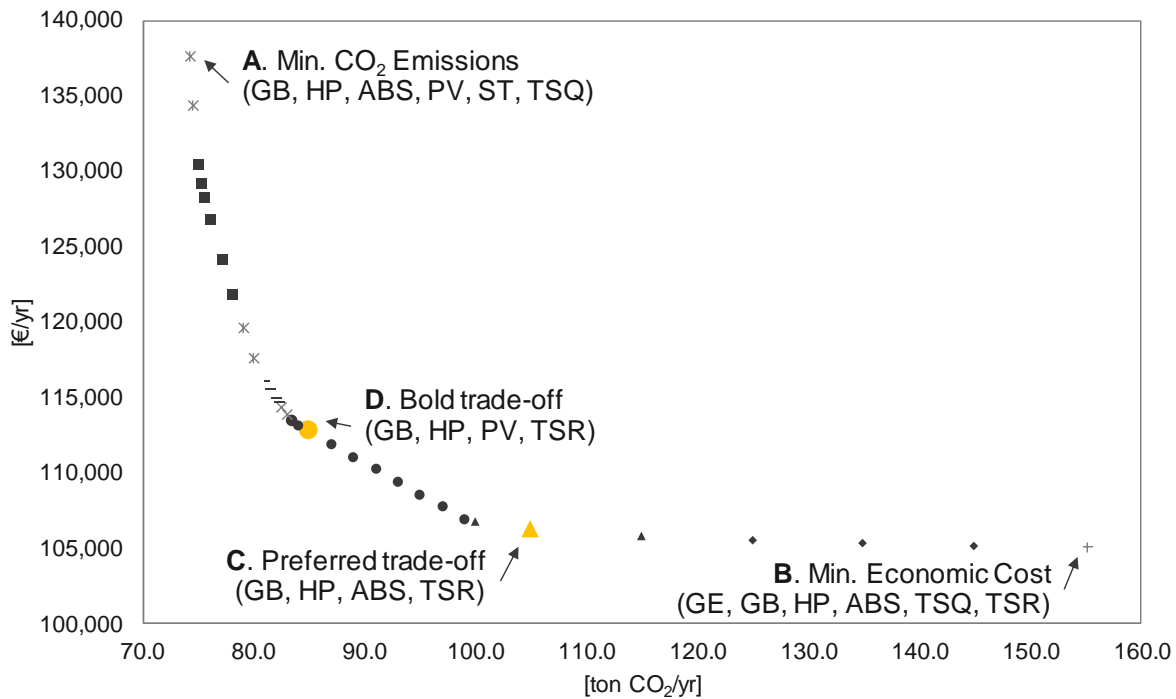
Figure 4.21: Pareto set considering the annual economic cost and the annual CO_2 emissions.

Table 4.15: Trade-off solutions between economic cost and CO_2 emissions.

| | ε-CO_2 tCO$_2$/yr | Economic cost €/yr | Installed capacities | | | | | | | | Marginal cost €/tCO$_2$ | Average cost €/tCO$_2$ |
			GE kW$_e$	GB kW	HP kW	ABS kW	PV m^2	ST m^2	TSQ kWh	TSR kWh		
(B)	155.1	105,067	4.2	204.8	162.1	94.0	-	-	0.4	39.9	-	-
	145.0	105,126	3.5	193.5	176.8	83.8	-	-	-	40.0	5.9	5.9
	135.0	105,254	3.1	171.6	201.9	66.3	-	-	-	40.2	12.8	9.3
	125.0	105,453	1.1	169.0	209.8	60.9	-	-	-	40.2	19.9	12.8
	115.0	105,771	-	163.6	218.7	54.7	-	-	-	40.3	31.9	17.6
(C)	105.0	106,266	-	140.0	244.6	36.7	-	-	-	40.4	49.5	24.0
	100.0	106,690	-	113.6	273.6	16.6	-	-	-	40.6	84.7	29.5
	99.0	106,916	-	91.8	297.6	-	1.5	-	-	40.7	226.6	33.0
	97.0	107,745	-	91.8	297.6	-	88.1	-	-	40.7	414.4	46.1
	95.0	108,574	-	91.8	297.6	-	174.7	-	-	40.7	414.4	58.4
	93.0	109,403	-	91.8	297.6	-	261.3	-	-	40.7	414.4	69.9
	91.0	110,232	-	91.8	297.6	-	347.9	-	-	40.7	414.4	80.6
	89.0	111,060	-	91.8	297.6	-	434.4	-	-	40.7	414.4	90.7
	87.0	111,889	-	91.8	297.6	-	521.0	-	-	40.7	414.4	100.2
(D)	85.0	112,718	-	91.8	297.6	-	607.6	-	-	40.7	414.4	109.2
	84.0	113,170	-	86.6	303.3	-	640.0	-	-	35.3	452.0	114.0
	83.5	113,472	-	75.3	315.6	-	640.0	-	-	23.6	604.3	117.4
	83.0	113,932	-	74.5	316.6	-	634.9	7.1	-	22.7	919.2	123.0
	82.5	114,392	-	74.5	316.6	-	629.4	14.6	-	22.7	920.5	128.5
	82.3	114,631	-	72.6	316.6	-	626.8	18.2	1.9	22.7	953.8	131.3
	82.0	114,884	-	69.7	317.3	-	624.5	21.4	4.8	22.0	1012.7	134.4
	81.5	115,424	-	63.2	320.9	-	620.3	27.1	11.4	18.6	1080.2	140.8
	81.0	116,005	-	59.8	320.8	0.4	615.0	34.5	18.5	18.1	1163.3	147.7
	80.0	117,605	-	56.1	312.6	19.2	603.9	49.7	43.1	-	1599.3	167.0
	79.0	119,643	-	55.8	296.4	30.4	589.2	70.0	89.4	-	2038.6	191.6
	78.0	121,862	-	55.6	285.2	37.4	570.5	95.8	121.1	0.9	2218.4	217.9
	77.0	124,221	-	54.7	267.8	39.3	552.9	120.0	172.6	14.8	2359.3	245.4
	76.0	126,850	-	52.9	260.4	41.4	530.4	151.1	201.1	19.0	2629.2	275.5
	75.5	128,282	-	52.8	253.2	42.7	520.2	165.1	228.8	24.0	2863.0	291.8
	75.3	129,301	-	62.7	265.0	47.8	519.3	166.3	231.0	5.8	4076.3	303.6
	75.0	130,498	-	63.0	269.6	48.8	513.4	174.5	247.2	-	4789.6	317.6
	74.5	134,365	-	54.3	269.6	48.8	480.2	220.2	267.0	-	7734.3	363.7
(A)	74.2	137,630	-	49.3	269.6	48.8	461.2	246.5	314.0	-	12,562.0	402.9
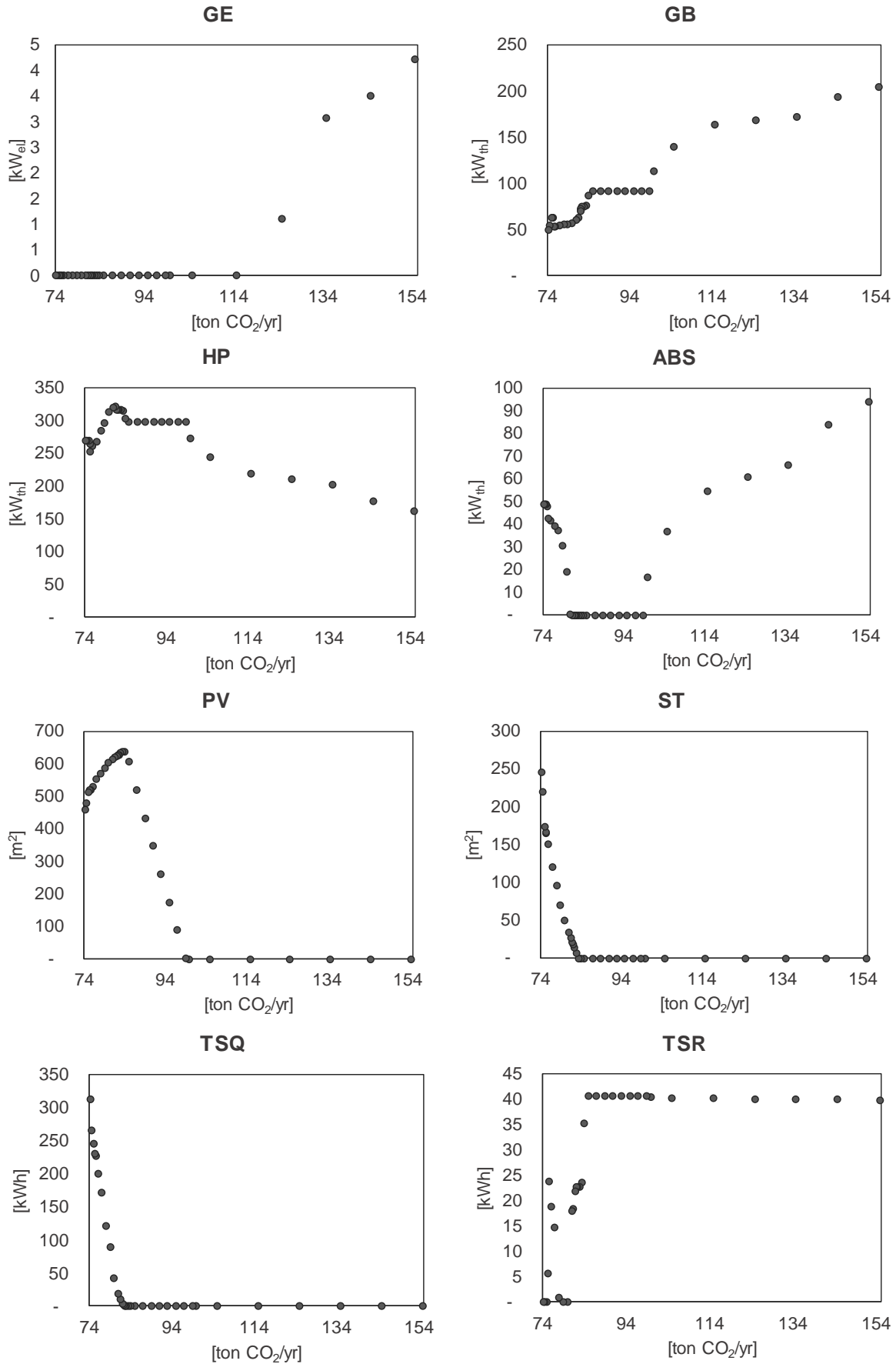
Figure 4.22: Installed capacities along the Pareto set.

Starting from the optimal total annual cost solution (B), as CO_2 emissions are forced down towards the environmental optimal (A), there is a shift in the installed capacities of GB and HP: the former decreases, while the latter increases. The GE is only included at CO_2 emissions levels higher than 125.0 ton CO_2/yr and even so with relatively small capacities. For total annual CO_2 emissions lower than 99.0 ton CO_2/yr, PV begins to be incorporated; its installed capacity increases until the maximum installable capacity corresponding to the available rooftop area is reached at 84.0 ton CO_2/yr. The rooftop area remains fully occupied from here on. By reducing CO_2 emissions from 83.0 ton CO_2/yr, then PV gives way to ST, which increases until the environmental optimal (A) is reached. TSQ closely follows the ST, being incorporated for lower values than 82.3 ton CO_2/yr.

There are two different ranges in which the ABS is included: for CO_2 emissions levels higher than 100.0 ton CO_2/yr and lower than 81.0 ton CO_2/yr. It is interesting to look into the role that the ABS plays in each scenario: at the higher CO_2 emissions range, the ABS is driven exclusively with heat produced with natural gas (GE cogenerated heat, Q_{cr}, and mostly GB conventional heat, Q_{ar}); on the other hand, at the lower range, the ABS is driven exclusively with heat from the ST collectors, Q_{str}.

The analysis of the trade-off solutions obtained also allowed for the identification of more interesting trade-off solutions than others, such as points C and D, in Table 4.15 and Figure 4.21. The results are gathered in Table 4.16.

Solution C was selected as preferred trade-off solution because of its good trade-off between both criteria: it achieves a 32.3% reduction in CO_2 emissions with an increase of only 1.1% in the total annual cost relative to the optimal cost configuration (B). Moreover, solution C includes only GB, HP, ABS, and TSR, thus constituting a simpler configuration than solutions A and B, that should be simpler and cheaper to operate and to maintain. Compared with the optimal annual cost solution (B), there is a reduction in the installed capacities of the GB and ABS, and an increase in the installed capacity of the HP. As a result, the system consumes 75.7% less natural gas and purchases 31.4% more electricity from the electric grid.

Solution D represents a higher commitment towards a more environmentally friendly solution: it achieves a 45.2% decrease in CO_2 emissions with an increase of 7.3% in the total annual cost relative to the optimal cost configuration (B). This solution includes GB, HP, PV, and TSR.

Table 4.16: Single-objective solutions and selected trade-off solutions comparison.

Results			Min. Economic cost (B)	Preferred trade-off (C)	Bold trade-off (D)	Min. CO_2 emissions (A)
GE	Cogeneration module	kW	4.2	-	-	-
GB	Gas boiler	kW	204.8	140.0	91.8	49.3
HP	Heat pump	kW	162.1	244.6	297.6	269.6
ABS	Absorption chiller	kW	94.0	36.7	-	48.8
PV	Photovoltaic panels	m²	-	-	607.6	461.2
ST	Solar thermal collectors	m²	-	-	-	246.5
TSQ	Hot water storage tank	kWh	0.4	-	-	314.0
TSR	Chilled water storage tank	kWh	39.9	40.4	40.7	-
Natural gas consumption, MWh/yr			363.3	88.1	52.8	0.1
Purchased electricity, MWh/yr			355.0	466.6	356.7	355.9
Sold electricity, MWh/yr			-	-	18.1	9.3
Annual operation cost, €/yr			75,225.0	77,548.6	54,672.6	53,108.7
Annual fixed cost, €/yr			29,841.9	28,717.7	58,045.6	84,521.6
Total annual cost, €/yr			105,066.9	106,266.3	112,718.2	137,630.2
Annual operation CO_2 emissions, kg CO_2/yr			152,275.9	102,063.8	73,304.3	61,558.5
Annual fixed CO_2 emissions, kg CO_2/yr			2789.8	2936.2	11,695.7	12,681.6
Total annual CO_2 emissions, kg CO_2/yr			155,066.7	105,000.0	85,000.0	74,240.1
Average cost (from solution B), €/ton CO_2			-	24.0	109.2	402.9

Table 4.15 also presents the marginal and the average costs of each solution, in €/ton CO_2. The marginal cost represents the economic cost of moving from one solution to the next in the Pareto set, while the average cost represents the cost of moving from the optimal cost solution (B) to any other in the set. These could be interesting indices to measure the effort the decision-maker is willing to make in order to move towards a more environmentally sound solution.

As can be seen from Table 4.15, it is no surprise that both the marginal and the average costs increase as the solutions shift towards lower CO_2 emissions levels. Moving from one optimum to the other (from B to A) would involve an average cost of 402.9 €/ton CO_2. However, taking the trade-off solution C into account, the average cost of moving from B to C is only 24.0 €/ton CO_2.

Based on the different conditions under which the system operates (e.g. climatic data, energy prices, local policies), local subsidies for CO_2 emissions savings and/or stock market prices for the CO_2 emissions could serve as indices to select among the various trade-off solutions based on their marginal costs. For example:

- The European Emission Allowances (EEX, 2018) value on August 4, 2018, was about 17.6 €/ton CO_2. Taking this value as reference, based on the marginal costs presented in Table 4.15 it would be possible to achieve a solution that is halfway between the optimal cost B and the trade-off C;

- An article published in the *The Economist* (2018) discusses a novel CO_2 removal system with a capture cost of about 100 €/ton CO_2. Taking this value as reference and comparing it to the marginal costs presented in Table 4.15, it would be possible to achieve a solution near to the trade-off C.

It becomes clear that ensuring an economic compensation for CO_2 emissions savings would enable trade-off solutions to be chosen, thus stimulating clean technology development and market innovation.

4.6 ECONOMIC COST ALLOCATION

Chapter 3 presented a methodological-oriented approach to the thermoeconomic analysis of a simple trigeneration system focusing on two fundamental aspects, namely: (i) the joint production of energy services in variable load operation; and (ii) the role of the TES unit in the optimal operation of the system. Section 4.6 extends the analysis to tackle trigeneration systems of higher complexity levels and with different operation conditions. In this regard, this section proposes cost allocation approaches to the following issues that have not been deeply studied in the field of thermoeconomics so far: (i) the inclusion of a component with different products for each operation mode, e.g. reversible heat pump producing heat in heating mode and cooling in cooling mode; (ii) the consumption of a free renewable energy source, such as the solar radiation; and (iii) the capital cost allocation for components operating at variable load conditions, especially regarding the heat pump and the TES units.

In order for the explanation to be as insightful as possible, thus allowing for more interesting results, a convenient trigeneration system was taken as an example for this section. The trigeneration system configuration and operational planning were obtained through a similar procedure to the one described in previous sections of this chapter, with the following simplifying assumptions: (i) the energy demands and the operation of the system are described by 12 representative days, one for each month of the year; therefore, no extreme-demand representative days are taken into account; and (ii) the electricity prices are constant.

Section 4.6.1 describes the trigeneration system, as well as the reference system defined for the present analysis. Then, Section 4.6.2 proposes and applies the thermoeconomic cost allocation approaches.

It is worth mentioning that even though the thermoeconomic analysis developed herein considers only the allocation of economic costs, the methodology could be easily extended to address aspects of a different nature, such as environmental burdens (e.g. CO_2 emissions).

4.6.1   Trigeneration system and reference system description

The trigeneration system analyzed herein is depicted in Figure 4.23, which also indicates the installed capacities of the technologies and the annual energy flows. The system is composed of a cogeneration module GE, a gas boiler GB, a single-effect absorption chiller ABS, photovoltaic panels PV, a reversible heat pump HP, a hot water storage tank TSQ, and a chilled water storage tank TSR.
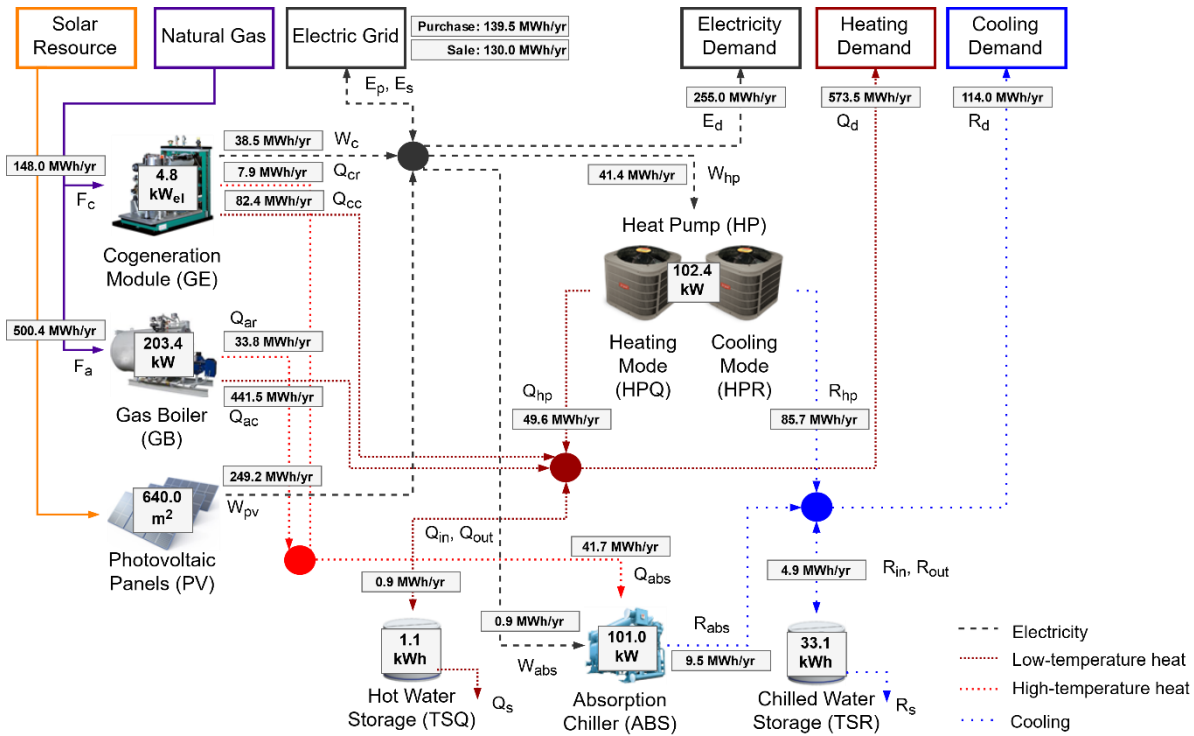
Figure 4.23: Trigeneration system diagram with installed capacities and annual energy flows.

It is assumed that the reference system considered herein is composed of a gas boiler GB and a heat pump operating in cooling mode only HPR. In this way, the electricity consumed by the HPR and delivered to the consumer center is covered by purchase from the electric grid. Figure 4.24 presents the reference system diagram with the corresponding installed capacities and annual energy flows.

For both systems, the technical parameters and the capital costs of the technologies are the same as the ones provided in Sections 4.2.3 and 4.2.4. Regarding the electricity prices, a constant purchase c_{ep} and selling c_{es} price of 0.140 €/kWh was considered from the Eurostat database (Eurostat, 2017). To maintain the same source of information, the natural gas purchase price c_g of 0.045 €/MWh (LHV) was also taken from the Eurostat database.
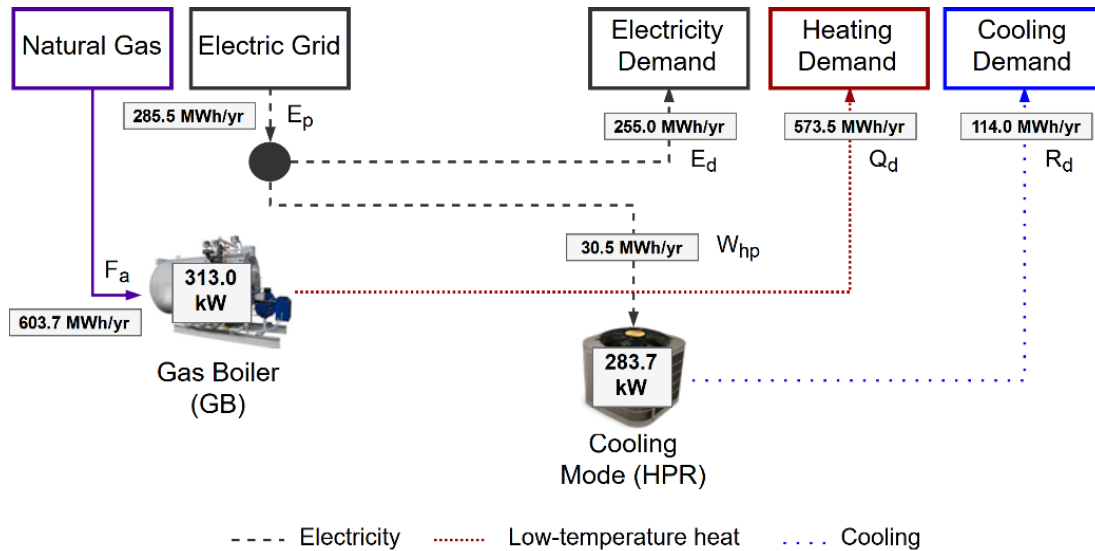
Figure 4.24: Reference system diagram with installed capacities and annual energy flows.

The capital costs for the trigeneration system and the reference system are presented in Table 4.17 and Table 4.18, respectively. Additional information regarding the annual consumption of energy resources and the total annual cost for both configurations are given in Table 4.19.

Table 4.17: Installed capacities and capital costs for the trigeneration system.

Technology	Installed capacity	Unit bare module cost	Investment cost, €	Annual fixed cost, €/yr
i	CAP	CI	INV	Z
GE	4.8 kW$_{el}$	2700 €/kW$_{el}$	15,497.9	2,324.7
GB	203.4 kW$_{th}$	77 €/kW$_{th}$	18,790.0	2,818.5
PV	640.0 m^2	264 €/m^2	202,368.0	30,355.2
ABS	101.0 kW$_{th}$	518 €/kW$_{th}$	62,773.2	9,416.0
TSQ	1.1 kWh	150 €/kWh	201.3	30.2
TSR	33.1 kWh	300 €/kWh	11,867.3	1,780.1
HP	102.4 kW$_{th}$	481 €/kW$_{th}$	59,079.2	8,861.9
Total	-	-	370,576.9	55,586.5

Table 4.18: Installed capacities and capital costs for the reference system.

Technology	Installed capacity	Unit bare module cost	Investment cost, €	Annual fixed cost, €/yr
i	CAP	CI	INV	Z
GB	313.0 kW$_{th}$	77 €/kW$_{th}$	28,921.2	4,338.2
HP	283.7 kW$_{th}$	481 €/kW$_{th}$	163,777.0	24,566.6
Total	-	-	192,698.2	28,904.7

Table 4.19: Total annual costs for the trigeneration and reference systems.

	Reference System	Trigeneration System
Natural gas consumption, MWh/yr	603.7	648.4
Purchased electricity, MWh/yr	285.5	139.5
Sold electricity, MWh/yr	-	130.0
Cost of natural gas, €/yr	27,166.0	29,176.5
Cost of purchased electricity, €/yr	39,967.0	19,531.2
Profit from the selling of electricity, €/yr	-	18,200.6
Annual operation cost CTE_{ope}, €/yr	67,132.9	30,507.0
Annual fixed cost CTE_{fix}, €/yr	28,904.7	55,586.5
Total annual cost CTE_{tot}, €/yr	96,037.7	86,093.5

The configuration of a trigeneration system is generally more complex than that of conventional energy systems and requires higher investment costs. Nevertheless, the higher investment is compensated by savings in the consumption of energy resources over the plant's operational lifetime. Indeed, from the information provided in Table 4.19, the trigeneration system analyzed herein presents savings of 36,626 €/yr in annual operation cost relative to the reference system. Conversely, as shown in Table 4.17 and Table 4.18, the additional investment cost corresponds to 177,879 €. Dividing the latter by the former results in a Simple Payback Period of 4.9 years.

The annual fixed cost of the system CTE_{fix} defined in Section 4.3.1 (Eq. (4.9)) can also be expressed as:

$$CTE_{fix} = \sum_i Z(i) = fam \cdot (1 + f_{IC}) \cdot \sum_i INV(i) = fam \cdot (1 + f_{IC}) \cdot \sum_i CI(i) \cdot CAP(i) \qquad (4.63)$$

where, $Z(i)$ is the annual fixed cost and $INV(i)$ is the investment cost of the technology i.

As previously mentioned, the hourly operation of the trigeneration system and the energy demands of the consumer center are described by 12 representative days (one representative day for each month of the year) that compose the year. An example of the operational planning is provided in Figure 4.25, which presents the hourly productions and energy demands of electricity and heating in January, and cooling in July.
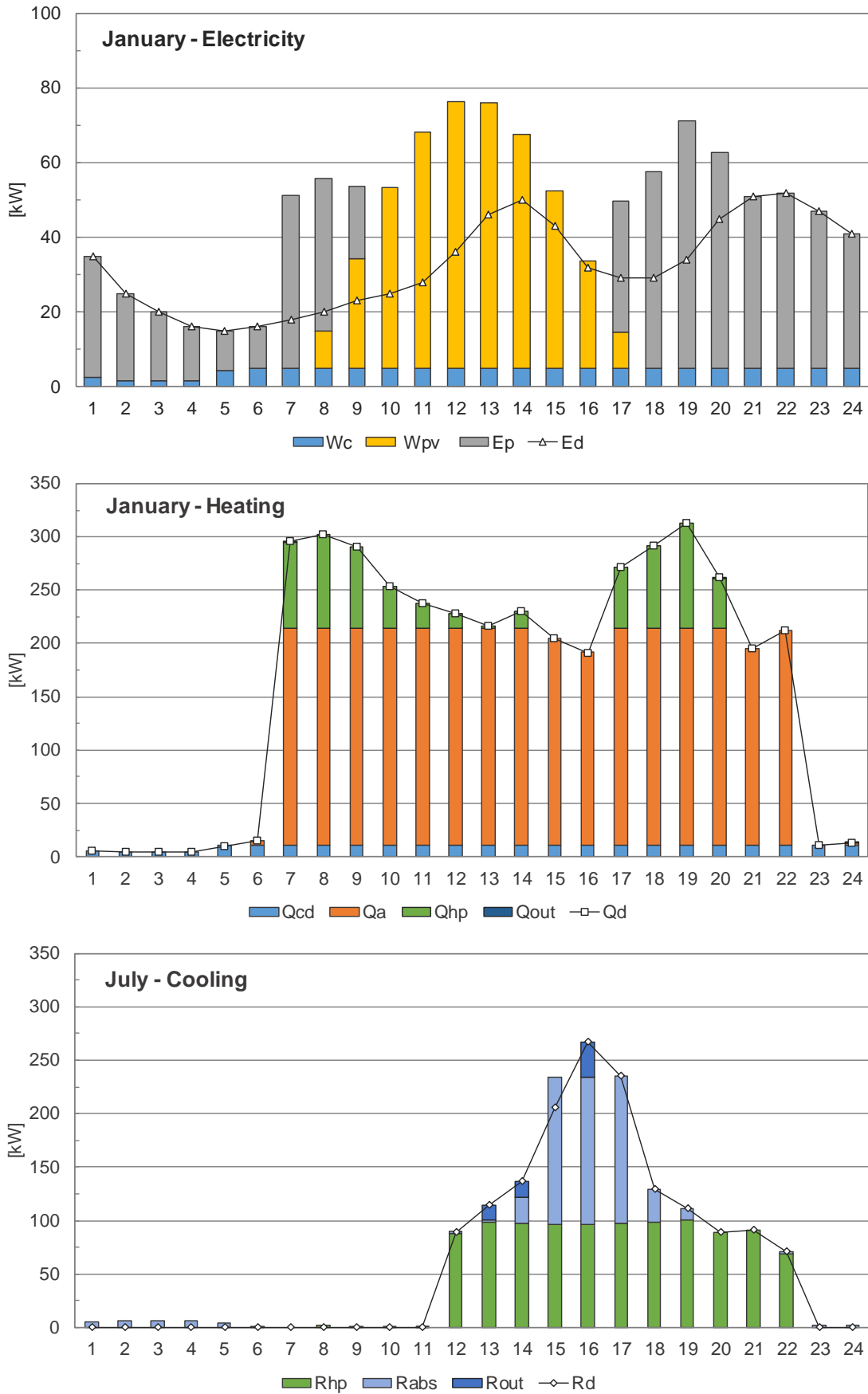
Figure 4.25: Hourly production and energy demands of electricity and heating in January, and cooling in July.

4.6.2   Thermoeconomic cost allocation

Based on the methodology proposed in Section 3.3, this section describes: (i) the definition of the productive structure, including the treatment for the combined production of electricity, heat, and cooling, and the disaggregation of energy flows and devices; (ii) the interconnection between hourly periods through the TES units; (iii) the capital cost allocation proposals; (iv) the cost allocation in the reference system; (v) the cost allocation proposals for the trigeneration system; and (vi) the results obtained.

4.6.2.1   Definition of the productive structure

The graphic representation of the productive structure proposed herein is depicted in Figure 4.26. Some flows identifiable in the productive structure have the same value and units as the ones in the physical structure of Figure 4.23. The determination of additional virtual flows is explained throughout this section.

In accordance with the description provided in Section 3.3.1, the productive structure of Figure 4.26 is composed of productive units (white rectangles), junctions (rhombs) and distributors (circles). The gray rectangles represent subsystems, which will be described in the following paragraphs.

Sold electricity subsystem

In the trigeneration system analyzed herein, the possibility of selling electricity to the grid provides an income that reduces the annual operation cost of the system. Given that electricity can be produced by the cogeneration module GE and the photovoltaic panels PV, when both are in operation it was proposed to proportionally distribute the sold electricity between them according to their power productions; by doing so, the income of selling electricity to the grid can be allocated to the internal flows and final products of the system.

For each hourly period h of each representative day d, the parameter δ_3 was defined for the sold electricity distribution, expressing the share of cogenerated electricity in proportion to the total electricity produced by the system:

$$\delta_3(h) = W_c(d,h)/\big(W_c(d,h) + W_{pv}(d,h)\big) \qquad (4.64)$$
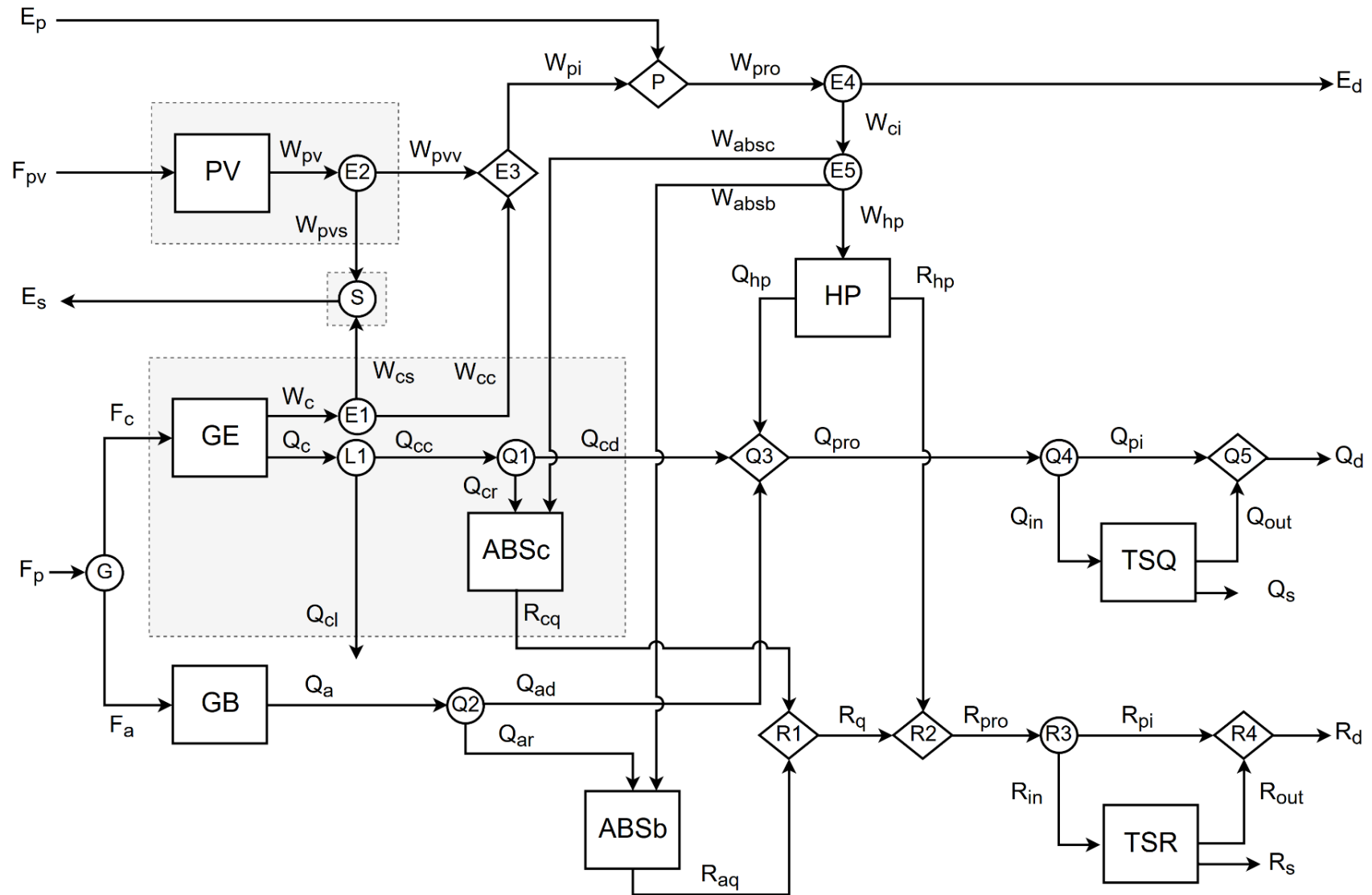
Figure 4.26: Productive structure of the trigeneration system.

The sold electricity E_s is distributed between the GE and PV accordingly:

$$W_{cs}(d,h) = \delta_3(d,h) \cdot E_s(d,h) \tag{4.65}$$
$$W_{pvs}(d,h) = (1 - \delta_3(d,h)) \cdot E_s(d,h) \tag{4.66}$$

The sold electricity subsystem is depicted in Figure 4.27. It is important to explain the choice for representing element S as a distributor (circle) instead of as a junction (rhomb): Even though the junction representation could be justified by the energy flows' directions (W_{cs} + W_{pvs} = E_s), the purpose of the sold electricity subsystem is to incorporate the income of selling electricity to the grid to the internal flows and final products of the system; therefore, despite the energy flows' directions, S functions as a distributor in which both energy flows W_{cs} and W_{pvs} receive the same electricity selling price c_{es}, whose value was defined in Section 4.6.1.
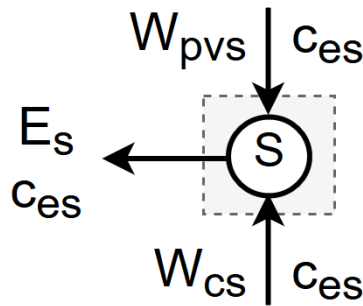
Figure 4.27: Sold electricity subsystem.

Photovoltaic subsystem

The photovoltaic subsystem, depicted in Figure 4.28, follows from the sold electricity subsystem previously described. In this way, the part of the photovoltaic electricity that is not sold W_{pvv} receives the benefit associated with the selling of W_{pvs}. The photovoltaic electricity that is not sold W_{pvv} is

$$W_{pvv}(d,h) = W_{pv}(d,h) - W_{pvs}(d,h) \tag{4.67}$$
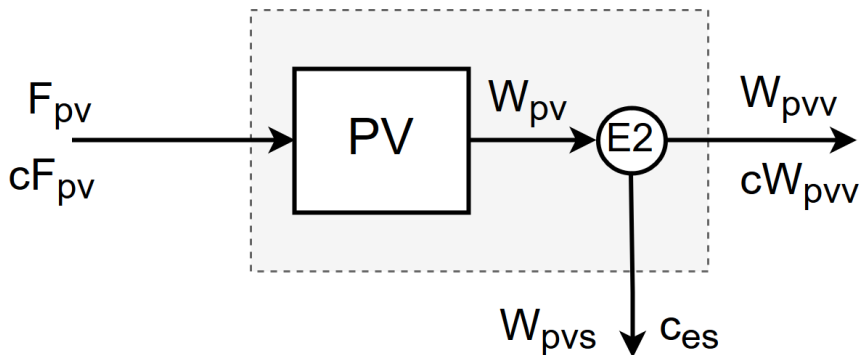
Figure 4.28: Photovoltaic subsystem.

Trigeneration subsystem

The trigeneration subsystem considered herein includes the cogeneration module GE and the conceptual disaggregation of the absorption chiller ABSc, as shown in Figure 4.29. It is evident that such trigeneration system is simpler than the one proposed in Section 3.3.1.1, which also includes the electric chiller EC. An analogous alternative would be to include the reversible heat pump HP, thus promoting its conceptual disaggregation. For the sake of clarity, however, it was decided not to disaggregate the HP, thus leaving it outside of the trigeneration subsystem. Lastly, it is worth noting that the trigeneration subsystem of Figure 4.29 mirrors the one originally proposed by Lozano et al. (Lozano et al., 2014, 2011).
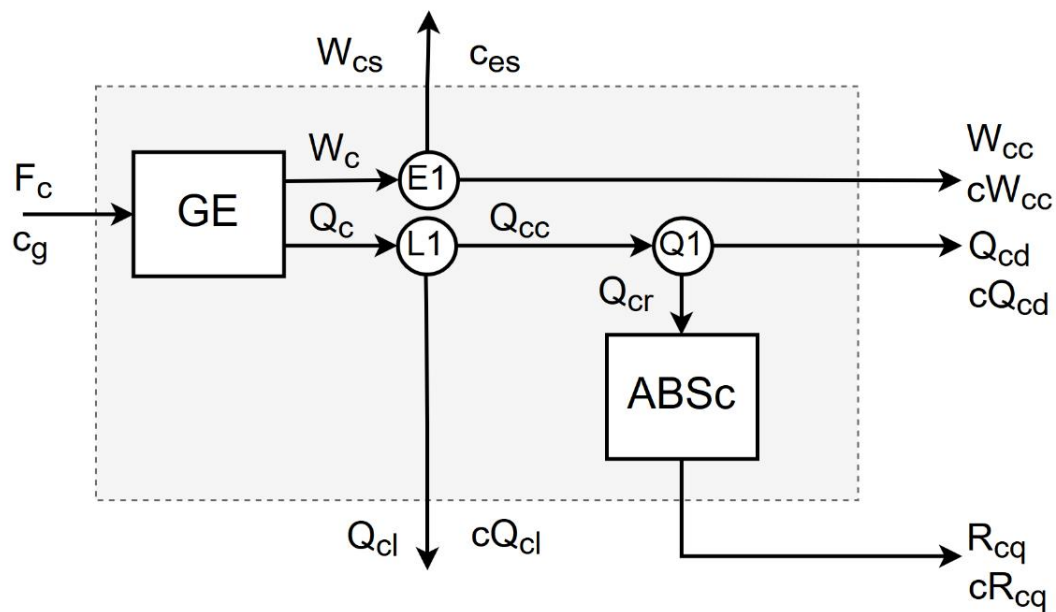
Figure 4.29: Trigeneration subsystem.

In the trigeneration subsystem the cogenerated electricity W_c is partly sold to the grid W_{cs} at price c_{es} and partly internally consumed by the system W_{cc} (Eq. (4.68)). The cogenerated heat Q_c can be: (i) used to attend the heat demand Q_{cd}; (ii) consumed in the ABSc for cooling production R_{cq}; and/or (iii) wasted into the environment Q_{cl}. As previously mentioned, the purchase price of natural gas c_g and the electricity selling price c_{es} are defined by the market (Section 4.6.1); moreover, heat dissipation takes place with no associated cost (cQ_{cl} = 0 €/kWh). Therefore, the three cogenerated products to which costs should be allocated are W_{cc}, Q_{cd} and R_{cq}.

$$W_{cc}(d, h) = W_c(d, h) - W_{cs}(d, h) \tag{4.68}$$

ABS conceptual disaggregation

The conceptual disaggregation of the ABS follows the methodology described in Section 3.3.1.2.

Other virtual flows

The electricity produced by the trigeneration subsystem W_{cc} and by the photovoltaic panels W_{pvv} compose the electricity produced in the hourly period W_{pi} (Eq. (4.69)). The electricity consumed in the hourly period W_{pro} (Eq. (4.70)) is composed of the electricity produced W_{pi} and the electricity purchased from the grid E_p. The electricity internally consumed by the system W_{ci} corresponds to the electricity consumed by the heat pump W_{hp} and by the absorption chillers W_{absc} and W_{absb}, and can be determined by the balance of Eq. (4.71).

$$W_{pi}(d,h) = W_{cc}(d,h) + W_{pvv}(d,h) \tag{4.69}$$
$$W_{pro}(d,h) = E_p(d,h) + W_{pi}(d,h) \tag{4.70}$$
$$W_{ci}(d,h) = W_{pro}(d,h) - E_d(d,h) \tag{4.71}$$

The heat produced by the heat pump Q_{hp}, by the trigeneration subsystem Q_{cd}, and by the gas boiler Q_{ad} compose the heat produced in the hourly period Q_{pro} for heating demand purposes (Eq. (4.72)). A part of Q_{pro} can be charged Q_{in} to the TES unit TSQ; the part that is not charged is the heat produced and consumed in the hourly period Q_{pi} (Eq. (4.73)).

$$Q_{pro}(d,h) = Q_{cd}(d,h) + Q_{ad}(d,h) + Q_{hp}(d,h) \tag{4.72}$$
$$Q_{pi}(d,h) = Q_{pro}(d,h) - Q_{in}(d,h) \tag{4.73}$$

The same reasoning applies to the determination of the cooling flows R_{pro} (Eq. (4.74)) and R_{pi} (Eq. (4.75)).

$$R_{pro}(d,h) = R_q(d,h) + R_{hp}(d,h) \tag{4.74}$$
$$R_{pi}(d,h) = R_{pro}(d,h) - R_{in}(d,h) \tag{4.75}$$

The TES units TSQ and TSR are explored in the following section.

4.6.2.2   Interconnection between hourly periods through the TES units

The methodology developed in Section 3.3.1.3 was applied for both TSQ and TSR. An example is presented for the interconnection between hourly periods through the TSR in July. As can be seen in Figure 4.30, the TSR is charged at hours 1-6, 8-12, 15, 23 and 24, and discharged at hours 13, 14 and 16. The energy charged at hour 2 $R_{in}(2)$ = 6.02 kWh is directed to hours 13 (*IN(2,13)* = 5.77 kWh) and 14 (*IN(2,14)* = 0.25 kWh), so that $R_{in}(h)$ is equal to the sum of all *IN(h,z)* leaving period h. The discharged energy at hour 14 $R_{out}(14)$ = 14.50 kWh proceeds from hours 2 (*OUT(2,14)* = 0.22 kWh), 3 (*OUT(3,14)* = 5.39 kWh), 4 (*OUT(4,14)* = 5.41 kWh), 5 (*OUT(5,14)* = 3.42 kWh) and 6 (*OUT(6,14)* = 0.07 kWh), in a way that $R_{out}(h)$ is equal to the sum of all *OUT(y,h)* arriving at period h. Energy losses r_s are evaluated along the pairs *(y,z)* and are proportional to the input *IN(y,z)*, an energy loss factor of 0.01 h^{-1} and the storage duration in hours. *LOSS(2,14)* = 0.03 kWh

corresponds to the energy losses along the pair *(2,14)*, which is determined by the sum of all r_s along the same pair. The energy losses associated with a discharge $LOSS_{out}(h)$ are obtained by the sum of all *LOSS* arriving at the discharge period *h*; for example, the energy losses due to the discharge at hour 14 are:

$$LOSS_{out}(14) = LOSS(2,14) + LOSS(3,14) + LOSS(4,14) + LOSS(5,14) + LOSS(6,14)$$
$$= 1.56 \, kWh$$

The $LOSS_{out}(h)$ values will be used in the capital cost allocation of the TSQ and TSR.

4.6.2.3   Capital cost allocation

This section discusses the adequate way to distribute the capital cost of each technology to its useful products considering variable annual operation. For technologies with constant production rates, a "consumption of capital resources per hour" *hZ* can be determined and used to assign the capital cost to product flows:

$$hZ(i) = Z(i) \, / \, HY(i) \tag{4.76}$$

where *HY(i)* is the annual operating hours of technology *i*.

It becomes evident that this consideration is not valid for variable load operation because it implies that all operating hours of the *i*th technology are assigned with the same capital cost. In this way, if the technology operates at partial load, its cost per unit product would increase dramatically, which does not make economic sense (Lozano et al., 2011; Piacentino and Cardona, 2007). By assuming the distribution of the capital cost of a technology based on its productivity, it is possible to assign the same capital cost value *kZ* to each unit produced. Therefore, the following expression follows:

$$kZ(i) = Z(i) \, / \, PY(i) \tag{4.77}$$

where *PY(i)* is the annual production of technology *i*. This is the approach considered for the GB, PV, and ABS. For components that produce more than one product in combined or joint production, the attribution is made based on the main product, e.g. the electricity in the GE.

		1	2	3	4	5	6	7	8	9	10	11	12	13	14	15	16	17..22	23	24	1...	LOSS
(1,13)	IN, OUT	5.26												4.66								
	rs		0.05	0.05	0.05	0.05	0.05	0.05	0.05	0.05	0.05	0.05	0.05	0.05								0.60
(2,13)	IN, OUT		5.77											5.17								
	rs			0.06	0.06	0.06	0.06	0.06	0.05	0.05	0.05	0.05	0.05	0.05								0.60
(2,14)	IN, OUT		0.25												0.22							
	rs			0.00	0.00	0.00	0.00	0.00	0.00	0.00	0.00	0.00	0.00	0.00	0.00							0.03
(3,14)	IN, OUT			6.02											5.39							
	rs				0.06	0.06	0.06	0.06	0.06	0.06	0.06	0.06	0.06	0.05	0.05							0.63
(4,14)	IN, OUT				5.98										5.41							
	rs					0.06	0.06	0.06	0.06	0.06	0.06	0.06	0.06	0.06	0.05							0.57
(5,14)	IN, OUT					3.74									3.42							
	rs						0.04	0.04	0.04	0.04	0.04	0.04	0.04	0.03	0.03							0.32
(6,14)	IN, OUT						0.08								0.07							
	rs							0.00	0.00	0.00	0.00	0.00	0.00	0.00	0.00							0.01
(6,16)	IN, OUT						1.23										1.12					
	rs							0.01	0.01	0.01	0.01	0.01	0.01	0.01	0.01	0.01	0.01					0.12
(8,16)	IN, OUT								1.99								1.84					
	rs									0.02	0.02	0.02	0.02	0.02	0.02	0.02	0.02					0.15
(9,16)	IN, OUT									0.33							0.31					
	rs										0.00	0.00	0.00	0.00	0.00	0.00	0.00					0.02
(10,16)	IN, OUT										0.33						0.31					
	rs											0.00	0.00	0.00	0.00	0.00	0.00					0.02
(11,16)	IN, OUT											0.33					0.31					
	rs												0.00	0.00	0.00	0.00	0.00					0.02
(12,16)	IN, OUT												0.33				0.32					
	rs													0.00	0.00	0.00	0.00					0.01
(15,16)	IN, OUT															28.83	28.54					
	rs																0.29					0.29
(23,13)	IN, OUT													2.10					2.42			
	rs	0.02	0.02	0.02	0.02	0.02	0.02	0.02	0.02	0.02	0.02	0.02	0.02	0.02						0.02		0.32
(24,13)	IN, OUT													1.83						2.09		
	rs	0.02	0.02	0.02	0.02	0.02	0.02	0.02	0.02	0.02	0.02	0.02	0.02	0.02								0.26
Rin(h)		5.26	6.02	6.02	5.98	3.74	1.31	-	1.99	0.33	0.33	0.33	0.33	-	-	28.83	-	-	2.42	2.09		-
Rout(h)		-	-	-	-	-	-	-	-	-	-	-	-	13.76	14.50	-	32.74	-	-	-		-
Rs(h)		0.04	0.10	0.16	0.21	0.27	0.31	0.32	0.31	0.33	0.33	0.33	0.33	0.33	0.19	0.04	0.33	-	-	0.02		3.96

Figure 4.30: Interconnection between charging and discharging periods through the TSR – energy flows, in kW.

The TES units require a different approach because these devices deal with two dimensions: quantity (stored energy) and time (storage duration). Allocating capital costs based on their productivity (annual discharged energy) would neglect the associated storage time. The storage time is important because the greater the storage time, the greater the energy losses. For example, discharging 1 kWh after a 1-hour storage time incurs less energy losses than discharging the same 1 kWh after a 12-hour storage time. Energy losses, on the other hand, relate both storage time and stored energy. Therefore, based on the methodology presented in Section 3.3.1.3, it is proposed herein to allocate more capital costs to discharges associated with larger storage times.

In this regard, a unit capital cost per energy loss unit $LZ(i)$ is defined, relating the annual capital cost $Z(i)$ and the annual energy losses $LY(i)$ for each TES unit i.

$$LZ(i) = Z(i) \, / \, LY(i) \tag{4.78}$$

It is evident that this assumption can only be applied when energy losses are considered. Otherwise, the approach based on productivity (kZ based on the annual discharged energy) would suffice.

The HP is a special case because it has two operation modes producing two different products at different times. Two different capital cost allocation approaches are proposed:

(i) HP capital cost allocation A: Main product

From the analysis of the operation of the system throughout the year, it can be seen that the HP's main product is the cooling R_{hp}. In fact, 75% of the annual cooling demand is covered by the HP, while only 8.6% of the annual heating demand is covered by this device. Moreover, the load factor of the HP in cooling mode is 27%, against 8% in heating mode, as shown in Table 4.20.

Therefore, a sensible capital cost allocation proposal is to allocate the entire HP annual capital cost $Z(HP)$ to the cooling R_{hp}. The approach based on the productivity (Eq. (4.77)), with $PY(HPR)$ as the annual R_{hp} production, would apply.

(ii) HP capital cost allocation B: Shared allocation

An alternative to the previous allocation proposal is to consider that there is not a main product and that the HP annual capital cost should be distributed between both heat Q_{hp} and cooling R_{hp} productions. Assuming that the HP's annual capital cost $Z(HP)$ can be expressed as the sum of the heat and cooling contributions:

$$Z(HP) = kZ(HPQ) \cdot PY(HPQ) + kZ(HPR) \cdot PY(HPR) \qquad (4.79)$$

where *kZ(HPQ)* and *kZ(HPR)* are the capital unit costs of the Q_{hp} and R_{hp}, respectively.

By assuming that the cost ratio between *kZ(HPQ)* and *kZ(HPR)* is equal to the HP's cooling/heating capacity ratio *rCAPhp = CAP(HPR)/CAP(HPQ) = 0.90* (Table 4.3) the following expression is obtained:

$$kZ(HPQ) = 0.90 \cdot kZ(HPR) \qquad (4.80)$$

Solving Equations (4.79) and (4.80) provides the capital unit costs of both HP products.

The values of the capital unit costs discussed in this section are presented in Table 4.20, for the trigeneration system, and Table 4.21, for the reference system.

Table 4.20: Capital unit costs for the trigeneration system.

Technology	Annual fixed cost, €/yr	Annual production, MWh/yr	Annual losses, MWh/yr	Capital unit cost per production, €/MWh	Capital unit cost per losses, €/MWh	Load factor, %
i	*Z*	*PY*	*LY*	*kZ*	*LZ*	
GE	2,324.68	38.48	-	60.41	-	91.84
GB	2,818.50	475.34	-	5.93	-	26.68
PV	30,355.20	249.23	-	121.80	-	17.10*
ABS	9,415.97	28.77	-	327.30	-	3.25
TSQ	30.20	-	0.03	-	1,198.28	25.64
TSR	1,780.10	-	0.50	-	3,579.18	17.17
(A) HP	8,861.88	85.72	-	103.38	-	35.44
(B) HPQ	3,034.63	49.60	-	61.18	-	8.01
(B) HPR	5,827.35	85.72	-	67.98	-	27.42

*considering nominal panel power.

Table 4.21: Capital unit costs for the reference system.

Technology	Annual fixed cost, €/yr	Annual production, MWh/yr	Annual losses, MWh/yr	Capital unit cost per production, €/MWh	Capital unit cost per losses, €/MWh	Load factor, %
i	*Z*	*PY*	*LY*	*kZ*	*LZ*	
GB	4,338.18	573.50	-	7.56	-	20.92
HPR	24,566.55	113.99	-	215.52	-	3.85

4.6.2.4   Cost allocation in the reference system

The conservation of costs applied to the productive structure of the system enables the cost formation process to be transparent throughout the system, from the resources consumed (energy and capital costs) to the final products. The unit costs of the internal flows and final products represent the amount of resources that must be consumed to produce one unit of the flow. Total unit costs account for both energy and capital components. By neglecting the capital term in the cost balances of the components, the unit energy costs are obtained.

The first and foremost requirement to performing cost allocation is the knowledge of the operational state of the system, which means that all energy flows in each hourly period h of each representative day d must be known. For the sake of clarity, the notation (d,h) will be omitted from the forthcoming equations.

The productive structure of the reference system is shown in Figure 4.31, which includes the corresponding annual energy flows and the prices of the energy resources consumed. The application of cost balances to the reference system is quite straightforward, as explained in the following paragraphs.
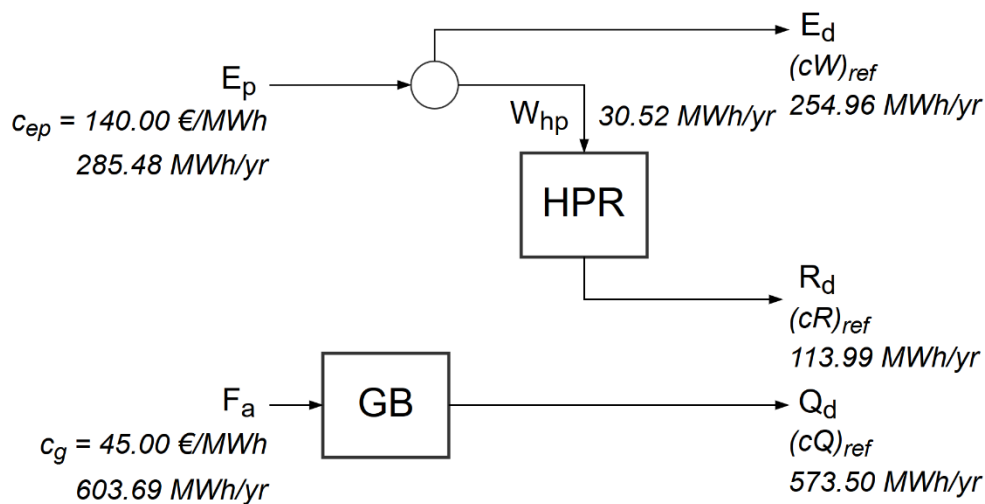
Figure 4.31: Productive structure of the reference system.

The purchased electricity E_p at price c_{ep} has two possible uses: (i) attend the electricity demand E_d; and (ii) drive the HPR for cooling production R_d. For the distributor (circle), a generally accepted accounting principle, which states that the unit costs of the products from the same line are equal, is applied. Therefore, the cost balance equation in the distributor is

$$c_{ep} \cdot E_p - cW_{hp} \cdot W_{hp} - (cW)_{ref} \cdot E_d = 0 \tag{4.81}$$

and the corresponding auxiliary equation is

$$cW_{hp} = (cW)_{ref} \tag{4.82}$$

Solving Equations (4.81) and (4.82) allows for the determination of the reference cost of electricity $(cW)_{ref} = cW_{hp} = c_{ep} = 140 \ €/\text{MWh}$ (Section 4.6.1).

As heat is exclusively produced in the GB with natural gas F_a at price c_g, all capital and energy costs are allocated to the produced heat; the cost balance in the GB is

$$c_g \cdot F_a - (cQ)_{ref} \cdot Q_d + kZ(GB) \cdot Q_d = 0 \tag{4.83}$$

which allows for the determination of the reference cost of heat $(cQ)_{ref} = 55 \ €/\text{MWh}$.

The cooling demand is attended by the HPR consuming purchased electricity. The cost balance applied to the HPR, considering capital and energy costs is

$$cW_{hp} \cdot W_{hp} - (cR)_{ref} \cdot R_d + kZ(HPR) \cdot R_d = 0 \tag{4.84}$$

which yields the reference cost of cooling $(cR)_{ref} = 253 \ €/\text{MWh}$.

Table 4.22 and Table 4.23 present the energy, capital, and total unit costs obtained for the reference system.

4.6.2.5 Cost allocation proposals for the polygeneration system

For the trigeneration system analyzed herein, all energy flows and market costs are known for each hourly period *h* of each representative day *d*. Electricity and natural gas prices were given in Section 4.6.1. As in Section 4.6.2.4, the notation *(d,h)* will be omitted from here on.

The cost conservation principle is applied to all productive units, junctions, distributors, and subsystems in the productive structure of the trigeneration system (Figure 4.26). For distributors, the accounting principle introduced in the previous section was considered, in which the unit costs of the products from the same line are considered equal. In the case of the junctions, provided that the unit costs of the entering flows are known, the unit cost of the junction's product is directly obtained from the cost balance equation. In the productive units with only one product, an energy transformation process takes place, so the unit cost of the product is directly obtained from the cost balance equation provided that the unit costs of the consumed flows are known.

However, as previously discussed, the trigeneration system analyzed herein imposes some difficulties to the cost allocation problem that have not been deeply studied in thermoeconomics so far. These difficulties are addressed accordingly:

(i) Joint production in the trigeneration subsystem

The cost allocation in the trigeneration subsystem follows the approach proposed in Section 3.3.2 with the necessary modifications concerning the capital cost of the technologies. The cost balance yields the following expression:

$$cF_c \cdot F_c + cW_{absc} \cdot W_{absc} - cW_{cs} \cdot W_{cs} - cW_{cc} \cdot W_{cc} - cQ_{cl} \cdot Q_{cl} - cQ_{cd} \cdot Q_{cd} - cR_{cq} \cdot R_{cq} \\ + kZ(GE) \cdot W_c + kZ(ABS) \cdot R_{cq} = 0 \tag{4.85}$$

As previously mentioned, no cost was allocated to the dissipation of cogenerated heat to the ambient ($cQ_{cl} = 0$). Considering that the resources consumed by the trigeneration subsystem must be allocated to its three useful cogenerated products (W_{cc}, Q_{cd}, R_{cq}) two auxiliary equations are needed to determine their unit costs (cW_{cc}, cQ_{cd}, cR_{cq}). Aiming at an equitable distribution of the benefits among the consumers, it was proposed to apply the same discount d to all cogenerated products with respect to a reference cost:

$$d = 1 - cW_{cc}/(cW)_{ref} = 1 - cQ_{cd}/(cQ)_{ref} = 1 - cR_{cq}/(cR)_{ref} \tag{4.86}$$

The reference costs considered herein are those of the reference system obtained in the previous section and shown in Table 4.23. From the criterion of equal discount, the two following auxiliary equations emerge:

$$cW_{cc}/(cW)_{ref} = cQ_{cd}/(cQ)_{ref} \tag{4.87}$$
$$cW_{cc}/(cW)_{ref} = cR_{cq}/(cR)_{ref} \tag{4.88}$$

(ii) Heat pump with a different product for each operation mode (heating or cooling mode)

In the case of the HP, the component consumes electricity to produce either heat or cooling, depending on the operation mode. The cost balance in the HP provides the following expression:

$$cW_{hp} \cdot W_{hp} - cQ_{hp} \cdot Q_{hp} - cR_{hp} \cdot R_{hp} + kZ(HPQ) \cdot Q_{hp} + kZ(HPR) \cdot R_{hp} = 0 \tag{4.89}$$

which is valid for both capital cost allocation approaches proposed in Section 4.6.2.3.

(iii) Free solar resource

By considering the solar resource as free of charge ($cF_{pv} = 0$) in the photovoltaic subsystem, only capital cost and the income of selling electricity ($cW_{pvs} = c_{es}$), when applicable, are allocated to its internal product cW_{pvv}:

$$cF_{pv} \cdot F_{pv} - cW_{pvv} \cdot W_{pvv} - cW_{pvs} \cdot W_{pvs} + kZ(PV) \cdot W_{pv} = 0 \tag{4.90}$$

(iv) TES units (TSQ and TSR)

The cost allocation in the TES units follows the methodology developed in Section 4.6.2.2, which considers the interconnection between hourly periods through the TES units as a charging and discharging network.

Regarding the cooling production, from the cost balance in distributor R3 it follows that the unit cost of the charged cooling cR_{in} is equal to the unit cost of the cooling produced in the hourly period cR_{pi}. This accounts for the fact that the energy stored in the TSR may have different unit costs according to the hourly period in which it was produced. Considering that the penalty for energy wasting must be allocated to its useful products, no cost was allocated to the energy losses R_s (cR_s = 0 €/kWh). The unit cost of the discharged cooling cR_{out} was obtained by tracing the discharged flow back to its origin periods according to the following Equation:

$$cR_{out}(h) \cdot R_{out}(h) = LZ(TSR) \cdot LOSS_{out}(h) + \sum_{z \neq h} cR_{in}(z) \cdot IN(z,h) \tag{4.91}$$

in which the first term of the right side corresponds to the capital cost of the TSR and the second to the energy costs.

The same reasoning applies to the TSQ.

4.6.2.6   Application to the polygeneration system

This section applies the cost allocation approaches presented in the previous sections and obtains the unit costs of the internal flows and final products of the trigeneration system for the 24 hourly periods of each representative day. The linear equation system proposed in Section 4.6.2.5 was solved using the software EES (2017). Based on the hourly unit costs, the aggregated monthly and annual values were obtained.

Section 4.6.2.3 proposed two capital cost allocation approaches for the heat pump HP, namely: (A) main product; and (B) shared allocation. Table 4.22 presents, for each proposal, the annual total unit costs obtained of the system's final products (electricity E_d, heat Q_d, and cooling R_d) and the HP's products (heat Q_{hp} and cooling R_{hp})

Table 4.22: Annual total unit cost comparison for different HP allocation proposals.

Energy flow	HP proposal A – Main product Total unit cost, €/MWh	HP proposal B – Shared allocation Total unit cost, €/MWh	Reference costs Total unit cost, €/MWh
E_d	123	123	140
Q_d	52	58	55
R_d	216	190	253
Q_{hp}	49	111	-
R_{hp}	135	100	-

From the analysis of the unit costs obtained, it can be seen that proposal A (cooling R_{hp} as the HP's main product, so that it receives all capital cost *Z(HP)*) leads to very different unit costs of the HP's products: Q_{hp} is 63% cheaper than R_{hp}; most importantly, the final products of the system Q_d and R_d are both cheaper than their respective reference costs *(cQ)ᵣₑf* and *(cR)ᵣₑf* : 5% and 15%, respectively. On the other hand, proposal B (HP capital cost *Z(HP)* is shared between both products Q_{hp} and R_{hp}) leads to similar unit costs of the HP's products: Q_{hp} is 11% more expensive than R_{hp}; but now Q_d is 5% more expensive than *(cQ)ᵣₑf*, while R_d is 25% cheaper than *(cR)ᵣₑf*.

A general conclusion from this is that proposal B leads to an overcharged heat due to a higher capital cost share, while proposal A produces more balanced unit costs in line with the reference costs. This analysis demonstrates the potential effect that different cost allocation approaches can have on the unit costs of the internal flows and final products obtained.

Additionally, the knowledge of the operational behavior of the system allows for a better understanding of which technology dominates the production of each energy service. From the data provided in Table 4.20, the HP produces 85.72 MWh/yr of cooling, while the absorption chiller ABS accounts for 28.77 MWh/yr; regarding the heat production, the HP produces 49.60 MWh/yr against the 475.34 MWh/yr produced by the gas boiler GB. It becomes clear that while the HP dominates the cooling production, it is only used in heating mode to cover heat peak demands. Thus, this information may be used to support the decision to allocate all HP capital cost to the cooling alone (proposal A).

In the light of the above discussion, HP capital cost allocation proposal A was selected as the most appropriate for this analysis and, thus, the results presented from here on are those obtained with this approach. Table 4.23 presents the main results on a yearly basis. As can be seen, the total annual cost has been distributed between the final products (electricity E_d, heat Q_d, and cooling R_d). It is interesting to notice how energy and capital costs contribute to the final cost of flows. For example, while cooling R_d is the cheapest product in terms of energy consumption, it becomes the most expensive one when capital costs are included. In fact, capital accounts for 94% of the total

cost of cooling. Conversely, the most expensive final product regarding energy consumption, heat Q_d, ends up with the lowest total unit cost (only 17% is due to capital cost).

Table 4.23: Annual energy flows, unit costs, and total costs of internal flows and final products of the trigeneration system.

	Energy flow, MWh/yr	Unit capital cost, €/MWh	Unit energy cost, €/MWh	Total unit cost, €/MWh	Total cost, €/yr
Reference system					
$(cW)_{ref}$	255	-	140	140	35,695
$(cQ)_{ref}$	574	8	47	55	31,504
$(cR)_{ref}$	114	216	37	253	28,839
Final products					
E_d	255	107	16	123	31,468
Q_d	574	9	43	52	29,973
R_d	114	203	14	216	24,654
Cogenerated products					
W_{cc}	31	34	95	130	3,995
Q_{cd}	82	18	30	48	3,959
R_{cq}	5	293	30	323	1,754
Other products					
W_{pvv}	127	239	-135	104	13,234
W_{pro}	297	106	18	124	36,760
Q_a	475	6	47	53	25,335
Q_{hp}	50	21	29	49	2,452
Q_{out}	1	53	33	87	76
Q_{pro}	574	9	43	52	29,943
R_{hp}	86	138	-3	135	11,594
R_{aq}	23	340	68	408	9,525
R_{out}	5	668	22	691	3,356
R_{pro}	114	186	13	200	22,873

Regarding the HP's products, the heat Q_{hp} turns out as competitive as the cogenerated heat Q_{cd}, while the cooling R_{hp} results as the best option for cooling production in the system. The absorption chiller ABS is only used to cover peak demands (low load factor), which, along with its high capital cost, leads to significantly high unit costs of the cooling produced: R_{cq} and R_{aq} are 28% and 61% more expensive than the reference cooling $(cR)_{ref}$. The unit costs of the discharged heat Q_{out} and cooling R_{out} from the TES units TSQ and TSR are also more expensive than their corresponding reference costs. The capital cost of the TSR accounts for almost the entirety of R_{out} total unit cost. Despite the high unit costs, it stands as a more profitable alternative to increasing installed capacity of other equipment.

The monthly energy and total unit costs and monthly energy consumptions of the internal flows and final products are presented in Table 4.24, Table 4.25 and Table 4.26, respectively.

Table 4.24. Monthly unit energy costs, €/MWh.

Month	E_d	Q_d	R_d	W_{cc}	Q_{cd}	R_{cq}	W_{pvv}	W_{pro}	Q_a	Q_{hp}	Q_{out}	Q_{pro}	R_{hp}	R_{aq}	R_{out}	R_{pro}
Jan	70	45	-	95	32	-	-54	75	47	35	39	45	-	-	-	-
Feb	35	45	-	93	31	-	-118	39	47	32	38	45	-	-	-	-
Mar	21	42	-	93	30	-	-126	21	47	7	29	42	-	-	-	-
Apr	-8	39	-	91	29	-	-179	-5	47	17	33	39	-	-	-	-
May	-30	38	-	90	29	-	-209	-30	47	-	29	38	-	-	-	-
Jun	-18	38	-5	98	30	30	-155	-23	47	-	31	38	-12	69	6	-5
Jul	-7	39	24	103	30	31	-132	-1	47	-	30	38	3	68	29	23
Aug	-7	37	16	101	30	30	-142	-6	47	-	30	37	-1	69	31	16
Sep	-2	38	-5	99	30	29	-156	-6	47	-	31	38	-8	-	17	-5
Oct	7	38	-	92	30	-	-178	8	47	46	37	38	-	-	-	-
Nov	33	46	-	93	31	-	-127	33	47	-	33	46	-	-	-	-
Dec	75	44	-	95	32	-	-40	75	47	30	39	44	-	-	-	-

Table 4.25. Monthly total unit costs, €/MWh.

Month	E_d	Q_d	R_d	W_{cc}	Q_{cd}	R_{cq}	W_{pvv}	W_{pro}	Q_a	Q_{hp}	Q_{out}	Q_{pro}	R_{hp}	R_{aq}	R_{out}	R_{pro}
Jan	130	53	-	121	47	-	115	130	53	52	83	53	-	-	-	-
Feb	125	53	-	120	47	-	106	126	53	51	75	53	-	-	-	-
Mar	123	51	-	120	47	-	105	123	53	41	59	51	-	-	-	-
Apr	119	50	-	120	46	-	99	120	53	43	60	50	-	-	-	-
May	116	50	-	119	46	-	95	116	53	-	61	50	-	-	-	-
Jun	120	52	186	139	49	317	102	119	53	-	115	51	133	408	740	160
Jul	123	53	235	156	52	331	105	124	53	-	123	53	137	408	553	225
Aug	123	53	220	152	53	322	103	123	53	-	128	53	136	408	803	207
Sep	123	52	180	142	51	315	102	122	53	-	121	52	133	-	793	146
Oct	121	50	-	120	46	-	99	121	53	47	81	49	-	-	-	-
Nov	125	53	-	120	47	-	105	125	53	-	60	53	-	-	-	-
Dec	130	53	-	121	47	-	117	130	53	51	80	53	-	-	-	-

Table 4.26. Monthly and annual energy flows, MWh.

Month	E_d	Q_d	R_d	W_{cc}	Q_{cd}	R_{cq}	W_{pvv}	W_{pro}	Q_a	Q_{hp}	Q_{out}	Q_{pro}	R_{hp}	R_{aq}	R_{out}	R_{pro}
Jan	24	126	0	3	7	0	10	31	99	19	0	126	0	0	0	0
Feb	22	94	0	2	7	0	9	24	82	5	0	94	0	0	0	0
Mar	24	59	0	2	7	0	11	26	47	5	0	59	0	0	0	0
Apr	21	32	0	2	7	0	10	22	21	4	0	32	0	0	0	0
May	22	14	0	2	7	0	10	22	7	0	0	14	0	0	0	0
Jun	19	13	17	3	7	1	12	23	7	0	0	13	15	1	1	17
Jul	19	11	48	3	6	2	14	28	26	0	0	11	32	14	2	48
Aug	19	10	35	3	6	2	13	27	16	0	0	10	26	8	1	36
Sep	19	11	14	3	7	1	11	22	5	0	0	11	13	0	1	14
Oct	22	13	0	2	7	0	9	22	6	0	0	13	0	0	0	0
Nov	21	70	0	2	7	0	8	21	63	0	0	70	0	0	0	0
Dec	24	120	0	3	7	0	10	30	97	15	0	120	0	0	0	0
Year	255	574	114	31	82	5	127	297	475	50	1	574	86	23	5	114

In Section 4.6.2.3, it was proposed to allocate the capital cost of the TSQ and TSR to the discharged energy in proportion to the energy losses associated with the discharge. This effect becomes clear when analyzing the monthly operation of the TSQ.

As can be seen from Table 4.25, the total unit cost of the discharged heat Q_{out} increases considerably during the summer months. This happens because of a change in the operation of the system: From June to September, the HP operates in cooling mode, which requires that the system maintain the TSQ charged for more hours than in the non-summer months. In fact, storage time triples in summer months. This increase in energy losses, due to longer storage periods, results in the allocation of more capital costs to the discharged heat.

For comparison's sake, the unit capital costs of the TSQ and TSR were also assessed with the productivity approach kZ (annual discharged energy), resulting in $kZ(TSQ)$ = 34.66 €/MWh and $kZ(TSR)$ = 366.35 €/MWh. A comparison of the monthly total unit costs of the discharged energy cQ_{out} and cR_{out} obtained with both approaches (A: productivity approach; B: annual energy losses approach) is presented in Figure 4.32. As can be seen, the productivity approach led to more stable total unit costs over the months; however, it does not account for the aforementioned changes in the operation of the TSQ and TSR.

Considering the interconnection between hourly periods, it was possible to evaluate the unit energy cost of the discharged energy from the TSQ and TSR. By knowing the origin periods of the discharged energy and the unit costs of the charged energy in those periods, the cR_{out} and cQ_{out} could be assessed. Similar to Figure 4.30, Figure 4.33 presents a sample of the unit energy costs of the discharged cooling from the TSR on a representative day of July.
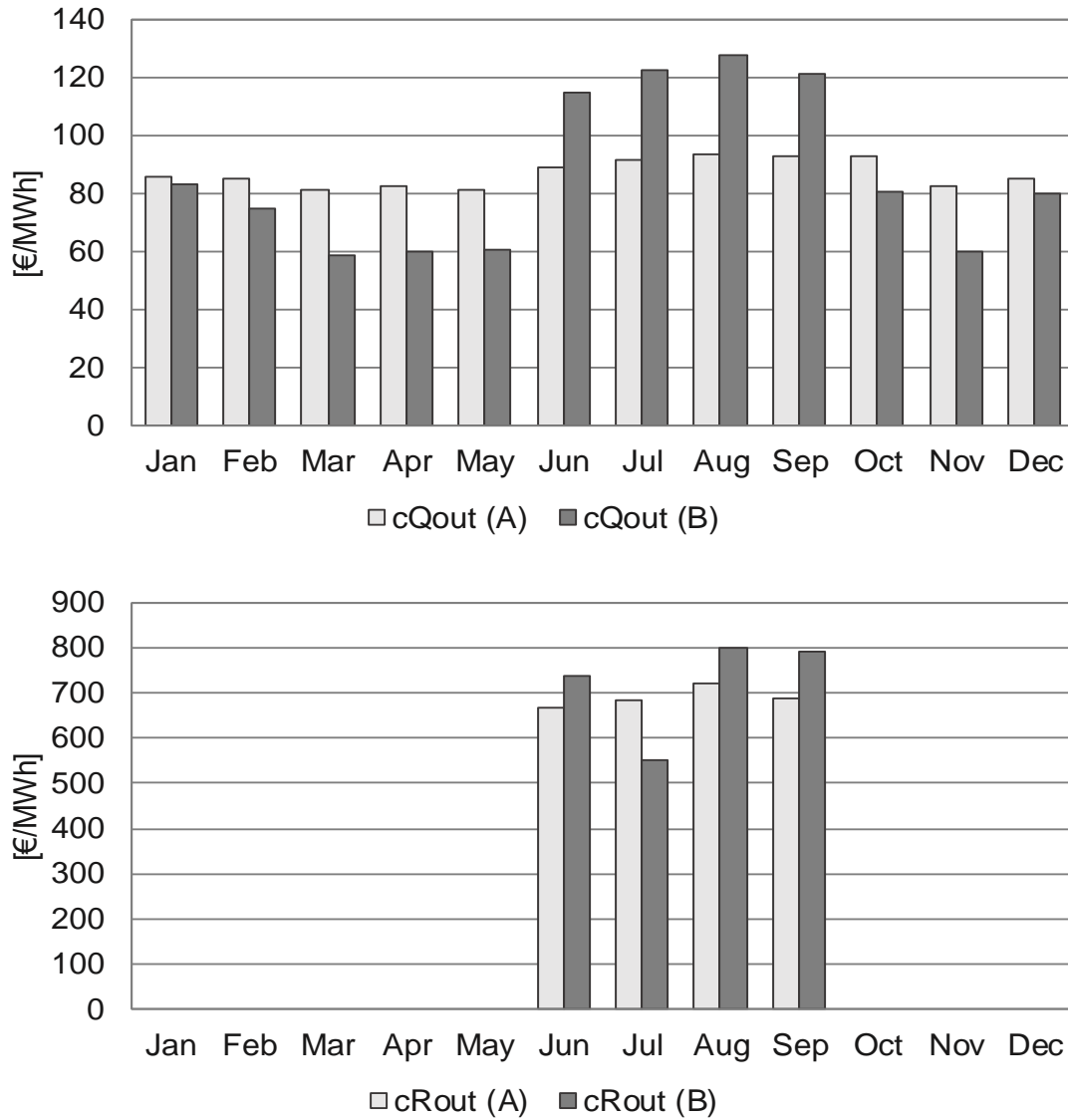
Figure 4.32: Monthly total unit costs of the discharged energy considering productivity approach (A) and annual energy losses approach (B) for the TSQ (top) and TSR (bottom).

		2	3	4	5	6	7	8	9	10	11	12	13	14
(2,14)	cIN, cOUT	0.0315												0.0356
(3,14)	cIN, cOUT		0.0315											0.0352
(4,14)	cIN, cOUT			0.0315										0.0348
(5,14)	cIN, cOUT				0.0291									0.0319
(6,14)	cIN, cOUT					0.0269								0.0291
cRin(h)		0.0315	0.0315	0.0315	0.0291	0.0269	-	-	-	-	-	-	-	-
cRout(h)		-	-	-	-	-	-	-	-	-	-	-	-	0.0343

Figure 4.33: Unit energy costs of the energy charged to and discharged from the TSR for selected hours of July.

Finally, it is interesting to analyze the annual cost savings distribution between the electricity, heating and cooling relative to the reference system. The energy, capital and total annual cost savings are presented in Table 4.27.

Table 4.27: Economic savings of the trigeneration system relative to reference system.

	E_d	Q_d	R_d	**Total**
Energy cost savings, €/yr	31,558	2,335	2,733	36,626
Capital cost savings, €/yr	-27,331	-804	1,451	-26,684
Total cost savings, €/yr	4,227	1,531	4,184	9,942
Unit energy cost savings, €/MWh	124	4	24	-
Unit capital cost savings, €/MWh	-107	-1	13	-
Total unit cost savings, €/MWh	17	3	37	-

As can be seen, the cooling and the electricity received the highest total annual savings, 37 €/MWh and 17 €/MWh, respectively, while the heat received only 3 €/MWh. In energy terms, electricity was the product with the highest energy cost savings, 124 €/MWh, followed by the cooling and the heating with 24 €/MWh and 4 €/MWh, respectively. Capital cost savings are negative because the trigeneration system requires higher investment and maintenance costs than the reference system; however, it was interesting to note that the cooling received a positive capital cost saving, which means that the optimal economic system attributes less capital cost to cooling than the reference system. This is due to the energy integration in the optimal economic system which allows for a lower HP installed capacity and higher load factor than the reference system.

4.7 CONCLUSIONS

A multi-objective optimization model formulated with MILP that determines the optimal configuration and operational strategy of a trigeneration system including RETs and TES was developed. The objective functions were the total annual cost (economic aspect) and the total annual CO_2 emissions (environmental aspect), both of which consisted of a fixed term, relative to the manufacturing and installation of the technologies, and a variable term, relative to the hourly operation of the system. The model carefully represented the dynamic conditions that govern the selection of technologies and the hour by hour operation of the system, which ultimately affect the objective function. Therefore, the results obtained were specific for the analyzed case study.

The model was applied to the case study of a multi-family building located in Zaragoza, Spain. A small capacity of cogeneration was installed in the optimal cost solution, while the RETs were not included. By reducing the CO_2 emissions along the Pareto set from the optimal cost to the optimal environmental solution, the cogeneration was rapidly displaced by the electric grid and the reversible heat pump. The multi-objective optimization procedure demonstrated the importance of the decision-maker's judgement in evaluating the different trade-off solutions. In this regard,

the marginal cost of moving from one solution to the next in the Pareto set was used to measure the effort the decision-maker is willing to make in order to move towards a more environmentally friendly solution. Finally, the thermoeconomic analysis of the trigeneration system was carried out, proposing cost allocation approaches for the joint production of energy services, the TES, RETs, and the reversible heat pump.

CHAPTER 5

Integration of renewable energy in polygeneration systems

5 INTEGRATION OF RENEWABLE ENERGY IN POLYGENERATION SYSTEMS

This chapter presents the application of mathematical programming techniques to the assessment of the technical, economic and environmental feasibility of renewable-based polygeneration systems in a Brazilian university hospital. Based on the multi-objective synthesis framework outlined in Chapter 2 and applied in Chapter 4 to a case study of a multi-family residential building in Zaragoza, Spain, a mixed integer linear programming (MILP) model is developed herein, incorporating an innovative approach to the thermal integration of technologies and utilities in the superstructure. In this way, Pinch Analysis, by means of the problem table algorithm, and mathematical programming, based on a MILP model, are combined to achieve a more realistic representation of the heat supply and demand in the system.

There is a great potential for the application of polygeneration systems in hospitals given their long operating hours, regular occupancy rate, high thermal energy requirements, and varied consumption of energy services (e.g. electricity, steam, hot water, space heating, space cooling) (Biglia et al., 2017; Gimelli and Muccillo, 2013; Guo et al., 2013; Lozano et al., 2009c). Moreover, there is an increasing interest in the need to ensure the quality and reliability of power supply, not only as regards maintaining life critical loads, but also the operation of the entire facility. Nevertheless, polygeneration systems do not eliminate the need for emergency generators, although they can contribute to reducing their installed capacities and numbers (Midwest CHP Application Center, 2007).

The cogeneration potential in Brazilian hospitals has been analyzed by Szklo et al. (2004), who have also identified implementation obstacles inherent to the Brazilian hospital sector. Presently, this situation is changing as new factors are taken into account, such as the normative for power exchange with the grid (ANEEL, 2015), the decreasing investment costs of photovoltaic panels and solar thermal collectors, subsidies to the price of natural gas for cogeneration purposes, and the increased opportunities for biomass.

These aspects have been systematically analyzed for the case study of the Brazilian university hospital in a set of conference papers derived from this thesis. A first approach to the MILP optimization model including realistic thermal integration considerations has been carried out by Pina et al. (2018c), in which the technical and economic feasibility of integrating cogeneration gas engines, gas boilers, mechanical chillers, absorption chillers, photovoltaic panels, flat-plate solar thermal collectors, and thermal energy storages was assessed. The results showed that cogeneration was, from the economic viewpoint, the most appropriate solution either with or without the permission to sell electricity to the grid, while the solar-based renewable energy technologies (RETs) were never included in the optimal solutions. In a subsequent study, Pina et

al. (2018d) proposed to analyze the technical, economic and environmental feasibility of a 100% renewable energy system; to this end, the cogeneration gas engine was replaced by biomass boilers and parabolic trough concentrators, and the technical-economic analysis was extended to include also the environmental aspects through the CO_2 emissions associated with the manufacturing of the equipment and the hourly operation of the system. Under the conditions considered in that study, biomass was the most economically interesting fuel for heat production, while cooling took place entirely with electricity purchased from the grid; the solar-based RETs, again, remained out of the optimal economic solutions. Finally, Pina et al. (2019) consolidated the two previous studies including all the previously mentioned technologies and proposing different modalities of interconnection with the electric grid.

The objective of this chapter is twofold: On the one hand, this chapter explains the MILP model developed, which reflects the complex characteristics of polygeneration systems (multiple energy resources, multiple energy products, multiple technology options, multiple operating periods, and multiple optimization criteria) and incorporates appropriate considerations for the thermal integration of technologies and utilities in the superstructure, aiming at an optimal match between the heat supply and demand. On the other hand, this chapter aims to apply the proposed methodology to assess the technical, economic and environmental feasibility of integrating RETs in a concrete case study of the university hospital in Brazil, considering locally available data. In this context, different scenarios of power exchange with the grid are analyzed, one of them corresponding to the current Brazilian policy, as well as the model's response to variations in boundary conditions, such as the purchase price of energy resources, the investment cost of RETs, the electricity CO_2 emission factors, and the permission to install or not fossil fuel-based technologies.

This chapter is structured as follows: Section 5.1 presents the case study of the Brazilian university hospital, including the description of the energy demands, local climatic data, economic and environmental data of fuels and electricity, as well as a brief account of the current regulatory framework for power exchange with the grid in Brazil. Section 5.2 introduces the superstructure of the renewable-based polygeneration system, provides the technical, economic and environmental parameters of the candidate technologies, in particular the thermal characteristics of the technologies and the thermal integration subsystem. Having defined the case study and the superstructure, Section 5.3 explains the mathematical model, including the objective functions and the system constraints. Section 5.4 presents and discusses the results obtained, comprising the economic cost and environmental optimal solutions, and the sensitivity analyses for the variation of some of the model's key parameters. Finally, Section 5.5 draws conclusions from the developed work.

5.1 CASE STUDY: UNIVERSITY HOSPITAL IN CAMPINAS

The case study corresponds to a medium-size university hospital with 403 beds and 65,000 m² constructed area located in Campinas in the southeastern region of Brazil (latitude -22.9°, longitude -47.0°). The hospital's energy demand data have been originally presented by Santo (2014, 2012). The analysis has been carried out for the period of one year, divided into 24 representative days *d* (one working day *wd* and one weekend/holiday *we* for each month of the year), each one composed of 24 consecutive periods of 1-hour duration. The number of representative days type *d* per year *NRY(d)* is shown in Table 5.1.

The main data of the case study are presented in the following subsections.

Table 5.1: Number of representative days type *d* per year *NRY*.

Day	Jan	Feb	Mar	Apr	May	Jun	Jul	Aug	Sep	Oct	Nov
wd	21	19	22	20	20	21	23	21	21	21	19
we	10	9	9	10	11	9	8	10	9	10	11

5.1.1 Energy demands

The hospital's energy demands consist of electricity, saturated steam at 180 °C for cooking, laundry and sterilization, hot water at 60 °C for sanitary purposes, and chilled water at 7 °C for air conditioning. It should be noted that the electricity demand accounts for lighting, elevators and other devices, thus excluding the consumption for thermal energy production (e.g. electricity consumption to produce cooling in mechanical chillers driven by electric motors).

The annual energy demands of the hospital are 9,633.5 MWh, hot water 518.7 MWh, steam 4,660.3 MWh, and chilled water 4,755.7 MWh. The energy demand profiles are available on hourly basis for a working day *wd* and a weekend/holiday *we* of each weather season: summer (from January to March), autumn (from April to June), winter (from July to September) and spring (from October to December). The daily energy demands of the hospital are given in Table 5.2 and the hourly energy demands for each weather season and type of day are depicted in Figure 5.1.

Table 5.2: Hospital's daily energy demands, kWh/day.

Energy demand	Summer (Jan-Mar)		Autumn (Apr-Jun)		Winter (Jul-Sep)		Spring (Oct-Dec)	
	wd	*we*	*wd*	*we*	*wd*	*we*	*wd*	*we*
Electricity	31,614	25,503	27,262	21,384	25,375	20,840	28,273	22,996
Steam	16,257	15,037	10,947	11,858	10,393	12,868	12,236	14,206
Hot water	1,178	889	1,788	1,077	2,039	1,225	1,438	822
Chilled water	18,321	16,412	12,116	11,580	8,424	7,896	14,788	13,205
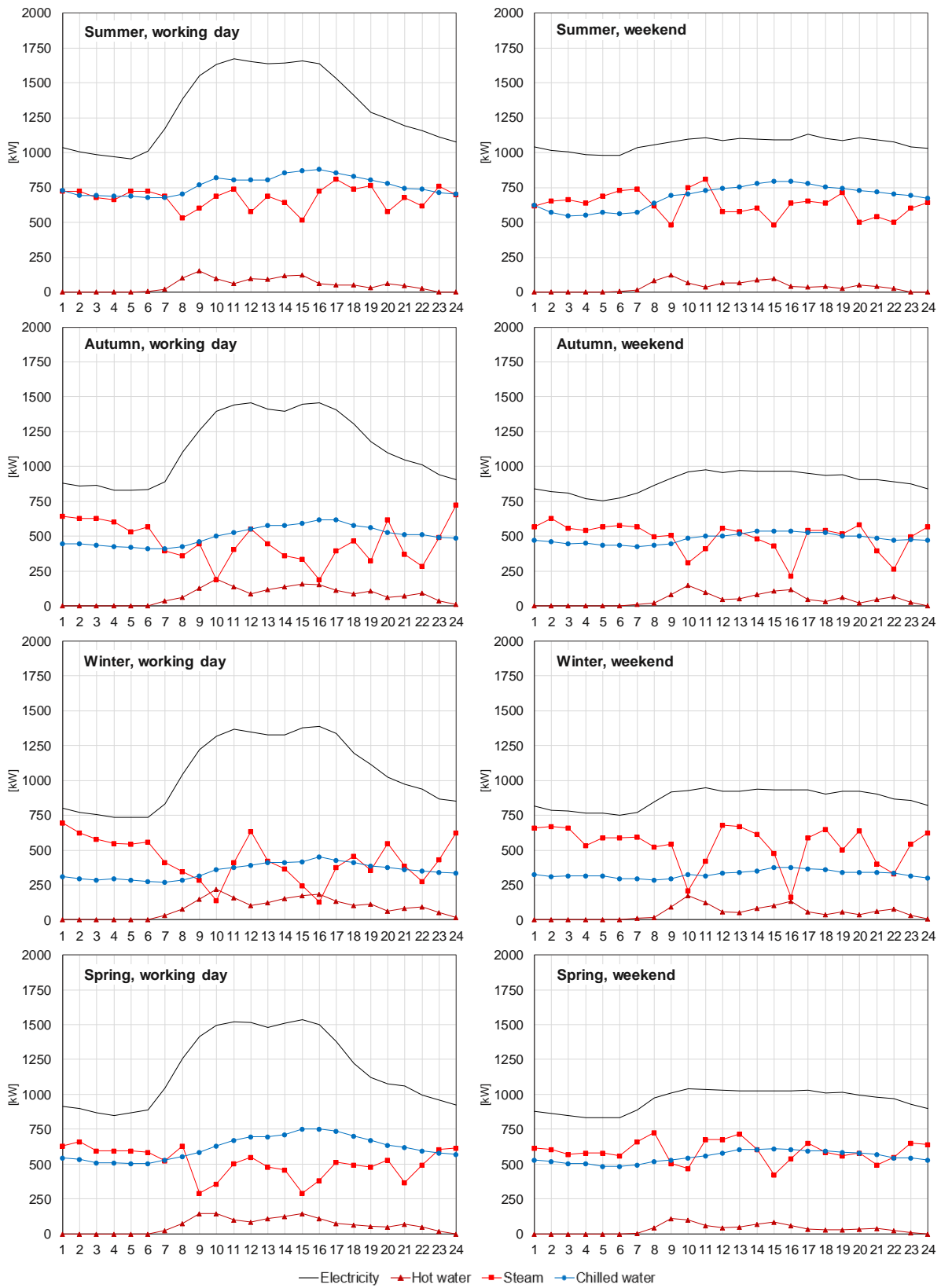
Figure 5.1: Hourly energy demands of working days and weekends/holidays for each weather season.

5.1.2   Local climatic data

Climatic data for the geographical location of Campinas was obtained from the software METEONORM (METEOTEST, 2018). This information includes the monthly mean hourly ambient temperature Ta, the monthly mean hourly global solar radiation on a surface tilted 20° facing north Q_r, and the hourly normal direct solar radiation Q_{Bn}, given in Table 5.3, Table 5.4 and Table 5.5, respectively.

Table 5.3: Monthly mean hourly ambient temperature Ta, °C.

Hour	Jan	Feb	Mar	Apr	May	Jun	Jul	Aug	Sep	Oct	Nov	Dec
1	20.8	21.2	21.3	19.9	16.8	15.9	15.5	17.0	17.8	19.6	19.4	20.3
2	20.3	20.7	20.7	19.3	16.2	15.2	14.8	16.3	17.1	19.0	18.8	19.7
3	20.0	20.3	20.2	18.7	15.6	14.6	14.1	15.6	16.5	18.6	18.5	19.4
4	19.8	20.0	19.9	18.4	15.3	14.3	13.8	15.2	16.2	18.2	18.2	19.1
5	19.6	19.7	19.6	18.1	15.0	13.9	13.4	14.9	15.8	18.0	18.0	18.9
6	19.6	19.7	19.4	17.8	14.8	13.7	13.2	14.6	15.7	18.0	18.1	19.0
7	20.3	20.1	19.6	17.9	14.8	13.7	13.2	14.6	16.0	19.1	19.4	20.3
8	21.5	21.5	21.1	19.4	16.0	14.8	14.2	16.2	17.8	20.6	20.9	21.6
9	22.7	22.9	22.7	21.1	17.7	16.6	15.9	18.3	19.5	22.3	22.3	23.1
10	23.9	24.2	24.3	22.7	19.4	18.5	17.8	20.3	21.2	23.8	23.7	24.5
11	25.0	25.5	25.7	24.1	20.8	20.3	19.6	22.0	22.7	25.2	24.9	25.7
12	25.8	26.4	26.7	25.3	22.0	21.7	21.1	23.4	23.9	26.3	25.6	26.4
13	26.4	27.1	27.4	26.2	22.9	22.7	22.2	24.4	24.8	27.0	26.1	27.0
14	26.8	27.5	27.9	26.6	23.5	23.3	22.8	25.1	25.4	27.5	26.4	27.2
15	26.9	27.7	28.0	26.7	23.7	23.5	23.0	25.3	25.6	27.6	26.5	27.3
16	26.8	27.6	27.9	26.4	23.4	23.1	22.7	25.0	25.3	27.4	26.2	27.1
17	26.4	27.3	27.3	25.6	22.5	22.1	21.8	24.0	24.5	26.7	25.6	26.5
18	25.7	26.5	26.3	24.5	21.3	20.8	20.5	22.6	23.2	25.6	24.7	25.8
19	24.8	25.5	25.2	23.7	20.6	20.1	19.7	21.8	22.3	24.5	23.6	24.7
20	24.1	24.7	24.5	23.0	20.0	19.4	19.0	20.9	21.5	23.6	22.9	24.0
21	23.4	24.0	23.8	22.3	19.3	18.7	18.3	20.1	20.7	22.8	22.2	23.2
22	22.7	23.3	23.1	21.7	18.6	18.0	17.6	19.3	19.9	21.9	21.4	22.4
23	22.0	22.4	22.4	21.0	18.0	17.2	16.9	18.5	19.1	21.1	20.7	21.6
24	21.3	21.7	21.7	20.3	17.3	16.5	16.2	17.7	18.4	20.2	20.0	20.8

Table 5.4: Hourly global solar radiation on surface tilted 20° facing north Q_r, W/m².

Hour	Jan	Feb	Mar	Apr	May	Jun	Jul	Aug	Sep	Oct	Nov	Dec
1-5	0	0	0	0	0	0	0	0	0	0	0	0
6	2	0	0	0	0	0	0	0	0	2	7	7
7	65	33	12	5	1	0	0	2	25	98	129	114
8	221	201	181	183	160	146	140	178	215	266	291	277
9	396	381	373	383	350	345	335	401	395	445	475	451
10	532	529	541	548	516	529	523	574	557	580	604	609
11	634	703	680	690	625	647	667	707	677	695	703	712
12	670	713	706	755	688	707	752	765	768	723	678	661
13	663	723	728	763	693	706	765	768	772	699	664	667
14	629	666	693	677	672	664	696	732	723	651	619	621
15	550	614	598	592	562	561	584	625	618	560	539	523
16	423	492	462	420	408	395	420	456	457	410	411	409
17	281	343	289	225	196	183	210	249	248	228	248	270
18	137	168	115	30	5	2	5	17	38	66	88	124
19	20	16	2	0	0	0	0	0	0	0	3	13
20-24	0	0	0	0	0	0	0	0	0	0	0	0

Table 5.5: Hourly normal direct solar radiation Q_{Bn}, W/m².

Hour	Jan	Feb	Mar	Apr	May	Jun	Jul	Aug	Sep	Oct	Nov	Dec
1-6	0	0	0	0	0	0	0	0	0	0	0	0
7	221	120	0	0	0	0	0	0	31	219	223	220
8	357	312	243	240	273	303	304	305	277	375	388	394
9	403	412	426	424	422	465	458	512	401	429	440	434
10	407	417	445	449	463	543	549	546	437	415	440	445
11	380	456	459	479	462	550	591	545	426	434	425	419
12	341	369	401	463	478	544	602	530	457	401	320	261
13	322	352	397	458	484	542	595	519	452	394	319	262
14	325	340	414	445	494	550	568	532	461	393	336	265
15	324	375	408	451	486	551	555	535	473	423	345	251
16	321	367	393	404	465	494	495	509	461	427	344	268
17	319	378	344	276	257	246	273	321	322	382	329	276
18	214	265	223	49	0	0	0	0	39	257	202	199
19	2	1	0	0	0	0	0	0	0	0	0	0
20-24	0	0	0	0	0	0	0	0	0	0	0	0

5.1.3   Economic and environmental data of fuels and electricity

For the economic and environmental assessment developed herein, the energy resources consumed by the system must be properly characterized in terms of their market-based energy prices and CO_2 emission factors. The energy resources available to the system are the following: locally available solar radiation, biomass pellets, natural gas, and the electricity from the national electric grid.

In Campinas, the local natural gas distributor is COMGAS, which offers a purchase price of *pcegas* = 0.035 €/kWh (LHV) (COMGAS, 2018). In the case of electricity, the local distributor CPFL Paulista offers a time-of-use tariff consisting on two pricing periods in which the purchase price *pelcom* varies according to the hour of the day and the month of the year as shown in Table 5.6. For this study, the contracted power tariff has been left out of the calculations. The electricity selling price *pelven* was assumed to be the purchase price at the corresponding hour minus a discount (penalization) of *penven* = 0.012 €/kWh, which accounts for the Tariff of Use of Distribution System (TUSD) relative to distribution and availability costs (CPFL, 2018). Finally, it was considered that biomass pellets were available at the purchase price of *pcebio* = 0.026 €/kWh (LHV) (Delgado et al., 2018). All the aforementioned energy prices include taxes.

Table 5.6: Hourly electricity prices with taxes (CPFL, 2018).

Annual period	On-peak		Off-peak	
	Hours	*pelcom*	**Hours**	*pelcom*
March to October	18-20	0.136 €/kWh	1-17, 21-24	0.094 €/kWh
November to February	19-21	0.136 €/kWh	1-18, 22-24	0.094 €/kWh

In terms of CO_2 emissions, the environmental impact associated with the consumption of the energy resources is assessed through: (i) the natural gas CO_2 emission factor $kgCO2_{gas}$ = 0.2020 kg CO_2/kWh (Rupp and Lamberts, 2017); (ii) the biomass pellets CO_2 emission factor $kgCO2_{bio}$ = 0.0506 kg CO_2/kWh (Delgado et al., 2018); and (iii) the CO_2 emission factor of the electricity in the national electric grid $kgCO2_{ele}$.

The CO_2 emission factors of the electricity in Brazil's power system are available on hourly basis for whole years since 2006 in (MCTIC, 2018). It is worth mentioning that these values are calculated based on generation records of plants centrally dispatched by the National Power System Operator (ONS) applying the methodological tool "Tool to calculate the emission factor for an electricity system". Such tool determines the CO_2 emission factor for the displacement of electricity generated by power plants in an electricity system by assessing the "combined margin" emission factor (CM) of the electricity system. The CM is the result of a weighted average of two emission factors pertaining to the electricity system: the operating margin (OM) and the build margin (BM). The OM is the emission factor that refers to the group of existing power plants whose current electricity production would be affected by the proposed new system. The BM is the emission factor that refers to the group of prospective power plants whose construction and future operation would be affected by the proposed new system (UN-FCCC, 2006).

For the present study, we have processed the data for the year 2016 to obtain the average hourly CO_2 emissions for each month of the year, which are shown in Figure 5.2 divided into wet period (December to April) and dry period (May to November) months. Considering the maximum and

the minimum hourly emission factors in each month of the year, the highest variation takes place in May (14.3%) and the lowest variation takes place in January (1.7%). The annual average value is 0.6228 kg CO_2/kWh. Considering the electricity generation of the whole national electric system, the annual average CO_2 emission factor is equal to 0.1581 kg CO_2/kWh.
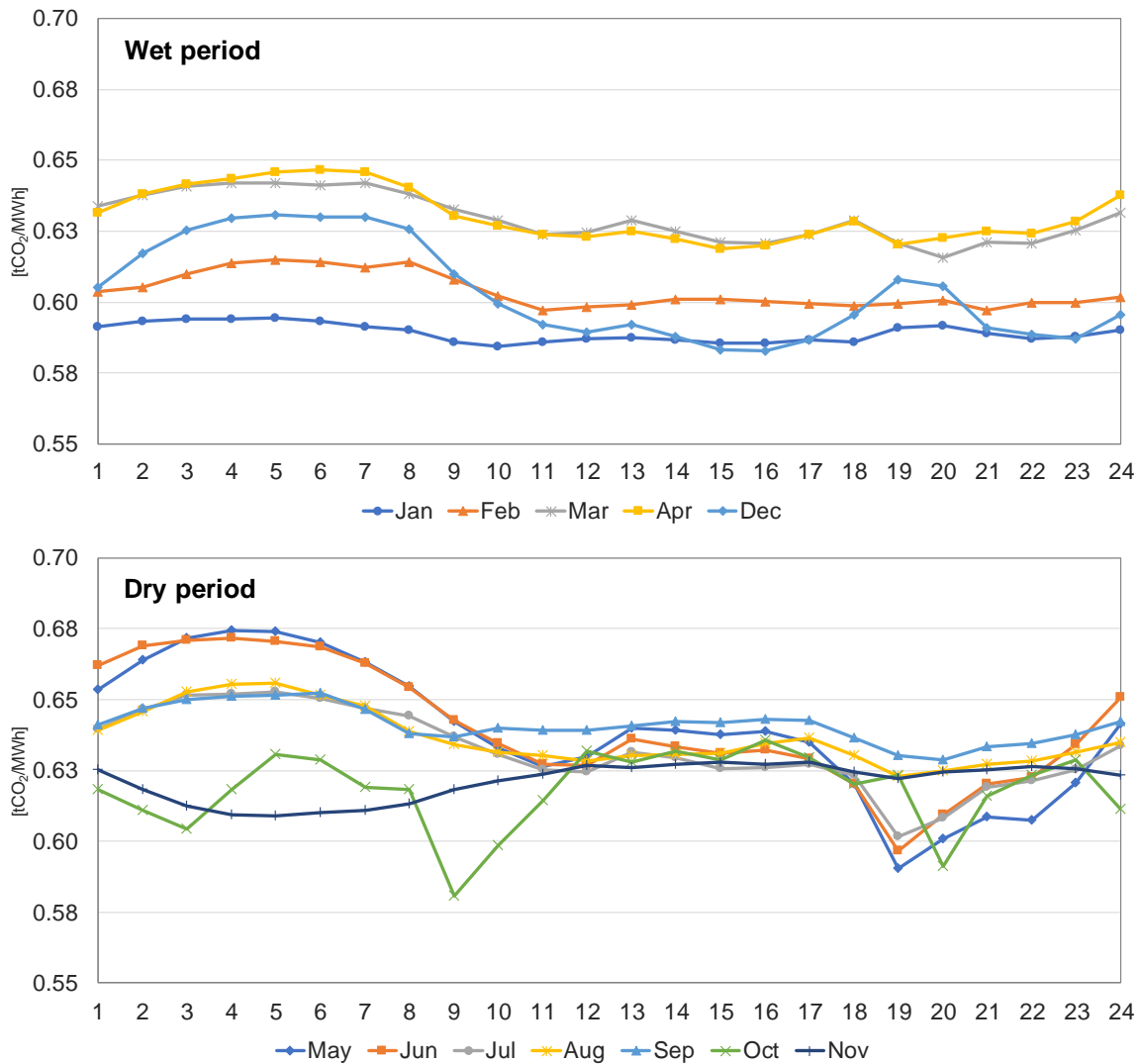
Figure 5.2: Hourly CO_2 emission factors of the electricity in the national electric grid in wet period (top) and dry period (bottom) months.

5.1.4 Electricity regulation in Brazil

A realistic representation of the case study must also take into account local policies and regulations, as they may have a significant influence on the optimal system's configuration and operational strategy. In the case of the university hospital analyzed herein, it is necessary to determine the conditions that allow the system to exchange electricity with the electric system. In this regard, the Brazilian Electricity Regulatory Agency (ANEEL) established the general conditions for the access of distributed microgeneration and minigeneration to the distribution

network and the Electrical Energy Compensation System (EECS) through the Normative Resolution 482/2012 (updated by the Normative Resolutions 687/2015 and 786/2017). This information is going to be used later in the mathematical model development.

The EECS is a system in which the injected electricity is transferred, by means of free loan, to the local distribution network generating energy credits in kWh that remain valid for a period of up to 60 months. The energy credits generated at a pricing period (e.g. on-peak) may be used to compensate electricity consumption at a different one (e.g. off-peak), in which case the ratio of the electricity tariff at the pricing period of injection to the electricity tariff at the pricing period of consumption must be used. After the 60 months any unused energy credits are lost.

One of the conditions to access the EECS is that the energy system must fit into the microgeneration or minigeneration category. The updated version of the Normative Resolution 482/2012 defines distributed micro and minigeneration as electricity production in small installations using any renewable source and/or qualified cogeneration connected to the distribution network through consumer unit facilities. Distributed microgeneration corresponds to power facilities with installed capacity less than or equal to 75 kW, while distributed minigeneration corresponds to power facilities with installed capacity greater than 75 kW and less or equal to 5 MW. The installed capacity of the distributed microgeneration and minigeneration is limited to the power availability in the local network distribution system.

5.2 RENEWABLE-BASED POLYGENERATION SYSTEM

This section describes the superstructure of the renewable-based polygeneration system analyzed, provides a detailed description of the technologies' technical, economic and environmental data, and presents the thermal integration subsystem, devised to allow for the optimal match between the heat supplied and demanded by the candidate technologies in the superstructure.

5.2.1 Superstructure

The superstructure of the polygeneration system is depicted in Figure 5.3. The energy resources available to the system include both renewable (solar radiation and biomass) and conventional (natural gas and electricity purchased from the electric grid) resources. The polygeneration system is designed to attend the hospital's energy demands, which consist of electricity E_d, saturated steam V_d at 180 °C, hot water Q_d at 60 °C, and chilled water R_d at 7 °C.

Figure 5.3: Superstructure of the renewable-based polygeneration system.

PV: Photovoltaic panels

BH: Biomass hot water boiler

AS: Single-effect absorption chiller

HS: Hot water storage tank

ST: Flat-plate solar thermal collectors

BV: Biomass steam boiler

AD: Double-effect absorption chiller

CS: Chilled water storage tank

PT: Parabolic trough concentrators

GH: Natural gas hot water boiler

EC: Mechanical chiller

GE: Cogeneration module

GV: Natural gas steam boiler

CT: Cooling tower

In accordance with the classification described in Chapter 2, the candidate technologies included in the superstructure can be divided into three groups:

- Generation technologies: Convert the energy resource into intermediate or final products. Depending on the energy resource's availability, the generation technologies may be classified as dispatchable (biomass hot water boiler BH, biomass steam boiler BV, natural gas hot water boiler GH, natural gas steam boiler GH, and natural gas cogeneration module GE) and non-dispatchable or intermittent (photovoltaic panels PV, flat-plate solar thermal collectors ST, and parabolic trough concentrators PT);

- Transformation technologies: Convert the energy resource or intermediate product into a final product. The technologies in the superstructure that fit into this description are the mechanical chiller EC, the single-effect absorption chiller AS, and the double-effect absorption chiller AD;

- Storage technologies: Store the energy product for later use. A hot water storage tank HS and a chilled water storage tank CS have been included in the superstructure.

The only exception to this classification is the cooling tower CT, which is a heat rejection technology that must be installed to dissipate to the ambient air the heat Q_{dis} from the transformation technologies ($Q_{dis,as}$, $Q_{dis,ad}$ and $Q_{dis,ec}$) and from the thermal integration subsystem $Q_{dis,int}$.

The cogeneration module GE consists of an internal combustion engine (based on the Wärtsilä 34DF model series) coupled to a heat recovery system. The GE consumes natural gas F_{ge} and produces cogenerated electricity W_{ge} and heat; the energy balance in the gas engine, based on technical data from the manufacturer's catalogue, identified four usable heat sources: exhaust gas Q_{eg}, charge air Q_{ac}, jacket water Q_{jw}, and lubricating oil Q_{lo}. The photovoltaic panels PV produce electricity W_{pv} from the global solar radiation on tilted surface Q_r. It is assumed that the system is connected to the electric grid, so electricity purchase E_p and sale E_s are allowed. Also, auxiliary electricity consumption W_{aux} was considered for most of the candidate technologies, as indicated in Figure 5.3.

The generation technologies (except for the PV) produce heat that can be used to attend the steam and hot water demands of the consumer center, as well as to drive the absorption chillers. The gas boilers GV and GH consume natural gas F_{gv} and F_{gh} and produce steam Q_{gv} and hot water Q_{gh}, respectively. The biomass boilers BV and BH consume biomass F_{bv} and F_{bh} and produce steam Q_{bv} and hot water Q_{bh}, respectively. Regarding the solar heat, flat-plate solar thermal collectors ST produce hot water Q_{st} from the global solar radiation on tilted surface Q_r, and parabolic trough

concentrators PT produce heat Q_{pt} from the normal direct solar radiation Q_{bn}. For cooling production, the mechanical chiller EC consumes electricity W_{ec} to produce cooling R_{ec}, while the simple-effect AS and double-effect AD absorption chillers consume heat Q_{as} and Q_{ad} to produce cooling R_{as} and R_{ad}, respectively.

Hot water Q_{hw} can be charged Q_{in} to and discharged Q_{out} from the hot water storage tank HS, with S_q being the energy stored in the time interval. Likewise, chilled water can be charged R_{in} to and discharged R_{out} from the chilled water storage tank CS, with S_r being the energy stored in the time interval. It is assumed that no energy losses take place in the TES units.

5.2.2   Equipment data

The candidate technologies included in the superstructure of Figure 5.3 are based on real, commercially available devices. The technical data correspond to a representative device of a series that was carefully selected to fit within the capacity range estimated based on the hospital's energy demands. The only exceptions are the PV, ST and PT, due to their modular assembly, so their technical parameters are those of a specific model. The complete information of the devices is provided in the Appendix B.

Table 5.7 shows the main technical parameters of the technologies, including the electric or thermal (LHV) efficiencies η, the coefficient of performance COP, the unit auxiliary electricity consumption CUe, the area to power ratio Rap of the solar-based RETs (in m^2 of module surface area per kW installed), and the maximum installable capacity PIN_{MAX}. Additional information about the photovoltaic panel, flat-plate solar thermal collector and parabolic trough concentrator is provided in Table 5.8, Table 5.9 and Table 5.10.

The operation of the technologies is limited to their installed capacities. In the case of the solar-based RETs, however, their productions are also limited by local environmental conditions, such as solar irradiance and ambient temperature, which vary hourly and daily. The unit production per m^2 of photovoltaic panel x_{pv} and flat-plate solar thermal collector x_{st}, module installed were calculated as described in SECTION A.4.3 assuming that they are fixed in place, facing north with a 20° tilt.

Table 5.7: Main technical data of the candidate technologies.

	Technology t	η	COP	CUe, kW_{el}/kW	Rap, m^2/kW	PIN_{MAX}, kW
PV	Photovoltaic panel	-	-	-	5.7070	10,000
ST	Flat-plate solar thermal collector	-	-	0.0050	1.4286	5000
PT	Parabolic trough concentrator	-	-	0.0164	1.5172	5000
GE	Cogeneration module	0.467 [1]	-	0.0300	-	5000
BH	Biomass hot water boiler	0.850	-	0.0050	-	5000
BV	Biomass steam boiler	0.850	-	0.0050	-	5000
GH	Natural gas hot water boiler	0.920	-	0.0050	-	5000
GV	Natural gas steam boiler	0.930	-	0.0050	-	5000
AS	Single-effect absorption chiller	-	0.635	0.0050	-	5000
AD	Double-effect absorption chiller	-	1.410	0.0050	-	5000
EC	Mechanical chiller	-	6.110	-	-	5000
CT	Cooling tower	1.000	-	0.0050	-	10,000
HS	Hot water storage tank	1.000	-	-	-	50,000 [2]
CS	Chilled water storage tank	1.000	-	-	-	50,000 [2]

[1] Electric efficiency; [2] kWh.

Table 5.8: Photovoltaic panel's technical data.

Parameters	Value
Manufacturer	Zytech
Model	ZT340P
P_{pv}: Maximum power	0.34 kWp
$A_{m,pv}$: Module surface area	1.94 m^2
η_{pv}: Module efficiency	0.1752
μ_T: Temperature coefficient of power	0.0038 °C^{-1}
$T_{c,NOCT}$: Cell temperature at NOCT conditions	45 °C

Table 5.9: Flat-plate solar thermal collector's technical data.

Parameters	Value
Manufacturer	OkoTech
Model	Gluatmugl HT
$A_{m,st}$: Module surface area	12 m^2
η_0: Thermal coefficient	0.806
k_1: Thermal coefficient	2.580 W/(m^2·K)
k_2: Thermal coefficient	0.009 W/(m^2·K^2)

Table 5.10: Parabolic trough concentrator's technical data.

Parameters	Value
Solar field	
Total aperture area	656 m²
Direct normal irradiance at design point	950 W/m²
Solar collector	
Model	SkyFuel SkyTrough
Orientation	North-South
Solar tracking	East-West
Tilt	0°
Solar Receiver	
Model	Schott PTR80
Heat transfer fluid (HTF)	Dowtherm RP
Inlet and outlet HTF temperature	185-225 ℃

Regarding the parabolic trough concentrator, the System Advisory Model (SAM) (NREL, 2018) was used to model and simulate the parabolic trough collector field. SAM is an open source software package which contains performance and economic models for concentrating solar power (CSP) systems, photovoltaic, solar hot water, and generic fuel-use technologies based on an hourly simulation engine integrated with TRNSYS (2019). An in-depth explanation of the model can be found in Wagner and Gilman (2011). The unit production per m² of PT installed x_{pt} was determined based on SAM's results.

Table 5.11, Table 5.12 and Table 5.13 present the x_{pv}, x_{pt} and x_{st} values, respectively, given as input data to the model.

Table 5.11: Unit production per m² of PV installed x_{pv}, W/m².

Hour	Jan	Feb	Mar	Apr	May	Jun	Jul	Aug	Sep	Oct	Nov	Dec
1-5	0	0	0	0	0	0	0	0	0	0	0	0
6	0	0	0	0	0	0	0	0	0	0	1	1
7	10	5	2	1	0	0	0	0	4	16	20	18
8	35	32	29	29	26	24	23	29	34	42	45	43
9	61	58	57	59	55	54	53	62	61	68	72	69
10	80	79	81	83	79	81	81	87	84	87	90	91
11	94	103	100	102	94	98	101	105	101	102	103	104
12	98	104	103	110	103	105	112	112	113	105	100	97
13	97	105	106	111	103	105	113	112	113	102	97	98
14	92	97	101	99	100	99	103	107	106	95	91	91
15	81	90	88	87	84	84	88	92	91	83	80	78
16	63	73	69	63	62	60	64	69	69	61	62	61
17	43	52	44	35	31	29	33	39	38	35	38	41
18	21	26	18	5	1	0	1	3	6	10	14	19
19	3	2	0	0	0	0	0	0	0	0	1	2
20-24	0	0	0	0	0	0	0	0	0	0	0	0

Table 5.12: Unit production per m^2 of PT installed x_{pt}, W/m^2.

Hour	Jan	Feb	Mar	Apr	May	Jun	Jul	Aug	Sep	Oct	Nov	Dec
1-6	0	0	0	0	0	0	0	0	0	0	0	0
7	3	0	0	0	0	0	0	0	0	3	20	16
8	136	99	45	6	1	0	0	3	53	171	173	174
9	187	210	189	200	161	148	149	227	220	213	198	201
10	192	212	203	230	217	250	258	282	236	202	207	213
11	189	222	214	242	206	241	270	269	224	215	205	209
12	177	187	190	234	213	231	267	257	240	202	166	145
13	162	183	194	230	218	230	264	251	237	198	166	147
14	165	177	208	228	217	239	260	262	246	194	174	149
15	162	202	203	235	235	259	269	274	258	213	176	140
16	162	197	193	221	247	255	257	274	255	223	176	146
17	166	202	184	151	84	66	99	164	195	222	175	157
18	119	135	60	24	27	26	26	26	25	46	65	94
19	16	22	20	16	18	18	18	17	17	19	19	19
20	10	15	13	9	10	9	9	9	9	12	12	12
21	5	7	6	1	0	0	0	0	1	6	5	6
22-24	0	0	0	0	0	0	0	0	0	0	0	0

Table 5.13: Unit production per m^2 of ST installed x_{st}, W/m^2.

Hour	Jan	Feb	Mar	Apr	May	Jun	Jul	Aug	Sep	Oct	Nov	Dec
1-7	0	0	0	0	0	0	0	0	0	0	0	0
8	0	0	0	0	0	0	0	0	0	0	13	4
9	105	93	86	88	49	40	29	91	92	142	167	151
10	219	218	228	227	188	196	189	239	229	258	276	283
11	305	363	345	347	282	298	312	353	331	355	361	371
12	338	374	370	404	338	351	386	405	409	382	343	333
13	334	385	390	413	345	355	400	411	416	366	333	339
14	308	341	363	346	330	323	347	385	379	328	299	303
15	245	299	288	278	243	241	258	299	295	255	234	225
16	141	200	177	138	117	106	124	162	164	133	130	132
17	26	79	35	0	0	0	0	0	0	0	0	17
18-24	0	0	0	0	0	0	0	0	0	0	0	0

The economic costs and environmental impacts of installing the candidate technologies are represented by the bare module cost CI and unit CO_2 emissions $CO2U$, respectively, as shown in Table 5.14. The CI corresponds to the purchase cost multiplied by a simple module factor, which accounts for transportation, installation, connection costs, etc. Additional economic data include the amortization and maintenance factor fam = 0.15 yr^{-1} and the indirect costs factor f_{IC} = 0.20 (Ramos, 2012). The $CO2U$ corresponds to the CO_2 emissions generated in the manufacturing process of the equipment. Also, it was considered that the plant's operational lifetime nyr = 20 years.

Table 5.14: Bare module cost and unit CO_2 emissions of the candidate technologies.

	Technology t	Bare module cost *CI* €/kW$_{nom}$	Unit CO_2 emissions *CO2U* kg CO_2/kW$_{nom}$
PV	Photovoltaic panel	1300 [2]	1840 [7]
ST	Flat-plate solar thermal collector	500 [3]	140 [3,8]
PT	Parabolic trough concentrator	425 [4]	130 [9,10]
GE	Cogeneration module	675 [5]	65 [11]
BH	Biomass hot water boiler	310 [6]	15 [1]
BV	Biomass steam boiler	375 [6]	20 [1]
GH	Natural gas hot water boiler	55 [5]	10 [11]
GV	Natural gas steam boiler	120 [5]	10 [11]
AS	Single-effect absorption chiller	260 [5]	165 [11]
AD	Double-effect absorption chiller	260 [5]	165 [11]
EC	Mechanical chiller	105 [5]	160 [11]
CT	Cooling tower	30 [5]	25 [11]
HS	Hot water storage tank	40 €/kWh [5]	150 kg CO_2/kWh [3]
CS	Chilled water storage tank	80 €/kWh [5]	300 kg CO_2/kWh [3]

References: [1](Delgado et al., 2018); [2](Lazard, 2016); [3](Guadalfajara, 2016); [4](Kurup and Turchi, 2015); [5](Ramos, 2012); [6](IEA, 2017); [7](Ito et al., 2009); [8](Raluy et al., 2014); [9](Burkhardt et al., 2011); [10](WEC, 2016); [11](Carvalho, 2011).

5.2.3 Thermal integration subsystem

For a realistic combination of technologies and thermal energy flows it becomes imperative that heat sources and demands are evaluated in terms of both quantity (kWh) and quality (temperature levels). Disregarding the flows' energy quality levels may result in a violation of the Second Law of Thermodynamics and unfeasible system configurations.

To address this issue, it is proposed herein to introduce in the superstructure depicted in Figure 5.3 a thermal integration subsystem, in which the hot flows supplied by the generation technologies and the cold flows consumed by transformation technologies and/or associated with the thermal energy demands of the consumer center exchange heat through a virtual network of heat exchangers. The thermal integration subsystem thus serves as interface between the heat supply and the heat demand in the system.

In order to impose sufficient thermal gradient for the heat transfer, a minimum temperature difference is set depending on the type of flow: 20 °C in the case of gas flows (e.g. exhaust gas, air) and 5 °C in the case of liquid flows (e.g. water, oil, HTF). As it was decided to keep the temperatures of the thermal energy services supplied to the consumer center unchanged, the minimum temperature differences have been carried out to the hot flows.

Table 5.15 presents the thermal characteristics of the different heat sources supplied by the technologies, namely the unit mass flow production *mui* in kg/s per kW of operating capacity,

specific heat *cpi*, latent heat *lhi*, temperature difference *ΔT*, initial (supply) T_{in} and final (target) T_{out} temperatures, and shifted temperatures T_{in}^* and T_{out}^*. The shifted temperatures are obtained by subtracting the previously mentioned minimum temperature differences from T_{in} and T_{out}. The hot flows *ibv* and *igv* provide latent heat at 180 °C.

Table 5.15: Thermal characteristics of hot flows.

Tech. t	Flow	Type	*mui* (kg/s)/kW	*cpi* kJ/(kg·K)	*lhi* kJ/kg	*ΔT* °C	T_{in} °C	T_{out} °C	T_{in}^* °C	T_{out}^* °C
GE	*ieg*	Gas	1.5808e-3	1.11	0	270	380	110	360	90
GE	*iac*	Air	1.5394e-3	1.01	0	170	215	40	195	20
GE	*ijw*	Water	3.0240e-3	4.20	0	10	95	85	90	80
GE	*ilo*	Oil	4.2612e-3	2.10	0	10	75	65	70	60
ST	*ist*	Water	7.9365e-3	4.20	0	30	95	65	90	60
PT	*ipt*	HTF	11.5218e-3	2.17	0	40	225	185	220	180
BH	*ibh*	Water	7.9365e-3	4.20	0	30	95	65	90	60
BV	*ibv*	Water	0.4179e-3	4.20	2015	90	185	95	180	90
GH	*igh*	Water	11.9048e-3	4.20	0	20	95	75	90	70
GV	*igv*	Water	0.4179e-3	4.20	2015	90	185	95	180	90

The hot flows supplied by the generation technologies are explained as follows. The cogeneration module GE provides four hot flows, each associated with one of its useful heat sources: (i) the exhaust gas is available at 380 °C and can be cooled until 110 °C (flow *ieg*), which is a limit established in order to avoid acid corrosion resulting from condensation within the heat recovery boiler; (ii) the charge air is available at 215 °C and must be cooled until 45 °C (flow *iac*); (iii) the jacket water is available at 95 °C and must be cooled until 85 °C (flow *ijw*); and (iv) the lubricating oil is available at 75 °C and must be cooled until 65 °C (flow *ilo*). The GV supplies saturated steam at 185 °C from hot water at 95 °C (flow *igv*). The GH supplies hot water at 95 °C from hot water at 75 °C (flow *igh*). The BV supplies saturated steam at 185 °C from hot water at 95 °C (flow *ibv*). The BH supplies hot water at 95 °C from hot water at 65 °C (flow *ibh*). The ST supply hot water at 95 °C from hot water at 65 °C (flow *ist*). Finally, the PT supply heat from 225 °C to 185 °C (flow *ipt*).

Analogously, Table 5.16 presents the thermal characteristics of the cold flows. The unit mass flow consumption *muj* is given in kg/s per kW of operating capacity in the case of the absorption chillers (flows *jas* and *jad*), and per kW of energy service consumed in the case of the hospital's steam (flow *jvd*) and hot water demands (*jqd*). The cold flows *jad* and *jvd* consume latent heat at 180 °C.

Table 5.16: Thermal characteristics of cold flows.

Tech. t	Flow	Type	muj (kg/s)/kW	cpj kJ/(kg·K)	lhj kJ/kg	ΔT °C	T_{in} °C	T_{out} °C	T_{in}^* °C	T_{out}^* °C
AS	jas	Water	12.4984e-3	4.20	0	30	60	90	60	90
AD	jad	Water	0.2964e-3	4.20	2015	90	90	180	90	180
VAP	jvd	Water	0.4037e-3	4.20	2015	110	70	180	70	180
DHW	jqd	Water	5.9524e-3	4.20	0	40	20	60	20	60

The cold flows consumed by transformation technologies and related to the steam and hot water demands of the consumer center are explained as follows. The AS produces chilled water at 7 °C consuming hot water at 90 °C and discharging it at 60 °C (flow *jas*). The AD produces chilled water at 7 °C consuming saturated steam at 180 °C and discharging it as hot water at 90 °C (flow *jad*). The steam demand corresponds to saturated steam at 180 °C that returns as hot water at 70 °C (flow *jvd*). The hot water demand is delivered at 60 °C and returns at 20 °C (flow *jqd*). Finally, the surplus heat $Q_{dis,int}$, if any, is dissipated in the cooling tower.

A detailed representation of the thermal integration subsystem is shown in Figure 5.4, indicating the hot and cold flows associated with each technology and/or energy demand, as well as their names and their initial (supply) and final (target) temperatures; a total of 10 temperature intervals were identified, the first being the hottest. Temperature interval $k = 4$ corresponds to the phase change from saturated water to saturated steam at 180 °C, in which the hot flows *ibv* and *igv* provide latent heat *lhi* and the cold flows *jad* and *jvd* consume latent heat *lhj*.
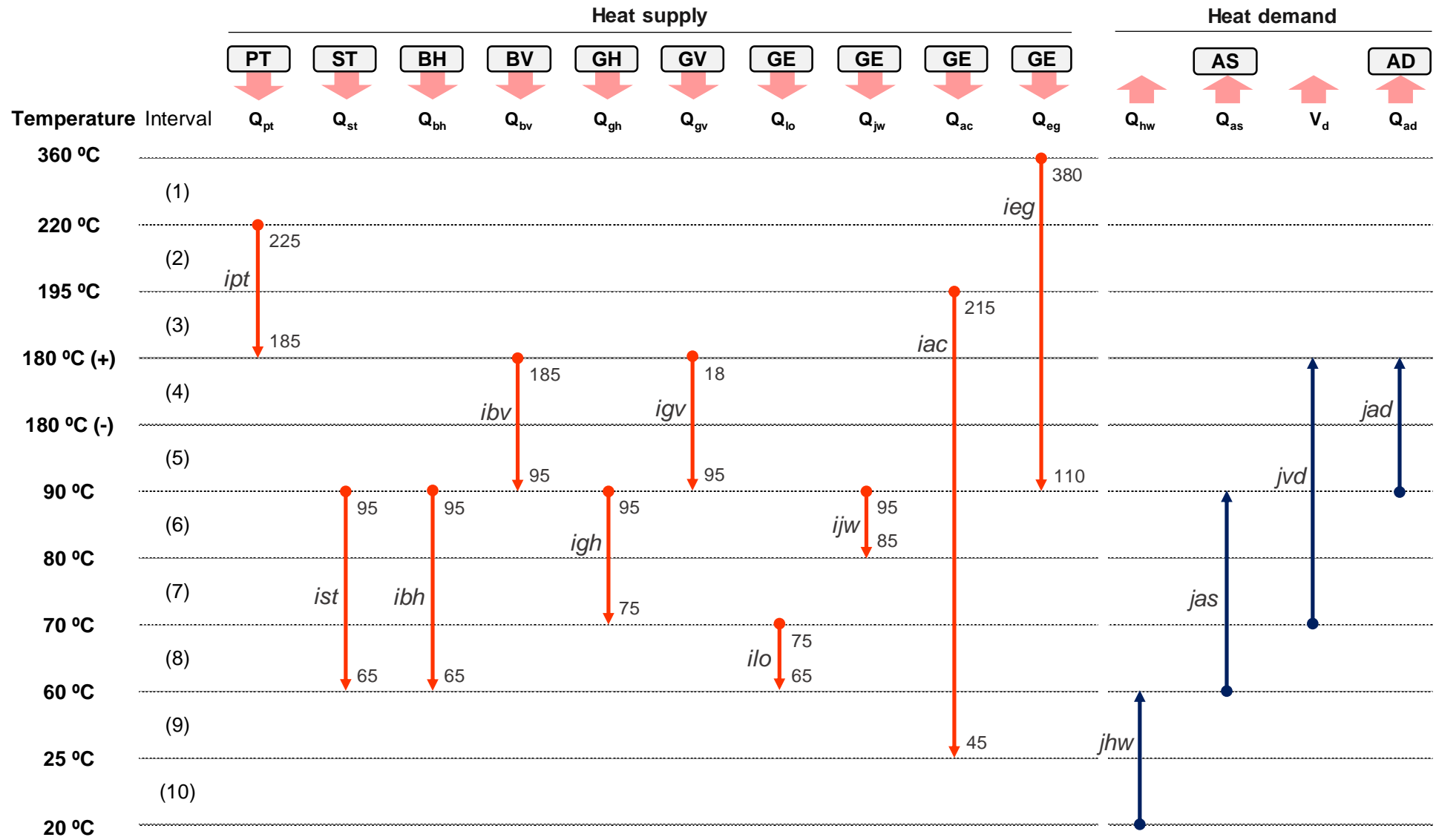
Figure 5.4: Thermal integration subsystem.

5.3 MATHEMATICAL MODEL

A MILP model was developed to determine the optimal configuration and operational planning of the renewable-based polygeneration system described in Section 5.2 for the case study analyzed herein. The optimization model is composed of decision variables representing: (i) the existence and size of the technologies; (ii) the operation load of each technology in each time interval; (iii) the energy resources exchanged with the market, i.e. electricity, natural gas and biomass; (iv) the TES units' capacities and the energy stored in each time interval; (v) the heat supply and demand in each temperature interval; and (vi) the heat surplus from one temperature interval to the next (heat cascade). The existence of technologies and external (legal) restrictions, such as the permission to sell electricity to the grid, are represented by binary variables, while all other variables are continuous.

5.3.1 Objective functions

The economic objective function is the total annual cost CTE_{tot}, which consists of the annual fixed cost CTE_{fix} and the annual variable cost CTE_{var}, calculated as

$$CTE_{tot} = CTE_{fix} + CTE_{var} \tag{5.1}$$

The annual fixed cost CTE_{fix} is given by Eq. (5.2), where $PIN(t)$ is the installed capacity of technology t.

$$CTE_{fix} = fam \cdot (1 + fic) \cdot \sum_t CI(t) \cdot PIN(t) \tag{5.2}$$

As previously mentioned, the operation of the system is described by 24 representative days (NRD = 24), each one composed of 24 consecutive periods (NP = 24) of 1-hour duration (NHP = 1). The annual variable cost CTE_{var} corresponds to the sum, for each hourly period h of each representative day d, of the costs of purchasing natural gas $CTE_{gas}(d,h)$, biomass $CTE_{bio}(d,h)$, and electricity $CTE_{ele}(d,h)$:

$$CTE_{var} = \sum_{d=1}^{NRD} \sum_{h=1}^{NP} NRY(d) \cdot NHP(h) \cdot \left(CTE_{gas}(d,h) + CTE_{bio}(d,h) + CTE_{ele}(d,h)\right) \tag{5.3}$$

$$CTE_{gas}(d,h) = pcegas \cdot \left(F_{gh}(d,h) + F_{gv}(d,h) + F_{ge}(d,h)\right) \tag{5.4}$$

$$CTE_{bio}(d,h) = pcebio \cdot \left(F_{bh}(d,h) + F_{bv}(d,h)\right) \tag{5.5}$$

$$CTE_{ele}(d,h) = pelcom(d,h) \cdot E_p(d,h) - pelven(d,h) \cdot E_s(d,h) \tag{5.6}$$

Analogous to the economic criterion, the environmental objective function corresponds to the total annual CO_2 emissions $CO2_{tot}$, which consists of the annual fixed emissions $CO2_{fix}$ and the annual variable emissions $CO2_{var}$.

$$CO2_{tot} = CO2_{fix} + CO2_{var} \tag{5.7}$$

The $CO2_{fix}$, annualized over the plant's operational lifetime *nyr* is expressed by

$$CO2_{fix} = \sum_t CO2U(t) \cdot PIN(t)/nyr \tag{5.8}$$

The $CO2_{var}$ consists of the terms relative to the consumption of natural gas $CO2_{gas}(d,h)$, biomass $CO2_{bio}(d,h)$, and electricity $CO2_{ele}(d,h)$:

$$CO2_{var} = \sum_{d=1}^{NRD} \sum_{h=1}^{NP} NRY(d) \cdot NHP(h) \cdot \left(CO2_{gas}(d,h) + CO2_{bio}(d,h) + CO2_{ele}(d,h)\right) \tag{5.9}$$

$$CO2_{gas}(d,h) = kgCO2_{gas} \cdot \left(F_{gh}(d,h) + F_{gv}(d,h) + F_{ge}(d,h)\right) \tag{5.10}$$

$$CO2_{bio}(d,h) = kgCO2_{bio} \cdot \left(F_{bh}(d,h) + F_{bv}(d,h)\right) \tag{5.11}$$

$$CO2_{ele}(d,h) = kgCO2_{ele}(d,h) \cdot \left(E_p(d,h) - E_s(d,h)\right) \tag{5.12}$$

5.3.2 System constraints

The objective functions are subject to equipment (capacity limits and production restrictions), energy balances, electric grid, local policies, and thermal integration constraints, described in the following subsections.

5.3.2.1 Installed capacity limits

For each technology *t*, the installed capacity *PIN(t)* is limited to the maximum installable capacity $PIN_{MAX}(t)$, as expressed by Eq. (5.13). The binary variable *yINS(t)* expresses the permission to install or not the technology *t*.

$$PIN(t) \leq yINS(t) \cdot PIN_{MAX}(t) \tag{5.13}$$

5.3.2.2 Production restrictions

The production restrictions of the candidate technologies are described below, applicable to each hourly period *h* of each representative day *d*.

Dispatchable generation technologies and transformation technologies

The production of the technology t is limited to its installed capacity *PIN(t)*. An example is given for the natural gas hot water boiler GH:

$$Q_{gh}(d,h) \leq PIN(GH) \tag{5.14}$$

Equality production restrictions relate the technology's energy consumption to its production. Moreover, a unit auxiliary electricity consumption *CUe* has been considered for most technologies. Examples of both restrictions are given below for the GH:

$$Q_{gh}(d,h) - \eta_{gh} \cdot F_{gh}(d,h) = 0 \tag{5.15}$$
$$W_{aux,gh}(d,h) = CUe(GH) \cdot Q_{gh}(d,h) \tag{5.16}$$

Solar-based RETs

Their productions depend on the hourly unit production per m² of module installed and area to power ratio, given as input data to the model. An example is given Eq. (5.17) for the flat-plate solar thermal collectors ST. The auxiliary electricity consumption is determined in the same way as explained for Eq. (5.16).

$$Q_{st}(d,h) \leq x_{st}(d,h) \cdot Rap(ST) \cdot PIN(ST) \tag{5.17}$$

Cooling tower

The heat dissipated $Q_{dis}(d,h)$ by the cooling tower CT is limited to its installed capacity according to Eq. (5.18). The CT dissipates heat from the transformation technologies ($Q_{dis,as}$, $Q_{dis,ad}$ and $Q_{dis,ec}$) and from the thermal integration subsystem $Q_{dis,int}$. The calculation of $Q_{dis,int}$ in Eq. (5.19) is explained in Section 5.3.2.6.

$$Q_{dis}(d,h) \leq PIN(CT) \tag{5.18}$$
$$Q_{dis}(d,h) = Q_{dis,as}(d,h) + Q_{dis,ad}(d,h) + Q_{dis,ec}(d,h) + Q_{dis,int}(d,h) \tag{5.19}$$
$$Q_{dis,as}(d,h) = R_{as}(d,h) \cdot \big(1 + CUe(AS)\big) + Q_{as}(d,h) \tag{5.20}$$
$$Q_{dis,ad}(d,h) = R_{ad}(d,h) \cdot \big(1 + CUe(AD)\big) + Q_{ad}(d,h) \tag{5.21}$$
$$Q_{dis,ec}(d,h) = R_{ec}(d,h) \cdot (1 + 1/COP_{ec}) \tag{5.22}$$

Thermal energy storage units

In the case of the TES units, for instance the hot water storage tank HS, the energy stored at the end of any hourly period $S_q(d,h)$, in kWh, is limited to the installed capacity *PIN(HS)*, according to Eq. (5.23). The energy balance in the HS is given by Eq. (5.24), in which the charged $Q_{in}(d,h)$ and discharged $Q_{out}(d,h)$ energy flows, in kW, are multiplied by the duration of the period *NHP(h)* in

order to convert them to the same unit as the stored energy $S_q(d,h)$. It should be noted that, for this analysis, there are no energy losses in the TES units.

$$S_q(d,h) \leq PIN(HS) \tag{5.23}$$
$$S_q(d,h-1) + \left(Q_{in}(d,h) - Q_{out}(d,h)\right) \cdot NHP(h) - S_q(d,h) = 0 \tag{5.24}$$

Considering the daily cyclical characteristic of the system operation, the energy stored in the TES units at the end of the representative day must be equal to the energy stored at the beginning of that day.

Considering the daily cyclical characteristic of the TES units, the energy stored at the beginning of the day must be equal to the energy stored at the end of the previous day.

The same reasoning is applied to the chilled water storage tank CS:

$$S_r(d,h) \leq PIN(CS) \tag{5.25}$$
$$S_r(d,h-1) + \left(R_{in}(d,h) - R_{out}(d,h)\right) \cdot NHP(h) - S_r(d,h) = 0 \tag{5.26}$$

5.3.2.3 Energy balances

Equations (5.27)-(5.29) express the electricity, hot water and cooling balances in each time interval, respectively.

$$E_p(d,h) + W_{pv}(d,h) + W_{ge}(d,h) - E_d(d,h) - E_s(d,h) - W_{ec}(d,h) - W_{aux}(d,h) = 0 \tag{5.27}$$
$$Q_{hw}(d,h) + Q_{out}(d,h) - Q_{in}(d,h) - Q_d(d,h) = 0 \tag{5.28}$$
$$R_{ec}(d,h) + R_{as}(d,h) + R_{ad}(d,h) + R_{out}(d,h) - R_{in}(d,h) - R_d(d,h) = 0 \tag{5.29}$$

5.3.2.4 General electric grid constraints

The sold $E_s(d,h)$ and purchased $E_p(d,h)$ electricity are limited according to Eqs. (5.30) and (5.31), in which the binary variables yEs and yEp indicate the permission to sell electricity to the grid and the permission to purchase electricity from the grid, respectively.

$$E_s(d,h) \leq yEs \cdot \left(W_{pv}(d,h) + W_{ge}(d,h)\right) \tag{5.30}$$
$$E_p(d,h) \leq yEp \cdot \left(E_d(d,h) + W_{ec}(d,h) + W_{aux}(d,h)\right) \tag{5.31}$$

5.3.2.5 Local policies constraints

The ANEEL Normative Resolution nº 235/2006 defines the requirements for the qualification of cogeneration facilities in Brazil. In this regard, two conditions must be fulfilled: a minimum equivalent electric efficiency *EEE*, based on established parameters according to the installed capacity and type of fuel, expressed by Eq. (5.32); and a minimum thermal efficiency $\eta_{ge,th}$, given by Eq. (5.33). The GE electric efficiency η_{ge} is shown in Table 5.7. The GE thermal efficiency $\eta_{ge,th}$ is

calculated as the annual useful cogenerated heat (difference between the annual heat produced by the cogeneration module Q_{ge_Y} and the annual heat dissipated from the thermal integrated subsystem Q_{dis,int_Y}) divided by the annual natural gas consumption F_{ge_Y}, according to Eq. (5.34).

$$EEE = \eta_{ge} + \eta_{ge,th}/2.14 \geq 41\% \tag{5.32}$$

$$\eta_{ge,th} > 15\% \tag{5.33}$$

$$\eta_{ge,th} = (Q_{ge\_Y} - Q_{dis,int\_Y})/F_{ge\_Y} \tag{5.34}$$

5.3.2.6 Thermal integration subsystem modelling

The thermal integration subsystem depicted in Figure 5.4 has been modelled based on the Transshipment model by Papoulias and Grossmann (1983), in which hot i and cold j flows exchange heat in temperature intervals k. The heat cascade and the heat balance in a general temperature interval k are shown in Figure 5.5. The modelling of the thermal integration subsystem is explained as follows, for each hourly period h of each representative day d.
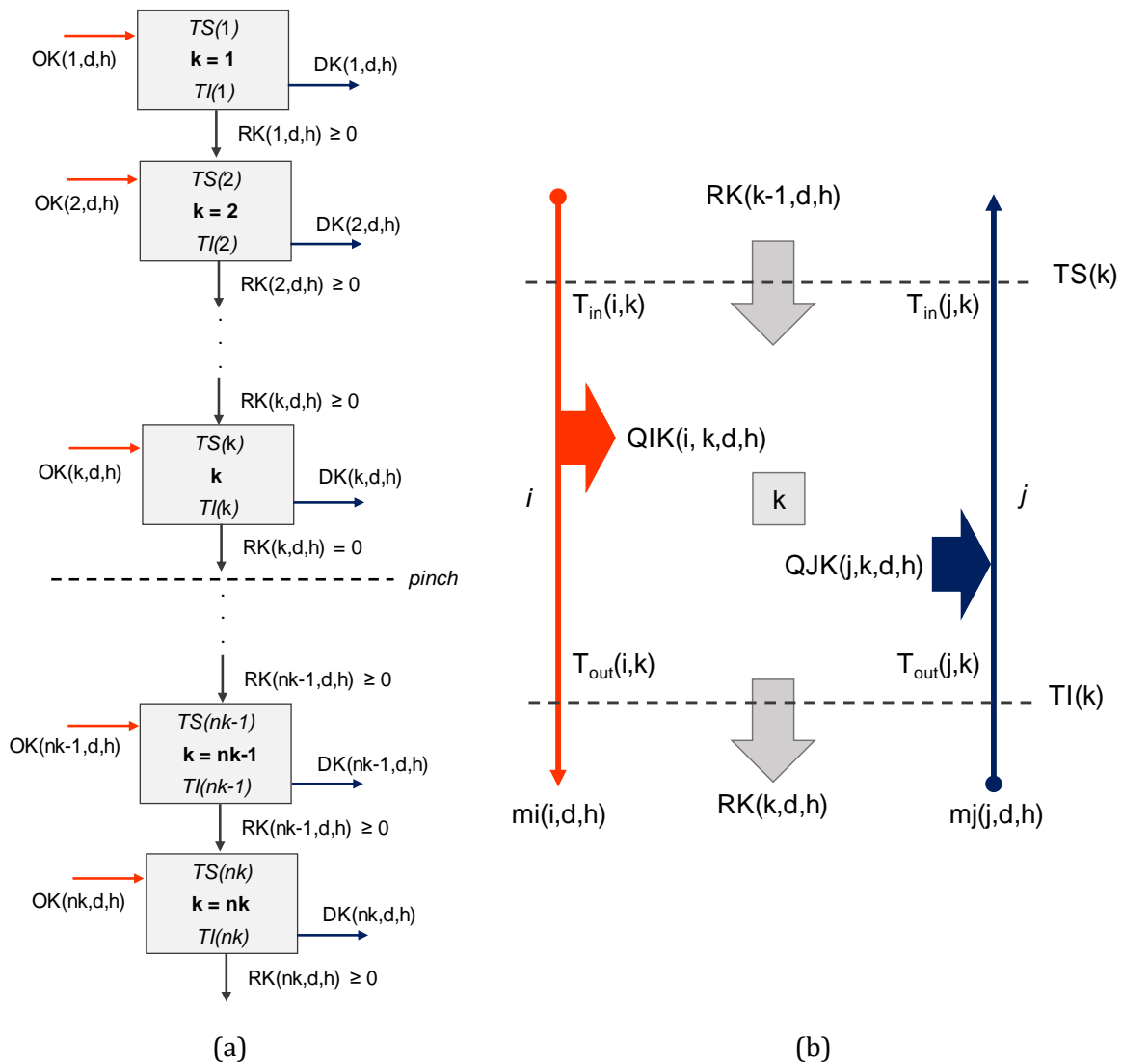
Figure 5.5: (a) Heat cascade, and (b) heat balance in a general temperature interval k.

The heat *QI(i,d,h)* supplied by a hot flow *i* is the sum of the heat *QIK(i,k,d,h)* transferred by the flow in each temperature interval *k* (Eq. (5.35)). The *QIK(i,k,d,h)* is, in turn, calculated according to Eq. (5.36). The hot flow mass rate *mi(i,d,h)* is determined as the product of the unit mass flow production *mui(i,t)* and the production of the main product *POP(t,d,h)* of technology *t* (Eq. (5.37)). The enthalpy change *Δhi(i,k)* of the hot flow *i* in the temperature interval *k* is expressed by Eq. (5.38), consisting of one component relative to the sensible heat (specific heat *cpi(i,k)* multiplied by the temperature difference of the temperature interval *ΔT(k)*) and another relative to the latent heat *lhi(i,k)*. The values of *mui(i,t)*, *cpi(i,k)* and *lhi(i,k)* were given in Table 5.15.

$$QI(i, d, h) = \sum_{k} QIK(i, k, d, h) \tag{5.35}$$

$$QIK(i, k, d, h) = mi(i, d, h) \cdot \Delta hi(i, k) \tag{5.36}$$

$$mi(i, d, h) = mui(i, t) \cdot POP(t, d, h) \tag{5.37}$$

$$\Delta hi(i, k) = cpi(i, k) \cdot \Delta T(k) + lhi(i, k) \tag{5.38}$$

To illustrate the modelling of Eqs. (5.35)-(5.38), examples are provided by Eqs. (5.39)-(5.42) for the hot flow *igh* associated with the natural gas hot water boiler GH. For the GH, the production of the main product *POP(t,d,h)* corresponds to the flow $Q_{gh}(d,h)$.

$$QI(igh, d, h) = \sum_{k} QIK(igh, k, d, h) \tag{5.39}$$

$$QIK(igh, k, d, h) = mi(igh, d, h) \cdot \Delta hi(igh, k) \tag{5.40}$$

$$mi(igh, d, h) = mui(igh, GH) \cdot Q_{gh}(d, h) \tag{5.41}$$

$$\Delta hi(igh, k) = cpi(igh, k) \cdot \Delta T(k) + lhi(igh, k) \tag{5.42}$$

For the cold flows *j*, Eqs. (5.43)-(5.46) are analogous to the ones presented for the hot flows. The values of *muj(j,t)*, *cpj(j,k)* and *lhj(j,k)* were given in Table 5.16.

$$QJ(j, d, h) = \sum_{k} QJK(j, k, d, h) \tag{5.43}$$

$$QJK(j, k, d, h) = mj(j, d, h) \cdot \Delta hj(j, k) \tag{5.44}$$

$$mj(j, d, h) = muj(j, t) \cdot POP(t, d, h) \tag{5.45}$$

$$\Delta hj(j, k) = cpj(j, k) \cdot \Delta T(k) + lhj(j, k) \tag{5.46}$$

Examples of Eqs. (5.43)-(5.46) are given by Eqs (5.47)-(5.50) for the cold flow *jas* associated with the single-effect absorption chiller AS. The production of the main product *POP(t,d,h)* of the AS corresponds to the flow $R_{as}(d,h)$.

$$QJ(jas, d, h) = \sum_{k} QJK(jas, k, d, h) \tag{5.47}$$

$$QJK(jas, k, d, h) = mj(jas, d, h) \cdot \Delta hj(jas, k) \tag{5.48}$$

$$mj(jas, d, h) = muj(jas, AS) \cdot R_{as}(d, h) \tag{5.49}$$

$$\Delta hj(jas, k) = cpj(jas, k) \cdot \Delta T(k) + lhj(jas, k) \tag{5.50}$$

The heat balance in a temperature interval k is expressed by Eq. (5.51), in which $RK(k,d,h)$ is the surplus heat of the corresponding temperature interval k, $RK(k-1,d,h)$ is the cascaded surplus heat from the previous (hotter) temperature interval $k-1$, $OK(k,d,h)$ is the heat supplied $QIK(i,k,d,h)$ by the hot flows i present in k (Eq. (5.52)), and $DK(k,d,h)$ is the heat consumed $QJK(j,k,d,h)$ by the cold flows j present in k (Eq. (5.53)). The fundamental condition of the Second Law of Thermodynamics is that the surplus heat must be greater than or equal to zero (Eq. (5.54)).

$$RK(k,d,h) + DK(k,d,h) = RK(k-1,d,h) + OK(k,d,h) \tag{5.51}$$

$$OK(k,d,h) = \sum_i QIK(i,k,d,h) \tag{5.52}$$

$$DK(k,d,h) = \sum_j QJK(j,k,d,h) \tag{5.53}$$

$$RK(k,d,h) \geq 0 \tag{5.54}$$

Finally, the surplus heat $RK(nk,d,h)$, if any, at the last (coldest) temperature interval nk, corresponds to the heat that must be dissipated $Q_{dis,int}(d,h)$ in the cooling tower. Also, there is no surplus heat into the first (hottest) temperature interval $k = 1$, so that $RK(0,d,h) = 0$.

$$Q_{dis,int}(d,h) = RK(nk,d,h) \tag{5.55}$$

5.3.3   Electrical energy compensation system modelling

This section modifies the optimization model described thus far by implementing the condition for the access to the EECS described in Section 5.1.4. This implementation will be used exclusively in the Brazilian grid modality D, described later in Section 5.4.

The permission to purchase electricity from the grid remains active (yEp = 1). On the other hand, selling electricity to the grid is no longer possible (yEs = 0), as now the power exchange with the grid is accounted in terms of energy credits. The binary variable $yEECS$ = 1 has been introduced to represent the access to the EECS.

In each time interval, the power exchange with the grid is represented by purchased electricity $E_p(d,h)$, imported electricity $E_{imp}(d,h)$, and exported electricity $E_{exp}(d,h)$. The electricity balance in the system expressed by Eq. (5.27) can be rewritten as

$$E_p(d,h) + E_{imp}(d,h) + W_{pv}(d,h) + W_{ge}(d,h) - E_d(d,h) - W_{ec}(d,h) - W_{aux}(d,h) - E_{exp}(d,h) = 0 \tag{5.56}$$

The $E_{exp}(d,h)$, $E_{imp}(d,h)$, and $E_p(d,h)$ are limited according to Eqs. (5.57)-(5.59).

$$E_{exp}(d,h) \leq yEECS \cdot \left(W_{pv}(d,h) + W_{ge}(d,h) \right) \tag{5.57}$$

$$E_{imp}(d,h) \leq yEECS \cdot \left(E_d(d,h) + W_{ec}(d,h) + W_{aux}(d,h) \right) \tag{5.58}$$

$$E_p(d,h) \leq yEp \cdot \left(E_d(d,h) + W_{ec}(d,h) + W_{aux}(d,h) - E_{imp}(d,h) \right) \tag{5.59}$$

Two additional binary variables $yIE(d,h)$ and $yEE(d,h)$ were introduced to prevent the system from simultaneously importing and exporting electricity. In order to avoid a nonlinearity, the constant *BIGM*, with a very large value (i.e. 1,000,000) was introduced. The following equations were obtained:

$$E_{exp}(d,h) \leq yEE(d,h) \cdot BIGM \tag{5.60}$$

$$E_{imp}(d,h) \leq yIE(d,h) \cdot BIGM \tag{5.61}$$

$$yEE(d,h) + yIE(d,h) \leq yEECS \tag{5.62}$$

The EECS can be represented in economic terms by computing the cost of the net electricity consumed by the system in the month; if the system exports more electricity than it consumes, the revenue is carried over to the next month, up to 60 months. In order to maintain an annual cyclic behavior to the system operation, it is considered herein that the revenue remains valid for only 12 months, after which any remaining revenue is lost. Therefore, the following constraint is defined for the annual balance of imported $E_{imp}(d,h)$ and exported $E_{exp}(d,h)$ electricity:

$$\sum_{d=1}^{NRD} \sum_{h=1}^{NP} NRY(d) \cdot NHP(h) \cdot pelcom(d,h) \cdot \left(E_{imp}(d,h) - E_{exp}(d,h) \right) \leq 0 \tag{5.63}$$

Regarding the objective functions, the electricity cost $CTE_{ele}(d,h)$ defined by Eq. (5.6) corresponds now only to the purchase cost, as expressed by Eq. (5.64). In the case of the environmental objective function, the $CO2_{ele}(d,h)$ defined by Eq. (5.12) can be rewritten as Eq. (5.65), which accounts for the CO_2 emissions associated with the electricity purchased, imported and exported.

$$CTE_{ele}(d,h) = pelcom(d,h) \cdot E_p(d,h) \tag{5.64}$$

$$CO2_{ele}(d,h) = kgCO2_{ele}(d,h) \cdot \left(E_p(d,h) + E_{imp}(d,h) - E_{exp}(d,h) \right) \tag{5.65}$$

5.4 RESULTS

The MILP optimization model developed in Section 5.3 was implemented and solved using the software LINGO (Schrage, 1999). As previously explained, binary variables are used in the optimization model to impose structural (regarding the permission to install technologies) and operational (regarding the permission to purchase/sell electricity) restrictions on the optimal solutions. For the optimal economic cost and environmental solutions analyzed herein, all candidate technologies in the superstructure depicted in Figure 5.3 were allowed to be installed

(*yINS(t)* = 1, for all technologies *t*). Moreover, four modalities of power exchange with the grid were proposed, as described by the binary variables and logical restrictions shown in Table 5.17.

Table 5.17: Modalities of power exchange with the grid.

Modality	Description
A Purchase only	Only purchase is allowed *yEp* = 1; *yEs* = 0
B Annual consumer	Purchase and sale are allowed with the condition of purchasing more electricity than it sells annually *yEp* = 1; *yEs* = 1 *Ep_Y – Es_Y* >= 0
C Unrestricted sale	Purchase and sale are allowed with no restraints. *yEp* = 1; *yEs* = 1
D Brazilian case	See Section 5.3.3

Modalities A, B and C correspond to general cases in which the permission to sell electricity to the grid is gradually improved from not allowed (modality A) to allowed with maximum limit (modality B) to allowed with no restraints (modality C). Modality D corresponds to the particular case of the Brazilian regulation in which electricity is no longer sold to the grid, but rather exported as free loan compensating the electricity purchase in later time intervals, as explained in Section 5.1.4 and modelled in Section 5.3.3. Therefore, modality D is not an extension of modalities A, B and C.

A reference system was defined to provide a basis for comparison. In this system only the gas boilers GH and GV, mechanical chiller EC, and the cooling tower CT were allowed to be installed (*yINS(t)* = 1, for *t* = GH, GV, EC, and CT; *yINS(t)* = 0, for the other technologies), and the system is allowed to purchase electricity from the grid (*yEp* = 1; *yEs* = 0).

The results obtained in this section are presented and discussed as follows: First, in Section 5.4.1, the optimal economic solutions are obtained under the different modalities of power exchange with the grid, including the Brazilian regulatory framework. Then, the incorporation of renewable energy technologies in the polygeneration systems is further analyzed in Section 5.4.2. The environmental criterion is introduced in Section 5.4.3. Finally, Section 5.4.4 poses the question as to the extent to which the electricity CO_2 emission factors affect the optimal environmental solutions analyzed herein.

5.4.1   Optimal economic cost solutions

The system configurations and the main results obtained for the optimal economic cost solutions are shown in Table 5.18 and Table 5.19.

Table 5.18: Configurations for the reference system and optimal cost polygeneration systems.

Technology t	Reference system			A – Purchase only			B – Annual consumer			C – Unrestricted sale			D – Brazilian case		
	PIN, kW	*fu,* %	*Z(t),* k€	*PIN,* kW	*fu,* %	*Z(t),* k€	*PIN,* kW	*fu,* %	*Z(t),* k€	*PIN,* kW	*fu,* %	*Z(t),* k€	*PIN,* kW	*fu,* %	*Z(t),* k€
GE	-	-	-	1,157	91.28	781.3	1,190	98.65	803.5	1,591	99.89	1,073.9	1,206	97.25	813.7
PV	-	-	-	0	-	-	0	-	-	0	-	-	0	-	-
PT	-	-	-	0	-	-	0	-	-	0	-	-	0	-	-
ST	-	-	-	0	-	-	0	-	-	0	-	-	0	-	-
GH	76	1.56	4.2	0	-	-	0	-	-	0	-	-	0	-	-
GV	780	75.61	93.6	314	38.85	37.7	301	25.97	36.1	139	6.50	16.7	295	25.12	35.3
BH	-	-	-	0	-	-	0	-	-	0	-	-	0	-	-
BV	-	-	-	0	-	-	0	-	-	0	-	-	0	-	-
EC	879	61.75	92.3	505	44.70	53.1	495	38.62	52.0	345	23.17	36.2	503	36.94	52.8
AS	-	-	-	350	90.50	91.1	364	96.73	94.5	489	90.49	127.2	368	97.04	95.7
AD	-	-	-	0	-	-	0	-	-	38	54.21	9.8	0	-	-
CT	1,023	61.75	30.7	1,492	75.22	44.7	1,514	78.28	45.4	1,753	85.31	52.6	1,535	76.79	46.0
HS, kWh	-	-	-	12	-	0.5	9	-	0.4	0	-	-	4	-	0.2
CS, kWh	-	-	-	39	-	3.1	33	-	2.6	31	-	2.5	8	-	0.7
Investment cost, k€			**220.8**			**1,011.4**			**1,034.5**			**1,318.8**			**1,044.4**

Note: *PIN*: installed capacity; *fu*: load factor; *Z(t)*: investment cost of technology *t*.

Table 5.19: Main results for the reference system and optimal cost polygeneration systems.

Results	Reference system	A – Purchase only	B – Annual consumer	C – Unrestricted sale	D – Brazilian case
Natural gas, MWh/yr	5,567,170	20,947,483	22,741,059	29,865,601	22,666,329
Biomass, MWh/yr	-	0	0	0	0
Purchased electricity, MWh/yr	10,465,556	1,048,062	**928,268**	98,261	0
Sold electricity, MWh/yr	-	-	**928,268**	3,767,648	-
Imported electricity, MWh/yr	-	-	-	-	1,041,609
Exported electricity, MWh/yr	-	-	-	-	1,033,145
Natural gas, kg CO_2/yr	1,124,568	4,231,392	4,593,694	6,032,851	4,578,598
Biomass, kg CO_2/yr	-	0	0	0	0
Purchased electricity, kg CO_2/yr	6,508,147	644,615	570,826	59,493	0
Sold electricity, kg CO_2/yr	-	-	-590,561	-2,368,923	-
Imported electricity, kg CO_2/yr	-	-	-	-	642,795
Exported electricity, kg CO_2/yr	-	-	-	-	-656,576
Annual variable CO_2 emissions, kg CO_2/yr	7,632,715	4,876,006	4,573,959	3,723,422	4,564,818
Annual fixed CO_2 emissions, kg CO_2/yr	8,741	13,391	13,436	15,001	13,197
Total annual CO_2 emissions, kg CO_2/yr	**7,641,456**	**4,889,397**	**4,587,395**	**3,738,423**	**4,578,015**
Natural gas, €/yr	194,851	733,162	795,937	1,045,296	793,322
Biomass, €/yr	-	0	0	0	0
Purchased electricity, €/yr	1,021,641	100,140	88,466	9,236	0
Sold electricity, €/yr	-	-	-77,680	-322,072	-
Annual variable cost, €/yr	1,216,492	833,302	806,723	732,461	793,322
Annual fixed cost, €/yr	39,753	182,058	186,210	237,392	188,000
Total annual cost, €/yr	**1,256,245**	**1,015,360**	**992,933**	**969,853**	**981,322**
Payback Period, yr	-	2.1	2.0	2.3	1.9

In the reference system the electricity demand as well as the internally consumed electricity were entirely covered by purchase from the electric grid; the steam and hot water demands were predominantly supplied by the natural gas steam boiler GV, while the natural gas hot water boiler GH covered only a few peak hours; and the cooling demand was attended by the mechanical chiller EC. The cooling tower CT was installed with the sole purpose of dissipating the heat from the EC. The total annual cost obtained was 1,256,245 €/yr, 96.8% of which corresponded to operation (variable) costs and the remaining 3.2% corresponded to installation (fixed) costs. Electricity purchase accounted for the largest part (84.0%) of the annual operation cost. Regarding the annual fixed cost, the GV and EC accounted for the largest shares (42.4% and 41.8%, respectively).

The optimal cost solution under modality A (purchase only) consisted of the cogeneration module GE, the natural gas steam boiler GV, the mechanical chiller EC, the single-effect absorption chiller AS, the cooling tower CT, and the TES units for hot water HS and for chilled water CS. The GE operated with a very high load factor (91.28%), which allowed it to cover most of the electricity (89.8%) and heat (88.8%) consumed by the system. Only 4.1% of the cogenerated heat was dissipated to the environment. The GV supported the operation of the GE. The AS produced 58.4% of the cooling demand and operated with a very high load factor close to the GE's. The EC, on the other hand, covered 41.6% of the cooling demand and operated with a lower load factor of 44.7%. The TES units presented rather small capacities compared to the other technologies. The total annual cost was equal to 1,015,360 €/yr, 82.1% of which corresponded to operation costs and 17.9% to installation costs. As opposed to the reference system, in this case electricity purchase accounted for only 12.0% of the annual operation cost, the remaining 88.0% was due to the consumption of natural gas. The largest share of the annual fixed cost was due to the installation of the GE (77.2%), followed by the AS (9.0%).

By further improving the permission to sell electricity to the grid, the optimal cost solution under modality B (annual consumer) achieved similar results to those under modality A. The same set of technologies was included, although with different installed capacities: there was a slight increase in the GE, AS and CT, and a slight decrease in the GV, EC, HS and CS. Moreover, the GE and the AS operated with even higher load factors (98.65% and 96.73%, respectively), covering a larger share of the electricity, heat, and cooling demands, while the GV and the EC functioned as auxiliary devices. Again, the TES units were negligible. It should be noted that the system sold as much electricity as it purchased, so the upper limit to the sale of electricity imposed in Table 5.17 was reached. A total annual cost of 992,933 €/yr was obtained, 81.2% of which accounted for operation costs and 18.8% accounted for investment costs. The permission to sell a part of the electricity produced allowed the system to generate 77,680 €/yr in revenue, thus reducing operation costs.

Compared to the previous optimal cost solutions A and B, the optimal cost solution under modality C (unrestricted sale) presented a more significant increase in the installed capacities of the GE, AS and CT, and a more significant decrease in the installed capacities of the GV and EC. Moreover, a small capacity of the double-effect absorption chiller AD was included, while the HS was eliminated. Because of the permission to freely sell electricity to the grid, the GE operated with the highest load factor (99.89%) and the system sold 38 times more electricity than it purchased, generating substantial revenue to partially compensate the operation costs. On the other hand, the higher operation of the GE also resulted in a higher dissipation of cogenerated heat, which reached 14.8%; that being said, the thermal efficiency of the GE remained way above (38.1%) the minimal legal requirement of 15% (Eq. (5.33)). The optimal cost solution achieved a total annual cost of 969,853 €/yr, 75.5% of which corresponded to operation costs and 24.5% of which corresponded to investment costs. The annual fixed cost followed a similar distribution to the previous cases, so that the GE accounted for the largest share (81.4%), followed by the AS (9.6%).

Shifting the focus to the Brazilian regulation (modality D), the optimal cost solution was rather similar to that under modality B, with the same set of technologies installed and almost the same load factors. Because electricity was exported to the grid as free loan, there was not any revenue generated. On the other hand, the quantity of exported electricity was enough to compensate all of the electricity purchased, so there was no cost associated with the purchase of electricity from the grid. As can be seen in Table 5.19, the imported electricity was greater than the exported electricity; the reason was that, as explained in Section 5.3.3, the balance was made in economic terms applying the electricity purchase price (on-peak or off-peak) at the corresponding time interval. Regarding the total annual cost, the optimal cost solution achieved 981,322 €/yr, 80.8% of which corresponded to operation costs and 19.2% corresponded to investment costs. In this case, the annual operation cost was entirely because of purchase of natural gas.

As can be seen, the GE was proved economically feasible for all modalities of power exchange with the grid, resulting in installed capacities between 1.1 and 1.6 MW and very high load factors. Relative to the reference system, the presence of the GE: (i) eliminated the natural gas hot water boiler GH; (ii) reduced the installed capacities of GV and EC by 40-60%; and (iii) enabled the installation of the AS.

In order to understand the role of the GE in the optimal operation of the system, it is important to consider its several heat sources at different temperature-levels. The case study analyzed has a greater demand for high-temperature heat (i.e. steam) than for low-temperature heat (i.e. hot water). The operation of the GE to cover the steam demand results in the simultaneous production of excess low-temperature heat, which is optimally used in the AS for cooling production. Therefore, there is a clear connection between the GE and the AS, whose installed capacities

increased/decreased accordingly. This also explains the model's preference for the AS over the double-effect absorption chiller AD, despite its higher COP.

Compared to a reference system, the more complex configuration of the polygeneration system requires a higher investment cost, which is compensated by savings in the consumption of energy resources. This was observed in the previous discussion about the different compositions of the total annual cost, in which the share of annual fixed cost increased, while the share of annual operation cost decreased, in the optimal cost solutions relative to the reference system. Taking, for example, the optimal cost solution under modality A, the ratio of the increased investment cost (1,011.4 – 220.8 = 790.6 k€) to the annual savings in operation costs (1,216.5 – 833.3 = 383.2 k€/yr) gives a payback period of 2.1 years, which is the period of time required to recoup the invested funds. The optimal cost solutions presented similar payback periods, the lowest one (1.9 years) was reached under modality D (Brazilian case).

Apart from the payback period relative to a reference system, it would also be interesting to assess the payback period of moving from one modality to another, e.g. from modality A (purchase only) to B (annual consumer), and from B to C (unrestricted sale). In this context, Figure 5.6 complements the information provided in Table 5.18 and Table 5.19 by showing the savings in operation costs and the additional investment cost of optimal cost solutions under modalities A through D relative to the reference system. The slope of the dotted lines in the main graph provides the inverse of the payback period of moving from the reference system to the optimal cost solutions; in the detailed graph, the dotted lines connect solutions A to B and B to C. It is interesting to notice the change in the slope: from A to B, the payback period required would be equal to 0.9 years, while from B to C it would be of 3.8 years.

Apart from the installed capacities and main results discussed thus far, the model also provides the annual and hourly energy operation planning of each representative day. The optimal cost solution under modality B is used as an example in this section. Complementing the information shown in Table 5.18 and Table 5.19, Figure 5.7 presents the system configuration and annual energy flows.
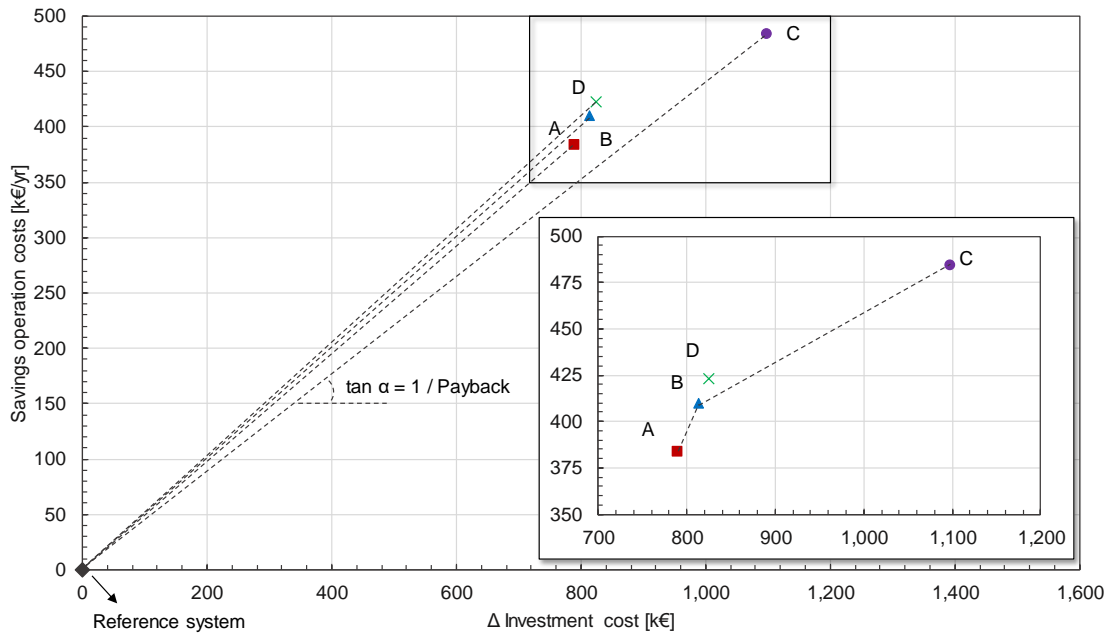
Figure 5.6: Additional investment cost and savings in operation cost of each solution.
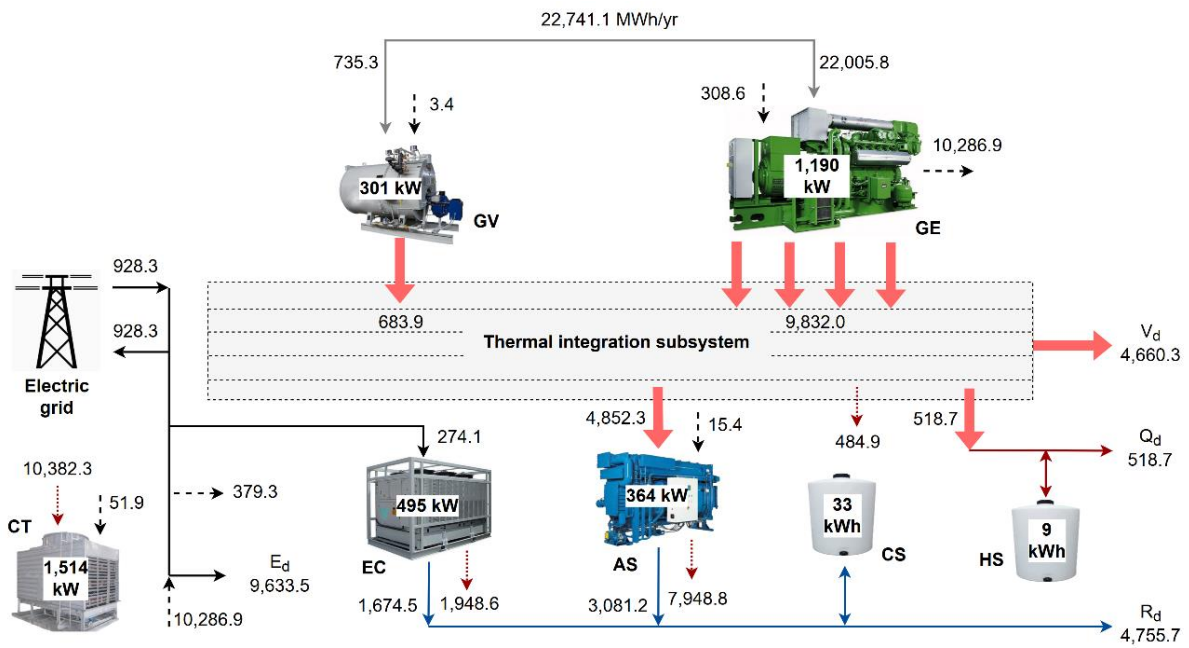
Figure 5.7: Annual energy flows for the optimal cost solution under modality B.

Regarding the annual operation of the system, the GE produced most of the electricity and heat consumed, while the GV and electric grid supported its operation. About 8% of the electricity produced by the GE was sold to the grid. The 10,515.9 MWh of produced heat produced were distributed between the AS (46.1%), steam demand V_d (44.3%), and hot water demand Q_d (4.9%); the remaining heat (4.7%) was dissipated to the environment through the CT. The AS covered about 65% of the cooling demand.

In terms of economic cost and CO_2 emissions, natural gas consumption was responsible for the greatest shares. Selling electricity to the grid resulted in an income that reduced the annual electricity cost by 88%. The annual investment cost accounted mostly to the GE (77.7%), followed by the AS (9.1%), and EC (5.0%). By contrast, the annual fixed CO_2 emissions were more evenly distributed between the EC (29.5%), GE (28.8%), and AS (22.3%).

The operation of the system at hour 11 of a working-day in January is shown in Figure 5.8. At this hour, the GE is operating at full load supported by the GV, and the system is purchasing electricity from the grid. About 33.7% of the electricity consumed by the system must be purchased from the grid. The EC supplies 57.2% of the cooling, 3.9% of which is stored in the CS. Regarding the heat production and consumption, the thermal integration subsystem is depicted in Figure 5.9. The GE and GV supply hot flows, providing the heat required by the cold flows associated with the AS, hot water Q_{hw}, and the steam demand V_d; no heat dissipation takes place at this hour. It is possible to divide the temperature intervals into two regions in which the heat supplied by the hot flows OK is entirely consumed by the cold flows DK. The limit between these regions indicate the existence of a pinch point at 180 °C, between temperature intervals 4 and 5. As can be seen, in the above-pinch region, the high-temperature heat flows supplied by the GE (Q_{eg} and Q_{ac}) and GV (Q_{gv}) cover the greatest part of steam production V_d, while in the below-pinch region the rest of the cold flows are attended.
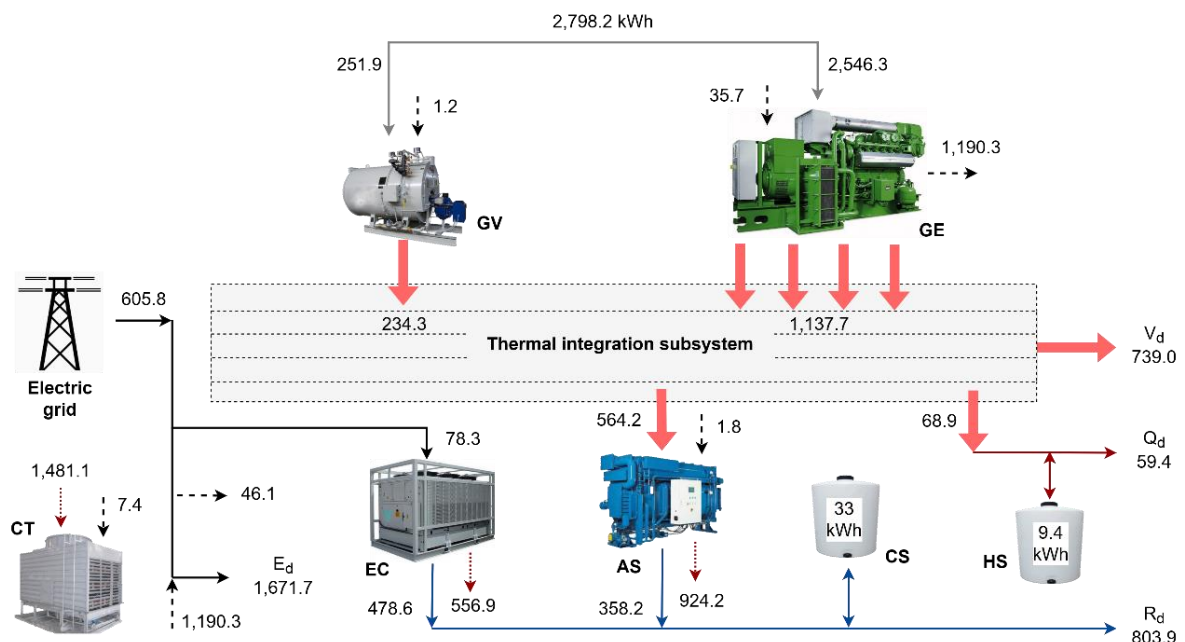
Figure 5.8: Hourly energy flows at hour 11 of a working day in January, for the optimal cost solution under modality B.
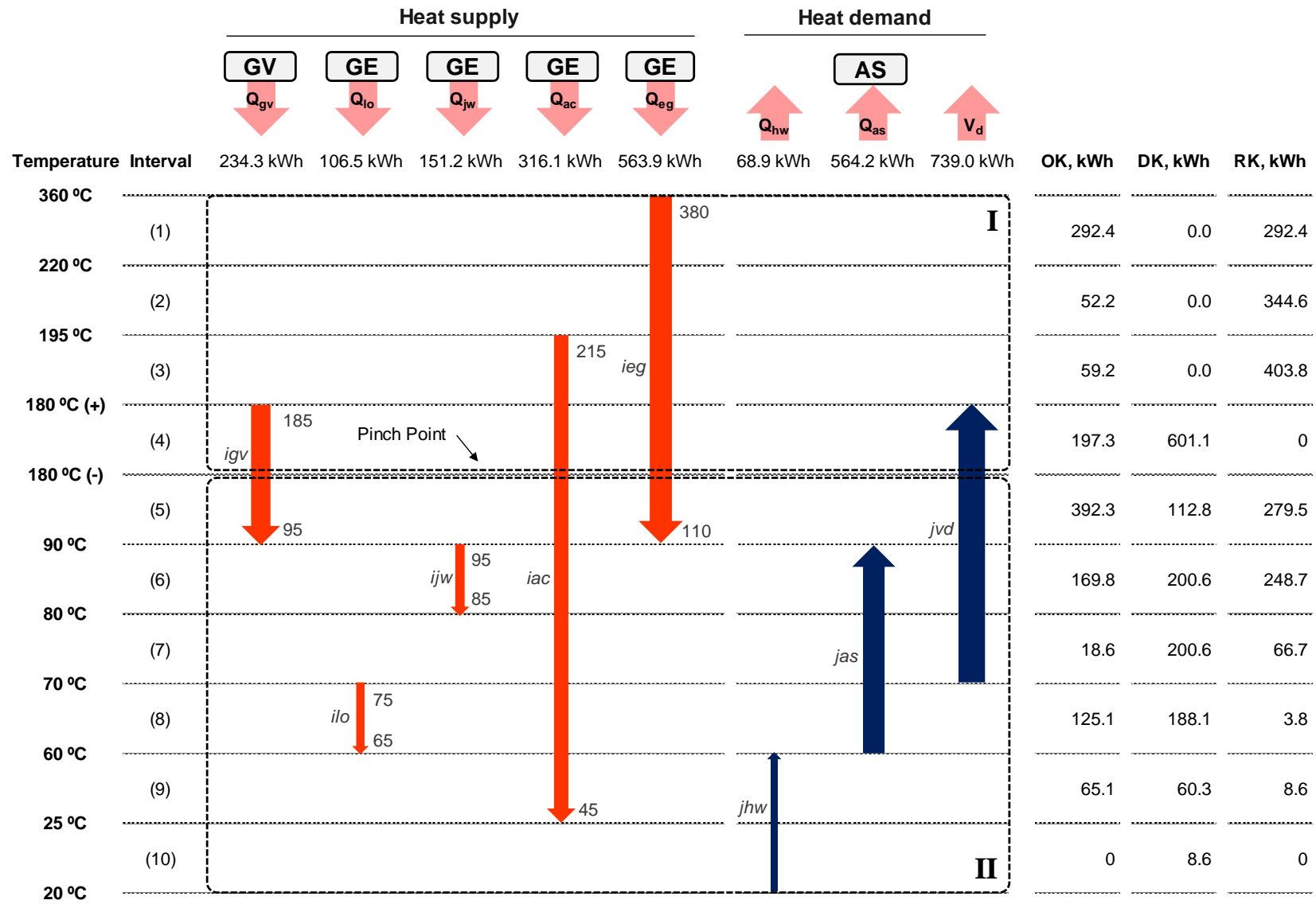
Figure 5.9: Thermal integration subsystem at hour 11 of a working day in January for the optimal cost solution under modality B.

5.4.2   Incorporation of renewable energy

The fact that none of the RETs were included in the optimal cost solutions called for an in-depth analysis of the parameters used in the optimization model. Moreover, it became clear that the cogeneration module GE was economically interesting either with or without the permission to sell electricity to the grid. In fact, it was observed that the more leeway the system was given to sell electricity (by shifting from modality A through C), the higher the GE's installed capacity and load factor.

In this regard, it was proposed to analyze the effect of changes in key parameters on the optimal cost solutions, throwing light on the conditions that would enable the incorporation of renewable energy sources in the polygeneration systems. These parameters include the purchase prices of energy resources (Section 5.4.2.1), the investment costs of the solar-based RETs (Section 5.4.2.2), and the condition of a ban on fossil fuels (Section 5.4.2.3).

5.4.2.1   Sensitivity analyses for the purchase prices of energy resources

This section carries out sensitivity analyses for the purchase price of natural gas *pcegas*, the purchase price of biomass *pcebio*, and the discount *penven* applied to the electricity selling price *pelven*, as given in 5.1.3.

The purchase price of natural gas *pcegas* considered in the previous analyses was equal to 0.035 €/kWh (LHV). This value was varied between 0.020 and 0.055 €/kWh (LHV). Figure 5.10 shows the total annual cost (objective function) and total annual CO_2 emissions obtained for the optimal cost solutions obtained under modalities A, C and D. As can be seen, as the *pcegas* increased, so did the total annual cost values. The increase was sharper under modality C, as the higher *pcegas* mitigated the revenue from selling electricity to the grid. For *pcegas* values greater than 0.040 €/kWh (LHV), the optimal solutions under the three modalities resulted practically the same. Interestingly, the total annual CO_2 emissions also increased with higher *pcegas* values, although with different trends. Modalities A and D fluctuated slightly for values below 0.045 €/kWh (LHV), then rose significantly. Under modality C the upward trend begun earlier at 0.030 €/kWh (LHV); in particular, between 0.030 and 0.035 €/kWh (LHV) there was a dramatic increase in the total annual emissions.

(a)

(b)
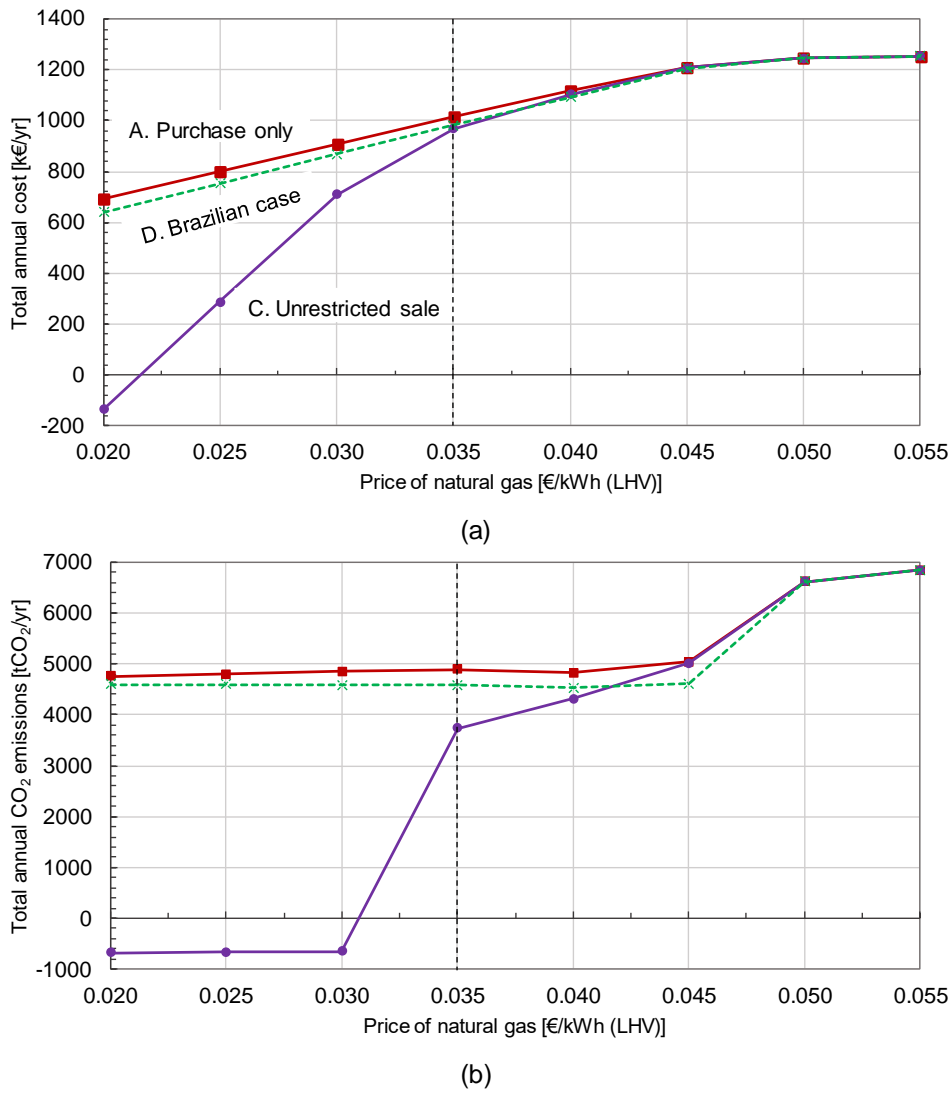
Figure 5.10: Sensitivity analysis for the price of natural gas, (a) total annual cost (objective function), and (b) total annual CO_2 emissions.

These results are directly linked to the system's configuration and operational planning. Therefore, this information can be used to provide further insight into the sensitivity analysis. In this regard, Figure 5.11 presents the installed capacities *PIN* of selected technologies, that is the cogeneration module GE, the biomass steam boiler BV, the single-effect absorption chiller AS, and the mechanical chiller EC.
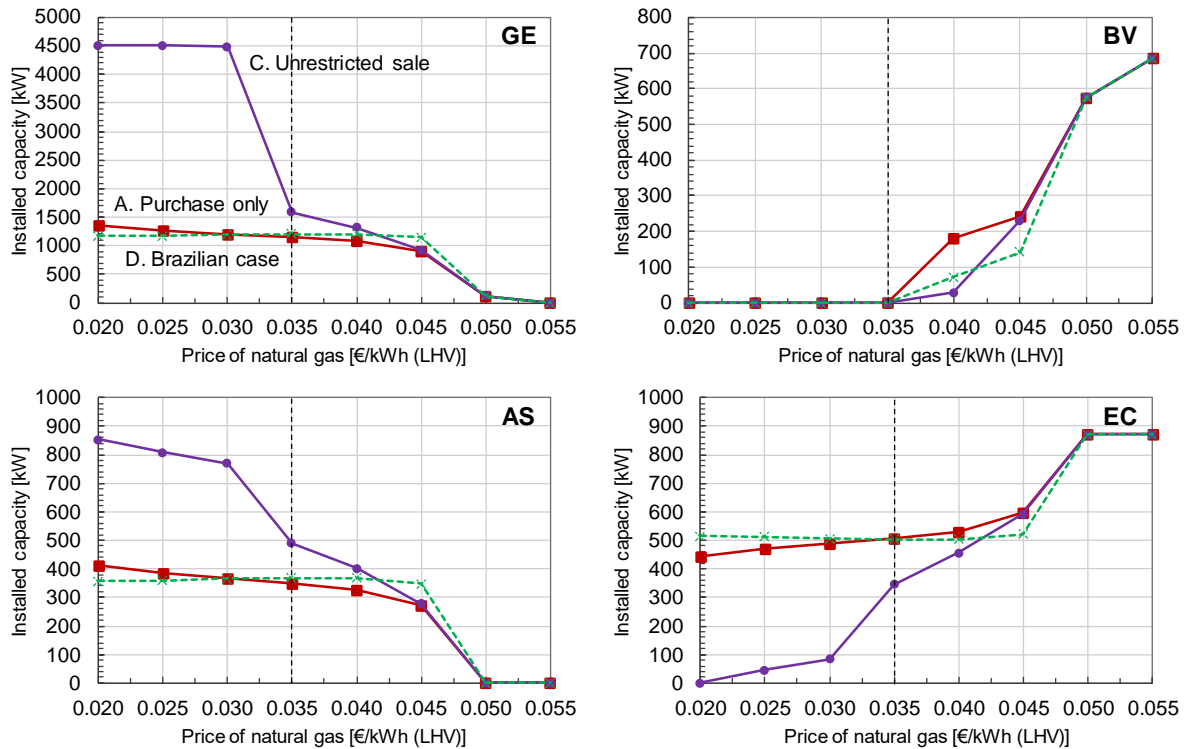
Figure 5.11: Sensitivity analysis for the price of natural gas, installed capacities.

As previously explained, there is a positive connection between the GE and the AS, so that their installed capacities follow similar trends. Under modality A, *PIN(GE)* and *PIN(AS)* decreased steadily with the increase in *pcegas* up to 0.045 €/kWh (LHV), then experienced a significant drop; the reduction in *PIN(AS)* was offset by an increase in the *PIN(EC)*. A similar trend was observed for the optimal solution under modality C, but the sharp drop took place after 0.030 instead of 0.045 €/kWh (LHV). By contrast, it is interesting to notice that under modality D, for *pcegas* values below 0.045 €/kWh (LHV), *PIN(GE)* and *PIN(AS)* presented a rather slight upward trend, then experienced a sharp fall, while the *PIN(EC)* presented a rather slight downward trend, then a dramatic increase. Under all modalities, the range between 0.045 and 0.050 €/kWh (LHV) represented a turning point for the system configuration, in which GE and AS were completely phased out, while EC and BV increased dramatically.

The sensitivity analysis for the purchase price of biomass *pcebio* was carried out by varying the current price of 0.026 down to 0.005 €/kWh (LHV). It made no sense to increase it, as biomass boilers were not included in the optimal economic cost solutions described in Section 5.4.1. The total annual cost (objective function) and total annual CO_2 emissions obtained under A, C and D are shown in Figure 5.12. As can be seen, under modalities A and D the total annual cost decreased with the reduction in the *pcebio*; under modality C, however, the reduction in the total annual cost was much more subtle and only took place between 0.005 and 0.010 €/kWh (LHV). The associated total annual CO_2 emissions fluctuated slightly, but in general were not significantly affected by a reduction in *pcebio*.

(a)

(b)
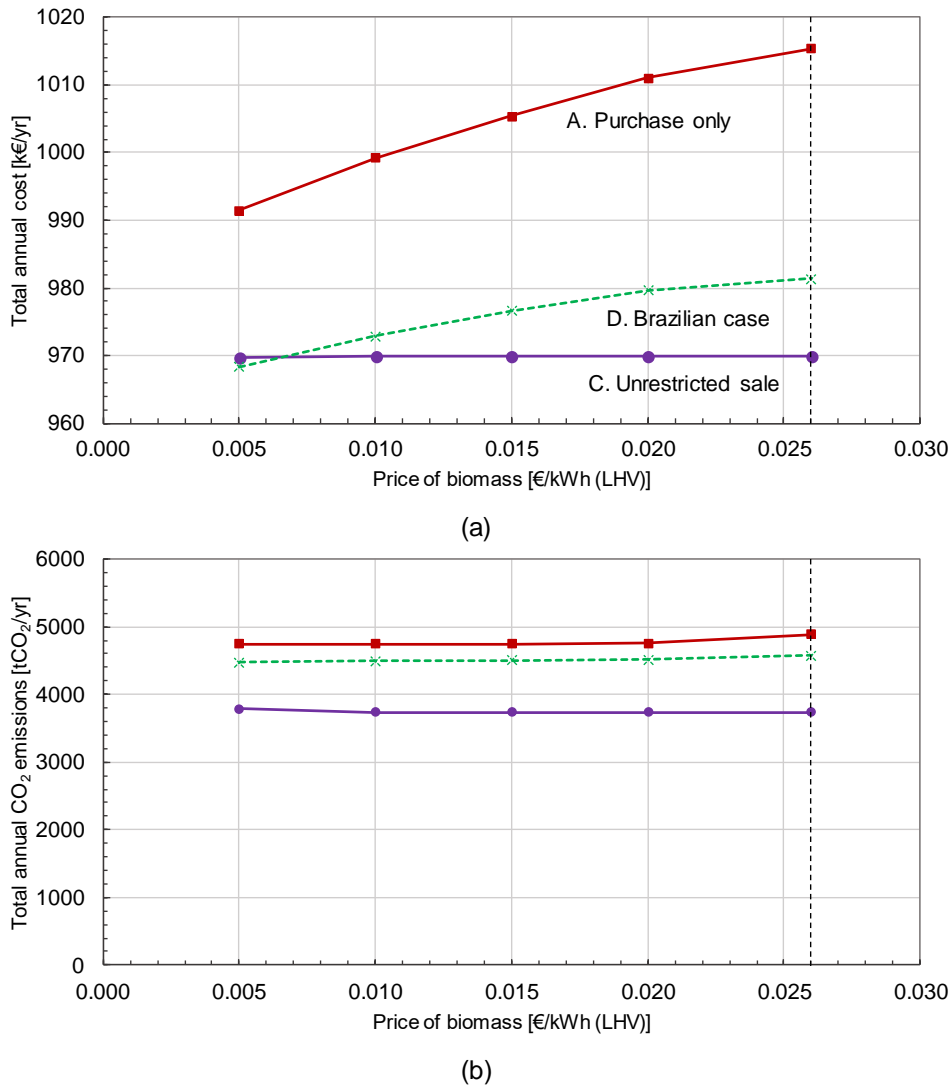
Figure 5.12: Sensitivity analysis for the price of biomass, (a) total annual cost (objective function), and (b) total annual CO_2 emissions.

Figure 5.13 presents the installed capacities *PIN* of the cogeneration module GE, natural gas steam boiler GV, double-effect absorption chiller AD, and mechanical chiller EC in the optimal cost solutions.

The results show that modalities A and D followed very similar trends: At 0.020 €/kWh (LHV), the BV was installed in both solutions, significantly displacing the GV. From 0.020 downwards, *PIN(BV)* increased and *PIN(GV)* decreased steadily. For *pcebio* values below 0.015 €/kWh (LHV), the use of AD became economically feasible, being driven by steam produced by the BV. Under modality F the optimal solution was much less susceptible to reductions in the *pcebio*. Only when the price was reduced to 0.005 €/kWh (LHV) that BV began to be included, accompanied by a slight increase in *PIN(AD)* and a reduction in *PIN(GV)*. Under all modalities, GE was only marginally displaced by the BV.
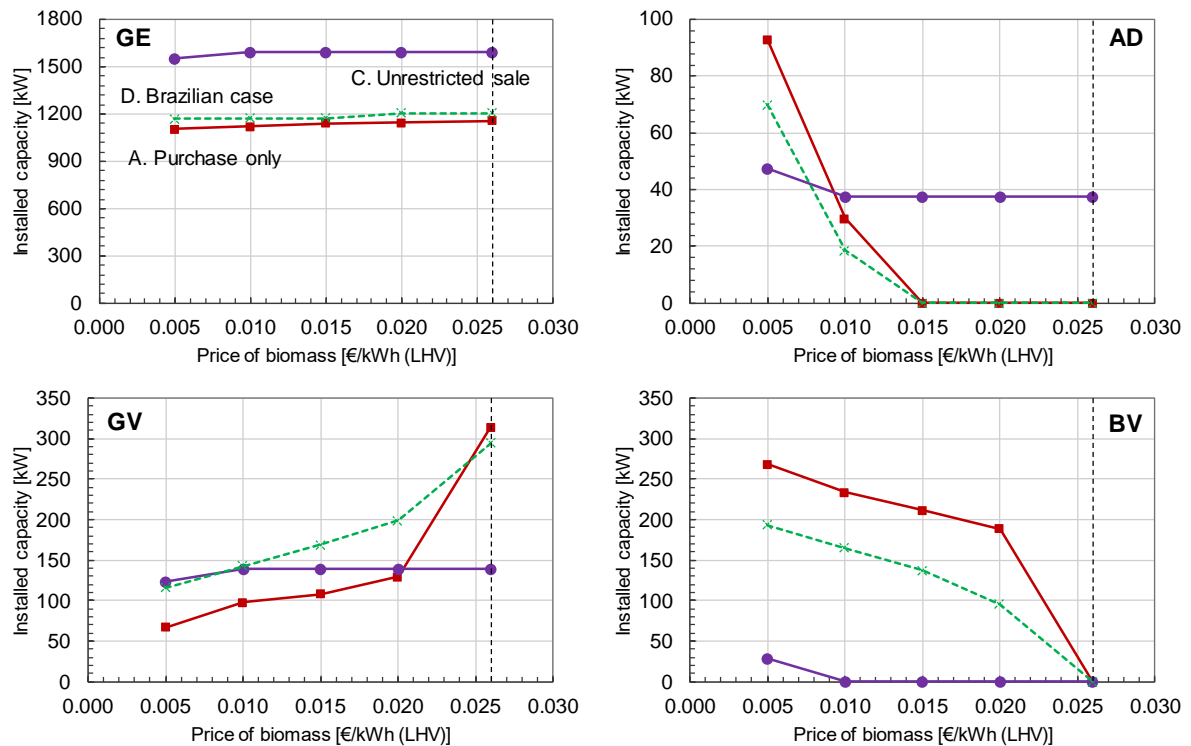
Figure 5.13: Sensitivity analysis for the price of biomass, installed capacities.

Regarding the discount *penven* applied to the electricity selling price *pelven*, the value originally used in the analyses was equal to 0.012 €/kWh and it was proposed to vary it between 0 (so that the selling price is equal to the purchase price) and 0.024 €/kWh. Figure 5.14 shows the total annual cost (objective function) and the total annual CO_2 emissions obtained for the optimal cost solutions under modality C. As can be seen, the total annual cost steadily decreased from *penven* 0.024 to 0.004 €/kWh, then the decrease until 0 was sharper. Regarding the associated total annual CO_2 emissions, there was also a steady decrease until 0.008 €/kWh, followed by a significant drop, which allowed the system to generated negative emissions.

(a)

(b)
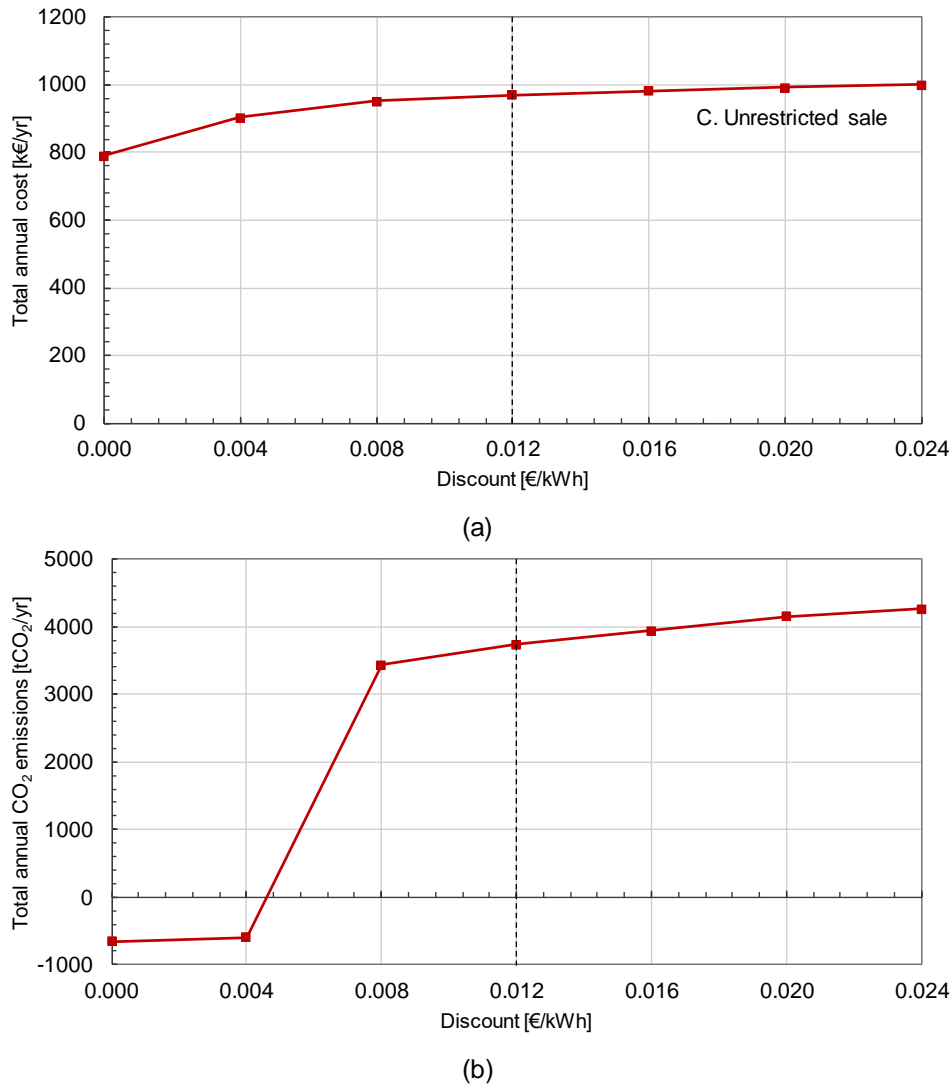
Figure 5.14: Sensitivity analysis for the discount to the electricity selling price, (a) total annual cost (objective function), and (b) total annual CO_2 emissions.

Figure 5.15 presents the installed capacities *PIN* of the cogeneration module GE, mechanical chiller EC, single-effect absorption chiller AS, and chilled water storage tank CS for the optimal cost solution under modality C.

The results showed that the reduction in the *penven* from 0.024 €/kWh downwards promoted a steady increase in the installed capacity of the GE until 0.008 €/kWh, after which it increased significantly and became level. Similar trends were observed in the AS and CS, and in the opposite direction in the case of the EC. It became clear that the range between 0.008 and 0.004 €/kWh represented a turning point for the system.
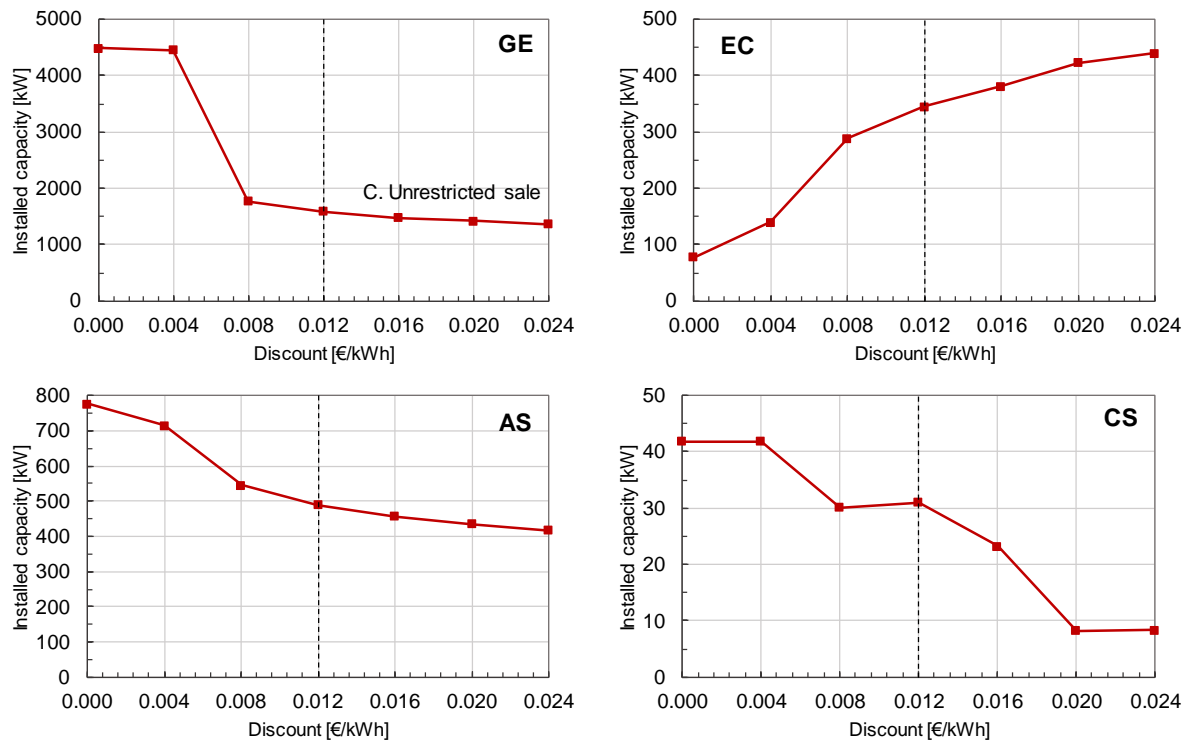
Figure 5.15: Sensitivity analysis for the discount to the electricity selling price, installed capacities.

5.4.2.2 Sensitivity analyses for the investment costs of the RETs

Regarding the solar-based RETs (i.e. photovoltaic panel PV, parabolic trough concentrator PT, and flat-plate solar thermal collector ST), it was proposed to carry out sensitivity analyses by decreasing their bare module costs CI by 80, 60, 40 and 20% in the optimal cost optimization.

Figure 5.16 shows the installed capacity PIN of PV and the total annual cost obtained by varying the $CI(PV)$ between its initial value of 1300 and 260 €/kWp. The optimal cost solution under modality A was the first in which PV began to be included, approximately at 800 €/kWp, then $PIN(PV)$ increased steadily. Under modality C, PV installation began for CI values lower than 770 €/kWp, then increased sharply, reaching the maximum installable capacity limit PIN_{MAX} of 10,000 kW. The optimal cost solution under modality D presented a similar trend to that of modality C, however, after the sharp increase, which took place between 770 and 520 €/kWp, the $PIN(PV)$ levelled off. Concerning the total annual cost, there was a downward trend under all modalities as the $PIN(PV)$ increased.

(a)

(b)
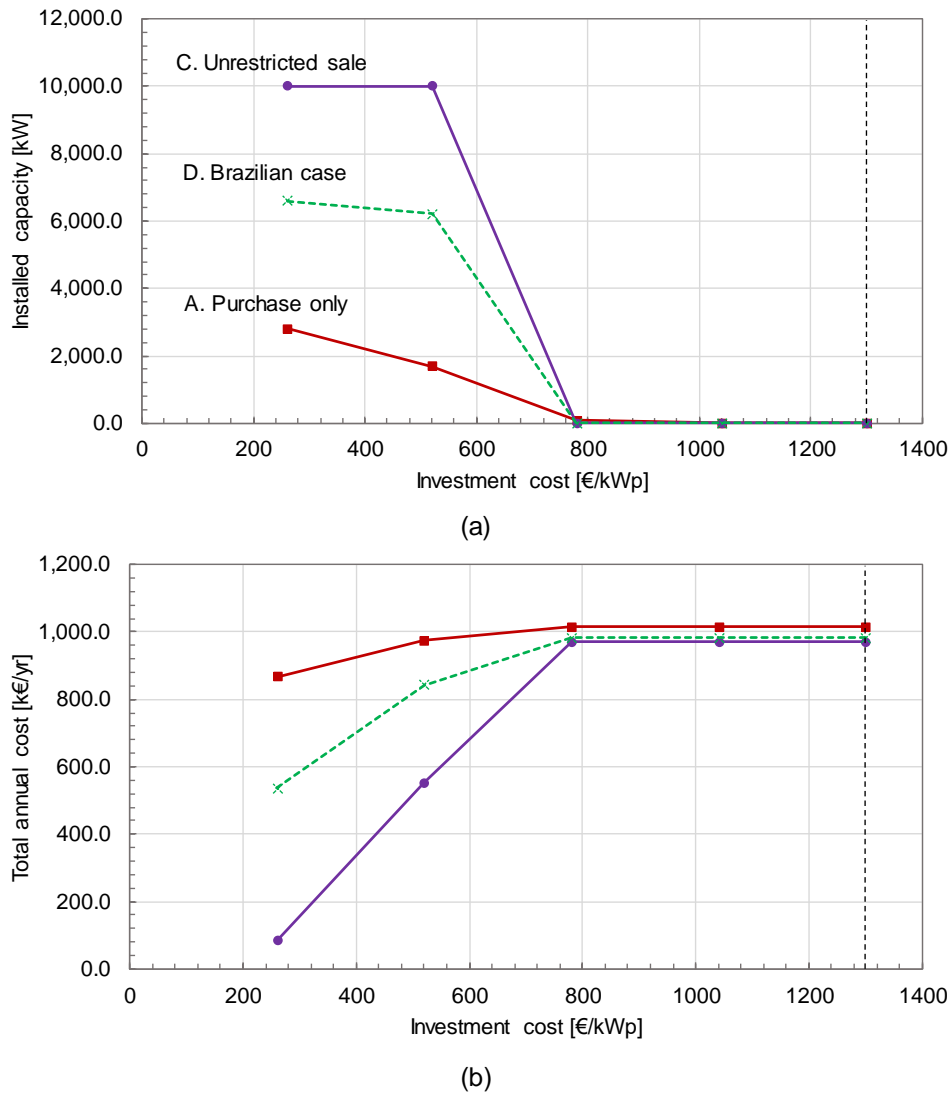
Figure 5.16: Sensitivity analysis for the bare module cost of PV, (a) installed capacity, and (b) total annual cost (objective function).

It is interesting to consider the ways in which the electric grid conditions influenced the integration of PV in the analyzed systems. For example, under modality C, the results suggest that the *PIN(PV)* would keep increasing indefinitely if there were no constraints to the maximum installable capacity; this can be explained by the simple fact that for *CI(PV)* values below 770 €/kWp the system generated revenue by selling electricity to the grid. On the other hand, under modality D, the system no longer sells electricity to the grid, but rather exports it as free loan for later consumption; the exported electricity that has not been consumed back after the period of one year is lost. Therefore, there is a balance between the exported and the imported electricity, so that the *PIN(PV)* leveled off even as *CI(PV)* decreased further. Finally, under modality A, *PIN(PV)* increased with the reduction in *CI(PV)* because the cheaper the PV panel, the higher the capacity that can be installed to cover peak demand periods, even if that means wasting electricity at other hours.

In the case of the PT, Figure 5.17 shows its installed capacity *PIN(PT)* and the total annual cost obtained by varying the *CI(PT)* between its initial value of 425 and 85 €/kW. In the optimal cost solution under modality A, the introduction of PT began for *CI(PT)* values lower than 140 €/kW. A similar trend was observed for the optimal solution under modality D, although with lower *PIN(PT)* and for *CI(PT)* values below 130 €/kW. In both cases, the presence of the PT displaced the cogeneration module GE. PT was never included in the optimal cost solution under modality C. Moreover, the installation of PT promoted a slight reduction in the total annual cost values.
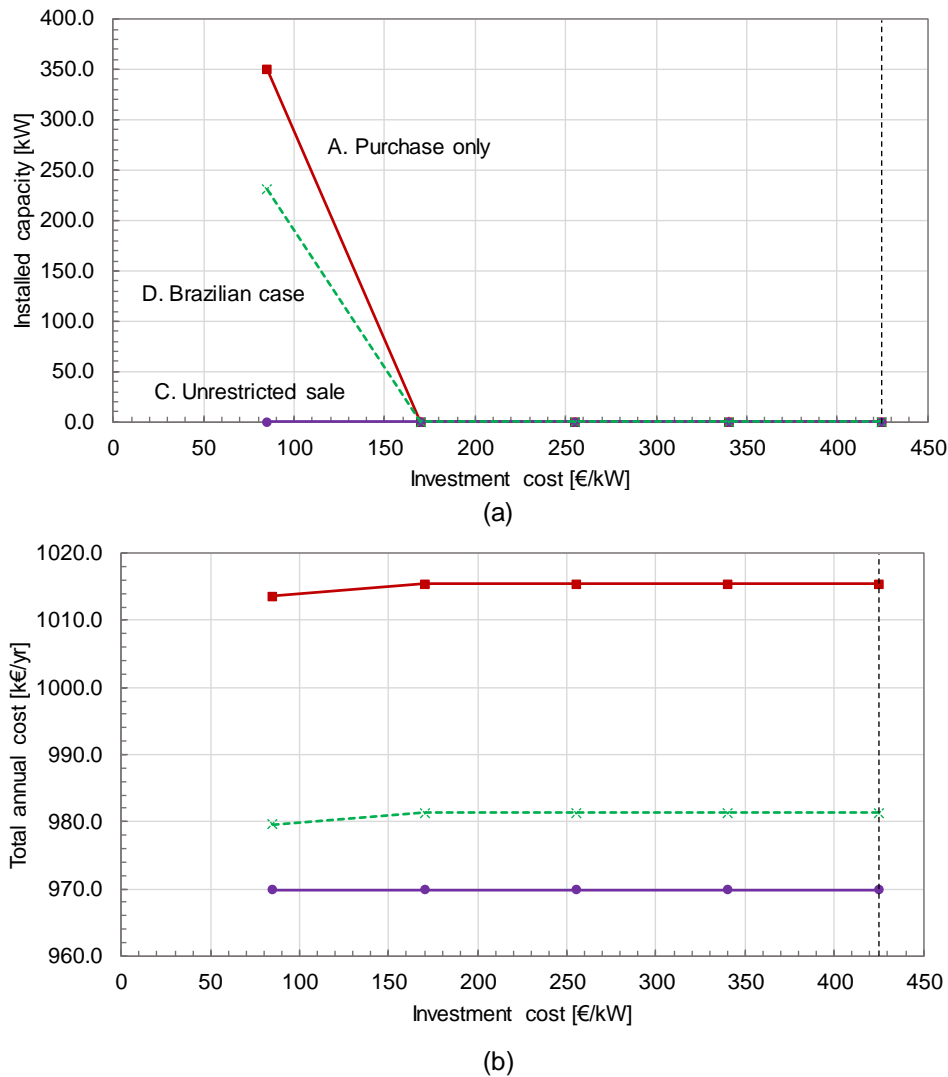
Figure 5.17: Sensitivity analysis for the bare module cost of the PT, (a) installed capacity, and (b) total annual cost (objective function).

As regards the ST, a sensitivity analysis was carried out by varying the *CI(ST)* between its initial value of 500 and 100 €/kWp. However, they were never installed in the optimal cost solutions. Apart from the suggested economic disadvantage, another reason was that, as previously mentioned, the case study analyzed herein had a greater demand for high-temperature heat than

for low-temperature heat, so that the ST would have to compete with the cogeneration module, which could simultaneously produce both heat qualities.

5.4.2.3   Effect of a total ban on fossil fuels

Finally, an additional situation was considered in which the fossil fuel-based technologies, namely the cogeneration module GE and the natural gas boilers GV and GH, were not allowed to be installed in the optimal economic cost solutions (*yINS(GE, GV, GH)* = 0). This could be, for instance, the result of a new governmental policy aiming at reducing the CO_2 emissions by phasing out fossil fuel-based technologies, such as natural gas boilers, fuel oil boilers, diesel engines, etc.

The results obtained are shown in Table 5.20. As can be seen, the optimal cost solutions were the same under the three modalities analyzed. Compared to their optimal economic cost solutions presented in Table 5.18 and Table 5.19, revoking the permission to install fossil fuel-based technologies led to the replacement of the GE and GV by the biomass steam boiler BV; also, cooling production became entirely electricity-based. As a consequence, there was a significant increase in both the total annual cost and total annual CO_2 emissions, in particular regarding the operation costs and emissions. It became clear that under these conditions cooling production in the mechanical chiller with electricity purchased from the grid was preferable in economic terms to cooling production in the absorption chiller with heat from biomass burning.

Nevertheless, compared to the reference system, the optimal cost solution without fossil fuels stands as a very interesting alternative, in which the total annual CO_2 emissions are reduced by 10.7% while the total annual costs remain practically unchanged (increase of only 0.05%).

Table 5.20: Optimal economic cost solution without fossil fuel-based technologies.

Results	A, C and D	
	PIN, kW	*fu*, %
BV	808	73.20
EC	871	62.34
CT	1,013	62.34
HS, kWh	49	-
CS, kWh	8	-
Biomass, MWh/yr		6,090.1
Purchased electricity, MWh/yr		10,465.6
Sold electricity, MWh/yr		-
Biomass, kg CO_2/kg		307,976
Purchased electricity, kg CO_2/kg		6,508,151
Sold electricity, kg CO_2/kg		-
Annual variable CO_2 emissions, kg CO_2/kg		6,816,127
Annual fixed CO_2 emissions, kg CO_2/kg		9,535
Total annual CO_2 emissions, kg CO_2/kg		**6,825,662**
Biomass, €/yr		158,342
Purchased electricity, €/yr		1,021,624
Sold electricity, €/yr		-
Annual variable cost, €/yr		1,179,966
Annual fixed cost, €/yr		76,921
Total annual cost, €/yr		**1,256,887**

5.4.3   Optimal environmental solutions

The optimization model was solved for the environmental aspect (total annual CO_2 emissions). The results obtained for the optimal environmental solutions under modalities A through D (see Table 5.17) are shown in Table 5.21 and Table 5.22. The reference system is the same as the one analyzed in Section 5.4.1.

Table 5.21: Configurations for the reference system and optimal environmental polygeneration systems.

Technology t	Reference system			A – Purchase only			B – Annual consumer			C – Unrestricted sale			D – Brazilian case		
	PIN, kW	fu, %	ZCO2(t), tCO$_2$	PIN, kW	fu, %	ZCO2(t), tCO$_2$	PIN, kW	fu, %	ZCO2(t), tCO$_2$	PIN, kW	fu, %	ZCO2(t), tCO$_2$	PIN, kW	fu, %	ZCO2(t), tCO$_2$
GE	-	-	-	1,344	44.26	87.4	0	-	0.0	**5,000**	90.14	325.0	**5,000**	90.14	325.0
PV	-	-	-	4,343	12.75	7,991.9	6,237	18.83	1,1475.9	**10,000**	18.83	18,400.0	**10,000**	18.83	18,400.0
PT	-	-	-	3,997	10.50	519.7	3,545	10.73	460.8	0	-	0.0	0	-	0.0
ST	-	-	-	0	-	0.0	0	-	0.0	0	-	0.0	0	-	0.0
GH	76	1.56	0.8	0	-	0.0	0	-	0.0	0	-	0.0	0	-	0.0
GV	780	75.61	7.8	0	-	0.0	0	-	0.0	0	-	0.0	0	-	0.0
BH	-	-	-	0	-	0.0	0	-	0.0	0	-	0.0	0	-	0.0
BV	-	-	-	535	30.02	10.7	756	42.98	15.1	0	-	0.0	0	-	0.0
EC	879	61.75	140.7	337	28.43	54.0	745	51.25	119.2	0	-	0.0	0	-	0.0
AS	-	-	-	372	55.39	61.4	0	-	0.0	879	61.75	145.1	879	61.75	145.1
AD	-	-	-	600	40.15	99.0	528	30.51	87.0	0	-	0.0	0	-	0.0
CT	1,023	61.75	25.6	1,574	71.05	39.4	1,180	61.06	29.5	5,058	84.27	126.4	5,058	84.27	126.4
HS, kWh	-	-	-	43	-	6.5	469	-	70.4	0	-	0.0	0	-	0.0
CS, kWh	-	-	-	667	-	200.1	0	-	0.0	0	-	0.0	0	-	0.0
Embedded CO$_2$ emissions, tCO$_2$			**174.8**			**9,069.9**			**12,258.0**			**18,996.5**			**18,996.5**

Note: *PIN*: installed capacity; *fu*: load factor; *ZCO2(t)*: embedded CO$_2$ emissions in the manufacturing of technology *t*.

Table 5.22: Main results for the reference system and optimal environmental polygeneration systems.

Results	Reference system	A – Purchase only	B – Annual consumer	C – Unrestricted sale	D – Brazilian case
Natural gas, MWh/yr	5,567,170	11,150,053	0	84,454,031	84,454,031
Biomass, MWh/yr	-	1,653,456	3,347,518	0	0
Purchased electricity, MWh/yr	10,465,556	0	**5,221,597**	0	0
Sold electricity, MWh/yr	-	-	**5,221,597**	44,947,470	-
Imported electricity, MWh/yr	-	-	-	-	0
Exported electricity, MWh/yr	-	-	-	-	44,947,470
Natural gas, kg CO_2/yr	1,124,568	2,252,311	0	17,059,714	17,059,714
Biomass, kg CO_2/yr	-	83,615	169,284	0	0
Purchased electricity, kg CO_2/yr	6,508,147	0	3,259,317	0	0
Sold electricity, kg CO_2/yr	-	-	-3,244,251	-28,143,031	-
Imported electricity, kg CO_2/yr	-	-	-	-	0
Exported electricity, kg CO_2/yr	-	-	-	-	-28,143,031
Annual variable CO_2 emissions, kg CO_2/yr	7,632,715	2,335,926	184,350	-11,083,317	-11,083,317
Annual fixed CO_2 emissions, kg CO_2/yr	8,741	453,494	612,899	949,825	949,825
Total annual CO_2 emissions, kg CO_2/yr	**7,641,456**	**2,789,420**	**797,249**	**-10,133,491**	**-10,133,491**
Natural gas, €/yr	194,851	390,252	0	2,955,891	2,955,891
Biomass, €/yr	-	42,990	87,035	0	0
Purchased electricity, €/yr	1,021,641	0	528,685	0	0
Sold electricity, €/yr	-	-	-428,171	-3,777,999	-
Annual variable cost, €/yr	1,216,492	433,242	187,550	-822,108	2,955,891
Annual fixed cost, €/yr	39,753	1,591,867	1,830,151	3,015,958	3,015,958
Total annual cost, €/yr	**1,256,245**	**2,025,109**	**2,017,701**	**2,193,850**	**5,971,849**
Investment cost, k€	220.8	8,843.7	10,167.5	16,755.3	16,755.3
Payback Period, yr	-	11.0	9.7	8.1	-

The optimal environmental solution under modality A (purchase only) consisted of the biomass steam boiler BV, photovoltaic panel PV and parabolic trough concentrator PT, the cogeneration module GE, the mechanical chiller EC, both absorption chillers AS and AD, and both TES units HS and CS. The system purchased natural gas and biomass, but not electricity from the grid. Apart from the previously mentioned correspondence between the GE and the AS, in this case there was also a positive relation between the PT, the AD and the CS. In this context, the heat produced by the PT was used in the AD to produce cooling, which was stored in the CS. The CO_2 emissions generated in the hourly operation of the system through the consumption of natural gas and biomass accounted for 83.7% of the total annual CO_2 emissions, while the CO_2 emissions associated with the manufacturing of the technologies accounted for the remaining 16.3%.

Moving to the optimal environmental solution under modality B (annual consumer), it was observed that the system (i) no longer consumed natural gas; (ii) purchased and sold electricity so that the annual net balance was zero, reaching the restriction imposed on the electricity sale in Table 5.17; and (iii) no longer installed the GE, AS, and CS. Interestingly, while the optimal environmental solution under modality A installed a great capacity of chilled water storage CS, this solution heavily relied on hot water storage HS. The total annual CO_2 emissions corresponded mostly to the manufacturing of the equipment (76.9%).

Under modality C (unrestricted sale), the optimal environmental solution included only the GE, PV, AS, and CT. This solution maximized the installed capacities of GE and PV, reaching their maximum installable capacities PIN_{MAX}. The reason was that the system was able to reduce the total annual CO_2 emissions by selling electricity to the grid, thus displacing grid CO_2 emissions. As a matter of fact, the annual operation CO_2 emissions are -11,083,317 kg CO_2/yr. Nevertheless, it should be noted that the operation of the GE to produce electricity resulted in a large quantity of dissipated cogeneration heat; as a consequence, the low the minimal legal requirement of 15% (Eq. (5.33)) was reached.

Changing the focus to the Brazilian case (modality D), the optimal environmental solution was virtually the same as the one under modality C, although with different annual variable cost values. This difference was because the system no longer sold electricity to the grid, so there was no revenue to reduce the annual operation cost of the system.

The results showed that selling/exporting electricity to the grid allowed the system to achieve significant reductions in the objective function (total annual CO_2 emissions). Moreover, the GE was environmentally interesting even when the system was not allowed to sell electricity to the grid (modality A). Relative to the optimal cost solutions, the optimal environmental solutions: (i)

included some of the RETs, namely the PV, PT and BV; and (ii) included relevant installed capacities of TES units.

Concerning the economic aspect in the optimal environmental solutions, it was observed that the investment costs required were very high, leading to long payback periods of 10 years on average, which seriously compromised their economic viability in real world applications. Therefore, it would be interesting to investigate trade-off solutions between both economic and environmental criteria, in search for acceptable solutions, following the methodology described in Chapter 2 and applied in Chapter 4.

5.4.4 Electric grid CO_2 emission factors

In the present study, the environmental criterion was described in terms of the CO_2 emissions associated with the manufacturing of the installed technologies and generated during the hourly operation of the system through the consumption of electricity, natural gas and biomass. As explained in Section 5.1.3, hourly CO_2 emission factors of the grid electricity $kgCO2_{ele}$ were employed with an annual average value equal to 0.6228 kg CO_2/kWh, corresponding to the emissions generated at the margin of operation and provided by the Brazilian Ministry of Science, Technology, Innovation and Communications (MCTIC, 2018). However, as of 2016, the annual average CO_2 emission factor of the whole Brazilian electric system was equal to 0.1581 kg CO_2/kWh, about four times lower.

Among other factors, the use of these high values of the CO_2 emission factors has led to some surprising results, such as: (i) the ability of the system to displace grid emissions with electricity produced in the GE with natural gas, so that the optimal environmental solutions under modalities C (unrestricted sale) and D (Brazilian case) maximized the installed capacity of GE (see Section 5.4.3); (ii) the increase in CO_2 emissions caused by a ban on fossil fuel-based technologies (see Table 5.20); and (iii) the increase in CO_2 emissions caused by higher natural gas purchase prices (see Figure 5.10). Therefore, it was proposed to carry out a sensitivity analysis for the hourly $kgCO2_{ele}$ in the optimal environmental solutions. In terms of annual average values, the $kgCO2_{ele}$ were reduced between 0.6228 and 0.1581 kg CO_2/kWh.

Figure 5.18 shows the total annual cost and total annual CO_2 emissions (objective function) obtained for the optimal environmental solutions under modalities A, C and D. By reducing the $kgCO2_{ele}$, the total annual cost under modalities A and C slightly increased and then decreased, peaking at 0.343 and 0.437 kg CO_2/kWh, respectively. By contrast, under modality D there was a sharp reduction in the total annual cost, especially between the initial value and 0.530 kg CO_2/kWh, owing to a decrease in the consumption of natural gas. The total annual CO_2 emissions

under modality A remained stable at first, then decreased steadily from 0.437 kg CO_2/kWh downwards. Under modalities C and D, however, an opposite trend was observed, in which the total annual CO_2 emissions increased sharply, especially between the initial value and 0.437 kg CO_2/kWh, in the case of modality C, and 0.530 kg CO_2/kWh, in the case of modality D.
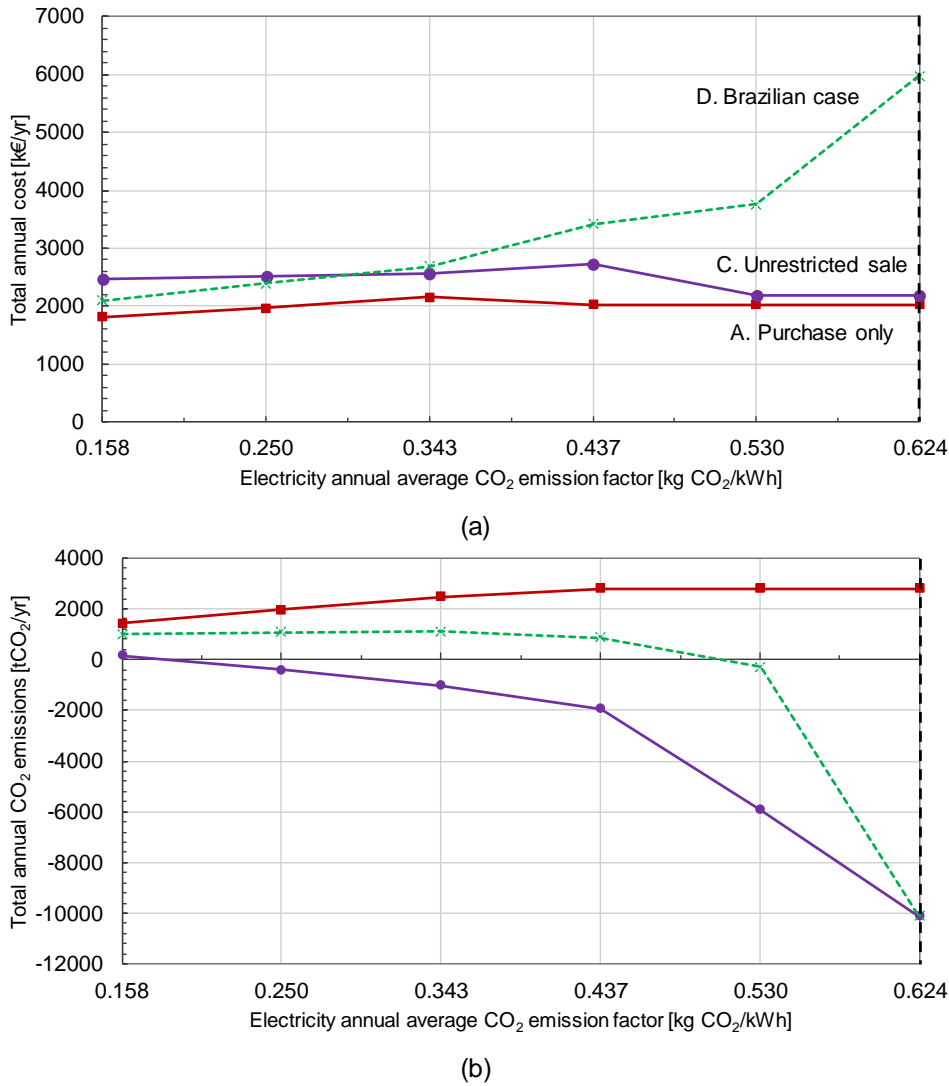
Figure 5.18: Sensitivity analysis for the electricity CO_2 emission factors, (a) total annual cost, and (b) total annual CO_2 emissions (objective function).

Figure 5.19 presents the installed capacities *PIN* under different modalities of the cogeneration module GE, photovoltaic panel PV, parabolic trough concentrator PT, mechanical chiller EC, single-effect AS and double-effect AD absorption, and hot water HS and chilled water CS storage tanks.
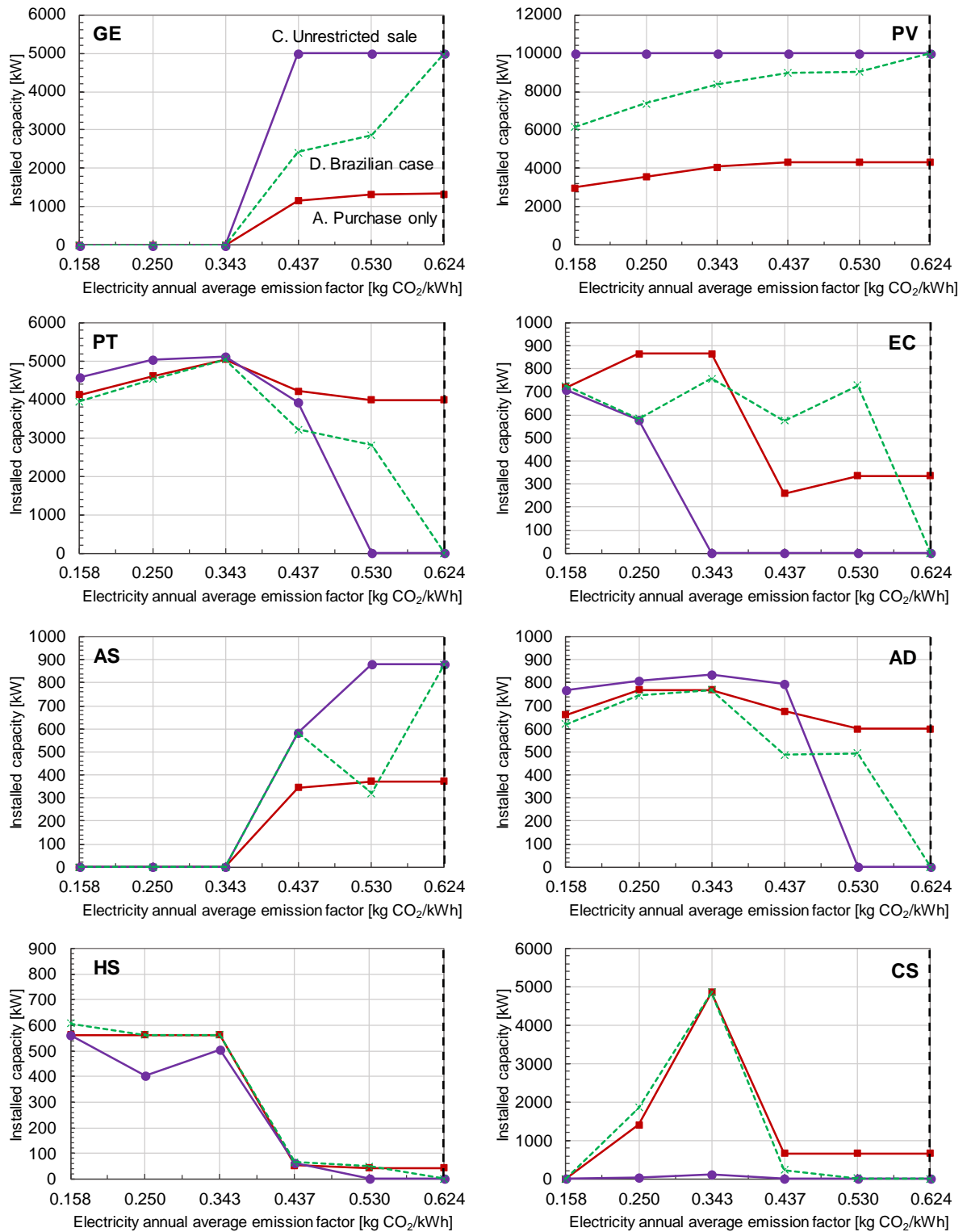
Figure 5.19: Sensitivity analysis for the electricity CO_2 emission factors, installed capacities.

Under all modalities, as in the previous analyses, there was a correspondence between the GE and the AS, both of which were completely phased out for $kgCO2_{ele}$ values below 0.437 kg CO_2/kWh; interestingly, there was also a correspondence between the PT and the AD, whose installed capacities peaked at 0.343 kg CO_2/kWh, except for the *PIN(AD)* under modality A, which peaked at 0.250 kg CO_2/kWh. Regarding the TES units, while the HS rose significantly from 0.437 to 0.343

kg CO_2/kWh, the CS peaked at 0.343 kg CO_2/kWh, then fell rapidly, being completely removed at 0.158 kg CO_2/kWh. PV presented similar trends under modalities A and D, in which their installed capacities steadily decreased from 0.437 kg CO_2/kWh downwards; on the other hand, under modality C the *PIN(PV)* remained unchanged at the maximum installable capacity limit.

5.5   CONCLUSIONS

A MILP model was developed herein to determine the optimal configuration and multi-period operational strategy of a polygeneration system that must attend the electricity, steam, hot water, and chilled water demands of a university hospital located in Campinas, Brazil. The optimization model included a detailed representation of the thermal integration of the heat supply and demand in the superstructure of the system. Additionally, the Brazilian regulatory environment for the exchange of electricity with the national electric grid was modelled. The optimal economic cost solutions were obtained for different modalities of power exchange with the grid, demonstrating the interest of cogeneration with natural gas under all modalities. Given the absence of the RETs, further analyses were carried out to evaluate on what future conditions the incorporation of renewable energies will have economic interest. In this regard, it was shown that the high investment cost of the solar-based RETs would have to be drastically reduced in order to promote their installation.

CHAPTER 6

Conclusions

6 CONCLUSIONS

Chapter 6 provides a synthesis of the work developed in this thesis, proclaims the contributions made, and presents future research directions.

6.1 SYNTHESIS

The overall aim of this thesis was to develop synthesis and operation optimization methodologies for polygeneration systems in residential-commercial applications. This task required, on the one hand, that the developed optimization models captured the dynamic operating conditions of buildings and their surroundings (e.g. variable energy demands, climatic conditions, energy and equipment prices, CO_2 emission factors), and on the other hand, that existing cost allocation approaches were complemented with respect to the integration of thermal energy storage (TES) and renewable energy sources (RES).

The opening chapter (Chapter 1) introduced the problem addressed and provided a background on the synthesis and operation optimization of polygeneration systems including RES and TES units for residential-commercial buildings. The review of the state of the art highlighted the interest and need of improving currently available synthesis and optimization techniques for buildings applications, especially in those cases of higher complexity levels in which RES and TES are included. This necessity was also demonstrated for the problem of allocating the costs of the resources consumed to the final products. Several research gaps were identified, thereby justifying the development of this thesis: multi-objective optimization models with balanced objective functions; accurate representation of dynamic operating conditions; realistic representation of the thermal requirements of the energy supply and demand in the superstructure; and rational cost allocation approaches that take into account dynamic operating conditions and the role of the TES.

The first part of the thesis included Chapters 2 and 3, which had a conceptual approach to the synthesis, optimization, and thermoeconomic analysis problems.

Chapter 2 outlined a multi-objective synthesis framework of polygeneration systems in buildings. The chapter began with an in-depth description about the potential benefits as well as the challenges associated with the introduction of different types of technologies in energy supply systems, such as cogeneration modules, thermally activated technologies, TES units, renewable energy technologies (RETs), and heat pumps. It was made clear that the gain in flexibility is accompanied by an increased system complexity, which requires an adequate optimization procedure that can address the many interrelated aspects of energy supply systems in buildings.

Thus, a comprehensive description was provided of the main steps that must be followed for the optimal synthesis of polygeneration systems, namely the superstructure definition, data compilation and elaboration, mathematical model development, and optimal decision-making.

Chapter 3 developed a thermoeconomic analysis of a simple trigeneration system assisted with TES based on marginal cost analysis and average costs calculation. First, the trigeneration system was modeled using a linear programming model that minimized the daily operation cost. The optimal operation of the system for a day of the year, composed of 24 hourly periods, was determined along with the marginal costs of the internal flows and final products of the system. The analysis of the marginal costs provided valuable insight into the operation of the system, explaining how and why the system operates given a change in external circumstances (e.g. increase in the consumer center's energy demands). The role of the TES in achieving the optimal solution was demonstrated. By studying the interconnection between the hourly periods through the TES, it was possible to identify time intervals in which the system takes advantage of its ability to store energy to achieve a more interesting economic result. For instance, there were hourly periods in which energy service production was advanced, so that the system produced the energy service in a previous cheaper hour and stored it for later consumption; on the other hand, there were periods in energy service production was postponed, so that the system used energy that was already stored.

In the second part of Chapter 3, cost allocation in the trigeneration system was tackled focusing on two important issues that had not been appropriately addressed until now: the joint production of energy services in polygeneration systems assisted with TES. The cost allocation proposal resulted in an equitable distribution of the benefits (e.g. revenue from electricity sale) and inefficiencies (e.g. penalty for energy wasting) of the combined production between the final products of the system. The TES added a new dimension to the cost allocation problem, as it became necessary to know not only the device in which the production took place but also the hourly period. Therefore, a novel cost allocation approach was proposed to trace the discharged energy back to its production period and, thus, connect the resources consumed to internal flows and final products.

The second part of the thesis consisted of Chapters 4 and 5, in which the methodologies proposed in the first part are complemented and applied to more realistic polygeneration systems in two case studies, one in Zaragoza (Spain) and another in Campinas (Brazil).

Chapter 4 developed a multi-objective optimization and thermoeconomic analysis of a trigeneration system for a multi-family building in Zaragoza. The mixed integer linear programming (MILP) model determines the optimal system configuration and hourly operational

planning from the economic and environmental viewpoints. The model carefully represented the dynamic conditions that govern the selection of technologies and the hour by hour operation of the system, which ultimately affect the objective function. In this context, a considerable effort was made to obtain the hourly-based CO_2 emission factors of the grid electricity in Spain, thus evaluating the environmental performance of the system in a more realistic way. Likewise, the environmental objective function accounted for the CO_2 emissions generated not only during the operation of the system, but also in the manufacturing of the technologies. An additional feature of the model was that the solar-based RETs were carefully modeled to capture the dynamic conditions of the solar availability and working temperatures. For the current conditions, the results showed that cogeneration with natural gas internal combustion engines had a low economic interest, as only a small capacity was installed in the optimal economic solution. Moreover, by reducing the CO_2 emissions from the optimal economic to the environmental solutions along the Pareto set, cogeneration was rapidly displaced by the electric grid and the reversible heat pump. This is explained by the increasing share of renewable energy in the national power mix, which reduces the CO_2 emission factor of the grid electricity, thus promoting the use of the reversible heat pump for heating and cooling.

Then, it was proposed to extend the cost allocation approaches of Chapter 3 to tackle the complex trigeneration systems analyzed in Chapter 4. The distribution of capital costs was carefully considered, especially regarding the TES units and the reversible heat pump. In the case of the heat pump, the knowledge of the operational behavior of the system was essential to identify the dominating device of each energy service production, leading in this case study to the consideration of cooling as the heat pump's main product, thus receiving all the heat pump's capital cost. Regarding the TES units, it was argued that capital cost allocation based on productivity (annual discharged energy) should be discouraged when energy losses are considered. In those cases, it is necessary to account for the history of the energy stored, as the longer duration of the storage (time difference between charge and discharge), the greater the energy losses generated. Therefore, it was proposed to allocate capital costs to the discharged energy based on its corresponding energy losses. In this way, more capital cost is allocated to the energy discharged after a long period of storage.

Chapter 5 assessed the technical, economic, and environmental feasibility of renewable-based polygeneration systems in a university hospital located in Campinas. A MILP model was developed to determine the optimal system configuration and hourly operational planning from the economic and environmental viewpoints. There are two main aspects that differentiate this model from the one developed in Chapter 4: First, the thermal integration of technologies and utilities was represented with a higher level of detail, aiming at an optimal match between the heat supply

and demand. This was achieved through the combination of Pinch Analysis, by means of the problem table algorithm, and mathematical programming techniques. Also, a comprehensive description of the thermal requirements of the technologies in the superstructure was carried out. Second, it included a careful representation of the Brazilian regulatory framework regarding the access of distributed micro/minigeneration to the distribution network and the Electrical Energy Compensation System (EECS). The analysis of the optimal cost solutions showed that under current conditions natural gas cogeneration was the most interesting solution for the Brazilian hospital either with or without the permission to sell electricity to the grid, while the RETs were never included. The detailed representation of the heat supply and demand in the superstructure became clear in the coupling between the cogeneration module and the single-effect absorption chiller: the high-temperature heat provided by the cogeneration module was used in the steam production, while the low-temperature heat was employed in the single-effect absorption chiller.

The absence of the RETs in the optimal cost solutions prompted a study on what future conditions the incorporation of renewable energies will have economic interest. In this context, it was demonstrated that the high investment cost of the solar-based RETs hindered their installation and a significant decrease would have to take place until they became economically feasible. Additionally, it became clear that under the current conditions the Brazilian EECS does not contribute to greater renewable energy deployment. In fact, it could be argued that such framework is lax and unsustainable in the long term. Finally, the CO_2 emissions of the electric grid at the operating margin provided by the Ministry of Science, Technology, Innovation and Communication of Brazil were proven to be too high, giving a window of opportunity for other technologies, more pollutant than RETs, such as natural gas-based cogeneration, to be installed.

6.2 CONTRIBUTIONS

Methodologies have been developed for the multi-objective synthesis and operation optimization of polygeneration systems assisted with renewable energy sources and thermal energy storage for residential-commercial buildings. The formulated MILP models addressed the many interrelated aspects of energy supply systems in buildings. The main contributions in this regard are the following:

- The optimization models were developed with a view to ensuring the same level of model detail for the optimization criteria (economic cost and CO_2 emissions). Therefore, both objective functions (total annual cost and total annual CO_2 emissions) were composed of two equivalent terms, one fixed (capital), relative to the installation of the technologies, and one variable (operation), relative to the hourly operation of the system. While the economic objective function accounted for the investment costs of installing the

technologies and the operation costs of consuming energy resources from the economic market, the environmental objective function was represented as the embedded CO_2 emissions generated in the manufacturing of the technologies installed and the CO_2 emissions generated during the operation of the system. In this way, the embedded CO_2 emissions were used as counterpart to the investment costs of the technologies, and the hourly CO_2 emission factors of the grid electricity were used as a counterpart to the hourly electricity purchase prices.

- The model was flexible as it allowed to: (i) incorporate local-based data, such as energy demands, energy resources, climatic data, CO_2 emission factors, among others; (ii) impose the installation/absence of technologies to obtain a specific system configuration; (iii) define operation modes of technologies for each month of the year; and (iv) introduce restrictions based on local regulations, such as the permission to buy/sell electricity to the grid and the minimum thermal efficiency for cogeneration units; in particular, this feature was used to model the current Brazilian regulatory environment for electricity exchange.

- The model carefully described the technologies and their interrelations. In this regard, the influence of dynamic climatic conditions (e.g. ambient air temperature and solar radiation) on the output of the technologies was accurately represented, especially the solar-based RETs. An innovative approach was developed to promote a more realistic representation of the thermal integration of technologies and utilities in the superstructure by combining Pinch Analysis, through the problem table algorithm, and mathematical programming, through MILP.

The main contributions in the context of the thermoeconomic analysis are the following:

- Thermoeconomic cost allocation methodologies for polygeneration systems in buildings applications have been proposed, contributing to some issues that had not been deeply studied until now: (i) the incorporation of TES units; (ii) deployment of free renewable energy resources (e.g. solar radiation); (iii) the introduction of components with different products for different operating modes (e.g. a reversible heat pump producing heat in heating mode and cooling in cooling mode); and (iv) the joint production of energy services in dynamic energy systems.

- A novel cost allocation method for the TES was developed that traces the discharged energy back to its production period and, thus, connects the resources consumed to internal flows and final products. Concerning the joint production of energy services, it was proposed to distribute the benefits and inefficiencies among all cogenerated products

by applying the same discount with respect to their reference costs. Additionally, the issue of allocating the capital costs of the technologies to their products was addressed, in particular concerning the TES units and the reversible heat pump. The cost allocation methodologies allowed all products of the polygeneration system to be economically competitive relative to a reference system, thus promoting their widespread social acceptance by society.

6.3   FUTURE WORK

This thesis has made important contributions to the ongoing work in the field of synthesis and operational optimization of polygeneration systems for residential-commercial buildings applications. Further research could follow several directions as highlighted below.

First, other technologies could be incorporated into the superstructure, such as different types of cogeneration prime movers (e.g. gas turbines, microturbines, fuel cells), renewable energy technologies (e.g. thermal hybrid collectors, evacuated tube collectors, Fresnel solar concentrator, wind turbines), thermally activated technologies (e.g. triple effect absorption chiller, gas fired absorption chiller), and energy storages (e.g. ice storage, electric battery), as well as solar thermal Organic Rankine Cycles (ORC). Innovative technology concepts could also be addressed, such as electric vehicles as mobile storage devices.

Second, the thermal integration of technologies and utilities in the superstructure could be enhanced, for example, by the optimal design of the heat exchangers network capable of operating with flexibility according to different operation modes as in the summer/winter seasons.

Third, the synthesis model could be extended to the design procedure so that, once the technologies to be installed have been selected and the part of the model that describes the performances of the technologies has been refined, the design model determines the number of devices and their corresponding installed capacities. As a result, this would enable the model to incorporate a dispatch schedule that takes into account the effect of partial load operation and start-up/ramp/shutdown of the devices on the system's performance.

Last, future research could use the features of the model to explore the effect of boundary conditions on the optimal solutions. In this regard, the regulatory environment for electricity exchange with the grid could be improved in order to compare different country's scenarios and evaluate the implementation of new ones. Moreover, the economic objective function could also reflect environmental concerns through a carbon emission tax or an added cost of carbon mitigation.

CAPÍTULO 6

Conclusiones

6 CONCLUSIONES

El Capítulo 6 proporciona un resumen del trabajo desarrollado en esta tesis, proclama las contribuciones realizadas, y da sugerencias para trabajos futuros.

6.1 SÍNTESIS

El objetivo general de esta tesis ha sido el de desarrollar metodologías de síntesis y optimización de la operación de sistemas de poligeneración en aplicaciones del sector residencial-comercial. Esta tarea ha requerido, por un lado, que los modelos de optimización desarrollados capturaran las condiciones dinámicas de operación del edificio y su entorno (demandas variables de energía, condiciones climáticas, precios de la energía y de los equipos, factores de emisión de CO_2), y, por otro lado, que los criterios existentes de reparto de costes se complementaran para tener en cuenta la integración de acumuladores de energía térmica (TES) y de fuentes de energía renovables (RES).

El capítulo inicial (Capítulo 1) ha presentado el problema de investigación abordado y ha contextualizado el tema de la síntesis y optimización de la operación de sistemas de poligeneración con RES y TES en edificios del sector residencial-comercial. La revisión de la literatura ha destacado el interés y la necesidad de mejorar las técnicas de síntesis y optimización disponibles en la actualidad para aplicaciones de edificios, especialmente en aquellos sistemas de mayor complejidad en los que se incluyen RES y TES. Dicha necesidad también se ha demostrado para el problema de la asignación de los costes de los recursos consumidos a los productos finales. Se identificaron varios objetivos de investigación insuficientemente estudiados hasta la fecha que justifican el desarrollo de esta tesis: modelos de optimización multiobjetivo con funciones objetivo equilibradas; representación precisa de las condiciones dinámicas de operación; representación realista de los requisitos térmicos de la oferta y demanda en la superestructura; y propuestas de asignación de costes para un reparto justo entre los consumidores finales que tengan en cuenta el papel de los TES.

La primera parte de la tesis ha comprendido los Capítulos 2 y 3 que han abordado conceptualmente los problemas de síntesis, optimización, y análisis.

El Capítulo 2 ha propuesto un marco para la síntesis multiobjetivo de sistemas de poligeneración en edificios. El capítulo comenzó con una descripción detallada de los beneficios potenciales y desafíos de la incorporación de diferentes tipos de tecnologías en sistemas energéticos, como módulos de cogeneración, tecnologías activadas térmicamente, TES, tecnologías de energía renovable (RETs), y bombas de calor. Se ha demostrado que el aumento de flexibilidad viene

acompañado por una mayor complejidad y requiere un procedimiento de optimización capaz de abordar la gran variedad de aspectos interrelacionados en los sistemas energéticos en edificios. Por lo tanto, se ha proporcionado una descripción completa de las tareas que deben seguirse para la síntesis óptima de sistemas de poligeneración; a saber, la definición de la superestructura, la compilación y elaboración de datos, el desarrollo del modelo matemático, y la toma de decisiones óptima.

El Capítulo 3 ha desarrollado el análisis termoeconómico de un sistema de trigeneración simple asistido con TES basado en el análisis de costes marginales y el cálculo de costes medios. Inicialmente, se ha modelado el sistema de trigeneración mediante un programa lineal que minimiza el coste de operación diario. Se ha determinado la operación óptima del sistema para un día del año compuesto de 24 periodos horarios junto con los costes marginales de los flujos internos y de los productos finales del sistema. El análisis de los costes marginales ha proporcionado una valiosa descripción de la operación, explicando cómo y por qué evoluciona el sistema bajo un cambio en las circunstancias externas (por ejemplo, un aumento de las demandas del centro consumidor). Se ha demostrado el papel que juega el TES para conseguir la solución óptima. Mediante el estudio de la interconexión operativa entre los periodos horarios a través del TES se ha hecho posible identificar intervalos de tiempo en los que el sistema aprovecha su capacidad de almacenar energía para lograr un resultado económico más interesante. Por ejemplo, hubo periodos en los que se adelantó la producción del servicio energético, de modo que el sistema produjo más barata la energía térmica en una hora anterior y la almacenó para su posterior consumo; por otro lado, hubo periodos en que se pospuso la producción de la energía térmica, y el sistema utilizó energía que ya estaba almacenada en el TES.

En la segunda parte del Capítulo 3, se ha abordado la asignación de costes en el sistema de trigeneración centrándose en aspectos fundamentales que no se habían tratado adecuadamente hasta ahora: la producción conjunta de servicios energéticos en sistemas de poligeneración asistida con TES. La propuesta de asignación de costes ha resultado en una distribución equitativa de los beneficios (como los ingresos por la venta de electricidad) y de las ineficiencias (como la penalización por despilfarrar energía) de la producción combinada entre los productos finales del sistema. El TES ha añadido una nueva dimensión al problema de reparto de costes, puesto que ha sido necesario considerar no sólo el equipo en el que tuvo lugar la producción, sino también el intervalo de tiempo. Por lo tanto, se propuso un abordaje novedoso de asignación de costes para rastrear la energía descargada hasta su período de producción y, así, conectar los recursos consumidos a los flujos internos y a los productos finales.

La segunda parte de la tesis ha comprendido los Capítulos 4 y 5, en los que las metodologías propuestas en la primera parte se han complementado y aplicado a sistemas de poligeneración más realistas en dos estudios de caso, uno en Zaragoza (España) y otro en Campinas (Brasil).

En el Capítulo 4 se ha desarrollado la optimización multiobjetivo y el análisis termoeconómico de un sistema de trigeneración para un edificio multifamiliar en Zaragoza. El modelo elaborado de programación lineal entera mixta (PLEM) permitió determinar la configuración óptima del sistema y la estrategia de operación horaria desde los puntos de vista económico y ambiental. El modelo ha representado detalladamente las condiciones dinámicas que gobiernan la selección de las tecnologías y la operación hora a hora del sistema, lo que finalmente afecta a la función objetivo. En este contexto, se hizo un esfuerzo considerable para obtener los factores horarios de emisión de CO_2 de la red eléctrica española, evaluando así el desempeño ambiental del sistema de manera realista. Asimismo, la función objetivo ambiental ha contabilizado las emisiones de CO_2 generadas no sólo durante la operación del sistema, sino también en la fabricación de los equipos. Una característica adicional del modelo ha sido que las RETs basadas en energía solar se han modelado cuidadosamente para considerar correctamente las condiciones dinámicas de la disponibilidad del recurso solar y las temperaturas de trabajo. Para las condiciones del caso, los resultados han demostrado que la cogeneración con motores de combustión interna de gas natural tenía un interés limitado, puesto que se ha instalado sólo una capacidad pequeña en la solución de mínimo coste económico. Además, al reducir las emisiones de CO_2 desde la solución de óptimo económico a la solución de óptimo ambiental a lo largo de la curva de Pareto, la cogeneración fue desplazada rápidamente por la red eléctrica y la bomba de calor reversible. Esto se puede explicar por la creciente participación de la energía renovable en la producción eléctrica peninsular, que reduce el factor de emisión de CO_2 de la electricidad disponible en la red, promoviendo así el uso de la bomba de calor reversible para calefacción y refrigeración.

A continuación, se han ampliado las propuestas de asignación de costes elaboradas en el Capítulo 3 para abordar el sistema de poligeneración complejo analizado en el Capítulo 4. La asignación de los costes de capital se ha considerado con atención, especialmente con respecto a los TES y la bomba de calor reversible. En el caso de la bomba de calor, el conocimiento del comportamiento de la operación del sistema ha sido fundamental para identificar el equipo dominante de cada servicio energético, lo que llevó, en este estudio de caso, a tomar la refrigeración como el producto principal de la bomba de calor, atribuyéndole así todo el coste de capital de este equipo. Acerca de los TES, se ha argumentado que la asignación de los costes de capital basada en la productividad (energía descargada anual) no es recomendable cuando se tienen en cuenta las pérdidas de energía. En esos casos, es necesario tener en cuenta el historial de la energía almacenada, puesto que a mayor duración del almacenamiento (diferencia de tiempo entre la carga y la descarga),

mayores serán las pérdidas de energía generadas. Por lo tanto, se ha propuesto asignar los costes de capital a la energía descargada en función de sus pérdidas de energía correspondientes. De esta manera, se asigna más coste de capital a la energía descargada tras un largo período de almacenamiento.

En el Capítulo 5 se ha evaluado la viabilidad técnica, económica y ambiental de sistemas de poligeneración que incorporan energías renovables en un hospital universitario en Campinas. Se ha desarrollado un modelo de PLEM para determinar la configuración óptima del sistema y la estrategia de operación horaria desde los puntos de vista económico y ambiental. Hay dos aspectos principales que diferencian este modelo del desarrollado en el Capítulo 4. Primero, la integración térmica de las tecnologías y utilidades se representó con mayor nivel de detalle, con el objetivo de conseguir una correspondencia óptima entre la oferta y la demanda de calor. Esto se ha logrado a través de la combinación del Análisis Pinch, mediante el algoritmo de la Tabla Problema, y las técnicas de programación matemática. Además, se realizó una descripción completa de los requisitos térmicos de las tecnologías en la superestructura. En segundo lugar, el modelo incluyó una representación detallada del marco regulatorio brasileño con respecto al acceso de micro/minigeneración distribuida a la red eléctrica y al Sistema de Compensación de Energía Eléctrica (EECS). El análisis de las soluciones de coste óptimo mostró que, en las condiciones actuales, la cogeneración con gas natural era la solución más interesante para el hospital brasileño, ya sea con o sin el permiso para vender electricidad, mientras que las RETs no se han incluido nunca. La representación detallada del suministro y de la demanda de calor en la superestructura ha quedado clara en el acoplamiento entre el módulo de cogeneración y la enfriadora de absorción de simple efecto: el calor de alta temperatura aportado por el módulo de cogeneración se ha utilizado en la producción de vapor, mientras que el calor de más baja temperatura se ha empleado en la enfriadora.

La ausencia de las RETs en las soluciones de mínimo coste económico ha motivado un estudio para determinar las condiciones en las que tendrá interés económico la incorporación de las energías renovables. En este contexto, se ha demostrado que el elevado coste de inversión de las RETs solares dificultaba su instalación y que tendría que producirse una disminución significativa hasta que fueran económicamente viables. Además, quedó claro que, en las condiciones actuales, el EECS brasileño no contribuye a un mayor uso de las energías renovables. De hecho, podría argumentarse que dicho marco es laxo e insostenible a largo plazo. Finalmente, se ha demostrado que los factores de emisión de CO_2 de la red eléctrica en el margen operativo proporcionados por el Ministerio de la Ciencia, Tecnología, Innovación y Comunicación de Brasil al ser demasiado altos, permiten que se instalen otras tecnologías más contaminantes que las RETs, como la cogeneración con gas natural.

6.2   CONTRIBUCIONES

Se han desarrollado metodologías de optimización multiobjetivo para la síntesis y operación de sistemas de poligeneración asistidos con fuentes renovables de energía y almacenamiento de energía térmica para edificios del sector residencial-comercial. Los modelos de PLEM formulados abordaron los distintos aspectos interrelacionados en los sistemas energéticos en los edificios. Las principales aportaciones a este respecto son las siguientes:

- Los modelos de optimización se han desarrollado con el fin de garantizar el mismo nivel de detalle para los dos criterios: coste económico y emisión de CO_2. Por lo tanto, se han formulado ambas funciones objetivo (coste total anual y emisión de CO_2 total anual) compuestas por dos términos equivalentes, uno fijo (capital), relativo a la instalación de las tecnologías, y otro variable (operación), relativo a la operación horaria del sistema. Si por un lado la función objetivo económica se ha representado como los costes de inversión y los costes de operación del consumo de los recursos energéticos comerciales, por el otro lado la función objetivo ambiental se ha representado como las emisiones de CO_2 generadas en la fabricación de los equipos instalados y las emisiones de CO_2 generadas durante la operación del sistema. De esta manera, las emisiones de CO_2 integradas se utilizaron como equivalente de los costes de inversión de las tecnologías, y los factores de emisión de CO_2 de la red eléctrica se usaron como equivalente de los precios horarios de compra de electricidad.

- El modelo es flexible, puesto que ha permitido: (i) incorporar datos locales, como demandas de energía, recursos energéticos, datos climáticos, factores de emisión de CO_2, entre otros; (ii) imponer la instalación/ausencia de tecnologías para obtener una configuración específica del sistema; (iii) definir distintos modos de operación de algunas tecnologías para cada mes del año; e (iv) introducir restricciones basadas en las regulaciones locales, como el permiso para comprar/vender electricidad a la red y el cumplimiento de una eficiencia térmica mínima para los módulos de cogeneración; en particular, esta característica se usó para modelar el marco actual regulatorio brasileño de intercambio de electricidad.

- El modelo ha descrito con detalle las tecnologías y sus interrelaciones. En este sentido, se representó con precisión la influencia de las condiciones climáticas dinámicas (por ejemplo, la temperatura ambiente y la radiación solar) en la producción de las tecnologías, especialmente las RETs basadas en energía solar. Se desarrolló un procedimiento innovador para promover una representación más realista de la integración térmica de tecnologías y utilidades en la superestructura mediante la combinación del Análisis Pinch,

a través del algoritmo de la Tabla Problema, y la programación matemática, a través de la PLEM.

Las principales aportaciones al análisis termoeconómico son las siguientes:

- Se han propuesto metodologías de asignación de costes para los sistemas de poligeneración en aplicaciones de edificios, con nuevas contribuciones en algunos aspectos que no se habían estudiado en profundidad hasta ahora: (i) la incorporación de TES; (ii) el uso de energías renovables gratuitas (por ejemplo, el recurso solar); (iii) la incorporación de equipos con diferentes productos en distintos modos de operación (por ejemplo, una bomba de calor reversible que produce calor en modo de calefacción y agua fría en modo de refrigeración); y (iv) la producción conjunta de servicios energéticos en sistemas energéticos dinámicos.

- Se desarrolló un nuevo método de asignación de costes para el TES que rastrea la energía descargada hacia su periodo de producción y, así, conecta los recursos consumidos a los flujos internos y productos finales. Con respecto a la producción conjunta de servicios energéticos, se propuso distribuir los beneficios y las ineficiencias entre todos los productos cogenerados aplicando el mismo descuento con relación a sus costes de referencia. Además, se abordó la cuestión del reparto de los costes de capital de las tecnologías a sus productos, en particular con respecto al TES y la bomba de calor reversible. Las metodologías de reparto de costes permitieron que todos los productos del sistema de poligeneración fueran económicamente competitivos en relación con el sistema de referencia, promoviendo así su aceptación por parte de la sociedad.

6.3   PERSPECTIVAS FUTURAS

Esta tesis ha hecho relevantes aportaciones al campo de la síntesis y optimización de sistemas de poligeneración en edificios del sector residencial-comercial. Hay algunas direcciones de estudio para extender el trabajo de esta tesis como se explica a continuación.

Primero, se podrían incorporar otras tecnologías en la superestructura, como diferentes tecnologías de cogeneración (turbinas de gas, microturbinas, pilas de combustible), tecnologías basadas en energías renovables (paneles solares híbridos, colectores solares de tubos de vacío, concentradores tipo Fresnel, aerogeneradores), tecnologías activadas térmicamente (enfriadoras de absorción de triple efecto, enfriadoras de absorción accionadas con gases de escape) y acumuladores de energía (acumuladores de hielo, baterías eléctricas), así como ciclos de potencia

y cogeneración ORC accionados con energía solar térmica. También podrían abordarse conceptos innovadores como los vehículos eléctricos como dispositivos móviles de almacenamiento.

Segundo, se podría mejorar la integración térmica de las tecnologías y utilidades en la superestructura, por ejemplo, mediante el diseño de la red de intercambiadores de calor capaz de operar con flexibilidad bajo distintos modos de operación, como verano/invierno.

Tercero, se podría extender el programa de síntesis hacia el diseño, de modo que, una vez realizada la selección de las tecnologías a instalar, y habiendo refinado la parte del modelo que describe las prestaciones de los equipos, el programa de diseño determinara el número de dispositivos y sus capacidades instaladas. Finalmente, esto permitiría avanzar hacia una programación del despacho que tuviera en cuenta el efecto en las prestaciones del sistema de la operación a carga parcial y arranque/rampa/parada de los equipos.

Por último, los trabajos futuros podrían utilizar la capacidad del modelo para evaluar el efecto de las condiciones de contorno en la solución óptima. En este sentido, se podría mejorar el marco regulatorio para el intercambio de electricidad con la red eléctrica, comparando los escenarios de distintos países y evaluando la implementación de nuevas condiciones. Además, la función objetivo económica podría reflejar el aspecto ambiental mediante la incorporación de una tasa a la emisión de carbono o de un sobrecoste por la mitigación de carbono.

REFERENCES

REFERENCES

Abusoglu, A., Kanoglu, M., 2009. Exergoeconomic analysis and optimization of combined heat and power production: A review. Renew. Sustain. Energy Rev. 13, 2295–2308.

AEMET, 2010. Guía Resumida del Clima en España 1981-2010 [WWW Document]. URL http://www.aemet.es/en/conocermas/recursos_en_linea/publicaciones_y_estudios/publicaciones/detalles/guia_resumida_2010 (accessed 8.30.16).

AENOR, 2007. UNE 94003:2007 - Datos climáticos para el dimensionado de instalaciones solares térmicas.

AENOR, 2005. UNE 94002:2005 - Thermal solar systems for domestic hot water production. Calculation method for heat demand.

Alarcon-Rodriguez, A., Ault, G., Galloway, S., 2010. Multi-objective planning of distributed energy resources: A review of the state-of-the-art. Renew. Sustain. Energy Rev. 14, 1353–1366.

Amundsen, E.S., Andersen, P., Jensen, F., 2011. Testing for cross-subsidisation in the combined heat and power generation sector: A comparison of three tests. Energy Econ. 33, 750–757.

Andiappan, V., 2017. State-Of-The-Art Review of Mathematical Optimisation Approaches for Synthesis of Energy Systems. Process Integr. Optim. Sustain. 1, 165–188.

ANEEL, 2015. Normative Resolution 687/2015, Brazilian Electricity Regulatory Agency.

Angrisani, G., Roselli, C., Sasso, M., 2012. Distributed microtrigeneration systems. Prog. Energy Combust. Sci. 38, 502–521.

Ardente, F., Cellura, M., 2012. Economic Allocation in Life Cycle Assessment. J. Ind. Ecol. 16, 387–398.

Arteconi, A., Hewitt, N.J., Polonara, F., 2012. State of the art of thermal storage for demand-side management. Appl. Energy 93, 371–389.

Ashouri, A., Fux, S.S., Benz, M.J., Guzzella, L., 2013. Optimal design and operation of building services using mixed-integer linear programming techniques. Energy 59, 365–376.

ASHRAE, 2015. Chapter 35 - Solar Energy Use, in: ASHRAE Handbook: HVAC Applications (SI).

ASHRAE, 2013. Chapter 14 - Climatic Design Information, in: Handbook - Fundamentals (SI).

ASHRAE, 2009. Chapter 19 - Energy Estimating and Modeling Methods General Considerations Models and Approaches, in: ASHRAE Handbook.

Azapagic, A., 2010. Assessing Environmental Sustainability: Life Cycle Thinking and Life Cycle Assessment, in: Sustainable Development in Practice. John Wiley & Sons, Ltd, Chichester, UK, pp. 56–80.

Azapagic, A., Clift, R., 1999. Allocation of environmental burdens in multiple-function systems. J. Clean. Prod. 7, 101–119.

Barberis, S., Rivarolo, M., Traverso, A., Massardo, A.F., 2016. Thermo-economic analysis of the energy storage role in a real polygenerative district. J. Energy Storage 5, 187–202.

Beretta, G.P., Iora, P., Ghoniem, A.F., 2014. Allocating resources and products in multi-hybrid multi-cogeneration: What fractions of heat and power are renewable in hybrid fossil-solar CHP? Energy 78, 587–603.

Bianchi, M., De Pascale, A., Melino, F., 2013. Performance analysis of an integrated CHP system with thermal and Electric Energy Storage for residential application. Appl. Energy 112, 928–938.

Biegler, L., Grossmann, I., 2004. Retrospective on optimization. Comput. Chem. Eng. 28, 1169–1192.

Biglia, A., Caredda, F. V., Fabrizio, E., Filippi, M., Mandas, N., 2017. Technical-economic feasibility of CHP systems in large hospitals through the Energy Hub method: The case of Cagliari AOB. Energy Build. 147, 101–112.

Brandoni, C., Renzi, M., 2015. Optimal sizing of hybrid solar micro-CHP systems for the household sector. Appl. Therm. Eng. 75, 896–907.

Bruno, J.C., Fernandez, F., Castells, F., Grossmann, I.E., 1998. A rigorous MINLP model for the optimal synthesis and operation of utility plants. Chem. Eng. Res. Des. 76, 246–258.

Buoro, D., Casisi, M., De Nardi, A., Pinamonti, P., Reini, M., 2013. Multicriteria optimization of a distributed energy supply system for an industrial area. Energy 58, 128–137.

Buoro, D., Pinamonti, P., Reini, M., 2014. Optimization of a Distributed Cogeneration System with solar district heating. Appl. Energy 124, 298–308.

Burkhardt, J.J., Heath, G.A., Turchi, C.S., 2011. Life cycle assessment of a parabolic trough concentrating solar power plant and the impacts of key design alternatives. Environ. Sci. Technol. 45, 2457–2464.

Cannistraro, G., 1995. Reduced weather data for building climatization and application to 29 European locations. Energy 20, 637–646.

Capuder, T., Mancarella, P., 2014. Techno-economic and environmental modelling and optimization of flexible distributed multi-generation options. Energy 71, 516–533.

Carvalho, M., 2011. Thermoeconomic and environmental analyses for the synthesis of polygeneration systems in the residential-commercial sector. PhD Thesis - University of Zaragoza, Department of Mechanical Engineering.

Carvalho, M., Lozano, M.A., Ramos, J., Serra, L.M., 2013. Synthesis of Trigeneration Systems: Sensitivity Analyses and Resilience. Sci. World J. 2013, 1–16.

Carvalho, M., Lozano, M.A., Serra, L.M., 2012. Multicriteria synthesis of trigeneration systems considering economic and environmental aspects. Appl. Energy 91, 245–254.

Casisi, M., Costanzo, S., Pinamonti, P., Reini, M., 2018. Two-Level Evolutionary Multi-objective Optimization of a District Heating System with Distributed Cogeneration. Energies 12, 114.

Catrini, P., Cipollina, A., Micale, G., Piacentino, A., Tamburini, A., 2017. Exergy analysis and thermoeconomic cost accounting of a Combined Heat and Power steam cycle integrated with a Multi Effect Distillation-Thermal Vapour Compression desalination plant. Energy Convers. Manag. 149, 950–965.

Chicco, G., Mancarella, P., 2009. Distributed multi-generation: A comprehensive view. Renew. Sustain. Energy Rev. 13, 535–551.

Collares-Pereira, M., Rabl, A., 1979. The average distribution of solar radiation-correlations between diffuse and hemispherical and between daily and hourly insolation values. Sol. Energy 22, 155–164.

COMGAS, 2018. Natural gas rates [WWW Document]. URL https://www.comgas.com.br/tarifas/

CPFL, 2018. Electricity rates [WWW Document]. CPFL Paul. URL https://www.cpflempresas.com.br/institucional/tarifas.aspx?emp=CPFL

Crespo Del Granado, P., Pang, Z., Wallace, S.W., 2016. Synergy of smart grids and hybrid distributed generation on the value of energy storage. Appl. Energy 170, 476–488.

CTE, 2013. CTE. Parte I, CTE: Código Técnico de la edificación, Documento Básico de eficiencia energética 4: DB-HE. FOM/1635/2013 update of Real Decreto 314/2006. BOE, September 12th.

da Gama Cerqueira, S.A.A., Nebra, S.A., 1999. Cost attribution methodologies in cogeneration systems. Energy Convers. Manag. 40, 1587–1597.

da Silva, J.A.M., Santos, J.J.C.S., Carvalho, M., de Oliveira, S., 2017. On the thermoeconomic and LCA methods for waste and fuel allocation in multiproduct systems. Energy 127, 775–785.

Darrow, K., Tidball, R., Wang, J., Hampson, A., 2015. Catalog of CHP Technologies. U. S. Environmental Protection Agency.

Delgado, D., Carvalho, M., Coelho, L., Chacartegui, R., 2018. Analysis of Biomass-fired Boilers in a Polygeneration System for a Hospital. Front. Manag. Res. 2, 1–13.

Deng, J., Wang, R., Wu, J., Han, G., Wu, D., Li, S., 2008. Exergy cost analysis of a micro-trigeneration system based on the structural theory of thermoeconomics. Energy 33, 1417–1426.

Deng, J., Wang, R.Z., Han, G.Y., 2011. A review of thermally activated cooling technologies for combined cooling, heating and power systems. Prog. Energy Combust. Sci. 37, 172–203.

Domínguez-Muñoz, F., Cejudo-López, J.M., Carrillo-Andrés, A., Gallardo-Salazar, M., 2011. Selection of typical demand days for CHP optimization. Energy Build. 43, 3036–3043.

Duffie, J.A., Beckman, W.A., Worek, W.M., 2013. Solar Engineering of Thermal Processes, 4th ed. ed, Journal of Solar Energy Engineering. Wiley.

EDP, 2017. Gas and Electricity Prices - Liberalized Market [WWW Document]. Gas Electr. Prices - Lib. Mark. URL http://www.edpenergia.es/es/hogares/gas-y-electricidad/precios/mercado-libre/ (accessed 8.31.17).

EEA, 2016. European Environment Agency - Progress on energy efficiency in Europe [WWW Document]. URL https://www.eea.europa.eu/data-and-maps/indicators/progress-on-energy-efficiency-in-europe-2/assessment-2 (accessed 3.24.18).

EES, 2017. Engineering Equation Solver. F-Chart Softw.

EEX, 2018. European Emissions Allowances [WWW Document]. URL https://www.eex.com/en/market-data/environmental-markets/spot-market/european-emission-allowances#!/2018/08/03 (accessed 8.4.18).

El-Sayed, Y.M., 2003. The Thermoeconomics of Energy Conversions. Elsevier Science.

El-Sayed, Y.M., Evans, R.B., 1970. Thermoeconomics and the Design of Heat Systems. J. Eng. Power 92, 27.

EnergyPlus, 2018. EnergyPlus Weather Data [WWW Document]. URL https://energyplus.net/weather (accessed 7.11.18).

Erbs, D.G., Beckman, W.A., Klein, S.A., 1983. Estimation of degree-days and ambient temperature bin data from monthly-average temperatures. ASHRAE J. 25:6, 60–65.

Erbs, D.G., Klein, S.A., Duffie, J.A., 1982. Estimation of the diffuse radiation fraction for hourly, daily and monthly-average global radiation. Sol. Energy 28, 293–302.

EU, 2010. Directive 2010/31/EU of the European Parliament and of the Council of 19 May 2010 on the energy performance of buildings (recast). Off. J. Eur. Union 13–35.

EU, 2012. Directive 2012/27/EU of the European Parliament and of the Council of 25 October 2012 on energy efficiency. Off. J. Eur. Union Dir. doi:http://data.europa.eu/eli/dir/2012/27/oj

Eurostat, 2017. Eurostat Energy Data [WWW Document]. URL http://ec.europa.eu/eurostat/web/energy/data/database (accessed 2.7.17).

Fazlollahi, S., Mandel, P., Becker, G., Maréchal, F., 2012. Methods for multi-objective investment and operating optimization of complex energy systems. Energy 45, 12–22.

Frangopoulos, C., 1987. Thermo-economic functional analysis and optimization. Energy 12, 563–571.

Frangopoulos, C.A., Spakovsky, M.R. Von, Sciubba, E., 2002. A Brief Review of Methods for the Design and Synthesis Optimization of Energy Systems. Int. J. Thermodyn. 5, 151–160.

Frederiksen, S., Werner, S., 2013. District Heating and Cooling. Studentlitteratur AB.

Frischknecht, R., 2000. Allocation in Life Cycle Inventory Analysis for Joint Production. Int. J. Life Cycle Assess. 5, 85–95.

REFERENCES

Gaggioli, R.A., 1983. Second Law Analysis for Process and Energy Engineering, in: Efficiency and Costing. ACS Symposium Series. pp. 3–50.

Gallo, A.B., Simões-Moreira, J.R., Costa, H.K.M., Santos, M.M., Moutinho dos Santos, E., 2016. Energy storage in the energy transition context: A technology review. Renew. Sustain. Energy Rev. 65, 800–822.

Gebreslassie, B.H., Guillén-Gosálbez, G., Jiménez, L., Boer, D., 2012. Solar assisted absorption cooling cycles for reduction of global warming: A multi-objective optimization approach. Sol. Energy 86, 2083–2094.

Gimelli, A., Muccillo, M., 2013. Optimization criteria for cogeneration systems: Multi-objective approach and application in an hospital facility. Appl. Energy 104, 910–923.

Giménez, J.M.M., 2004. Evaluación de alternativas para el abastecimiento energético de una urbanización residencial en Zaragoza. Proyecto de Fin de Carrera, CPS, Universidad de Zaragoza.

Gluesenkamp, K., Hwang, Y., Radermacher, R., 2013. High efficiency micro trigeneration systems. Appl. Therm. Eng. 50, 1480–1486.

Gochenour, C., 2003. Regulation of Heat and Electricity Produced in Combined Heat and Power Plants.

Gong, J., You, F., 2015. Sustainable design and synthesis of energy systems. Curr. Opin. Chem. Eng. 10, 77–86.

González, A., Riba, J.-R., Rius, A., 2016. Combined heat and power design based on environmental and cost criteria. Energy 116, 922–932.

González, A., Sala, J.M., Flores, I., López, L.M., 2003. Application of thermoeconomics to the allocation of environmental loads in the life cycle assessment of cogeneration plants. Energy 28, 557–574.

Gordon, C., Fung, A., 2009. Hourly emission factors From the electricity generation sector - A tool for analyzing the impact of renewable technologies In ontario. Trans. Can. Soc. Mech. Eng. 33, 105–118.

Grossmann, I.E., Halemane, K.P., Swaney, R.E., 1983. Optimization strategies for flexible chemical processes. Comput. Chem. Eng. 7, 439–462.

Guadalfajara, M., 2016. Economic and environmental analysis of central solar heating plants with seasonal storage for the residential sector. PhD Thesis - University of Zaragoza, Department of Mechanical Engineering.

Guadalfajara, M., Lozano, M.A., Serra, L.M., 2015. Simple calculation tool for central solar heating plants with seasonal storage. Sol. Energy 120, 72–86.

Guo, L., Liu, W., Cai, J., Hong, B., Wang, C., 2013. A two-stage optimal planning and design method for combined cooling, heat and power microgrid system. Energy Convers. Manag. 74, 433–445.

Haeseldonckx, D., Peeters, L., Helsen, L., D'haeseleer, W., 2007. The impact of thermal storage on the operational behaviour of residential CHP facilities and the overall CO2 emissions. Renew. Sustain. Energy Rev. 11, 1227–1243.

Hamming, R.W., 1973. Numerical Methods for Scientists and Engineers, Dover books on engineering. Dover.

Harvey, L., 2012. A handbook on low-energy buildings and district-energy systems: fundamentals, techniques and examples. Routledge.

Hemmes, K., Zachariahwolf, J., Geidl, M., Andersson, G., 2007. Towards multi-source multi-product energy systems. Int. J. Hydrogen Energy 32, 1332–1338.

Hennen, M., Postels, S., Voll, P., Lampe, M., Bardow, A., 2017. Multi-objective synthesis of energy systems: Efficient identification of design trade-offs. Comput. Chem. Eng. 97, 283–293.

Hinojosa, L.R., Day, A.R., Maidment, G.G., Dunham, C., Kirk, P., 2007. A comparison of combined heat and power feasibility models. Appl. Therm. Eng. 27, 2166–2172.

Holmberg, H., Tuomaala, M., Haikonen, T., Ahtila, P., 2012. Allocation of fuel costs and CO_2-emissions to heat and power in an industrial CHP plant: Case integrated pulp and paper mill. Appl. Energy 93, 614–623.

Horngren, C.T., 2009. Cost Accounting: A Managerial Emphasis, 13/e. Pearson Education.

Houwing, M., 2010. Smart Heat and Power: Utilizing the Flexibility of Micro Cogeneration. Technology, Policy and Management - Delft University of Technology.

Hui, C.W., 2000. Determining marginal values of intermediate materials and utilities using a site model. Comput. Chem. Eng. 24, 1023–1029.

IDAE, 2016. Factores de emisión de CO_2 y coeficientes de paso a energía primaria de diferentes fuentes de energía final consumidas en el sector de edificios en España, Documento Reconocido del Reglamento de Instalaciones Térmicas en los Edificios (RITE).

IDAE, 2011. Energía Solar Fotovoltaica: Pliego de Condiciones Técnicas de Instalaciones Conectadas a Red. IDAE 46.

IDAE, 2009. Escala de calificación energética. Edificios de nueva construcción. Group of Thermotechnics, Engineering School of Seville, IDAE.

IEA, 2017. District Energy Systems in China.

IEA, 2017a. Energy Efficiency 2017. IEA. doi:10.1787/9789264284234-en

IEA, 2017b. Energy Efficiency Indicators Highlights, Energy Efficiency Indicators Highlights (2017 edition).

IEA, 2017c. Energy Technology Perspectives 2017 - Executive Summary.

IEA, 2018. Key World Energy Statistics. IEA.

INE, 2018. National Statistics Institute [WWW Document]. URL http://www.ine.es/dyngs/INEbase/listaoperaciones.htm (accessed 6.5.18).

Itami, H., Kaplan, R.S., 1980. An Activity Analysis Approach to Unit Costing with Multiple Interactive Products. Manage. Sci. 26, 826–839.

Ito, K., Shiba, T., Yokoyama, R., 1994. Optimal Operation of a Cogeneration Plant in Combination With Electric Heat Pumps. J. Energy Resour. Technol. 116, 56.

Ito, M., Komoto, K., Kurokawa, K., 2009. A comparative LCA study on potential of very-large scale PV systems in Gobi desert. Conf. Rec. IEEE Photovolt. Spec. Conf.

Iyer, R.R., Grossmann, I.E., 1998. Synthesis and operational planning of utility systems for multiperiod operation. Comput. Chem. Eng. 22, 979–993.

Jana, K., Ray, A., Majoumerd, M.M., Assadi, M., De, S., 2017. Polygeneration as a future sustainable energy solution – A comprehensive review. Appl. Energy 202, 88–111.

Jiménez Navarro, J.P., Cejudo López, J.M., Connolly, D., 2017. The effect of feed-in-tariff supporting schemes on the viability of a district heating and cooling production system. Energy 134, 438–448.

Jradi, M., Riffat, S., 2014. Tri-generation systems: Energy policies, prime movers, cooling technologies, configurations and operation strategies. Renew. Sustain. Energy Rev. 32, 396–415.

Kalogirou, S.A., 2014. Solar Energy Engineering Processes and Systems. Second Edition.

Kaltschmitt, M., Streicher, W., Wiese, A., 2007. Renewable energy: technology, economics and environment. Springer Science & Business Media.

Kemp, I., 2007. Pinch analysis and process integration: A user guide on process integration for the efficient use of energy, 2nd ed. ed. Butterworth-Heinemann/ Elsevier.

Khan, I., Jack, M.W., Stephenson, J., 2018. Analysis of greenhouse gas emissions in electricity systems using time-varying carbon intensity. J. Clean. Prod. 184, 1091–1101.

Khan, K.H., Rasul, M.G., Khan, M.M.K., 2004. Energy conservation in buildings: cogeneration and cogeneration coupled with thermal energy storage. Appl. Energy 77, 15–34.

Knight, I., Ugursal, I., Beausoleil-Morrison, I., 2005. Residential Cogeneration Systems : A Review of The Current Technologies, Annex 42 of the International Energy Agency, Energy Conservation in Buildings and Community Systems Programme.

Konak, A., Coit, D.W., Smith, A.E., 2006. Multi-objective optimization using genetic algorithms: A tutorial. Reliab. Eng. Syst. Saf. 91, 992–1007.

Kopsakangas-Savolainen, M., Mattinen, M.K., Manninen, K., Nissinen, A., 2017. Hourly-based greenhouse gas emissions of electricity – cases demonstrating possibilities for households and companies to decrease their emissions. J. Clean. Prod. 153, 384–396.

Kurup, P., Turchi, C.S., 2015. Parabolic Trough Collector Cost Update for the System Advisor Model (SAM). Tech. Rep. NREL/TP-6A20-65228 Natl. Renew. Energy Lab. 1–40.

Lai, S.M., Hui, C.W., 2009. Feasibility and flexibility for a trigeneration system. Energy 34, 1693–1704.

Lai, S.M., Hui, C.W., 2010. Integration of trigeneration system and thermal storage under demand uncertainties. Appl. Energy 87, 2868–2880.

Lazard, 2016. Lazard's Levelized Cost of Energy Analysis - 10.

Lazzaretto, A., Tsatsaronis, G., 2006. SPECO: A systematic and general methodology for calculating efficiencies and costs in thermal systems. Energy 31, 1257–1289.

Lewis, M., 2004. Integrated design for sustainable buildings. Building for the future. A Suppl. to ASHRAE Journals 46, 2–3.

Li, G., Zheng, X., 2016. Thermal energy storage system integration forms for a sustainable future. Renew. Sustain. Energy Rev. 62, 736–757.

Li, H., Sun, Q., Zhang, Q., Wallin, F., 2015. A review of the pricing mechanisms for district heating systems. Renew. Sustain. Energy Rev. 42, 56–65.

Li, L., Mu, H., Gao, W., Li, M., 2014. Optimization and analysis of CCHP system based on energy loads coupling of residential and office buildings. Appl. Energy 136, 206–216.

Liew, P.Y., Theo, W.L., Wan Alwi, S.R., Lim, J.S., Abdul Manan, Z., Klemeš, J.J., Varbanov, P.S., 2017. Total Site Heat Integration planning and design for industrial, urban and renewable systems. Renew. Sustain. Energy Rev. 68, 964–985.

Linnhoff, B., Townsend, D.W., Boland, D., Hewitt, D.F., Thomas, B.E.A., Guy, A.R., Al., E., 1982. User guide on process integration for the efficient use of energy. Institution of Chemical Engineers. Rugby, UK: IchemE.

Liu, B.Y.H., Jordan, R.C., 1963. The long-term average performance of flat-plate solar-energy collectors. Sol. Energy 7, 53–74.

Liu, B.Y.H., Jordan, R.C., 1960. The interrelationship and characteristic distribution of direct, diffuse and total solar radiation. Sol. Energy 4, 1–19.

Liu, M., Shi, Y., Fang, F., 2014. Combined cooling, heating and power systems: A survey. Renew. Sustain. Energy Rev. 35, 1–22.

Liu, P., Georgiadis, M.C., Pistikopoulos, E.N., 2013. An energy systems engineering approach for the design and operation of microgrids in residential applications. Chem. Eng. Res. Des. 91, 2054–2069.

Liu, P., Gerogiorgis, D.I., Pistikopoulos, E.N., 2007. Modeling and optimization of polygeneration energy systems. Catal. Today 127, 347–359.

Liu, W., Chen, G., Yan, B., Zhou, Z., Du, H., Zuo, J., 2015. Hourly operation strategy of a CCHP system with GSHP and thermal energy storage (TES) under variable loads: A case study. Energy Build. 93, 143–153.

Lozano, M.A., 2001. Diseño óptimo de sistemas simples de cogeneración. Inf. Tecnol. 12, 53–58.

Lozano, M.A., Bartolomé, J.L., Valero, A., Reini, M., 1994. Thermoeconomic diagnosis of energy systems. Flowers 94, 149–156.

Lozano, M.A., Carvalho, M., Ramos, J.C., Serra, L.M., 2009a. Thermoeconomic analysis of simple trigeneration systems. Int. J. Thermodyn. 12, 147–153.

Lozano, M.A., Carvalho, M., Serra, L.M., 2009b. Operational strategy and marginal costs in simple trigeneration systems. Energy 34, 2001–2008.

Lozano, M.A., Carvalho, M., Serra, L.M., 2011. Allocation of economic costs in trigeneration systems at variable load conditions. Energy Build. 43, 2869–2881.

Lozano, M.A., Carvalho, M., Serra, L.M., 2014. Tackling environmental impacts in simple trigeneration systems operating under variable conditions. Int. J. Life Cycle Assess. 19, 1087–1098.

Lozano, M.A., Pina, E.A., Serra, L.M., 2019. Thermal integration in polygeneration energy systems for buildings, in: XI National and II International Engineering Thermodynamics Congress (11-CNIT). Albacete, Spain.

Lozano, M.A., Ramos, J., 2010. Thermodynamic and Economic Analysis for Simple Cogeneration Systems. Cogener. Distrib. Gener. J. 25, 63–80.

Lozano, M.A., Ramos, J.C., Carvalho, M., Serra, L.M., 2009c. Structure optimization of energy supply systems in tertiary sector buildings. Energy Build. 41, 1063–1075.

Lozano, M.A., Ramos, J.C., Serra, L.M., 2010. Cost optimization of the design of CHCP (combined heat, cooling and power) systems under legal constraints. Energy 35, 794–805.

Lozano, M.A., Valero, A., 1993. Theory of the exergetic cost. Energy 18, 939–960.

Lozano, M.A., Valero, A., Serra, L., 1996. Local optimization of energy systems. Am. Soc. Mech. Eng. Adv. Energy Syst. Div. AES 36, 241–250.

Mancarella, P., 2014. MES (multi-energy systems): An overview of concepts and evaluation models. Energy 65, 1–17.

Manfren, M., Caputo, P., Costa, G., 2011. Paradigm shift in urban energy systems through distributed generation: Methods and models. Appl. Energy 88, 1032–1048.

Maréchal, F., 1995. Mèthode d'analyse et de synthèse énergétiques des procédés industriels. Faculté des Sciences Appliquées, Collection des publications n. 124, Université de Liège.

Maroufmashat, A., Elkamel, A., Fowler, M., Sattari, S., Roshandel, R., Hajimiragha, A., Walker, S., Entchev, E., 2015. Modeling and optimization of a network of energy hubs to improve economic and emission considerations. Energy 93, 2546–2558.

Martinez-Sanchez, V., Hulgaard, T., Hindsgaul, C., Riber, C., Kamuk, B., Astrup, T.F., 2016. Estimation of marginal costs at existing waste treatment facilities. Waste Manag. 50, 364–375.

MCTIC, 2018. Fatores de emissão da margem de operação pelo método da análise de despacho [WWW Document]. [In Port. URL http://www.mctic.gov.br/mctic/opencms/ciencia/SEPED/clima/textogeral/emissao_despacho.html (accessed 7.2.18).

Mendes, G., Ioakimidis, C., Ferrão, P., 2011. On the planning and analysis of Integrated Community Energy Systems: A review and survey of available tools. Renew. Sustain. Energy Rev. 15, 4836–4854.

Messagie, M., Mertens, J., Oliveira, L., Rangaraju, S., Sanfelix, J., Coosemans, T., Van Mierlo, J., Macharis, C., 2014. The hourly life cycle carbon footprint of electricity generation in Belgium, bringing a temporal resolution in life cycle assessment. Appl. Energy 134, 469–476.

METEOTEST, 2018. METEONORM [WWW Document]. URL http://www.meteonorm.com/

Midwest CHP Application Center, 2007. Combined Heat & Power (CHP) Resource Guide for Hospital Applications.

Modi, A., Bühler, F., Andreasen, J.G., Haglind, F., 2017. A review of solar energy based heat and power generation systems. Renew. Sustain. Energy Rev. 67, 1047–1064.

Murugan, S., Horák, B., 2016. A review of micro combined heat and power systems for residential applications. Renew. Sustain. Energy Rev. 64, 144–162.

Ng, K.S., Martinez Hernandez, E., 2016. A systematic framework for energetic, environmental and economic (3E) assessment and design of polygeneration systems. Chem. Eng. Res. Des. 106, 1–25.

Nielsen, J.E., 2014. A booming market for solar district heating, in: SHC 2014, International Conference on Solar Heating and Cooling for Buildings and Industry, Beijing, China.

NREL, 2018. System Advisor Model (SAM) [WWW Document]. URL https://sam.nrel.gov/

Olsthoorn, D., Haghighat, F., Mirzaei, P.A., 2016. Integration of storage and renewable energy into district heating systems: A review of modelling and optimization. Sol. Energy 136, 49–64.

Ortiga, J., Bruno, J.C., Coronas, A., 2011. Selection of typical days for the characterisation of energy demand in cogeneration and trigeneration optimisation models for buildings. Energy Convers. Manag. 52, 1934–1942.

Papoulias, S.A., Grossmann, I.E., 1983. A structural optimization approach in process synthesis—II: Heat recovery networks. Comput. Chem. Eng. 7, 707–721.

Pehnt, M., Cames, M., Fischer, C., Praetorius, B., Schneider, L., Schumacher, K., Voß, J.P., 2006. Micro cogeneration: towards decentralized energy systems. Springer Science & Business Media.

Peuser, F.A., Remmers, K.-H., Schnauss, M., 2005. Sistemas solares térmicos: diseño e instalación. Solarpraxis.

Pfenninger, S., Hawkes, A., Keirstead, J., 2014. Energy systems modeling for twenty-first century energy challenges. Renew. Sustain. Energy Rev. 33, 74–86.

Piacentino, A., Cardona, F., 2007. On thermoeconomics of energy systems at variable load conditions: Integrated optimization of plant design and operation. Energy Convers. Manag. 48, 2341–2355.

Picón-Núñez, M., Medina-Flores, J.M., 2013. Process Integration Techniques for Cogeneration and Trigeneration Systems, in: Handbook of Process Integration (PI). Elsevier, pp. 484–504.

Pina, E.A., Lozano, M.A., Serra, L.M., 2017. Optimal operation and marginal costs in simple trigeneration systems including thermal energy storage. Energy 135, 788–798.

Pina, E.A., Lozano, M.A., Serra, L.M., 2018a. Allocation of economic costs in trigeneration systems at variable load conditions including renewable energy sources and thermal energy storage. Energy 151, 633–646.

Pina, E.A., Lozano, M.A., Serra, L.M., 2018b. Thermoeconomic cost allocation in simple trigeneration systems including thermal energy storage. Energy 153, 170-184.

Pina, E.A., Lozano, M.A., Serra, L.M., 2018c. Optimal design of polygeneration systems supported with renewable energy sources and energy storage for a Brazilian hospital, in: Proceedings of ECOS 2018. Guimaraes, Portugal.

Pina, E.A., Lozano, M.A., Serra, L.M., 2018d. Opportunities for the Integration of Solar Thermal Heat, Photovoltaics and Biomass in a Brazilian Hospital, in: Proceedings of the EuroSun 2018, September 10-13, 2018, Rapperswil, Switzerland. Rapperswil, Switzerland.

Pina, E.A., Lozano, M.A., Serra, L.M., 2019. Technical, economic and environmental feasibility of renewable-based energy systems in a Brazilian university hospital, in: Proceedings of the XI National and II International Engineering Thermodynamics Congress. Albacete, Spain.

Pintarič, Z.N., Kravanja, Z., 2006. Selection of the Economic Objective Function for the Optimization of Process Flow Sheets. Ind. Eng. Chem. Res. 45, 4222–4232.

Pintarič, Z.N., Kravanja, Z., 2015. The importance of proper economic criteria and process modeling for single- and multi-objective optimizations. Comput. Chem. Eng. 83, 35–47.

Poncelet, K., Member, S., Hanspeter, H., Member, S., Delarue, E., Virag, A., William, D., 2017. Selecting Representative Days for Capturing the Implications of Integrating Intermittent Renewables in Generation Expansion Planning Problems 32, 1936–1948.

Quelhas, A.M., Gil, E., McCalley, J.D., 2006. Nodal prices in an integrated energy system. Int. J. Crit. Infrastructures 2, 50–69.

Raluy, R.G., Serra, L.M., Guadalfajara, M., Lozano, M.A., 2014. Life cycle assessment of central solar heating plants with seasonal storage. Energy Procedia 48, 966–976.

Ramos, J.C., 2012. Optimización del diseño y operación de sistemas de cogeneración para el sector residencial comercial. PhD Thesis - University of Zaragoza, Department of Mechanical Engineering.

REE, 2018. Real-time demand and generation [WWW Document]. Red Eléctrica España - Spanish Penins. Electr. demand Track. real time. URL http://www.ree.es/en/activities/realtime-demand-and-generation (accessed 5.25.18).

Reini, M., Taccani, R., 2004. On the Thermoeconomic Approach to the Diagnosis of Energy System Malfunctions: The Role of the Fuel Impact Formula. Int.J. Thermodyn. 7, 61–72.

Rivarolo, M., Greco, A., Massardo, A.F., 2013. Thermo-economic optimization of the impact of renewable generators on poly-generation smart-grids including hot thermal storage. Energy Convers. Manag. 65, 75–83.

Rong, A., Lahdelma, R., 2016. Role of polygeneration in sustainable energy system development challenges and opportunities from optimization viewpoints. Renew. Sustain. Energy Rev. 53, 363–372.

Rong, A., Su, Y., 2017. Polygeneration systems in buildings: A survey on optimization approaches. Energy Build. 151, 439–454.

Rossiter, A.P., Ranade, S.M., 1988. Marginal costs set the scene for profitable operation and investment in pinch retrofits, in: Understanding Process Integration II - IChemE Symposium Series No. 109. pp. 283–301.

Rovira, A., Sánchez, C., Muñoz, M., Valdés, M., Durán, M.D., 2011. Thermoeconomic optimisation of heat recovery steam generators of combined cycle gas turbine power plants considering off-design operation. Energy Convers. Manag. 52, 1840–1849.

Rubio-Maya, C., Uche-Marcuello, J., Martínez-Gracia, A., Bayod-Rújula, A.A., 2011. Design optimization of a polygeneration plant fuelled by natural gas and renewable energy sources. Appl. Energy 88, 449–457.

Rupp, R.F., Lamberts, R., 2017. Relatório: Fatores de conversão de energia elétrica e térmica em energia primária e em emissões de dióxido de carbono a serem usados na etiquetagem de nível de eficiência energética de edificações.

Safaei, A., Freire, F., Antunes, C.H., 2013. A model for optimal energy planning of a commercial building integrating solar and cogeneration systems. Energy 61, 211–223.

Sanaye, S., Sarrafi, A., 2015. Optimization of combined cooling, heating and power generation by a solar system. Renew. Energy 80, 699–712.

Santo, D.B.D.E., 2012. Energy and exergy efficiency of a building internal combustion engine trigeneration system under two different operational strategies. Energy Build. 53, 28–38.

Santo, D.B.D.E., 2014. An energy and exergy analysis of a high-efficiency engine trigeneration system for a hospital: A case study methodology based on annual energy demand profiles. Energy Build. 76, 185–198.

Savic, D., 2002. Single-objective vs . Multiobjective Optimisation for Inte- grated Decision Support. Integr. Assess. Decis. Support 1, 7–12.

Schrage, L., 1999. Optimization modeling with LINGO. Lindo Syst. Lindo Systems.

Serra, L.M., Lozano, M.A., Ramos, J., Ensinas, A. V., Nebra, S.A., 2009. Polygeneration and efficient use of natural resources. Energy 34, 575–586.

Sigarchian, S.G., Malmquist, A., Martin, V., 2018. Design optimization of a complex polygeneration system for a hospital. Energies 11, 1071, 2–24.

Sjödin, J., Henning, D., 2004. Calculating the marginal costs of a district-heating utility. Appl. Energy 78, 1–18.

Sonar, D., Soni, S.L., Sharma, D., 2014. Micro-trigeneration for energy sustainability: Technologies, tools and trends. Appl. Therm. Eng. 71, 790–796.

Spanish Industry Office, 2007. Order ITC/2794/2007, September 27th, 2007. Spain's Off. J. BOE No. 23, 39690–39698.

Szklo, A.S., Borghetti Soares, J., Tiomno Tolmasquim, M., 2004. Energy consumption indicators and CHP technical potential in the Brazilian hospital sector. Energy Convers. Manag. 45, 2075–2091.

Tereshchenko, T., Nord, N., 2015. Uncertainty of the allocation factors of heat and electricity production of combined cycle power plant. Appl. Therm. Eng. 76, 410–422.

The Economist, 2018. Extracting carbon dioxide from the air is possible. But at what cost? [WWW Document]. URL https://www.economist.com/science-and-technology/2018/06/07/extracting-carbon-dioxide-from-the-air-is-possible.-but-at-what-cost?fsrc=scn/tw/te/bl/ed/extractingcarbon dioxidefromtheairispossiblebutatwhatcostclimatechange (accessed 20.06.2019).

Thomas, A.L., 1969. The allocation problem in financial accounting theory, Studies in accounting research. American Accounting Association.

TRNSYS, 2019. A Transient System Simulation tool [WWW Document]. Sol. Energy Lab. Univ. Wisconsin-Madison. URL http://sel.me.wisc.edu/trnsys/ (accessed 2.21.19).

Tsatsaronis, G., Winhold, M., 1985. Exergoeconomic Analysis and Evaluation of Energy-Conversion Plants. Energy 10, 69–80.

Ubando, A.T., Culaba, A.B., Aviso, K.B., Tan, R.R., 2013. Simultaneous carbon footprint allocation and design of trigeneration plants using fuzzy fractional programming. Clean Technol. Environ. Policy 15, 823–832.

UN, 2017. World population projected to reach 9.8 billion in 2050, and 11.2 billion in 2100 [WWW Document]. United Nations - World Popul. Prospect. 2017. URL https://www.un.org/development/desa/en/news/population/world-population-prospects-2017.html (accessed 3.16.18).

Ünal, A.N., Ercan, S., Kayakutlu, G., 2015. Optimisation studies on tri-generation: a review. Int. J. Energy Res. 39, 1311–1334.

UN-FCCC, 2006. Tool to calculate the emission factor for an electricity system TOOL07.

Varbanov, P., Perry, S., Makwana, Y., Zhu, X.X., Smith, R., 2004. Top-level Analysis of Site Utility Systems. Chem. Eng. Res. Des. 82, 784–795.

Varbanov, P.S., Klemeš, J.J., 2011. Integration and management of renewables into Total Sites with variable supply and demand. Comput. Chem. Eng. 35, 1815–1826.

Verda, V., Borchiellini, R., 2007. Exergy method for the diagnosis of energy systems using measured data. Energy 32, 490–498.

Viti, A., 1996. DTIE 1.01, preparación de agua caliente para usos sanitarios. ATECYR, Madrid.

Voll, P., Jennings, M., Hennen, M., Shah, N., Bardow, A., 2015. The optimum is not enough: A near-optimal solution paradigm for energy systems synthesis. Energy 82, 446–456.

Voorspools, K.R., D'Haeseleer, W.D., 2002. The evaluation of small cogeneration for residential heating. Int. J. Energy Res. 26, 1175–1190.

Voorspools, K.R., D'haeseleer, W.D., 2003. The impact of the implementation of cogeneration in a given energetic context. IEEE Trans. Energy Convers. 18, 135–141.

Wagner, M.J., Gilman, P., 2011. Technical manual for the SAM physical trough model, NREL Technical report.

Wakui, T., Kawayoshi, H., Yokoyama, R., 2016. Optimal structural design of residential power and heat supply devices in consideration of operational and capital recovery constraints. Appl. Energy 163, 118–133.

Wang, J., Mao, T., 2015. Cost allocation and sensitivity analysis of multi-products from biomass gasification combined cooling heating and power system based on the exergoeconomic methodology. Energy Convers. Manag. 105, 230–239.

Wang, J., Yang, Y., Mao, T., Sui, J., Jin, H., 2015. Life cycle assessment (LCA) optimization of solar-assisted hybrid CCHP system. Appl. Energy 146, 38–52.

Wang, J.J., Jing, Y.Y., Zhang, C.F., Zhao, J.H., 2009. Review on multi-criteria decision analysis aid in sustainable energy decision-making. Renew. Sustain. Energy Rev. 13, 2263–2278.

Wang, Y., Lior, N., 2007. Fuel allocation in a combined steam-injected gas turbine and thermal seawater desalination system. Desalination 214, 306–326.

WEC, 2016. World Energy Resources: Solar 2016, World Energy Council. doi:https://www.worldenergy.org/wp-content/uploads/2013/10/WER_2013_8_Solar_revised.pdf

WEC, 2016. World Energy Trilemma 2016 Defining Measures To Accelarate the Energy Transition. World Energy Counc. Rep. 1–113.

Wu, D.W., Wang, R.Z., 2006. Combined cooling, heating and power: A review. Prog. Energy Combust. Sci. 32, 459–495.

Yokoyama, R., Ito, K., Kamimura, K., Miyasaka, F., 1994. Development of a General-Purpose Optimal Operational Planning System for Energy Supply Plants. J. Energy Resour. Technol. 116, 290.

Yokoyama, R., Shinano, Y., Taniguchi, S., Ohkura, M., Wakui, T., 2015. Optimization of energy supply systems by MILP branch and bound method in consideration of hierarchical relationship between design and operation. Energy Convers. Manag. 92, 92–104.

APPENDIX A

Case study in Spain – Data elaboration

A. CASE STUDY IN SPAIN – DATA ELABORATION

This appendix describes the case study in Spain and the elaboration of the input data for the multi-objective optimization model developed in Chapter 4. First, the consumer center's geographic and building characteristics are described in Section A.1. Then, the local climatic data are assessed in Section A.2, including the hourly ambient temperature, the hourly wet-bulb temperature, and the hourly solar radiation. The energy demands for the representative days of the months of the year are estimated in Section A.3 from annual reference values and monthly and hourly distribution profiles. Finally, a technical description of the technologies included in the superstructure of the trigeneration system is provided in Section A.4.

A.1 CONSUMER CENTER DESCRIPTION

The case study consists of a multi-family residential building complex located in the city of Zaragoza (latitude 41.6°), Spain. The complex is composed of 100 dwellings, each one with 100 m² of surface area. It was assumed that the dwellings are distributed between five identical buildings consisting of: (i) five floors per building; (ii) four dwellings per floor; and (iii) a square-shaped rooftop with 20-meter length and width. Thus, the complex's available rooftop area for the installation of photovoltaic panels and solar thermal collectors was estimated to be 2000 m².

Table A.1 collects the main geographic and structural parameters of the consumer center used throughout this Appendix.

Table A.1: Parameters of the case study in Zaragoza, Spain.

Type	Parameter	Nomenclature	Value
Geographic location	Latitude	ϕ	41.6°
	Ground reflectance (albedo)	ρ_g	0.2
Building characteristics	Number of dwellings	N	100 dwellings
	Surface area of each dwelling	S	100 m²/dwelling
	Square rooftop length and width	L	20 m
	Available rooftop surface area	AA	2000 m²

The analysis carried out in Chapter 4 covered the period of one year. It was considered that the energy demands and the operation of the system are described by 12 representative days, each one composed of 24 consecutive periods of 1-hour duration. Each representative day was attributed to a month of the year and no distinction was made between working days and weekends/holidays; in this way, the number of representative days type d per year $NRY(d)$ is equal to the number of days in the corresponding month, as shown in Table A.2. Additionally, Table A.2 provides the recommended average day of the month $\bar{n}(d)$ for latitudes between ±66.5° obtained from Duffie et al. (2013), used in Section A.2.2 to estimate the hourly solar radiation.

Table A.2: Representative days of the months of the year.

Month	Representative day d	Recommended average day of the month $\bar{n}(d)$	Number of representative days type d per year $NRY(d)$
January	1	17	31
February	2	47	28
March	3	75	31
April	4	105	30
May	5	135	31
June	6	162	30
July	7	198	31
August	8	228	31
September	9	258	30
October	10	288	31
November	11	318	30
December	12	344	31

A.2 CLIMATIC DATA

Local climatic data are necessary for the determination of the consumer center's energy demands, and the technologies' adjustment factors and production rates. Therefore, for the geographic location of Zaragoza, Spain, the following climatic data must be obtained: (i) hourly ambient temperature Ta and hourly wet-bulb temperature Twb, as described in Section A.2.1; and (ii) hourly solar radiation on a tilted surface Q_r, as described in Section A.2.2.

Following the methodology described by Guadalfajara et al. (2015) and Guadalfajara (2016), the estimation of the hourly Ta, Twb and Q_r is done with monthly average values, which have been obtained from multiple sources and are shown in Table A.3: (i) average of daily medium Ta_{ave}, minimum Ta_{min}, and maximum Ta_{max} ambient temperatures, obtained from AEMET (2010); (ii) cold water temperature of the supply network T_{CW}, obtained from UNE 94.002 (AENOR, 2005); (iii) dew point temperature Tdp, obtained from EnergyPlus (2018); and (iv) average daily global radiation on a horizontal surface $\bar{H}$, obtained from UNE 94.003 (AENOR, 2007).

Table A.3: Monthly climatic data for Zaragoza, Spain.

Month	Ta_{ave}, °C	Ta_{min}, °C	Ta_{max}, °C	T_{CW}, °C	Tdp, °C	$\bar{H}$, MJ/(m²·day)
January	6.4	2.4	10.3	8.0	1.6	6.4
February	8.4	3.5	13.3	9.0	1.8	9.8
March	10.9	5.2	16.6	10.0	2.7	13.8
April	13.0	7.4	18.7	12.0	4.2	17.4
May	17.2	11.2	23.2	15.0	6.7	21.5
June	21.3	14.3	27.7	17.0	9.5	23.8
July	24.5	17.5	31.5	20.0	11.8	25.3
August	24.4	17.8	31.0	19.0	13.1	22.5
September	20.7	14.7	26.7	17.0	12.0	16.5
October	15.5	10.3	20.7	14.0	9.3	11.6
November	10.0	5.8	14.3	10.0	5.7	7.5
December	7.1	3.5	10.7	8.0	2.4	5.7

A.2.1 Hourly ambient and wet-bulb temperatures

For each hourly period h of each representative day d, the hourly ambient temperature $Ta(d,h)$ is estimated from monthly average temperatures through the Erbs's correlation (Erbs et al., 1983), according to Eq. (A.1).

$$Ta(d,h) = Ta_{ave}(d) + A(d) \cdot \left(\sum_{k=1}^{4} a_k \cdot \cos(k \cdot \tau(h) - b_k) \right) \tag{A.1}$$

where $Ta_{ave}(d)$ is given in Table A.3, $A(d)$ is the amplitude of the diurnal variation, as expressed by Eq. (A.2), and $\tau(h)$ is the angular hour of the day, in rad, given by Eq. (A.3). The adjustment coefficients a_k and b_k, presented in Table A.4, were determined by Cannistraro (1995) based on the data from 29 European cities.

$$A(d) = Ta_{max}(d) - Ta_{min}(d) \tag{A.2}$$
$$\tau(h) = \frac{2\pi \cdot (\theta(h) - 1)}{24} \tag{A.3}$$

The values of $Ta_{min}(d)$ and $Ta_{max}(d)$ in Eq. (A.2) are shown in Table A.3. In Eq. (A.3), $\theta(h)$ is the solar hour, with 1 corresponding to 1 a.m. and 24 corresponding to midnight.

Table A.4: Adjustment coefficients for European cities (Cannistraro, 1995).

	1	2	3	4
a_k	0.3454	0.0732	0.0079	0.0057
b_k	3.7270	0.4320	1.3370	3.4530

The hourly ambient temperature $Ta(d,h)$ for the representative days of the months of the year obtained for Zaragoza, Spain, are given in Table A.5.

Table A.5: Hourly ambient temperature *Ta(d,h)*, °C.

Hour	Jan	Feb	Mar	Apr	May	Jun	Jul	Aug	Sep	Oct	Nov	Dec
1	5.3	6.8	10.4	12.8	16.5	20.9	24.1	24.0	20.2	15.1	9.6	5.6
2	5.1	6.6	10.2	12.6	16.3	20.7	24.0	23.8	20.0	15.0	9.4	5.3
3	5.0	6.5	10.1	12.5	16.1	20.5	23.8	23.7	19.9	14.8	9.3	5.2
4	4.8	6.3	10.0	12.4	15.9	20.3	23.7	23.6	19.8	14.7	9.2	5.0
5	4.7	6.2	9.8	12.3	15.8	20.1	23.6	23.5	19.7	14.6	9.1	4.9
6	4.6	6.1	9.8	12.2	15.7	20.1	23.6	23.4	19.6	14.6	9.1	4.8
7	4.8	6.3	9.9	12.3	15.8	20.2	23.7	23.5	19.7	14.7	9.2	5.0
8	5.1	6.6	10.3	12.6	16.3	20.7	24.0	23.8	20.0	15.0	9.4	5.4
9	5.7	7.3	10.8	13.1	17.0	21.5	24.5	24.3	20.5	15.5	9.9	6.0
10	6.5	8.1	11.5	13.7	17.9	22.5	25.2	24.9	21.1	16.1	10.5	6.9
11	7.3	8.9	12.2	14.4	18.8	23.5	25.9	25.6	21.8	16.8	11.2	7.8
12	8.0	9.7	12.9	14.9	19.7	24.4	26.5	26.1	22.3	17.4	11.7	8.6
13	8.5	10.3	13.4	15.4	20.3	25.1	27.0	26.6	22.8	17.8	12.1	9.2
14	8.9	10.7	13.7	15.7	20.7	25.6	27.3	26.9	23.1	18.1	12.4	9.6
15	9.1	10.8	13.9	15.8	20.9	25.8	27.5	27.0	23.2	18.3	12.6	9.7
16	9.0	10.8	13.8	15.7	20.8	25.7	27.4	26.9	23.1	18.2	12.5	9.7
17	8.7	10.5	13.6	15.5	20.5	25.4	27.2	26.7	22.9	18.0	12.3	9.4
18	8.3	10.0	13.1	15.1	20.0	24.8	26.8	26.3	22.5	17.6	11.9	8.8
19	7.7	9.4	12.6	14.7	19.3	24.0	26.3	25.9	22.1	17.1	11.5	8.2
20	7.1	8.7	12.1	14.2	18.6	23.3	25.7	25.4	21.6	16.6	11.0	7.6
21	6.6	8.2	11.6	13.8	18.0	22.6	25.3	25.0	21.2	16.2	10.6	7.0
22	6.2	7.7	11.2	13.4	17.5	22.0	24.9	24.6	20.8	15.8	10.2	6.5
23	5.8	7.4	10.9	13.2	17.1	21.6	24.6	24.4	20.6	15.5	10.0	6.1
24	5.5	7.1	10.6	12.9	16.7	21.2	24.4	24.1	20.3	15.3	9.8	5.8

The wet-bulb temperature *Twb(d,h)* in each hourly period *h* of each representative day *d* was obtained from the Engineering Equation Solver (EES, 2017) using the *wetbulb* function. The following considerations were made: (i) the atmospheric air pressure *patm* is considered constant and equal to 1.013 bar; (ii) the monthly dew point temperature *Tdp(d)* is given in Table A.3 and considered constant throughout the day; and (iii) the dry ambient air temperature corresponds to *Ta(d,h)*, given in Table A.5. The *Twb(d,h)* obtained are given in Table A.6.

A.2.2 Hourly solar radiation on a tilted surface

The methodology described herein is based on ASHRAE (2015, 2013), Kalogirou (2014) and Duffie et al. (2013). First, Section A.2.2.1 explains the sun-earth geometry and the several angles that can be defined to position the sun relative to a plane on the surface of the earth. Then, Section A.2.2.2 describes the methodology for assessing the extraterrestrial solar radiation on a horizontal surface, which is the base for the assessment of the terrestrial solar radiation described in Section A.2.2.3. Finally, Section A.2.2.4 describes the Isotropic Sky Model, by Liu and Jordan (1963), used to calculate the radiation on tilted surfaces on the earth.

Table A.6: Hourly wet-bulb temperature *Twb(d,h)*, °C.

Hour	Jan	Feb	Mar	Apr	May	Jun	Jul	Aug	Sep	Oct	Nov	Dec
1	3.6	4.5	6.7	8.4	11.2	14.2	16.5	17.1	15.2	11.8	7.6	4.1
2	3.5	4.4	6.6	8.4	11.1	14.1	16.5	17.1	15.1	11.7	7.5	4.0
3	3.5	4.3	6.6	8.3	11.0	14.0	16.4	17.0	15.1	11.7	7.5	3.9
4	3.4	4.3	6.5	8.2	10.9	14.0	16.4	17.0	15.0	11.6	7.4	3.8
5	3.3	4.2	6.4	8.2	10.8	13.9	16.3	16.9	15.0	11.6	7.4	3.8
6	3.3	4.2	6.4	8.2	10.8	13.9	16.3	16.9	15.0	11.6	7.3	3.7
7	3.4	4.2	6.5	8.2	10.9	13.9	16.3	17.0	15.0	11.6	7.4	3.8
8	3.6	4.4	6.6	8.4	11.1	14.1	16.5	17.1	15.1	11.8	7.5	4.0
9	3.9	4.8	6.9	8.6	11.4	14.4	16.7	17.2	15.3	12.0	7.8	4.4
10	4.3	5.2	7.2	8.9	11.7	14.8	16.9	17.4	15.5	12.2	8.0	4.8
11	4.7	5.6	7.6	9.2	12.1	15.2	17.1	17.7	15.8	12.5	8.3	5.3
12	5.1	6.0	7.9	9.4	12.5	15.5	17.3	17.8	16.0	12.7	8.6	5.7
13	5.3	6.3	8.1	9.6	12.7	15.8	17.5	18.0	16.1	12.9	8.8	6.0
14	5.5	6.5	8.3	9.8	12.9	16.0	17.6	18.1	16.2	13.0	8.9	6.2
15	5.6	6.6	8.4	9.8	13.0	16.0	17.7	18.1	16.3	13.1	9.0	6.3
16	5.6	6.5	8.3	9.8	12.9	16.0	17.6	18.1	16.3	13.1	9.0	6.2
17	5.4	6.4	8.2	9.7	12.8	15.9	17.6	18.0	16.2	13.0	8.9	6.1
18	5.2	6.1	8.0	9.5	12.6	15.7	17.4	17.9	16.0	12.8	8.7	5.8
19	4.9	5.8	7.8	9.3	12.3	15.4	17.2	17.8	15.9	12.6	8.5	5.5
20	4.6	5.5	7.5	9.1	12.0	15.1	17.1	17.6	15.7	12.4	8.3	5.2
21	4.3	5.2	7.3	8.9	11.8	14.8	16.9	17.5	15.6	12.3	8.1	4.9
22	4.1	5.0	7.1	8.7	11.6	14.6	16.8	17.3	15.4	12.1	7.9	4.6
23	3.9	4.8	6.9	8.6	11.4	14.5	16.7	17.2	15.3	12.0	7.8	4.4
24	3.8	4.7	6.8	8.5	11.3	14.3	16.6	17.2	15.2	11.9	7.7	4.3

A.2.2.1 Sun-earth geometry

The earth revolves around the sun in an elliptical orbit, in which the sun occupies one of its focuses. It takes the earth 365.25 days to complete a revolution and 24 hours to make one rotation around its axis, which is tilted at an angle of 23.45° to the plane of the elliptic, as can be seen in Figure A.1. In this way, the angle between the earth's equator and the plane that connects the centers of the sun and the earth is constantly changing.
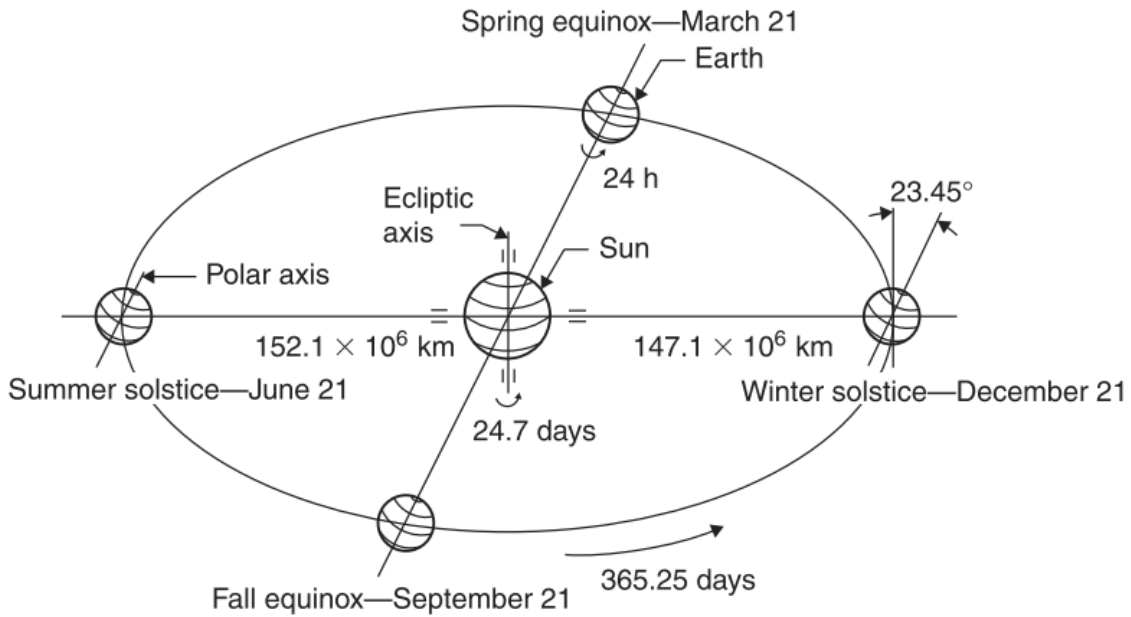
Figure A.1: Movement of the earth around the sun (Kalogirou, 2014).

Every day, the arc traced by the sun as it moves across the sky reaches its highest point at midday. From winter to summer, the days grow longer as the sun's path gets higher in the sky. As depicted in Figure A.2 in the Northern Hemisphere, on June 21, the sun is at is most northerly position and daytime is at a maximum; this day is called summer solstice. By contrast, on December 21 the sun is at its most southerly position and daytime is at a minimum; this day is called winter solstice. Around March 21 and September 21, daytime and nighttime have equal lengths; these days are known as spring and fall equinoxes, respectively. In the Southern Hemisphere, summer and winter solstices are the opposite: the former takes place on December 21 and the latter on June 21.

According to Kalogirou (2014), the earth receives only a tiny fraction of the total energy emitted by the sun, equal to $1.7 \cdot 10^{14}$ kW; it is estimated that 84 minutes of this energy is equal to the world energy demand for one year (about 900 EJ). In order to estimate the solar radiation that reaches the surface of the earth at a given moment and location, it is essential to know the path of the sun across the sky.
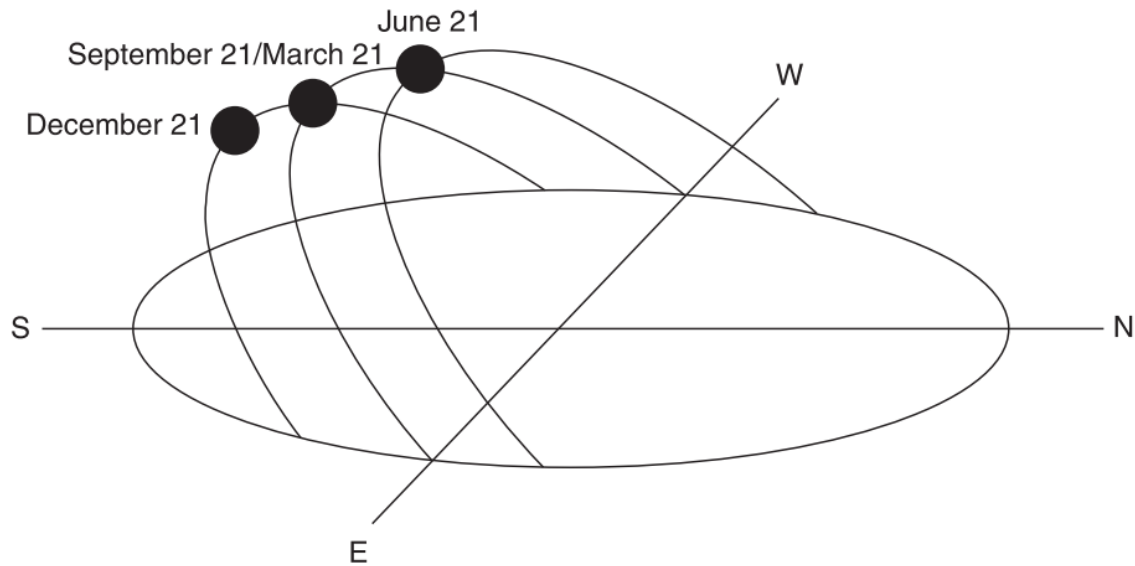
Figure A.2: Annual changes in the sun's position in the sky (Northern Hemisphere) (Kalogirou, 2014).

At any time, the position of the sun relative to a plane of any orientation in relation to the earth can be described in terms of several angles, as explained below, some of which are indicated in Figure A.3.

Latitude ϕ: The angular location north or south of the equator, -90° ≤ ϕ ≤ 90° (north positive).

Tilt β: The angle between the plane of the surface in question and the horizontal, 0° ≤ β ≤ 180° (β > 90° means that the surface is facing downward). The optimum tilt for the maximum annual insolation of a fixed collector is generally equal to the latitude of the location, with angle variations of about 10 to 15°, depending on the application (Kalogirou, 2014).

Declination δ: The earth axis of rotation is tilted 23.45° to the plane of the earth's orbital plane and the sun's equator. Declinations north of the equator (summer in the Northern Hemisphere) are considered positive, whereas those south are negative. The declination angle ranges from +23.45° at the summer solstice to -23.45° at the winter solstice; at spring and fall equinoxes, δ = 0° (Kalogirou, 2014).

The declination angle varies with the day of the year n as the earth rotates around the sun according to Eq. (A.4):

$$\delta(n) = 23.45° \cdot \sin\left(360 \cdot \frac{284 + n}{365}\right) \tag{A.4}$$
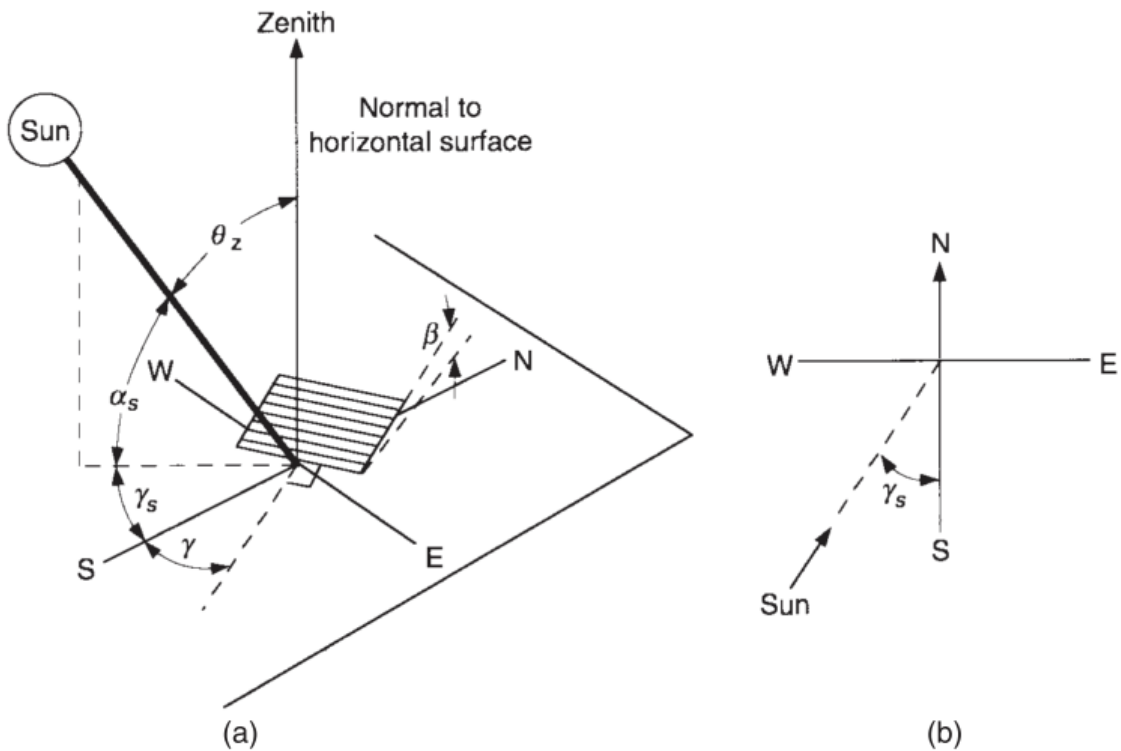
Figure A.3: (a) Zenith angle θ_z, surface tilt angle β, surface azimuth angle γ, and solar altitude angle α_s; and (b) plan view showing solar azimuth angle γ_s. (Duffie et al., 2013).

Hour angle ω: The angular displacement of the sun east or west of the local meridian due to the rotation of the earth on its axis takes place at 15° per hour h. By convention, the hour angle is 0° at the solar noon ($t = 12$), negative in the morning and positive in the afternoon (Kalogirou, 2014).

$$\omega(t) = (t - 12) \cdot 15 \tag{A.5}$$

Solar altitude angle α_s: The angle between the sun's rays and the horizontal plane on the earth. This angle is the complement of the *zenith angle θ_z*, which is the angle between the sun's rays and the vertical.

Solar azimuth angle γ_s: The angular deviation from the local meridian of the projection on the horizontal plane of the earth-sun line. By convention, west variations are considered positive and east variations are negative (Kalogirou, 2014). At solar noon, the sun is exactly on the meridian ($\omega = 0°$) and thus $\gamma_s = 0°$.

Surface azimuth angle γ: The deviation of the projection on a horizontal plane of the normal to the surface from the local meridian, with zero due south, east negative, and west positive. Fixed collectors should be oriented toward the equator, facing south in the Northern Hemisphere and north in the Southern Hemisphere.

Incidence angle θ: The angle between the solar beam radiation on a surface and the normal to that surface. Eq. (A.6) relates the $\theta(n,t)$ to the previously described angles for the time period t of the corresponding day of the year n:

$$
\begin{aligned}
\cos\theta(n,t) = {} & \sin\delta(n)\cdot\sin\phi\cdot\cos\beta - \sin\delta(n)\cdot\cos\phi\cdot\sin\beta\cdot\cos\gamma + \cos\delta(n)\cdot\cos\phi \\
& \cdot\cos\beta\cdot\cos\omega(t) + \cos\delta(n)\cdot\sin\phi\cdot\sin\beta\cdot\cos\gamma\cdot\cos\omega(t) + \cos\delta(n) \\
& \cdot\sin\beta\cdot\sin\gamma\cdot\sin\omega(t)
\end{aligned}
\tag{A.6}
$$

For horizontal surfaces (tilt β = 0°), the incidence angle is equal to the zenith angle $\theta(n,t) = \theta_z(n,t)$. Its value must be between 0° and 90° when the sun is above the horizon. In this way, Eq. (A.6) becomes:

$$
\cos\theta_z(n,t) = \cos\delta(n)\cdot\cos\phi\cdot\cos\omega(t) + \sin\delta(n)\cdot\sin\phi
\tag{A.7}
$$

Sunrise and sunset hour angles: When the sun sets ($t = t_{ss}$), the solar altitude is $\alpha_s(n,t_{ss})$ = 0° and, thus, the zenith angle is $\theta_z(n,t_{ss})$ = 90°. The sunset hour angle $\omega_{ss}(n)$ for a day of the year n is obtained by solving Eq. (A.7) with $\theta_z(n,t)$ = 90°:

$$
\omega_{ss}(n) = \cos^{-1}\left(-\frac{\sin\phi\cdot\sin\delta(n)}{\cos\phi\cdot\cos\delta(n)}\right) = \cos^{-1}(-\tan\phi\cdot\tan\delta(n))
\tag{A.8}
$$

The sunrise hour angle $\omega_{sr}(n)$ is the negative of $\omega_{ss}(n)$.

The equations presented in this section for the solar angles can be applied for any time t. For the next sections the hourly period h will be used, corresponding to the time interval between t_1 and t_2 equal to 1 hour. In this way, the days of the year can be divided into 24 consecutive periods h, each one with 1-hour duration.

A.2.2.2   Extraterrestrial solar radiation

Before presenting the methodology to assess the extraterrestrial solar radiation on a horizontal plane, it is important to clarify the concepts of *irradiance*, *irradiation*, and *insolation*, according to Duffie et al. (2013).

Irradiance, in W/m², is the rate of radiant energy incident on a surface per unit area. The symbol G is used specifically for solar irradiance.

Irradiation, in J/m², is the incident energy on a surface per unit area, determined by integrating the irradiance over any time period comprehended by t_1 and t_2. *Insolation* is the term applied to the solar energy irradiation. The symbols H and I are used to represent the insolation for a day

and for an hour of the year, respectively. In addition, the overbar (e.g. $\overline{H}$) indicates a monthly mean value.

In accordance with Duffie et al. (2013), the subscripts on *G*, *H*, and *I* are as follows: *o* refers to the extraterrestrial radiation; *b* and *d* represent beam and diffuse radiation, respectively; *T* and *n* refer to radiation on a tilted plane and on a plane normal to the direction of propagation, respectively. If neither *T* nor *n* appears, the radiation is on a horizontal plane.

Throughout the year, the earth-sun distance varies and so does the extraterrestrial solar irradiance G_{on} measured on a horizontal plane normal to the radiation propagation in the range of ±3.3%. The $G_{on}(n)$ value for a day of the year *n* is given by Eq. (A.9).

$$G_{on}(n) = G_{sc} \cdot \left[1 + 0.033 \cdot \cos\left(\frac{360 \cdot n}{365}\right)\right] \tag{A.9}$$

where G_{sc} is the solar constant, defined as the amount of solar energy per unit time on a unit area of a surface normal to the sun's rays, just beyond the earth's atmosphere at the mean earth-sun distance. In accordance with Duffie et al. (2013), a G_{sc} = 1367 W/m² is used in this work.

When the plane is set parallel to the ground, the extraterrestrial solar irradiance $G_o(n,t)$ for the time period *t* of the day of the year *n* is given by Eq. (A.10):

$$G_o(n, t) = G_{on}(n) \cdot \cos\theta_z(n, t) \tag{A.10}$$

Combining Eq. (A.7) with Eq. (A.10) gives the $G_o(n,t)$ for a horizontal surface at any time between sunrise and sunset.

$$G_o(n, t) = G_{sc} \cdot \left[1 + 0.033 \cdot \cos\left(\frac{360 \cdot n}{365}\right)\right] \cdot [\cos\delta(n) \cdot \cos\phi \cdot \cos\omega(t) + \sin\delta(n) \cdot \sin\phi] \tag{A.11}$$

Integrating Eq. (A.11) over the period between sunrise and sunset gives the extraterrestrial insolation on a horizontal surface $H_o(n)$ for the day of the year *n*:

$$\begin{aligned}
H_o(n) = &\frac{24 \cdot 3600 \cdot G_{sc}}{\pi} \cdot \left[1 + 0.033 \cdot \cos\left(\frac{360 \cdot n}{365}\right)\right] \\
&\cdot \left[\cos\delta(n) \cdot \cos\phi \cdot \sin\omega_{ss}(n) + \frac{\pi \cdot \omega_{ss}(n)}{180} \cdot \sin\delta(n) \cdot \sin\phi\right]
\end{aligned} \tag{A.12}$$

Analogously, integrating Eq. (A.11) over the time period between t_1 and t_2, which define the hourly period *h* of the day of the year *n*, gives the extraterrestrial insolation on a horizontal surface $I_o(n,h)$:

$$I_o(n,h) = \frac{12 \cdot 3600 \cdot G_{sc}}{\pi} \cdot \left[1 + 0.033 \cdot \cos\left(\frac{360 \cdot n}{365}\right)\right]$$
$$\cdot \left[\cos \delta(n) \cdot \cos \phi \cdot (\sin \omega_2(h) - \sin \omega_1(h)) + \frac{\pi(\omega_2(h) - \omega_1(h))}{180} \cdot \sin \delta(n) \cdot \sin \phi\right] \quad \text{(A.13)}$$

The hour angles $\omega_1(h)$ and $\omega_2(h)$ are defined as follows:

$$\omega_1(h) = (h - 12 - 1) \cdot 15 \qquad \text{(A.14)}$$
$$\omega_2(h) = (h - 12) \cdot 15 \qquad \text{(A.15)}$$

And the hour angle $\omega(h)$ is calculated for the midpoint of the hour h for which the calculation is made:

$$\omega(h) = (h - 12 - 0.5) \cdot 15 \qquad \text{(A.16)}$$

Also, $\omega_1(h)$ and $\omega_2(h)$ must be corrected to the sunrise $\omega_{sr}(n)$ and sunset $\omega_{ss}(n)$ hour angles in the corresponding day of the year n, so that before dawn $\omega_1(h) = \omega_{sr}(n)$ and after twilight $\omega_2(h) = \omega_{ss}(n)$:

For $\omega_1(h) < \omega_{sr}(n)$, $\omega_1(h) = \omega_{sr}(n)$ (A.17)
For $\omega_1(h) > \omega_{ss}(n)$, $\omega_1(h) = \omega_{ss}(n)$ (A.18)
For $\omega_2(h) < \omega_{sr}(n)$, $\omega_2(h) = \omega_{sr}(n)$ (A.19)
For $\omega_2(h) > \omega_{ss}(n)$, $\omega_2(h) = \omega_{ss}(n)$ (A.20)

A.2.2.3 Terrestrial irradiation

The methodology described thus far has considered the solar radiation on any day n of the year. However, the same procedure can be followed for the representative days d of the months of the year. In this case, as shown in Table A.2, the representative day d associated with a month of the year corresponds to the recommended average day of that month $\bar{n}(d)$. Using the recommended average day gives the monthly mean value, indicated by the overbar (e.g. $\bar{H}$). For the sake of clarity, from here on the notation will indicate only the representative days d, for instance $\bar{H}(d) = \bar{H}(\bar{n}(d))$.

As the extraterrestrial solar radiation travels through the earth's atmosphere, a part of it is scattered and absorbed. Some of the scattered radiation reaches the earth's surface from the entire sky vault, this is called diffuse radiation. The solar radiation that comes directly through the atmosphere is called direct or beam radiation. The sum of both the diffuse and beam radiations compose the total radiation received by a surface on earth (Kalogirou, 2014).

The effects due to scattering and absorption in the atmosphere are variable with time as atmospheric conditions and air mass change, for example in clear or cloudy days. For any day n of

the year, the ratio of the daily total insolation on a terrestrial horizontal surface $H(n)$ to the daily total extraterrestrial insolation $H_o(n)$ is the clearness index $K_T(n)$.

Analogously, the ratio of the monthly mean daily total insolation on a terrestrial horizontal surface $\bar{H}(d)$ to the monthly mean daily total extraterrestrial insolation $\bar{H}_o(d)$ is the monthly mean clearness index $\bar{K}_T(d)$, for the representative day d of the month of the year:

$$\bar{K}_T(d) = \frac{\bar{H}(d)}{\bar{H}_o(d)} \tag{A.21}$$

where the representative day d associated with a month of the year refers to the recommended average day of that month $\bar{n}(d)$. Therefore, the value of $\bar{H}_o(d)$ for the representative day d is obtained by solving Eq. (A.12) with n equal to the average day of the month $\bar{n}(d)$. The value of $\bar{H}(d)$ can be obtained through in situ measurement at meteorological stations; for the preset study, its values are given in Table A.3.

The monthly mean daily insolation $\bar{H}(d)$ can be distributed into its beam and diffuse components. The monthly fraction that is diffuse $\bar{H}_d(d)/\bar{H}(d)$, can be estimated as a function of $\bar{K}_T(d)$ by the correlation proposed by Erbs et al. (1982):

For $\omega_{ss}(d) \leq 81.4°$:

$$\frac{\bar{H}_d(d)}{\bar{H}(d)} = 1.391 - 3.560 \cdot \bar{K}_T(d) + 4.189 \cdot \bar{K}_T^2(d) - 2.137 \cdot \bar{K}_T^3(d) \tag{A.22}$$

For $\omega_{ss}(d) > 81.4°$:

$$\frac{\bar{H}_d(d)}{\bar{H}(d)} = 1.311 - 3.022 \cdot \bar{K}_T(d) + 3.427 \cdot \bar{K}_T^2(d) - 1.821 \cdot \bar{K}_T^3(d) \tag{A.23}$$

Thus, knowing $\bar{K}_T(d)$ and $\bar{H}(d)$ for the representative day d, the monthly mean daily diffuse insolation $\bar{H}_d(d)$ can be obtained. The monthly mean daily direct insolation $\bar{H}_b(d)$ is determined as the difference $\bar{H}(d) - \bar{H}_d(d)$.

Daily radiation data can be used to estimate hourly radiation numbers. As stated by Duffie et al. (2013), this is not an exact process and it leads to conservative results; however, it works best for clear days, which are the days that produce most of the output of solar processes.

The ratio $r_t(d,h)$ of the hourly total insolation $I(d,h)$ to the monthly mean daily insolation $\bar{H}(d)$

$$r_t(d,h) = \frac{I(d,h)}{\bar{H}(d)} \tag{A.24}$$

is expressed by the correlation of Collares-Pereira and Rabl (1979), as presented by Duffie et al. (2013):

If $\omega(h) > \omega_{ss}(d)$ or $\omega(h) < \omega_{sr}(d)$, then $r_t(d,h) = 0$. Else,

$$r_t(d,h) = \frac{\pi}{24} \cdot (a(d) + b(d) \cdot cos\,\omega(h)) \cdot \frac{cos\,\omega(h) - cos\,\omega_{ss}(d)}{sin\,\omega_{ss}(d) - \frac{\pi \cdot \omega_{ss}(d)}{180} \cdot cos\,\omega_{ss}(d)} \tag{A.25}$$

The coefficients $a(d)$ and $b(d)$ are given by:

$$a(d) = 0.409 + 0.5016 \cdot sin(\omega_{ss}(d) - 60) \tag{A.26}$$
$$b(d) = 0.6609 - 0.4767 \cdot sin(\omega_{ss}(d) - 60) \tag{A.27}$$

Thus the hourly total insolation on a surface on earth $I(d,h)$ is determined.

Analogously, the ratio $r_d(d,h)$ of the hourly diffuse insolation $I_d(d,h)$ to the monthly mean daily diffuse insolation $H_d(d)$

$$r_d(d,h) = \frac{I_d(d,h)}{\overline{H}_d(d)} \tag{A.28}$$

is determined by the correlation proposed by Liu and Jordan (1960), as presented by Duffie et al. (2013):

If $\omega(h) > \omega_{ss}(d)$ or $\omega(h) < \omega_{sr}(d)$, then $r_d(d,h) = 0$. Else,

$$r_d(d,h) = \frac{\pi}{24} \cdot \frac{cos\,\omega(h) - cos\,\omega_{ss}(d)}{sin\,\omega_{ss}(d) - \frac{\pi \cdot \omega_{ss}(d)}{180} \cdot cos\,\omega_{ss}(d)} \tag{A.29}$$

Solving Eq. (A.28) and Eq. (A.29) yields the hourly diffuse insolation $I_d(d,h)$.

Finally, the hourly beam insolation $I_b(d,h)$ is determined by the difference between the hourly total $I(d,h)$ and hourly diffuse $I_d(d,h)$ insolation:

$$I_b(d,h) = I(d,h) - I_d(d,h) \tag{A.30}$$

A.2.2.4 Radiation on a tilted surface (Isotropic Sky Model)

The Isotropic Sky Model, derived by Liu and Jordan (1963) and presented by Duffie et al. (2013), considers the insolation on a tilted surface $I_T(d,h)$ as composed of three components: beam, isotropic diffuse, and solar radiation diffusely reflected from the ground.

$$I_T(d,h) = I_b(d,h) \cdot R_b(d,h) + I_d(d,h) \cdot F_{c,s} + I(d,h) \cdot \rho_g \cdot F_{c,g} \tag{A.31}$$

Where $I_b(d,h)$ is the hourly beam insolation, $R_b(d,h)$ is the geometric factor, $I_d(d,h)$ is the hourly diffuse insolation, $F_{c,s}$ is the view factor to the sky, ρ_g is the reflectance of the ground or the albedo, and $F_{c,g}$ is the view factor to the ground. The value of ρ_g for the case study considered herein is given in Table A.1.

The geometric factor $R_b(d,h)$ is the ratio of the radiation on the tilted surface to that on a horizontal surface at any time:

$$R_b(d,h) = \frac{\cos\theta(d,h)}{\cos\theta_z(d,h)} \tag{A.32}$$

where, as previously mentioned, d refers to $\bar{n}(d)$ given in Table A.2.

The view factors to the sky and to the ground are determined by Eq. (A.33) and Eq. (A.34), respectively.

$$F_{c,s} = \frac{1+\cos\beta}{2} \tag{A.33}$$
$$F_{c,g} = \frac{1-\cos\beta}{2} \tag{A.34}$$

Finally, dividing the insolation on a tilted surface $I_T(d,h)$ by 3600 changes its base from J/(h·m²) to W/m², thus giving the hourly solar radiation on tilted surface required for the optimization model $Q_r(d,h)$:

$$Q_r(d,h) = I_T(d,h) \cdot \frac{1}{3600} \tag{A.35}$$

For the case study considered herein, the photovoltaic panels and the flat-plate solar thermal collectors have the same solar azimuth value (orientation south) but different tilt values, as shown in Table A.7. Therefore, the hourly solar radiation on tilted surface was assessed for both technologies. The results obtained for the photovoltaic panels $Q_{r,pv}(d,h)$ and flat-plate solar thermal collectors $Q_{r,st}(d,h)$ are presented in Table A.8 and Table A.9, respectively.

Table A.7: PV and ST tilt and orientation values.

Technology	Parameter	Nomenclature	Value
Photovoltaic panels	Tilt	β_{pv}	35°
	Orientation azimuth south	γ_{pv}	0°
Solar thermal collectors	Tilt	β_{st}	30°
	Orientation azimuth south	γ_{st}	0°

Table A.8: Hourly solar radiation on tilted surface $Q_{r,pv}(d,h)$, photovoltaic panels with 35° tilt and solar azimuth 0°, W/m².

Hour	Jan	Feb	Mar	Apr	May	Jun	Jul	Aug	Sep	Oct	Nov	Dec
1	0.00	0.00	0.00	0.00	0.00	0.00	0.00	0.00	0.00	0.00	0.00	0.00
2	0.00	0.00	0.00	0.00	0.00	0.00	0.00	0.00	0.00	0.00	0.00	0.00
3	0.00	0.00	0.00	0.00	0.00	0.00	0.00	0.00	0.00	0.00	0.00	0.00
4	0.00	0.00	0.00	0.00	0.00	0.00	0.00	0.00	0.00	0.00	0.00	0.00
5	0.00	0.00	0.00	0.00	0.00	0.00	0.00	0.00	0.00	0.00	0.00	0.00
6	0.00	0.00	0.00	3.36	32.35	44.51	37.20	14.99	0.00	0.00	0.00	0.00
7	0.00	0.00	44.82	91.34	131.92	150.98	151.93	122.82	69.29	0.00	0.00	0.00
8	62.89	122.70	178.21	227.07	276.86	301.34	319.95	293.19	218.13	153.24	85.10	50.50
9	184.83	267.82	331.79	375.78	429.94	457.62	495.28	475.81	385.41	311.06	219.36	168.73
10	310.47	412.90	481.02	516.15	571.14	600.28	655.76	645.88	545.71	466.97	356.35	291.60
11	413.48	529.92	599.47	625.68	679.78	709.32	778.62	777.50	671.93	591.89	468.07	392.78
12	471.40	595.19	665.00	685.72	738.87	768.42	845.28	849.33	741.46	661.33	530.73	449.80
13	471.40	595.19	665.00	685.72	738.87	768.42	845.28	849.33	741.46	661.33	530.73	449.80
14	413.48	529.92	599.47	625.68	679.78	709.32	778.62	777.50	671.93	591.89	468.07	392.78
15	310.47	412.90	481.02	516.15	571.14	600.28	655.76	645.88	545.71	466.97	356.35	291.60
16	184.83	267.82	331.79	375.78	429.94	457.62	495.28	475.81	385.41	311.06	219.36	168.73
17	62.89	122.70	178.21	227.07	276.86	301.34	319.95	293.19	218.13	153.24	85.10	50.50
18	0.00	0.00	44.82	91.34	131.92	150.98	151.93	122.82	69.29	0.00	0.00	0.00
19	0.00	0.00	0.00	3.36	32.35	44.51	37.20	14.99	0.00	0.00	0.00	0.00
20	0.00	0.00	0.00	0.00	0.00	0.00	0.00	0.00	0.00	0.00	0.00	0.00
21	0.00	0.00	0.00	0.00	0.00	0.00	0.00	0.00	0.00	0.00	0.00	0.00
22	0.00	0.00	0.00	0.00	0.00	0.00	0.00	0.00	0.00	0.00	0.00	0.00
23	0.00	0.00	0.00	0.00	0.00	0.00	0.00	0.00	0.00	0.00	0.00	0.00
24	0.00	0.00	0.00	0.00	0.00	0.00	0.00	0.00	0.00	0.00	0.00	0.00

Table A.9: Hourly solar radiation on tilted surface $Q_{r,st}(d,h)$, solar thermal collectors with 30° tilt and solar azimuth 0°, W/m².

Hour	Jan	Feb	Mar	Apr	May	Jun	Jul	Aug	Sep	Oct	Nov	Dec
1	0.00	0.00	0.00	0.00	0.00	0.00	0.00	0.00	0.00	0.00	0.00	0.00
2	0.00	0.00	0.00	0.00	0.00	0.00	0.00	0.00	0.00	0.00	0.00	0.00
3	0.00	0.00	0.00	0.00	0.00	0.00	0.00	0.00	0.00	0.00	0.00	0.00
4	0.00	0.00	0.00	0.00	0.00	0.00	0.00	0.00	0.00	0.00	0.00	0.00
5	0.00	0.00	0.00	0.00	0.00	0.00	0.00	0.00	0.00	0.00	0.00	0.00
6	0.00	0.00	0.00	3.41	32.85	45.15	37.68	15.19	0.00	0.00	0.00	0.00
7	0.00	0.00	44.02	95.18	141.25	163.77	165.39	130.75	70.20	0.00	0.00	0.00
8	56.79	116.89	176.76	231.34	287.00	315.02	334.01	301.29	218.59	147.77	78.12	44.24
9	175.65	259.53	329.18	379.97	440.40	471.72	509.46	483.55	384.89	303.25	209.22	159.12
10	298.34	402.14	477.05	519.94	581.59	614.46	669.72	652.96	543.98	456.78	343.17	278.81
11	399.01	517.16	594.31	629.02	690.07	723.41	792.28	783.93	669.12	579.77	452.49	377.49
12	455.64	581.31	659.15	688.77	749.04	782.43	858.73	855.35	738.02	648.13	513.82	433.14
13	455.64	581.31	659.15	688.77	749.04	782.43	858.73	855.35	738.02	648.13	513.82	433.14
14	399.01	517.16	594.31	629.02	690.07	723.41	792.28	783.93	669.12	579.77	452.49	377.49
15	298.34	402.14	477.05	519.94	581.59	614.46	669.72	652.96	543.98	456.78	343.17	278.81
16	175.65	259.53	329.18	379.97	440.40	471.72	509.46	483.55	384.89	303.25	209.22	159.12
17	56.79	116.89	176.76	231.34	287.00	315.02	334.01	301.29	218.59	147.77	78.12	44.24
18	0.00	0.00	44.02	95.18	141.25	163.77	165.39	130.75	70.20	0.00	0.00	0.00
19	0.00	0.00	0.00	3.41	32.85	45.15	37.68	15.19	0.00	0.00	0.00	0.00
20	0.00	0.00	0.00	0.00	0.00	0.00	0.00	0.00	0.00	0.00	0.00	0.00
21	0.00	0.00	0.00	0.00	0.00	0.00	0.00	0.00	0.00	0.00	0.00	0.00
22	0.00	0.00	0.00	0.00	0.00	0.00	0.00	0.00	0.00	0.00	0.00	0.00
23	0.00	0.00	0.00	0.00	0.00	0.00	0.00	0.00	0.00	0.00	0.00	0.00
24	0.00	0.00	0.00	0.00	0.00	0.00	0.00	0.00	0.00	0.00	0.00	0.00

A.3 ENERGY DEMANDS

This section calculates the annual, monthly, and hourly energy demands of the consumer center considered in this study. The energy demands of the multi-family building complex consist of electricity, heating, and cooling. The heating demand is composed of both domestic hot water DHW and space heating SH. Moreover, the electricity demand excludes the consumption of electricity for thermal production, e.g. electric chiller for cooling production, electric heat pump for heat production; therefore, the electricity demand considers only the dwellings' electric consumption for home appliances, lighting, etc.

The following information is necessary for the estimation of the energy demands: (i) reference values of annual energy consumption; (ii) building characteristics, such as number of dwellings, occupancy rates, and surface area per dwelling; (iii) local climatic data, such as hourly ambient temperature and monthly cold water temperature of the supply network; and (iv) monthly and hourly energy demands distribution factors.

The reference values for the estimation of the annual energy demands presented in Table A.10 have been obtained from different sources: (i) the reference annual demand of electricity D_{ELE} was obtained from the research developed by Giménez (2004); (ii) the reference annual domestic hot water DHW demand D_{DHW} was obtained from CTE (2013); and (iii) the reference annual space heating SH demand D_{SH} and the reference annual cooling demand D_{REF} were obtained from IDAE (2009).

Table A.10: Reference values for the estimation of the annual energy demands.

Parameter	Nomenclature	Value
Reference annual SH demand	D_{SH}	40.6 kWh/(m²·yr)
Reference annual DHW demand	D_{DHW}	28 l/(day·person)
Reference annual electricity demand	D_{ELE}	25.5 kWh/(m²·yr)
Reference annual cooling demand	D_{REF}	11.4 kWh/(m²·yr)

The consumer center's building characteristics, such as number of dwellings N and surface area per dwelling S, have been described in Section A.1 and are given in Table A.1. In addition, according to the National Statistics Institute in Spain (INE), the average area per occupant in Spanish residential buildings is *apo* = 33.3 m²/occupant (INE, 2018).

The climatic data for the geographic location of Zaragoza, Spain, includes the hourly ambient temperature *Ta(d,h)*, calculated in Section A.2.1 and shown in Table A.5, and the monthly cold water temperature of the supply network $T_{CW}(d)$, given in Table A.3.

The general procedure for the estimation of the energy demands is depicted in the flow chart of Figure A.4.
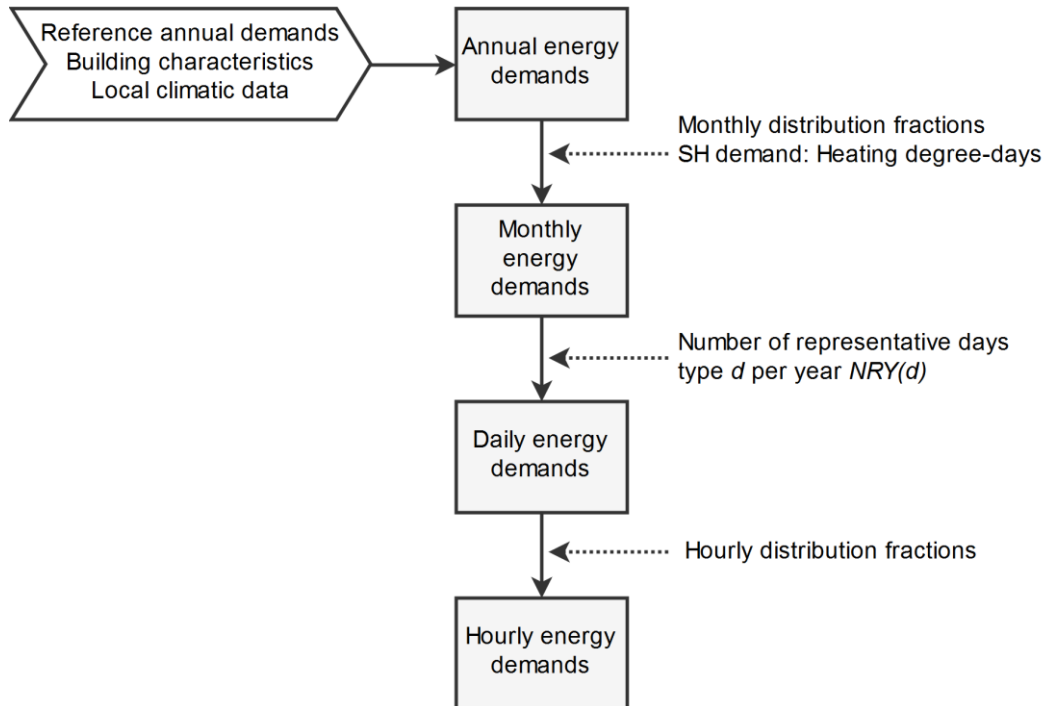
Figure A.4: Information flow chart for the calculation of the energy demands.

First, the annual energy demands are estimated based on the reference annual demand values and building characteristics. Then, the annual energy demands are distributed between the months of the year through monthly distribution fractions. The monthly fractions $fm_{VDHW}(d)$, $fm_{Ed}(d)$, and $fm_{Rd}(d)$ presented in Table A.11 are used to distribute the annual DHW, electricity, and cooling demands. In the case of the SH demand, the monthly fraction $fm_{SH}(d)$ is calculated in Section A.3.2 following the heating degree-days method, as described in Guadalfajara (2016).

Table A.11: Monthly fractions for the DHW, electricity and cooling demands.

Representative day d	$fm_{VDHW}(d)$ (Viti, 1996)	$fm_{Ed}(d)$ (Giménez, 2004)	$fm_{Rd}(d)$ (Ramos, 2012)
1	0.0952	0.0944	0.0000
2	0.0830	0.0852	0.0000
3	0.0876	0.0944	0.0000
4	0.0897	0.0817	0.0000
5	0.0884	0.0844	0.0000
6	0.0831	0.0737	0.1474
7	0.0765	0.0761	0.4184
8	0.0663	0.0761	0.3112
9	0.0749	0.0737	0.1230
10	0.0799	0,0844	0.0000
11	0.0839	0.0817	0.0000
12	0.0914	0.0944	0.0000

For the representative days d of the months of the year, the daily energy demands are obtained by dividing the corresponding monthly energy demands by the number of representative days type d per year *NRY(d)*. Note that, as explained in Section A.1, the *NRY(d)* is equal to the number of days in the corresponding month.

Finally, the daily energy demands are distributed between the hourly periods that compose the day through hourly distribution factors. The hourly distribution factors fh_{SH} for SH, fh_{DHW} for DHW, fh_{Ed} for electricity, and fh_{Rd} for cooling are given in Table A.12 to Table A.15, respectively.

The mathematical formulations for the estimation of the electricity, heating, and cooling demands are described in Sections A.3.1, A.3.2, and A.3.3, respectively.

Table A.12: Hourly fractions of the SH demand for each representative day (Ramos, 2012).

Hour	Jan	Feb	Mar	Apr	May	Jun	Jul	Aug	Sep	Oct	Nov	Dec
1	0.0000	0.0000	0.0000	0.0000	-	-	-	-	-	-	0.0000	0.0000
2	0.0000	0.0000	0.0000	0.0000	-	-	-	-	-	-	0.0000	0.0000
3	0.0000	0.0000	0.0000	0.0000	-	-	-	-	-	-	0.0000	0.0000
4	0.0000	0.0000	0.0000	0.0000	-	-	-	-	-	-	0.0000	0.0000
5	0.0000	0.0000	0.0000	0.0000	-	-	-	-	-	-	0.0000	0.0000
6	0.0000	0.0000	0.0000	0.0000	-	-	-	-	-	-	0.0000	0.0000
7	0.0784	0.0817	0.0893	0.0966	-	-	-	-	-	-	0.0828	0.0855
8	0.0756	0.0787	0.0861	0.0931	-	-	-	-	-	-	0.0798	0.0824
9	0.0711	0.0740	0.0809	0.0875	-	-	-	-	-	-	0.0750	0.0774
10	0.0664	0.0692	0.0757	0.0818	-	-	-	-	-	-	0.0702	0.0724
11	0.0634	0.0660	0.0722	0.0781	-	-	-	-	-	-	0.0669	0.0691
12	0.0615	0.0640	0.0700	0.0757	-	-	-	-	-	-	0.0649	0.0670
13	0.0584	0.0608	0.0665	0.0720	-	-	-	-	-	-	0.0617	0.0637
14	0.0566	0.0589	0.0644	0.0697	-	-	-	-	-	-	0.0597	0.0616
15	0.0534	0.0556	0.0608	0.0657	-	-	-	-	-	-	0.0564	0.0582
16	0.0492	0.0513	0.0561	0.0607	-	-	-	-	-	-	0.0520	0.0537
17	0.0718	0.0537	0.0420	0.0288	-	-	-	-	-	-	0.0527	0.0553
18	0.0697	0.0620	0.0445	0.0288	-	-	-	-	-	-	0.0597	0.0551
19	0.0610	0.0633	0.0521	0.0395	-	-	-	-	-	-	0.0629	0.0552
20	0.0608	0.0582	0.0523	0.0409	-	-	-	-	-	-	0.0624	0.0546
21	0.0460	0.0438	0.0331	0.0298	-	-	-	-	-	-	0.0367	0.0396
22	0.0567	0.0589	0.0540	0.0512	-	-	-	-	-	-	0.0562	0.0493
23	0.0000	0.0000	0.0000	0.0000	-	-	-	-	-	-	0.0000	0.0000
24	0.0000	0.0000	0.0000	0.0000	-	-	-	-	-	-	0.0000	0.0000

Table A.13: Hourly fractions of the DHW demand for each representative day (Viti, 1996).

Hour	Jan	Feb	Mar	Apr	May	Jun	Jul	Aug	Sep	Oct	Nov	Dec
1	0.0102	0.0102	0.0102	0.0102	0.0102	0.0102	0.0102	0.0102	0.0102	0.0102	0.0102	0.0102
2	0.0070	0.0070	0.0070	0.0070	0.0070	0.0070	0.0070	0.0070	0.0070	0.0070	0.0070	0.0070
3	0.0070	0.0070	0.0070	0.0070	0.0070	0.0070	0.0070	0.0070	0.0070	0.0070	0.0070	0.0070
4	0.0070	0.0070	0.0070	0.0070	0.0070	0.0070	0.0070	0.0070	0.0070	0.0070	0.0070	0.0070
5	0.0164	0.0164	0.0164	0.0164	0.0164	0.0164	0.0164	0.0164	0.0164	0.0164	0.0164	0.0164
6	0.0266	0.0266	0.0266	0.0266	0.0266	0.0266	0.0266	0.0266	0.0266	0.0266	0.0266	0.0266
7	0.0391	0.0391	0.0391	0.0391	0.0391	0.0391	0.0391	0.0391	0.0391	0.0391	0.0391	0.0391
8	0.0668	0.0668	0.0668	0.0668	0.0668	0.0668	0.0668	0.0668	0.0668	0.0668	0.0668	0.0668
9	0.0746	0.0746	0.0746	0.0746	0.0746	0.0746	0.0746	0.0746	0.0746	0.0746	0.0746	0.0746
10	0.0375	0.0375	0.0375	0.0375	0.0375	0.0375	0.0375	0.0375	0.0375	0.0375	0.0375	0.0375
11	0.0281	0.0281	0.0281	0.0281	0.0281	0.0281	0.0281	0.0281	0.0281	0.0281	0.0281	0.0281
12	0.0234	0.0234	0.0234	0.0234	0.0234	0.0234	0.0234	0.0234	0.0234	0.0234	0.0234	0.0234
13	0.0227	0.0227	0.0227	0.0227	0.0227	0.0227	0.0227	0.0227	0.0227	0.0227	0.0227	0.0227
14	0.0563	0.0563	0.0563	0.0563	0.0563	0.0563	0.0563	0.0563	0.0563	0.0563	0.0563	0.0563
15	0.0320	0.0320	0.0320	0.0320	0.0320	0.0320	0.0320	0.0320	0.0320	0.0320	0.0320	0.0320
16	0.0336	0.0336	0.0336	0.0336	0.0336	0.0336	0.0336	0.0336	0.0336	0.0336	0.0336	0.0336
17	0.0359	0.0359	0.0359	0.0359	0.0359	0.0359	0.0359	0.0359	0.0359	0.0359	0.0359	0.0359
18	0.0852	0.0852	0.0852	0.0852	0.0852	0.0852	0.0852	0.0852	0.0852	0.0852	0.0852	0.0852
19	0.1758	0.1758	0.1758	0.1758	0.1758	0.1758	0.1758	0.1758	0.1758	0.1758	0.1758	0.1758
20	0.0867	0.0867	0.0867	0.0867	0.0867	0.0867	0.0867	0.0867	0.0867	0.0867	0.0867	0.0867
21	0.0609	0.0609	0.0609	0.0609	0.0609	0.0609	0.0609	0.0609	0.0609	0.0609	0.0609	0.0609
22	0.0250	0.0250	0.0250	0.0250	0.0250	0.0250	0.0250	0.0250	0.0250	0.0250	0.0250	0.0250
23	0.0188	0.0188	0.0188	0.0188	0.0188	0.0188	0.0188	0.0188	0.0188	0.0188	0.0188	0.0188
24	0.0234	0.0234	0.0234	0.0234	0.0234	0.0234	0.0234	0.0234	0.0234	0.0234	0.0234	0.0234

Table A.14: Hourly fractions of the electricity demand for each representative day (Giménez, 2004).

Hour	Jan	Feb	Mar	Apr	May	Jun	Jul	Aug	Sep	Oct	Nov	Dec
1	0.0451	0.0451	0.0451	0.0432	0.0432	0.0431	0.0431	0.0431	0.0431	0.0432	0.0432	0.0451
2	0.0322	0.0322	0.0322	0.0360	0.0360	0.0367	0.0367	0.0367	0.0367	0.0360	0.0360	0.0322
3	0.0258	0.0258	0.0258	0.0288	0.0288	0.0319	0.0319	0.0319	0.0319	0.0288	0.0288	0.0258
4	0.0206	0.0206	0.0206	0.0259	0.0259	0.0288	0.0288	0.0288	0.0288	0.0259	0.0259	0.0206
5	0.0193	0.0193	0.0193	0.0245	0.0245	0.0272	0.0272	0.0272	0.0272	0.0245	0.0245	0.0193
6	0.0206	0.0206	0.0206	0.0245	0.0245	0.0272	0.0272	0.0272	0.0272	0.0245	0.0245	0.0206
7	0.0232	0.0232	0.0232	0.0259	0.0259	0.0288	0.0288	0.0288	0.0288	0.0259	0.0259	0.0232
8	0.0258	0.0258	0.0258	0.0288	0.0288	0.0304	0.0304	0.0304	0.0304	0.0288	0.0288	0.0258
9	0.0296	0.0296	0.0296	0.0317	0.0317	0.0319	0.0319	0.0319	0.0319	0.0317	0.0317	0.0296
10	0.0322	0.0322	0.0322	0.0331	0.0331	0.0335	0.0335	0.0335	0.0335	0.0331	0.0331	0.0322
11	0.0361	0.0361	0.0361	0.0375	0.0375	0.0383	0.0383	0.0383	0.0383	0.0375	0.0375	0.0361
12	0.0464	0.0464	0.0464	0.0476	0.0476	0.0463	0.0463	0.0463	0.0463	0.0476	0.0476	0.0464
13	0.0593	0.0593	0.0593	0.0576	0.0576	0.0575	0.0575	0.0575	0.0575	0.0576	0.0576	0.0593
14	0.0644	0.0644	0.0644	0.0634	0.0634	0.0591	0.0591	0.0591	0.0591	0.0634	0.0634	0.0644
15	0.0554	0.0554	0.0554	0.0548	0.0548	0.0543	0.0543	0.0543	0.0543	0.0548	0.0548	0.0554
16	0.0412	0.0412	0.0412	0.0432	0.0432	0.0463	0.0463	0.0463	0.0463	0.0432	0.0432	0.0412
17	0.0374	0.0374	0.0374	0.0389	0.0389	0.0383	0.0383	0.0383	0.0383	0.0389	0.0389	0.0374
18	0.0374	0.0374	0.0374	0.0375	0.0375	0.0367	0.0367	0.0367	0.0367	0.0375	0.0375	0.0374
19	0.0438	0.0438	0.0438	0.0375	0.0375	0.0399	0.0399	0.0399	0.0399	0.0375	0.0375	0.0438
20	0.0580	0.0580	0.0580	0.0432	0.0432	0.0479	0.0479	0.0479	0.0479	0.0432	0.0432	0.0580
21	0.0657	0.0657	0.0657	0.0533	0.0533	0.0575	0.0575	0.0575	0.0575	0.0533	0.0533	0.0657
22	0.0670	0.0670	0.0670	0.0634	0.0634	0.0543	0.0543	0.0543	0.0543	0.0634	0.0634	0.0670
23	0.0606	0.0606	0.0606	0.0620	0.0620	0.0543	0.0543	0.0543	0.0543	0.0620	0.0620	0.0606
24	0.0528	0.0528	0.0528	0.0576	0.0576	0.0495	0.0495	0.0495	0.0495	0.0576	0.0576	0.0528

Table A.15: Hourly fractions of the cooling demand for each representative day (Ramos, 2012).

Hour	Jan	Feb	Mar	Apr	May	Jun	Jul	Aug	Sep	Oct	Nov	Dec
1	-	-	-	-	-	0.0000	0.0000	0.0000	0.0000	-	-	-
2	-	-	-	-	-	0.0000	0.0000	0.0000	0.0000	-	-	-
3	-	-	-	-	-	0.0000	0.0000	0.0000	0.0000	-	-	-
4	-	-	-	-	-	0.0000	0.0000	0.0000	0.0000	-	-	-
5	-	-	-	-	-	0.0000	0.0000	0.0000	0.0000	-	-	-
6	-	-	-	-	-	0.0000	0.0000	0.0000	0.0000	-	-	-
7	-	-	-	-	-	0.0000	0.0000	0.0000	0.0000	-	-	-
8	-	-	-	-	-	0.0000	0.0000	0.0000	0.0000	-	-	-
9	-	-	-	-	-	0.0000	0.0000	0.0000	0.0000	-	-	-
10	-	-	-	-	-	0.0000	0.0000	0.0000	0.0000	-	-	-
11	-	-	-	-	-	0.0000	0.0000	0.0000	0.0000	-	-	-
12	-	-	-	-	-	0.0577	0.0580	0.0582	0.0592	-	-	-
13	-	-	-	-	-	0.0740	0.0744	0.0747	0.0759	-	-	-
14	-	-	-	-	-	0.0881	0.0886	0.0889	0.0904	-	-	-
15	-	-	-	-	-	0.1327	0.1333	0.1338	0.1360	-	-	-
16	-	-	-	-	-	0.2526	0.1733	0.2062	0.2746	-	-	-
17	-	-	-	-	-	0.2305	0.1527	0.1768	0.2347	-	-	-
18	-	-	-	-	-	0.0561	0.0842	0.0716	0.0502	-	-	-
19	-	-	-	-	-	0.0413	0.0720	0.0587	0.0297	-	-	-
20	-	-	-	-	-	0.0245	0.0582	0.0480	0.0188	-	-	-
21	-	-	-	-	-	0.0205	0.0593	0.0469	0.0165	-	-	-
22	-	-	-	-	-	0.0220	0.0460	0.0362	0.0140	-	-	-
23	-	-	-	-	-	0.0000	0.0000	0.0000	0.0000	-	-	-
24	-	-	-	-	-	0.0000	0.0000	0.0000	0.0000	-	-	-

A.3.1 Electricity demand

Following the procedure described in the opening of Section A.3, Equations (A.36)-(A.39) determine, respectively, the annual electricity demand E_{d_Y}, in MWh/yr, the monthly electricity demand $E_{d\_M}(d)$, in MWh/month, the daily electricity demand $E_{d\_D}(d)$ of each representative day d of the months of the year, in MWh/day, and the hourly electricity demand $E_d(d,h)$, in MWh.

$$E_{d\_Y} = D_{ELE} \cdot N \cdot S \cdot 10^{-3} \tag{A.36}$$
$$E_{d\_M}(d) = fm_{Ed}(d) \cdot E_{d\_Y} \tag{A.37}$$
$$E_{d\_D}(d) = E_{d\_M}(d) / NRY(d) \tag{A.38}$$
$$E_d(d,h) = fh_{Ed}(d,h) \cdot E_d(d) \tag{A.39}$$

The annual E_{d_Y}, monthly $E_{d\_M}(d)$ and daily $E_{d\_D}(d)$ electricity demands for the representative days d of the months of the year are presented in Table A.16. The hourly electricity demands $E_d(d,h)$ are given in Table A.17.

Table A.16: Annual, monthly, and daily electricity demands.

Representative day d	$E_{d\_M}(d)$, MWh/month	$E_{d\_D}(d)$, MWh/day
1	24.06	0.7761
2	21.73	0.7760
3	24.06	0.7761
4	20.83	0.6943
5	21.51	0.6940
6	18.78	0.6260
7	19.41	0.6260
8	19.41	0.6260
9	18.78	0.6260
10	21.51	0.6940
11	20.83	0.6943
12	24.06	0.7761
Year E_{d_Y}, MWh/yr	254.96	-

Table A.17: Hourly electricity demand values for each representative day, kW.

Hour	Jan	Feb	Mar	Apr	May	Jun	Jul	Aug	Sep	Oct	Nov	Dec
1	35.00	35.00	35.00	30.00	30.00	27.00	27.00	27.00	27.00	30.00	30.00	35.00
2	25.00	25.00	25.00	25.00	25.00	23.00	23.00	23.00	23.00	25.00	25.00	25.00
3	20.00	20.00	20.00	20.00	20.00	20.00	20.00	20.00	20.00	20.00	20.00	20.00
4	16.00	16.00	16.00	18.00	18.00	18.00	18.00	18.00	18.00	18.00	18.00	16.00
5	15.00	15.00	15.00	17.00	17.00	17.00	17.00	17.00	17.00	17.00	17.00	15.00
6	16.00	16.00	16.00	17.00	17.00	17.00	17.00	17.00	17.00	17.00	17.00	16.00
7	18.00	18.00	18.00	18.00	18.00	18.00	18.00	18.00	18.00	18.00	18.00	18.00
8	20.00	20.00	20.00	20.00	20.00	19.00	19.00	19.00	19.00	20.00	20.00	20.00
9	23.00	23.00	23.00	22.00	22.00	20.00	20.00	20.00	20.00	22.00	22.00	23.00
10	25.00	25.00	25.00	23.00	23.00	21.00	21.00	21.00	21.00	23.00	23.00	25.00
11	28.00	28.00	28.00	26.00	26.00	24.00	24.00	24.00	24.00	26.00	26.00	28.00
12	36.00	36.00	36.00	33.10	33.00	29.00	29.00	29.00	29.00	33.00	33.10	36.00
13	46.00	46.00	46.00	40.00	40.00	36.00	36.00	36.00	36.00	40.00	40.00	46.00
14	50.00	50.00	50.00	44.00	44.00	37.00	37.00	37.00	37.00	44.00	44.00	50.00
15	43.00	43.00	43.00	38.10	38.00	34.00	34.00	34.00	34.00	38.00	38.10	43.00
16	32.00	32.00	32.00	30.00	30.00	29.00	29.00	29.00	29.00	30.00	30.00	32.00
17	29.00	29.00	29.00	27.00	27.00	24.00	24.00	24.00	24.00	27.00	27.00	29.00
18	29.00	29.00	29.00	26.00	26.00	23.00	23.00	23.00	23.00	26.00	26.00	29.00
19	34.00	34.00	34.00	26.00	26.00	25.00	25.00	25.00	25.00	26.00	26.00	34.00
20	45.00	45.00	45.00	30.00	30.00	30.00	30.00	30.00	30.00	30.00	30.00	45.00
21	51.00	51.00	51.00	37.00	37.00	36.00	36.00	36.00	36.00	37.00	37.00	51.00
22	52.00	52.00	52.00	44.00	44.00	34.00	34.00	34.00	34.00	44.00	44.00	52.00
23	47.10	47.00	47.10	43.10	43.00	34.00	34.00	34.00	34.00	43.00	43.10	47.10
24	41.00	41.00	41.00	40.00	40.00	31.00	31.00	31.00	31.00	40.00	40.00	41.00

A.3.2   Heating demand

The annual heating demand Q_{d_Y} corresponds to the sum of the annual SH demand Q_{SH_Y} and the annual DHW demand Q_{DHW_Y}:

$$Q_{d\_Y} = Q_{SH\_Y} + Q_{DHW\_Y} \tag{A.40}$$

The annual Q_{SH_Y}, in MWh/yr, is calculated by to Eq. (A.41).

$$Q_{SH\_Y} = D_{SH} \cdot N \cdot S \cdot 10^{-3} \tag{A.41}$$

As explained in the opening of Section A.3, the SH monthly fractions $fm_{SH}(d)$ are determined according to the monthly heating-degree days method (Erbs et al., 1983; Frederiksen and Werner, 2013).

The monthly heating degree-days $DD_{SH\_M}(d)$, in °C·day/month, are assessed according to Eq.(A.42).

$$DD_{SH\_M}(d) = \left(\sum_{h=1}^{24} Max\left(T_{base\_SH} - T_a(d,h); 0\right) \right) \cdot \frac{NRY(d)}{24} \tag{A.42}$$

where T_{base_SH} is the reference temperature for the location of Zaragoza, considered 15 °C.

In accordance with Guadalfajara (2016), in order to avoid SH production when the demand is too low, the SH supplied is considered zero in those months in which the $DD_{SH\_M}(d)$ is lower than the number of days in the month $NRY(d)$:

If $DD_{SH\_M}(d) < NRY(d)$, then

$$DD'_{SH\_M}(d) = 0 \tag{A.43}$$

Else,

$$DD'_{SH\_M}(d) = DD_{SH\_M}(d) \tag{A.44}$$

Therefore, the SH monthly fraction $fm_{SH}(d)$ and the monthly demand $Q_{SH\_M}(d)$ are determined according to Eq. (A.45) and Eq. (A.46), respectively.

$$fm_{SH}(d) = \frac{DD'_{SH\_M}(d)}{\sum_{d=1}^{12} DD'_{SH\_M}(d)} \tag{A.45}$$

$$Q_{SH\_M}(d) = fm_{SH}(d) \cdot Q_{SH\_Y} \tag{A.46}$$

The daily SH demand $Q_{SH\_D}(d)$ of each representative day d is obtained by dividing the corresponding monthly value $Q_{SH\_M}(d)$ by the number of representative days type d in the year $NRY(d)$, as expressed by Eq. (A.47).

$$Q_{SH\_D}(d) = Q_{SH\_M}(d)/NRY(d) \tag{A.47}$$

Table A.18 shows the adjusted heating degree-days $DD'_{SH\_M}(d)$, the monthly fractions $fm_{SH}(d)$ and demands $Q_{SH\_M}(d)$, and the daily demands $Q_{SH\_D}(d)$.

Table A.18: Adjusted heating degree-days, and monthly and daily SH demands.

Representative day d	$DD'_{SH\_M}(d)$, °C·day/month	$fm_{SH}(d)$, -	$Q_{SH\_M}(d)$, MWh/month	$Q_{SH\_D}(d)$, MWh/day
1	260.40	0.2667	108.30	3.4934
2	190.40	0.1950	79.20	2.8280
3	105.40	0.1080	43.84	1.4140
4	40.03	0.0410	16.65	0.5549
5	0.00	0.0000	0.00	0.0000
6	0.00	0.0000	0.00	0.0000
7	0.00	0.0000	0.00	0.0000
8	0.00	0.0000	0.00	0.0000
9	0.00	0.0000	0.00	0.0000
10	0.00	0.0000	0.00	0.0000
11	132.00	0.1352	54.89	1.8299
12	248.00	0.2540	103.15	3.3271
Year, MWh/yr	976.23	1.0000	406.03	-

The hourly distribution of the daily SH demand $Q_{SH\_D}(d)$ was done according to Eq. (A.48). The hourly space heating demands $Q_{SH}(d,h)$ are given in Table A.21.

$$Q_{SH}(d,h) = fh_{SH}(d,h) \cdot Q_{SH\_D}(d) \tag{A.48}$$

In the case of the DHW, the volumetric annual V_{DHW_Y}, in m³/yr, and monthly $V_{DHW\_M}(d)$ demands are determined by to Eq. (A.49) and Eq. (A.50), respectively.

$$V_{DHW\_Y} = D_{DHW} \cdot N \cdot \frac{S}{apo} \cdot 365 \cdot 10^{-3} \tag{A.49}$$

$$V_{DHW\_M}(d) = fm_{VDHW}(d) \cdot V_{DHW\_Y} \tag{A.50}$$

The monthly fraction $fm_{VDHW}(d)$ was obtained from Viti (1996) and was given in Table A.11.

Based on the monthly volumetric value $V_{DHW\_M}(d)$, the monthly DHW energy demand $Q_{DHW\_M}(d)$, in MWh/month, are calculated considering the thermal input necessary to take the water from the supply network temperature $T_{CW}(d)$ to 60 °C (minimum temperature required of the DHW for sanitary reasons).

$$Q_{DHW\_M}(d) = V_{DHW\_M}(d) \cdot \rho \cdot cp \cdot (60 - T_{CW}(d)) \cdot \frac{1}{3600} \cdot 10^{-3} \tag{A.51}$$

where, the density of the liquid water is ρ = 1000 kg/m³, and the specific heat of the liquid water is c_p = 4.18 kJ/(kg·K).

The DHW annual demand Q_{DHW_Y} corresponds to the sum of its monthly components, as expressed by Eq. (A.52). The DHW daily demand $Q_{DHW\_D}(d)$ is obtained according to Eq. (A.53) and the DHW hourly demand $Q_{DHW}(d,h)$ is obtained from Eq. (A.54).

$$Q_{DHW\_Y} = \sum_{d=1}^{12} Q_{DHW\_M}(d) \tag{A.52}$$

$$Q_{DHW\_D}(d) = Q_{DHW\_M}(d)/NRY(d) \tag{A.53}$$

$$Q_{DHW}(d,h) = fh_{DHW}(d,h) \cdot Q_{DHW\_D}(d) \tag{A.54}$$

The DHW annual Q_{DHW_Y}, monthly $Q_{DHW\_M}(d)$ and daily $Q_{DHW}(d)$ demands for the representative days d of the months of the year are presented in Table A.19. The hourly DHW demands $Q_{DHW}(d,h)$ are given in Table A.22.

Table A.19: Monthly and daily DHW demands.

Representative day d	$Q_{DHW\_M}(d)$, MWh/month	$Q_{DHW\_D}(d)$, MWh/day
1	17.62	0.5685
2	15.07	0.5382
3	15.59	0.5030
4	15.33	0.5109
5	14.16	0.4568
6	12.72	0.4240
7	10.90	0.3514
8	9.68	0.3122
9	11.46	0.3822
10	13.09	0.4221
11	14.93	0.4978
12	16.92	0.5458
Year Q_{DHW_Y}, MWh/yr	167.49	-

Finally, the heating demands are obtained by adding up the SH and the DHW components. Table A.20 presents the annual Q_{d_Y}, monthly $Q_{d\_M}(d)$, daily $Q_{d\_D}(d)$ heating demands. The hourly values $Q_d(d,h)$ for the hourly periods h of the representative days d are given in Table A.23.

Table A.20: Monthly and daily heating demands.

Representative day d	$Q_{d\_M}(d)$, MWh/month	$Q_{d\_D}(d)$, MWh/day
1	125.92	4.0619
2	94.27	3.3662
3	59.42	1.9170
4	31.98	1.0658
5	14.16	0.4568
6	12.72	0.4240
7	10.90	0.3514
8	9.68	0.3122
9	11.46	0.3822
10	13.09	0.4221
11	69.83	2.3277
12	120.07	3.8729
Year Q_{d_Y}, MWh/yr	573.50	-

Table A.21: Hourly SH demand for each representative day, kW.

Hour	Jan	Feb	Mar	Apr	May	Jun	Jul	Aug	Sep	Oct	Nov	Dec
1	0.00	0.00	0.00	0.00	-	-	-	-	-	-	0.00	0.00
2	0.00	0.00	0.00	0.00	-	-	-	-	-	-	0.00	0.00
3	0.00	0.00	0.00	0.00	-	-	-	-	-	-	0.00	0.00
4	0.00	0.00	0.00	0.00	-	-	-	-	-	-	0.00	0.00
5	0.00	0.00	0.00	0.00	-	-	-	-	-	-	0.00	0.00
6	0.00	0.00	0.00	0.00	-	-	-	-	-	-	0.00	0.00
7	273.90	231.10	126.30	53.60	-	-	-	-	-	-	151.50	284.50
8	264.10	222.60	121.70	51.70	-	-	-	-	-	-	146.00	274.20
9	248.40	209.30	114.40	48.60	-	-	-	-	-	-	137.20	257.50
10	232.00	195.70	107.00	45.40	-	-	-	-	-	-	128.50	240.90
11	221.50	186.60	102.10	43.30	-	-	-	-	-	-	122.40	229.90
12	214.80	181.00	99.00	42.00	-	-	-	-	-	-	118.80	222.90
13	204.00	171.90	94.00	40.00	-	-	-	-	-	-	112.90	211.90
14	197.70	166.60	91.10	38.70	-	-	-	-	-	-	109.20	204.90
15	186.60	157.20	86.00	36.50	-	-	-	-	-	-	103.20	193.60
16	171.90	145.10	79.30	33.70	-	-	-	-	-	-	95.20	178.70
17	250.80	151.90	59.40	16.00	-	-	-	-	-	-	96.40	184.00
18	243.50	175.30	62.90	16.00	-	-	-	-	-	-	109.20	183.30
19	213.10	179.00	73.70	21.90	-	-	-	-	-	-	115.10	183.70
20	212.40	164.60	74.00	22.70	-	-	-	-	-	-	114.20	181.70
21	160.70	123.90	46.80	16.50	-	-	-	-	-	-	67.20	131.80
22	198.10	166.60	76.40	28.40	-	-	-	-	-	-	102.80	164.00
23	0.00	0.00	0.00	0.00	-	-	-	-	-	-	0.00	0.00
24	0.00	0.00	0.00	0.00	-	-	-	-	-	-	0.00	0.00

Table A.22: Hourly DHW demand for each representative day, kW.

Hour	Jan	Feb	Mar	Apr	May	Jun	Jul	Aug	Sep	Oct	Nov	Dec
1	5.80	5.50	5.10	5.20	4.70	4.30	3.60	3.20	3.90	4.30	5.10	5.60
2	4.00	3.80	3.50	3.60	3.20	3.00	2.50	2.20	2.70	3.00	3.50	3.80
3	4.00	3.80	3.50	3.60	3.20	3.00	2.50	2.20	2.70	3.00	3.50	3.80
4	4.00	3.80	3.50	3.60	3.20	3.00	2.50	2.20	2.70	3.00	3.50	3.80
5	9.30	8.80	8.20	8.40	7.50	7.00	5.80	5.10	6.30	6.90	8.20	9.00
6	15.10	14.30	13.40	13.60	12.20	11.30	9.30	8.30	10.20	11.20	13.20	14.50
7	22.20	21.00	19.70	20.00	17.90	16.60	13.70	12.20	14.90	16.50	19.50	21.30
8	38.00	36.00	33.60	34.10	30.50	28.30	23.50	20.90	25.50	28.20	33.30	36.50
9	42.40	40.10	37.50	38.10	34.10	31.60	26.20	23.30	28.50	31.50	37.10	40.70
10	21.30	20.20	18.90	19.20	17.10	15.90	13.20	11.70	14.30	15.80	18.70	20.50
11	16.00	15.10	14.10	14.40	12.80	11.90	9.90	8.80	10.70	11.90	14.00	15.30
12	13.30	12.60	11.80	12.00	10.70	9.90	8.20	7.30	8.90	9.90	11.60	12.80
13	12.90	12.20	11.40	11.60	10.40	9.60	8.00	7.10	8.70	9.60	11.30	12.40
14	32.00	30.30	28.30	28.80	25.70	23.90	19.80	17.60	21.50	23.80	28.00	30.70
15	18.20	17.20	16.10	16.30	14.60	13.60	11.20	10.00	12.20	13.50	15.90	17.50
16	19.10	18.10	16.90	17.20	15.30	14.20	11.80	10.50	12.80	14.20	16.70	18.30
17	20.40	19.30	18.10	18.30	16.40	15.20	12.60	11.20	13.70	15.20	17.90	19.60
18	48.40	45.90	42.90	43.50	38.90	36.10	29.90	26.60	32.60	36.00	42.40	46.50
19	99.90	94.60	88.40	89.80	80.30	74.50	61.80	54.90	67.20	74.20	87.50	96.00
20	49.30	46.70	43.60	44.30	39.60	36.80	30.50	27.10	33.10	36.60	43.20	47.30
21	34.60	32.80	30.60	31.10	27.80	25.80	21.40	19.00	23.30	25.70	30.30	33.20
22	14.20	13.50	12.60	12.80	11.40	10.60	8.80	7.80	9.60	10.60	12.40	13.60
23	10.70	10.10	9.50	9.60	8.60	8.00	6.60	5.90	7.20	7.90	9.40	10.30
24	13.30	12.60	11.80	12.00	10.70	9.90	8.20	7.30	8.90	9.90	11.60	12.80

Table A.23: Hourly heating demand for each representative day, kW.

Hour	Jan	Feb	Mar	Apr	May	Jun	Jul	Aug	Sep	Oct	Nov	Dec
1	5.80	5.50	5.10	5.20	4.70	4.30	3.60	3.20	3.90	4.30	5.10	5.60
2	4.00	3.80	3.50	3.60	3.20	3.00	2.50	2.20	2.70	3.00	3.50	3.80
3	4.00	3.80	3.50	3.60	3.20	3.00	2.50	2.20	2.70	3.00	3.50	3.80
4	4.00	3.80	3.50	3.60	3.20	3.00	2.50	2.20	2.70	3.00	3.50	3.80
5	9.30	8.80	8.20	8.40	7.50	7.00	5.80	5.10	6.30	6.90	8.20	9.00
6	15.10	14.30	13.40	13.60	12.20	11.30	9.30	8.30	10.20	11.20	13.20	14.50
7	296.10	252.10	145.90	73.60	17.90	16.60	13.70	12.20	14.90	16.50	171.00	305.80
8	302.10	258.50	155.30	85.80	30.50	28.30	23.50	20.90	25.50	28.20	179.30	310.60
9	290.80	249.40	151.90	86.70	34.10	31.60	26.20	23.30	28.50	31.50	174.40	298.20
10	253.30	215.90	125.90	64.50	17.10	15.90	13.20	11.70	14.30	15.80	147.10	261.30
11	237.50	201.80	116.20	57.70	12.80	11.90	9.90	8.80	10.70	11.90	136.40	245.20
12	228.10	193.60	110.80	54.00	10.70	9.90	8.20	7.30	8.90	9.90	130.40	235.70
13	216.90	184.20	105.40	51.60	10.40	9.60	8.00	7.10	8.70	9.60	124.20	224.30
14	229.70	196.90	119.40	67.40	25.70	23.90	19.80	17.60	21.50	23.80	137.30	235.70
15	204.70	174.50	102.10	52.80	14.60	13.60	11.20	10.00	12.20	13.50	119.10	211.10
16	191.00	163.20	96.20	50.80	15.30	14.20	11.80	10.50	12.80	14.20	111.90	197.00
17	271.20	171.20	77.40	34.30	16.40	15.20	12.60	11.20	13.70	15.20	114.30	203.60
18	291.90	221.20	105.80	59.50	38.90	36.10	29.90	26.60	32.60	36.00	151.70	229.80
19	313.00	273.60	162.10	111.70	80.30	74.50	61.80	54.90	67.20	74.20	202.60	279.60
20	261.70	211.30	117.60	67.00	39.60	36.80	30.50	27.10	33.10	36.60	157.30	229.00
21	195.30	156.60	77.40	47.70	27.80	25.80	21.40	19.00	23.30	25.70	97.50	165.00
22	212.30	180.00	88.90	41.20	11.40	10.60	8.80	7.80	9.60	10.60	115.30	177.70
23	10.70	10.10	9.50	9.60	8.60	8.00	6.60	5.90	7.20	7.90	9.40	10.30
24	13.30	12.60	11.80	12.00	10.70	9.90	8.20	7.30	8.90	9.90	11.60	12.80

A.3.3　Cooling demand

Following the procedure described in the opening of Section A.3, Equations (A.55)-(A.58) determine, respectively, the annual R_{d_Y}, in MWh/yr, the monthly $R_{d\_M}(d)$, the daily $R_{d\_D}(d)$, and the hourly cooling demand $R_d(d,h)$.

$$R_{d\_Y} = D_{REF} \cdot N \cdot S \cdot 10^{-3} \tag{A.55}$$
$$R_{d\_M}(d) = fm_{Rd}(d) \cdot R_{d\_Y} \tag{A.56}$$
$$R_{d\_D}(d) = R_{d\_M}(d) \,/NRY(d) \tag{A.57}$$
$$R_d(d,h) = fh_{Rd}(d,h) \cdot R_{d\_D}(d) \tag{A.58}$$

The monthly $fm_{Rd}(d)$ and the hourly $fh_{Rd}(d,h)$ factors were obtained from Ramos (2012) and were given in Table A.11 and Table A.15, respectively.

The annual R_{d_Y}, monthly $R_{d\_M}(d)$ and daily $R_{d\_D}(d)$ cooling demands for the representative days d of the months of the year are presented in Table A.24. The hourly cooling demands $R_d(d,h)$ are given in Table A.25.

Table A.24: Annual, monthly, and daily electricity demands.

Representative day d	$R_{d\_M}(d)$, MWh/month	$R_{d\_D}(d)$, MWh/day
1	0.00	0.0000
2	0.00	0.0000
3	0.00	0.0000
4	0.00	0.0000
5	0.00	0.0000
6	16.80	0.5600
7	47.69	1.5387
8	35.47	1.1445
9	14.03	0.4673
10	0.00	0.0000
11	0.00	0.0000
12	0.00	0.0000
Year R_{d_Y}, MWh/yr	113.99	-

Table A.25: Cooling demand values for each representative day, kW.

Hour	Jan	Feb	Mar	Apr	May	Jun	Jul	Aug	Sep	Oct	Nov	Dec
1	-	-	-	-	-	0.00	0.00	0.00	0.00	-	-	-
2	-	-	-	-	-	0.00	0.00	0.00	0.00	-	-	-
3	-	-	-	-	-	0.00	0.00	0.00	0.00	-	-	-
4	-	-	-	-	-	0.00	0.00	0.00	0.00	-	-	-
5	-	-	-	-	-	0.00	0.00	0.00	0.00	-	-	-
6	-	-	-	-	-	0.00	0.00	0.00	0.00	-	-	-
7	-	-	-	-	-	0.00	0.00	0.00	0.00	-	-	-
8	-	-	-	-	-	0.00	0.00	0.00	0.00	-	-	-
9	-	-	-	-	-	0.00	0.00	0.00	0.00	-	-	-
10	-	-	-	-	-	0.00	0.00	0.00	0.00	-	-	-
11	-	-	-	-	-	0.00	0.00	0.00	0.00	-	-	-
12	-	-	-	-	-	32.30	89.20	66.60	27.70	-	-	-
13	-	-	-	-	-	41.40	114.50	85.50	35.50	-	-	-
14	-	-	-	-	-	49.30	136.30	101.70	42.30	-	-	-
15	-	-	-	-	-	74.30	205.10	153.10	63.60	-	-	-
16	-	-	-	-	-	141.50	266.60	236.10	128.30	-	-	-
17	-	-	-	-	-	129.10	234.90	202.20	109.70	-	-	-
18	-	-	-	-	-	31.40	129.60	81.90	23.50	-	-	-
19	-	-	-	-	-	23.10	110.80	67.20	13.90	-	-	-
20	-	-	-	-	-	13.70	89.50	54.90	8.80	-	-	-
21	-	-	-	-	-	11.50	91.20	53.70	7.70	-	-	-
22	-	-	-	-	-	12.30	70.80	41.40	6.50	-	-	-
23	-	-	-	-	-	0.00	0.00	0.00	0.00	-	-	-
24	-	-	-	-	-	0.00	0.00	0.00	0.00	-	-	-

A.4 TECHNICAL DATA

This section elaborates the technical data that are used as input data to the multi-objective optimization model developed in Chapter 4. First, the technical specifications of the technologies included in the superstructure of the trigeneration system are given in Section A.4.1. Then, taking into account the local climatic data calculated in Section A.2, Section A.4.2 evaluates adjustment factors to correct the operation performance of the reversible heat pump and the single-effect absorption chiller; and Section A.4.3 assesses the hourly specific productions of the photovoltaic panels and solar thermal collectors per m² of module installed. Lastly, Section A.4.4 estimates the rooftop area usage of the aforementioned solar energy technologies based on the consumer center's building characteristics.

A.4.1 Technical specifications of the technologies in the superstructure

The superstructure of the trigeneration system analyzed in Chapter 4 is composed of a cogeneration module GE, a gas boiler GB, a simple-effect absorption chiller ABS, a reversible heat pump HP, photovoltaic panels PV, flat-plate solar thermal collectors ST, a hot water storage tank TSQ, and a chilled water storage tank TSR. These technologies are all based on real, commercially available devices, whose technical specifications at nominal conditions are presented in Table A.26 to Table A.32. The selection of the devices and their corresponding capacities has been made in accordance with the types, quantities, and qualities of energy demands of the consumer center. In Chapter 4, the technical coefficients will be considered constant as provided herein, while the installed capacities will be free in the optimization process.

Table A.26: Technical specifications – cogeneration module GE.

Technical specifications at nominal operation		
Manufacturer	-	Senertec
Model	-	Dachs
Fuel	-	Natural gas
Fuel consumption (LHV)	kW	20.50
Electrical power	kW	5.50
Thermal power	kW	12.50
Auxiliary electric consumption	kW	0.12
Electrical efficiency	%	26
Thermal efficiency	%	61
Overall efficiency	%	88

Table A.27: Technical specifications – gas boiler GB.

Technical specifications at nominal operation		
Manufacturer	-	Baxi
Model	-	CPA-BTH 100
Fuel	-	Natural gas
Thermal power	kW	100
Thermal efficiency (LHV)	%	95

Table A.28: Technical specifications – single-effect absorption chiller ABS.

Technical specifications at nominal operation		
Manufacturer	-	Thermax
Model	-	Cogenie
Heat source	-	Hot water
Cooling capacity	kW	105
Coefficient of performance	-	0.69
Unit electricity consumption	-	0.03
Inlet/outlet chilled water temperatures	°C	12.2 / 6.7
Inlet/outlet cooling water temperatures	°C	29.4 / 36.6
Inlet/outlet hot water temperatures	°C	90.6 / 85.0
Chilled water flow rate	m³/h	16.5
Cooling water flow rate	m³/h	30.0
Hot water flow rate	m³/h	23.2

Table A.29: Technical specifications – reversible heat pump HP.

Technical specifications at nominal operation		
Manufacturer	-	Ferroli
Model	-	RLA HE
Type	-	Air-Water
Heating mode		
Heating capacity	kW	242.0
Absorbed power	kW	74.6
Coefficient of performance	-	3.24
Ambient air temperature	°C	7
Inlet/outlet hot water temperatures	°C	40 / 45
Cooling mode		
Cooling capacity	kW	234.0
Absorbed power	kW	73.3
Energy efficiency ratio	-	3.19
Ambient air temperature	°C	35
Inlet/outlet chilled water temperatures	°C	12 / 7

Table A.30: Technical specifications – photovoltaic panels PV.

Technical specifications at nominal operation		
Manufacturer	-	SolarWorld
Model	-	SW 260 poly
Module length	m	1.675
Module width	m	1.001
Surface area	m^2	1.67
Maximum power	kW	0.26
Module efficiency	%	15.51
Temperature coefficient of power	$°C^{-1}$	0.0041
Irradiation at SRC conditions	kW/m^2	1.00
Cell temperature at SRC conditions	°C	25
Ambient temperature at NOCT conditions	°C	20
Cell temperature at NOCT conditions	°C	47
Irradiation at NOCT conditions	kW/m^2	0.80

Table A.31: Technical specifications – flat-plate solar thermal collectors ST.

Technical specifications at nominal operation		
Manufacturer	-	Solar Energy
Model	-	GK 5000
Module length	m	2.059
Module width	m	2.441
Surface area	m^2	5.04
Thermal coefficient k_0	-	0.789
Thermal coefficient k_1	$W/(m^2{\cdot}K)$	3.834
Thermal coefficient k_2	$W/(m^2{\cdot}K^2)$	0.011

Table A.32: Technical specifications –hot water TSQ and chilled water TSR storage tanks.

Technical specifications at nominal operation		
Manufacturer	-	Idrogas
Capacity	m^3	5
Energy loss factor	h^{-1}	0.01

A.4.2 Adjustment factors estimation

The technical specifications of the technologies provided in Section A.4.1 are for nominal operation conditions. Nevertheless, different operation conditions than the nominal have been considered for some of the technologies included in the superstructure, thus affecting their performances. In particular, the reversible heat pump HP and the single-effect absorption chiller ABS are highly susceptible to changes in, for example, the ambient air temperature, which is considered to change on hourly and monthly basis.

Therefore, it is proposed herein to assess the adjustment factors for the operation at off-design conditions of the ABS (Section A.4.2.1) and the HP (Section A.4.2.2).

A.4.2.1   Adjustment factors for the ABS

Table A.33 presents the ABS's operation parameters at nominal conditions and the ones considered in the case study. As can be seen, based on the technical specifications provided in Table A.28, the nominal operation of the ABS considers: (i) a constant inlet cooling water temperature of 29.4 °C; (ii) a constant inlet hot water temperature of 90.6 °C; and (iii) a constant temperature difference in the hot water circuit of 5.6 °C. On the other hand, for the case study: (i) the inlet cooling water temperature $T_{cw,in}(d,h)$ is considered to vary on hourly and monthly basis, being estimated by a simple model of an evaporative cooling tower to be 5 °C above the hourly wet-bulb temperature $Twb(d,h)$ (calculated in Section A.2.1); (ii) the inlet hot water temperature $T_{hw,in}$ is equal to 85 °C; and (iii) the temperature difference in the hot water circuit ΔT_{hw} is equal to 10 °C.

Table A.33: Operation conditions for the ABS.

Parameter	Nominal	Case study
Inlet cooling water temperature	29.4 °C	$T_{cw,in}(d,h) = Twb(d,h) + 5\,°C$
Inlet hot water temperature	90.6 °C	85 °C
Temperature difference in the hot water circuit	5.6 °C	10 °C

Therefore, the ABS's cooling capacity and COP must be adjusted according to the three aforementioned parameters. Nevertheless, due to a lack of technical information provided by the manufacturer, the COP of the ABS was considered constant regardless of the operation conditions.

The adjustment factor for the cooling capacity $fCAP_{abs}(d,h)$ is composed of three terms:

$$fCAP_{abs}(d, h) = fcapa_{Thw,in} \cdot fcapa_{\Delta Thw} \cdot fcapa_{Tcw,in}(d, h) \tag{A.59}$$

where $fcapa_{Thw,in}$, $fcapa_{\Delta Thw}$, and $fcapa_{Tcw,in}(d,h)$ are the adjustment factors relative to the $T_{hw,in}$, ΔT_{hw}, and $T_{cw,in}(d,h)$, respectively.

These adjustment factors for the cooling capacity are determined by the graphs in Figure A.5, obtained from the manufacturer's catalogues. The corresponding adjustment factors are given in Table A.34.
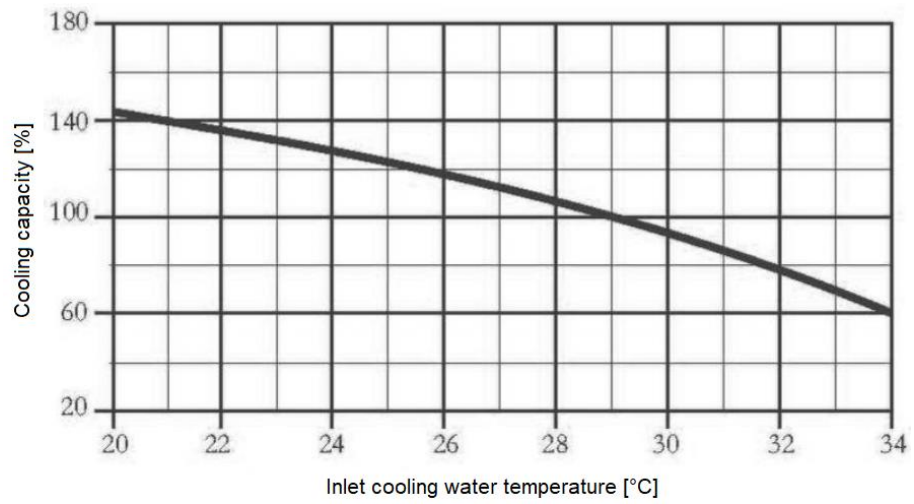
(a)
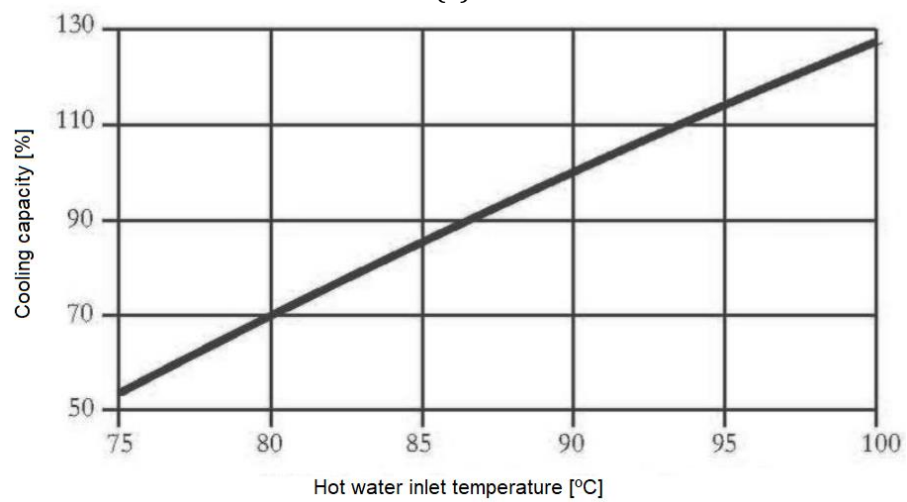
(b)
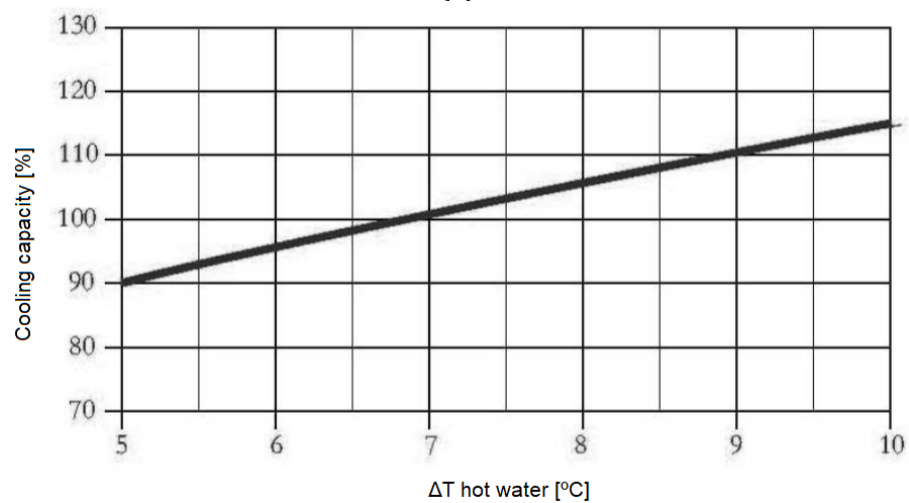
(c)

Figure A.5: Adjustment factors for the absorption chiller's capacity: (a) inlet cooling water temperature; (b) inlet hot water temperature; and (c) temperature difference in the hot water circuit.

Table A.34: Adjustment factors for the absorption chiller's cooling capacity.

Adjustment factor	Value
$fcapa_{Thw,in}$	0.87
$fcapa_{\Delta Thw}$	1.15
$fcapa_{Tcw,in}(d,h)$	See Eq. (A.60)

In the case of the $fcapa_{Tcw,in}(d,h)$, Eq. (A.60) was obtained by drawing the adjustment factors from Figure A.5 (a) in a Parametric Table and regressing them as a function of $T_{cw,in}$ using the linear regression tool from the software EES (2017).

$$fcapa_{Tcw,in}(d,h) = 0.3311 + 0.1211 \cdot T_{cw,in}(d,h) - 0.0033 \cdot T^2_{cw,in}(d,h) \tag{A.60}$$

It should be noted that Figure A.5 (a) has an inlet cooling water temperature range from 20 to 34 °C. Given that the $T_{cw,in}(d,h)$ may be higher or lower than that in certain hours of the day:

If $T_{cw,in}(d,h) \leq 20\,°C$, then $T_{cwl,in}(d,h) = 20\,°C$

If $T_{cw,in}(d,h) \geq 34\,°C$, then $T_{cwl,in}(d,h) = 34\,°C$

Finally, Eq. (A.59) can be rewritten as:

$$fCAP_{abs}(d,h) = 0.3311 + 0.1211 \cdot T_{cwl,in}(d,h) - 0.0033 \cdot T^2_{cwl,in}(d,h) \tag{A.61}$$

The results obtained for each hourly period of each representative day are presented in Table A.38.

A.4.2.2 Adjustment factors for the HP

The HP has two operation modes: heating HPQ and cooling HPR modes. Regarding the heating mode, Table A.35 presents the operation parameters at nominal conditions and the ones considered in the case study. As can be seen, based on the technical specifications provided in Table A.29, the nominal operation of the HP in heating mode considers: (i) a constant ambient air temperature of 7 °C; and (ii) the production of hot water at 45 °C. On the other hand, for the case study: (i) the ambient air temperature $Ta(d,h)$ is supposed to change on hourly and monthly basis, as calculated in Section A.2.1; and (ii) the hot water is produced at $T_{hw,out}$ = 55 °C.

Table A.35: Operation conditions for the heat pump in heating mode.

Parameter	Nominal	Case study
Ambient air temperature	7 °C	$Ta(d,h)$
Outlet hot water temperature	45 °C	55 °C

Therefore, the HP's heating capacity and COP must be adjusted according to these two parameters. The manufacturer provides two graphs with adjustment factors for the heating capacity *fcapq* and absorbed power *fconq*, which are depicted in Figure A.6.
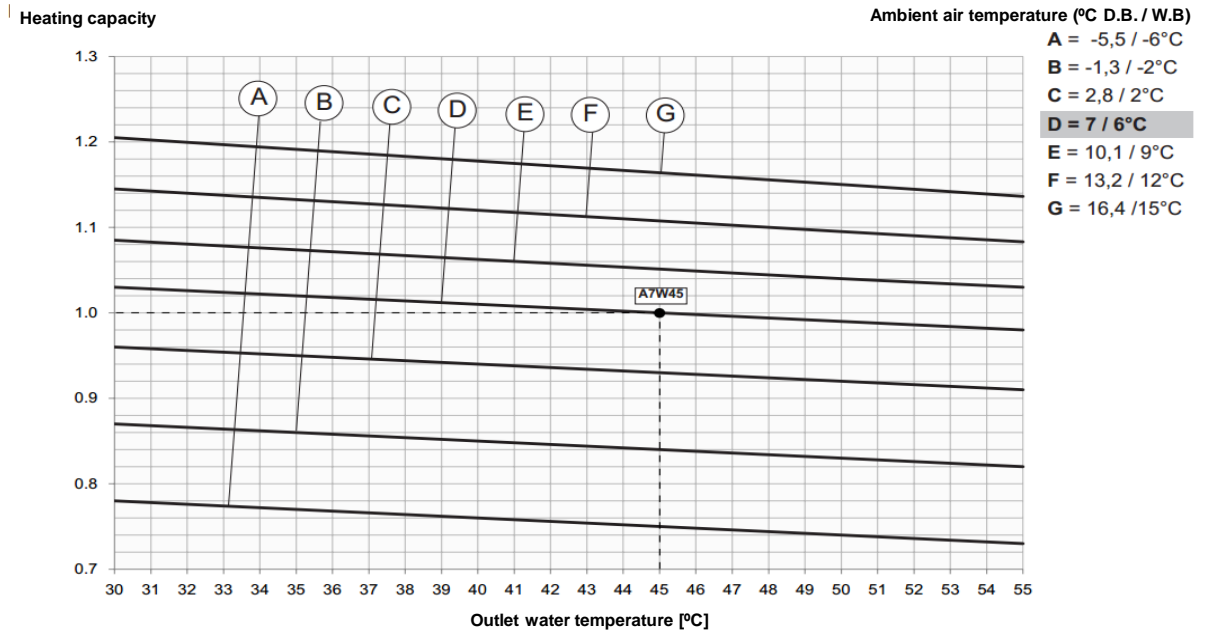
(a)
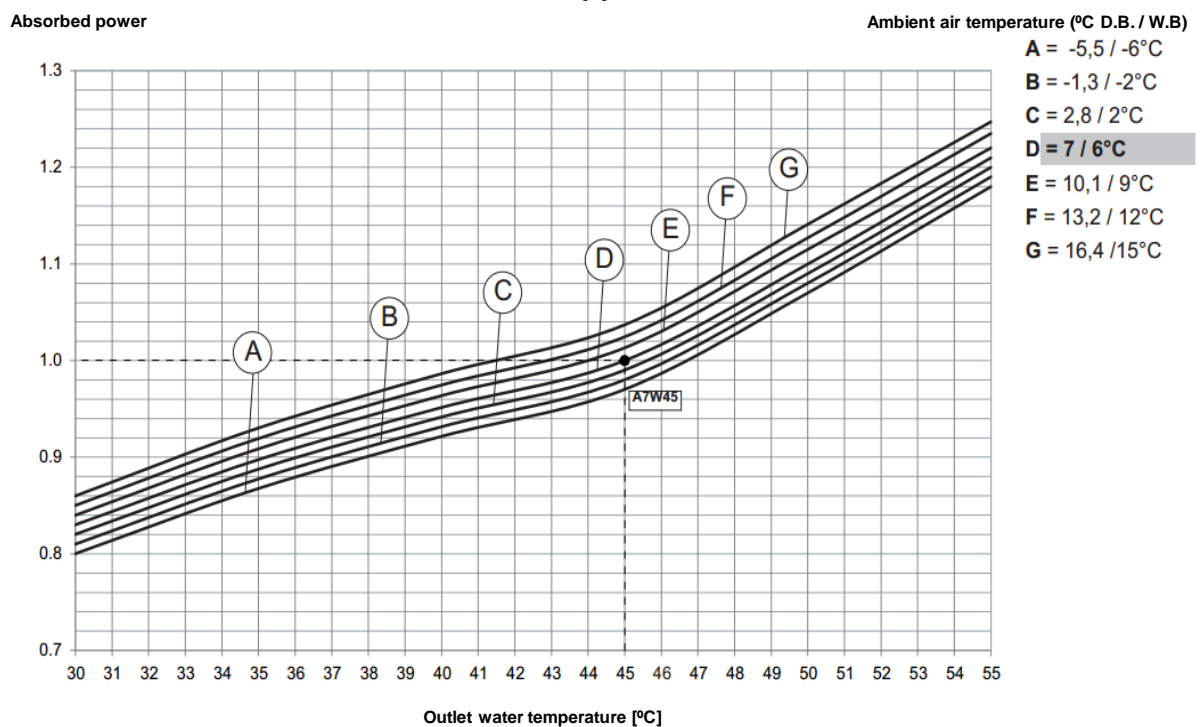
(b)

Figure A.6: Adjustment factors for the heat pump's (a) capacity and (b) absorbed power, in heating mode.

For the outlet hot water temperature of 55 °C, the corresponding adjustment factors are given in Table A.36. The adjustment factor of the COP *fcopq* is determined as the division *fcapq/fconq*.

Table A.36: Adjustment factors for the heat pump in heating mode, $T_{hw,out}$ = 55 °C.

Ambient air temperature Ta	Adjustment factor for the heating capacity $fcapq$	Adjustment factor for the absorbed power $fconq$	Adjustment factor for the COP $fcopq$
-5.5	0.73	1.18	0.62
-1.3	0.82	1.19	0.69
2.8	0.91	1.20	0.76
7	0.98	1.21	0.81
10.1	1.03	1.22	0.84
13.2	1.08	1.23	0.88
16.4	1.13	1.25	0.91

Similar to the procedure described for the ABS in Section A.4.2.1, the adjustment factors for the HP's capacity *fCAP_hpq(d,h)* and COP *fCOP_hpq(d,h)* in heating mode were obtained by drawing their values in a Parametric Table and regressing them as a function of *Ta* using the linear regression tool from the software EES (2017).

$$fCAP_{hpq}(d, h) = 0.8435 + 0.0184 \cdot Ta(d, h) \tag{A.62}$$
$$fCOP_{hpq}(d, h) = 0.7050 + 0.0133 \cdot Ta(d, h) \tag{A.63}$$

It should be noted that Figure A.6 (a) and (b) have an ambient air temperature range from -5.5 to 16.4 °C. Given that *Ta(d,h)* may be higher than that in certain hours of the day:

If $Ta(d, h) \geq 16.4\,°C$,

Then, $fCAP_{hpq}(d, h) = fcapq(16.4\,°C)$ and $fCOP_{hpq}(d, h) = fcopq(16.4\,°C)$

The *fCAP_hpq(d,h)* and *fCOP_hpq(d,h)* obtained for each hourly period of each representative day are presented in Table A.39 and Table A.40, respectively.

Regarding the cooling mode, the only difference in the operation conditions is the hourly ambient temperature: its nominal value is a constant 35 °C, while it is considered that *Ta(d,h)* varies on hourly and monthly basis, as previously explained.

Thus, the HP's cooling capacity and EER must be adjusted according to the ambient air temperature. Figure A.7 presents the adjustment factors for the cooling capacity *fcapr* and absorbed power *fconr* obtained from the manufacturer's catalogues.
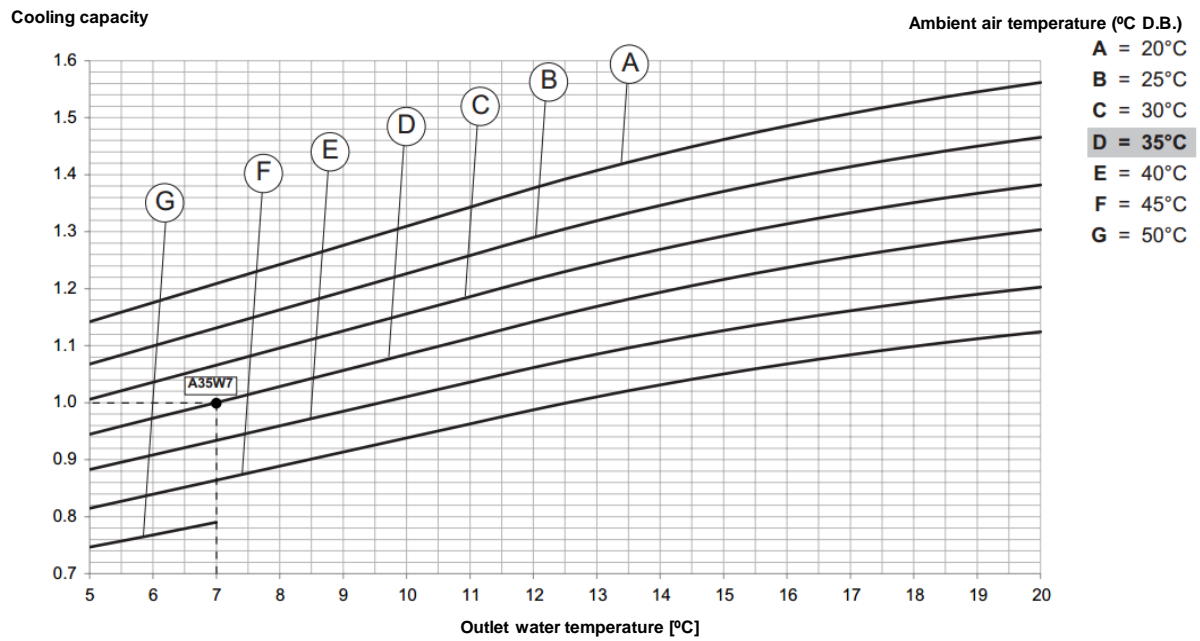
(a)
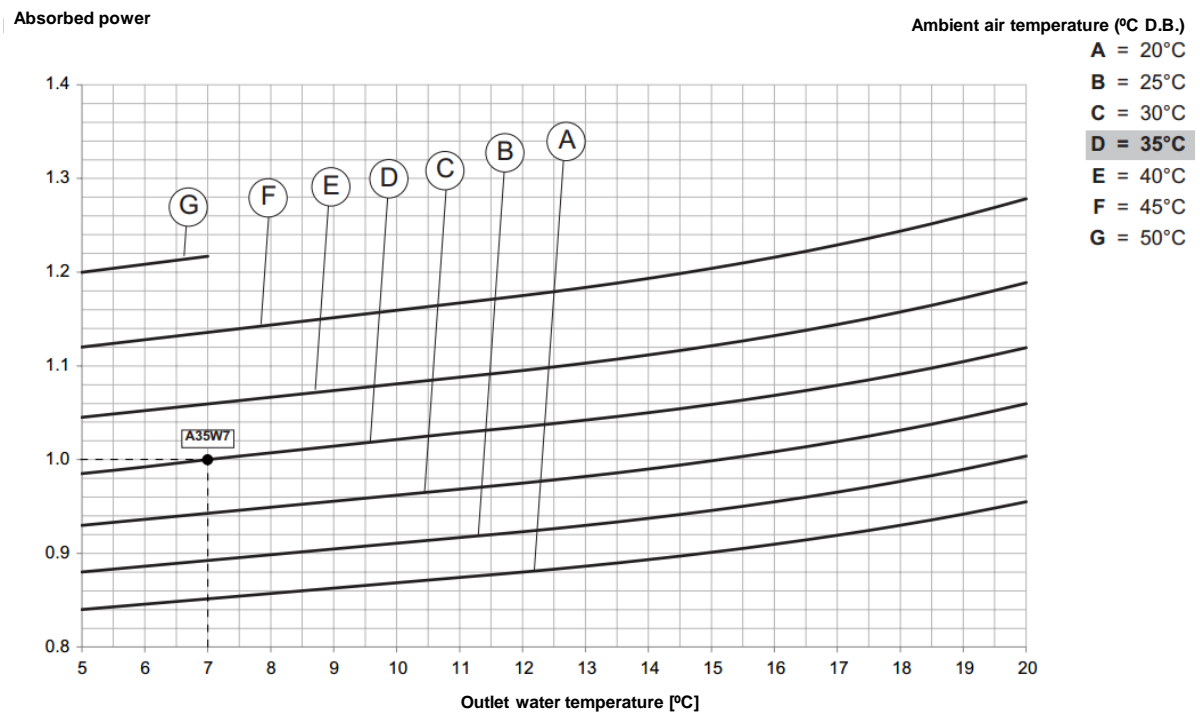
(b)

Figure A.7: Correction factors for the heat pump's (a) capacity and (b) absorbed power, in cooling mode.

Table A.37 presents the adjustment factors *fcapr* and *fconr* for the nominal chilled water production temperature of 7 °C. The adjustment factor of the EER *feerr* is determined as the division *fcapr/fconr*.

Table A.37: Adjustment factors for the heat pump in cooling mode.

Ambient air temperature Ta	Adjustment factor for the heating capacity fcapr	Adjustment factor for the absorbed power fconr	Adjustment factor for the EER feerr
20	1.21	0.85	1.42
25	1.13	0.89	1.27
30	1.07	0.94	1.14
35	1.00	1.00	1.00
40	0.94	1.06	0.88
45	0.86	1.14	0.76
50	0.79	1.22	0.65

Analogous to the heating mode, for each hourly period h of each representative day d, the adjustment factors for the HP's capacity $fCAP_{hpr}(d,h)$ and EER $fEER_{hpr}(d,h)$ in cooling mode are obtained by Eq. (A.64) and Eq. (A.65).

$$fCAP_{hpr}(d,h) = 1.4825 - 0.0138 \cdot Ta(d,h) \tag{A.64}$$
$$fEER_{hpr}(d,h) = 1.9146 - 0.0256 \cdot Ta(d,h) \tag{A.65}$$

It should be noted that Figure A.7 (a) and (b) have an ambient air temperature range from 20 to 50 °C. Given that $Ta(d,h)$ may be lower than that in certain hours of the day:

If $Ta(d,h) \leq 20 \,°C$,

Then, $fCAP_{hpr}(d,h) = fcapr(20 \,°C)$ and $fEER_{hpr}(d,h) = feerr(20 \,°C)$

The $fCAP_{hpr}(d,h)$ and $fEER_{hpr}(d,h)$ obtained for each hourly period of each representative day are presented in Table A.41 and Table A.42, respectively.

Table A.38: Hourly adjustment factors for the cooling capacity of the absorption chiller $fCAP_{abs}$.

Hour	Jan	Feb	Mar	Apr	May	Jun	Jul	Aug	Sep	Oct	Nov	Dec
1	1.4300	1.4300	1.4300	1.4300	1.4300	1.4300	1.4300	1.4300	1.4300	1.4300	1.4300	1.4300
2	1.4300	1.4300	1.4300	1.4300	1.4300	1.4300	1.4300	1.4300	1.4300	1.4300	1.4300	1.4300
3	1.4300	1.4300	1.4300	1.4300	1.4300	1.4300	1.4300	1.4300	1.4300	1.4300	1.4300	1.4300
4	1.4300	1.4300	1.4300	1.4300	1.4300	1.4300	1.4300	1.4300	1.4300	1.4300	1.4300	1.4300
5	1.4300	1.4300	1.4300	1.4300	1.4300	1.4300	1.4300	1.4300	1.4300	1.4300	1.4300	1.4300
6	1.4300	1.4300	1.4300	1.4300	1.4300	1.4300	1.4300	1.4300	1.4300	1.4300	1.4167	1.4117
7	1.3929	1.3942	1.3953	1.3962	1.3971	1.3974	1.3965	1.3941	1.3898	1.3842	1.3780	1.3722
8	1.3785	1.3799	1.3810	1.3820	1.3829	1.3832	1.3823	1.3797	1.3752	1.3694	1.3631	1.3572
9	1.4169	1.4176	1.4182	1.4188	1.4300	1.4300	1.4190	1.4176	1.4151	1.4117	1.4079	1.4042
10	1.4300	1.4300	1.4300	1.4300	1.4300	1.4300	1.4300	1.4300	1.4300	1.4300	1.4300	1.4300
11	1.4300	1.4300	1.4300	1.4300	1.4300	1.4300	1.4300	1.4300	1.4300	1.4300	1.4300	1.4300
12	1.4300	1.4300	1.4300	1.4300	1.4300	1.4300	1.4300	1.4300	1.4300	1.4300	1.4300	1.4300
13	1.4300	1.4300	1.4300	1.4300	1.4300	1.4300	1.4300	1.4300	1.4300	1.4300	1.4300	1.4300
14	1.4300	1.4300	1.4300	1.4300	1.4300	1.4300	1.4300	1.4300	1.4300	1.4300	1.4300	1.4300
15	1.4300	1.4300	1.4300	1.4300	1.4300	1.4300	1.4300	1.4300	1.4300	1.4300	1.4300	1.4300
16	1.4300	1.4300	1.4300	1.4300	1.4300	1.4300	1.4300	1.4300	1.4300	1.4300	1.4300	1.4300
17	1.4300	1.4300	1.4300	1.4300	1.4300	1.4300	1.4300	1.4300	1.4300	1.4300	1.4300	1.4300
18	1.4300	1.4300	1.4300	1.4300	1.4300	1.4300	1.4300	1.4300	1.4300	1.4300	1.4167	1.4117
19	1.3929	1.3942	1.3953	1.3962	1.3971	1.3974	1.3965	1.3941	1.3898	1.3842	1.3780	1.3722
20	1.3785	1.3799	1.3810	1.3820	1.3829	1.3832	1.3823	1.3797	1.3752	1.3694	1.3631	1.3572
21	1.4169	1.4176	1.4182	1.4188	1.4300	1.4300	1.4190	1.4176	1.4151	1.4117	1.4079	1.4042
22	1.4300	1.4300	1.4300	1.4300	1.4300	1.4300	1.4300	1.4300	1.4300	1.4300	1.4300	1.4300
23	1.4300	1.4300	1.4300	1.4300	1.4300	1.4300	1.4300	1.4300	1.4300	1.4300	1.4300	1.4300
24	1.4300	1.4300	1.4300	1.4300	1.4300	1.4300	1.4300	1.4300	1.4300	1.4300	1.4300	1.4300

Table A.39: Hourly adjustment factors for the heat pump's capacity in heating mode $fCAP_{hpq}$.

Hour	Jan	Feb	Mar	Apr	May	Jun	Jul	Aug	Sep	Oct	Nov	Dec
1	0.9253	0.9177	0.9110	0.9045	0.8986	0.8953	0.8981	0.9098	0.9303	0.9558	0.9810	1.0021
2	0.9534	0.9441	0.9357	0.9277	0.9203	0.9162	0.9197	0.9343	0.9597	0.9913	1.0225	1.0487
3	0.9922	0.9812	0.9715	0.9622	0.9536	0.9488	0.9529	0.9699	0.9995	1.0362	1.0725	1.1029
4	1.0313	1.0204	1.0108	1.0016	0.9931	0.9883	0.9923	1.0092	1.0385	1.0749	1.1109	1.1410
5	1.1054	1.0938	1.0836	1.0738	1.0648	1.0597	1.0640	1.0819	1.1130	1.1339	1.1339	1.1339
6	1.1339	1.1339	1.1339	1.1392	1.1291	1.1235	1.1282	1.1339	1.1339	1.1339	1.1339	1.1339
7	1.1339	1.1339	1.1339	1.1339	1.1339	1.1339	1.1339	1.1339	1.1339	1.1339	1.1339	1.1339
8	1.1339	1.1339	1.1339	1.1339	1.1339	1.1339	1.1339	1.1339	1.1339	1.1339	1.1339	1.1339
9	1.1339	1.1339	1.1339	1.1382	1.1292	1.1241	1.1284	1.1339	1.1339	1.1339	1.1339	1.1339
10	1.0814	1.0714	1.0625	1.0540	1.0462	1.0418	1.0455	1.0610	1.0880	1.1215	1.1339	1.1339
11	0.9888	0.9807	0.9734	0.9665	0.9601	0.9565	0.9595	0.9722	0.9942	1.0216	1.0487	1.0714
12	0.9414	0.9345	0.9283	0.9224	0.9170	0.9140	0.9165	0.9273	0.9460	0.9692	0.9921	1.0113
13	0.9253	0.9177	0.9110	0.9045	0.8986	0.8953	0.8981	0.9098	0.9303	0.9558	0.9810	1.0021
14	0.9534	0.9441	0.9357	0.9277	0.9203	0.9162	0.9197	0.9343	0.9597	0.9913	1.0225	1.0487
15	0.9922	0.9812	0.9715	0.9622	0.9536	0.9488	0.9529	0.9699	0.9995	1.0362	1.0725	1.1029
16	1.0313	1.0204	1.0108	1.0016	0.9931	0.9883	0.9923	1.0092	1.0385	1.0749	1.1109	1.1410
17	1.1054	1.0938	1.0836	1.0738	1.0648	1.0597	1.0640	1.0819	1.1130	1.1339	1.1339	1.1339
18	1.1339	1.1339	1.1339	1.1392	1.1291	1.1235	1.1282	1.1339	1.1339	1.1339	1.1339	1.1339
19	1.1339	1.1339	1.1339	1.1339	1.1339	1.1339	1.1339	1.1339	1.1339	1.1339	1.1339	1.1339
20	1.1339	1.1339	1.1339	1.1339	1.1339	1.1339	1.1339	1.1339	1.1339	1.1339	1.1339	1.1339
21	1.1339	1.1339	1.1339	1.1382	1.1292	1.1241	1.1284	1.1339	1.1339	1.1339	1.1339	1.1339
22	1.0814	1.0714	1.0625	1.0540	1.0462	1.0418	1.0455	1.0610	1.0880	1.1215	1.1339	1.1339
23	0.9888	0.9807	0.9734	0.9665	0.9601	0.9565	0.9595	0.9722	0.9942	1.0216	1.0487	1.0714
24	0.9414	0.9345	0.9283	0.9224	0.9170	0.9140	0.9165	0.9273	0.9460	0.9692	0.9921	1.0113

Table A.40: Hourly adjustment factors for the heat pump's coefficient of performance in heating mode $fCOP_{hpq}$.

Hour	Jan	Feb	Mar	Apr	May	Jun	Jul	Aug	Sep	Oct	Nov	Dec
1	0.7640	0.7585	0.7536	0.7490	0.7447	0.7423	0.7443	0.7528	0.7676	0.7860	0.8041	0.8193
2	0.7843	0.7775	0.7715	0.7657	0.7604	0.7574	0.7599	0.7704	0.7888	0.8115	0.8340	0.8529
3	0.8122	0.8043	0.7973	0.7906	0.7844	0.7809	0.7838	0.7961	0.8174	0.8439	0.8701	0.8920
4	0.8403	0.8325	0.8256	0.8189	0.8128	0.8094	0.8123	0.8244	0.8455	0.8718	0.8977	0.9195
5	0.8937	0.8854	0.8780	0.8710	0.8645	0.8608	0.8639	0.8768	0.8993	0.9099	0.9099	0.9099
6	0.9099	0.9099	0.9099	0.9181	0.9109	0.9068	0.9102	0.9099	0.9099	0.9099	0.9099	0.9099
7	0.9099	0.9099	0.9099	0.9099	0.9099	0.9099	0.9099	0.9099	0.9099	0.9099	0.9099	0.9099
8	0.9099	0.9099	0.9099	0.9099	0.9099	0.9099	0.9099	0.9099	0.9099	0.9099	0.9099	0.9099
9	0.9099	0.9099	0.9099	0.9174	0.9109	0.9073	0.9103	0.9099	0.9099	0.9099	0.9099	0.9099
10	0.8764	0.8693	0.8628	0.8567	0.8511	0.8479	0.8506	0.8618	0.8812	0.9054	0.9099	0.9099
11	0.8097	0.8039	0.7986	0.7936	0.7890	0.7864	0.7886	0.7978	0.8137	0.8334	0.8529	0.8693
12	0.7756	0.7706	0.7661	0.7619	0.7580	0.7558	0.7577	0.7654	0.7789	0.7956	0.8121	0.8260
13	0.7640	0.7585	0.7536	0.7490	0.7447	0.7423	0.7443	0.7528	0.7676	0.7860	0.8041	0.8193
14	0.7843	0.7775	0.7715	0.7657	0.7604	0.7574	0.7599	0.7704	0.7888	0.8115	0.8340	0.8529
15	0.8122	0.8043	0.7973	0.7906	0.7844	0.7809	0.7838	0.7961	0.8174	0.8439	0.8701	0.8920
16	0.8403	0.8325	0.8256	0.8189	0.8128	0.8094	0.8123	0.8244	0.8455	0.8718	0.8977	0.9195
17	0.8937	0.8854	0.8780	0.8710	0.8645	0.8608	0.8639	0.8768	0.8993	0.9099	0.9099	0.9099
18	0.9099	0.9099	0.9099	0.9181	0.9109	0.9068	0.9102	0.9099	0.9099	0.9099	0.9099	0.9099
19	0.9099	0.9099	0.9099	0.9099	0.9099	0.9099	0.9099	0.9099	0.9099	0.9099	0.9099	0.9099
20	0.9099	0.9099	0.9099	0.9099	0.9099	0.9099	0.9099	0.9099	0.9099	0.9099	0.9099	0.9099
21	0.9099	0.9099	0.9099	0.9174	0.9109	0.9073	0.9103	0.9099	0.9099	0.9099	0.9099	0.9099
22	0.8764	0.8693	0.8628	0.8567	0.8511	0.8479	0.8506	0.8618	0.8812	0.9054	0.9099	0.9099
23	0.8097	0.8039	0.7986	0.7936	0.7890	0.7864	0.7886	0.7978	0.8137	0.8334	0.8529	0.8693
24	0.7756	0.7706	0.7661	0.7619	0.7580	0.7558	0.7577	0.7654	0.7789	0.7956	0.8121	0.8260

Table A.41: Hourly adjustment factors for the heat pump's capacity in cooling mode $fCAP_{hpr}$.

Hour	Jan	Feb	Mar	Apr	May	Jun	Jul	Aug	Sep	Oct	Nov	Dec
1	1.2100	1.2100	1.2100	1.2100	1.2100	1.2100	1.2100	1.2100	1.2100	1.2100	1.2100	1.2100
2	1.2100	1.2100	1.2100	1.2100	1.2100	1.2100	1.2100	1.2100	1.2100	1.2100	1.2100	1.2100
3	1.2100	1.2100	1.2100	1.2100	1.2100	1.2100	1.2100	1.2100	1.2100	1.2100	1.2100	1.2100
4	1.2100	1.2100	1.2100	1.2100	1.2100	1.2100	1.2100	1.2100	1.2100	1.2100	1.2100	1.2100
5	1.2100	1.2100	1.2100	1.2100	1.2100	1.2100	1.2100	1.2100	1.2100	1.2100	1.2100	1.1990
6	1.2100	1.2100	1.2100	1.2100	1.2100	1.2100	1.2100	1.2100	1.2100	1.1958	1.1638	1.1370
7	1.1925	1.2026	1.2100	1.2100	1.2100	1.2100	1.2100	1.2100	1.1858	1.1520	1.1186	1.0906
8	1.1911	1.2006	1.2100	1.2100	1.2100	1.2100	1.2100	1.2100	1.1848	1.1530	1.1214	1.0951
9	1.2100	1.2100	1.2100	1.2100	1.2100	1.2100	1.2100	1.2100	1.2100	1.2033	1.1747	1.1507
10	1.2100	1.2100	1.2100	1.2100	1.2100	1.2100	1.2100	1.2100	1.2100	1.2100	1.2100	1.2100
11	1.2100	1.2100	1.2100	1.2100	1.2100	1.2100	1.2100	1.2100	1.2100	1.2100	1.2100	1.2100
12	1.2100	1.2100	1.2100	1.2100	1.2100	1.2100	1.2100	1.2100	1.2100	1.2100	1.2100	1.2100
13	1.2100	1.2100	1.2100	1.2100	1.2100	1.2100	1.2100	1.2100	1.2100	1.2100	1.2100	1.2100
14	1.2100	1.2100	1.2100	1.2100	1.2100	1.2100	1.2100	1.2100	1.2100	1.2100	1.2100	1.2100
15	1.2100	1.2100	1.2100	1.2100	1.2100	1.2100	1.2100	1.2100	1.2100	1.2100	1.2100	1.2100
16	1.2100	1.2100	1.2100	1.2100	1.2100	1.2100	1.2100	1.2100	1.2100	1.2100	1.2100	1.2100
17	1.2100	1.2100	1.2100	1.2100	1.2100	1.2100	1.2100	1.2100	1.2100	1.2100	1.2100	1.1990
18	1.2100	1.2100	1.2100	1.2100	1.2100	1.2100	1.2100	1.2100	1.2100	1.1958	1.1638	1.1370
19	1.1925	1.2026	1.2100	1.2100	1.2100	1.2100	1.2100	1.2100	1.1858	1.1520	1.1186	1.0906
20	1.1911	1.2006	1.2100	1.2100	1.2100	1.2100	1.2100	1.2100	1.1848	1.1530	1.1214	1.0951
21	1.2100	1.2100	1.2100	1.2100	1.2100	1.2100	1.2100	1.2100	1.2100	1.2033	1.1747	1.1507
22	1.2100	1.2100	1.2100	1.2100	1.2100	1.2100	1.2100	1.2100	1.2100	1.2100	1.2100	1.2100
23	1.2100	1.2100	1.2100	1.2100	1.2100	1.2100	1.2100	1.2100	1.2100	1.2100	1.2100	1.2100
24	1.2100	1.2100	1.2100	1.2100	1.2100	1.2100	1.2100	1.2100	1.2100	1.2100	1.2100	1.2100

Table A.42: Hourly adjustment factors for the heat pump's energy efficiency ratio in cooling mode $fEER_{hpr}$.

Hour	Jan	Feb	Mar	Apr	May	Jun	Jul	Aug	Sep	Oct	Nov	Dec
1	1.4235	1.4235	1.4235	1.4235	1.4235	1.4235	1.4235	1.4235	1.4235	1.4235	1.4235	1.4235
2	1.4235	1.4235	1.4235	1.4235	1.4235	1.4235	1.4235	1.4235	1.4235	1.4235	1.4235	1.4235
3	1.4235	1.4235	1.4235	1.4235	1.4235	1.4235	1.4235	1.4235	1.4235	1.4235	1.4235	1.4235
4	1.4235	1.4235	1.4235	1.4235	1.4235	1.4235	1.4235	1.4235	1.4235	1.4235	1.4235	1.4235
5	1.4235	1.4235	1.4235	1.4235	1.4235	1.4235	1.4235	1.4235	1.4235	1.4235	1.4235	1.3872
6	1.4235	1.4235	1.4235	1.4235	1.4235	1.4235	1.4235	1.4235	1.4235	1.3813	1.3218	1.2720
7	1.3752	1.3939	1.4235	1.4235	1.4235	1.4235	1.4235	1.4235	1.3627	1.2999	1.2377	1.1856
8	1.3727	1.3903	1.4235	1.4235	1.4235	1.4235	1.4235	1.4235	1.3609	1.3017	1.2430	1.1940
9	1.4235	1.4235	1.4235	1.4235	1.4235	1.4235	1.4235	1.4235	1.4235	1.3954	1.3421	1.2975
10	1.4235	1.4235	1.4235	1.4235	1.4235	1.4235	1.4235	1.4235	1.4235	1.4235	1.4235	1.4235
11	1.4235	1.4235	1.4235	1.4235	1.4235	1.4235	1.4235	1.4235	1.4235	1.4235	1.4235	1.4235
12	1.4235	1.4235	1.4235	1.4235	1.4235	1.4235	1.4235	1.4235	1.4235	1.4235	1.4235	1.4235
13	1.4235	1.4235	1.4235	1.4235	1.4235	1.4235	1.4235	1.4235	1.4235	1.4235	1.4235	1.4235
14	1.4235	1.4235	1.4235	1.4235	1.4235	1.4235	1.4235	1.4235	1.4235	1.4235	1.4235	1.4235
15	1.4235	1.4235	1.4235	1.4235	1.4235	1.4235	1.4235	1.4235	1.4235	1.4235	1.4235	1.4235
16	1.4235	1.4235	1.4235	1.4235	1.4235	1.4235	1.4235	1.4235	1.4235	1.4235	1.4235	1.4235
17	1.4235	1.4235	1.4235	1.4235	1.4235	1.4235	1.4235	1.4235	1.4235	1.4235	1.4235	1.3872
18	1.4235	1.4235	1.4235	1.4235	1.4235	1.4235	1.4235	1.4235	1.4235	1.3813	1.3218	1.2720
19	1.3752	1.3939	1.4235	1.4235	1.4235	1.4235	1.4235	1.4235	1.3627	1.2999	1.2377	1.1856
20	1.3727	1.3903	1.4235	1.4235	1.4235	1.4235	1.4235	1.4235	1.3609	1.3017	1.2430	1.1940
21	1.4235	1.4235	1.4235	1.4235	1.4235	1.4235	1.4235	1.4235	1.4235	1.3954	1.3421	1.2975
22	1.4235	1.4235	1.4235	1.4235	1.4235	1.4235	1.4235	1.4235	1.4235	1.4235	1.4235	1.4235
23	1.4235	1.4235	1.4235	1.4235	1.4235	1.4235	1.4235	1.4235	1.4235	1.4235	1.4235	1.4235
24	1.4235	1.4235	1.4235	1.4235	1.4235	1.4235	1.4235	1.4235	1.4235	1.4235	1.4235	1.4235

A.4.3 Solar production estimation

The photovoltaic and solar thermal productions depend on the technologies' technical parameters, as described in Section A.4.1, as well as on local climatic data, such as the hourly ambient temperature and hourly solar radiation, as calculated in Sections A.2.1 and A.2.2, respectively. Based on this information, the present section assesses the hourly specific productions of the photovoltaic panels PV and solar thermal collectors ST per m² of module installed.

A.4.3.1 Photovoltaic panels specific productions

The technical specifications of the PV are given in Table A.30. For each hourly period h of each representative day d, the PV specific production $x_{pv}(d,h)$ is determined according to Eq. (A.66), based on the methodology described by Duffie et al. (2013).

$$x_{pv}(d,h) = \frac{P_{pv}}{A_{pv}} \cdot \frac{Q_{r,pv}(d,h)}{Q_{r,SRC}} \cdot F_{top}(d,h) \cdot \eta_e \tag{A.66}$$

where the maximum power P_{pv}, the surface area A_{pv}, and the irradiation at SRC conditions $Q_{r,SRC}$ are given in Table A.30; the hourly solar radiation on tilted surface $Q_{r,pv}(d,h)$ was calculated in Section A.2.2 and is given in Table A.8. The efficiency of power-conditioning equipment is $\eta_e = 0.9$.

The hourly temperature correction factor $F_{top}(d,h)$ is calculated by Eq. (A.67)

$$F_{top}(d,h) = 1 + \mu_T \cdot \left(T_{c,pv}(d,h) - T_{c,SRC}\right) \tag{A.67}$$

where the temperature coefficient of power μ_T and the cell temperature at SRC conditions $T_{c,SRC}$ are given in Table A.30.

The hourly cell temperature $T_{c,pv}(d,h)$ is calculated according to Eq. (A.68).

$$T_{c,pv}(d,h) = Ta(d,h) + \left(T_{c,NOCT} - T_{a,NOCT}\right) \cdot \frac{Q_{r,pv}(d,h)}{Q_{r,NOCT}} \cdot \left(1 - \frac{\eta_{pv} \cdot F_{top}(d,h)}{0.9}\right) \tag{A.68}$$

where the module efficiency η_{pv} and the ambient temperature $T_{a,NOCT}$, cell temperature $T_{c,NOCT}$ and irradiation $Q_{r,NOCT}$ at NOCT conditions are given in Table A.30; and the hourly ambient air temperature $Ta(d,h)$ was calculated in Section A.2.1 and is given in Table A.5.

The hourly PV specific productions $x_{pv}(d,h)$ obtained are given in Table A.43.

A.4.3.2   Flat-plate solar thermal collectors unit productions

The technical specifications of the flat-plate solar thermal collectors ST are given in Table A.31. As explained in Chapter 4, the solar thermal collector is considered to operate in two temperature levels: low-temperature heat production to attend the consumer center's heating demand, and high-temperature heat production to drive the single-effect absorption chiller. Thus, the ST specific productions must be calculated according to the operation temperature.

For each hourly period h of each representative day d, the general Eq. (A.69) gives the specific productions $x_{stq}(d,h)$ and $x_{str}(d,h)$ for a collector's operation temperature $T_{ST} = 60$ °C (low-temperature operation) and $T_{ST} = 80$ °C (high-temperature operation), respectively.

$$x_{st}(d, h) = Max\left(k_0 \cdot Q_{r,st}(d, h) - k_1 \cdot (T_{ST} - Ta(d, h)) - k_2 \cdot (T_{ST} - Ta(d, h))^2; 0\right) \qquad \text{(A.69)}$$

where the thermal coefficients k_0, k_1 and k_2 are given in Table A.31; the hourly ambient temperature $Ta(d,h)$ was calculated in Section A.2.1 (Table A.5); and the hourly solar radiation on tilted surface $Q_{r,st}(d,h)$ was calculated in Section A.2.2 (Table A.9).

The hourly ST specific productions $x_{stq}(d,h)$ and $x_{str}(d,h)$ obtained are given in Table A.44 and Table A.45, respectively.

Table A.43: Hourly photovoltaic specific production x_{pv}, W/m^2.

Hour	Jan	Feb	Mar	Apr	May	Jun	Jul	Aug	Sep	Oct	Nov	Dec
1	0.00	0.00	0.00	0.00	0.00	0.00	0.00	0.00	0.00	0.00	0.00	0.00
2	0.00	0.00	0.00	0.00	0.00	0.00	0.00	0.00	0.00	0.00	0.00	0.00
3	0.00	0.00	0.00	0.00	0.00	0.00	0.00	0.00	0.00	0.00	0.00	0.00
4	0.00	0.00	0.00	0.00	0.00	0.00	0.00	0.00	0.00	0.00	0.00	0.00
5	0.00	0.00	0.00	0.00	0.00	0.00	0.00	0.00	0.00	0.00	0.00	0.00
6	0.00	0.00	0.00	0.50	4.74	6.43	5.32	2.14	0.00	0.00	0.00	0.00
7	0.00	0.00	6.71	13.50	19.13	21.54	21.42	17.36	9.97	0.00	0.00	0.00
8	9.49	18.30	26.24	32.98	39.37	42.11	44.07	40.48	30.78	22.18	12.64	7.60
9	27.42	39.15	47.76	53.38	59.70	62.34	66.30	63.82	53.01	44.01	31.99	24.99
10	45.22	59.02	67.58	71.60	77.35	79.62	85.19	84.03	73.02	64.45	50.91	42.43
11	59.24	74.27	82.42	85.01	90.09	91.90	98.53	98.50	87.76	79.92	65.67	56.26
12	66.80	82.32	90.11	91.87	96.48	97.96	105.06	105.67	95.27	87.99	73.56	63.76
13	66.56	81.95	89.63	91.37	95.91	97.31	104.31	104.96	94.71	87.55	73.27	63.55
14	58.61	73.27	81.10	83.65	88.51	90.06	96.42	96.51	86.20	78.73	64.90	55.72
15	44.44	57.73	65.82	69.73	75.16	77.04	82.24	81.30	70.92	62.90	49.95	41.76
16	26.80	38.04	46.16	51.58	57.51	59.74	63.35	61.15	51.04	42.64	31.20	24.48
17	9.25	17.73	25.27	31.75	37.78	40.18	41.93	38.62	29.53	21.42	12.30	7.43
18	0.00	0.00	6.47	13.02	18.39	20.59	20.42	16.59	9.58	0.00	0.00	0.00
19	0.00	0.00	0.00	0.49	4.59	6.19	5.10	2.06	0.00	0.00	0.00	0.00
20	0.00	0.00	0.00	0.00	0.00	0.00	0.00	0.00	0.00	0.00	0.00	0.00
21	0.00	0.00	0.00	0.00	0.00	0.00	0.00	0.00	0.00	0.00	0.00	0.00
22	0.00	0.00	0.00	0.00	0.00	0.00	0.00	0.00	0.00	0.00	0.00	0.00
23	0.00	0.00	0.00	0.00	0.00	0.00	0.00	0.00	0.00	0.00	0.00	0.00
24	0.00	0.00	0.00	0.00	0.00	0.00	0.00	0.00	0.00	0.00	0.00	0.00

Table A.44: Solar thermal specific production (low-temperature operation) x_{stq}, W/m².

Hour	Jan	Feb	Mar	Apr	May	Jun	Jul	Aug	Sep	Oct	Nov	Dec
1	0.00	0.00	0.00	0.00	0.00	0.00	0.00	0.00	0.00	0.00	0.00	0.00
2	0.00	0.00	0.00	0.00	0.00	0.00	0.00	0.00	0.00	0.00	0.00	0.00
3	0.00	0.00	0.00	0.00	0.00	0.00	0.00	0.00	0.00	0.00	0.00	0.00
4	0.00	0.00	0.00	0.00	0.00	0.00	0.00	0.00	0.00	0.00	0.00	0.00
5	0.00	0.00	0.00	0.00	0.00	0.00	0.00	0.00	0.00	0.00	0.00	0.00
6	0.00	0.00	0.00	0.00	0.00	0.00	0.00	0.00	0.00	0.00	0.00	0.00
7	0.00	0.00	0.00	0.00	0.00	0.00	0.00	0.00	0.00	0.00	0.00	0.00
8	0.00	0.00	0.00	0.00	21.73	61.24	90.44	65.49	0.00	0.00	0.00	0.00
9	0.00	0.00	32.98	83.53	150.97	193.89	238.16	218.04	123.95	36.17	0.00	0.00
10	0.00	88.33	159.52	203.67	272.47	317.60	376.01	362.47	259.42	166.13	49.99	0.00
11	83.07	187.50	261.72	299.23	367.96	414.40	483.87	476.32	367.89	271.81	143.49	69.11
12	133.46	245.11	320.91	354.27	422.70	469.95	545.53	541.40	430.33	332.93	197.91	118.20
13	137.74	250.37	326.94	360.19	428.86	476.67	552.44	547.93	436.39	338.33	202.45	122.10
14	96.10	203.48	280.05	317.24	386.70	434.88	504.91	496.19	386.32	288.21	157.27	80.96
15	18.51	114.97	190.10	233.70	303.73	351.78	411.16	395.65	290.16	193.48	72.96	4.77
16	0.00	2.79	73.81	123.63	192.72	239.58	285.14	262.39	165.02	72.68	0.00	0.00
17	0.00	0.00	0.00	3.98	69.20	113.23	143.93	115.96	31.37	0.00	0.00	0.00
18	0.00	0.00	0.00	0.00	0.00	0.00	4.95	0.00	0.00	0.00	0.00	0.00
19	0.00	0.00	0.00	0.00	0.00	0.00	0.00	0.00	0.00	0.00	0.00	0.00
20	0.00	0.00	0.00	0.00	0.00	0.00	0.00	0.00	0.00	0.00	0.00	0.00
21	0.00	0.00	0.00	0.00	0.00	0.00	0.00	0.00	0.00	0.00	0.00	0.00
22	0.00	0.00	0.00	0.00	0.00	0.00	0.00	0.00	0.00	0.00	0.00	0.00
23	0.00	0.00	0.00	0.00	0.00	0.00	0.00	0.00	0.00	0.00	0.00	0.00
24	0.00	0.00	0.00	0.00	0.00	0.00	0.00	0.00	0.00	0.00	0.00	0.00

Table A.45: Solar thermal specific production (high-temperature operation) x_{str}, W/m².

Hour	Jan	Feb	Mar	Apr	May	Jun	Jul	Aug	Sep	Oct	Nov	Dec
1	0.00	0.00	0.00	0.00	0.00	0.00	0.00	0.00	0.00	0.00	0.00	0.00
2	0.00	0.00	0.00	0.00	0.00	0.00	0.00	0.00	0.00	0.00	0.00	0.00
3	0.00	0.00	0.00	0.00	0.00	0.00	0.00	0.00	0.00	0.00	0.00	0.00
4	0.00	0.00	0.00	0.00	0.00	0.00	0.00	0.00	0.00	0.00	0.00	0.00
5	0.00	0.00	0.00	0.00	0.00	0.00	0.00	0.00	0.00	0.00	0.00	0.00
6	0.00	0.00	0.00	0.00	0.00	0.00	0.00	0.00	0.00	0.00	0.00	0.00
7	0.00	0.00	0.00	0.00	0.00	0.00	0.00	0.00	0.00	0.00	0.00	0.00
8	0.00	0.00	0.00	0.00	0.00	0.00	0.00	0.00	0.00	0.00	0.00	0.00
9	0.00	0.00	0.00	0.00	49.94	94.53	140.15	120.07	24.45	0.00	0.00	0.00
10	0.00	0.00	56.64	101.72	172.36	219.27	279.08	265.50	160.85	65.29	0.00	0.00
11	0.00	84.30	159.71	198.15	268.77	317.09	388.00	380.36	270.24	171.77	40.91	0.00
12	29.77	142.54	219.63	253.90	324.27	373.49	450.56	446.28	333.44	233.56	95.88	14.73
13	34.44	148.26	226.21	260.36	331.01	380.87	458.15	453.45	340.07	239.45	100.83	18.98
14	0.00	101.71	179.72	217.81	289.26	339.53	411.09	402.17	290.42	189.70	55.94	0.00
15	0.00	13.41	90.00	134.50	206.54	256.71	317.63	301.90	194.51	95.18	0.00	0.00
16	0.00	0.00	0.00	24.47	95.57	144.55	191.66	168.68	69.40	0.00	0.00	0.00
17	0.00	0.00	0.00	0.00	0.00	17.94	50.17	21.99	0.00	0.00	0.00	0.00
18	0.00	0.00	0.00	0.00	0.00	0.00	0.00	0.00	0.00	0.00	0.00	0.00
19	0.00	0.00	0.00	0.00	0.00	0.00	0.00	0.00	0.00	0.00	0.00	0.00
20	0.00	0.00	0.00	0.00	0.00	0.00	0.00	0.00	0.00	0.00	0.00	0.00
21	0.00	0.00	0.00	0.00	0.00	0.00	0.00	0.00	0.00	0.00	0.00	0.00
22	0.00	0.00	0.00	0.00	0.00	0.00	0.00	0.00	0.00	0.00	0.00	0.00
23	0.00	0.00	0.00	0.00	0.00	0.00	0.00	0.00	0.00	0.00	0.00	0.00
24	0.00	0.00	0.00	0.00	0.00	0.00	0.00	0.00	0.00	0.00	0.00	0.00

A.4.4   Rooftop area usage

As explained in Section A.1, the available rooftop surface area for the installation of PV and ST was estimated to be 2000 m². The PV and ST thus compete for surface area. The present section assesses the rooftop surface area occupied by each m² of module installed. The PV and ST technical parameters used in this section can be found in Table A.30 and Table A.31, respectively.

Figure A.8 depicts the side view of the module installation. Following the procedure described in IDAE (2011), the minimum row spacing d between two modules of height h should be that which ensures at least 4 hours of sun around noontime on the winter's solstice.
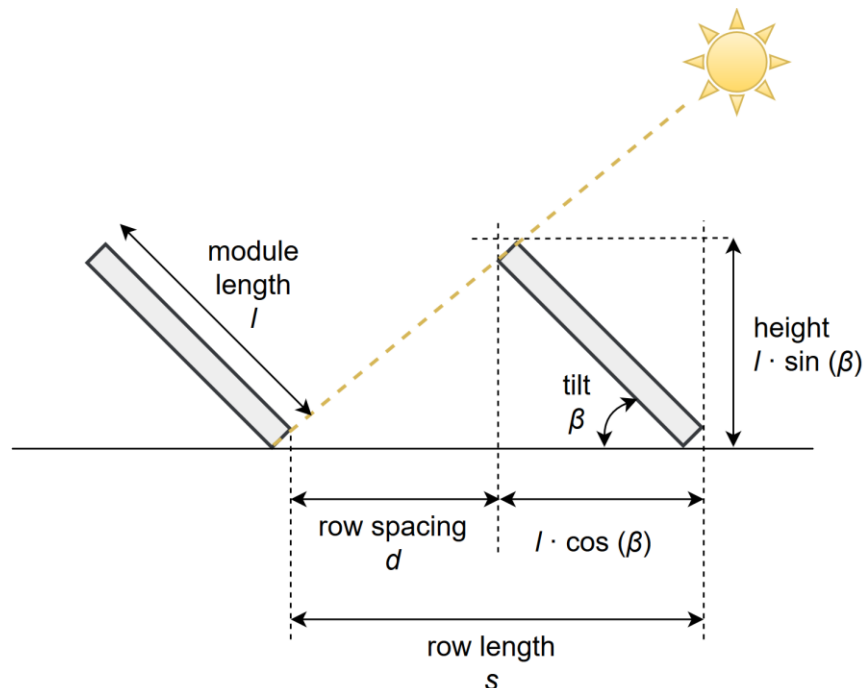

Figure A.8: Minimum distance between rows.

Generally, the row spacing d must be at least equal to the product of $h \cdot k$, in which h is the height of the module, determined by Eq. (A.70), and k is a dimensionless parameter, determined by Eq. (A.71) (IDAE, 2011).

$$h = l \cdot sin(\beta) \tag{A.70}$$
$$k = \frac{1}{tan(61° - \phi)} \tag{A.71}$$

where l is the module length; β is the tilt of the module, given in Table A.7; and Φ is the latitude, given in Table A.1 for the location of Zaragoza, Spain.

The row length s thus can be calculated as

$$s = d + l \cdot \cos(\beta) \tag{A.72}$$

The following row length values were obtained: 4.11 m for the PV and 4.72 m for the ST.

Now, knowing that the buildings have a square-shaped rooftop with 20-meter side L, the total number of PV and ST modules can be estimated:

For the PV, the number of modules per row is roughly $L/s \approx 5$ and the number of rows per building is about $L/w \approx 16$, in which w is the PV module width; thus, 400 PV modules can be installed in the five buildings, which corresponds to 640 m^2 of PV panels; dividing the available rooftop surface area by the total PV surface area yields the PV unit rooftop area usage rpv equal to 3.1250 m^2 roof/m^2 PV.

Analogously, for the ST the number of modules per row is about $L/s \approx 5$ and the number of rows per building is approximately $L/w \approx 7$; thus, 175 modules can be installed in the five buildings, which corresponds to 882 m^2 of ST collectors; the ST unit rooftop area usage rst obtained is equal to 2.2676 m^2 roof/m^2 ST.

APPENDIX B

Case study in Brazil – Technical data

B.   CASE STUDY IN BRAZIL – TECHNICAL DATA

As explained in Chapter 5, for some technologies included in the superstructure depicted in Fig. 5.3, their technical data were obtained from a representative device of a series that was carefully selected to fit within the estimated capacity range according to the hospital's energy demands. Appendix B provides the information of the concrete pieces of equipment, namely the cogeneration module GE (natural gas engine), the hot water and steam natural gas boilers GH and GV, the single- and double-effect absorption chillers AS and AD, and the mechanical chillers, described in Tables B.1-B.6. The technical specifications of the biomass boilers BH and BV were obtained from Delgado et al. (2018).

Table B.1: Technical specifications – cogeneration module GE (Ramos, 2012).

Technical specifications at nominal operation		
Manufacturer	-	Wärtsilä
Model series	-	34DF
Fuel	-	Natural gas
Fuel consumption (LHV)	kW	6,225
Gross electrical power	kW	3,000
Net electrical power	kW	2,910
Auxiliary electric consumption	kW_{el}/kW	0.03
Exhaust gas heat recovery	kW	1,378
Charge air heat recovery	kW	770
Jacket water heat recovery	kW	370
Lubricating oil heat recovery	kW	260
Exhaust gas mass flow	kg/s	4.6

Table B.2: Technical specifications – natural gas hot water boiler GH (Ramos, 2012).

Technical specifications at nominal operation		
Manufacturer	-	Viessmann
Model series	-	Vitomax 200 – LW
Fuel	-	Natural gas
Fuel consumption (LHV)	kW	3,900
Thermal efficiency	%	92
Auxiliary electric consumption	kW_{el}/kW	0.005

Table B.3: Technical specifications – natural gas steam boiler GV (Ramos, 2012).

Technical specifications at nominal operation		
Manufacturer	-	Viessmann
Model series	-	Vitomax 200 – HS
Fuel	-	Natural gas
Fuel consumption (LHV)	kW	4,000
Thermal efficiency	%	93
Auxiliary electric consumption	kW_{el}/kW	0.005

Table B.4: Technical specifications – mechanical chiller EC (Ramos, 2012).

Technical specifications at nominal operation		
Manufacturer	-	Mitsubishi
Model series	-	AART – 145EX
Cooling capacity	kW	5,978
COP (includes auxiliary electric consumption)	-	6.11

Table B.5: Technical specifications – single-effect absorption chiller AS (Ramos, 2012).

Technical specifications at nominal operation		
Manufacturer	-	World Energy
Model series	-	2AB 420
Cooling capacity	kW	1,476
Heat source	-	Hot water
COP	-	0.635
Auxiliary electric consumption	kW_{el}/kW	0.005

Table B.6: Technical specifications – double-effect absorption chiller AD (Ramos, 2012).

Technical specifications at nominal operation		
Manufacturer	-	Broad Air Conditioning
Model series	-	BYS 250
Cooling capacity	kW	1,476
Heat source	-	Saturated steam
COP	-	1.41
Auxiliary electric consumption	kW_{el}/kW	0.005